ORIGIN OF A-TYPE GRANITES IN EAST CHINA: EVIDENCE FROM HF-O-LI ISOTOPES

By Yuya GAO

A thesis submitted for the degree of Doctor of Philosophy,

Department of Earth and Planetary Sciences,

Macquarie University

June, 2015

ABSTRACT

A-type granites are a distinct group of granites which have great metallogenic significance and are the only granitoid type found on other terrestrial planets. Several petrogenetic models have been proposed to account for the mineralogical, geochemical and unique O-isotopic characteristics of A-type granites in eastern China.

This study elucidates the origin of Cretaceous A-type granites in eastern China using a non-traditional geochemical tracer, lithium isotopic composition, in addition to conventional geochemical data. This required improvement of *in situ* lithium isotopic analytical methods, laid the groundwork for understanding Li isotope behavior in granites and in zircons, and developed Hf-O-Li isotope fingerprints as a useful geochemical tracer for future studies of granite petrogenesis.

Six A-type granite plutons (Nianzishan, Houshihushan, Laoshan, Suzhou, Taohuadao, and Putuoshan) along eastern China were examined systematically for their geochronology, petrography, whole-rock geochemistry, whole-rock Li isotope compositions, and *in situ* zircon Hf-O-Li isotopes. The different stability of the U-Pb isotopic and oxygen-isotope systems in zircon have been re-evaluated. A screening criterion (D_{dpa}) has been developed to quantify the degree of radiation damage by taking both time and [U], [Th] into consideration. This makes it possible to obtain more reliable U-Pb and O isotope data from highly evolved high-U granites. The correlation between D_{dpa}, U-Pb ages and $\delta^{18}O$ values strongly suggests that anomalously high U-Pb ages and depleted oxygen isotope compositions are caused by different mechanisms related to different D_{dpa} thresholds. The screened isotopic results suggest that the Suzhou, Laoshan, and Houshihushan plutons formed in a single magmatic period and

are not really "low-$\delta^{18}O$" granites as previous assumed.

Whole-rock and *in situ* Li isotopes are applied to constrain the source region of the granites. Though extreme isotopic variations of Li have been observed during *in situ* SIMS (Secondary Ion Mass Spectrometry) analysis of zircon, Li isotopes in zircon are potentially useful for studying the origin of its host rock if the zircon grains are large enough. Detailed ion imaging and *in situ* profiles indicate that the large variations of [Li] and extreme fractionation of δ^7Li (~20‰) in zircons were only observed at the rim of the zircon and were generated by diffusion during cooling from igneous temperatures. Homogeneous δ^7Li in the cores of large zircon grains most likely carry reliable information about the isotopic signatures of their source magmas.

Geochemical evidence from Hf-O-Li isotopes indicates that the source region of Cretaceous A-type granites in eastern China has a more complex history than previously thought. This source region could be generated from partial melting of a juvenile upper crustal source (Nianzishan), re-melting of ancient igneous protoliths, triggered by input of depleted mantle-derived magmas (Suzhou, Putuoshan), a hybrid origin from metasomatized mantle and lower crust (Laoshan, Taohuadao), or dehydrated mantle source mixed with some component of lower crustal-derived magmas (Houshihushan). Their production was most likely triggered by the upwelling of the asthenosphere related to the delamination of a flat-subducting oceanic slab and the thinning of the subcontinental lithosphere.

Keywords: A-type granites eastern China, granite geochronology, granite geochemistry, granite O isotopes, Li isotopes, zircon radiation damage, post-orogenic granites

DECLARATION

This Thesis is based on work carried out in the ARC Centre of Excellence for Core to Crust Fluid Systems (CCFS) and the GEMOC National Key Centre, in the Department of Earth and Planetary Sciences of Macquarie University (Australia) and in the Institute of Geology and Geophysics, China Academy of Sciences, Beijing (China) over the period Feb 2012 to June 2015. I hereby declare that all data and interpretations presented in this thesis are my own work except for information cited from published or unpublished work of others that have been fully acknowledged.

This thesis is submitted to both Macquarie University, Australia and the Institute of Geology and Geophysics, China Academy of Sciences, China, under the conditions of the Cotutelle agreement for this PhD program between these institutions. No part of this thesis has previously been submitted for any other degree at any other university or educational institution.

Yuya Gao

1 June 2015

ACKNOWLEDEGEMENTS

First and foremost, I would like to thank my supervisor Sue O' Reilly for her patience and efforts in helping me finish my Ph.D, for the opportunity to use the cutting-edge instrumental facilities at GEMOC, for providing opportunities to attend conferences and workshops, and for all the financial support during my stay in Macquarie University.

I must truly express my gratitude for another supervisor Bill Griffin who gave me as much guidance as I needed and as much freedom as I wanted during my PhD, and for me this was the best form of supervision. He has encouraged me to think independently when I originally felt under-qualified, and allowing my accomplishments to feel substantial. I deeply thank his endless patience for correcting my Chinglish and incredible prompt reading and editing of any material I sent him -- never more than 48 hours. Moreover, his sense of humor made my learning experience at MQ more than enjoyable.

Norm Pearson was solely responsible for introducing me to the lab work. He was always accessible for discussions, and I much benefited from his expertise in analytical work and dealing with the multiple-collector ICPMS.

I am also grateful to my supervisor in China Xian-hua Li for his patience, for entrusting me with this work, and for all the academic and non-academic support. He is a diligent, precise, open-minded person, and always strict; sometimes a little aggressive when involved in scientific problems. Xianhua set me a great example in how to do research.

Meifei Chu deserves special mention for introducing me into the world of lithium analysis. She always answers my questions without any reservation. Her attitude to the lab work deeply impressed me and I have learned so much from her.

Both I and my thesis have benefited enormously from helpful suggestions by Jin-Hui Yang, Qiu-Li Li and Fu-yuan Wu. Special thanks to Yan-Jie Tang for his insightful comments. The thesis profited significantly from helpful suggestions and comments by Steve Clement, Ian Williams, Craig Lundstrom and Trevor Ireland which have greatly improved the thesis.

I am also grateful to Peter Wieland for his help in all chemical issues. He did a wonderful job preparing all the stuff I need in the lab. I would like to particularly thank Yu Liu, Guo-Qiang Tang and Hong-xia Ma for assistance with analytical work in the Chinese Academy of Sciences.

For the four field trips in China, there are too numerous of people to thank, but in particular I must recognize the extraordinary efforts of Ya-fei Wang, Xiao-yan Jiang, and Wei Dan who helped me collect samples. I would like to thank Sláma Jiří for providing the Plešovice zircon standards.

A big thank you also goes to Oliver Gaul, Sally-Ann Hodgekiss, Will Powell and the staff of the HDR office for their friendly and prompt help in the non-academic issues. I would also like to broadly thank all the staff and students of Earth and Science department in MQ for providing a friendly work atmosphere, and sharing not only their knowledge and experience, but also good times off the campus.

Finally, I thank and love my parents who have always supported me unselfishly, unquestioningly and unwaveringly and always have faith in me. The love and encouragement I received from family and friends was so invaluable.

TABLE OF CONTENTS

ABSTRACT ..... **I**

DECLARATION ..... **III**

ACKNOWLEDEGEMENTS ..... **V**

TABLE OF CONTENTS ..... **VII**

LIST OF FIGURES ..... **XIII**

LIST OF TABLES ..... **XXIII**

CHAPTER 1. INTRODUCTION **1**

1.1. BACKGROUND 1

1.1.1 A short review of A-type granites *1*

1.1.2 Low $\delta^{18}O$ A-type granites in East China *8*

1.1.3 Development of lithium isotope analysis *10*

1.1.4 The key scientific issues *14*

1.2. RESEARCH TOPIC AND SIGNIFICANCE 21

1.2.1 Research Focuses *21*

1.2.2 Significance *22*

1.3 THESIS OUTLINE 23

CHAPTER 2. GEOLOGICAL BACKGROUND AND SAMPLING **25**

2.1. INTRODUCTION 25

2.1.1 Tectonic context *25*

2.1.2 Cretaceous A-type granites in East China *28*

2.2 LOW $\Delta^{18}O$ A-TYPE GRANITES IN EAST CHINA 29

2.2.1 Nianzishan *29*

2.2.2 Houshihushan *32*

2.2.3 Laoshan *33*

2.2.4 Suzhou pluton *36*

2.2.5 Taohuadao *39*

2.2.6 Putuoshan *39*

CHAPTER 3. METHODOLOGY 43

3.1 PRE-TREATMENTS 43

3.1.1 Whole-rocks *43*

3.1.2 Zircons *44*

3.2 WHOLE ROCK GEOCHEMISTRY 44

3.2.1 Major-element analyses *45*

3.2.2 Trace-element analyses *45*

3.2.3 Whole-rock Li isotopes *46*

3.3 *IN SITU* ANALYSES 47

3.3.1 U-Pb dating of zircons *48*

3.3.2 In situ O-isotope analyses *49*

3.3.3 SIMS in situ analysis of Li isotopes *50*

3.3.4 Raman spectrometry *51*

3.3.5 SIMS ion imaging *51*

3.3.6 LA-MC-ICPMS Hf isotope analysis of zircon *52*

CHAPTER 4. THE LOW-δ^{18}O SUZHOU A-TYPE GRANITE REVISITED: THE EFFECTS OF HIGH U CONTENT ON ZIRCON O-ISOTOPES AND SIMS U-Pb DATING **55**

4.1 INTRODUCTION 57

4.2 GEOLOGICAL BACKGROUND 59

4.3 RESULTS 60

4.3.1 Imaging of zircons *60*

4.3.2 SIMS U-Pb ages *61*

4.3.3 In situ zircon and quartz oxygen isotopes *62*

4.3.4 Raman spectroscopy *65*

4.4 DISCUSSION 66

4.4.1 Uranium influence on SIMS zircon dating *66*

4.4.2 Influence of radiation damage on zircon oxygen isotopes *71*

4.3.3 Protocols for screening zircon data *77*

4.5 CONCLUSIONS 82

CHAPTER 5. SIMS ANALYSIS OF LI ISOTOPES IN ZIRCON: TOPOGRAPHY /CHARGE EFFECTS AND OPTIMIZATION OF ANALYTICAL PARAMETERS **85**

5.1 INTRODUCTION 85

5.2 SIMS ZIRCON *IN SITU* LI ISOTOPE ANALYSIS 86

5.3 RESULTS 89

5.4 DISCUSSION AND CONCLUDING REMARKS 92

5.4.1 Topography effect and Charge effect *92*

5.4.2 Refinements in techniques *93*

CHAPTER 6. LITHIUM ISOTOPES BEHAVIOR IN ZIRCON 96

6.1 INTRODUCTION 96

6.2 SAMPLE INFORMATION 97

6.2.1 Plešovice *98*

6.2.2 Qinghu *98*

6.2.3 Temora *100*

6.3 RESULTS 100

6.3.1 Plešovice *101*

6.3.2 Qinghu *103*

6.3.3 Temora *107*

6.4 DISCUSSION 109

6.4.1 Intra-granular heterogeneity in [Li] and δ^7Li *109*

6.4.2 Modeling of diffusion-driven fractionation of Li isotopes *111*

6.4.3 Speculations on Li isotopic data in zircons *116*

6.5 CONCLUSIONS 120

CHAPTER 7. ORIGIN OF CRETACEOUS A-TYPE GRANITES IN EAST CHINA 123

7.1 GEOCHEMICAL DATA 123

7.1.1 Major and Trace element 123

7.1.2 SIMS in situ U-Pb dating results of A-type granites 134

7.1.3 In situ Hf-O-Li isotopes 143

7.1.4 Whole-rock Lithium isotopes 151

7.2 DISCUSSION 151

7.2.1 The A-type granite magmatic episode 151

7.2.1 Oxygen isotopes of A-type granites 154

7.2.3 Fingerprinting the sources of low-$\delta^{18}O$ A-type granites with Li isotopes 157

7.2.4 Origin and Petrogenesis of A-type granites in Eastern China 161

7.3 CONCLUSIONS 167

CHAPTER 8. CONCLUSIONS 169

REFERENCES 174

APPENDIX TABLE i. List of samples studied 199

APPENDIX TABLE ii. Whole-rock chemical compositions 202

APPENDIX TABLE iii. *In situ* zircon U-Th-Pb isotope compositions 213

APPENDIX TABLE iv. *In situ* zircon Hf isotope compositions 217

APPENDIX TABLE v. *In situ* zircon O isotope compositions 223

APPENDIX TABLE vi. *In situ* quartz O isotope compositions 233

APPENDIX TABLE vii. *In situ* zircon Li isotope compositions 242

APPENDIX TABLE viii. Whole-rock Li isotope compositions 247

APPENDIX TABLE ix. SIMS zircon U-Pb isotopic data..... 249

APPENDIX TABLE x. Zircon oxygen-isotopic composition and calculated D_{dpa}..... 254

APPENDIX TABLE xi. SIMS in situ quartz oxygen isotopic results..... 258

APPENDIX TABLE xii. In situ M257 Li isotope compositions..... 259

APPENDIX TABLE xiii. In situ Plesovice and Qinghu Li isotopes 262

PUBLICATIONS..... 200

LIST OF FIGURES

Figure 1.1 Lithium isotopic composition of various reservoirs, modified after Tang et al. (2010).....11

Figure 1.2 Li isotopes fractionation during cation exchange (modified from Tomascak, 2004).....13

Figure 1.3 Values of δ^7Li: a) Jack Hills detrital zircons; b) Continental crust zircons; and whole rock values for: c) products of continental weathering; d) continental crust; e) altered ocean crust, marine sediment; f) Primitive igneous rocks (modified from Ushikubo et al., 2008).....18

Figure 1.4 Summary of Li diffusion data for minerals. Li diffusion in zircon is considerably slower than Li diffusion in other minerals for which diffusion data exist (Cherniak and Watson, 2010). 19

Figure 1.5 Summary of diffusion data for zircon: a) Li diffusion is considerably faster than diffusion of other cations in zircon, and b) faster than diffusion of oxygen under most circumstances, except at low temperatures under hydrothermal conditions. In addition, Li diffusion is much slower than the diffusion of helium (Cherniak and Watson, 2010).....20

Figure 2.1 Geological map and six selected late Mesozoic A-type granites along the continental margin in eastern China. Modified after Wang et al. (1995)

and Sun et al. (2007) 27

Figure 2.2 a) Sketch geological map of China; b) Distribution of Mesozoic igneous rocks in NE China. Modified from Wu et al. (2003b); c) Geological map of Nianzishan Pluton (modified from Wei, 2008); d) Outcrop of Nianzishan K-feldspar granite; e) Typical photomicrograph of Nianzishan K-feldspar granite. 30

Figure 2.3 a) Sketch geological map of China; b) Distribution of Mesozoic igneous rocks in North China Craton. Modified from Yang et al. (2003); c) Geological map of Houshihushan Pluton (modified from Wei, 2008); d) Outcrop of Houshihushan K-feldspar granite; e) Typical photomicrograph of Houshihushan K-feldspar granite. 32

Figure 2.4 a) Sketch geological map of E.China; b) the Laoshan granitic complex in the Jiaodong Peninsula. Modified from Goss et al. (2010); c) Geological map of Laoshan Pluton. Modified from Zhao et al. (1998). 34

Figure 2.5 a) Outcrop of Laoshan Alkaline granite; b) Photomicrograph of Laoshan Alkaline granite; c, d) Examples of mafic microgranular enclaves occurring within A-type granites in the Laoshan granitic complex. 35

Figure 2.6 a) Location of South China; b) Geological map showing distribution of Mesozoic intrusions in the South China. Modified from (Zhou et al., 2006); and c) Simplified geological map of Suzhou pluton.....37

Figure 2.7 a) Outcrop of Amphibole-bearing porphyritic K-feldspar granite; b)

Photomicrograph of ampibole bearing granite; c) Outcrop of biotite-enriched K-feldspar granite in Baieshan (west of Suzhou granite); d) Photomicrograph of biotite with K-feldspar; e) Miarolitic cavities in coarse-grained biotite-K-feldspar granite; f) Interstitial habit of biotite in biotite-K-feldspar granite; g) Ablitized K-feldspar; h) Porphyritic texture of quartz and hypersolvus feldspar. 38

Figure 2.8 a) Sketch geological map of China; b) Geological map of Taohuadao pluton. Modified from (Qiu et al., 1996); c) Geological map of Putuoshan Pluton. Modified from (Xie et al., 2005); d) Outcrop of Taohuadao biotite alkaline -feldspar granite; e, f) Typical photomicrograph of Taohuadao K-feldspar granite; g) Outcrop of Putuoshan K-feldspar granite; h,i) Typical photomicrograph of Putuoshan K-feldspar granite.....40

Figure 4.1 Cathodoluminescence (CL) images of representative zircons analysed for U-Pb, and O-isotopes. 61

Figure 4.2 a) Concordia zircon grains from the Suzhou granite (includes zircons from all three rock types); b) U-Pb relative probability; c) weighted average, and d) Concordia diagrams for group 1 zircons. Analyses are shown with 2σ errors and uncertainties in weighted mean ages are quoted at the 95% confidence level. 62

Figure 4.3 a) Plot of zircon [U] vs $^{206}Pb/^{238}U$ age; b) Plot of zircon D_{dpa} vs $^{206}Pb/^{238}U$ age; The D_{dpa} is calculated based on the [U], [Th] obtained from

the corresponding SIMS spots. Grey vertical dashed lines mark turning point at $D_{dpa} \approx 0.08$; c) Plot of zircon U content vs $\delta^{18}O$; d) Plot of zircon D_{dpa} vs $\delta^{18}O$. Grey vertical dashed lines mark turning point at $D_{dpa} \approx 0.03$. 63

Figure 4.4 a) Histogram of $\delta^{18}O$ values for zircons; typical cathodoluminescence images and transmitted-light photos of zircon crystals with "mantle" $\delta^{18}O$ (right) and low-$\delta^{18}O$ zircon crystals (left); b) Weighted average diagram of $\delta^{18}O$ values for zircons. Data of zircons with [U] >1500 ppm are in blue color. 64

Figure 4.5 a) Histogram diagram, and b) Weighted average of $\delta^{18}O$ values for quartz with reflected-light and transmitted-light photo; Data of "dirty quartz" are in orange color.....66

Figure 4.6 Raman spectra of zircons with different [U] and [Th]. Spectra obtained from the standards and other zircons with [U] < 1500 ppm all show the distinctive zircon peaks (grey vertical dashed lines). However, zircons with [U] >1500 ppm generally show patterns with broad indistinct peaks, indicating that these zircons have an amorphous or semi-amorphous structure. This most likely reflects partial to complete metamictization through radiation damage. 67

Figure 4.7 Oxygen isotope fractionation between quartz and zircon from the Suzhou pluton. Thin solid bar of data points represents the 2SD. Solid isotherms are from Valley et al. (2003).....74

Figure 4.8 Histograms of $\delta^{18}O$ values for zircon-quartz pairs from the Suzhou granite. a) amphibole-bearing porphyritic alkali-feldspar granite; b) coarse-grained alkali-feldspar granite; c) fine-grained alkali-feldspar granite; d) altered alkali-feldspar granite. 76

Figure 4.9 Plot of zircon U-Pb age vs $\delta^{18}O$ values. 78

Figure 4.10 Correlation between U concentration and U-Pb ages, along with assigned D_{dpa} of 0.03, 0.08, and 0.5. Dashed lines Th/U = 0.1; solid lines Th/U = 1. The area between dashed and solid lines with same D_{dpa} includes all zircons with Th/U = 0.1 ~ 1. 79

Figure 5.1 Examples of analytical spots of M257 zircon standard. 90

Figure 5.2 A single spot 80-cycle analysis of zircon standard M257 94

Figure 6.1 a) Trace outlines of Plešovice-R to show the position of the Li isotopic and [Li] measurements by SIMS; b) The ion image of the variation of Li and Y content (bright colors = higher content); c) $\delta^{7}Li$ vs Relative distance to the rim; d) [Li] vs Relative distance to the rim. 2 SE error bars for the isotope ratio measurements are shown. Typical analytical uncertainty of $\delta^{7}Li$ is ~2‰ for the 20 μm pits, ~2.5 ‰ for the 10 μm pits and ~5‰ for 5 μm pits (2 SD). Distance to rim is calculated by the X-Y position of the analytical spot to the nearest rim.....102

Figure 6.2 a) Trace outlines of Plešovice-L to show the position of the Li isotopic and [Li] measurements; b) Ion image of the variation of Li, Y, P and U

concent (bright colors = higher concentration); c) δ^7Li vs X position of AA' profile; d) [Li] vs X position of AA' profile; e) δ^7Li vs Relative distance to the rim; f) [Li] vs Relative distance to the rim. 104

Figure 6.3 a) Ion image of the variation of Li and Y concent (bright colors = higher concentration); b) δ^7Li vs Relative distance to the rim; c) [Li] vs Relative distance to the rim. 105

Figure 6.4 Plots of δ^7Li and [Li] vs Relative distance to the rim of seven Qinghu zircons. 106

Figure 6.5 a) Analytical spots on Temora zircon; b) ion image of Li, P, Y, Yb; c) δ^7Li profile through zircon; d) [Li] profile through zircon. 108

Figure 6.6 One-dimensional diffusion model for Plešovice zircons, calculated change in Li concentration as a function of distance a) PlesoviceL-10μm; b) All the Plesovice data.....113

Figure 6.7 One-dimensional diffusion model for Qinghu zircons, calculated change in Li concentration as a function of distance a) [Li]data of Qinghu_1; b) All the other Qinghu [Li] data.....113

Figure 6.8 One-dimensional diffusion model for Temora zircon, calculated change in Li concentration as a function of distance. 114

Figure 6.9 Effects of different β values on diffusion fractionation model.....115

Figure 6.10 a) [Li] and δ^7Li as a function of distance for a one dimensional diffusion model. The depth, width and the position of the trough of the Li

profile is a function of β, diffusivity and time; b) Modeled variation in δ^7Li vs Li concentration (ppm). The left side of the dashed line shows a negative correlation between δ^7Li and [Li] while the right side of the dashed line presents a possitive correlation. 117

Figure 6.11 a) Compiled data for all the analysed spots on Plešovice zircons; b) Probability density plot and c) Weighted average of analysed spots more than 100 μm from the rim. 118

Figure 6.12 a) Compiled data for all the analysed spots on Qinghu zircons; b) Probability density plot and c) Weighted average of analysed spots more than 50 μm from the rim. 120

Figure 7.1 Discrimination diagrams for six A-type granites a) Alkalis vs Silica plot (Ewart, A., 1982); b) A/NK vs A/CNK plot (Maniar and Piccoli, 1989). A = Al_2O_3, N = Na_2O, K = K_2O, C = CaO (all in molar proportions; c) SiO_2 vs $FeO_t/(FeO_t + MgO)$ diagram (Frost et al., 2001). Above the FeO_t line is the field of Fe-granitoids corresponding to A-type.; d) 10000Ga/A1 vs Zr plot. The coordinates of the M-I-S type granite fields are X=2.6, Y=250 (Whalen et al., 1987). 124

Figure 7.2 Nb-Y-Ce Classification diagrams for the studied A-type granites (Eby, 1992). 125

Figure 7.3 Primitive mantle-normalized plot of spidergrams for the: a) Nianzishan and b) Houshihushan pluton. Normalization values are from Sun and

McDonough (1989); Chondrite-normalized plot of rare-earth element abundances: c) Nianzishan and d) Houshihushan pluton. Chondritic values are from Sun and McDonough (1989). 126

Figure 7.4 Harker diagrams showing the chemical variations within the Houshihushan Pluton. Reference values are from Wen et al. (2013).....127

Figure 7.5 Harker diagrams showing the chemical variations of the Laoshan Pluton. Reference values are from Yan and Shi (2014).....129

Figure 7.6 Primitive mantle-normalized plot of spidergrams for the: a) Laoshan and b) Suzhou pluton. Normalization values are from Sun and McDonough (1989); Chondrite-normalized plot of rare-earth element abundances: c) Laoshan and d) Suzhou pluton. Chondritic values are from Sun and McDonough (1989).....130

Figure 7.7 Harker diagrams showing the chemical variations of the Suzhou pluton. 131

Figure 7.8 Primitive mantle-normalized plot of spidergrams for the: a) Putuoshan and b) Taohuadao pluton. Normalization values are from Sun and McDonough (1989); Chondrite-normalized plot of rare-earth element abundances: c) Putuoshan d) Taohuadao pluton. Chondritic values are from Sun and McDonough (1989).....132

Figure 7.9 Harker diagrams showing the chemical variations of the Putuoshan Pluton. Reference values are from (Qiu et al., 1999).....134

Figure 7.10 CL images of representative zircons analysed for in situ U-Pb, Hf-O-Li isotopes. Small red blue and yellow ellipses indicate the SIMS analysis spots for U-Pb, O and Li isotopes, respectively, and the big orange circles denote the LA-MC-ICPMS analysis spots for Hf isotopes. 135

Figure 7.11 U-Pb concordia diagram for zircons from the six A-type granites....136

Figure 7.12 Weighted average of the a) Nianzishan and b) Laoshan plutons.....137

Figure 7.13 Weighted average of the a) Taohuadao and b) Putuoshan plutons 139

Figure 7.14 a) Histogram and weighted average of $\varepsilon Hf_{(t)}$ values for the Nianzishan zircons; b) Weighted average of δ^7Li values for Nianzishan zircons; Histogram and weighted average of $\delta^{18}O$ values for the Nianzishan: c) zircon and d) quartz. 144

Figure 7.15 a) Histogram and weighted average of $\varepsilon Hf_{(t)}$ values for the Houshihushan zircons; b) Weighted average of δ^7Li values for Houshihushan zircons; Histogram and weighted average of $\delta^{18}O$ values for the Houshihushan: c) zircon and d) quartz. 145

Figure 7.16 Histogram and weighted average of $\varepsilon Hf_{(t)}$ valuse of zircon from the Laoshan a) A-type granite; b) Histogram and weighted average of $\delta^{18}O$ values for Laoshan c) zircon from A-type granite; d) zircon from I-type granite; e) quartz from A-type granite; f) Weighted average of δ^7Li values of zircons from Laoshan A-type granite. 146

Figure 7.17 a) Histogram and weighted average of $\varepsilon Hf_{(t)}$ values for the Suzhou

zircons; b) Weighted average of δ^7Li values for Suzhou zircon; Histogram and weighted average δ^{18}O values for the Suzhou c) zircon and d) quartz. 147

Figure 7.18 a) Histogram and weighted average of $\varepsilon Hf_{(t)}$ values for the Taohuadao zircons; b) Weighted average of δ^7Li values for Taohuadao zircons; Histogram and weighted average δ^{18}O for the Taohuadao: c) zircon and d) quartz.....149

Figure 7.19 Histogram and weighted average of $\varepsilon Hf_{(t)}$ value of zircon from the Putuoshan a) A-type granite; b) I-type granite; Histogram and weighted average of δ^{18}O values for the Putuoshan c) zircon from A-type granite; d) zircon from I-type granite; e) quartz from A-type granite; f) Weighted average of δ^7Li value of zircons from Putuoshan A-type granite. 150

Figure 7.20 Oxygen isotope fractionation between quartz and zircon from the six studied plutons. Thin solid bar of data points represents the 2SD. Solid isotherms are from Valley et al. (2003). The mantle range is shown by the pink box. 156

Figure 7.21 δ^{18}O variation during magma degassing under different temperatures 159

LIST OF TABLES

Table 1-1 Comparisons of the different analytical methods for lithium isotopes...15

Table 2-1 Summary of the studied A-type granites in eastern China 31

Table 4-1 Calculated D_{dpa} for zircon U-Pb age standards.....80

Table 5-1 Summary of instrumental conditions for SIMS δ^7Li determinations 87

Table 5-2 Summary of δ^7Li data for NIST-614 glass and M257 zircon 91

Table 5-3 Summary of the data with 40 cycles and 80 cycles 95

Table 6-1 Information on the studied standards.....99

Table 6-2 SIMS Li isotopes summary 101

Table 6-3 Temora zircon data.....107

Table 6-4 Model parameter for Plesovice, Qinghu and Temora zircon 116

Table 7-1 Summaries of Hf-O-Li isotopes of six studied plutons 141

Table 7-2 present dating results of studied A-type granites.....153

Table 7-3 Summaries the oxygen isotope of whole-rock, bulk zircon and quartz in the previous studies.....154

CHAPTER 1. INTRODUCTION

1.1. BACKGROUND

1.1.1 A short review of A-type granites

The formation and evolution of the continental crust is an important field of geological research. Granites, acidic intrusive rocks mainly composed of feldspar, quartz and mica, are the major constituent of the continental crust. They can be divided into S (supracrustal or sedimentary), I (infracrustal or igneous), A-type (alkaline, anorogenic and anhydrous) according to their source region (Chappell and White, 1974; White, 1979) or tectonic environment (Loiselle and Wones, 1979) and have been widely studied to identify mineralization processes, to investigate crust-mantle interaction, to model geodynamic processes, and to understand the transmission and transformation of matter and energy during the differentiation of the continental crust (Clarke, 1992; Clarke, 1996; Bonin et al., 1998; Barbarin, 1999; Bonin, 2007).

The definition and discrimination of A-type granites

A-type granites are a distinct group of granites that are volumetrically insignificant, compared with the dominant I- and S-type granites, but are found in both continental and oceanic crust (Bonin, 2007). They have attracted a great deal of attention since the term was proposed because of their unusual mineralogy and chemistry and their potential value in reconstructing tectonic settings (Loiselle and Wones, 1979; Collins et al., 1982; Clemens et al., 1986; Whalen et al., 1987; Eby, 1990; Creaser et al., 1991;

Turner et al., 1992; Skjerlie and Johnston, 1993; King et al., 1997b; King et al., 2001; Frost et al., 2002; Klimm et al., 2003; Martin, 2006; Yang et al., 2006; Dall'Agnol and Ramo, 2009; Frost and Frost, 2010; Magna et al., 2010a). A-type granites were originally defined by Loiselle and Wones (1979) as relatively dry (anhydrous) granites, characterized by high contents of alkali metals and most high-field-strength trace elements. Alkali mafic minerals, such as riebeckite, arfvedsonite, aegirine-augite, fayalite and sodic pyroxene are essential to discriminate A-type granites. However, some of the A-type granites are metaluminous or weakly peraluminous and do not contain alkali mafic minerals. Based on 148 analyses of A-type granites compared to 1569 analyses of I- and S-type granites from the Lachlan Fold Belt (LFB) of Australia, Whalen et al. (1987) proposed several discrimination diagrams. The most effective parameters to diagnose A-type granites are high Ga/Al ($10000 \times Ga/Al > 2.6$) and Zr (Zr > 250 ppm, Zr + Nb + Y + Ce > 350 ppm). Plots of $K_2O + Na_2O$, Nb and Zr *vs* Ga/Al are particularly useful in diagnosing of A-type granites for strongly alkaline to peralkaline analyses. The $(K_2O + Na_2O)/CaO$ *vs* (Zr + Nb + Y + Ce) diagram roughly distinguishes A-type granites from fractionated I- and S-type granites; Sylvester (1989) used the diagram of $(Al_2O_3 + CaO)/(FeO^* + Na_2O + K_2O)$ *vs* $100 \times (MgO + FeO^* + TiO_2)/SiO_2$, which is fairly effective in discriminating alkaline granites from calc-alkaline and strongly peraluminous granites.

However, the discrimination diagrams above fail to identify highly fractionated A- and I-type granites. As fractionation increases, the chemical and mineralogical compositions of different granite types converge (Whalen et al., 1987). Highly

fractionated A-, I-, S-type granites may have similar high Ga/Al, FeO*/MgO and low CaO contents and plot in the same area. Moreover, although the Zr contents of the least-evolved A-type granites are distinctively high, the most felsic A-type granites have lower Zr contents (~100 ppm) than I-type due to removal of zircon during fractionation to lower temperatures (King et al., 2001). Consequently, it is essentially impossible to classify them using one chemical discrimination diagram (King et al., 1997b; King et al., 2001; Yang et al., 2006). One possible criterion is FeO_t content. A-type granites have FeO_t > 1% while highly evolved I-types have FeO_t < 1%. Another possible way to discriminate highly fractionated A- and I- types is by calculating magmatic temperatures. The temperatures required for extraction of melts produced during anhydrous partial melting are higher than those of highly-evolved I type granites (~760^{o}C) (Wang et al., 2000). Clemens et al. (1986) favour the formation of A-type granites by partial melting at elevated temperatures (> 900^{o}C) of a melt-depleted I-type source with essentially low to moderate water content of 2.4 – 4.3 wt%; Creaser et al. (1991) reported temperatures of 900 – 1010^{o}C and water contents of 1 – 2 wt% for A-type volcanic rocks (Creaser and White, 1991).

The validity and limitations of various kinds of methods to identify A-type granites (especially geochemical discrimination diagrams) are not always clear. Cautions should be used when they are applied to help discriminate the types of granite. In summary, we recommend following steps to discriminate A-type granites: 1). Examine the mineral assemblage of the granites; 2). Use discrimination diagrams -- Ga/Al, Zr and FeO_t are the chief criteria for identifying A-type compositions; 3). See if there are associated

mafic rocks; 4). Discriminate highly-evolved A-, I-, and S-types by combining geochemical characteristics and calculating magmatic temperatures.

Subdivision of the A-type granitoids

The A-type granitoids can be divided into subgroups based on different criteria. The most common method of defining granite types is in terms of mineralogical and/or chemical compositions.

Eby (1990, 1992) suggested a two-fold subdivision based on the geochemistry of trace elements. Group A_1 is characterized by element ratios similar to those observed for OIB (Oceanic Island Basalt), and represents differentiation of magmas derived from continental rifts, hotspots or mantle plumes. Group A_2 is characterized by ratios that vary from those observed for continental crust to those observed for IAB (Island Arc Basalt), which relates them to continent-continent collision or island-arc magmatism. Therefore, A_1 and A_2 are also known as AA (anorogenic A-type granites) and PA (post-orogenic A-type granites) (Hong et al., 1995; Yuan, 2001).

Although this classification has been widely used, it is essentially a chemical classification which has developed some deficiencies with further research; for instance, typical anorogenic granitoids sometimes fall in the A_2 or near the A_1-A_2 boundary (Wu et al., 2002), or even outside both fields. Thus, there are limitations in the A_1-A_2 discriminant diagrams. They are unable to cover all the A-type granites; many A-type granites plot in the A_1-A_2 transition zone or overlap in both regions, and some are not consistent with their geological setting.

King et al. (1997b) compared the A-type granites in Lachlan Fold Belt (LFB) of

southeastern Australia with some peralkaline granites, and argue that aluminous (metaluminous to weakly peraluminous) granites from the LFB rocks are very different from with traditional "alkaline" A-type rocks. They suggest that the origin and petrogenesis of aluminous A-type granites are very different from peralkaline A-type granites and that the two types should not be grouped (King et al., 1997b). This classification scheme is well-accepted and widely used (Bonin, 2007). Aluminous and peralkaline A-type granites can be recognized on the basis of their mineralogical and geochemical characteristics. The peralkaline subgroup contains alkali mafic minerals, such as riebeckite, arfvedsonite, aegirine-augite, fayalite and sodic pyroxene, while the aluminous subgroup contains annite and Fe-rich calcic- or sodic-calcic amphibole. Geochemically, the two subgroups can be discriminated in the Al/(Ca + Na+ K) - Al/(Na + K) diagram. Compared to the peralkaline subgroup, the aluminous type contains higher Al_2O_3, MgO, CaO, Ba and Sr, but lower Rb, Ga and REE.

So far, the differences in origin and petrogenesis between these two varieties of A-type granites are not clear. King et al. (1997) proposed that the two types were derived from different sources; aluminous A-type granites were produced by high-temperature partial melting of a felsic infracrustal source while peralkaline A-type granites were associated with mafic magmas. Rajesh (2000) investigated A-type ring complexes at Ambalavayal in South India and suggests that aluminous and peralkaline A-type granites are generated from the same source. Alkaline A-type involved partial melting of a charnockitic mafic-intermediate lower crust while aluminous features could reflect the loss of a peralkaline fluid phase during limited fractional crystallization of

the magma in a high-level chamber. King et al. (2001) emphasized the petrogenetic differences in forming two types of granites. They proposed that both A-type magmas were produced by high-temperature, partial melting of quartzo-feldspathic crustal rocks. Their chemical variability is probably related to the efficiency of fractional crystallization and emplacement along a major fault at shallow levels. Wu et al. (2002) examined the paragenesis of A-type granites in North China, and concluded that no isotopic difference between these two subgroups of A-type granites has been demonstrated in NE China. Their origin is thought to have involved partial melting of an underplated lower crustal source.

Besides the traditional classification of A_1-A_2 and Alkaline-Aluminous subdivisions, another classification regarding reduced and oxidized A-type granites has been proposed. Until recently, little attention has been given to the oxidized magnetite-series A-type granites. This group was first defined by Anderson and Bender (1989). However, this classification is problematic as it does not strictly follow the original definition of A-type granites, and approaches calc-alkaline and I-type granites in some aspects (Dall'Agnol and de Oliveira, 2007). Early researchers suggested that the redox state of granite cannot be inherited from the source rocks, but only reflects the physical and chemical conditions of the magma chamber. Recent studies indicate that silicic magmas with small amounts of iron and large amounts of water do not have their redox states reset, and that these presumably reflect their generation (Carmichael, 1991; Blevin and Chappell, 1995). Experimental data indicate that, besides pressure, the nature of A-type granites is dependent on f_{O2} conditions and the water content of

magma sources. These developments have resulted in the classification of "reduced" and "oxidized" A-type granites (Frost and Frost, 1997; Dall'Agnol et al., 1999; Frost et al., 1999; Frost et al., 2001; Dall'Agnol and de Oliveira, 2007).

A-type granites: origin and petrogenesis

There appears to be a consensus that A-type granites are commonly emplaced in an extensional tectonic regime (Loiselle and Wones, 1979), but their origin and genesis are still an issue of hot debate (Yang et al., 2006; Bonin, 2007). Numerous petrogenetic models of A-type granites have been proposed during last 35 years. The crucial and fundamental question is whether such granitoids are exclusively crustally- derived or whether they require significant involvement of mantle material; or even whether they can be generated directly by fractional crystallization of basalt (Yang et al., 2006). The most widely accepted models can summarised as follow:

(i) Partial melting of a F- and/or Cl-enriched, dry, lower crustal granulitic residue left after an earlier extraction of I-type granitic melts (Collins et al., 1982; Clemens et al., 1986);

(ii) Anatexis of relatively refractory intermediate calc-alkaline meta-igneous crust (Creaser et al., 1991; Skjerlie and Johnston, 1993; Patiño Douce, 1997);

(iii) Derivation from mixed OIB-crustal sources (Eby, 1990; Eby, 1992);

(iv) Extreme fractionation of mantle-derived magmas emplaced to shallower crustal levels (Turner et al., 1992; Barbarin, 1999);

(v) Involvement of a depleted upper mantle modified by slab-derived fluids

(Liégeois et al., 1987);

(vi) Remelting of a lower crustal (meta-)igneous source metasomatized by mantle-derived fluids (Martin, 2006).

(vii) Hybridization between anatectic granitic and mantle-derived mafic magmas (Yang et al., 2006).

The above petrogenetic models for A-type granites indicate that the source regions of A-type granites might be very complicated. Huang et al. (2011) identified one A-type granite pluton with a high $\delta^{18}O$, up to 11‰, which suggests a contribution from metasedimentary rocks. They proposed that the physical conditions (the high-temperature and low f_{H2O}) might play a more critical role than the chemical composition of the source regions in the genesis of this unique rock type (Huang et al., 2011).

1.1.2 Low $\delta^{18}O$ A-type granites in East China

Mesozoic A-type granites are widely distributed in eastern China (Wang et al., 1995; Hu et al., 2005). They are divided into peralkaline and aluminous subgroups which differ in their mineral assemblages, mineral compositions, geochemical features and suggest derivation from diverse sources (Qiu et al., 2004; Wong et al., 2009; Jiang et al., 2011; Li et al., 2011a; Yang et al., 2012). This region is thus the ideal laboratory for the study of A-type granites. The most interesting discovery is that some of them have distinctive $\delta^{18}O$ values that are lower than normal mantle values (Fu et al., 1996; Wei et al., 2001a; Wei et al., 2002; Valley, 2003; Yuan et al., 2003; Wei et al., 2008; Zhang and Zheng, 2011). Oxygen is the most abundant element in the Earth's crust.

Igneous fractionation has negligible effects on oxygen-isotope composition, because the Si-O bonds in the silicate melt and in silicate minerals are essentially identical. Magmatic rocks with low $\delta^{18}O$ therefore may have tectonic implications, although they have been reported from only few areas (Hildreth et al., 1991; King et al., 1997a; Balsley and Gregory, 1998; Bindeman and Valley, 2000; Bindeman and Valley, 2001; Monani and Valley, 2001; Bindeman and Valley, 2003; Bindeman et al., 2007; Bindeman et al., 2008)，they usually occur in rift zones, associated with the development of caldera collapse and subsequent re-melting of low-$\delta^{18}O$ rocks. This melting involves high-T interaction between magmas and crustal water, or the assimilation of low-$\delta^{18}O$ rocks during magma emplacement. However, water-saturated magmas typically either erupt explosively or quench as subsurface porphyries before the magmatic $\delta^{18}O$ can be lowered by assimilation (Balsley and Gregory 1998). As a result, granites crystallized from low-$\delta^{18}O$ magmas are even rarer.

Several models have been proposed for the origin of low $\delta^{18}O$ A-type granites in East China. The most widely accepted one was proposed by Wei et. al. (2008), based on integration of Sr-Nd-O isotope data on whole-rock samples or bulk zircon separates. Their formation was attributed to the involvement of ^{18}O-depleted materials in the magma source, and the authors speculated that this represented a reworking or recycling of oceanic or continent crust (Wei et al., 2002; Wei et al., 2008). However, the initial Sr-isotope ratios of A-type granites are difficult to measure precisely due to extremely low Sr concentrations and high Rb/Sr; the bulk mineral analysis may obscure by mineral defects and carries some misleading information; all these hampers their use in

deciphering the origins of the magmas.

In recent years, the combined *in situ* analysis of Hf and O isotopes in zircon has provided a new approach to tracing the origin of granites, and has shifted the focus toward the involvement of mantle-derived magmas in granite genesis (Yang et al., 2006; Kemp et al., 2007; Li et al., 2009a; Li et al., 2010b; Zhu et al., 2011; Chen et al., 2013). However, an origin of A-type granites from altered oceanic crust cannot be totally ruled out through the use of Hf-O isotopes, as Hf isotopes provide similar constrain as Nd isotopes (Sun, 2010; Chen, 2015). Therefore, a non-traditional isotopic system, lithium isotopes, has been introduced in order to further constrain the sources of A-type granites.

1.1.3 Development of lithium isotope analysis

Physicochemical characteristics of Li

Lithium is the lightest lithophile element. It has two stable isotopes ^{7}Li and ^{6}Li, with relative abundances about 92.4% and 7.6%, respectively. Lithium isotope ratios are commonly presented using delta notation ($\delta^{7}Li= [(^{7}Li/^{6}Li_{sample}/^{7}Li/^{6}Li_{L\text{-}svec}) - 1] \times 1000$). Li has many unique chemical characteristics which make it a useful geological tracer (Chan et al., 1994; Pistiner and Henderson, 2003; Elliott et al., 2004; Rudnick and Nakamura, 2004; Rudnick et al., 2004; Teng et al., 2004; Tomascak, 2004; Teng, 2005; Elliott et al., 2006; Tang et al., 2007; Teng et al., 2009; Vlastelic et al., 2009; Magna et al., 2010a): 1). Lithium has a significant relative mass difference between its two isotopes (*ca.* 16%) coupled with broad elemental dispersion in Earth and planetary materials. In addition, there is *ca.* 8% natural mass fractionation in natural system

among different materials (Figure 1.1), caused by diffusive, hydrothermal and weathering processes; 2). Unlike the better-established light stable isotope systems (e.g., C, O & S), Li is a trace cation and does not form an integral part of hydrological, atmospheric or biological cycles; 3). Lithium is not a nutrient and does not participate in biologically mediated reactions; its isotopic composition is not influenced by redox reactions; 4). Lithium is also moderately incompatible in mafic silicate minerals in magmatic processes which likely to provide different information than is available from the more commonly used isotope systems; 5). Lithium isotopes are a potentially ideal tracer to constrain the role of hydrothermally-altered lower oceanic crust, as they are sensitive geochemical tracer of fluid/melt-mineral interactions from the Earth's surface to the mantle.

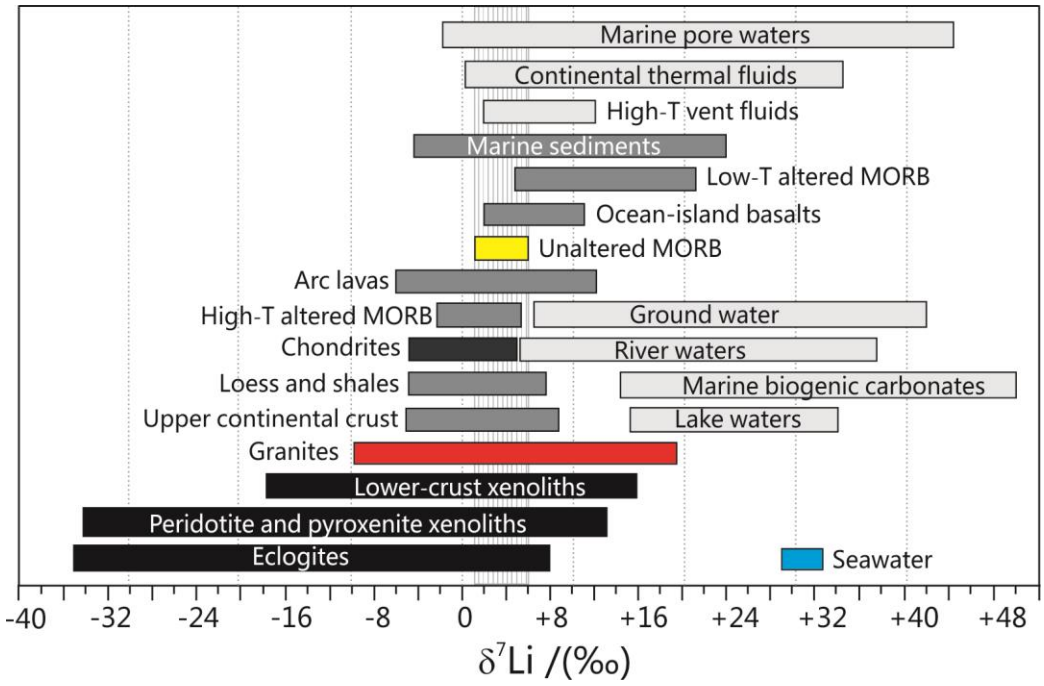


Figure 1.1 Lithium isotopic composition of various reservoirs, modified after Tang et al. (2010)

The applications of Li isotopes

As a newly developed isotopic system with so much potential, the applications of Li isotopes cover a wide range of geological processes, which includes: 1). Material cycling between mantle and crust (Jeffcoate et al., 2004; Seitz et al., 2004; Magna et al., 2006a; Aulbach and Rudnick, 2009; Halama et al., 2009); 2). Continental weathering (Huh et al., 2001; Pistiner and Henderson, 2003; Rudnick et al., 2004; Ushikubo et al., 2008); 3). Fluid transfer processes in subduction zones (Moriguti and Nakamura, 1998; Tomascak et al., 2000; Chan et al., 2002; Zack et al., 2003; Magna et al., 2006a; Marschall et al., 2006); 4). Seafloor alteration and crustal recycling at active continental margins (Chan et al., 1992; Chan et al., 2002); 5). Magmatism (Parkinson et al., 2006; Parkinson et al., 2007; Schuessler et al., 2009); 6). Cosmic events (Magna et al., 2006c; Magna et al., 2006b; Seitz et al., 2007; Magna et al., 2010b).

Determination of the Li isotope composition

Despite these merits of Li isotopic tracing, the very property that makes Li geochemically interesting makes quantification of its isotopic composition extraordinarily challenging: 1). To enable tracing, the accurate Li ratio has to be obtained, which necessitates a complete separation and purification of the Li in the sample before any measurement. The significant Li isotopic fractionation requires 100% recovery yield of Lithium in the column separation (Figure 1.2). The Li concentration of natural geological bodies is very low and significant interference is expected during separation (as an active metal cation lithium easily forms complex molecules with many elements) (Tomascak et al., 1999; Bouman et al., 2002; Magna et al., 2004; le Roux,

2009; le Roux, 2010); 2). Not many standard samples are available and settings may vary from one laboratory to another (Moriguti and Nakamura, 1998; James and Palmer, 2000); 3). Li isotopes are subject to great mass fractionation, which may lead to changes in the original isotopes of samples during analysis (Oi et al., 1991; Ooi et al., 1999; Tomascak et al., 1999; Magna et al., 2004); and 4). Li is highly diffusible and sensitive to subsequent geological processes, making it difficult to retain its original isotopic compoaition (Beck et al., 2006; Parkinson et al., 2006; Teng et al., 2006a; Cherniak and Watson, 2010; Dohmen et al., 2010). As such, it becomes very difficult to measure the accurate Li isotopic composition of geological samples. Nor is it easy to interpret the results of Li isotopic analysis.

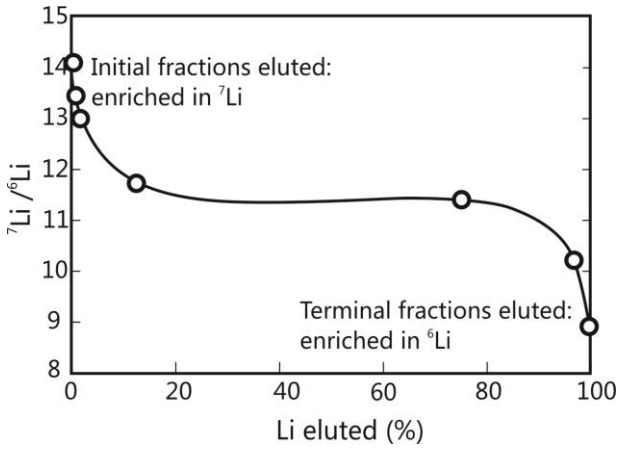


Figure 1.2 Li isotopes fractionation during cation exchange (modified from Tomascak, 2004)

The advantages of Li isotopes in identify the sources of A-type granites in E. China

Li is soluble in fluids, hence is widely distributed in all types of rocks. Intensive fractionation of Li isotope during weathering and fluid processes resulted in significant

divergences in the Li isotopic compositions of crustal sediments, sea water and altered oceanic crust from mantle, and the igneous rocks that have never undergone surface alteration (see Elliott et al., 2006; Tang et al., 2010 and reference within). Compared with granite Sr-Nd or Hf-O isotopic studies, Li isotopes are more sensitive to fluid processes or supracrustal materials, hence providing effective constraint for investigating the contribution made by fluids and surface weathering to granite diagenesis. As such, Li isotopes can serve as a sensitive tracer to identify whether magmatic rocks came from altered crust, whether they are mixed by supracrustal sediments or are simply the re-melted product of mantle-derived basic rocks. This could be very helpful to further constraining the material source and rock genesis of the Mesozoic A-type granites (especially those with low-$\delta^{18}O$ or abnormally high-$\delta^{18}O$) in East China.

1.1.4 The key scientific issues

At present, the combination of Hf and O isotopes is the most popular tool for tracing granite source regions(Kemp et al., 2007; Be'eri-Shlevin et al., 2010; Li et al., 2010b; Li et al., 2010c; Zhu et al., 2011; Dan et al., 2012; Chen et al., 2013; Jiang and Li, 2014). In zircon, oxygen is the major element, and magmatic differentiation hardly changes its oxygen isotopic composition. As a stable isotope, it is time-independent but is subject to pre-magmatic hydrothermal alteration; Hf isotopes are immune to low-temperature water-rock interactions in the source rock, but are sensitive to magma differentiation and radioactive growth. A combination of the two can provide useful information on granite source regions, however, Hf-O isotopic tracing has not provided

an unambiguous answer to problem of the source regions of low $\delta^{18}O$ A-type granites in China (Sun and 孙金凤, 2010; Chen, 2015).

Continuously improvement in the analytical procedures has made it possible to measure Li isotopes accurately as well as precisely. So far, three high-accuracy Li isotope measurement methods are widely accepted: 1). Thermal Ionization Mass Spectrometry (TIMS) (Oi et al., 1997; Moriguti and Nakamura, 1998; Chan and Frey, 2003; Kasemann et al., 2005; Nakamura et al., 2008); 2). Multi-collector Inductively Coupled Plasma Mass Spectrometry (MC-ICP-MS) (Magna et al., 2004; Seitz et al., 2004; Kasemann et al., 2005; Elliott et al., 2006; Jochum et al., 2006; Huang et al., 2010); 3). Secondary Ion Mass Spectrometry (SIMS) (Kasemann et al., 2005; Jochum et al., 2006). The advantages of the different methods are compared as follow：

Table 1-1 Comparisons of the different analytical methods for lithium isotopes

Analytical method	TIMS	MC-ICP-MS	SIMS
Type	Whole-rock/bulk mineral	Whole-rock/bulk mineral	*In situ*
Sample required	～250mg	～20mg	～10ng
precision(2σ)	±0.5‰	～0.12–1.1‰	~0.26-4.8‰
Sample prep.	time consuming	time consuming	easily prepared
Analytical time	slow	fast	fast

Whole-rock Li-isotope analysis involves complex sample preparation processes and long analysis cycles. It is sensitive to the freshness levels of the samples, often is unable to reveal the heterogeneity of complex samples and even gives misleading

information. SIMS Li-isotope analysis is superior in terms of sample preparation, spatial resolution and interpretation of analysis results; yet its analytical precision requires further improvement. So far, the most widely applied areas are olivine in mantle xenoliths (Woodland et al., 2002; Seitz et al., 2004; Sonntag et al., 2007; Bell et al., 2009), pyroxene from meteorites (Seitz et al., 2004; Beck et al., 2006; Marks et al., 2008); glass in basalt (Kobayashi et al., 2003; Kobayashi et al., 2004) and synthetic glass (Richter et al., 2003; Lundstrom et al., 2005). Application to continental crustal granitic rocks has been limited and highly debated (Teng et al., 2006b; Teng et al., 2008; Ushikubo et al., 2008; Teng et al., 2009).

Teng et al. (2004, 2008) conducted research on the isotopic composition and concentration of lithium in the continental curst. The estimated Li isotope composition of the upper continental crust is δ^7Li = 0 ± 2‰ with [Li] = 35 ± 11 ppm. The Li isotopes of lower continental crust show a large variation which ranges from −17.9 to +15.7‰, with an average of δ^7Li= +2.5‰ and [Li] = 8 ppm. The average δ^7Li of the bulk continental crust is around +1‰, which is lower than fresh mid-ocean ridge basalts (δ^7Li= +3.4‰, [Li] = 6 ppm), lithospheric mantle (δ^7Li = +3.4‰, [Li] = 1-2 ppm) and oceanic crust (δ^7Li= +5‰, [Li] = 7-33 ppm) (Tomascak, 2004).

The worldwide variation of δ^7Li in granites is −9 to +21‰ (Magna et al., 2010a and references within). Most granites lie in the range −4 to +9‰, with an average of +2.0 ± 2.3‰ (1σ, n = 130) (Teng et al., 2009 and references therein), which is equivalent to the mean value for the continental crust. Teng et al. (2009) examined the whole-rock Lithium isotopes of A-, S-, and I-type granite worldwide. They claimed that

Li isotopes do not fractionate significantly during the differentiation of granitic magmas, and that the spread in δ^7Li values is similar in all three types of granite, with the whole-rock δ^7Li ranging from −5 to +10‰. This would suggest that Li in granites mainly comes from the crust, with little contribution from mantle-derived Li.

Zircon is a weathering-resistant, silicate mineral with a high closure temperature for diffusion; it occurs widely in many types of rocks. At present, zircon is the most important mineral with respect to U-Pb dating and Hf-O isotopic tracing (Kemp et al., 2007). The ground-breaking work of Ushikubo et al. (2008) showed that the Li isotopic composition of zircon has great potential for tracing weathering processes and the recycling of crustal materials. The study gave a wide range of δ^7Li values (over 30‰) for Jack Hills zircons with ages of 4348-3362 Ma. They concluded that the Jack Hills zircons have retained the Li-isotope signature of the magma source, because Li diffusion in zircon is limited by the diffusion of REE^{3+} which substitutes on the Zr^{4+} site.

However, controversy arose because the δ^7Li range of the Hadean zircons discovered in Jack Hills (Figure 1.3a), is larger than the worldwide whole-rock δ^7Li variation in granites (Figure 1.3d), implying that zircon contains more information than whole-rock samples. Yet little research on *in situ* microanalysis of Li isotopes has been carried out after this initial breakthrough. This is attributable to the limited precision of the SIMS analyses on the one hand, and the lack of standard zircons with homogeneous Li-isotope ratios on the other hand. The δ^7Li value of the Xinjiang zircon standards used by Ushikubo et al. (2008) range from 3.1 to 11.6‰ (2σ = 4.8‰), with average Li

concentrations of 6.4 ± 6.6 ppm (2σ). Inhomogeneous standard samples could compromise the analytical results. The accuracy and standards of SIMS constitutes a major constraint on *in situ* analysis of Li isotopes in zircon.

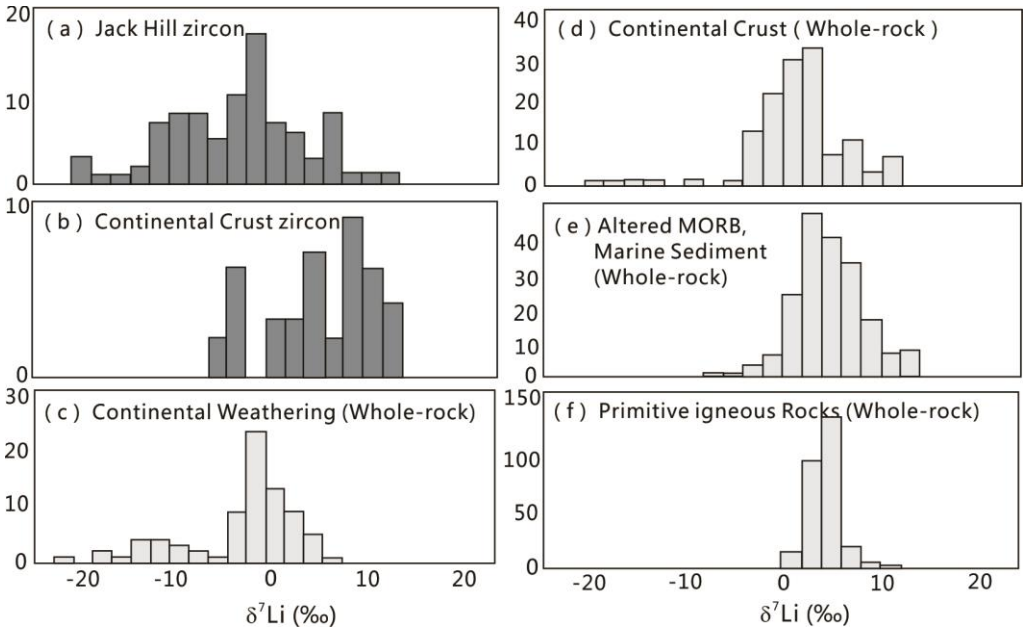


Figure 1.3 Values of δ^7Li: a) Jack Hills detrital zircons; b) Continental crust zircons; and whole rock values for: c) products of continental weathering; d) continental crust; e) altered ocean crust, marine sediment; f) Primitive igneous rocks (modified from Ushikubo et al., 2008)

The contrast in Li-isotope variability between whole-rock and *in situ* zircon has aroused great interest. Cherniak and Watson (2010) conducted experiments on Li diffusion rates in different minerals. The results (Figure 1.4) revealed that Li diffusion is slower in zircon than in any other minerals, so that zircon is the mineral that best preserves Li and consequently the most reliable mineral for examining the Li isotopic system in magmatic rocks.

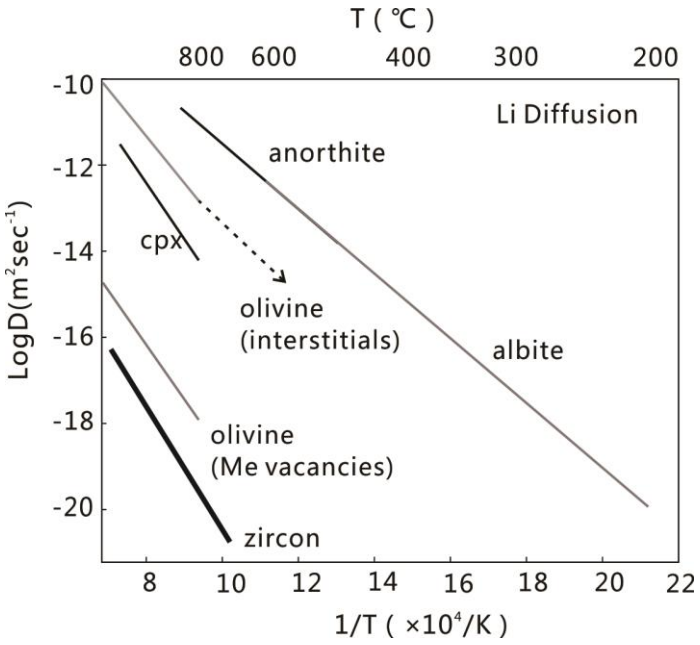


Figure 1.4 Summary of Li diffusion data for minerals. Li diffusion in zircon is considerably slower than Li diffusion in other minerals for which diffusion data exist (Cherniak and Watson, 2010).

Cherniak and Watson (2010) also compared the Li diffusion in zircons under different conditions of temperature and fluid availability. Their results indicated that Li diffusion is slower in zircon than in other cations, second to only the rare gas He, and equivalent to O under medium or low-temperature water-bearing conditions (Figure 1.5), but it still diffuses at a considerable rate. Hence, while the zircon Li-isotope system cannot remain closed under high-grade metamorphism, it can be preserved under mid-crustal metamorphic temperatures. This, in turn, offers favorable conditions for the preservation of Li isotope in the source regions of granitic magmas.

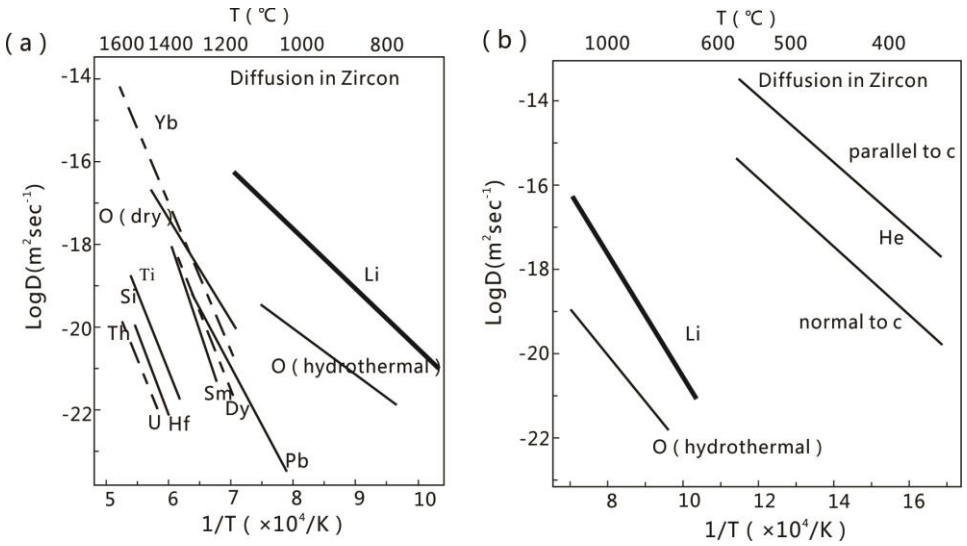


Figure 1.5 Summary of diffusion data for zircon: a) Li diffusion is considerably faster than diffusion of other cations in zircon, and b) faster than diffusion of oxygen under most circumstances, except at low temperatures under hydrothermal conditions. In addition, Li diffusion is much slower than the diffusion of helium (Cherniak and Watson, 2010)

A recent study of I-, S- and A-type granites from the Variscan belt in Western Carpathians of Slovakia shows results that contrast with those of Teng et al. (2004, 2008, 2009). While I-type granites have very limited range of δ^7Li (δ^7Li = −1.2 to +0.5‰), large variations of lithium isotopes (δ^7Li = −3 to +9‰) are found in S-type granites. More interestingly, a unique heavy Li-isotope signature (δ^7Li > 4.7‰) is found in A-type granites. The high δ^7Li and Li concentration of A-type granites from the Variscan belt is conflict with most current petrogenetic models, including remelting of residual granulitic sources, meta-igneous or calc-alkaline metaigneous compositions, involvement of mixed OIB-crust sources and derivation from mantle-derived mafic and intermediate magmas. However, these data are consistent with the new model of Martin (2006), in which the Variscan A-type granites were generated by anatexis of

metasomatised lower crust. Nevertheless, the use of Li isotopes to unravel the origin of A-type granites needs further investigations.

China was relatively late in starting Li isotopic geochemical studies. Since 2005, some laboratories and researchers have turned their eyes to the research and application of Li isotopic analysis methods. Wang (2006) was the first to establish a procedure for MC-ICP-MS Li chemical separation and measurement of the isotopic composition. Tang et al. (2007, 2009, 2011) and (Zhang et al., 2007) examined the Li isotopes of mantle xenoliths from basalts in North China and investigated the fractionation mechanisms of Li isotopes. Zhang et al. (2009) set up a microprobe *in situ* isotopic analysis method for olivine and pyroxene on the Cameca 1280 SIMS of Institute of Geology and Geophysics, Chinese Academy of Sciences (IGG-CAS). They also studied mantle xenoliths from the Jiaodong area, and presented evidence that the old lithospheric mantle of North China was once metasomatized by melts. Li et al. (2011b) developed a zircon standards for Li-isotope analysis (M257; δ^7Li = 2.1 ± 1.0‰ (2σ), Li = 0.86 ± 0.18 ppm (2σ)), making it possible to perform accurate *in situ* microanalysis of Li isotopes in zircon .

1.2. RESEARCH TOPIC AND SIGNIFICANCE

1.2.1 Research Focuses

Significant variations in Li-isotope compositions, due to either involvement of different sources or diffusion-driven isotopic fractionation, make explanation of the data difficult. The aim of this study is to shed new light on the origin and petrogenesis of A-type granites in eastern China, through a systematic investigation of several

unique A-type granites, including a comprehensive integration of petrological, geochemical and traditional (Hf-O) and non-traditional isotopic (Li) data on zircons. This study will:

1. Provide new data for insufficiently-characterized A-type granites, in order to shed new light on the origin and petrogenesis of Cretaceous A-type granites in East China.
2. Re-evaluate the effect of radiation damage in zircons and develop tools for screening the quality of U-Pb and O isotopic data in highly-evolved A-type granites.
3. Determine whether Li-isotope variations in zircon are caused by different sources, diffusion-driven fractionation or both.
4. Investigate the feasibility of *in situ* analysis of Li isotopes in zircon as a geochemical tracer to identify distinct origins of A-type granites.

1.2.2 Significance

A-type granites have great metallogenic significance and economic potential. The origin and petrogenesis of A-type granites can provide important information related to geodynamics. It will help to understand the growth of continental crust, lithospheric evolution and the development of regional tectonics. This project has developed improved methods for *in situ* lithium-isotope analysis and a new understanding of the behavior of lithium in both granites and zircons. This development of Hf-O-Li isotope fingerprints provides a powerful geochemical tracer for future studies of granite petrogenesis.

1.3 THESIS OUTLINE

This thesis is divided into 8 chapters. Chapter 1 presents the significance of this research and the main objectives of the study. Chapter 2 presents an overview of the geological setting of the research area. Chapter 3 provides the details of analytical methods used in this work, including sample preparation and different types of chemical and isotopic analyses. Chapter 4 evaluates the effect of radiation damage in zircon and presents a technique for screening U-Pb and O- isotope data on highly evolved A-type granites. Chapter 5 optimized analytical parameters and procedures to achieve the best possible precision with best possible high spatial resolution in SIMS Li-isotope ratio determinations and discuss the "Topography/charge-compensation effect" in zircon *in situ* Li-isotope analysis. Chapter 6 presents experimental results on Li diffusion designed to understand the behavior of Li in zircon. Chapter 7 re-evaluates the evidence for the origins of A-type granites from previous work and provides new constraint using Hf-O-Li isotopes based on the work of this thesis. Chapter 8 summarizes the conclusions reached in this study.

CHAPTER 2. GEOLOGICAL BACKGROUND AND SAMPLING

2.1. INTRODUCTION

2.1.1 Tectonic context

East China is composed of the Central Asian Orogenic Belt (CAOB) (Xing-Meng Orogenic belt) in the north, the North China Craton (NCC) in the center and the Southeast Orogenic Belt (SOB) in the south and east (Figure 2.1). The whole area became an active continental margin before Jurassic time (Zhou and Li, 2000; Li and Li, 2007), during the subduction of the Pacific plate from Late Jurassic to Cretaceous in the south, and subduction of the Izanagi plate in the north (Zhou, 2006; Zhou et al., 2006). It is distinguished by the widespread occurrence of Phanerozoic granitic rocks, making it an ideal place to study granites.

Eastern China is well known for the Phanerozoic removal of the subcontinental lithospheric mantle root (Griffin et al., 1998; Xu, 2001; Wu et al., 2003a; Gao et al., 2004; Wu et al., 2005). Sr-Nd isotopic studies of Cenozoic basalts and their mantle xenoliths indicate that the present lithospheric mantle in Eastern China is mildly depleted and recently formed or refertilized. The “lithospheric thinning” in eastern China has been a hot topic in the last decade. However, the timing, mechanisms and tectonic controlling factors for this geodynamic phenomenon are still unclear. It is suggested that the lithospheric thinning took place in the Late Mesozoic, and that the SCLM was maximally thinned in Early Cretaceous (120 to 130 Ma) (Wu and Sun, 1999). Some suggest that the lithospheric thinning was related to the subduction of Pacific plate in the east, which resulted first in lithospheric thickening and subsequent delamination (Wu et al., 2003a). Others suggest that the lithospheric destruction started

during the Jurassic, probably due to the loss of the physical integrity of the craton as a result of the Triassic collision between the North China and Yangtze blocks (Deng and Macdougall, 1992). Other models include extension (Li, 2000), subduction-related transpression (Zhou, 2006; Zhou et al., 2006), thermal erosion (Xu, 2001) and crustal delamination/foundering (Gao et al., 2004; Wu et al., 2005), etc.

Eastern China was dominated by roughly north to southward extension and rifting in the Early Cretaceous (from ~140 to ~125 Ma), producing a series of well-known extensional basins with abundant volcanic rocks, intrusive rocks and corresponding ore deposits (e.g., Lu-Zong, Ning-Zhen with abundant Cu, as well as Ag, Au, Pb, Zn, Mo mineralizations) (Mao and Wang, 2000; Sun et al., 2007). In the late Early Cretaceous (from ~125 Ma to ~110 Ma), the extension was replaced by southeast-northwestward transpression, and magmatism in east China generally ceased during this period (Li, 2000).

A giant Late Mesozoic A-type granitoids zone can be recognised in eastern China. The A-type granites are closely associated with calc-alkaline granites and are the product of the late magmatic evolution. From south to north, the distribution of these granites covers the Fujian, Guangdong, Min-Zhe coast, lower Yangtze, Sulu coast, Hebei and Heilongjiang areas and constitute a giant granite belt with NNE direction parallel to the continental margin of eastern China.

Hundreds of A-type granites are recognized in this granitoid belt. They have distinct mineralogical, petrological and geochemical characteristics. Their petrogenesis can provide important information on continental dynamics, and are the key to understanding the formation and reworking of continental crust and regional tectonic evolution.

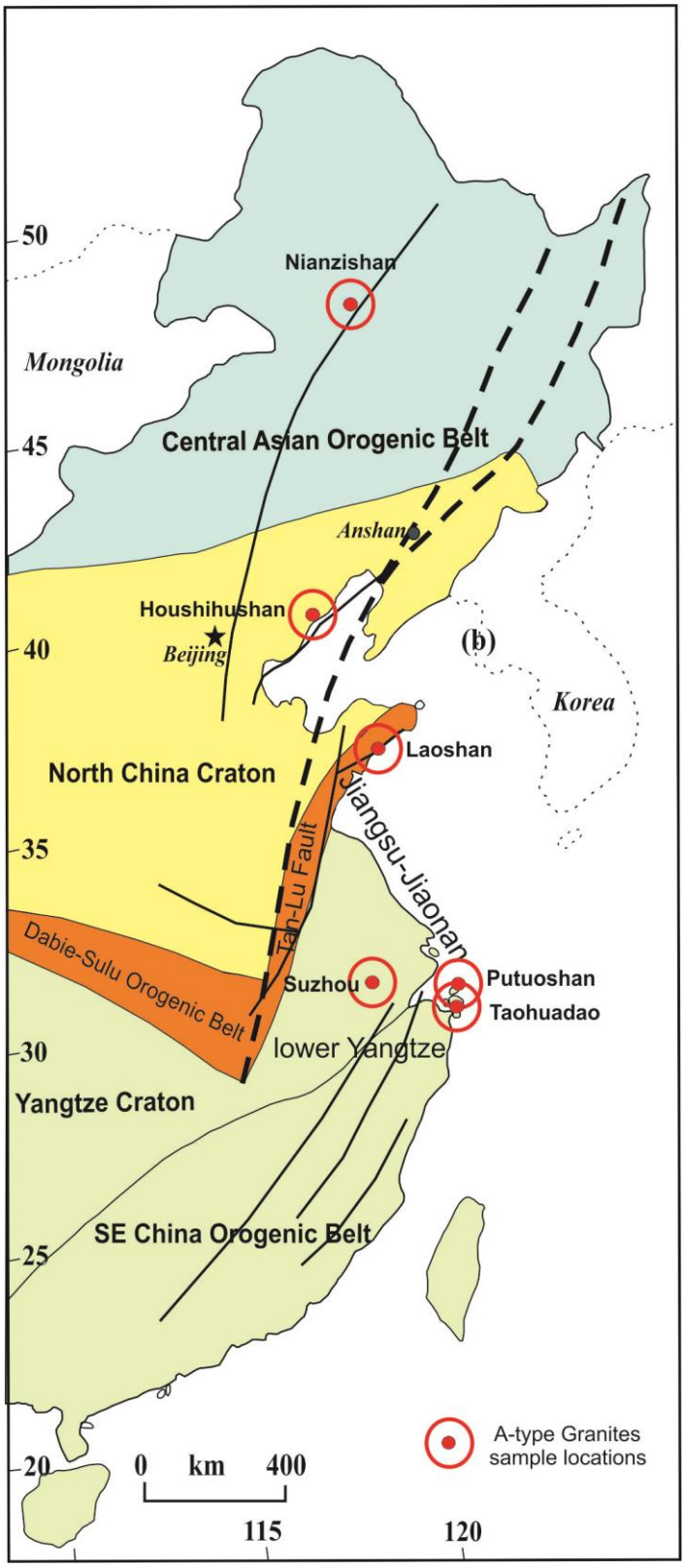


Figure 2.1 Geological map and six selected late Mesozoic A-type granites along the continental margin in eastern China. Modified after Wang et al. (1995) and Sun et al. (2007)

2.1.2 Cretaceous A-type granites in East China

According to existing geochronological data, A-type granites in eastern China may have been intruded in two episodes. The first episode is from 135 to 120 Ma and includes the lower Yangtze zone in the SOB, Northern Jiangsu-Jiaonan in the NCC, and Shanhaiguan and Nianzishan in the CAOB. The second one is from 100 to 70 Ma and is concentrated on the southeastern coast. They exhibit not only a variety of rock assemblages but also obvious regional variations in their emplacement patterns. Based on different criteria, sub-types of these A-type granitic rocks have been identified, i.e., peralkaline/aluminous A-type granite, A_1/A_2 A-type granite (many A-type granites fall in the A_1-A_2 transition zone or overlap in both regions) and Reduced/Oxidized A-type granites (the definition and classifications of A-type granites are in Chapter 1). Most of the aluminous and peralkaline A-type granites are nearly coeval (123 to 126 Ma). These ages are consistent with the peak of the Mesozoic magmatism in eastern China, and are also coeval with the mineralization in large-scale gold deposits and the formation of the metamorphic core complexes in the eastern North China Craton (Wu et al., 2003a). These geological observations all indicate an extensional setting for eastern China during the Early Cretaceous.

Field observations, sample collection and geochemical analysis have been carried out on six typical low $\delta^{18}O$ A-type granite plutons in eastern China, distributed as shown in Figure 2.1. Based on their mineral assemblages and geochemical characteristics, the six plutons can be classified into two subtypes -- peralkaline granite containing ferromagnesian minerals, and miarolitic K-feldspar granites relatively rich in aluminous minerals (Wang et al., 1995; Hu et al., 2005). Their geochemistry and main rock-forming minerals show a clear distinction. The peralkaline A-type contains abundant allanite, chevkinite and Fe-Ti minerals (titanomagnetite, ilmenite and

pyrophanite), while the accessory mineral assemblage for aluminous A-type is monazite and Fe-Ti oxide minerals dominated by magnetite, rutile and pyrophanite. Major elements of rock samples feature high contents of silicon and alkali metals but low Fe, Mg and Ca while the trace elements are mainly poor in Sr, Ba, P and Ti but rich in Rb, Th and U, which are typical characteristics of A-type granites. The chondrite-normalized distribution of rare earth elements follows the classic gull-shaped pattern, with Eu negative anomaly. The following gives detailed descriptions about their petrographic characteristics respectively.

2.2 LOW $\delta^{18}O$ A-TYPE GRANITES IN EAST CHINA

2.2.1 Nianzishan

The Nianzishan pluton is located on the western margin of the Songliao basin, southeast of the Great Xing'an range, and west of the Qiqihar City in Heilongjiang Province (Figure 2.2a, b). It is one of the representative low $\delta^{18}O$ Mesozoic A-type granites along the continental margin of eastern China, and also the smallest pluton of the studied six A-type granites with an outcrop area of about $15km^2$ (Figure 2.2 c) . The pluton is composed of medium- to fine-grained alkaline granite with no recognizable zonation in the field. The common occurrence of centimeter size miarolitic cavities indicates its high-level emplacement. Major minerals include quartz (25-30%), alkali feldspar (~70%), arfvedsonite (2-5%) and aegirine-augite (1-2%). The country rocks are the Cretaceous andesitic volcanic rocks.

Due to its shallow emplacement in the crust, relatively small scale and high permeability of the andesitic surrounding rocks, the Nianzishan granites experienced very complex late magmatic and postmagmatic isotopic exchanges, compared to other Mesozoic A-type granites in eastern China (Wei et al., 2001a). Previous studies show that the Nianzishan A-type granites underwent strong hydrothermal alteration during

magmatic emplacement (Li and Yu, 1993). The whole-rock has large variations in $\delta^{18}O$ and most of the quartz samples have lower $\delta^{18}O$ values than the normal mantle (Yu et al., 1990; Li et al., 1992; Wei et al., 2001a; Zhao et al., 2001). Oxygen isotopes show significant disequilibrium fractionation between common rock-forming minerals . There has been controversy as to whether the large variation in $\delta^{18}O$ and ^{18}O-depleted feature are due to the post-magmatic alteration or partial melting of lower-$\delta^{18}O$ values protolith.

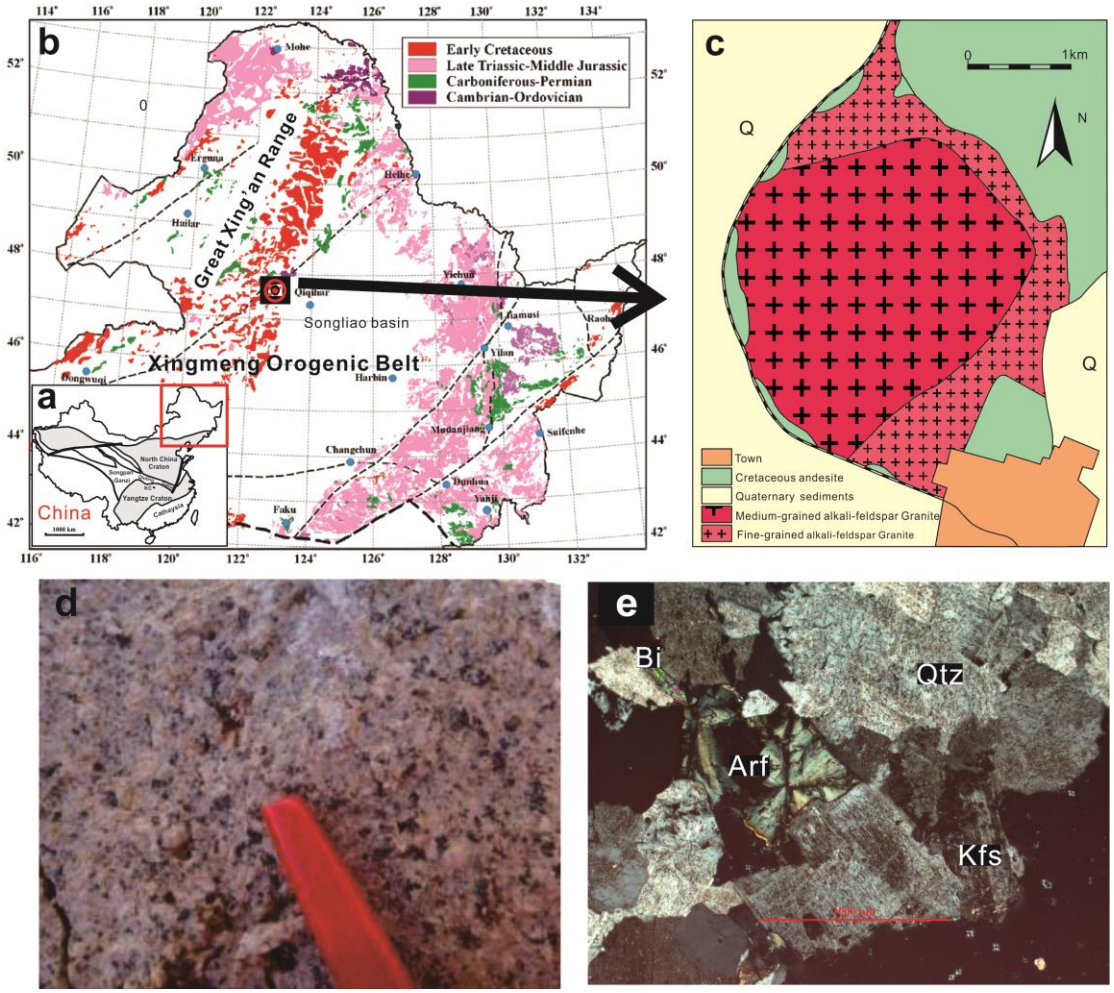


Figure 2.2 a) Sketch geological map of China; b) Distribution of Mesozoic igneous rocks in NE China. Modified from Wu et al. (2003b); c) Geological map of Nianzishan Pluton (modified from Wei, 2008); d) Outcrop of Nianzishan K-feldspar granite; e) Typical photomicrograph of Nianzishan K-feldspar granite.

Table 2-1 Summary of the studied A-type granites in eastern China

Contents	Nianzishan	Houshihushan	Laoshan	Suzhou	Taohuadao	Putuoshan
Latitude (N)	47°32′52″	40°02′44″	36°09′05″	31°15′32″	29°48′43.9″	29°58′50.4″
Longitude (E)	112°51′36″	119°44′24″	120°40′03″	120°30′09″	122°17′26.6″	122°23′08.7″
Area (A-type) (km2)	15	30	260	60	17	20
Emplacement level*	High	Very high	Moderate	Moderate	High	High
Grain size	Medium to fine	Fine to medium	Fine to medium	Medium to coarse	Medium to coarse	Coarse
Petrography	Alkaline granite	Alkaline granite	Alkaline granite	Alkaline granite	Alkaline granite	Alkaline granite
Diameter of miarolitic cavities (cm)	1–2	0.5	0.5	1–50	1–30	2–15
Enclaves	Common	Less common	Rare	Very common	Less common	Very common
Common minerals	Quartz, alkali-feldspar	Quartz, alkali-feldspar	Quartz, alkali-feldspar	Quartz,alkali-feldspar	Quartz, Perthite	Quartz, alkali-feldspar
	Aegirine	Aegirine	Magnetite	Annite	Aegirine	Magnetite
	Arfvedsonite	Arfvedsonite		Magnetite	Arfvedsonite	Titanite
	Magnetite	Magnetite				Apatite
Age of country rocks	Cretaceous	Late Jurassic, Precambrian	Cretaceous and Precambrian	Devonian	Late Jurassic	Jurassic
lithology of country rocks	andesite	rhyolite, gneiss	sandstone, rhyolite, gneiss	sandstone	andesitic/rhyolitic volcaniclastic rocks	diorite
Permeability of countryrocks	High	High to moderate	Moderate to low	Low	Moderate to low	Moderate to low
Isotopic age (Ma)	123	113	110	123	90	90

2.2.2 Houshihushan

The Houshihushan pluton (also called Shanhaiguan pluton in some previous studies) lies on the eastern edge of the Shanhaiguan area, 4km north of Shanhai Pass (Figure 2.3a, b). It is exposed over an area of about 45 km^2 and has intrusive contacts with the Baiqi formation of the upper Jurassic (J3b). It is a large igneous ring complex which varies from alkaline rhyolitic tuff, rhyolite, and alkaline granite to alkali-feldspar syenite (Figure 2.3c).

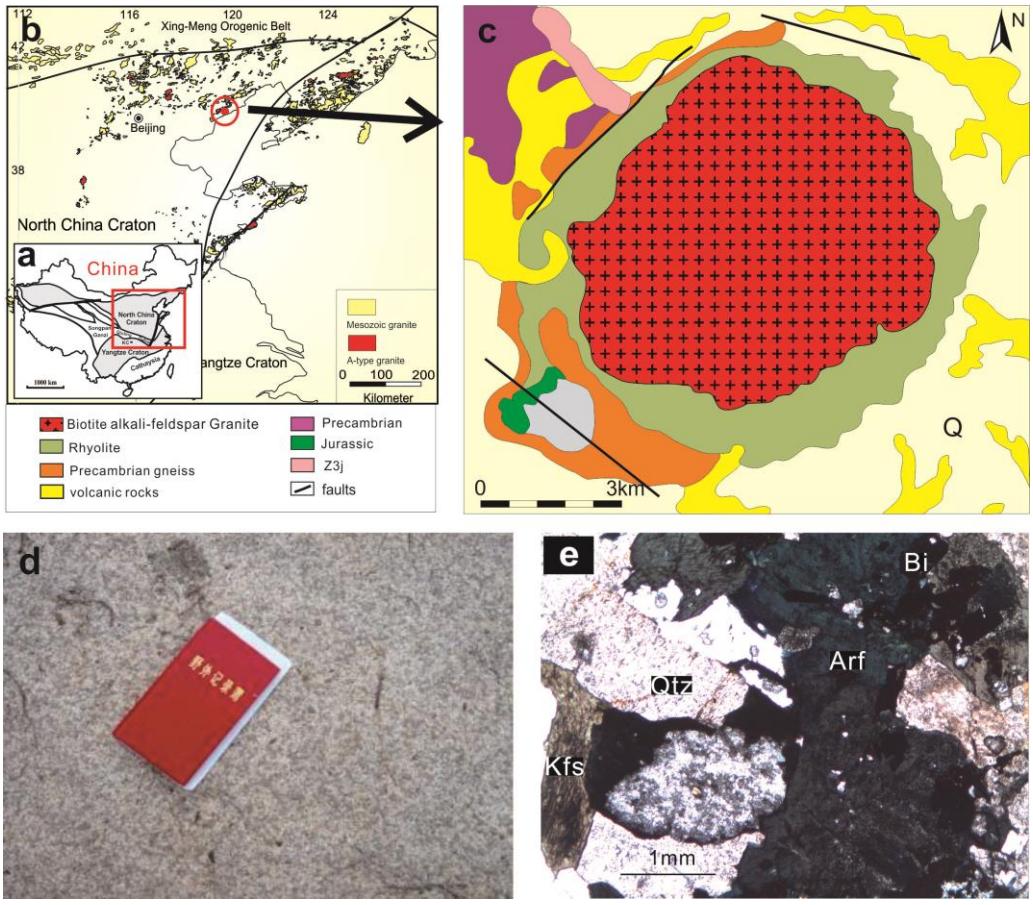


Figure 2.3 a) Sketch geological map of China; b) Distribution of Mesozoic igneous rocks in North China Craton. Modified from Yang et al. (2003); c) Geological map of Houshihushan Pluton (modified from Wei, 2008); d) Outcrop of Houshihushan K-feldspar granite; e) Typical photomicrograph of Houshihushan K-feldspar granite.

The miarolitic A-type granite is in the middle of the granitoid ring complex. The

grain size at the edges is slightly smaller. The major rock-forming minerals of the A-type granite are ~20% quartz, ~70% alkali feldspar, ~10% Na-rich amphibole (Figure 2.3d, e). Miarolitic cavities are usually less than 1 cm in diameter, and enclaves are relatively rare. The country rocks are Archean gneisses on the western and eastern borders, and andesitic and rhyolitic volcanic rocks on the southern margins.

2.2.3 Laoshan

The Laoshan granitic complex occurs in the central part of the Su-Lu UHP metamorphic belt of eastern China and is one of the important components of Yanshan Granitic Zone in the Jiangsu-Jiaodong area (Figure 2.4a, b). It is a typical Mesozoic granitic complex composed of calc-alkaline and peralkaline rocks exposed over an area of about 600 km^2. In the north and southeast, the plutons intrude the Cretaceous arkose sandstone of the Laiyang Group and thermal metamorphism is obvious at the contact sites; at the northeast and west, the plutons intrude into the Proterozoic metamorphic basement of the Jiaonan Group (mainly biotite-plagioclase gneiss and granulite-amphibolite); in the northwest (separated by the NE-trending Cangkou fault zone) they are associated with the late Mesozoic shoshonite series and rhyolitic volcanic rocks (Figure 2.4c).

Detailed field and petrographic studies have shown that the calc-alkaline group includes three units of granitic rocks: quartz-monzonitic granite, biotite-monzonitic granite and quartz syenite, while the peralkaline group shows a strong A-type affinity. The major mineral composition of the quartz-monzonitic granite are K-feldspar (30%), plagioclase (40%, $An_{31\sim34}$), quartz (18%) and amphibolite (10%). Albite twinning could be observed on plagioclase. The assemblage of accessory minerals includes titanite, apatite, magnetite and zircon. The biotite-monzonitic granite is found mainly in the western part of the intrusion. It is gray to pink in color, and medium- to fine-grained.

The mineral assemblage consists of K-feldspar (35%), plagioclase (30%, $An_{16\sim22}$), quartz (28%), biotite (5%) and small amount of Amphibolite. Most of the biotite is euhedral with partly chloritization.

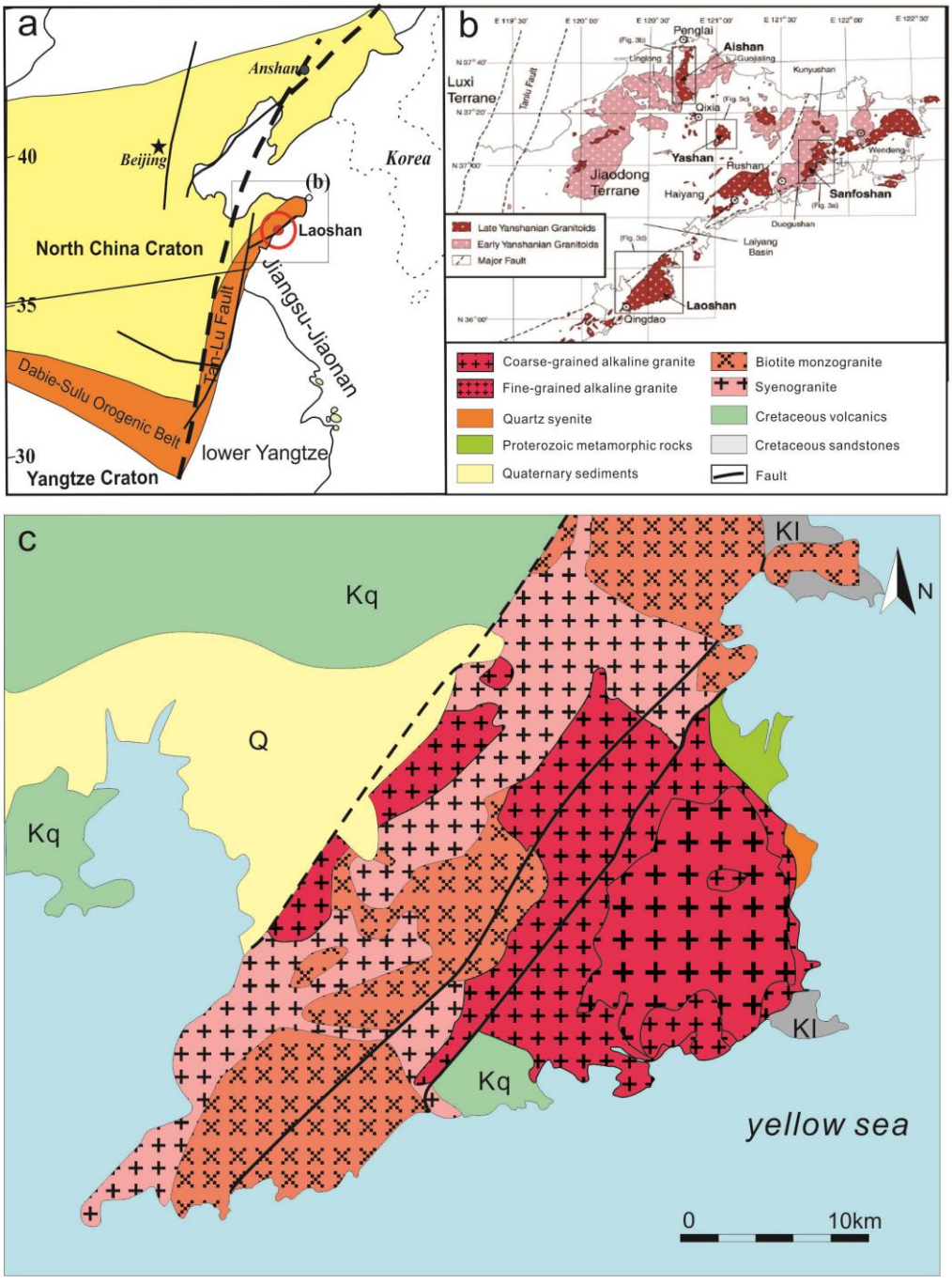


Figure 2.4 a) Sketch geological map of E.China; b) the Laoshan granitic complex in the Jiaodong Peninsula. Modified from Goss et al. (2010); c) Geological map of Laoshan Pluton. Modified from Zhao et al. (1998).

The assemblages of accessory minerals include titanite, apatite, magnetite, ilmenite and zircon. The quartz syenite is pink in color and has a coarse-medium graphic texture, miarolitic structure. The mineral assemblage consists of K-feldspar (50%), plagioclase (12%), quartz (35%) and biotite (< 3%). Feldspars show some degree of kaolinization while biotites develop chloritization or sericitization. The assemblage of accessory minerals includes titanite, apatite, magnetite, zircon and fluorite.

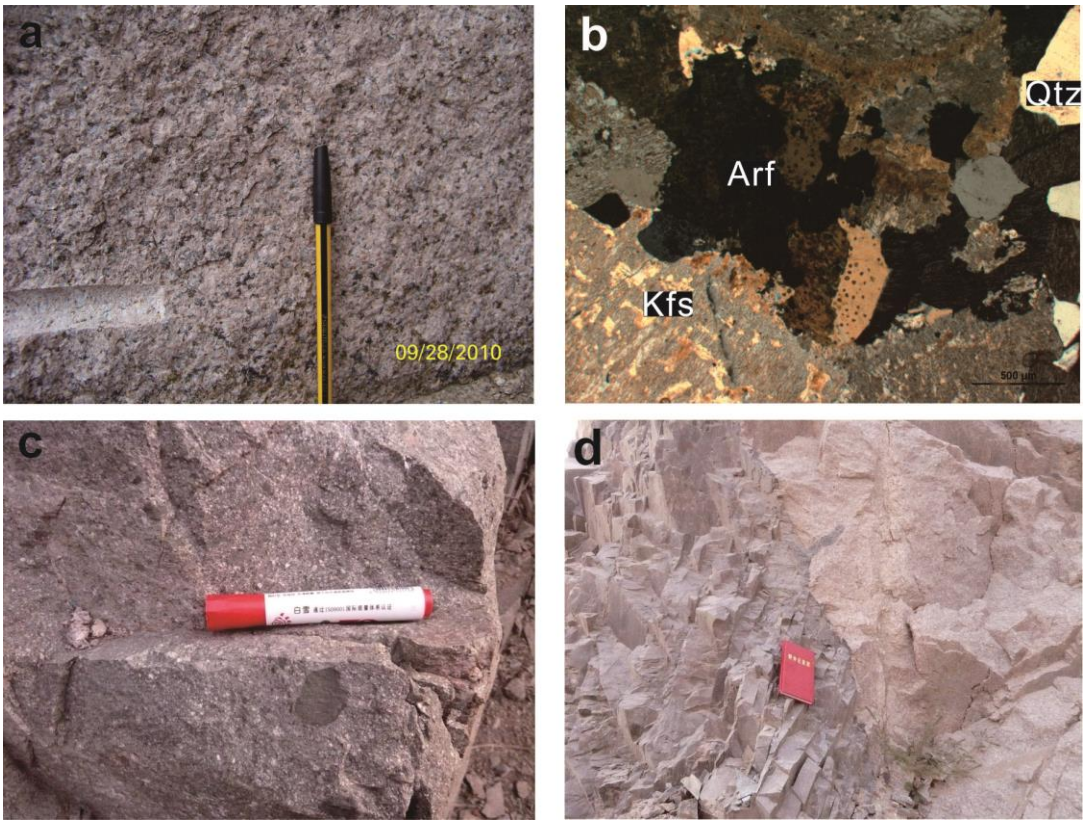


Figure 2.5 a) Outcrop of Laoshan Alkaline granite; b) Photomicrograph of Laoshan Alkaline granite; c, d) Examples of mafic microgranular enclaves occurring within A-type granites in the Laoshan granitic complex.

The peralkaline group is considered the main body of Laoshan complex (Figure 2.5a, b). The paragenesis is characterized by quartz (25 – 30%), alkali feldspar (65 – 70%), a small amount of alkaline melantic minerals (< 5%) such as arfvedsonite and aegirine together with accessory phases (magnetite, fluorite, mica, titanite and zircon) in the miarolitic cavities. Plagioclase and micas are scarce. Mafic enclaves are ubiquitous

in the complex with very different shapes. Feldspar exhibits mainly hypersolvus textures. Numerous mafic microgranular enclaves occur within granites (Figure 2.5c, d). The numerous miarolitic structure and common granophyric textures of quartz indicate rapid cooling and shallow-level emplacement.

2.2.4 Suzhou pluton

The Suzhou intrusion (Figure 2.6), located at the conjunction of the lower Yangtze magmatic belt and the Southeastern coast magmatic belt of China, was originally described by Zhang et al. (1988) and Charoy and Raimbault (1994). It is elliptical in shape, exposed over 60 km^2, and was intruded into Permian to Jurassic sandstones. The Suzhou granite has long been considered as an example of multiple intrusions, and has been divided into two (Sun, 1958) or three (Wang et al., 1997) magmatic stages as well as several granite phases according to the petrology.

Three main phases are observed in the field: 1). Amphibole-bearing porphyritic K-feldspar granite can be seen only in the Daluoshan- Baieshan area, and is considered to be the early phase of the intrusion (Figure 2.7a, b). The mineral assemblage consists of 60% subhedral alkali feldspar ($Or_{53}Ab_{47}$), 0 – 5% plagioclase (An_{38-2}), 35% anhedral quartz (some is vermicular), 1 – 5% biotite, and <1% hornblende as well as accessory minerals, including zircon and apatite; 2). coarse-grained biotite-K-feldspar granite with anhedral quartz and biotite dominates the exposed pluton and is considered the main phase in the previous studies.

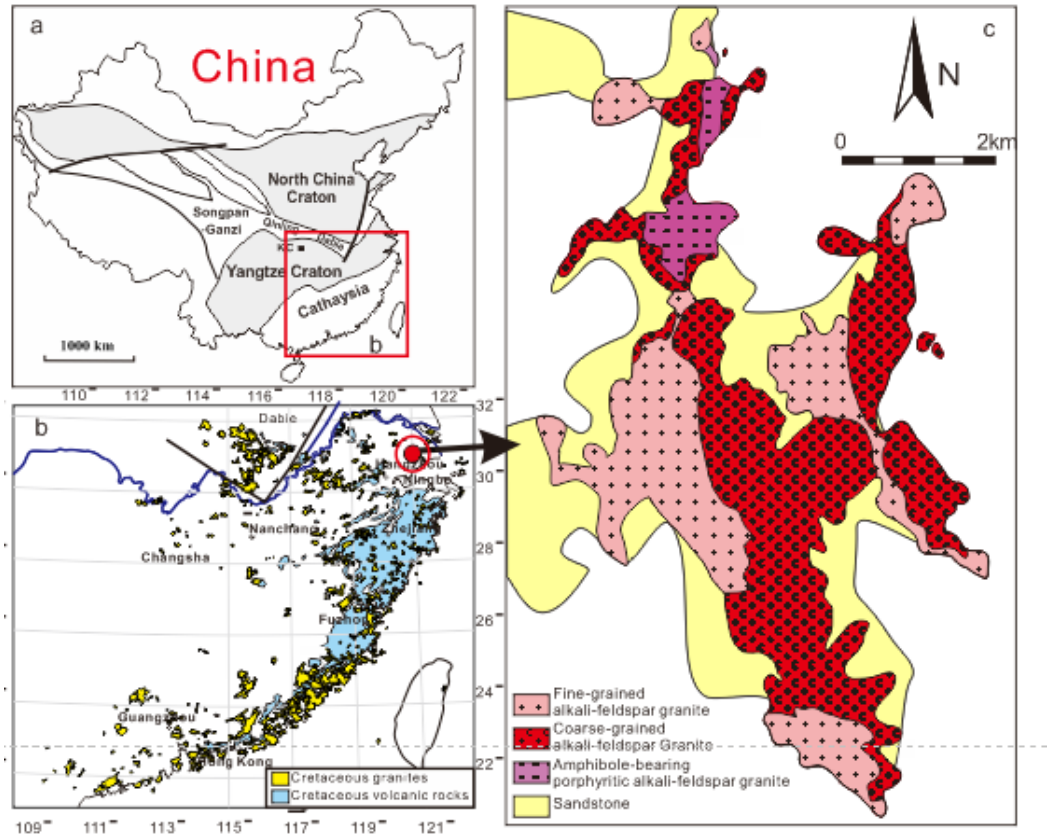


Figure 2.6 a) Location of South China; b) Geological map showing distribution of Mesozoic intrusions in the South China. Modified from (Zhou et al., 2006); and c) Simplified geological map of Suzhou pluton

Rock-forming minerals include plagioclase, K-feldspar, quartz and biotite; the accessory minerals include magnetite, titanite, zircon and apatite. Numerous miarolitic cavities are developed in this phase (Figure 2.7c). Feldspar exhibits mainly hypersolvus textures (Figure 2.7d) crystallized before the emplacement of the magma; (3) albitized K-feldspar granite shows a fine-grained porphyritic texture (Figure 2.7 e, f), and is found mainly in the western part of the intrusion. It is composed mainly of perthite, orthoclase, microcline, plagioclase (An_{25}), and quartz. Most feldspar in this phase developed sub-, trans-, or hypersolvus structures, and albite twinning could be observed. Biotite in this phase is mostly annite (Charoy and Raimbault, 1994; Zhang et al., 1988; Wang and Ding, 1995; Zhang et al., 1987). The melanocratic mineral of the all phases is

mainly biotite which develops an interstitial habit, suggesting a low initial water activity. The miarolitic cavities and common granophyric textures of quartz indicate rapid cooling and shallow-level emplacement.

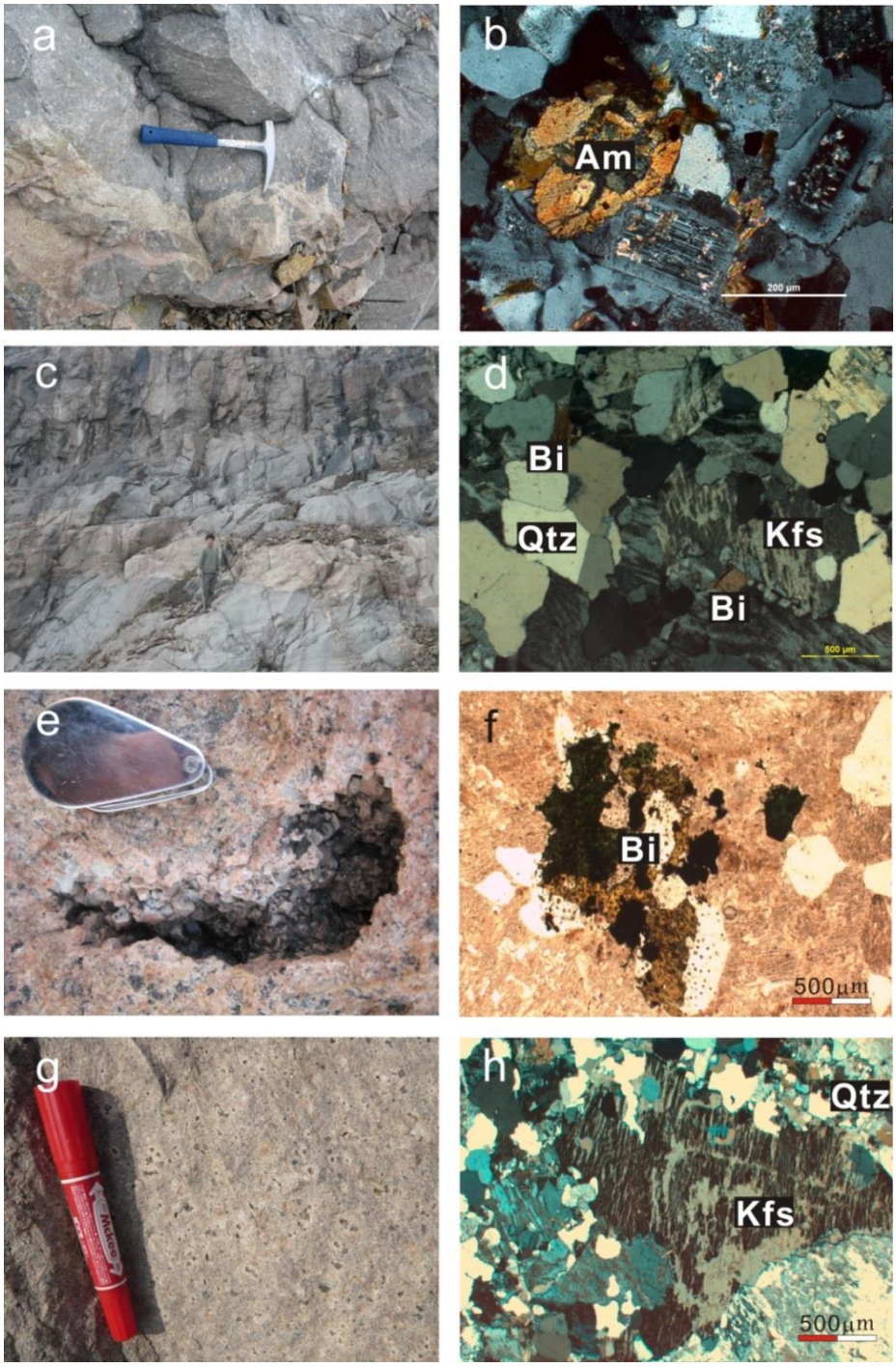


Figure 2.7 a) Outcrop of Amphibole-bearing porphyritic K-feldspar granite; b) Photomicrograph of ampibole bearing granite; c) Outcrop of biotite-enriched K-feldspar granite in Baieshan (west of Suzhou granite); d) Photomicrograph of biotite with

K-feldspar; e) Miarolitic cavities in coarse-grained biotite-K-feldspar granite; f) Interstitial habit of biotite in biotite-K-feldspar granite; g) Ablitized K-feldspar; h) Porphyritic texture of quartz and hypersolvus feldspar.

2.2.5 Taohuadao

Taohuadao pluton is located at the northeast edge of the Zhenhai-Wenzhou fracture zone in the southern part of Taohuadao, Putuo District, Zhoushan, Zhejiang province (Figure 2.8a, b). The pluton is a typical alkaline A-type granite in the Mesozoic Yanshanian magmatic belt in Zhejiang and Fujian coastal area.

The size of the Taohuadao pluton exposed above the sea level is limited, with an outcrop area of about 17 km^2. The northern part of the pluton is intruded into the andesitic volcaniclastic rocks of the Chawan group (J3c) and the southern part into the upper rhyolitic volcaniclastic rocks of the Xishantou group (J3x4) (Figure 2.8b). NW- and NE-trending fault structures are well developed in the region. Detailed field and petrographic studies have shown that the lithology of Taohuadao pluton is simply gray miarolitic alkaline granite (Figure 2.8d, e). The assemblages of major minerals are quartz (～25%), perthite (～70%); the melanocratic minerals are short prismatic aegirine (2%) and needle-like arfvedsonite (4%) which develops an interstitial habit. Quartz and alkali feldspar develop graphic texture. Miarolitic structures are common and have different sizes and irregular shapes.

Previous research on mineralogy, trace element, rare earth element and isotope geochemistry show that Taohuadao pluton is a typical postorogenic A-type granite, signifying the end of the Mesozoic orogenesis in China's South-East coastal region.

2.2.6 Putuoshan

The Putuoshan granitic pluton is located in the eastern part of the Zhoushan region in Zhejian (Figure 2.8a, c). It is a typical multi-stage I-A granite composite body with

an outcrop area of approximately 30 km^2. The K-feldspar granite body intrudes into early diorite which can be found on the northern and eastern parts of the island. There are also sporadic occurrences of Yanshanian volcanic rocks on the Putuo island which represent the latest stage of magmatic activity in the region (Qiu et al., 1999).

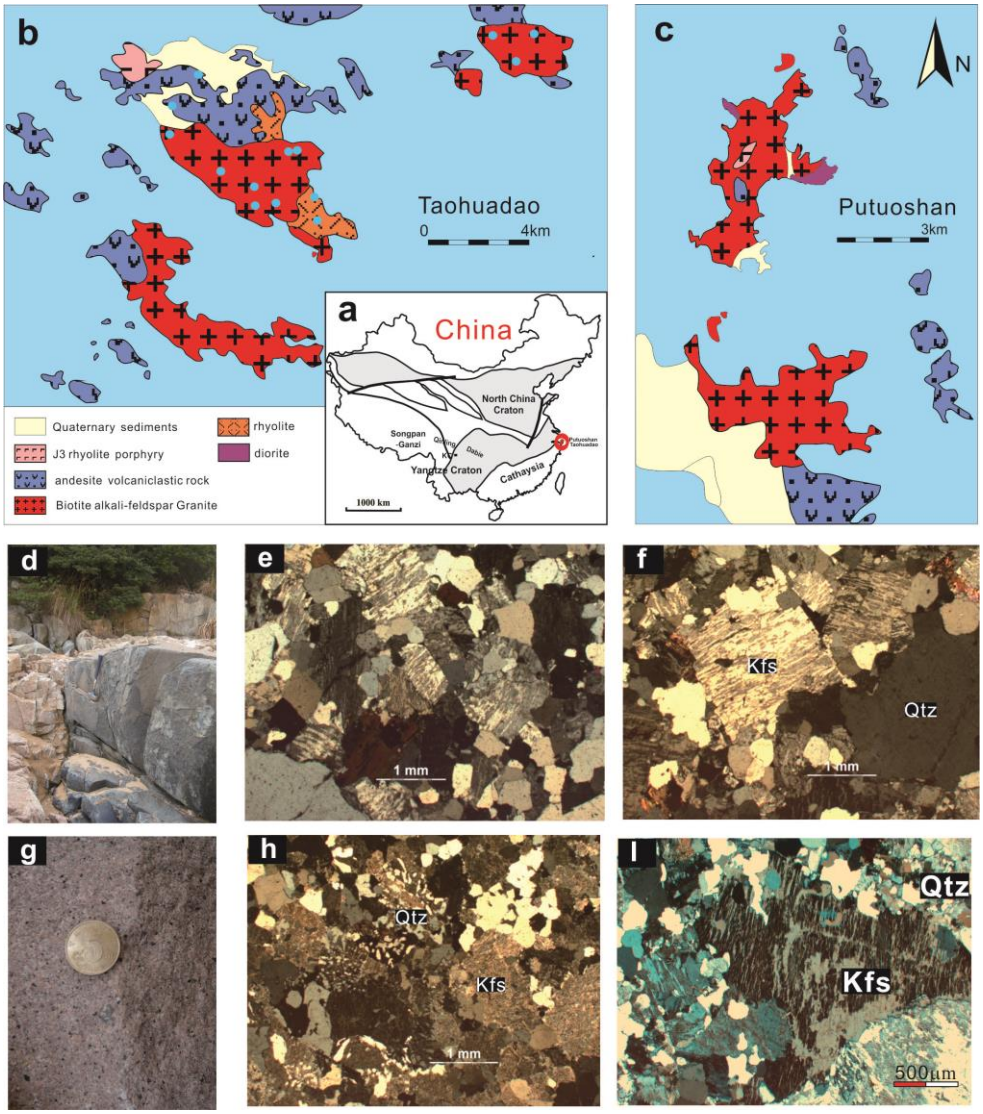


Figure 2.8 a) Sketch geological map of China; b) Geological map of Taohuadao pluton. Modified from (Qiu et al., 1996); c) Geological map of Putuoshan Pluton. Modified from (Xie et al., 2005); d) Outcrop of Taohuadao biotite alkaline -feldspar granite; e, f) Typical photomicrograph of Taohuadao K-feldspar granite; g) Outcrop of Putuoshan K-feldspar granite; h,i) Typical photomicrograph of Putuoshan K-feldspar granite.

The main phase is a coarse-grained biotite-K-feldspar granite (Figure 2.8g, h, i). The mineral assemblage consists of ~65% alkali feldspar (microcline), ~10 plagiolase (An = 10-14), 25% subhedral quartz, ~5% biotite and very little hornblende (< 1%) as well as accessory minerals including magnetite, titanite, zircon and apatite. The quartz has developed an interstitial habit to the feldspar and some of it has a vermicular structure. Numerous miarolitic cavities are developed in the pluton. Their infill consists of feldspar, quartz and almandine. The miarolitic cavities and common granophyric textures of quartz indicate rapid cooling and shallow-level emplacement. Microgranular dioritic inclusions of MME type are distributed in the northern part of the island. The inclusions are mainly 10 to 30 cm in diameter with different shapes, and show pronounced plastic rheology. They usually have a clear-cut contact relationship with the host rocks but some transitional or fuzzy contacts are also seen. They have similar mineral assemblages to those of the host rocks, but contain more mafic minerals: ~50% plagioclase ($An_{31\sim35}$), ~15% quartz, ~25% alkali feldspar and ~10% hornblende (mostly altered). The accessory minerals are apatite, titanite and ilmenite. Needle-like apatite is the main accessory mineral in MME. It has a length to width ratio larger than 10, which indicates rapid crystallization.

CHAPTER 3. METHODOLOGY

One hundred and eight fresh samples were selected from six A-type granitic plutons for petrographic, whole-rock geochemical and isotopic studies (sample details are listed in Appendix Table i). Samples collected in the field are generally *ca.* 20×20 ×20 cm^3 in sizes, fresh, undeformed/unmetamorphosed, and vary from pale-grey to brick-red in colour.

Laboratory studies have included thin-section preparation and examination, rock crushing, loss on ignition (LOI) determination, major-element determination by XRF (X-Ray Fluorescence Spectrometer), trace element determination by ICP-MS (Inductively Coupled Plasma Mass Spectrometry), whole-rock Li isotope determination by MC-ICP-MS (Multi-Collector Inductively Coupled Plasma Mass Spectrometry), cathodoluminescence (CL) imaging of zircons by SEM (Scanning Electron Microscopy), Raman spectra by micro-Raman spectrometer, ion microprobe for *in situ* U-Pb dating and O-Li isotope analysis (Cameca IMS-1280 SIMS), and isotopic analysis of Hf isotopes in zircon by LA-MC-ICP-MS (MC-ICP-MS with an attached laser ablation system). Detailed analytical procedures are given below.

3.1 PRE-TREATMENTS

3.1.1 Whole-rocks

Hand specimens have been thin-sectioned and were crushed into centimeter-scale

grains using hammers after detailed petrographic examination. Fresh grains were hand-picked to avoid surface alteration and contamination and then cleaned using purified water before they were further ground to < 200 mesh with grinding sets made of tungsten carbide.

Sample powders were dried at 105 ℃ for two hours. To determine the loss on ignition (LOI), about 1 gram (precision is 0.0001 gram) powder of each sample was carefully weighed before and after being roasted at 900 ℃ for two hours in a furnace. Half a gram (± 0.0001, after LOI determination) of each sample was weighed and mixed with 4.5000 ± 0.0001 grams of lithium tetraborate. Well-mixed powders were fused to produce glass discs for major-element determination.

3.1.2 Zircons

Zircon grains were separated by conventional magnetic and density techniques to concentrate non-magnetic heavy fractions. Zircon grains, together with zircon standards Plešovice, 91500 and Penglai, were mounted in epoxy and polished to half of the crystal thickness to expose their interiors for analyses. Transmitted- and reflected-light photomicrographs were taken to document the interior and exterior structures of zircons using a camera attached to a Leica microscope. Cathodoluminescence (CL) images were produced using a LEO1450VP Secondary Electron Microprobe attached with a Mini CL to reveal the structures. These images were used to choose appropriate target sites (free of inclusions, fractures and surface contamination) for *in situ* analyses.

3.2 WHOLE ROCK GEOCHEMISTRY

Whole-rock analytical methods include major-trace elements and Li isotopes.

3.2.1 Major-element analyses

Major element oxides were determined by X-ray fluorescence on fused glass beads using a Rigaku RIX 2000 X-ray fluorescence spectrometer at the Guangzhou Institute of Geochemistry, Chinese Academy of Sciences. Analytical procedures were those described by Li et al. (2000). Glass discs were made from melting dehydrated sample powders. Calibration lines used in quantification were produced by bivariate regression of data from 36 reference materials encompassing a large range of silicate compositions (Li et al., 2005). Analytical uncertainties are between 1% and 5% (2σ).

3.2.2 Trace-element analyses

Trace elements were analysed using an Agilent 7500a ICP-MS at the Institute of Geology and Geophysics, Chinese Academy of Sciences (IGG-CAS), Beijing. Analytical procedures were similar to those described by Li et al. (2000). About 50 mg of powdered sample were dissolved in a high-pressure Teflon bomb for 48 h using an HF + HNO3 mixture at ~90^{o}C, followed by evaporation to dryness, then refluxing in 7N HNO_3 for 12 h at ~100^{o}C and finally diluting the sample solution with 2% HNO_3. An internal standard solution containing the single element Rh was used to monitor signal drift during ICP-MS measurements, which showed a good stability range with ~10% variation. A set of USGS and Chinese national rock standards, including BHVO-2, BIR-1, AGV-2, RGM-2, GSP-2, JG-1 and JG-2 was used for calibration.

Analytical precision typically is better than 5% (2σ). Major- and trace-element results are combined in Appendix Table ii.

3.2.3 Whole-rock Li isotopes

The Li-isotope composition and [Li] of whole-rock samples were measured using solution MC–ICPMS methods at the Geochemical Analysis Unit, Department of Earth and Planetary Sciences, Macquarie University. Approximately 50 mg of each rock powder was digested in Savillex® screw-top beakers with 2ml concentrated HF and 2 ml concentrated HNO_3 for 72 h on a hot plate at ~140 ^{0}C. After evaporation of the solution, the residue was re-dissolved and dried down twice in concentrated HNO_3 to remove fluorides completely. Then the samples were dried down twice in 7M HCl. Finally, the sample was dissolved and stored in 0.36ml 5M HNO_3. An aliquot (1/2 of the solution, equivalent to ~25 mg of the original sample powder) from the 5M HNO_3 solution was then evaporated and dissolved in 0.9 ml of 1M HNO_3 in methanol. The final concentration of methanol in the solution is ~80% (v/v). This solution was used for Li separation by ion-exchange chromatography.

The procedure used for purification of the dissolved solution is similar to those described by Seitz et al. (2004). Teflon columns with a volume of 1.6 ml were packed with BioRad® AG 50W–X8 (200 - 400 mesh) cation exchange resin. The resin was cleaned before the first use by repeated rinsing with 7M HCl and de-ionized water. Prior to loading of a sample, the column was rinsed with 6 ml HCl and 6 ml de-ionized water and pre-conditioned with 6 ml eluent. The sample was loaded onto the resin in 0.9

ml of eluent. Subsequently cations were eluted with 17.1 ml eluent. The eluates (pre-cut, cut and post-cut) are then evaporated to dryness. Finally, samples were dissolved in 2% HNO_3 for analysis on Agilent 7500c/s Quadrupole ICPMS to calculate recovery yield and then diluted to 15 ppb. Li recovery was typically > 99.9% in the course of our separation procedure. The procedural blank was usually less than 20 pg Li.

Impurities in the eluted samples were assessed before isotope analysis (e.g. Na/Li ratios $\ll 1$ in this study) by Q-ICP-MS analyses. The purified 15 ppb Li solution was analysed twice using a Nu Plasma MC-ICP-MS (Nu034) to further evaluate reproducibility. The isotopic analysis of each unknown sample was bracketed by two 15 ppb L-SVEC standard solutions ($^{7}Li/^{6}Li = 12.039 \pm 0.03$) (Chan et al., 1992) to correct for mass fractionation. Li concentration was determined by comparison of signal intensity between sample solutions and measurements of L-SVEC. An additional ACR Li single-element standard solution was measured multiple times as a secondary check on instrument performance ($\delta^{7}Li = 12.3 \pm 1.0‰$; 2σ). The accuracy of the results was monitored using international rock standards RGM and GSP-2, which gave results (average $\delta^{7}Li$ values of $+2.3 \pm 1.2‰$, and $-0.5‰ \pm 1.4‰$, respectively) (Schuessler et al., 2009) in agreement with the published values. To summarise, our average reproducibility based on samples and standards is $\pm 1.0‰$ (2σ). The analytical data are listed in Appendix Table viii.

3.3 *IN SITU* ANALYSES

In situ studies include zircon U-Pb analysis, Hf-O-Li isotope analysis, Raman

spectrometry and ion imaging and quartz O isotopes.

3.3.1 U-Pb dating of zircons

All the zircon mounts were vacuum-coated with high-purity gold prior to analysis by SIMS. Measurements of U, Th and Pb were conducted using the Cameca IMS-1280 SIMS at IGG-CAS. U-Th-Pb ratios and absolute abundances were determined relative to the standard zircon Plešovice (Sláma et al., 2008) and 91500 (Wiedenbeck et al., 1995), respectively, analyses of which were interspersed with those of unknown grains, using operating- and data- processing procedures similar to those described by Li et al. (2009b). Uncertainty of 1% (1 RSD) for $^{206}Pb/^{238}U$ measurements of the standard zircons was propagated to the unknowns (Li et al., 2010a). Measured compositions were corrected for common Pb using the abundance of non-radiogenic ^{204}Pb. Corrections are sufficiently small to be insensitive to the choice of common-Pb composition, so an average present-day crustal composition (Stacey and Kramers, 1975) was adopted for the common Pb, assuming that the common Pb is largely surface contamination introduced during sample preparation. Uncertainties on individual analyses in data tables are reported at a 1σ level; mean ages for pooled U/Pb analyses are quoted with 95% confidence interval. Data processing was carried out by the Cameca Customisable Ion Probe Software (CIPS). Statistical reduction and plotting of the data (include calculated ages, uncertainties, weighted means, and the generation of U-Pb concordia plots) were carried out using the Isoplot/Ex v. 2.49 program (Ludwig, 2001). The full data set is presented in Appendix dataset iv.

3.3.2 *In situ* O-isotope analyses

In situ oxygen-isotope analyses were conducted on zircons that were previously dated, using the same Cameca IMS-1280 SIMS at IGG-CAS. After U-Pb dating, the sample mount was repolished to ensure that any oxygen implanted in the zircon surface from the O_2^- beam used for U-Pb analysis was removed. The Cs^+ primary ion beam was accelerated to 10 kV, with an intensity of *ca.* 2 nA corresponding to a beam size of ~10 μm in diameter. A normal-incidence electron flood gun was used to compensate for sample charging during analysis with homogeneous electron density over a 100 μm oval area. A 60 eV energy window was used, together with a mass resolution of *ca.* 2500. Negative secondary ions were extracted at a –10 kV potential. The sample was at –10 kV and extracted to real ground. Oxygen isotopes were measured using the multi-collection mode on two off-axis Faraday cups. The intensity of the ^{16}O beam was typically ~1×10^9 cps. One analysis consists of 20 cycles, with an internal precision generally better than 0.4‰ (2SE) on the $^{18}O/^{16}O$ ratio. The detailed analytical procedures are similar to those reported by Li et al. (2010b). Measured $^{18}O/^{16}O$ values were normalized to the Vienna Standard Mean Ocean Water composition (VSMOW, $^{18}O/^{16}O = 0.0020052$). The instrumental mass fractionation factor (IMF) was corrected using the Penglai zircon standard with a $\delta^{18}O$ value of 5.3‰ (Li et al., 2010b), which was mounted close to each zircon sample to avoid the geometrical effects ('X-Y' effect) as proposed by Kita et al. (2009). The IMF was corrected as follows:

$$IMF = (\delta^{18}O)_{M(standard)} - (\delta^{18}O)_{VSMOW}$$

$\delta^{18}O_{Sample} = (\delta^{18}O)_M - IMF$

A second zircon standard (91500, mounted at the centre) was analysed as an unknown to ascertain the veracity of the IMF. Measurements of the 91500 zircon during the course of the study yielded a weighted mean of $\delta^{18}O = 10.0 \pm 0.4‰$ (2SD), which is consistent with the reported value of 9.9 ‰ (Wiedenbeck et al., 2004). The analytical procedures for measuring oxygen isotopes in quartz are the same as those used for zircon. The IMF has been corrected using the NBS-28 standard with a $\delta^{18}O$ value of 9.5‰ (Matsuhisa, 1974). The full data set is presented in Appendix dataset v and vi.

3.3.3 SIMS *in situ* analysis of Li isotopes

Lithium isotopic measurements on zircon were performed using the Cameca IMS 1280HR SIMS at IGG–CAS. Zircon crystals and standard M257 (Li et al., 2011b) were cast in epoxy mounts. The mounts were vacuum-coated with high-purity gold prior to SIMS analysis. The O^- primary ion beam was accelerated at –13 kV, with an intensity of *ca.* 20 to 30 nA. The Kohler illumination mode was used with a *ca.* 200 μm aperture to produce even sputtering over the entirely analysed area.

Positive secondary ions were extracted at a 10 kV potential. Detailed secondary-ion optics parameters follow the description of Li et al. (2011b), and include an entrance slit width of 400 μm, maximum area of 125 μm, field aperture of 5000 μm square, and energy slit width of 60 eV together with a mass resolution of 1300 (at 10% peak height). A single ion-counting electron multiplier (EM) was used as the detection device. The raw δ^7Li values of unknowns are expressed as:

$$\delta^7Li=[(R_m/R_0)-1]\times1000‰$$

where R_m is the measured raw $^7Li/^6Li$ value, and R_0 (= 12.039) is the literature $^7Li/^6Li$ ratio of NIST L-SVEC Lithium carbonate (Chan et al., 1992).

Drift of δ^7Li values in the M257 standard over repeated analyses is typically < 2‰ in a single analytical session with an internal precision between 1.5 and 2.0 ‰ (2SE) for a single spot. Measurements of Li isotopes and concentrations were conducted in several separate sessions. The full data set is presented in Appendix dataset vii, and the summary data for the M257 zircon standard and other three zircons (Plešovice, Qinghu and Temora 2) are given in Table 6-2.

3.3.4 Raman spectrometry

Raman spectra were collected to determine the relationship between zircon crystallinity and U concentration. Zircons were analysed on an inVia-Reflex micro-Raman spectrometer at the Technical Institute of Physics and Chemistry, Chinese Academy of Science. The instrument was configured to use ~80 μW of power and a laser wavelength of 532 nm. The analyses were recorded at room temperature from a 4 μm laser spot over 100 second increments. This setup did not cause any sample degradation. Each Raman analysis was measured immediately adjacent to the shallow ablation pit created by the SIMS oxygen-isotope analysis, to allow comparison against a known [U].

3.3.5 SIMS ion imaging

Secondary ion images were obtained for construction of Li concentration maps on selected zircon grains. Before each scanning analysis, the sample was pre–sputtered over a 200 μm × 200 μm area by rastering for 300 s in order to eliminate surface contamination. The lateral resolution of an ion image is limited by the size of the primary beam; we used a focused beam of O^- with a diameter of 5 μm (~1 nA) to scan a 150 μm × 150 μm area. Each image was collected as 128 × 128 pixels (~1μm/pixel). The Dynamic Transfer Optical System was applied to obtain a wide field of view and $^7Li^+$ was detected by the electron multiplier. Other mass spectrometric conditions were similar to those used for isotopic analyses of the samples.

3.3.6 LA-MC-ICPMS Hf isotope analysis of zircon

Analysis of Lu-Hf isotopes in zircon has been revolutionized by recent advances in plasma-source mass spectrometry and laser-ablation micro-sampling techniques (Griffin et al., 2000; Kemp et al., 2007). *In situ* zircon Hf isotopic analyses were carried out at the IGG-CAS using a Neptune multi-collector-ICPMS equipped with a Geolas-193 laser-ablation system. Lu-Hf isotopic measurements were made on the same zircon grains previously analysed for U-Pb and Oxygen isotopes. During analyses, the spot sizes of 63 and 80 Am and a laser repetition rate of 8 Hz with 100 mJ were used. Details of the analytical procedures are described by (Xu et al., 2004; Wu et al., 2006). Analyses of double standard zircons 91500 and Penglai or Mud Tank and GJ-1 were interspersed with unknowns. The results of standard 91500 or Mud Tank were used for external correction. The weighted average $^{176}Hf/^{177}Hf$ ratios of standard 91500 and Mud

Tank analysed during the whole session are identical within analytical errors to their accepted values (0.282306 ±8 and 0.282507 ±6 for 91500 and Mud Tank, respectively; (Woodhead and Hergt, 2005), no further external adjustment was made. $(^{176}Lu/^{177}Hf)_{CHUR}$ = 0.0332 and $(^{176}Hf/^{177}Hf)_{CHUR,0}$ = 0.282772 (Blichert-Toft and Albarede, 1997), $(^{176}Lu/^{177}Hf)_{DM}$ = 0.0384 and $(^{176}Hf/^{177}Hf)_{DM}$ = 0.28325; $(^{176}Lu/^{177}Hf)_c$= 0.015, $\lambda=1.867\times10^{-11}yr^{-1}$ (Soderlund et al., 2004) was used in our calculations.

Isobaric interferences by ^{176}Lu and ^{176}Yb on the ^{176}Hf signal were subtracted by monitoring the intensity of ^{175}Lu and ^{172}Yb signals, using $^{176}Lu/^{175}Lu$ = 0.026549 and $^{176}Yb/^{172}Yb$ = 0.5886 (Chu et al., 2002). Independent mass bias factors for Hf and Yb (β_{Hf} and β_{Yb}) in the isobaric interference correction were used. Measured $^{176}Hf/^{177}Hf$ ratios were normalized to $^{179}Hf/^{177}Hf$ = 0.7325 (Griffin et al., 2000).

CHAPTER 4. THE LOW-δ^{18}O SUZHOU A-TYPE GRANITE REVISITED: THE EFFECTS OF HIGH U CONTENT ON ZIRCON O-ISOTOPES AND SIMS U-Pb DATING

(This chapter includes results published in a paper by Gao, Y.-Y., et al. (2014). "Screening criteria for reliable U–Pb geochronology and oxygen isotope analysis in uranium-rich zircons: A case study from the Suzhou A-type granites, SE China." Lithos 192-195: 180-191. All data, otherwise acknowledged in the published paper, were produced by myself under supervision. Results and conclusions were made through collaboration of myself with the three other authors.)

Igneous fractionation has negligible effects on oxygen-isotope composition, but theoretical calculations suggest that high-T water-rock interaction can significantly decrease the oxygen isotope ratios of silicate rocks. However, water-saturated magmas typically either erupt explosively or quench as subsurface porphyries before the magmatic $\delta^{18}O$ can be lowered by assimilation (Balsley and Gregory, 1998). As a result, granites crystallized from low-$\delta^{18}O$ magmas are rare.

Wei et al. (2008), using bulk analysis of zircon separates, reported five ^{18}O-depleted A-type granites ($\delta^{18}O$ = 3.1 to 5.4‰) along the east coast of China. Their formation was attributed to a reworking or recycling of oceanic or continent crust (Wei

et al., 2001a; Wei et al., 2001b; Wei et al., 2008).

However, the nature and proportions of the source components, and the role of mantle-derived magmas, have proved almost impossible to resolve from whole-rock compositions (Hawkesworth and Kemp, 2006) or, as in this case, bulk zircon isotopic compositions. One of the well-documented low-$\delta^{18}O$ A-type granites in E. China, the Suzhou pluton, displays a scattered range of $\delta^{18}O$ from +3.5 to 9.2‰ which has led to some confusion regarding its origin (Charoy and Raimbault, 1994; Fu et al., 1996; Wang et al., 1998; Wei et al., 1999; Wei et al., 2001b; Wei et al., 2002; Wei et al., 2008). Whether these $\delta^{18}O$ variations reflect the magma sources, or are only "noise" is worthy of further investigation. Many studies indicate there are limitations on the degree to which zircons with high uranium contents can retain isotopic information (Booth et al., 2005). Considering the rarity of low-$\delta^{18}O$ granites and this possible relation between the U content and O isotopes, the Suzhou A-type granites were re-examined to determine if they actually are true low-$\delta^{18}O$ A-type granites.

This chapter presents a SIMS (Cameca IMS-1280) *in situ* study of the links between the U-Pb age of zircon, the $\delta^{18}O$ of zircon and the $\delta^{18}O$ of quartz from the Suzhou "low-$\delta^{18}O$" A-type granite, Eastern China. The use of D_{dpa} (Displacement per atom) of the single zircon grains has been evaluated to quantify the degree of radiation damage, taking both time and [U], [Th] into consideration. Conclusion can be made by integrating *in situ* data with the whole-rock and bulk zircon data, Raman spectra and calculated D_{dpa}, that the Suzhou pluton formed in a single magmatic period and is not really a "low-$\delta^{18}O$" granite as previously assumed. The correlation between D_{dpa}, U-Pb

ages and $\delta^{18}O$ values strongly suggests that anomalously high U-Pb ages and apparent depleted oxygen-isotope compositions are caused by different mechanisms which have different D_{dpa} thresholds.

4.1 INTRODUCTION

Zircon ($ZrSiO_4$) is a common U-rich accessory mineral occurring in a wide range of rock types. It has long been recognized as a key geochronometer based on the radioactive decay of U to Pb and the premier geochemical tracer in terms of Hf and O isotopes because of its resistance to alteration and post-magmatic metamorphism. These "reliable" zircon data are crucial for providing insights into global-scale processes such as early planetary cooling, rates of crustal recycling over time, and the history of continental lithosphere/hydrosphere interactions. However, the conservative behavior of Hf, Pb and O in zircon is controlled by their diffusion rates and the degree of radiation-damage of the zircon. Therefore, the resistance of zircon to alteration and post-magmatic metamorphism is sometimes overestimated. The reliability of data on zircon U-Pb isotopic systems has been attracting increasing attention in recent years. A number of studies indicate that the U-Pb isotopic system in zircons with high U contents commonly shows discordance (Wetherill, 1956; Silver and Sarah, 1963; Krogh, 1982; McLaren et al., 1994; Utsunomiya et al., 2007). It appears that "high-U" or "old" zircons might have suffered significant radiation damage and metamictization, which limit their usefulness as a geochronometer (Aines and Rossman, 1986; Geisler et al., 2002; Ewing et al., 2003; Cavosie et al., 2004; Carter et al., 2006; Sol á et al., 2009).

Although disturbance of the U-Pb system can be detected as isotopic discordance, it is more difficult to know if the oxygen-isotopes have been disturbed. Early studies indicated that non-metamict zircons are highly retentive of oxygen isotope signatures even under high-grade metamorphism (Valley et al., 1994). However, a few studies on bulk zircon separates have shown that zircons with discordant U-Pb ages also have a large range of oxygen-isotope compositions, which suggested that the resilience of the oxygen-isotope system in zircon may be overestimated (Silver, 1963; Bibikova et al., 1982; Valley et al., 1994).

Most zircon studies have qualitatively ascribed U-Pb discordance and disturbed oxygen isotopes to the process of zircon metamictization. Nevertheless, it is difficult to quantitatively specify the minimum U content that causes metamictization, because the radiation damage is accumulated through time and can be annealed out. Moreover, little attention has been focused on the reliability of oxygen-isotope analyses of concordant zircons. The development of SIMS has allowed targeting of specific domains within individual zircon crystals and made it possible to avoid metamict zones as far as possible, effectively reducing the proportion of unreliable data used in zircon dating and isotopic tracing. Nevertheless, even zircons with perfect oscillatory zoning may contain narrow high-U zones that are metamict and hence are not easily detectable in CL images. High-U zircons often yield apparently older U-Pb ages (McLaren et al., 1994; Williams and Hergt, 2000; White and Ireland, 2012) and lower oxygen-isotope values (Booth et al., 2005) in SIMS *in situ* analyses.

The aim of this chapter is to further investigate the influence of U on SIMS U-Pb

dating and oxygen-isotope analysis, and to provide a rigorous assessment of how high the U content can be before we must begin to suspect the reliability of zircon isotopic data. The screening criteria are based on a case study of the A-type granite from Suzhou. This is a highly evolved Cretaceous A-type granite containing zircons with a range of U and Th contents (hereafter [U], [Th]), and minimal natural "fading" or annealing of radiation damage, making it appropriate for this study. The relationship between [U], [Th], and the measured U-Pb ages and $\delta^{18}O$ in zircons provides robust constraints for the interpretation of relevant zircon isotopic data in the followed studies.

4.2 GEOLOGICAL BACKGROUND

The Suzhou granite is located at the junction of the Dabie-Lower Yangtze Reach magmatic belt and the coastal magmatic belt of southeastern China. It is a Cretaceous A-type granite enriched in REE, HFSE, U, and Th, and considered to be one of the "low-$\delta^{18}O$" A-type granites recently defined in eastern China (Wei et al., 2008).

The Suzhou pluton can be divided into three magmatic phases on the basis of petrography and isotopic ages which are discribed in Chapter 2. The first phase is an amphibole-bearing porphyritic alkali-feldspar granite that occurs in the northern part of the pluton; the second phase, which is the dominant rock-type of the Suzhou granite, is a coarse-grained alkali-feldspar granite with numerous miarolitic cavities; the third phase is a fine-grained alkali-feldspar granite that occurs mainly in the western part of the pluton. Hydrothermal alteration and weathering occurs along the pluton margins. Both quartz and alkaline feldspar in such rocks display a cloudy or "dirty" appearance

under crossed polarizers.

4.3 RESULTS

4.3.1 Imaging of zircons

Zircons separated from representative samples of the three phases are colorless to dark pinkish brown and 50 to 300 μm in length, with aspect ratios of 1:1 to 3:1. Fluid- and mineral inclusions are commonly seen in transmitted light. Zircons from the amphibole-bearing porphyritic alkali-feldspar granite phase (Sz1) are generally prismatic, while zircons from the coarse-grained alkali-feldspar granite phase (Sz2, Sz4: slightly altered) are smaller in size and mostly euhedral to subhedral. The fine-grained alkali-feldspar granite phase (Sz3) has more zircons with dark CL than the other phases.

Based on reflected-light photos and CL and BSE imagery, the zircons can be divided into two groups: 1). Group 1 zircons, which are colourless, transparent and characterized by clear oscillatory zoning under CL (Figure 4.1, yellow and red spots), and 2). Group 2, which appear fractured in reflected-light photos and nearly black under CL, indicative of very high U and Th contents and accompanying metamictization (Figure 4.1, orange and pink spots). Igneous zonation and small fluid inclusions are visible in most crystals. Many zircon surfaces show evidence of pitting, which may reflect partial dissolution during alteration.

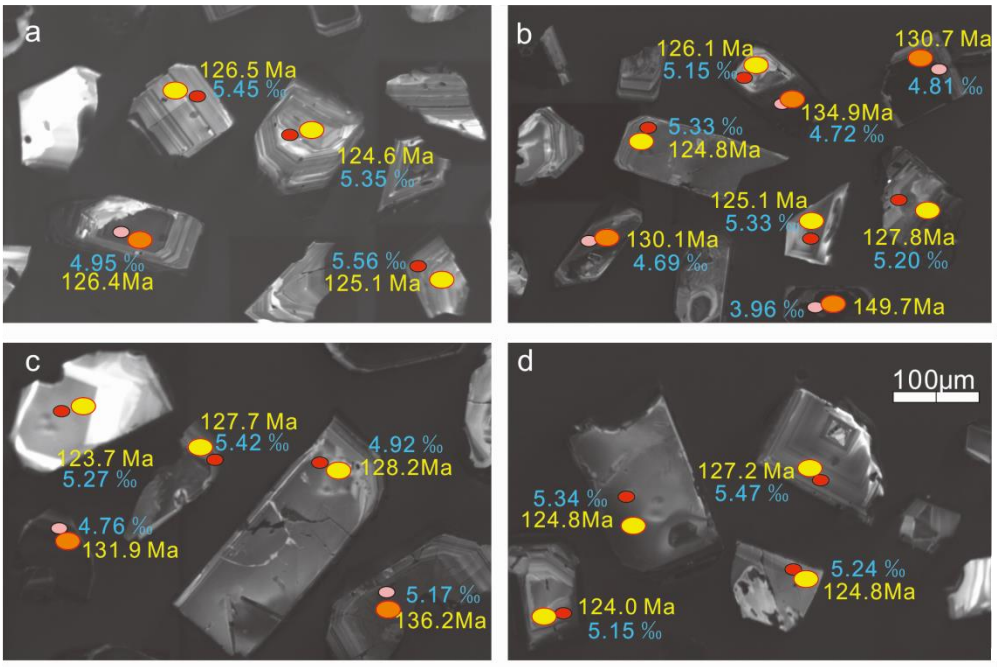


Figure 4.1 Cathodoluminescence (CL) images of representative zircons analysed for U-Pb, and O-isotopes.

4.3.2 SIMS U-Pb ages

One hundred and fifty analyses were conducted on 141 zircons (Appendix table ix). U-Pb data were calibrated through the Pb^+/U^+ vs UO_2^+/U^+ scheme. The measured [U], [Th] of the Suzhou zircons range from 33 to 13,433 ppm and 23 to 17,028 ppm, respectively. The group 1 zircons (115 analyses), have moderate [U] (< 3000 ppm) and [Th] (< 3820 ppm), with Th/U ratios of 0.2 - 1.7. Most zircons have low common-Pb contents, with values for f_{206} (based on the $(^{204}Pb/^{206}Pb)_{measured}/(^{204}Pb/^{206}Pb)_{common}$) of ≤ 2.0%. Thirteen spots with high f_{206} (2 to 58%) were eliminated from the final age calculation because the high common Pb resulted in large uncertainties in the calculation of the radiogenic Pb content and composition (listed in grey color in

Appendix table ix). The remaining 102 analyses gave concordant U/Pb ratios within analytical uncertainties, yielding a weighted mean $^{206}Pb/^{238}U$ age of 126.1 ± 0.5 Ma (MSWD = 1.16) (Figure 4.2b, c, d).

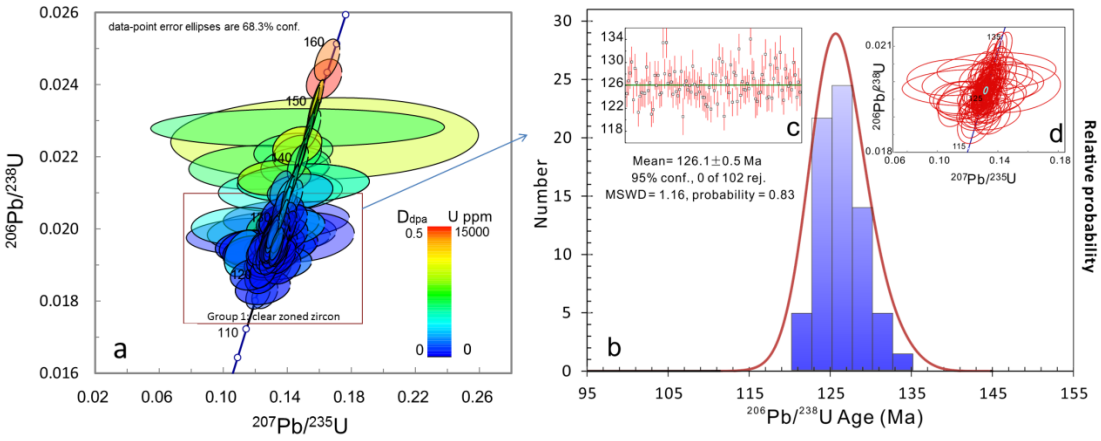


Figure 4.2 a) Concordia zircon grains from the Suzhou granite (includes zircons from all three rock types); b) U-Pb relative probability; c) weighted average, and d) Concordia diagrams for group 1 zircons. Analyses are shown with 2σ errors and uncertainties in weighted mean ages are quoted at the 95% confidence level.

The analysed Group 2 zircons (35 spots, Figure 4.2a) have very high and variable contents of [U] (3027 to 13,433ppm) and [Th] (457 to 17,028 ppm), with Th/U ratios of 0.2 to 1.6. There is a strong correlation between the ^{204}Pb-corrected $^{206}Pb/^{238}U$ ages and [U] (Figure 4.3a). The slope of the correlation line is approximately 2.2 ± 0.3% per 1000 ppm U, which is similar to the correlation slope measured by White and Ireland (2012) and Williams and Hergt (2000).

4.3.3 *In situ* zircon and quartz oxygen isotopes

One hundred and fifty *in situ* O-isotope analyses were conducted on the same zircon zones next to the sites of the U-Pb analysis. The two groups of zircon have

distinct oxygen-isotope characteristics that are closely related to [U] (Figure 4.4a). The weighted average $\delta^{18}O$ of each sample is listed in Appendix table x. Zircons with [U] < 1500 ppm have a very homogeneous O isotopic composition, with $\delta^{18}O$ ranging from 4.76‰ to 5.95‰ and forming a Gaussian distribution with an average $\delta^{18}O$ = 5.34 ± 0.46‰ (2SD; Figure 4.4b). The $\delta^{18}O$ values of this group are independent of [U]. In contrast, zircons with [U] > 1500 ppm have variously low $\delta^{18}O$ (3.73 to 5.35‰) (Figure 4.4b), and there is a negative correlation between [U] and $\delta^{18}O$ (Figure 4.3c).

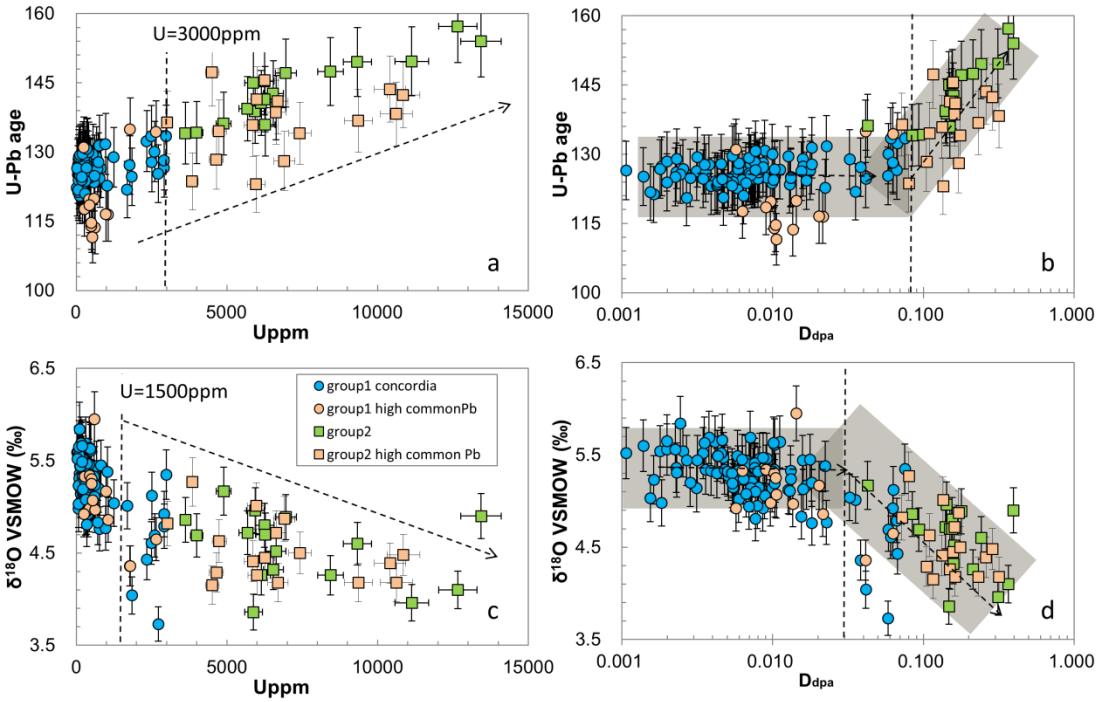


Figure 4.3 a) Plot of zircon [U] vs $^{206}Pb/^{238}U$ age; b) Plot of zircon D_{dpa} vs $^{206}Pb/^{238}U$ age; The D_{dpa} is calculated based on the [U], [Th] obtained from the corresponding SIMS spots. Grey vertical dashed lines mark turning point at $D_{dpa} \approx 0.08$; c) Plot of zircon U content vs $\delta^{18}O$; d) Plot of zircon D_{dpa} vs $\delta^{18}O$. Grey vertical dashed lines mark turning point at $D_{dpa} \approx 0.03$.

SIMS analyses of oxygen isotopes were carried out on quartz coexisting with the

zircons, to investigate the magmatic $\delta^{18}O$ value of the Suzhou A-type granite as well as the extent of subsolidus exchange of oxygen isotopes between non-U-bearing minerals. Eighty-four *in situ* O analyses were conducted on 76 quartz grains (Appendix table xi). Quartz grains from samples Sz1, Sz2, and Sz3 are irregular in shape, 300-500 μm in diameter and clear in transmitted light; a very few of them show partial damage or alteration (a "dirty" appearance under reflected light and nearly opaque under transmitted light). Quartz grains from sample Sz4 are "dirtier" than the others. Analyses were done on both clear and "dirty" quartz. Except for the 8 dirtiest ones in sample Sz4 (excluded from weighted average calculation), most quartz grains give a tight range of $\delta^{18}O$ values from 7.1 to 8.3‰ with an average $\delta^{18}O = 7.70 \pm 0.52$‰ (2SD), defining a Gaussian distribution (Figure 4.5a, b). O isotope fractionation between quartz and group 1 zircons varies from 2.07 to 2.44, *vs* 2.93 to 3.31 for quartz and the group 2 zircons.

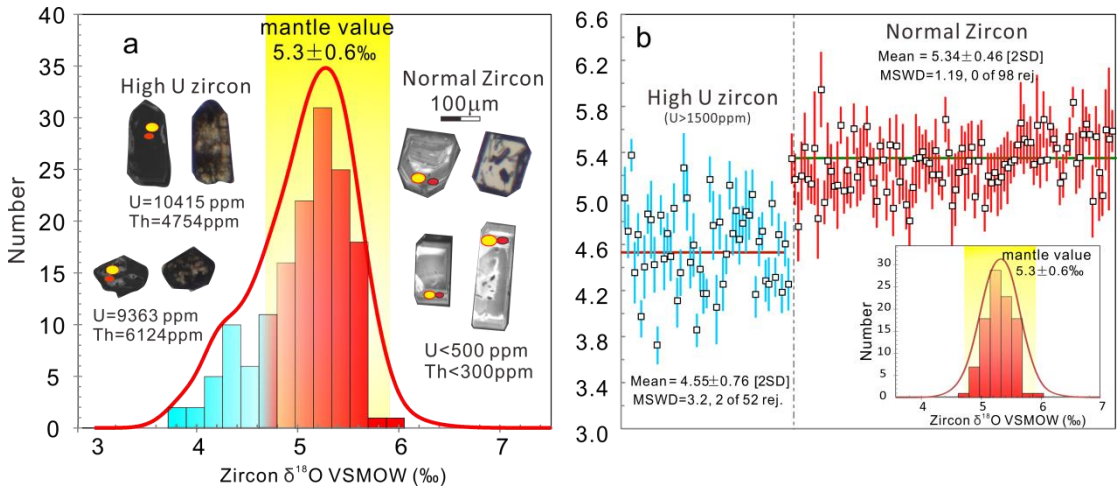


Figure 4.4 a) Histogram of $\delta^{18}O$ values for zircons; typical cathodoluminescence images and transmitted-light photos of zircon crystals with "mantle" $\delta^{18}O$ (right) and low-$\delta^{18}O$ zircon crystals (left); b) Weighted average diagram of $\delta^{18}O$ values for zircons. Data of zircons with [U] >1500 ppm are in blue color.

4.3.4 Raman spectroscopy

Raman spectra were measured of 3 zircon standards (Plešovice, Penglai and 91500) and 30 grains of zircons from the Suzhou pluton. The spectra of selected Raman analyses are presented in Figure 4.6.

They show a regular change in the spectrum that can be directly related to differences in [U]. All the standards yield spectra similar to (or only shifted slightly from) spectra of crystalline zircon that has experienced very few alpha decay/recoil events (Zhang et al., 2000). In zircons with [U] < 1500 ppm, peaks are well-defined and sharp. Three dominant peaks occur at *ca.* 350, 450 and 1010 cm^{-1} with the most intense peak at 1010 cm^{-1}; these peaks are interpreted as representing the internal vibrations of SiO_4 tetrahedra (Nasdala et al., 2001). With increasing U concentration, the Raman spectra of zircons change gradually. In grains with [U] > 5000 ppm, the peaks change again, and show a broad peak from 400 to 900 cm^{-1} with a maximum at 500 cm^{-1}. These spectra are characteristic of amorphous silica/glass (McMillan, 1984; McLaren et al., 1994). Not all zircons with [U] > 3000 ppm fit this pattern, which could be attributed to late annealing of zircon, partly erasing the effects of radiation damage.

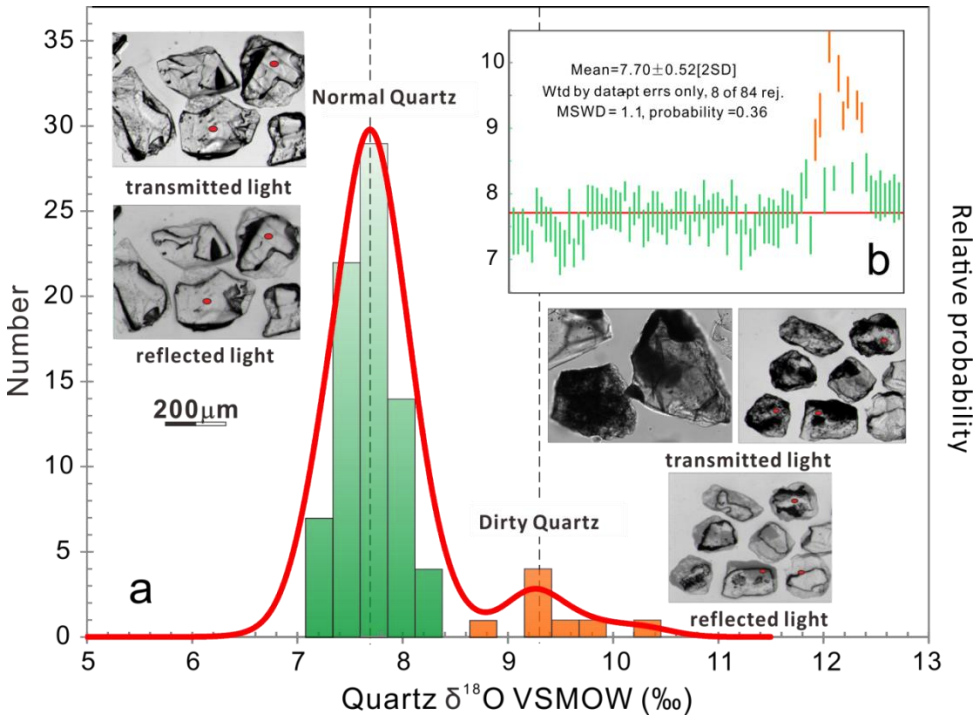


Figure 4.5 a) Histogram diagram, and b) Weighted average of $\delta^{18}O$ values for quartz with reflected-light and transmitted-light photo; Data of "dirty quartz" are in orange color.

4.4 DISCUSSION

4.4.1 Uranium influence on SIMS zircon dating

(1) The age of the Suzhou granite

The Suzhou A-type pluton has long been regarded as consisting of multiple intrusions that can be divided into 3 stages according to the petrography and field relations. Published radiometric age data using different methods give results that are not entirely consistent. Several Rb-Sr whole-rock studies have produced isochron ages ranging from 114 to 140 Ma (Ouyang, 1985; Wang et al., 1993).(Chen et al., 1993) suggested that the ^{40}Ar-^{39}Ar age of amphibolite-bearing granite, biotite K-feldspar granite and albite

granite crystallized at 122.7 ± 1.4 Ma, 122.6 ± 0.4 Ma, and 123.1 ± 0.1 Ma (2SD), respectively. However, the ^{40}Ar-^{39}Ar ages determined by Charoy and Raimbault (1994) are 123.1 ± 0.4 Ma, 123.4 ± 0.8 Ma and 133 ± 1 Ma (2SD), with an age gap of 10 Ma between the last two stages.

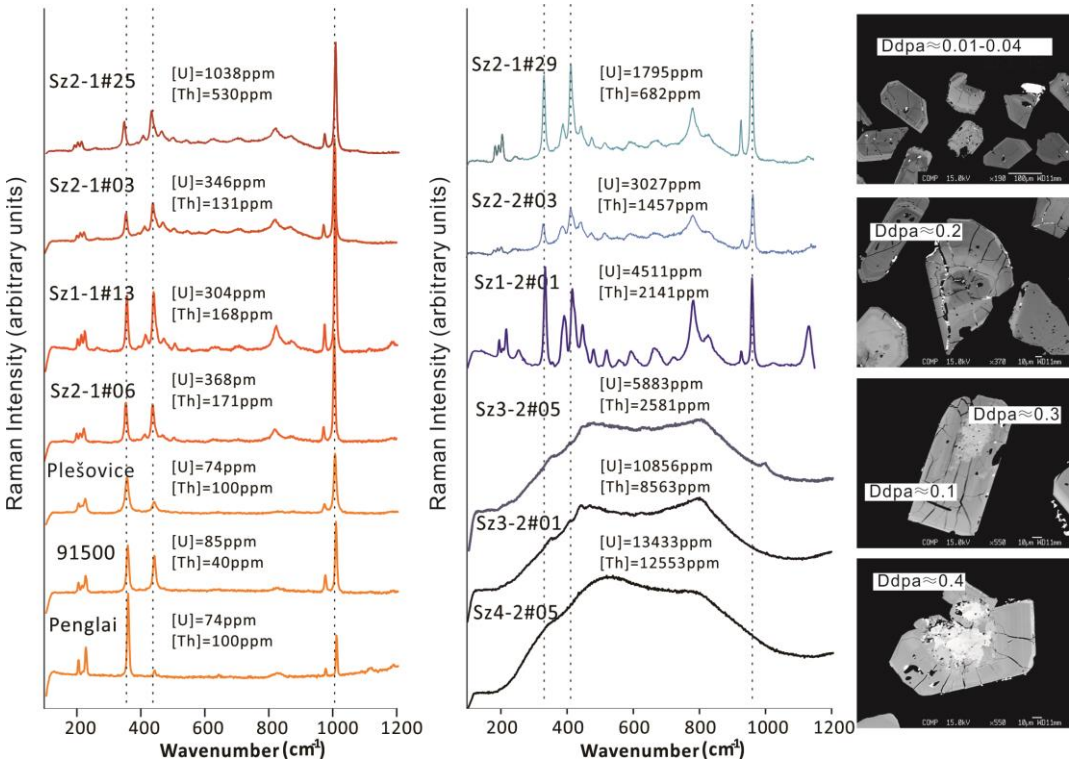


Figure 4.6 Raman spectra of zircons with different [U] and [Th]. Spectra obtained from the standards and other zircons with [U] < 1500 ppm all show the distinctive zircon peaks (grey vertical dashed lines). However, zircons with [U] >1500 ppm generally show patterns with broad indistinct peaks, indicating that these zircons have an amorphous or semi-amorphous structure. This most likely reflects partial to complete metamictization through radiation damage.

SIMS U-Pb dating of zircons from the Suzhou granites in the present study shows a range in [U] and [Th] and complex relationships to the age data. Such a wide range of apparent zircon crystallization ages is unreasonable for a simple igneous rock.

Generally, high U (and Th) concentrations lead to discordance in the U-Pb isotopic system, often attributed to the loss of radiogenic lead related to changes in the physical properties of zircon caused by radiation damage and subsequent alteration (McLaren et al., 1994; King et al., 2001; Utsunomiya et al., 2007). Moreover, high-U zircons have more cracks than normal zircon and higher common Pb, which causes spurious ^{204}Pb corrections. In our SIMS results, zircon grains with U contents > 3000 ppm are more likely to contain high common Pb and to be discordant. However, even without those high levels of common Pb, analyses of zircons that are strongly metamict still show a broad correlation between [U] and U-Pb age (Figure 4.3a). This phenomenon is known as the "high-U matrix effect" and was first mentioned by Williams and Hergt (2000). It is generally accepted that the higher apparent U-Pb ages found in SIMS analyses might be caused by preferential sputtering related to differences in the zircon matrix (Williams and Hergt, 2000; Butera et al., 2001; White and Ireland, 2012).

(2) The cause of the "high-U matrix effect"

Although the "high-U matrix effect" is commonly cited in SIMS zircon U-Pb dating studies, there is no consensus on the threshold of [U] which will cause the matrix effect. Williams and Hergt (2000) suggested that a relationship between SIMS zircon age and [U] was only apparent above 2500 ppm; Butera et al. (2001) corrected for U-dependent calibration bias by 2.0% per 1000 ppm U above 2500 ppm; Leech (2008) reported that zircons with [U] > 4000 ppm have high apparent ages. White and Ireland (2012) pointed out that young zircons even with [U] > 10000 ppm do not show the "high-U matrix effect", strongly suggesting that the radiation damage needs to

accumulate through time. That means that to define "high-U" zircon, we also need to specify its age.

A matrix effect could be caused by high U in the matrix affecting the ionization yield, or by metamictization. Compared with the matrix difference caused by high U^{4+} substituting for Zr^{4+}, the degree of metamictization of zircon is more critical in controlling the preferential sputtering. As mentioned above, young high-U zircons do not show the effect and this implies that U substitution is not causing the fractionation. This also is confirmed by Raman spectra, which show that zircons with increasing degrees of damage have gradually changing peaks and higher values of half-width height, indicating that the U-rich zircons are in a metamict state (Nasdala et al., 2002a; Nasdala et al., 2002b). According to the spectra for the Suzhou pluton, [U] > 3000 ppm greatly "softens" the microstructure of the zircon lattice and has a significant impact on the measured U-Pb age. In other words, the "high-U matrix effect" only appears when the analysed zircons have reached a certain degree of radiation damage. Therefore, it is essential to use "the degree of radiation damage" instead of U content to describe the matrix effect. Experimental data suggest that a radiation dose of one unit (10^{18}α-decays events/g) could produce 10-20% of an amorphous component (R ǿs et al., 2000). Electron diffraction and HRTEM imaging indicate that when the radiation dose reaches 10^{19}α-decays events/g, the zircon will be fully metamict (Nasdala et al., 2001; Ewing et al., 2003; Palenik et al., 2003).

(3) The effect of the "Degree of radiation damage" on the calibration

For natural zircons, U-Th concentrations and age can be used to evaluate the

approximate radiation dose absorbed by a zircon. The degree of radiation damage can be calculated from the radiation dose by assuming no annealing has taken place afterwards. The degree of lattice damage can be expressed in terms of "displacements-per-atom (dpa)". D_{dpa} is the dose in dpa, and we can use the following formula to make a quantitative estimate of the amount of radiation damage in minerals:

$$D_{dpa} = D\alpha\ W\ n/(a\ A)$$

where A is Avogadro's number, W is the molecular weight of the mineral, n is the average number of displacements per α−decay, a is the number of atoms per formula unit and Dα is the dose in units of α-decays/g. In the case of zircon an approximate value of n = 94000 can be used, according to previous computer simulations (Palenik et al., 2003). For natural zircons, the U-Th concentrations and the age can be used to calculate the radiation dose:

$$D\alpha = 8\ N_{238}\ [\exp(t/\tau_{238}) - 1] + 7\ N_{235}\ [\exp(t/\tau_{235}) - 1] + 6\ N_{232}\ [\exp(t/\tau_{232}) - 1]$$

where N_{238}, N_{235}, and N_{232} are the measured numbers of atoms/g of ^{238}U, ^{235}U and ^{232}Th; $\tau_{(238)}$, $\tau_{(235)}$, and $\tau_{(232)}$ are their respective half-lives; *t* is the geological age (Ewing et al., 2003). The half-lives and age need to be in the same time units. D_{dpa} directly reflects the highest possible degree of metamictization (amorphization) of a zircon. Thus, because D_{dpa} is a parameter which combines [U], [Th] and the time span of decay, a "high D_{dpa} effect" might provide a better descriptor of the influence of [U] on the SIMS U-Pb age determination.

Figure 4.3b shows calculated D_{dpa} *vs* U-Pb age. The results with $D_{dpa} > 0.08$ should be discarded and not used in the age calculations. Therefore, all the Pb-U ratios for the

screened zircons are concordant within analytical errors; zircons from four samples from the all the main phases present a very consistent crystallization age at 126.1 ± 0.5 Ma. This is the best age obtained up to now and indicates that the Suzhou granites were formed in a single magmatic episode.

4.4.2 Influence of radiation damage on zircon oxygen isotopes

(1) Oxygen isotopes composition of the Suzhou granite

Previous bulk zircon analyses have been used to argue that Suzhou granite is ^{18}O-depleted. Wei et al. (2008) used the laser-fluorination technique to analyze bulk zircon samples from 12 different rocks in the Suzhou pluton. The measured $\delta^{18}O$ ranged from 4.79 to 5.06‰, with an average value for the entire Suzhou suite cited as 4.92 ± 0.26‰ (2SD). However, most of our SIMS *in situ* oxygen-isotopic analyses of zircon indicate that the Suzhou granites have a normal mantle $\delta^{18}O$ value (5.3 ± 0.6‰, 2SD, Valley et al., 1998; Cavosie et al. 2009); only 1/3 of the *in situ* analyses in this study have $\delta^{18}O < 5.1$‰, and these show a strong linear correlation of $\delta^{18}O$ with both [U] and U-Pb age (Figure 4.3c).

The correlation between $\delta^{18}O$ and [U] might in principle be attributed to the presence of: 1). Inherited zircons; 2). Change of IMF (instrumental mass fractionation); 3). Change of the zircons' structure by radiation damage, or 4). Radioactive damage and later alteration. In the discussion above, we concluded that all the zircons crystallized at the same time from one magmatic event and we did not observe zircons with inherited cores or overgrowth rims in the CL images; thus it is unlikely that the low-$\delta^{18}O$ is

related to heterogeneous domains within the zircon grains. Peck et al. (2001) reported five zircon standards with variable HfO_2 and suggest that IMF varies about 1‰ for each 1 wt % HfO_2. However, in the Suzhou granite, HfO_2 ranges from 0.5 to 1.5 %, which is in the same range as the standard zircon. Therefore, the Hf IMF correction will be minor and negligible. Compared to the matrix difference caused by [Hf^{4+}] substituting for Zr^{4+}, the degree of metamictization of zircon is more critical in controlling the preferential sputtering.

It is important to distinguish between the real value of zircon $\delta^{18}O$ and a matrix-dependent ionization effect in the SIMS analysis. In the analysis of $\delta^{18}O$ in bulk zircon separates by laser fluorination, there is no mineral-specific fractionation and no matrix effect and therefore the results can be regarded as the true composition of the bulk zircons. However, this may not represent the true original magmatic value, if the bulk sample is made up of more than one population. Our SIMS *in situ* analyses have identified two groups; the weighted average $\delta^{18}O$ of high-U zircon (1/3 of the grains having $\delta^{18}O \approx 4.55‰$) and normal zircon (2/3 of the grains having $\delta^{18}O \approx 5.34‰$) is 5.08 ± 0.45‰, identical within error to the previous laser-fluorination bulk analyses (4.92 ± 0.26‰). Thus, the bulk zircon result can be attributed to mixing between the high-U and normal-U zircons described above.

It is noteworthy that the low $\delta^{18}O$ values found in the SIMS analyses are also the true values of the high-U zircon grains, which might suggest that a matrix effect cannot be the major cause of low $\delta^{18}O$ values in SIMS analysis. Valley (2009) proved that there are no systematic differences observed for ion microprobe data from individual zircon

grains *vs* laser-fluorination analyses of bulk samples comprising hundreds of zircon grains. This suggests that the SIMS data can be compared with laser fluorination data. Wei et al (2008) analysed unaltered samples from the same pluton using the laser fluorination technique. They have solid evidence to show their low $\delta^{18}O$ is a real composition and can be used to prove that low-$\delta^{18}O$ zircon actually exists in the Suzhou pluton. That also means that the low $\delta^{18}O$ values in SIMS analysis are not instrument-dependent. Therefore, an explanation is required for the lower $\delta^{18}O$ values of high-U zircons: have these low-$\delta^{18}O$ zircons crystallized from low-$\delta^{18}O$ magmas or do they reflect later alteration?

From the O-isotope fractionation diagram (Figure 4.7), except for the 8 dirtiest quartz grains from sample Sz4, quartz and group 1 zircon have oxygen-isotope temperatures between 771 and 856^{o}C, consistent with their Zr saturation temperatures (T_{Zr}: 865 ± 110^{o}C, calculated from Charoy and Raimbault, 1994; Wei et al., 2008). Therefore, group 1 zircon and quartz equilibrated at high temperatures. In contrast, quartz and group 2 zircon have oxygen-isotope temperatures ranging from 618 to 692^{o}C, which are much lower than T_{Zr}. Thus, group 2 zircon does not represent the $\delta^{18}O$ values of the original magma.

Because of their shallow depth of emplacement, as evidenced by the presence of miarolitic cavities, some rocks may have been affected by post-magmatic hydrothermal alteration. Late hydrothermal alteration of sample Sz4 apparently led to an increase of $\delta^{18}O$ in quartz while zircon was not affected. Histograms of $\delta^{18}O$ for Suzhou zircon-quartz pairs (Figure 4.8) show that, aside from a few highly altered quartz grains

in sample Sz4, the unaltered to mildly altered quartz has very homogeneous $\delta^{18}O$ values of ~7.6‰, while high-U zircons show a larger variation. This suggests that quartz can preserve the O-isotope ratios of magmas better than high-U zircon can. We conclude that normal quartz (clear and unaffected by later hydrothermal alteration) and zircon with [U] < 1500 ppm from the Suzhou granites are in oxygen-isotope equilibrium; this indicates that the parental magmas of the Suzhou granite were not depleted in ^{18}O as previously reported. Compared with zircon, except in very U-rich rocks, quartz seldom suffers radiation damage, which could make it a good candidate to constrain the oxygen-isotope compositions of the granitic magmas. This then enables us to evaluate the measured oxygen-isotope composition of zircon by examining the quartz-zircon pair, if we can establish that quartz and zircon are in mutual contact and temporally related to each other.

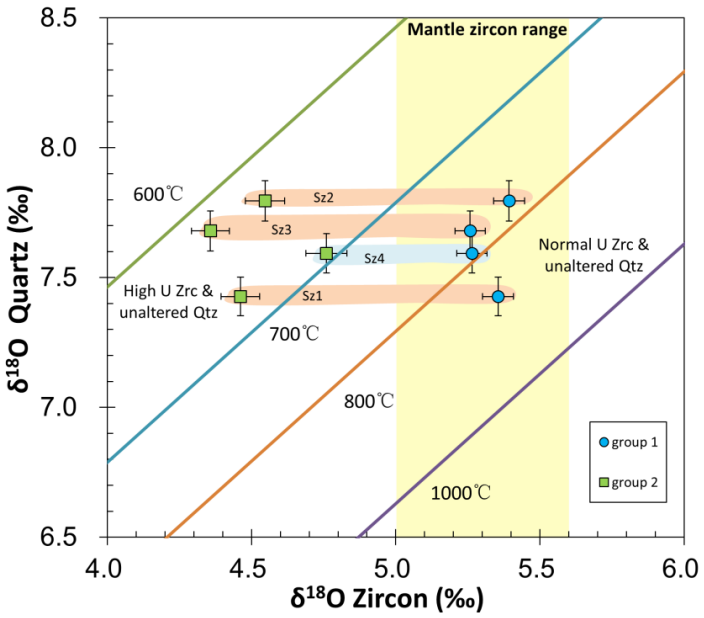


Figure 4.7 Oxygen isotope fractionation between quartz and zircon from the Suzhou pluton. Thin solid bar of data points represents the 2SD. Solid isotherms are from Valley

et al. (2003).

The $\delta^{18}O$ values of equilibrium quartz-zircon pairs are interpreted to reflect the primary magmatic oxygen isotopic compositions. Based on the correlation of $\delta^{18}O$ values between zircon and whole rock: $\delta^{18}O_{(Zrc\text{-}WR)} = \delta^{18}O_{(Zrc)} - \delta^{18}O_{(WR)} \approx -0.0612$ (wt% SiO_2) + 2.5 (Valley et al., 2005), the calculated whole-rock $\delta^{18}O$ values of the Suzhou pluton range from 6.5 to 7.6‰. Therefore, the Suzhou A-type granites were generated either by extreme fractionation of mantle-derived magmas, or by re-melting of mafic to intermediate igneous protoliths with little, if any, involvement of supracrustal material.

(2) Mechanism of formation of "low-$\delta^{18}O$ zircon"

The discussion above indicates that the low $\delta^{18}O$ values are the true values of the zircons in their present state, but do not represent magmatic values. Igneous zircons are highly retentive and potentially preserve oxygen-isotope compositions in equilibrium with the magma at the time of their crystallization (King et al., 1997; Monani and Valley, 2001; Valley, 2003; Valley et al., 1994). However, this would not be true if zircons are subjected to strong radiation damage. The relationship between U-Pb systematics and oxygen isotopes has been examined by Bibikova (1982), Valley (1994, 2003) and Booth (2005). They concluded that zircons with disturbed U-Pb systematics are often variably depleted in ^{18}O (Booth et al., 2005; Valley, 2003; Valley et al., 1994). However, little caution has been taken in the evaluation of zircon oxygen isotopes and effects on the U-Pb system remain unexplored.

The discussion above suggests that the zircon oxygen-isotope system has a lower

tolerance for radiation damage than U-Pb system, and that oxygen isotopes thus may develop open-system behavior, with the low $\delta^{18}O$ values in high-U zircon simply reflecting the effects of radiation damage.

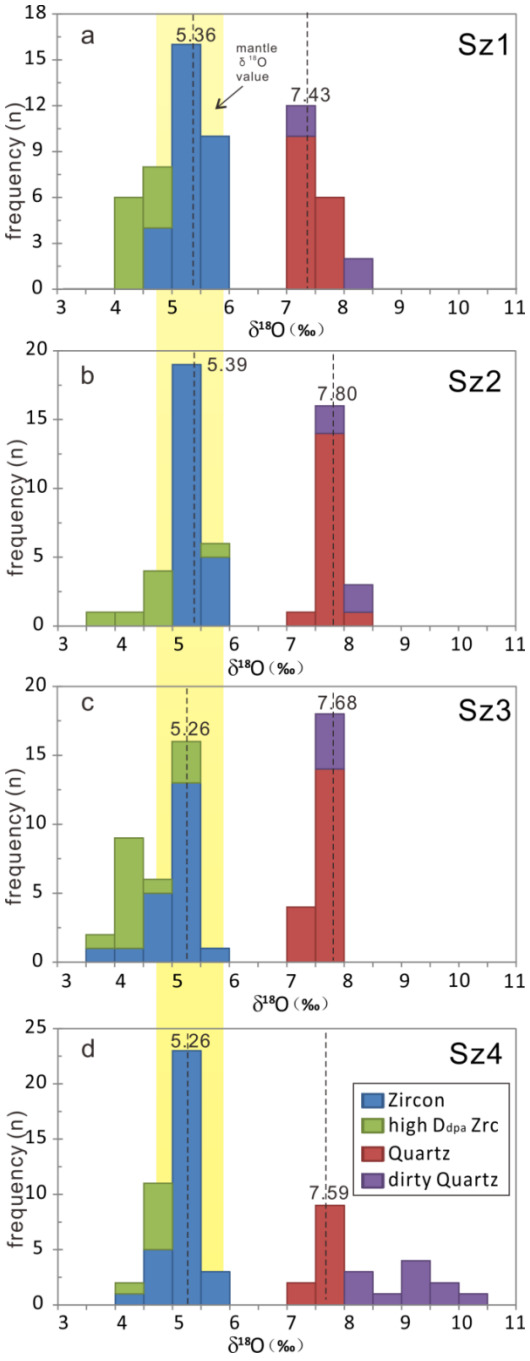


Figure 4.8 Histograms of $\delta^{18}O$ values for zircon-quartz pairs from the Suzhou granite. a) amphibole-bearing porphyritic alkali-feldspar granite; b) coarse-grained

alkali-feldspar granite; c) fine-grained alkali-feldspar granite; d) altered alkali-feldspar granite.

A likely explanation for the depleted $\delta^{18}O$ is that zircon becomes metamict due to crystal lattice expansion and decreased crystallinity caused by accumulated damage to the crystal structure. Metamictization ultimately produces an amorphous matrix that may be open to the infiltration of hydrous fluids into the damaged structure and/or along cracks and grain boundaries (Woodhead et al., 1991). Metamict zircons commonly contain easily detectable OH^-, and the OH^- groups in these zircons appear to be involved in the local charge balance of the disrupted lattice (Aines and Rossman, 1986). Analyses of the zircons from the Suzhou granite demonstrate that large amounts of U in the zircon matrix will greatly damage the chemical durability of the zircon with respect to oxygen. Trace water can enter the zircon structure after a certain threshold of damage ($D_{dpa} > 0.03$) is reached. The OH^- probably comes from surface water, which could be extremely depleted in ^{18}O. Oxygen easily diffuses in both hydrous and amorphous zircon glass (Watson and Cherniak, 1997; Cherniak and Watson, 2003; Cherniak, 2010), and therefore lowers the $\delta^{18}O$ of the entire zircon grain.

4.3.3 Protocols for screening zircon data

In the Suzhou pluton, about 1/4 of the zircons have older U-Pb apparent ages, 1/3 have anomalously low $\delta^{18}O$ values, and U-Pb apparent age and $\delta^{18}O$ are negatively correlated (Figure 4.9).

The isotopic characteristics of these anomalous grains have been affected by

metamictization, and do not represent the magmatic value. Therefore it is useful to have a quantitative tool to evaluate the effect of metamictization on zircon oxygen-isotope values before making petrogenetic interpretations. White and Ireland (2012) noted that the "high-U matrix effect" is likely to be both sample-dependent and instrument-dependent. As metamictization is caused by radiation damage, [U], [Th] and age should all be considered. Therefore, while the screening criterion of [U] < 3000 ppm for reliable U-Pb ages could only apply to the Suzhou pluton and other zircons with similar ages, the value of $D_{dpa} < 0.08$ can be applied to other samples. Using the above formula to calculate D_{dpa}, we can quantify the relationships of [U]-[Th]-Age-D_{dpa}. (Figure 4.10)

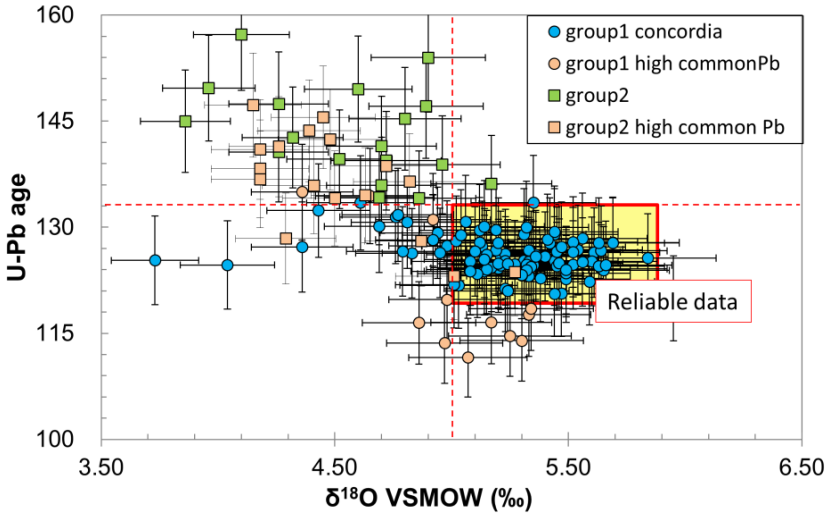


Figure 4.9 Plot of zircon U-Pb age vs $\delta^{18}O$ values.

Figure 4.10 shows [U] versus age for each degree of radiation damage (different D_{dpa}). Th content is also considered in this figure, and the area between the dashed and solid lines with the same D_{dpa} includes all zircons with Th/U from 0.1 to 1. From Figure

4.10, the minimum U content that causes a certain D_{dpa} level decreases with increasing age; in another word, to achieve the same degree of radiation damage, the threshold of the "High-U effect" decreases with increasing age. For old zircons (> 4 Ga), even those with low [U] (< 200 ppm) and [Th], the radiation damage accumulated through geological time would be extensive, assuming the lattice was not annealed (e.g. by metamorphic heating).

For the Suzhou granite, zircon grains with [U] > 1500 ppm have low $\delta^{18}O$ values. Application of this criterion to other zircon populations requires an assessment of the approximate radiation dose absorbed by a zircon. The D_{dpa} of the Suzhou pluton is from 0.00~0.40. For D_{dpa} > 0.03, the correlation of $\delta^{18}O$ with [U] shows a "high D_{dpa} effect". Figure 4.10 shows that nearly all of the zircon standards lie below the threshold of D_{dpa} = 0.03. In combination with the Raman spectra, the zircon $\delta^{18}O$ data suggest that the threshold for atomic displacements and defect formation in zircon should be around D_{dpa} = 0.03, where the zircon lattice "softens".

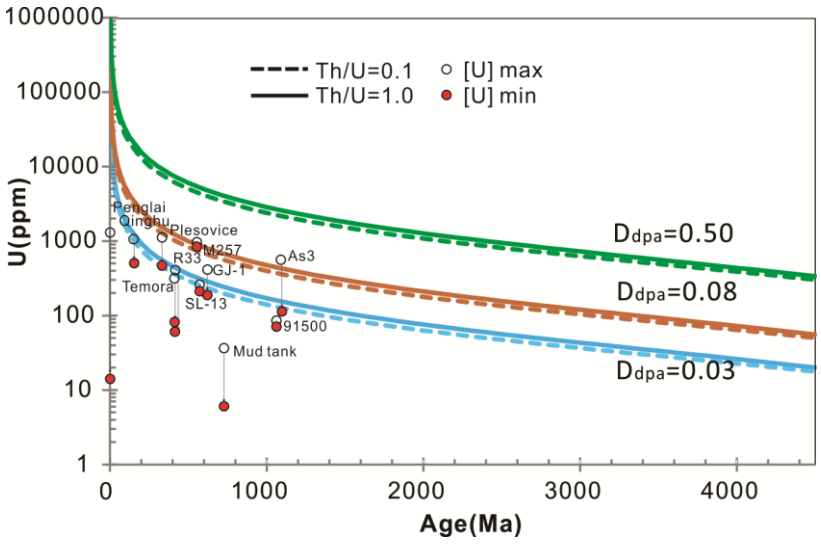


Figure 4.10 Correlation between U concentration and U-Pb ages, along with assigned

D_{dpa} of 0.03, 0.08, and 0.5. Dashed lines Th/U = 0.1; solid lines Th/U = 1. The area between dashed and solid lines with same D_{dpa} includes all zircons with Th/U = 0.1 ~ 1.

Table 4-1 is a summary of the calculated D_{dpa} of zircon standards and data from other studies of [U]-$\delta^{18}O$ or [U]-age relationships. Combining these data with those from this study, we propose that those zircons with $D_{dpa} > 0.03$ may have disturbed $\delta^{18}O$, and that $D_{dpa} > 0.08$ may cause "high-U matrix effect". The data above the threshold should be used for petrogenetic studies only with great care.

Table 4-1 Calculated D_{dpa} for zircon U-Pb age standards

Reference	Age(Ma)	U(ppm)	Th(ppm)	Reference	Calculated D_{dpa}
Penglai	4.4	14～1297	5～747	Li et al. (2010)	～0.00
Qinghu	159.5	1042±387	544±288	Li et al. (2009, 2013)	0.02～0.04
Plešovice	337.1	465～1106	44～183	Slama et al. (2008)	0.03～0.06
Temora1	416.8	64～846	23～534	Black et al. (2003）	0.00～0.07
Temora2	416.8	130±21	54±10	Black et al. (2004）	0.01～0.02
R33	419.3	148±20	100±20	Ratcliffe and Aleinikoff(2000)	～0.01
M257	516.3	840±60	~227	Nasdala et al. (2008)	0.07～0.08
Z6266(Br266	559.0	871～958	191～212	Stern (2003)	0.08～0.09
SL13	572.1	210～238	18～21	Lee et al. (1997)	～0.02
GJ-1	609.0	212～422	6～13	Jackson et al. (2004)	0.02～0.04
Mudtank	732.0	6～36	~17	Black and Gulson (1978)	～0.00
91500	1065.0	71～98	~40	Wiedenbeck et al. (1995, 2004)	0.01～0.02
AS3	1099.1	360±80	233±54	Paces and Miller (1993)	0.06～0.09
QGNG	1842.0	212±23	188±26	Black et al. (2003, 2004）	0.07～0.10

This provides a new procedure for screening both zircon $\delta^{18}O$ values and SIMS U-Pb ages to improve the quality of datasets. D_{dpa} is equivalent to [U] for plutons with a single age, but will be more useful in distinguishing zircons with disturbed O-isotope systematics, and thus eliminating confusing data from detrital-zircon populations.

Radiation damage is a complicated effect, which integrates both accumulated lattice damage and annealing over geological time (Lumpkin and Ewing, 1988; Meldrum et al., 1998; Balan et al., 2001). Thus the calculated D_{dpa} may not be the same as the actual D_{dpa} in zircon. For zircons with very old ages, the threshold of D_{dpa} will be more complex, as the lattice defects will incorporate hydroxide species, and the presence of trace water will hasten the annealing process. There will probably be a balance between radiation damage and annealing; as a result, zircons may appear less damaged than estimated from the calculated D_{dpa} (Yamada et al., 1995; Nasdala et al., 2001; Nasdala et al., 2002a; Nasdala et al., 2002b). Nasdala et al. (2001) have suggested that zircon samples from Sri Lanka do not preserve the full damage that would be expected based on the calculated dose. This finding is consistent with previous work showing that Sri Lankan zircon crystals are less metamict than would be expected from their α-decay dose (Holland and Gottfried, 1955; Murakami et al., 1991). For example, a 561 Ma annealed gem-quality zircon from Sri Lanka has a damage dose equivalent to that of a ~375 Ma un-annealed zircon (Palenik et al., 2003). Therefore, is it is necessary to use both the calculated D_{dpa} and Raman spectroscopy to identify the actual degree of damage and to ensure that the analysed zircons are fully crystalline.

4.5 CONCLUSIONS

The degree of radiation damage accumulated by a zircon crystal through geological time is rarely negligible. SIMS analyses of zircons with extreme radiation damage can show an apparent increase in Pb/U age and a real decrease in $\delta^{18}O$ that are correlated with the D_{dpa}. We can draw the following conclusions:

1. The higher apparent U-Pb ages and lower $\delta^{18}O$ values typical of high-U zircon are both related to radiation damage, but are caused by different mechanisms. The "high D_{dpa} effect" on SIMS U-Pb age determinations is a matrix effect specific to SIMS analysis, while the low-$\delta^{18}O$ zircons reflect compositional (oxygen-isotope) exchange due to oxygen diffusion in hydrous (metamict) zircons. The U-Pb isotope system in zircon is more stable than the oxygen-isotope system, and zircons with concordant U-Pb ages may thus have disturbed $\delta^{18}O$ values.

2. The threshold of the "high-U matrix effect" decreases with increasing age; the D_{dpa} may be a better screen for choosing zircons for O-isotope analysis and dating. Raman spectroscopy can be used to measure the crystallinity of zircons and should be used together with D_{dpa} to select zircons for isotopic studies. The recommended threshold for reliable oxygen-isotope data is set at $D_{dpa} < 0.03$ to eliminate the low-$\delta^{18}O$ zircons affected by diffusion, whereas D_{dpa} should be less than 0.08 for U-Pb dating of zircon to avoid significant age distortions. This discriminant may be especially useful in detrital-zircon studies.

3. Integration of Raman spectra and oxygen-isotope analyses of coexisting quartz reveals that low $\delta^{18}O$ values are due to the effects of radiation damage in the zircons and later interaction with OH-bearing fluids, infiltration and diffusion were facilitated in the radiation-damaged areas.

4. The Suzhou granite formed in a single magmatic episode at 126.1 ± 0.5 Ma. Oxygen isotopes of normal zircons have mantle values of 5.34 ± 0.46‰ (2SD) that are in equilibrium with quartz. Compared with high-U zircon, quartz can better preserve the primary O-isotope ratios of magmas. The Suzhou pluton is not a primary "low-$\delta^{18}O$ A-type granite" as previously suggested.

CHAPTER 5. SIMS ANALYSIS OF LI ISOTOPES IN ZIRCON: TOPOGRAPHY /CHARGE EFFECTS AND OPTIMIZATION OF ANALYTICAL PARAMETERS

5.1 INTRODUCTION

SIMS has become a major technique employed in geochemistry for its high resolution, high sensitivity and high spatial resolution. It has been designed to undertake isotopic analysis of minerals in sub-micron spots, which can reveal valuable geological information. Li isotopes have become increasingly recognized as a useful tracer in many geochemical applications; however, the mechanism of Li diffusion and the phenomenon of Li-isotope fractionation in zircon are poorly understood. It is vital to understand Li behavior in zircon in order to make valid interpretations of *in situ* data.

In contrast to $\delta^{18}O$ determinations, Li is a trace element (~1-100 ppm) in major rock-forming minerals and in accessory minerals, which leads to the following complications (Layne, 2009): 1). Substantial matrix effects caused by variable major-element concentrations. In order to calibrate the Instrumental Mass Fractionation (IMF) correctly, one or more reference materials that are adequately matched to the range of sample compositions to be analysed are required; 2). Li itself may be extremely variable in concentration within samples. Care must be taken to maintain detector linearity; 3). IMF can vary for individual analyses if care is not taken to stabilize the effective sample potential during analysis. Care must be taken to monitor and stabilize drift in sample potential when large primary beam currents are used in focused spots. Therefore, the low concentration of Li makes it difficult to achieve ± 0.1‰ precision as in the $\delta^{18}O$ determinations.

Kita et al. (2009) found that values of $\delta^{18}O$ obtained from zircon *in situ* oxygen

isotope analysis vary depending on the amount of relief, rims of mineral grans, sample geometry and the inclination of the mount surface, which can result in $\delta^{18}O$ elevated by ~ 4‰. This "topography effect" should also be evaluated in Li isotopic analysis. Moreover, there are charging effects that can occur due to removal of the Au coat that can influence the apparent concentrations measured; the standardization protocol to mitigate against this "charge -compensation effect" is also discussed in this chapter.

The NIST-614 glass standard and M257 zircon standard are chosen to conduct this study as they are homogeneous in Li concentration and isotope ratio (Li et al., 2011b). A 5 μm, 10 μm and 20 μm primary beam were used to focus on the NIST-614 glass standard and M257 zircon standard, in order to study the topography /charge-compensation effect. The aim is to achieve the best possible precision with best possible high spatial resolution in SIMS Li-isotope ratio determinations, by careful optimization of instrument transmission and sensitivity, analytical parameters and analytical procedures.

5.2 SIMS ZIRCON *IN SITU* LI ISOTOPE ANALYSIS

The instrumental conditions for δ^7Li determinations in published studies are summarised below (Table 5-1). All the analyses involved sputtering with a primary beam of O^-, for higher extraction of Li^+ secondary ions from the sample. Most studies have opted to use a single collector and to use primary beam currents of 10 to 30 nA. The sputtered craters are often 20 to 30 μm in diameter. Except for Bell et al. (2009), Mass Resolving Power (MRP) has been maintained at values > 1100, to ensure effective separation of $^6LiH^+$ from $^7Li^+$.

Optimization of instrument Transmission and Sensitivity

In this study, we used the CAMECA IMS-1280HR for the lithium isotopic analysis. It is the latest model, and combines the former IMS-1280 with an ultra-high sensitivity

magnetic sector. We opted to use primary beam currents of 20-30 nA in Kohler mode, with sputtered craters of 20 × 30 μm and 5-10 nA in Gauss mode with sputtered craters ≤ 10 μm.

Table 5-1 Summary of instrumental conditions for SIMS δ^7Li determinations

Study	Instru-ment	Samples	Primary Beam(nA)	Beam size(μm)	MRP*	Time	Cycles
Bell et al (2009)	IMS 3f/6f	Olivine	15–30	30–50	~600	6Li+(10s); 7Li+(1s)	50–200
Vigier et al (2007)	IMS 1270	Foraminifera	~60	20–30	~3000	6Li+(12s); 7Li+(10s)	40–60
Kasemann et al (2005)	IMS 1270	Ref Mat (glass)	10	25	2400	6Li+(5s); 7Li+(2s)	100
Kasemann et al (2005)	IMS 4f	Ref Mat (glass)	20	25	1200	6Li+(5s); 7Li+(2s)	120
Decitre et al (2002)	IMS 3f	Ref Mat (glass & mafic mineral)	10–20	~20	1100	6Li+(6s); 7Li+(3s)	120
Chaussidon & Robert (1998)	IMS 3f	Semarkona / Meteorite / chondrules	(10kV)	~25	~1600	6Li+(8s); 7Li+(4s)	150–200
Ushikubo et al (2008)	IMS 1280 multicoll	Zircon	0.5–3.0	10–15	2200	400 s;	6Li+ (L2); 7Li+ (H2)
Kobayashi et al (2004)	IMS 1270 multicoll	Olivine-hosted melt incl.	15	20	~2000	550 s; ;	6Li+ (L2); 7Li+ (H2)

To maximize transmission for any given setup, Layne (2009) suggested to deploy: i) the largest available Contrast Aperture, ii) as wide an Energy Slit setting as practical (minimum ±25 eV) and, iii) the widest Entrance Slit and Exit Slit settings possible. Therefore, Entrance Slit and Energy Slit have been maintained at widths 300 μm and 60 eV respectively. MRP has been maintained at 1300 (almost 100% transmission efficiency can be reached with 2000 mass resolution).

Because of the large mass difference between ^{6}Li and ^{7}Li (~16.7%), $^{7}Li^{+}$ and $^{6}Li^{+}$ lie just within the maximum dispersion of the multicollector array, so the collectors are far from the optical axis and experience increasing distortion. As a result, in multicollector mode it is difficult to obtain a flat peak, and this puts a limit on precision. Moreover, the multicollector array produced a drift of up to 4 ‰ in the calculated IMF over a 10 hour analytical session (Ushikubo et.al, 2008). Therefore, a single ion-counting electron multiplier (EM) was used as the detection device.

Other procedures were also used to improve signal and reproducibility. A pre-sputter of 30 seconds was applied to ensure removal of surface contamination before data collection. The ^{7}Li signal was then used as reference peak for centering secondary ion beams in order to obtain maximum secondary-ion signal and reduce the analytical error caused by sample topography. Scanning and adjusting the sample offset limited any drift due to sample charging during analysis.

Kobayashi et al. (2004) noted that the sensitivities for IMS 1270 instruments (with no sample offset voltage applied) are 2000 cps/ppm/nA for basaltic glass; Ushikubo et al. (2008) present sensitivities for the IMS 1280 of 2345 cps/ppm/nA for zircon and 1125 cps/ppm/nA for NIST 612. In our study, the Li+ yield is ~5000 cps/ppm/nA for zircon.

Li concentration determinations

The intensity of the primary ion can be used as an internal reference to calculate Li concentration. There is a linear relationship between signal intensity of Li and the intensity of the primary beam. Therefore, Li concentrations can be estimated by comparing the signal intensity of ^{7}Li in the samples to that in a standard (Kasemann et al., 2005; Ushikubo et al., 2008; Layne, 2009):

$$[Li]_{(ppm)} = [^{7}Li^{+}_{yield}]_{measure}/[^{7}Li^{+}_{yield}]_{standard} \times [Li]_{standard}$$

$$[^{7}Li^{+}_{yield}] = {}^{7}Li^{+}_{signal}/I_{primary\ beam\ current}$$

Instrumental Mass Fractionation

Instrumental Mass Fractionation (IMF) is the deviation of the measured isotopic ratio from the true value as the lighter isotope is generally ionized preferentially to the heavier isotope. IMF is the major analytical issue in SIMS analysis. The IMF can be determined by measuring the ratio of interest within a standard and then applying a fractional correction to the unknown sample ratio:

$$= {}^{measure}(^{7}Li/^{6}Li)_{standard}/{}^{true}(^{7}Li/^{6}Li)_{standard}$$

$$IMF\ (‰) = 1000 \times (1 - \quad)$$

The isotopic value of the unknown sample can be calculated as:

$${}^{true}(^{7}Li/^{6}Li)_{sample} = {}^{measure}(^{7}Li/^{6}Li)_{sample}/$$

The IMF is a complex process, and the principles governing secondary-ion extraction are not well understood. A variety of factors, such as sample matrix, instrument type and/or specific settings, can lead to variable transmission of ion beams. As mentioned above, the Matrix Effect during $\delta^{7}Li$ determinations is more substantial than for $\delta^{18}O$. For example, zircon M257 and NIST-614 glass standard have ~40‰ difference in the IMF correction (Li et al., 2011b). Even compositionally zoned minerals might have matrix effects at the intra-mineral level (Bell et al., 2009). Therefore, consideration of matrix effects is especially important for $\delta^{7}Li$ determinations. External fractionation correction can be used only when sample and standard have the same IMF. Matrix-matched reference materials are crucial for accurate Li isotope measurements by SIMS.

5.3 RESULTS

The 5 μm, 10 μm and 20 μm primary beam were applied on the NIST-614 glass

and M257 zircon respectively in order to discuss the topography/charge-compensation effect.

For the 5 μm primary beam, twenty-nine analyses were conducted on the M257 zircon standard, fourteen of which are scattered spots; eight are lined spots (Figure 5.1) to characterize the charge-compensation effect; and seven are at the rim of the M257 zircon in order to characterize the topography effect. The measured δ^7Li values of the scattered spots range from -1.5 to 5.7‰ forming a Gaussian distribution pattern with a mean δ^7Li of 2.1 ± 2.3 ‰ (1σ). Variation of the $^7Li^+$ count rate (the ratio of ^{7}Li intensity to the primary ion current) is around 2% (Table 5-2).

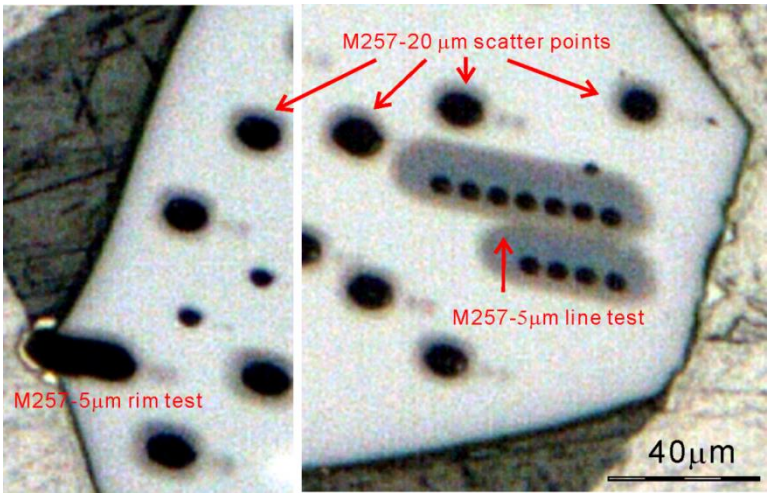


Figure 5.1 Examples of analytical spots of M257 zircon standard.

The measured δ^7Li values of the lined spots range from -2.2 to 4.6‰ with average δ^7Li of 1.5 ± 2.8 ‰ (1σ). While the δ^7Li value seems within error with scattered spots, the $^7Li^+$ count rate for the lined spots (7444 ± 1018) are much lower than that of scattered spots (8638 ± 696), which suggests that the charge accumulation somehow limits the Li+ yield. For the M257-rim spots, both [Li] and δ^7Li value are abnormal. The δ^7Li value is depleted with extremely large standard error (up to 4.9‰) and $^7Li^+$ count rate (3345 ± 1647) is dramatically lower than the M257-scatter.

The same phenomenon is also observed on the NIST-614 glass standard. The

measured δ^7Li values of NIST-614-scatter range from 13.0 to 21.3‰ forming a Gaussian distribution pattern with a mean δ^7Li of 16.3 ± 2.4 ‰(1σ). The $^7Li^+$ count rate is 6321 ± 304 cps. The measured δ^7Li values of NIST-614-line spots have the similar range (12.8 to 20.3‰) as the scattered spots, with same average δ^7Li of 16.3 ± 2.5 ‰ (1σ). The $^7Li^+$ count rate (5555 ± 368) for the lined spots is also lower than that of the scattered spots. The NIST-614-rim spots also have dramatically lower [Li] ($^7Li^+$ count rate = 3510 ±1505) and δ^7Li values than the scattered spots.

The rim and charge effects can be repeated in 10 μm and 20 μm M257 and NIST-614. The data are summarised in Table 5-2.

Table 5-2 Summary of δ^7Li data for NIST-614 glass and M257 zircon

	Average (1SD)	Standard error	Difference	Average count rate
5 μm Primary Beam				
M257-scatter (14)	2.1 ±2.3	~1.4 - 1.9‰	7.1‰	8638 ±696
M257-line (7)	1.5 ±2.8	~1.7 - 2.2‰	6.8‰	7444 ±1018
M257-rim (8)	-1.5 ±8.7	~2.3 - 4.9‰	25.6‰	3345 ±1647
NIST-614-scatter	16.3 ±2.4	~1.8 - 2.4‰	8.3‰	6321 ±304
NIST-614-line (7)	16.3 ±2.5	~2.0 - 3.2‰	7.5‰	5555 ±368
NIST-614-rim (3)	7.3 ±20.7	> 3.1‰	29.3‰	3510 ±1505
10 μm Primary Beam				
M257-scatter (14)	2.1 ±1.5	~1.0 - 1.4‰	5.7‰	8017 ±376
M257-line (7)	1.9 ±1.4	~1.0 – 1.5‰	3.7‰	6873 ±134
M257-rim (6)	-5.9 ±4.5	~0.7 – 1.0‰	11.3‰	7262 ±1472
20 μm Primary Beam				
M257-scatter (15)	2.1 ±1.3	~0.5-0.9‰	3.4‰	6843 ±545
M257-rim (7)	2.1 ±2.1	~0.5-0.6‰	6.1‰	5338 ±132
NIST-614-scatte (6)	10.6 ±1.6	~0.5-0.6‰	3.9‰	3610 ±37

*scatter/line/rim refers to figure 5-1

For the experiments with a 10 μm primary beam, twenty-seven analyses were

conducted on the M257 zircon standard; fourteen are scattered spots, seven are lined spots and six are at the rim. The measured δ^7Li values of scattered spots range from 0 to 6.7‰ forming a Gaussian distribution pattern with a mean δ^7Li of 2.1 ± 1.5 ‰ (1σ).Variation of the $^7Li^+$ count rate is around 2%. The measured δ^7Li values of lined spots range from 0.1 to 3.7 ‰ with average δ^7Li of 1.9 ± 1.4 ‰ (1σ). The average $^7Li^+$ count rate is 6873 ± 134 cps. For the M257-rim spots, δ^7Li has a negative mean value of -5.9 ± 4.5 and the average $^7Li^+$ count rate (7262 ± 1472) is lower than that of the scattered spots (8017 ± 376).

For the experiments with a 20 μm primary beam, the measured δ^7Li values of M257-scatter range from -0.1 to 6.0‰, forming a Gaussian distribution pattern with a mean δ^7Li of 2.1± 1.3 ‰ (1σ). The $^7Li^+$ count rate is 6843 ± 545. NIST-614-rim have average δ^7Li of 10.6 ± 1.6and $^7Li^+$ count rate of 3610 ± 37, similar with NIST-614-rim 5μm analysis results. Compared with 5μm data, δ^7Li values obtained with the 10 μm and 20 μm spots have much better precision.

5.4 DISCUSSION AND CONCLUDING REMARKS

5.4.1 Topography effect and Charge effect

The results show that when the analytical spots are too close to each other, their count rates decrease. The most probable explaination is that the yield of the secondary Li^+ ion is supressed by the charge accumulation. No significant isotopic fractionation is observed during this process. The charge effect lowers the [Li] to a certain extent while the δ^7Li value is not affected. The topography effect has great impact on the [Li] and δ^7Li and both of the [Li] and δ^7Li reduced to varying degrees. The analytical errors also increased significantly at the rim. Therefore, special attention is required when dealing with the data from the rim in a profile analysis. The count rate and error of the rim data should be compared with those from the scattered spots, in order to avoid those affected

by the rim and charge accumulation.

5.4.2 Refinements in techniques

While the standard bracketing method can be applied to improve the data accuracy and correction to IMF, a number of other factors may also affect data precision. In general, there is a trade-off between precision, which may be limited by the number of ions counted, spatial resolution and analytical time. The formula for the theoretical counting statistics error on $^{7}Li/^{6}Li$ can be described as follows:

$$\sigma = \sqrt{\frac{1}{{}^{6}Li_{total\ ion\ counts}} + \frac{1}{{}^{7}Li_{total\ ion\ counts}}}$$

The total ion count for ^{7}Li (or ^{6}Li) is:

$$^{7(6)}Li_{\text{ Total ion counts}} = {}^{7(6)}Li_{concentration} \times {}^{7(6)}Li_{yield} \times I_{\text{primary beam current}} \times t_{\text{ integration time}}$$

According to the formula for counting-statistics errors, the higher the ion signal and the longer the integration time, the lower counting-statistics error will be.

Spatial resolution *vs* Precision

Spot size can varied for ion microprobe analysis; the beam size can be focused to a diameter of 3 μm on the IMS1280 instrument (Liu et al., 2011). However, the primary beam current and the ion yield vary with spot size, and the beam is generally defocused to a larger diameter in order to generate more secondary ions for analysis. The Cameca IMS 1280HR SIMS routinely undertakes *in situ* isotopic microanalysis at relatively high precision (~1‰, 1) and high spatial resolution (~20 × 30 × 2 μm^3). Generally, the higher spatial resolution is, the lower the analytical precision. We have compared data from 20 × 30 μm sputtered craters in Kohler mode with ≤ 10 μm sputtered craters in Gauss mode. The typical values for the 2SD reproducibility of $\delta^{7}Li$ for multiple analyses of a standard material are ± 1.5‰ at 20 μm, ± 2‰ at 10 μm, and ± 5‰ at < 5 μm. As Li shows a large range in isotopic composition in natural system, ~2‰

analytical precision is sufficient to meet the needs of most Li-isotope studies. Therefore, considering charge effect and highly variable δ^7Li at the zircon rim, a 10 μm spot size is preferentially used in the following studies.

Precision vs Intergration time/cycles

From the formula above, theoretically, the statistical error should decrease if we increase the analytical time. However, the stability of the primary beam, beam density and depth fractionation will offset the benefits from longer integration time. The primary beam current will be steadier over a short period. Moreover, high beam density might cause depth fractionation if the analytical time is too long. Figure 5.2 demonstrates a single analysis spot of 80 cycles of M257 zircon standard. For the first 40 cycles, the ^{7}Li/^{6}Li have a more steady value; after the 40 cycles, the ^{7}Li/^{6}Li decrease because of the depth fraction. Table 5.3 summaries the data with 40 cycles and 80 cycles. The data with 40 cycles usually have precision equal to or better than those with 80 cycles.

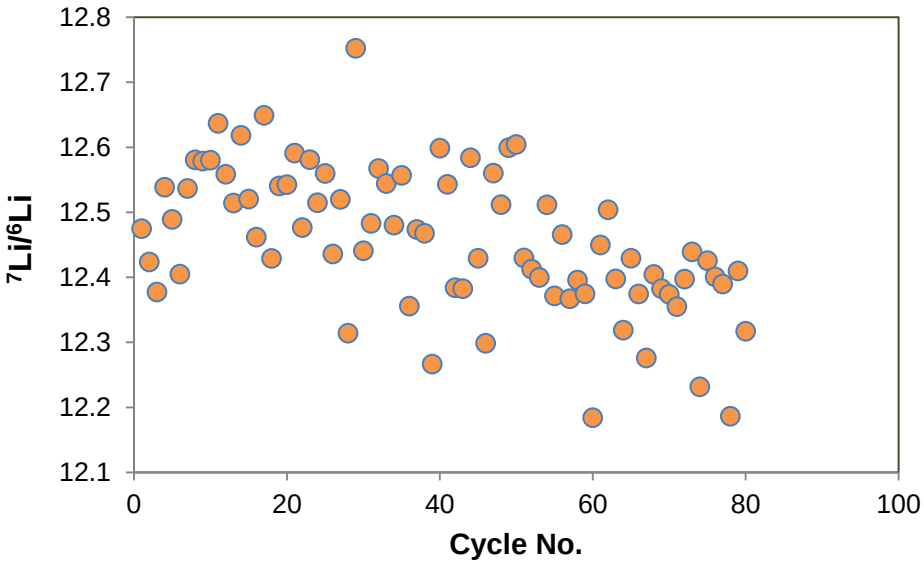


Figure 5.2 A single spot 80-cycle analysis of zircon standard M257

Accuracy and precision can be improved by carefully balancing the beam size and

analysis time. In the following study, ≤ 10 μm primary beam at 5-10 nA with 40 cycle×18 s/cycle integration time are applied in Gaussian mode to facilitate the analysis of a complex zircon rim.

Table 5-3 Summary of the data with 40 cycles and 80 cycles

	Mean	SD.	SE.	Poisson	Reject	Integrated
M257-10 μm-40 cycle						
$^{7}Li/^{6}Li$	12.5	0.0	0.10	0.09	1.0	12.549
^{7}Li	795	934	1.86	0.04	0.0	79530
M257-10 μm-80 cycle						
$^{7}Li/^{6}Li$	12.5	0.0	0.08	0.06	4.0	12.488
^{7}Li	935	116	1.42	0.03	3.0	92536

Compared to other elements, Li has an intrinsically high ion yield of Li^{+} under O^{-} sputtering. The $^{7}Li^{+}$ yield of NIST-614 synthetic glass ($[^{7}Li] \approx 1.5$ ppm, $[^{6}Li] \approx 0.1$ ppm) can achieve 2000 cps/nA/ppm under a ~20 nA O^{-} beam bombardment. Therefore, for the total integration time of 600 s, the theoretical counting- statistics error of Li isotopes on NIST-614 glass is $\sigma \approx 0.6‰$. The best reproducibility reported to date was ± 0.5 ‰ in synthetic basalt glass using a Cameca IMS 1270 in mono-collection mode (Kasemann et al. 2005).

The same procedure can be used to calculate the theoretical counting-statistics error of zircon standard M257 ([Li] = 0.86 ppm, Li et al., 2011b). Although [Li] is lower in M257 than in NIST-614, the sensitivities for IMS 1280 instruments can achieve 5000 cps/ppm/nA for zircon (Li et al., 2011b, this study) which lead to almost equal precision to NIST-614 glass. For the 10 μm beam size, the $^{7}Li/^{6}Li$ ratio of M257 zircon standard can be analysed with an internal precision of 2.0‰ (2SE), and an external precision around 2.5‰ (2SD).

CHAPTER 6. LITHIUM ISOTOPES BEHAVIOR IN ZIRCON

(This chapter includes results submit to Scientific Reports by **Gao, Y.-Y., et al. (2015). " Extreme lithium isotopic fractionation in three zircon standards (Plešovice, Qinghu and Temora)".** All data were produced by myself under supervision.)

6.1 INTRODUCTION

Lithium isotopes are a potentially powerful tracer in a wide range of geochemical processes because of their significant relative mass difference (*ca.* 16.7%), lithium's broad elemental dispersion and moderately incompatibility (Tang et al., 2007; Tomascak et al., 2008; Ushikubo et al., 2008; Teng et al., 2009; Teng et al., 2010). It is highly soluble and very sensitive to fluid/melt–mineral interactions, and can display up to 80‰ isotopic fractionation in natural systems (Rudnick et al. 2004; Tomascak, 2004). However, the factors that make Li geochemically useful also make the quantification and interpretation of its isotopic composition extraordinarily challenging (Tomascak 2004). It is still controversial to what extent Li isotopic signatures and abundances will be preserved in whole-rock samples and minerals, as there are major differences between the whole-rock and *in situ* results (see chapter 1). While the spread in δ^7Li values is similar in granites world-wide, with whole-rock δ^7Li ranging from –5 to +10‰ (Teng et al., 2009), the zircons from Jack Hills show a wide range of δ^7Li values, over 30‰ (Ushikubo et al., 2008). This contrast in Li isotopic variations between whole-rock samples and zircons has aroused great interest. Cherniak and Watson (2010) conducted experiments on Li diffusion in zircon at different temperatures and with different fluid compositions. Their results indicated that Li diffusion is slower in zircon

than in other major rock-forming minerals, but it still diffuses at a considerable rate, so that zircons will be only '*moderately retentive of Li signatures at mid-crustal metamorphic temperatures*.'

Bouvier et al. (2011) conducted the first systematic Li isotopes and trace elements analysis in igneous zircons in order to characterize Li character from typical Archean continental crust. They suggest that Li substitutes in interstitial sites in zircon, and charge compensates for trivalent cations. This results in a relatively slow diffusion rate of Li. Moreover, they estimated partition coefficient between zircon and evolved melt ($D_{Li\ zircon/melt}$ of ~0.3). However, no data exist for direct comparison between whole-rock and zircon lithium-isotope compositions to calculate the partition coefficient and to understand the relations between their Li isotopes.

This chapter presents new results for Li isotopes and concentrations in three well-studied zircon standards (Plešovice, Qinghu and Temora) commonly used for U-Pb and Hf-O isotopic analysis. We have analysed both whole-rock and zircon δ^7Li and Li abundance ([Li]), while also imaging the distribution of seven trace elements (Li, P, Ti, Yb, Y, U, and Th) in well-studied zircon standards commonly used for U-Pb and Hf-O isotopic analysis. The aim of this study is to shed light on Li behavior in zircons, to find out whether the lithium-isotope variation reflects differences in source values or is caused by diffusion, or both. This is fundamental to evaluating the feasibility of using Li-isotope analysis of *in situ* zircon as a geochemical tracer to identify the source regions of magmas.

6.2 SAMPLE INFORMATION

Three standard zircons (Plešovice, Qinghu and Temora) have been chosen for this study, as they (i) are homogeneous and concordant in terms of radiogenic Pb/U ratios, (ii) are homogeneous in Hf-O isotopic composition, (iii) have crystalline (nonmetamict)

structures, and (iv) occur as mm–cm sized grains. The isotopic characteristics of the zircons are summarised in Table 6-1.

6.2.1 Plešovice

Plešovice zircons were extracted from a high-temperature potassic granulite in the southern Bohemian Massif of the Czech Republic. The content of zircon in the granulite is up to 0.6 wt.%, and it is variable on the scale of tens of centimeters (Vrána, 1989; Janoušek et al., 2007). The Plešovice zircon is homogeneous in terms of U-Pb age and Hf isotopes, thus, widely used as a standard for microbeam isotopic analyses (Sláma et al. 2008). Zircon grains are prismatic, pale pink to brown euhedral crystals and have been tested for Li-isotope homogeneity in a previous study, which turned out to show heterogeneous Li-isotope compositions (~10‰ variation in δ^7Li) (Li et al., 2011b). Two grains (2094 μm and 1770 μm, respectively) were selected and mounted to acquire detailed diffusion profiles.

6.2.2 Qinghu

The Qinghu monzonite is located in the southwestern part of the Nanling Range in south China (Li et al., 2009a). The rock types of the pluton are coarse-grained hornblende monzonite, medium-grained quartz-bearing hornblende monzonite and fine-grained quartz monzonite (Li et al., 2013) Zircons from the Qinghu monzonite are euhedral, range from 100 to 500 μm in length, and have length/width ratios mostly between 1:2 and 1:4. Most zircons show a clear euhedral concentric zoning under cathodoluminscence (CL). Previous studies indicate that Qinghu zircon is quite homogeneous and can be used as a working reference standard for SIMS U-Pb and Hf-O isotopic analysis (Li et al., 2013).

Table 6-1 Information on the studied standards

	M257	Reference	Plešovice	Reference	Qinghu	Reference	Temora	Reference
Rock type	gem	Nasdala, 2007	granulite	Sláma, 2008	syenite	Li, 2013	diorite	Black, 2003
Zircon Radius	megacryst	This study	megacryst	This study	~400 μm	This study	~400 μm	This study
Age (Ma)	561.3 ± 0.3	Nasdala, 2008	337.1 ± 0.4	Sláma, 2008	159.5 ± 0.2	Li, 2013	416.8	Black, 2003
$^{176}Hf/^{177}Hf$	0.281544 ± 18	Hu, 2012	0.282482 ± 13	Sláma, 2008	0.283002 ± 04	Li, 2013	0.282693 ± 14	Sláma, 2008
$\delta^{18}O$ (‰)	13.9 ± 0.1	Nasdala, 2008	8.2 ± 0.2	IGGCAS lab	5.4 ± 0.2	Li, 2013	8.1	Black, 2004
whole-rock[Li]	-	-	53	This study	23	This study	12	This study
whole-rock δ^7Li (‰)*	-	-	-0.1	-	1.45	-	1.1	-
Zircon [Li] (ppm)	~ 0.86	Li, 2011	0.5 - 13.8	This study	0.1 - 25.8	This study	0.1 - 0.9	This study
Zircon δ^7Li (‰)*	~ +2.1	Li, 2011	-21.5 - +8.0	This study	-37.6 - +1.7	This study	-13.6 - +13.1	This study
modeled [Li] (ppm)	-	Li, 2011	32	This study	21	This study	13	This study
modeled δ^7Li (‰)*	-	Li, 2011	1.5	This study	-4	This study	9	This study

*δ^7Li (‰) = [($^7Li/^6Li$)/12.039)-1]×1000.

6.2.3 Temora

Temora zircons are extracted from the Middledale Gabbroic Diorite of the Tasman Oragenic Belt, Australia. It is medium– to coarse–grained, relatively unaltered and composed dominantly of labradoritic plagioclase and brown pargasitic hornblende (partially replaced by chlorite) (Kemp et al., 2005). Some augite and hypersthene are also present; the former is partially replaced by cummingtonite, and the latter by actinolite. Opaque minerals (hematite, ilmenite and lesser magnetite) are relatively common and give the intrusion a strong positive magnetic signature (Black et al., 2003). Zircons are mostly euhedral, and the range of grain size is 100–550 microns. It is clear under both reflected and transmitted light and show sector zoning under cathodoluminescence image. Temora zircons are widely used as U-Pb age and Hf-O isotope microanalyses (Black et al. 2004; Woodhead and Hergt 2005).

6.3 RESULTS

Zircons with euhedral crystal shapes were picked and analysed for both Li isotopic composition and element mapping. The abundance and isotopic composition of Li were measured along 17 traverses across eleven zircon grains (2 Plešovice, 8 Qinghu and 1 Temora). Nine ion-imaging analyses were used to partially map the zircon grains. Typical analytical (~10 μm) uncertainty of δ^7Li is ~1.5‰ (2SD). Traverses of 5 to 15 analytical spots at 10 to 200 μm intervals were performed across selected grains in order to investigate the degree of homogeneity. A smaller primary ion beam (~5 μm) was used to conduct a more thorough study of the rim phenomena, with analytical uncertainty of ~3.0‰ (1SD). Detailed information for all the measurements is listed in appendix table xiii. Generally, all the zircon grains have a 5–20 μm wide rim with extremely high [Li], about 5 to 10 times higher than the core. There is extreme isotopic fractionation (~20‰) at the zircon rims on a small scale (~50 μm).

Table 6-2 SIMS Li isotopes summary

		δ^7Li (‰)					
Sample name	**Spot size**	**Min**	**Max**	**Fractionation**	**Min**	**Max**	**Average**
PlesoviceR	**(20μm)**	-10.7	3.7	14.8	0.5	2.3	0.4
	(10μm	-8.9	3.3	12.2	0.8	8.7	--
	(5μm)	-14.1	3.4	17.6	0.5	9.5	--
PlesoviceL	**(20μm)**	-4	3.3	7.3	0.7	1.9	0.3
	(10μm)	-14.3	3.7	18.0	0.7	14.4	--
	(5μm)	-13.7	-1	12.7	0.5	13.3	--
Plesovice-inter grains		-14.3	3.7	18.0	0.5	14.4	--
Qinghu-1	**(10&20μm)**	-18.3	1.4	19.7	0.31	1.97	--
Qinghu-6	**(10&20μm)**	-8.1	0.2	8.3	0.64	9.26	--
Qinghu-9	**(10μm)**	-15.2	-1.4	13.8	1.05	14.38	--
Qinghu-a	**(10μm)**	-21.4	0.3	21.6	0.64	11.2	--
Qinghu-b	**(10μm)**	-7.9	-0.7	7.2	0.69	10.27	--
Qinghu-c	**(10μm)**	-10.1	0.7	10.8	0.88	9.52	--
Qinghu-d	**(10μm)**	-22.8	0.1	22.9	0.6	5.13	--
Qinghu-e	**(10μm)**	-14.4	-0.3	14.1	1.06	6.95	--
Qinghu-inter grains		-22.8	1.4	24.2	0.31	14.38	--
Temora	**(20μm)**	1.1	13.1	12	0.02	0.29	
	(10μm)	-4.7	16.1	20.8	0.03	6.84	

Both positive and negative correlations between [Li] and δ^7Li were encountered. Variability in δ^7Li, related to cracks with higher Li content, was also observed and these spots were eliminated when defining the diffusion model.

6.3.1 Plešovice

Four whole-rock samples of Plešovice have been analysed. The [Li] of Plešovice are ~53 ppm. The δ^7Li values range from -1.6 to -0.6 ‰ (± 0.5, 2SD). The whole-rock data are listed in appendix table 6-1. Two Plešovice megacrysts (Plešovice L & R) have

been studied in detail. ~20 μm, ~10 μm and ~5 μm beam spots were used to traverse each grain. [Li] profiles across the two megacrysts are nearly flat at the center, but dramatically increased at the rim (Figure 6-1, 6-2). The overall [Li] ranges from 0.5～14.4 ppm. The δ^7Li values range from -14.3–+4.1‰. Fractionation of Li isotopes is up to 18‰ in a single grain. Both Plešovice megacrysts show a plateau of constant δ^7Li in their cores, but striking heterogeneity at the rims.

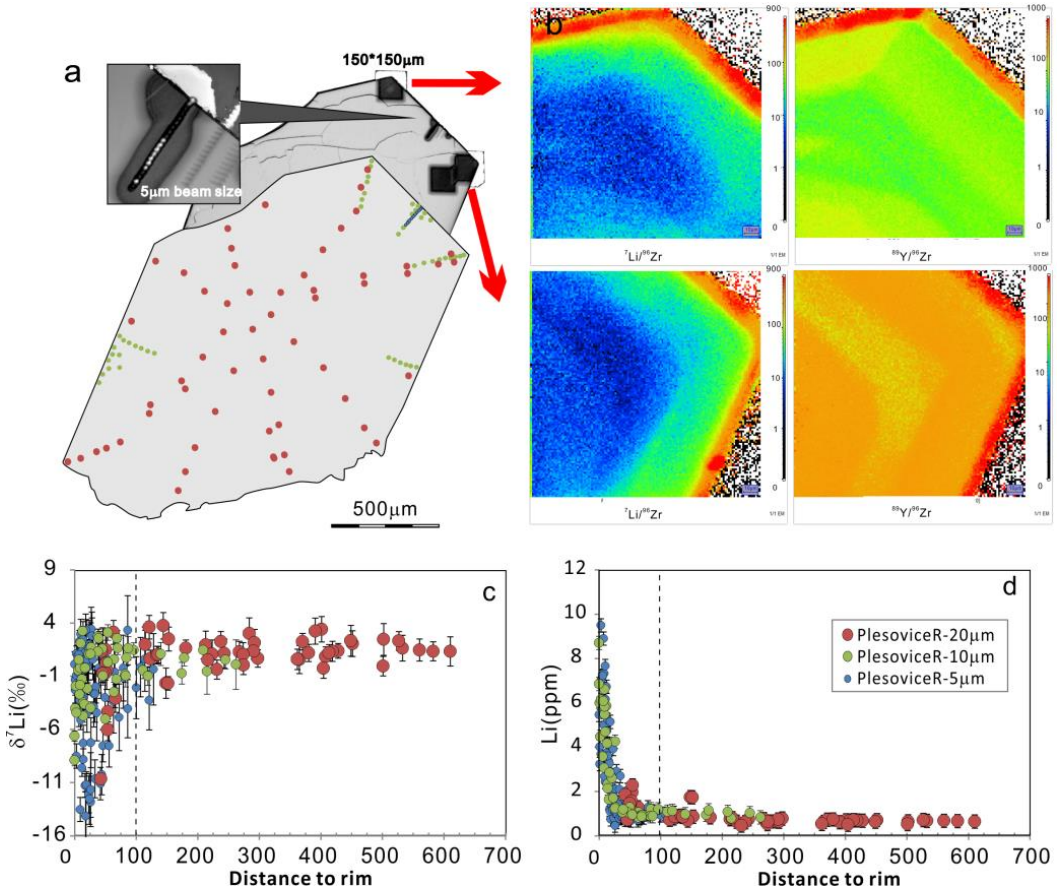


Figure 6.1 a) Trace outlines of Plešovice-R to show the position of the Li isotopic and [Li] measurements by SIMS; b) The ion image of the variation of Li and Y content (bright colors = higher content); c) δ^7Li vs Relative distance to the rim; d) [Li] vs Relative distance to the rim. 2 SE error bars for the isotope ratio measurements are shown. Typical analytical uncertainty of δ^7Li is ~2‰ for the 20 μm pits, ~2.5 ‰ for the 10 μm pits and ~5‰ for 5 μm pits (2 SD). Distance to rim is calculated by the X-Y position of the analytical spot to the nearest rim.

For the PlešoviceR zircon, the [Li] ranges from 0.5 – 9.5 ppm and δ^7Li values range from -14.1 – +4.1‰. The δ^7Li values in the rim of PlešoviceR show very complex spatial variation; therefore, ~10 μm and the ~5 μm beam spot were used to map the changes in Li isotopes over small areas. The ion image is a visual display of [Li] and [Y] changes at the rim. Both [Li] and δ^7Li become stable with distance to rim >100 μm (Figure 6.1).

For the PlešoviceL zircon, [Li] ranges from 0.5 – 14.4 ppm and δ^7Li from -14.3 – +3.7‰. The ion image displays [Li] and [Y] at a broken rim. Profile AA' along the zircon demonstrates the Li isotope change across the entire zircon. [Li] shows a rimward increase, while δ^7Li is negatively correlated with [Li] and characterized by a typical diffusion profile. Both [Li] and δ^7Li become stable with distance from rim of > 100 μm (Figure 6.2). Compared to PlešoviceR, PlešoviceL has a better shape and fewer cracks, and δ^7Li at the rim of PlešoviceL is less complex than in PlešoviceR.

6.3.2 Qinghu

The whole–rock [Li] of the Qinghu monzonite is ~23ppm; δ^7Li values range from 0.9–+2.5‰ (± 0.5, 2SD). Two zircon grains have been traversed using both ~20 μm and ~10 μm beams. [Li] ranges from 0.6 to 14.4 ppm and δ^7Li values range from -22.8 to +1.4‰ (Table 6-2). Compared to the Plešovice samples, Qinghu zircons have higher [Li] in the cores, mostly around 1–2 ppm. Qinghu zircons also have extremely high [Li] in their rims, usually 10x higher than in the core. The maximum [Li] at the rim is approximately equal to the whole-rock [Li].

For the Qinghu_1 zircon, the [Li] ranges from 0.31 – 1.97 ppm and δ^7Li from -18.3 –+1.4‰. The ion image indicates that [Li] and [Y] are to some extent correlated to each other. It also shows higher [Li] near cracks while [Y] remains unaffected. The [Li] of Qinghu_1 shows a rimward increase. The δ^7Li values of Qinghu_1 obtained

using the ~20 μm and ~10 μm beam spot are negatively correlated with [Li] and define a typical diffusion profile (Figure 6.3).

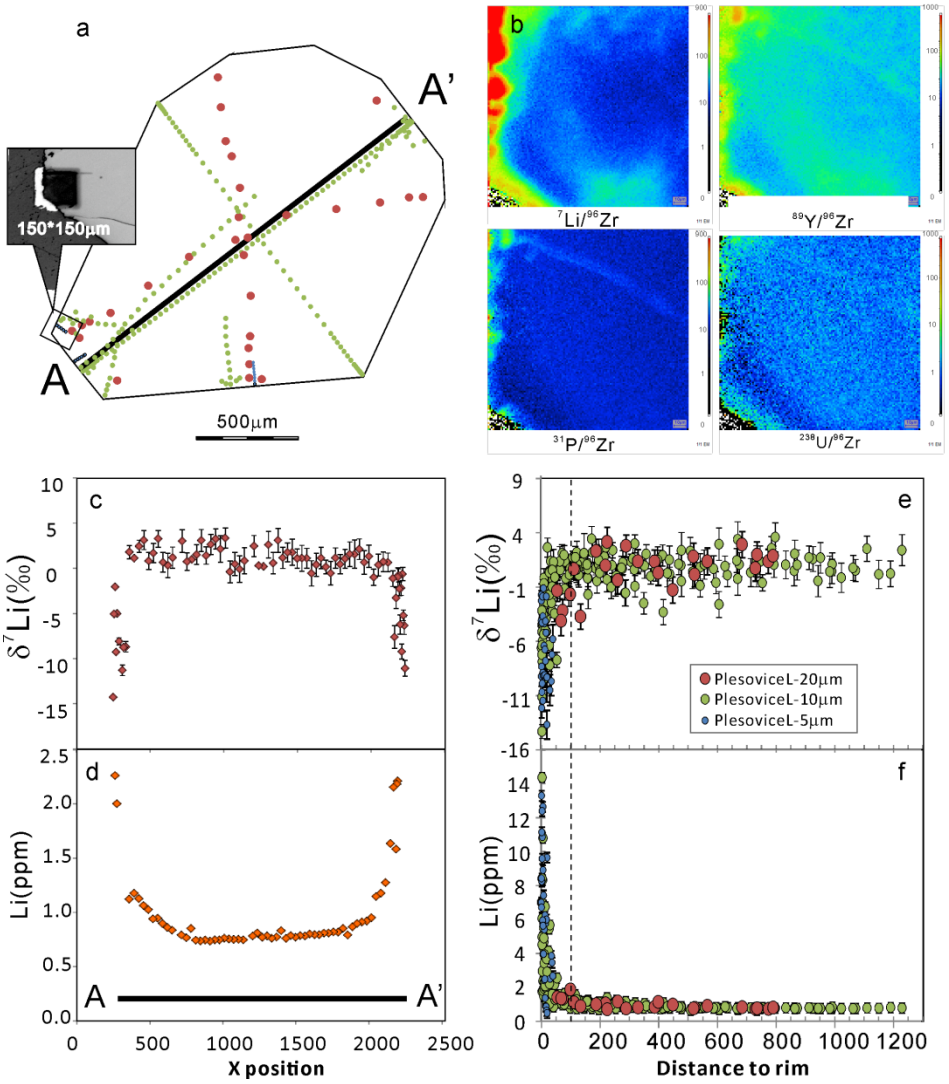


Figure 6.2 a) Trace outlines of Plešovice-L to show the position of the Li isotopic and [Li] measurements; b) Ion image of the variation of Li, Y, P and U concent (bright colors = higher concentration); c) δ^{7}Li vs X position of AA' profile; d) [Li] vs X position of AA' profile; e) δ^{7}Li vs Relative distance to the rim; f) [Li] vs Relative distance to the rim.

Another seven Qinghu zircons were traversed using a ~10 μm beam spot. In all of these grains, [Li] shows a rimward increase and become stables at distances from rim of > 50 μm (Figure 6.4). The δ^{7}Li profiles are more complicated, and show larger fractionation than the Plešovice zircons. Generally, the δ^{7}Li values are higher and more homogeneous in the core than at the rim.

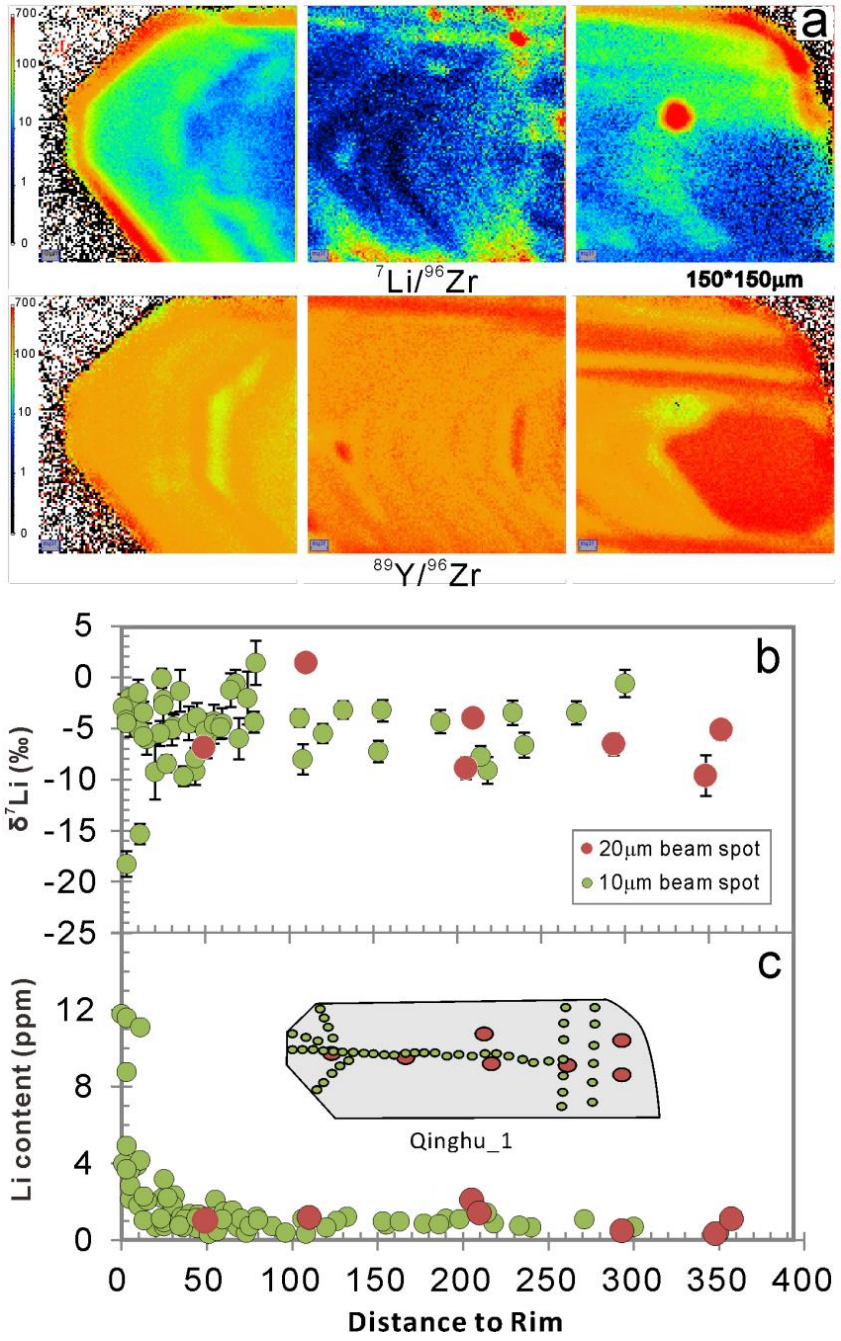


Figure 6.3 a) Ion image of the variation of Li and Y concent (bright colors = higher concentration); b) δ^{7}Li vs Relative distance to the rim; c) [Li] vs Relative distance to the rim.

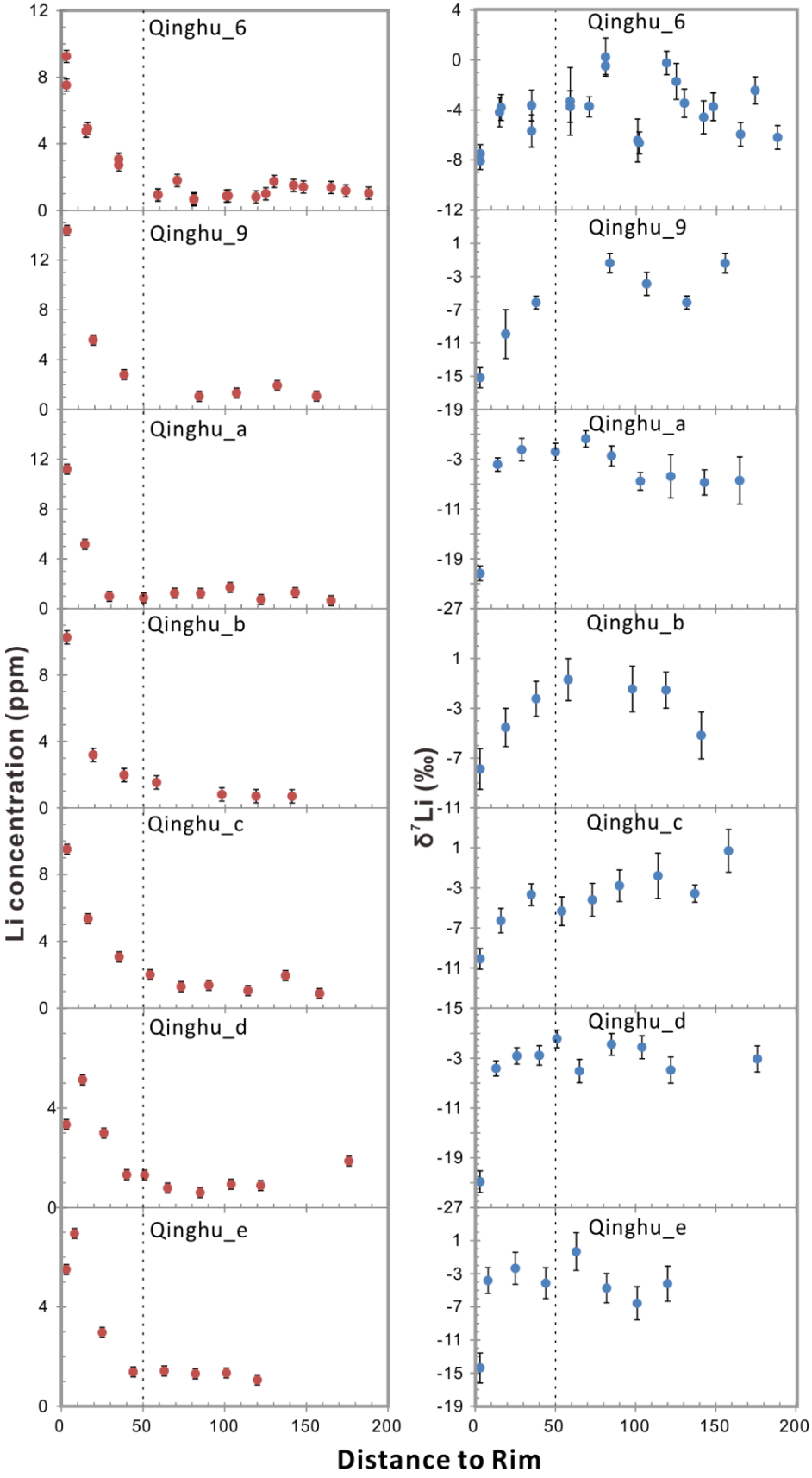


Figure 6.4 Plots of δ^7Li and [Li] vs Relative distance to the rim of seven Qinghu zircons.

6.3.3 Temora

The whole rock [Li] of Temora is ~12 ppm, and δ^7Li values range from 0.7–1.5‰. The Temora zircon grains have been traversed using 20 μm and 10 μm beam sizes. All the data are shown in Table 6-3. Li, P, Y, Yb ion images are shown in Figure 6.3b. The ion image demonstrates a very high [Li] rim on Temora zircons, which can only covered by the ~10 μm beam. Y and Yb positively correlated to [Li] while P is quite homogeneous from the rim to core.

Table 6-3 Temora zircon data

Name	IP	X Position	Y Position	distance to rim	δ7Li	1σ	ppm	1σ	note
Tem2-20μm _1		-3069	-283	153	1.07	0.71	0.29	0.000	
Tem2-20μm_2		-3134	-268	89	6.1	1.6	0.06	0.000	
Tem2-20μm_3		-3222	-280	0	13.06	2.82	0.02	0.000	low [Li]
Tem2-20μm_4		-3312	-306	-94	7.45	1.53	0.06	0.001	
Tem2-20μm_5		-3365	-267	-144	5.26	1.22	0.10	0.001	
Temora_10μm-01	8.27	-3439	6	193	-4.67	1.97	6.84	0.203	
Temora_10μm-02	8.45	-3418	3	172	4.75	2.89	0.15	0.001	
Temora_10μm-03	8.37	-3397	0	151	0.98	2.77	0.10	0.001	
Temora_10μm-04	8.30	-3376	-3	130	8.34	3.1	0.09	0.001	
Temora_10μm-05	8.20	-3355	-6	109	5.07	3.49	0.07	0.001	
Temora_10μm-06	7.91	-3334	-9	87	10.87	2.83	0.10	0.002	
Temora_10μm-07	7.98	-3313	-12	66	3.57	3.41	0.09	0.001	
Temora_10μm-08	7.46	-3291	-14	44	10.58	3.05	0.08	0.001	
Temora_10μm-09	7.56	-3269	-16	22	-	-	0.03	0.000	low [Li]
Temora_10μm-10	7.18	-3247	-18	0	5.88	5.74	0.03	0.000	low [Li]
Temora_10μm-11	7.02	-3225	-20	-22	-	-	0.03	0.000	low [Li]
Temora_10μm-12	7.08	-3203	-22	-44	-	-	0.05	0.000	low [Li]
Temora_10μm-13	7.09	-3181	-24	-66	16.07	3.09	0.10	0.002	

Temora_10μm-14	6.96	-3159	-26	-88	6.64	4.01	0.06	0.001
Temora_10μm-15	7.13	-3137	-28	-110	3.05	4.35	0.07	0.001
Temora_10μm-16	7.04	-3115	-30	-133	6.72	4.51	0.06	0.001
Temora_10μm-17	6.62	-3093	-32	-155	11.68	3.64	0.10	0.001
Temora_10μm-18	6.09	-3071	-34	-177	-0.23	1.24	1.60	0.013
Temora_10μm-19	6.23	-3049	-36	-199	-1.8	0.62	5.01	0.026

Temora zircons have quite low Li contents, which leads to relatively larger analytical errors. For all the twenty-four analytical spots, [Li] ranges from 0.02 – 6.84 ppm and δ^7Li values range from -4.7 – +16.1‰. There is a typical diffusion profile with gradually decreasing [Li] and increasing δ^7Li from rim to core (Figure 6.5 c, d). Except for the spots with very low [Li], the δ^7Li is relatively homogeneous (with a weighted average of 7.0 ± 1.8 ‰) in the centers of grains within 150 μm.

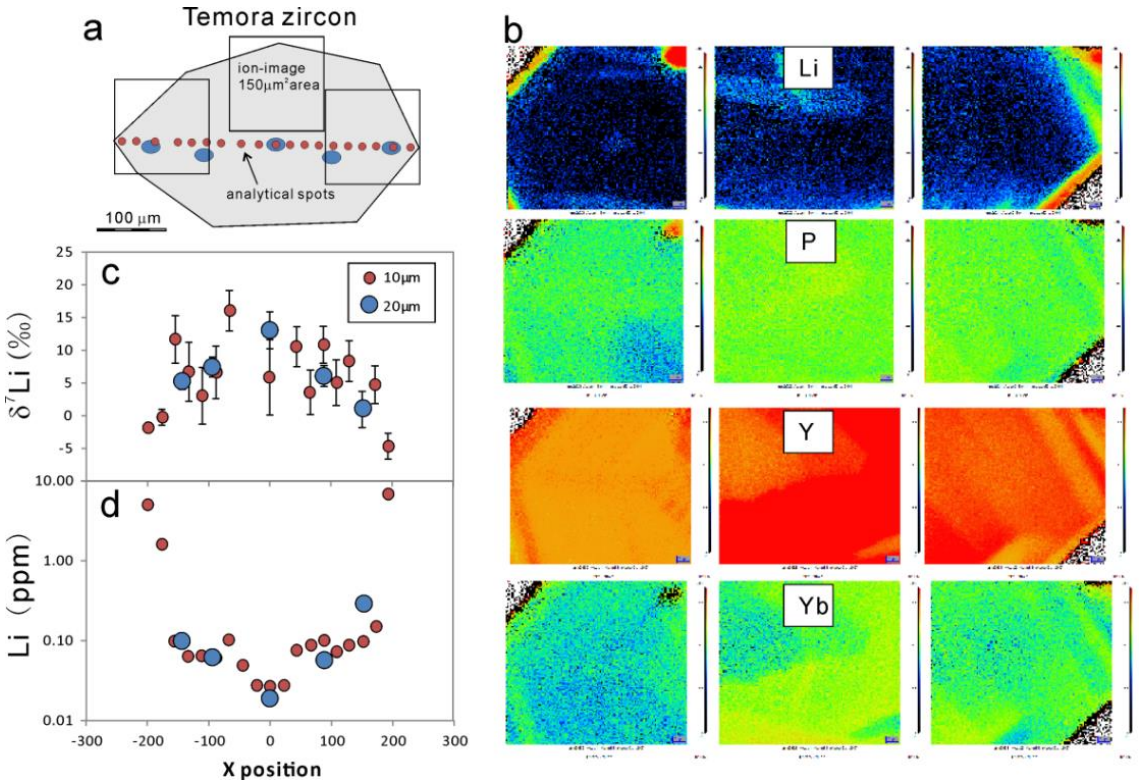


Figure 6.5 a) Analytical spots on Temora zircon; b) ion image of Li, P, Y, Yb; c) δ^7Li profile through zircon; d) [Li] profile through zircon.

6.4 DISCUSSION

6.4.1 Intra-granular heterogeneity in [Li] and δ^7Li

The question of whether Li-isotope variations in zircon reflect differences in sources, metasomatism or diffusion-driven isotopic fractionation requires a thorough discussion. To date, only a few studies on the isotopic composition of Li in zircons have been carried out (Ushikubo et al., 2008; Cherniak and Watson, 2010; Bouvier et al., 2011; Li et al., 2011b). The results of these studies are by no means conclusive with respect to either diffusion fractionation or zircon-melt isotopic fractionation. Our results show that Li-isotope heterogeneity occurs on both intra- and inter-granular levels. There is up to ~20‰ isotopic fractionation within ~50 microns of the rim of a single grain (Figure 6.4). Extreme Li-isotope fractionation (~35‰, ~48‰) also has been observed in olivine (Su et al., 2012; Tang et al., 2014) and orthopyroxene (~40‰) (Jeffcoate et al., 2007). One outcome from these studies is that such extreme fractionation cannot be produced by equilibrium fractionation. The processes responsible may include metasomatism of mantle rocks by silicate and carbonatite melts and hydrous fluids (Su et al., 2012), preservation or modification of fluid/melt fractionation derived from recycled oceanic crust (Tang et al., 2014), diffusion-driven fractionation and emplacement-related alteration coupled with isotopic exchange (Jeffcoate et al., 2007).

Our results show that the largest fractionations (～20‰) are found at the zircon grain boundaries. The most negative abnormal values equate with the lowest δ^7Li value in nature (Tomascak, 2004), which indicates that diffusion-driven fractionation might be a key process in producing such negative values. To confirm that the data at the rims are robust, we examined the Li isotopes in the epoxy and on the rim of the sloped surface of M257 and the NIST standard in order to check the following possibilities: 1). contamination by the epoxy (due to large size of the secondary beam relative to the rim

width) that imparts a high δ^7Li on zircons with low [Li]; 2). analytical artifacts (topography effect and charge effect) from sample geometry and topography (See discussion in chapter 5).

The measured [Li] and δ^7Li of the epoxy are 11.5 ppm and 202 ‰, respectively. It is important to note that the IMF is corrected against M257 zircon standard, which does not reflect the true value of the epoxy. The analysis of Li isotopes in the epoxy is simply to prove that the abnormal data are not caused by accidental sampling of the epoxy. The [Li] in the epoxy is lower than that in the zircon rim, while δ^7Li is much heavier than that in the zircon (< 10‰). This implies that one can easily recognize the effects of even a small volume of epoxy incorporated in the analysis.

The charge effect was carefully avoided in the analysis. The sample mount has been taken out and re-coated if the analytical spots were too close to each other. Data have been screened by ion yield and analytical errors in order to avoid topography effect (See discussion in chapter 5). Moreover, the high-[Li] zones at the rim are not observed in the M257 zircon and are not present where the zircon grain is bounded by a broken surface (Figure 6.2a); it is only seen at growth surfaces (crystal faces). Since both types of grain boundary stand up from the epoxy mount, the high-[Li] zones cannot be ascribed to a topographic effect; therefore, they must represent processes affecting the original boundary between the zircon crystal and its host rock. Li is also concentrated in fissures and interstices of the zircon grains. Considering the high Li abundance in the corresponding whole rock, multiple sources are probable, including contamination by Li-rich mineral phases on cracks and surfaces, and exchange with a high-δ^7Li fluid phase. Therefore, the high [Li] and extreme δ^7Li at the rim is most likely driven by diffusion, caused by a dramatic gradient in [Li].

6.4.2 Modeling of diffusion-driven fractionation of Li isotopes

Many studies have provided examples of large isotopic fractionations developed during the chemical diffusion of lithium under both low- and high-temperature conditions (Richter et al., 2003; Rudnick et al., 2004; Lundstrom et al., 2005; Richter et al., 2009). The general phenomenon of diffusive fractionation of Li isotopes in solid phases is poorly understood at present. Diffusion models for Li-isotope fractionation have been constructed for minerals such as olivine and pyroxene (Dohmen et al., 2010; Tang et al., 2014). As Li diffuses more slowly in zircon than in any other minerals (Cherniak and Watson, 2010), we have modeled Li- isotope diffusion in zircon to understand to what extent the fractionation can be driven by diffusion.

Mathematical Formulation for the Diffusion of Lithium

The diffusion model is based on Fick's first and second law:

$$\frac{\partial \phi}{\partial t} = \nabla \cdot (D \nabla \phi) \quad \text{.....(1)}$$

As diffusion in minerals and melts is complicated and difficult to describe due to multiple components in the system, complex boundary conditions and highly non-ideal mixing (Zhang, 2010), simplifications are usually made in order to obtain analytical solutions. Considering the high Li content and large volume of the melt, the Li concentration in the melt can be taken as constant; since the diffusion distance (the rim) is much smaller than the grain size of the zircon, the medium can be treated as semi-infinite (Zhang, 2010). Here, we assume a diffusion-couple solution for Li diffusion between zircon and melt/surrounding minerals (no convection is considered in the melt). The diffusion problem is simplified to a one-dimensional diffusion-couple model in infinite space. D is considered constant and independent of C and x.

From the above assumptions, we can derive the initial conditions and boundary conditions as follows:

Initial conditions: at t = 0, if x > 0, then C = C1; if x < 0, then C = C2

Boundary conditions: at t ≥ 0, when x = ∞, C = C1; when x = −∞, then C = C2

Here, C1 and C2 present the initial concentration of melt/surrounding mineral and zircon, respectively. The final analytical solution can be easily calculated and simulated in an Excel spreadsheet:

$$C = \frac{C_1+C_2}{2} + \frac{C_1-C_2}{2} \cdot erf \frac{x}{\sqrt{4Dt}} \quad \text{.....(2)}$$

where *erf* is the error function：

$$\mathrm{erf}(x) = 1 - \frac{2}{\sqrt{\pi}} \int_x^{\infty} e^{-t^2}\, dt$$

This one-dimensional diffusion-couple model is a simplification of the real diffusion occurring in the geological situation but should capture the essence of the problem.

Simulation of diffusion-driven fractionation of Li in zircon

The calculated change in [Li] as a function of distance for a one-dimension model of a melt-mineral diffusion couple is firstly based on an initial concentration gradient fixed by $[Li]_{\text{whole rock}}/[Li]_{\text{zircon}}$. The observed profile of Temora is qualitatively consistent with that expected for initial $[Li]^i$ = 11 ppm diffusing to [Li] = 0.08ppm, while the modeled initial [Li] of Qinghu (30 ppm) and Plešovice (26ppm) are different from their whole-rock [Li] (23ppm and 53ppm, respectively). This suggests that the whole-rock Li isotopes may have been modified by later processes or the initial diffusion condition is most likely controlled by the [Li] of the mineral adjacent to the zircon, rather than a melt.

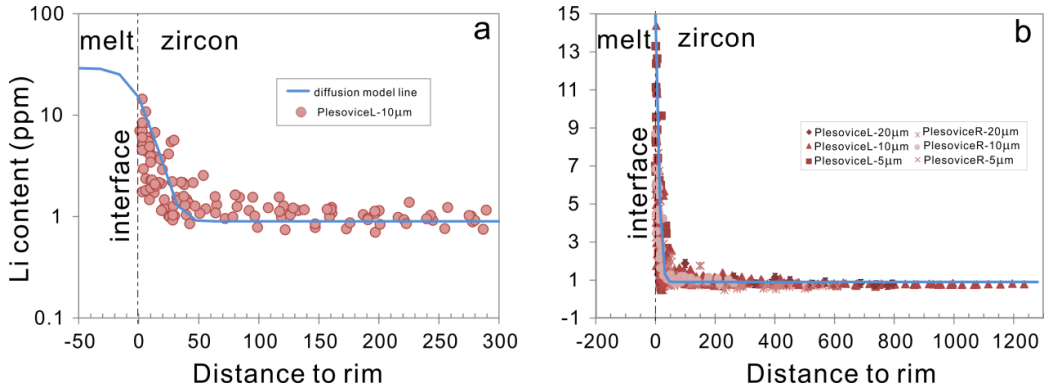


Figure 6.6 One-dimensional diffusion model for Plešovice zircons, calculated change in Li concentration as a function of distance a) PlesoviceL-10μm; b) All the Plesovice data.

For the data obtained from the Plešovice zircons, concentrations drop from ~15 to 1 ppm over a very narrow zone at rim (< 100 μm, Figure 6.6); in the Qinghu zircons, concentrations drop from ~13 to 1 ppm over an even narrower zone (< 50 μm, Figure 6.7). Generally, there are five factors controlling chemical diffusion: the size of the grain, time, the activity gradient, temperature and cooling rate. According to the model, the Plešovice zircon probably underwent diffusion at a lower temperature than the Qinghu zircon.

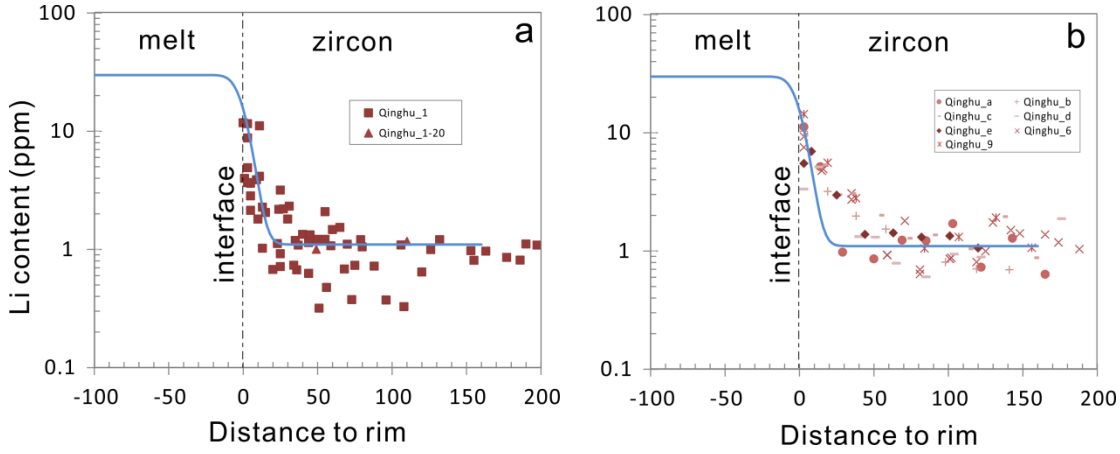


Figure 6.7 One-dimensional diffusion model for Qinghu zircons, calculated change in Li concentration as a function of distance a) [Li]data of Qinghu_1; b) All the other Qinghu [Li] data.

In the Temora zircons, concentrations drop from ~10 to 0.08 ppm over ~50 μm zone at rim (Figure 6.8). The fitted diffusion coefficients indicate that diffusion in the Temora zircon was the slowest of the three examples, especially considering the older age which leads to longer diffusion time.

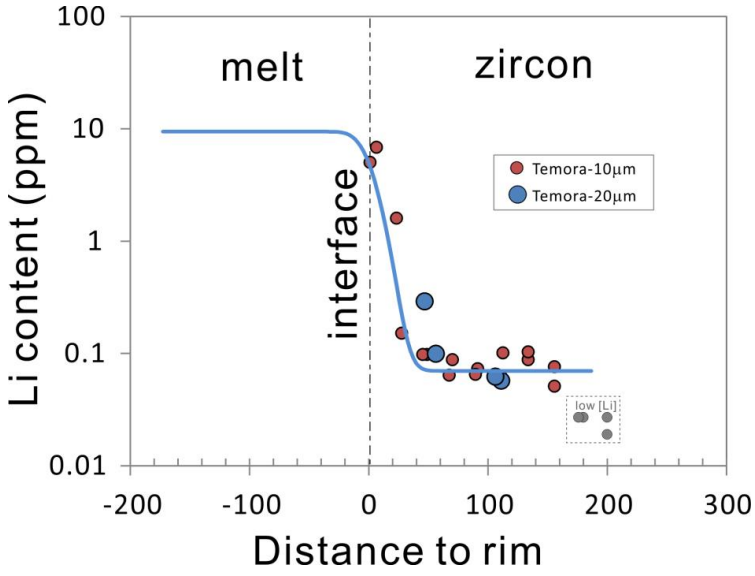


Figure 6.8 One-dimensional diffusion model for Temora zircon, calculated change in Li concentration as a function of distance.

A series of diffusion coefficients were applied to model the [Li] as a function of distance (Figure 6.6, 6.7, 6.8). When the measured Li contents are modeled by Equation (2), a diffusion coefficient value of D = 9.73E-27 m^2s^{-1} provides the best fit for the [Li] of the Plešovice zircon (SIMS Li analysis data are available in the Appendix dataset; error bars are at 2σ), while D = 1.82E-26 m^2s^{-1} provides the best fit for the Qinghu data and D = 5.12E-27 m^2s^{-1} provides the best fit for the Temora data. Using empirical formula of Cherniak and Watson (2010), the calculated temperatures corresponding to these D values should be around 450 ^oC, 460 ^oC and 440 ^oC, respectively. The model parameters are listed in Table 6-4.

While the [Li] data show good consistency with the model, the δ^7Li values are difficult to model, as the relative diffusion rates of ^6Li and ^7Li in zircon have not been

experimentally constrained. In the absence of a theoretical basis for the relationship between the diffusivity and the mass in zircon, here we assume, following Richter et al. (1999), that the effective diffusion coefficients of ^{6}Li and ^{7}Li are related to their masses by:

$$\frac{D_{i,1}}{D_{i,2}} = \left(\frac{m_{i,2}}{m_{i,1}}\right)^{\beta} \quad \text{(3)}$$

where the kinetic fractionation parameter β is an empirical parameter that controls the degree of isotopic fractionation (Figure 6.9). The modeled δ^{7}Li profile has a "trough", the depth of which is controlled by β. The factor β For the Li isotopes in a silica melt has been experimentally determined to be 0.215 (Richter et al., 2003). However, as the diffusion coefficients are media-dependent (Richter et al. 2003), this value might not be applicable to zircon. In order to give a qualitative evaluation of how extreme the fractionation can be driven only by diffusion, we have calculated apparent fractionations for core and rim compositions of the model.

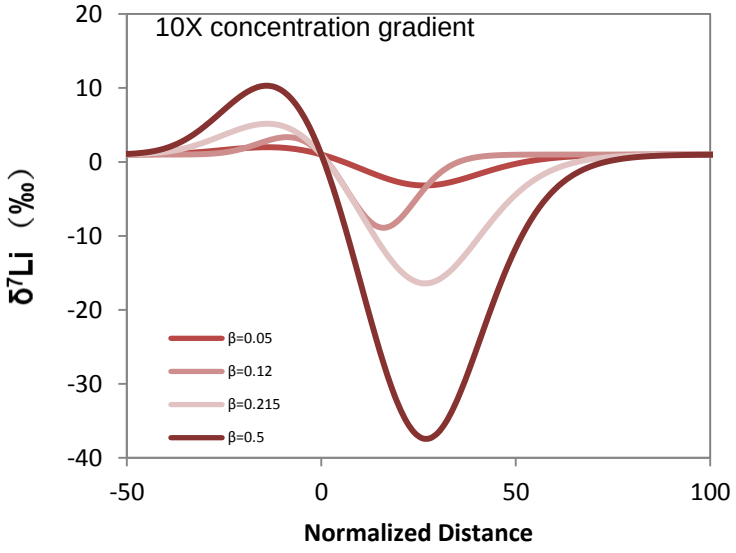


Figure 6.9 Effects of different β values on diffusion fractionation model

The diffusion model shows that large differences in both the Li concentration gradient and Li diffusivities can lead to significant Li isotopic fractionation. When β =

0.215, the model predicts up to 36‰ fractionation within a single grain for the Qinghu zircon, 33‰ for the Plešovice zircon and 68‰ for the Temora zircon. When β = 0.12, the fractionation calculated from the model is 21‰, 19‰ and 31‰, respectively, which is broadly consistent with the SIMS data: 24‰, 18‰, and 20‰.

Table 6-4 Model parameter for Plesovice, Qinghu and Temora zircon

Sample Name	**Diffusion coefficient**	**Age(Ma)**	**Melt**		**Zircon Core**	
			initial [Li]	Initial δ^7Li	initial [Li]	initial δ^7Li
Plesovice	9.73E-27	337.1	26.0	1.2	0.9	1.2
Qinghu	1.82E-26	159.5	30.0	-4.2	1.0	-4.2
Temora	5.12E-27	417.6	11	9	0.08	9

6.4.3 Speculations on Li isotopic data in zircons

Interpretation of Li isotopic data in zircons

The Plešovice and Qinghu zircons have good crystalline structure and are homogeneous in terms of radiogenic Pb/U ratios and Hf-O isotopic compositions. The discussion in the previous section suggests that their Li isotopes probably were also homogeneous initially, and then were fractionated by diffusion-driven processes. Therefore, the δ^7Li data of zircons should be treated carefully to assure recognition of the primary Li isotope values.

Theoretically, in zircon grains without good crystal shape, plots of [Li] *vs* δ^7Li can show a positive correlation, a negative correlation or no correlation. This might be the case if only a portion of the diffusion profile is sampled (Figure 10a, b).

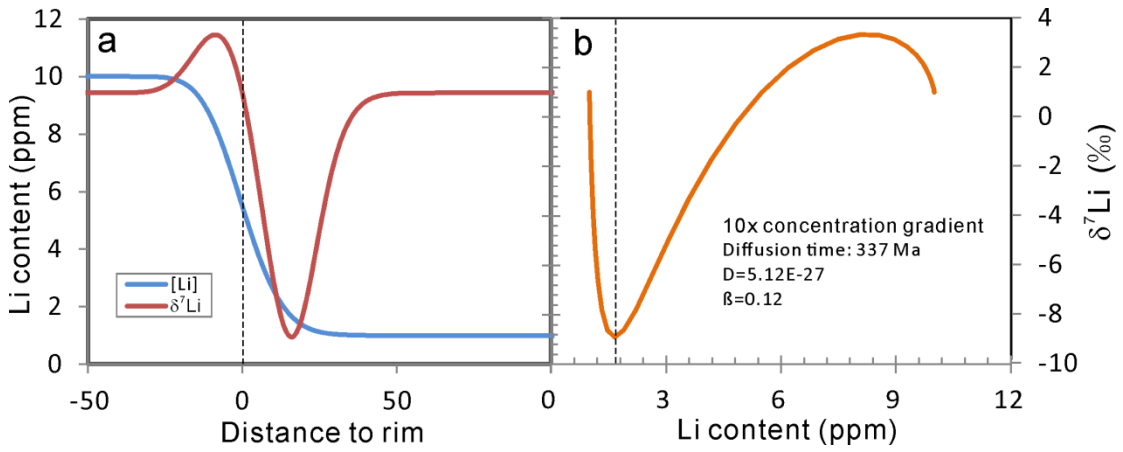


Figure 6.10 a) [Li] and δ^7Li as a function of distance for a one dimensional diffusion model. The depth, width and the position of the trough of the Li profile is a function of β, diffusivity and time; b) Modeled variation in δ^7Li vs Li concentration (ppm). The left side of the dashed line shows a negative correlation between δ^7Li and [Li] while the right side of the dashed line presents a possitive correlation.

Usually, Li-isotope heterogeneities are easily re-homogenized in a zircon < 100 µm in size after a few million years at lower-crust temperatures (Cherniak and Watson, 2010). Rapid diffusion will produce a positive correlation between [Li] *vs* δ^7Li, and there will be no "trough" as the diffusion is completed. If initial isotopic equilibrium between zircon and melt is assumed, and [Li] is positively correlated with δ^7Li, the highest values of δ^7Li may represent the initial δ^7Li of the magma, as observed in this study. A negative correlation can be produced at the rim when Li-isotope equilibrium between zircon and melt is not achieved. In this case, the data at the high δ^7Li - low [Li] end will most probably be closest to the original values. Thus, for both positive and negative correlations, the higher δ^7Li will be most similar to the original magmatic value.

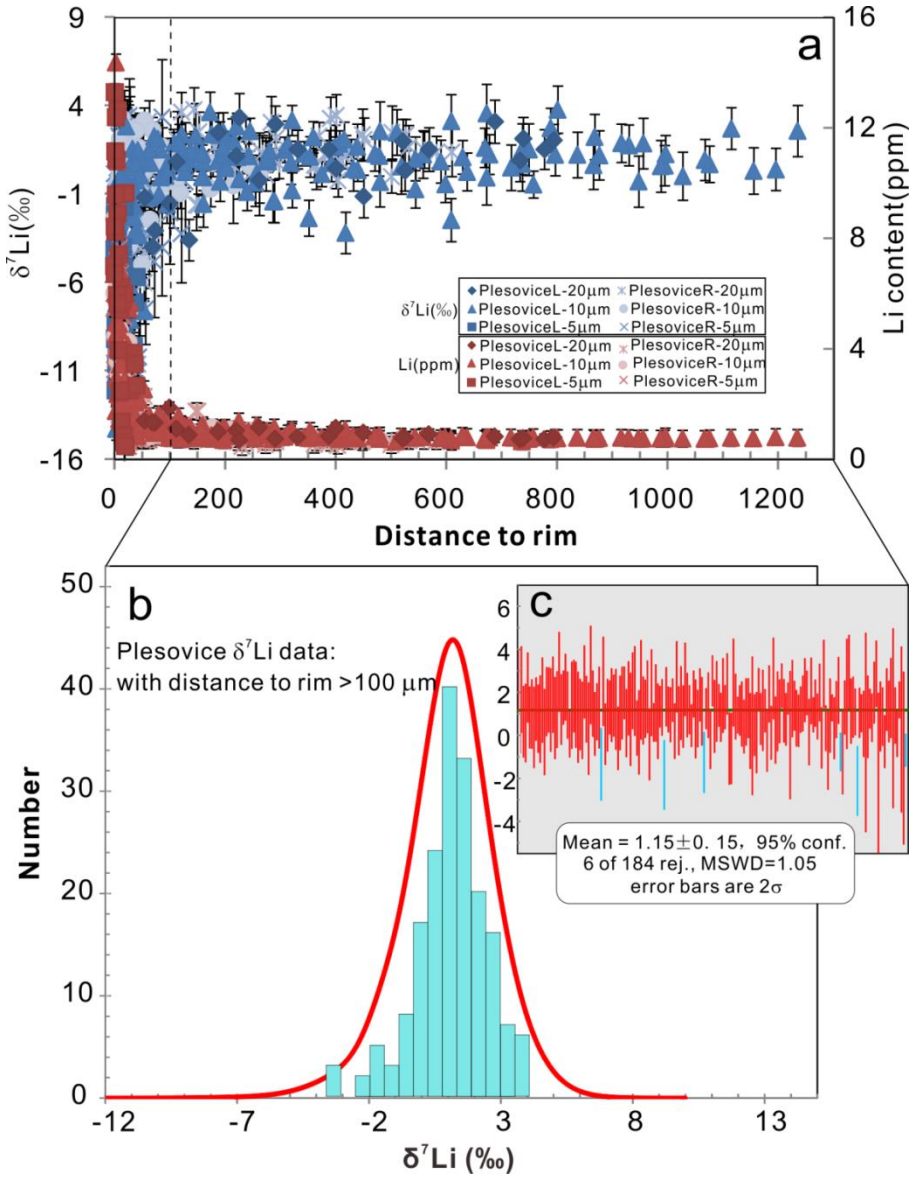


Figure 6.11 a) Compiled data for all the analysed spots on Plešovice zircons; b) Probability density plot and c) Weighted average of analysed spots more than 100 μm from the rim.

Idealy, the diffusion fractionation will produce a trough in δ^7Li. The SIMS results show low δ^7Li at the rim, but do not clearly match the "trough" produced by the basic diffusion model. The complex δ^7Li values might be caused by superposition of different mechanisms. Kinetic isotope fractionation can occur both during and after cooling, and a "two-stage diffusion" process might occur. 1). Diffusion between melt and zircon: zircon crystallizes and equilibrates with magma, then Li starts to diffuse from the melt

into zircon grains during magmatic cooling, driven by the large Li gradient. 2). Diffusion between solid mineral phases: after the melt has fully crystallized, Li starts to diffuse from the adjacent minerals with high [Li] (feldspar/biotite/quartz, etc) into zircon. The preservation of the original Li isotopic composition in zircon will depend on the cooling rate. Slow cooling rates might greatly modify the original "equilibrium" Li isotopes. In spite of this, if the zircon grain is large enough or the diffusion period is short enough, the Li isotopes in the core will retain the primary δ^7Li of the melt from which the zircon crystalized. As the Plešovice, Qinghu and Temora zircons are homogeneous in terms of radiogenic Pb/U ratios and Hf-O isotopic compositions, one can assume their parental melts remained constant and no fluid or melt was added during the crystallization of the zircon. Therefore, the δ^7Li plateau in the diffusion profiles should represent the primary value. Figure 6.11 shows the compiled data for all the analysed spots on the Plešovice zircons. The analysed spots more than 100 μm from the rim show a good Gaussian distribution, with weighted average δ^7Li = 1.15 ± 0.15‰ (1σ). This should be the best estimate of the primary δ^7Li of the Plešovice zircon.

For the Qinghu zircon (Figure 6.12), the analysed spots more than 50 μm from the rim show a Gauss distribution, with a weighted average δ^7Li = -4.2 ± 0.4‰ (1σ). This is taken as the best estimate of the primary δ^7Li of the Qinghu zircon. Where zircon grains are small (e.g. Temora zircon) or do not have well-defined crystal shapes, only a portion of the diffusion profile is sampled, and the δ^7Li value in the center of the grain cannot present the primary Li isotope value.

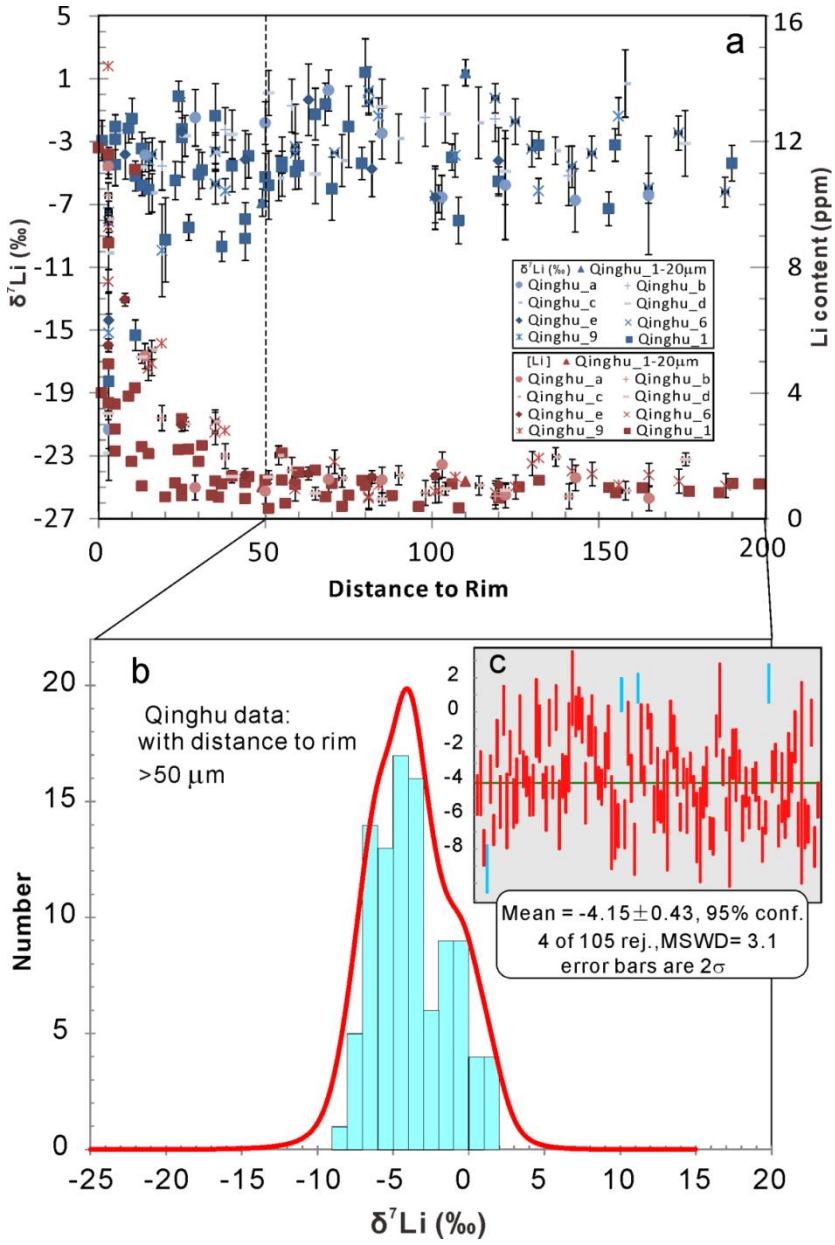


Figure 6.12 a) Compiled data for all the analysed spots on Qinghu zircons; b) Probability density plot and c) Weighted average of analysed spots more than 50 μm from the rim.

6.5 CONCLUSIONS

This study has corroborated the hypothesis of diffusion-driven fractionation of Li isotopes in zircon, using ion imaging and analysis at high spatial resolution with ～20 μm, 10 μm and 5 μm SIMS beams. We suggest that the observed large variations of [Li] and the extreme fractionation of δ^7Li in zircons were generated by diffusion during

cooling from igneous temperatures. Interpreting the significance of δ^7Li values in zircons requires much more effort in understanding of the possible effects of the late diffusion fractionation on [Li] and δ^7Li distribution in zircons.

1. Diffusive ingress of Li from a melt into zircon grains is accompanied by extreme kinetic fractionation of Li isotopes. Extremely large isotopic variations of Li in zircons can be caused by diffusion as [Li] increases rapidly at the rim. The heterogeneity (δ^7Li variations ~20‰ within individual grains) indicates that bulk analysis of Li isotopes in mineral separates may produce misleading data.
2. It is important to analyze profiles to identify whether the δ^7Li signature in a given zircon is caused by diffusion. Homogeneous δ^7Li in the cores of large zircon grains most likely carries reliable information about the isotopic signature of the source magmas.
3. For the Plešovice zircon, the δ^7Li value of the analytical spots more than 100 μm from the rim is homogeneous. The initial δ^7Li of the Plešovice host rock was around 1.15 ± 1.3‰ (1σ); the Qinghu zircon, the δ^7Li value of the analytical spots more than 50 μm from the rim is homogeneous. The initial δ^7Li of the Plešovice host rock was around -4.15 ± 2.0‰ (1σ).
4. Diffusion coefficients of Li in zircons are different for Plešovice, Temora and Qinghu zircons, which imply that they have different thermal histories.

CHAPTER 7. ORIGIN OF CRETACEOUS A-TYPE GRANITES IN EAST CHINA

For the past 20 years, the Yanshanian granitic plutons in eastern China have been the subject of extensive geological investigations, as they represent one of the biggest granite provinces worldwide. Although several studies have reported aspects of the geochronology, mineralogy, petrography and geochemistry (Li and Yu, 1993; Qiu et al., 1996), there is still controversy concerning the age and petrogenesis of these alkali igneous rocks, especially for those with low $\delta^{18}O$ values (Wang et al., 1998; Wei et al., 2000; Wei et al., 2001a; Zhao et al., 2001; Wei et al., 2006; Wei et al., 2008; Yang et al., 2008). A primary purpose of this chapter is to use non-traditional Li isotopes as well as *in situ* Hf-O isotopes to provide a new window into the sources and petrogenesis of several A-type granites, particularly deciphering the involvement of recycled-crust in granite genesis. In this chapter we: 1). Present systematic major- and trace-element compositions, whole-rock Li isotopic data, *in situ* zircon U-Pb age and Hf-O-Li isotopic data of six A-type granites from eastern China; 2). Use these tracers to constrain the time of emplacement and sources of magma.

7.1 GEOCHEMICAL DATA

7.1.1 Major and Trace element

A total of one hundred and five samples from the six plutons were analysed for major- and trace-element compositions. The geological background of these rocks is described in chapter 2. The results are listed in Appendix table ii and plotted in Figure 7.1-7.9.

Available geochemical data for the six plutons show their pronounced A-type

affinity. Major-element data show that most samples are acidic with ferroan compositions. They are high in SiO_2, $Fe_2O_3^T$ and Na_2O+K_2O, have high K/Na, Fe/Mg, Ga/Al ratios and low Al_2O_3, TiO_2, MgO and CaO contents. According to the plot of alkalis *vs* silica (Ewart, 1982), most of the A-type granite samples plot in the region of the sub-alkaline series and the high-K calc-alkaline series (Figure 7.1).

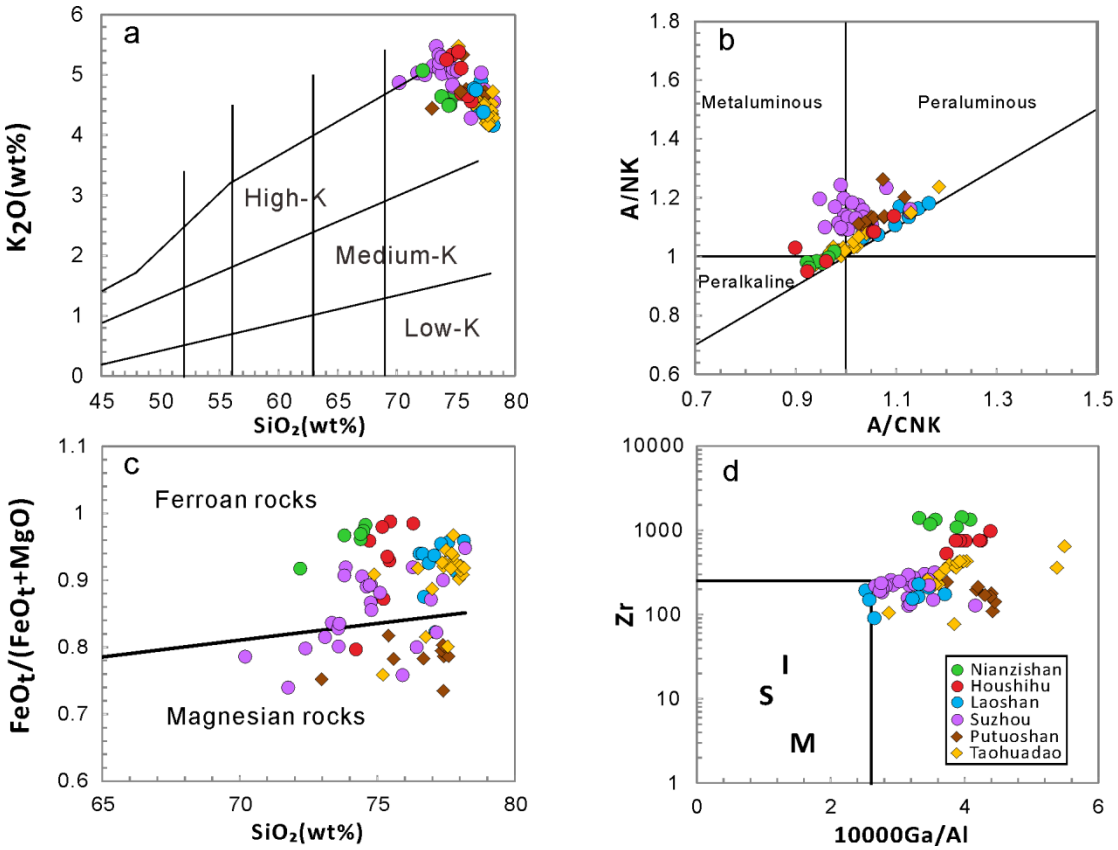


Figure 7.1 Discrimination diagrams for six A-type granites a) Alkalis vs Silica plot (Ewart, A., 1982); b) A/NK vs A/CNK plot (Maniar and Piccoli, 1989). A = Al_2O_3, N = Na_2O, K = K_2O, C = CaO (all in molar proportions; c) SiO_2 vs $FeO_t/(FeO_t + MgO)$ diagram (Frost et al., 2001). Above the FeO_t line is the field of Fe-granitoids corresponding to A-type.; d) 10000Ga/A1 vs Zr plot. The coordinates of the M-I-S type granite fields are X=2.6, Y=250 (Whalen et al., 1987).

The studied plutons thus geochemically resemble published A-type granites worldwide, but show distinctive difference with respect to M-, I-, and S-type granites (see in chapter 1). Except for the Suzhou granites, most samples plot within the field of

A_1-type granites, suggesting within-plate and/or post-orogenic extensional settings (Figure 7.2).

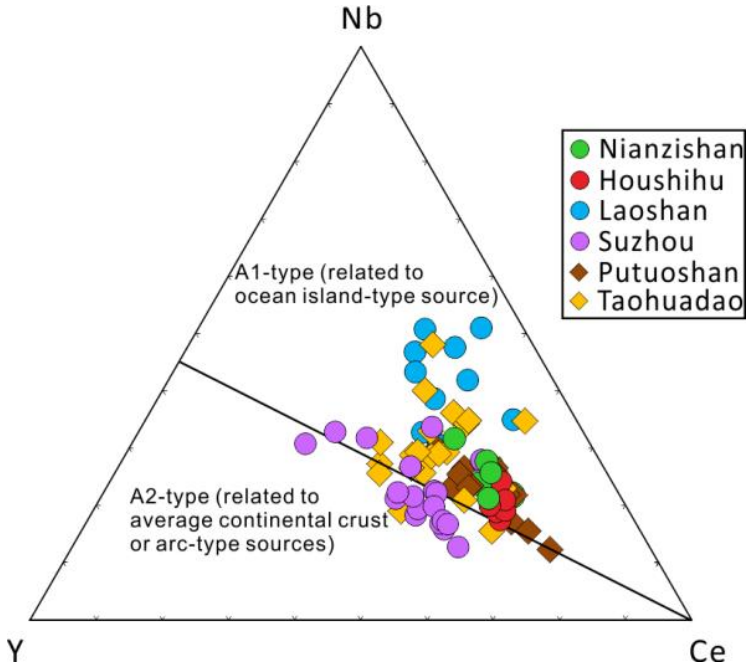


Figure 7.2 Nb-Y-Ce Classification diagrams for the studied A-type granites (Eby, 1992).

Nianzishan

Rocks from the Nianzishan pluton are quite fresh. They are high in silica and total alkalis, with SiO_2 ranging from 72.2 wt% to 74.6 wt%, and total K_2O + Na_2O varying from 8.7 to 10.3 wt% ($Na_2O \approx K_2O$). They fall within the high-K calc- alkaline field based on the K_2O versus SiO_2 diagram (Figure 7.1a). According to the aluminum saturation index (ASI), the Nianzishan granites are peralkaline (Maniar and Piccoli, 1989), with A/CNK and A/NK (molar ratio of $Al_2O_3/[CaO+Na_2O+K_2O]$ and $Al_2O_3/[Na_2O+K_2O]$) values clustering mostly around 0.92 - 0.98 (Figure 7.1b) . They all plot in the field of ferroan granitoids, and in the field of A-type granites (Figure 7.1c, d). They have low contents of CaO (< 0.5 wt%), MgO (< 0.11 wt%) and TiO_2 (< 0.3 wt%), and high FeO_t/MgO ratios (> 11).

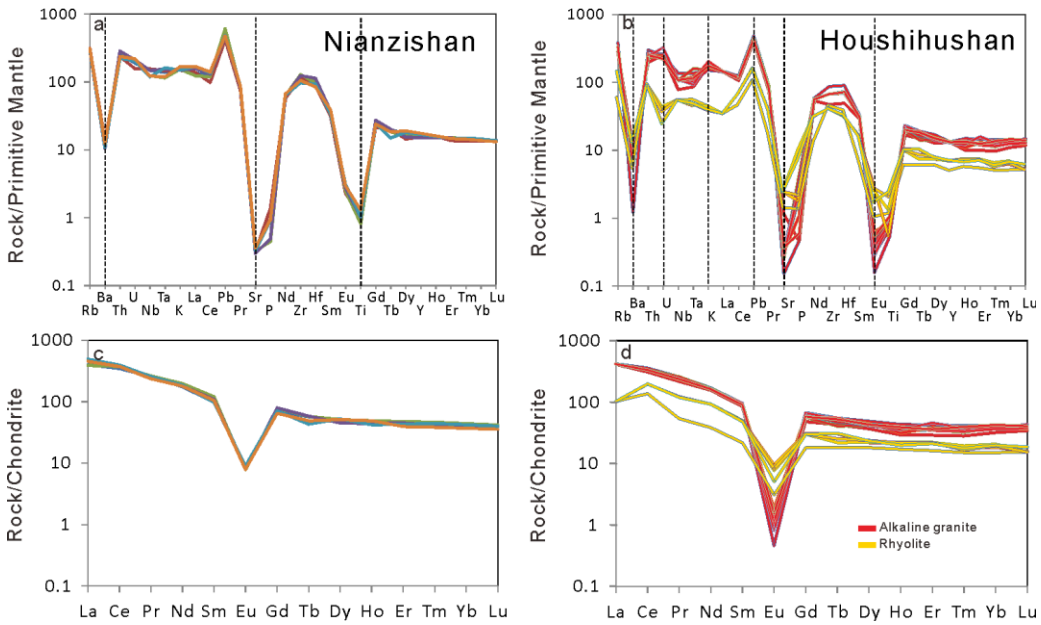


Figure 7.3 Primitive mantle-normalized plot of spidergrams for the: a) Nianzishan and b) Houshihushan pluton. Normalization values are from Sun and McDonough (1989); Chondrite-normalized plot of rare-earth element abundances: c) Nianzishan and d) Houshihushan pluton. Chondritic values are from Sun and McDonough (1989).

The Nianzishan granites are enriched in some large-ion lithophile elements (LILE, such as Rb and Th) and high field strength elements (HFSE, such as Zr and Hf); and depleted in Sr, Ba, and Ti. The total REE are ~ 566 ppm, $(La/Yb)_N$ = 7.6 to 14.0 (Chondrite-normalized). The granite thus has a relatively high rare earth element (REE) content, with significant negative Eu anomalies (Eu/Eu* = 0.08 – 0.11). The Ga concentrations range from 22 to 27 ppm, yielding high 10000 × Ga/Al ratios (3.3 – 4.1) and fall within the typical A-type granite range in this discrimination diagram (Whalen et al., 1987) (Figure 7.1d). Zircon-saturation temperatures (T_{Zr}) calculated from bulk-rock compositions (Miller et al., 2003) range from 972 ^{o}C – 1008 ^{o}C.

Houshihushan

Nine alkaline granite samples and five rhyolite samples have been analysed. The alkaline granites are high in silica, with SiO_2 ranging from 74.2 to 76.3 wt%, and K_2O > Na_2O with total K_2O + Na_2O varying from 8.4 to 10.0 wt%; they plot in the fields of the

sub-alkaline series and high-K calc-alkaline series (Figure 7.1a). The rhyolite has lower silica and alkalis, ranging from 68.5 to 74.0 wt% and 6.3 to 8.7 wt%, respectively. It follows the same geochemical trends as the alkaline granites in the Harker diagrams (Figure 7.4). The percentages of Al_2O_3, CaO, MgO, P_2O_5, Fe_2O_3 and TiO_2 are low and all are negatively correlated with SiO_2.

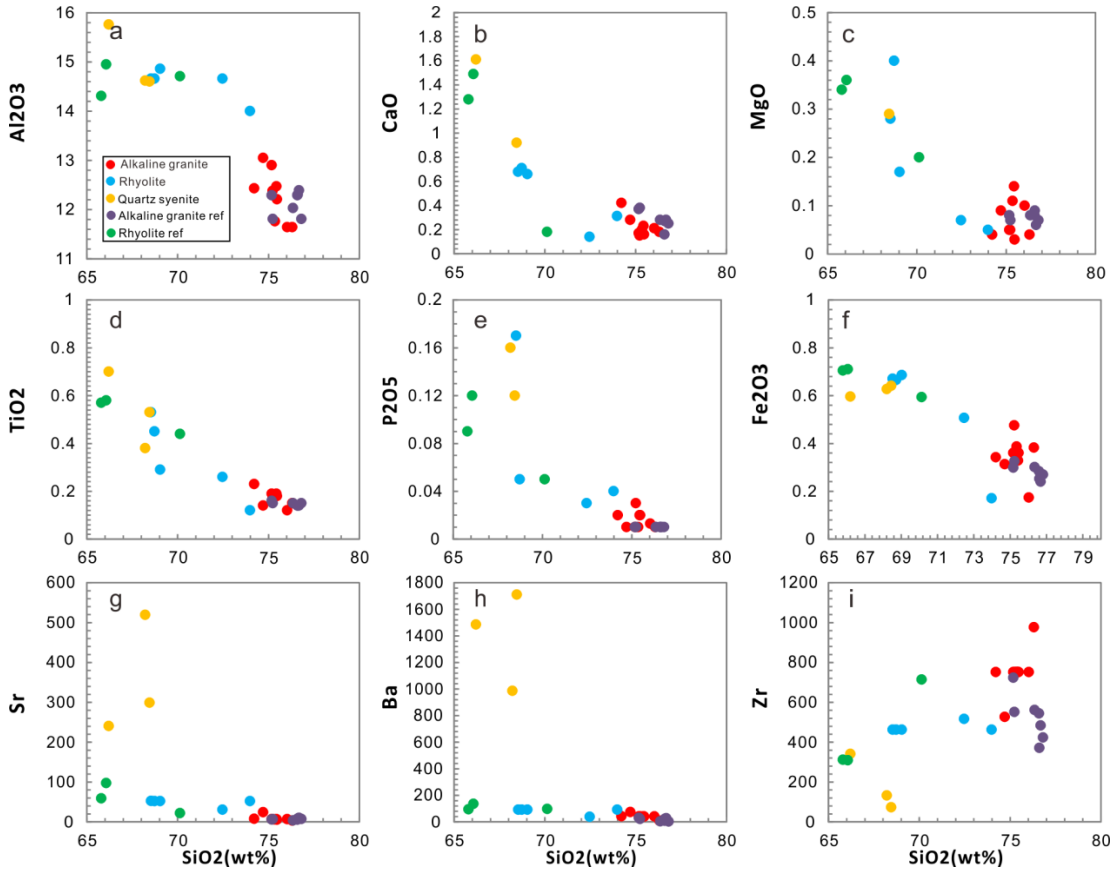


Figure 7.4 Harker diagrams showing the chemical variations within the Houshihushan Pluton. Reference values are from Wen et al. (2013).

The alkaline granites have a total REE of ~514 ppm, with LREE enrichment and relatively flat HREE patterns (La_N/Yb_N = 9.8 – 12.9) and strongly negative Eu anomaly (Eu/Eu*~ 0.02) (Figure 7.3). The rhyolite has a relatively low total REE content (~242 ppm) and a smaller Eu anomaly (0.15 – 0.24) than the alkaline granites. In the primitive mantle-normalized spidergrams (Figure 7.3), these rocks show variable enrichment in Rb, Th, U, Pb, Zr and Hf and depletion in Sr, Ba and Eu, which decrease with

increasing SiO_2 (Figure 7.4). The alkaline granites also have higher 10000 × Ga/Al (3.7 – 4.4) than the rhyolite (3.4 – 3.7) (Figure 7.1d). Both of them plot within the A-type granite field in the 10000 × Ga/Al vs Zr discrimination diagram (Whalen et al., 1987). According to the bulk-rock composition, zircon-saturation temperatures (T_{Zr}) suggest a minimum crystalization temperature > 900 ^{o}C (Miller et al., 2003).

Laoshan

The Laoshan granites are composite batholiths of I- and A-type plutons; ten alkaline granite samples and eight quartz syenite samples have been analysed. The samples are fairly fresh which is confirmed by LOI ranging from 0.22 – 0.51 wt%. Both phases are characterized by high silica and alkali contents, with SiO_2 ranging from 72.5 to 78.2 wt% and $K_2O > Na_2O$ with total alkalis ($K_2O + Na_2O$) varying from 8.2 to 9.6 wt%. They plot in the fields of the high-K calc-alkaline series and alkaline series (Figure 7.1a). In terms of ASI (Figure 7.1b), the molar ratios of A/CNK and A/NK ratios ranging from 1.02 to 1.17, plot in the metaluminous to peraluminous region (Maniar and Piccoli, 1989). They have low total Al_2O_3, CaO, MgO, P_2O_5, Fe_2O_3 and TiO_2 and all are negatively correlated with SiO_2 (Figure 7.5).

In trace element abundances, they are highly enriched in light rare-earth elements (LREEs) and have typical high 10000 × Ga/Al ratios (2.3 – 3.7). Samples from the two phases show similar Chondrite-normalized REE patterns ($\sum$REE = 70 – 363, La_N/Yb_N = 6.3 – 26.0, and Eu/Eu* = 0.14 – 0.56) and identical primitive-mantle-normalized spider diagrams (Figure 7.6). Most samples show strong but variable negative Ba, Sr, P and Ti anomalies and positive anomalies in Rb, Th, K, Pb, Zr and Hf (Figure 7.6a). Zircon-saturation temperatures (T_{Zr}) calculated from bulk-rock compositions (Miller et al., 2003) range from 753^{o}C – 883^{o}C, providing minimum estimates of crystallization temperature.

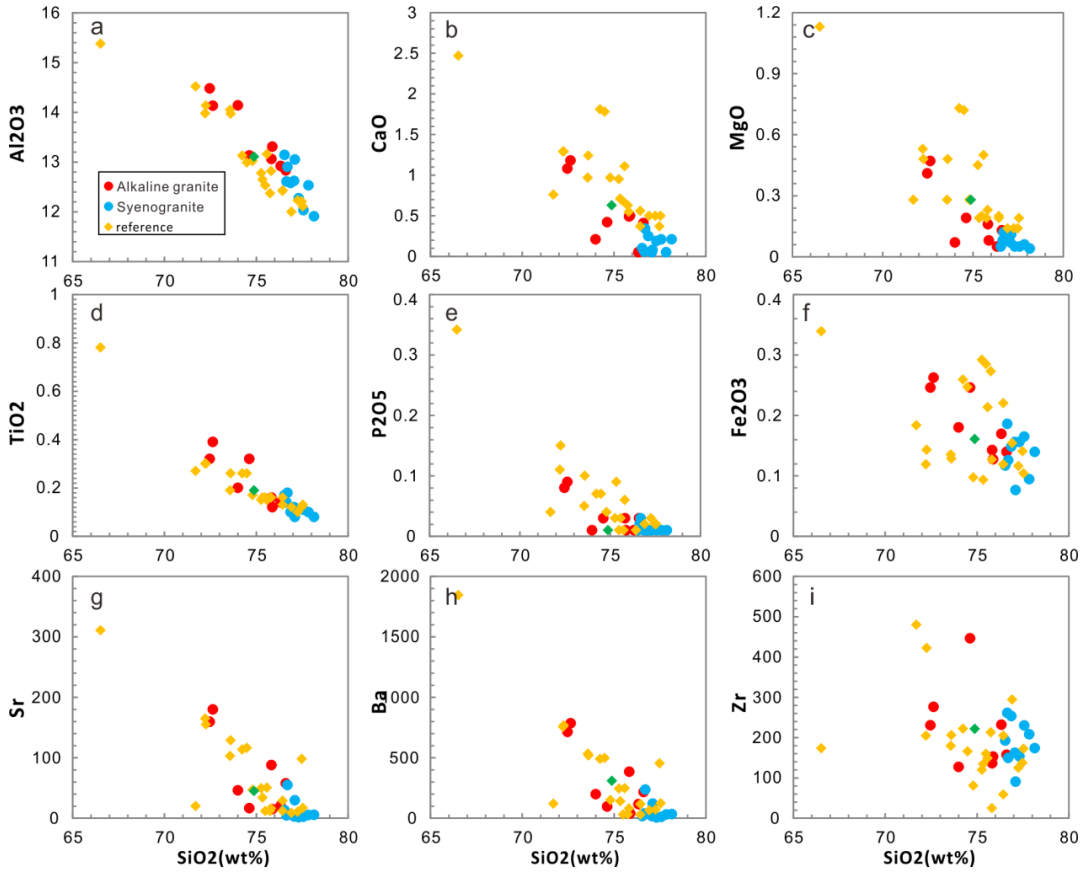


Figure 7.5 Harker diagrams showing the chemical variations of the Laoshan Pluton. Reference values are from Yan and Shi (2014).

Suzhou

Inspection of thin sections shows that the samples from the Suzhou pluton are relatively fresh to slightly altered. This observation is confirmed by LOI values of less than 1 wt % except for 09YY092, 09YY103 and 09YY110, which are 1.28 wt%, 1.01 wt% and 1.07 wt%, respectively. In general, all three phases samples from the Suzhou pluton are high in silica and alkalis, with SiO_2 ranging from 70.2 to 78.2 wt.%; K_2O > Na_2O with total K_2O + Na_2O varying from 7.9 to 9.4 wt%, and the samples plot in the region of the sub-alkaline series and high-K calc-alkaline series (Figure 7.1).

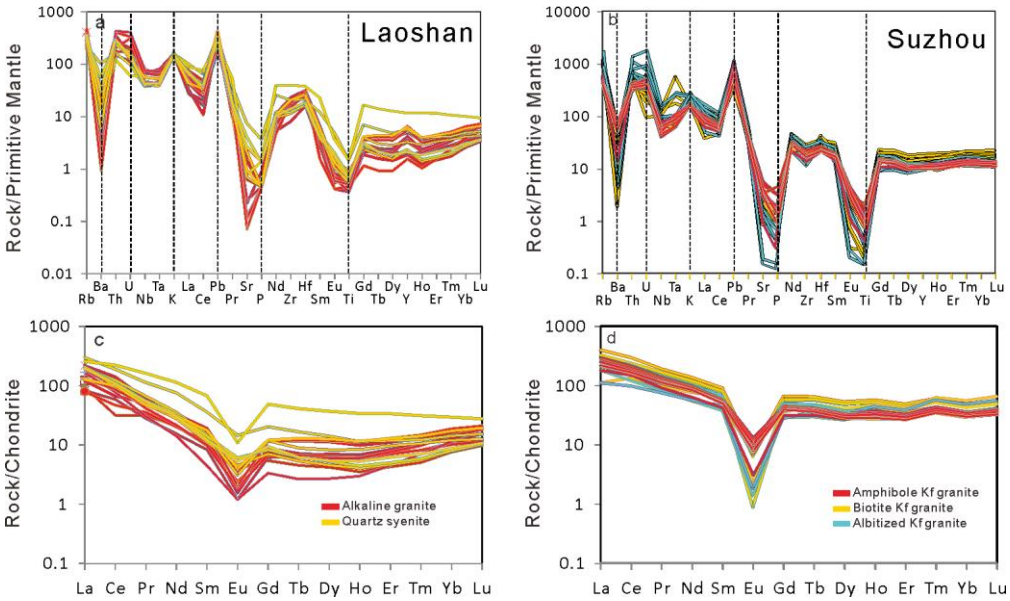


Figure 7.6 Primitive mantle-normalized plot of spidergrams for the: a) Laoshan and b) Suzhou pluton. Normalization values are from Sun and McDonough (1989); Chondrite-normalized plot of rare-earth element abundances: c) Laoshan and d) Suzhou pluton. Chondritic values are from Sun and McDonough (1989).

The amphibole-bearing early phase has lower SiO_2 than the other two phases, but it still follows the geochemical trends with other two phases of rocks in the Harker diagrams (Figure 7.7). The albitized granite is slightly higher in Na_2O than biotite-bearing K-feldspar granite but there is no distinguishable difference in trace elements. In terms of ASI (Figure 7.1b), the molar ratios of $Al_2O_3/[CaO+Na_2O+K_2O]$ and $Al_2O_3/[Na_2O+K_2O]$ ratios ranging from 0.95 to 1.13, plot in the metaluminous to peraluminous region (Maniar and Piccoli, 1989). The percentages of CaO, MgO, P_2O_5, Fe_2O_3 and TiO_2 are low and all are negatively correlated with SiO_2 (Figure 7.7).

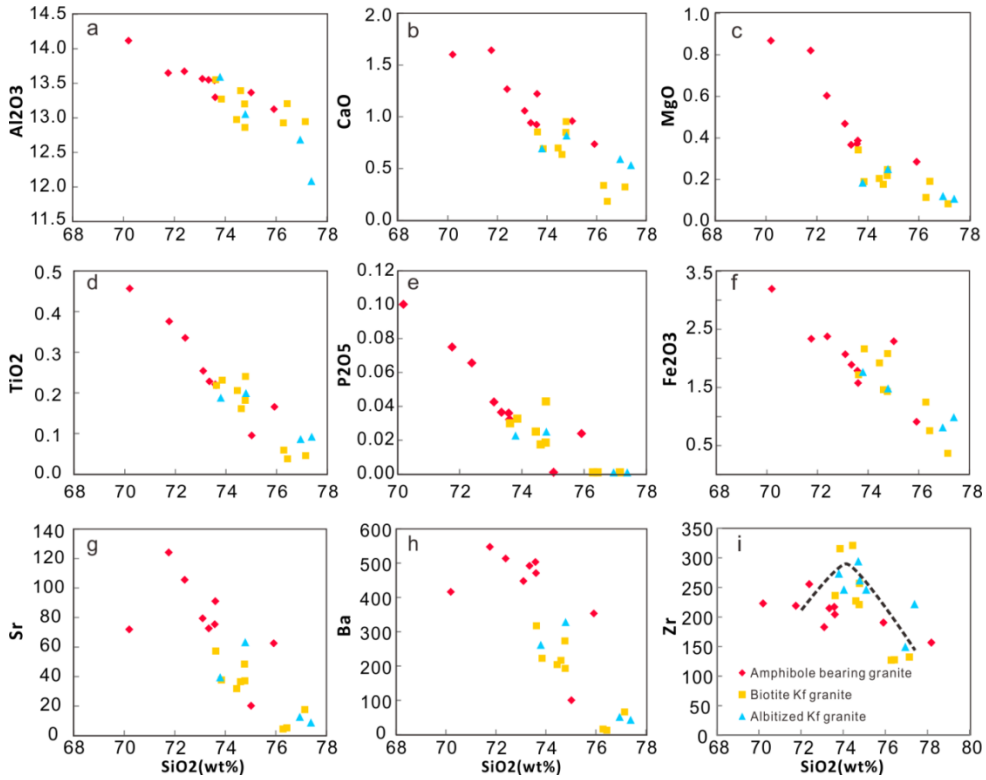


Figure 7.7 Harker diagrams showing the chemical variations of the Suzhou pluton.

Samples from all three phases show similar Chondrite-normalized REE patterns, with variable LREE enrichment and flat HREE patterns (La_N = 85 – 120, Yb_N = 10.3 – 13.7 and La_N/Yb_N = 2.0 – 9.9; subscript N denotes the Chondrite-normalized) and strongly Eu anomaly (Eu/Eu* = 0.02 – 0.26) (Figure 7.8). Thus, crystal fractionation of feldspars probably played a significant role in the magmatic evolution. In the primitive mantle-normalized incompatible trace element spidergrams (Figure 7.8), these rocks show variable enrichment in Rb, Th, U, Ta, Pb, and LREE and depletion in Sr, Ba and Eu which decrease with increasing SiO_2. The Ga concentrations range from 19 to 25 ppm, yielding high 10000 × Ga/Al ratios (2.7 – 4.2) (Figure 7.1d). High abundances of Zr, Nb, Ce, Y and the high Ga/Al ratio classify the Suzhou granite as a typical A-type granite (Whalen et al., 1987). Zr increases to SiO_2 = 74%, then decreases with increasing SiO_2. Zircon-saturation temperatures (T_{Zr}) calculated from bulk-rock compositions (Miller et al., 2003) range from 771 ^{o}C – 847 ^{o}C, providing minimum

estimates of temperature.

Taohuadao

Twenty-two samples of the Taohuadao granites have been analysed. They are high in silica with SiO_2 ranging from 74.9 to 78.2 wt%. They are potassium-rich with K_2O/Na_2O ratios ranging from 0.96 to 1.78, and total K_2O+Na_2O varying from 7.9 to 10.1 wt%, and they plot within the region of high-K calc-alkaline series. According to the ASI classification, the granites are metaluminous to weakly peraluminous with A/CNK and A/NK values of 0.94 – 1.19 and 0.97 – 1.24, respectively. They exhibit a ferroan signature with $FeO_t/(FeO_t + Mg)$ (molar ratios) ranging from 0.76 to 0.97 (Frost et al., 2001). The percentages of CaO, MgO, P_2O_5, Fe_2O_3 and TiO_2 are low while FeO_t/MgO (3.1 – 29.4) and Ga/Al (2.9 – 6.3) are high.

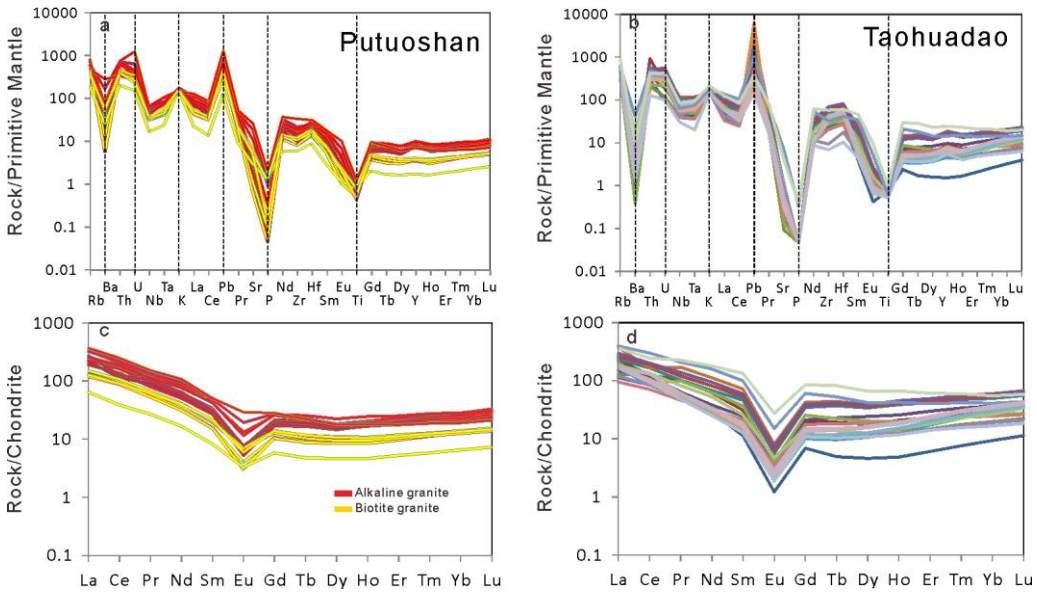


Figure 7.8 Primitive mantle-normalized plot of spidergrams for the: a) Putuoshan and b) Taohuadao pluton. Normalization values are from Sun and McDonough (1989); Chondrite-normalized plot of rare-earth element abundances: c) Putuoshan d) Taohuadao pluton. Chondritic values are from Sun and McDonough (1989).

The Taohuadao granites have high REE contents, with total REE ~247 ppm. All the samples show coherent rare earth element (REE) patterns, characterized by

depletion of HREE relative to LREE $(La/Yb)_N$ = 3.9 – 12.1) and significant negative Eu anomalies (Eu/Eu* = 0.13 – 0.26). The primitive mantle normalized spider diagrams (Figure 7.8a) show that these rocks are enriched in highly incompatible elements such as LREE and large ion lithophile elements (LILE), but depleted in high field strength elements (HFSE), with prominent negative anomalies of Ba, Sr, Eu and Ti. The T_{Zr} ranges from 727 – 945 ^{o}C

Putuoshan

Nine alkaline granite samples and six biotite granite samples of the Putuoshan granites have been analysed. The alkaline granites and biotite granites have similar silica and alkali content. The SiO_2 ranges from 73.0 – 78.1 wt% with total $K_2O + Na_2O$ varying from 8.5 to 9.0 wt %; they plot in the region of high-K calc-alkaline series. The rocks are mostly peraluminous with A/CNK ratios ranging from 1.0 to 1.1 and A/NK ranging from 1.10 to 1.26. In the Harker diagrams, SiO_2 has obvious negative correlations with Al_2O_3, CaO, MgO, TiO_2 and P_2O_5 (Figure 7.9).

All the samples show similar REE patterns, with LREE enrichment relative to HREE; $(La/Yb)_N$ = 6.5 – 19.4 for alkaline granites and 9.1 – 11.9 for biotite granites. The alkaline granites have relatively higher REE contents (~ 224 ppm) and stronger negative Eu anomalies (Eu/Eu* = 0.17 – 0.77) than biotite granites (total REE ~ 130 ppm, Eu/Eu* = 0.31 – 0.47) and thus lie above the relevant curves in Figure 7.8. They show enrichment of LILE, and depletion of HFSE with negative anomalies of Ba, Ta, P and Ti in the primitive mantle-normalized spider diagrams. The biotite granites exhibit Ga/Al = 1.26 – 2.48 and plot in the field of I-type granites. The alkaline granites have higher Ga/Al (2.65 – 4.78) and fall within field of the A-type granites. Zircon-saturation temperatures (T_{Zr}) calculated from bulk-rock compositions (Miller, McDowell et al. 2003) range from 758 ^{o}C – 869 ^{o}C for alkaline granites and 719 – 777 ^{o}C for biotite

granites.

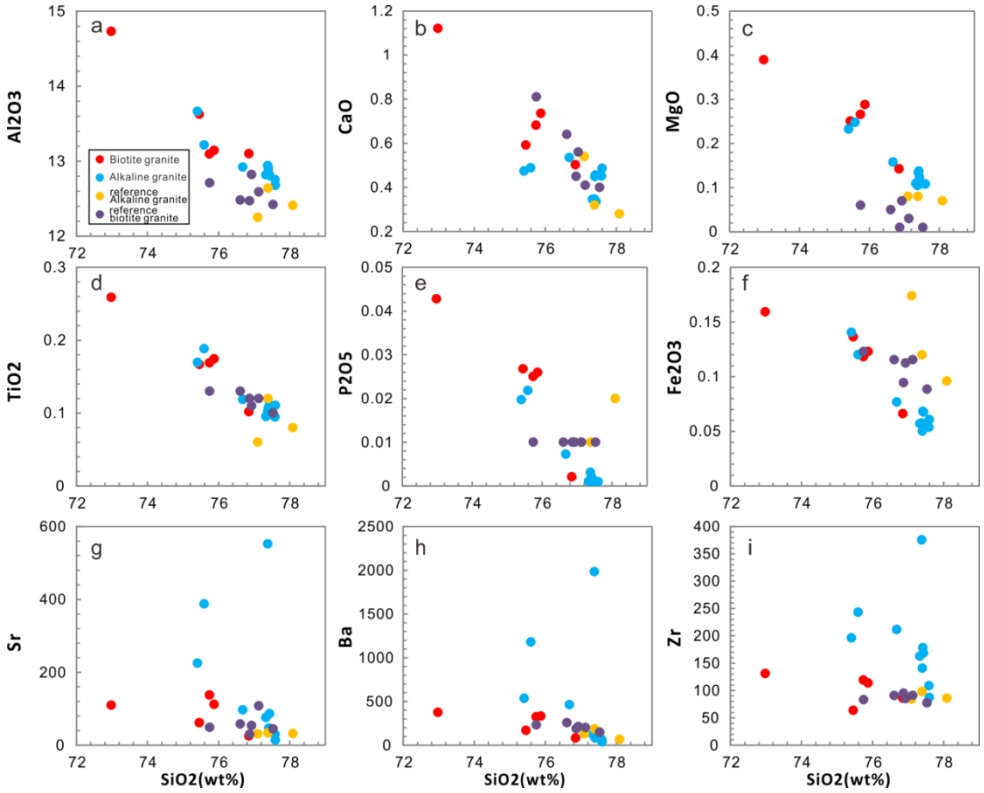


Figure 7.9 Harker diagrams showing the chemical variations of the Putuoshan Pluton. Reference values are from (Qiu et al., 1999).

7.1.2 SIMS *in situ* U-Pb dating results of A-type granites

Zircons from fourteen samples were analysed by Cameca IMS 1280; all the measured Pb-U ratios are concordant within analytical errors.

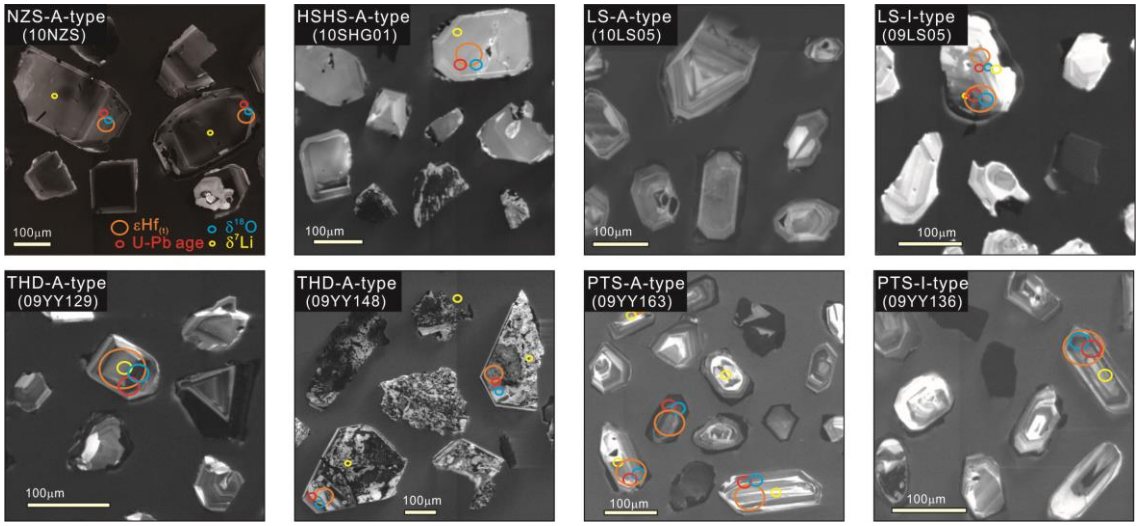


Figure 7.10 CL images of representative zircons analysed for in situ U-Pb, Hf-O-Li isotopes. Small red blue and yellow ellipses indicate the SIMS analysis spots for U-Pb, O and Li isotopes, respectively, and the big orange circles denote the LA-MC-ICPMS analysis spots for Hf isotopes.

Nianzishan

Zircons from the Nianzishan alkaline granite (NZS) are mostly euhedral, range from 100 to 400 μm in length, and have length to width ratios mostly between 1:1 and 1:3. Two samples have been analysed for U-Pb age. Fourteen analyses of 14 zircons from 10NZS were obtained. These zircons have moderate contents of U (127 – 352 ppm) and Th (55 –219 ppm). All analyses give Th/U ratios between 0.43 and 0.62. Most the grains have low f_{206} (the proportion of common ^{206}Pb in total measured ^{206}Pb) values < 0.6 %. The measured Pb/U isotopic ratios are concordant within analytical errors. The weighted mean of $^{206}Pb/^{238}U$ is 0.01869 ± 0.00031 (1SD), corresponding to a concordia age of 119.3 ± 1.0 (MSWD = 0.9, 2σ, Figure 7.11a). Thirteen analyses were obtained of 13 zircons from 10NZS03. Except for two grains with higher U and Th contents, these zircons have moderate contents of U (52 – 323 ppm) and Th (21 – 179 ppm), with Th/U ratios 0.32 – 0.84. Expect for three grains (which were eliminated from the Concordia plot), most of the analytical spots have low common Pb, with f_{206} values 0.0 – 0.6%. The measured Pb/U isotopic ratios are concordant within analytical errors. The weighted mean of $^{206}Pb/^{238}U$ is 0.01874 ± 0.00044 (1SD), corresponding to a Concordia age of 119.6 ± 1.6 (MSWD = 1.6, 2σ, Figure 7.11b). Therefore, the crystallization age for the Nianzishan alkaline granite is taken as 119.4 ± 1.0 Ma (2σ, Figure 7.12a).

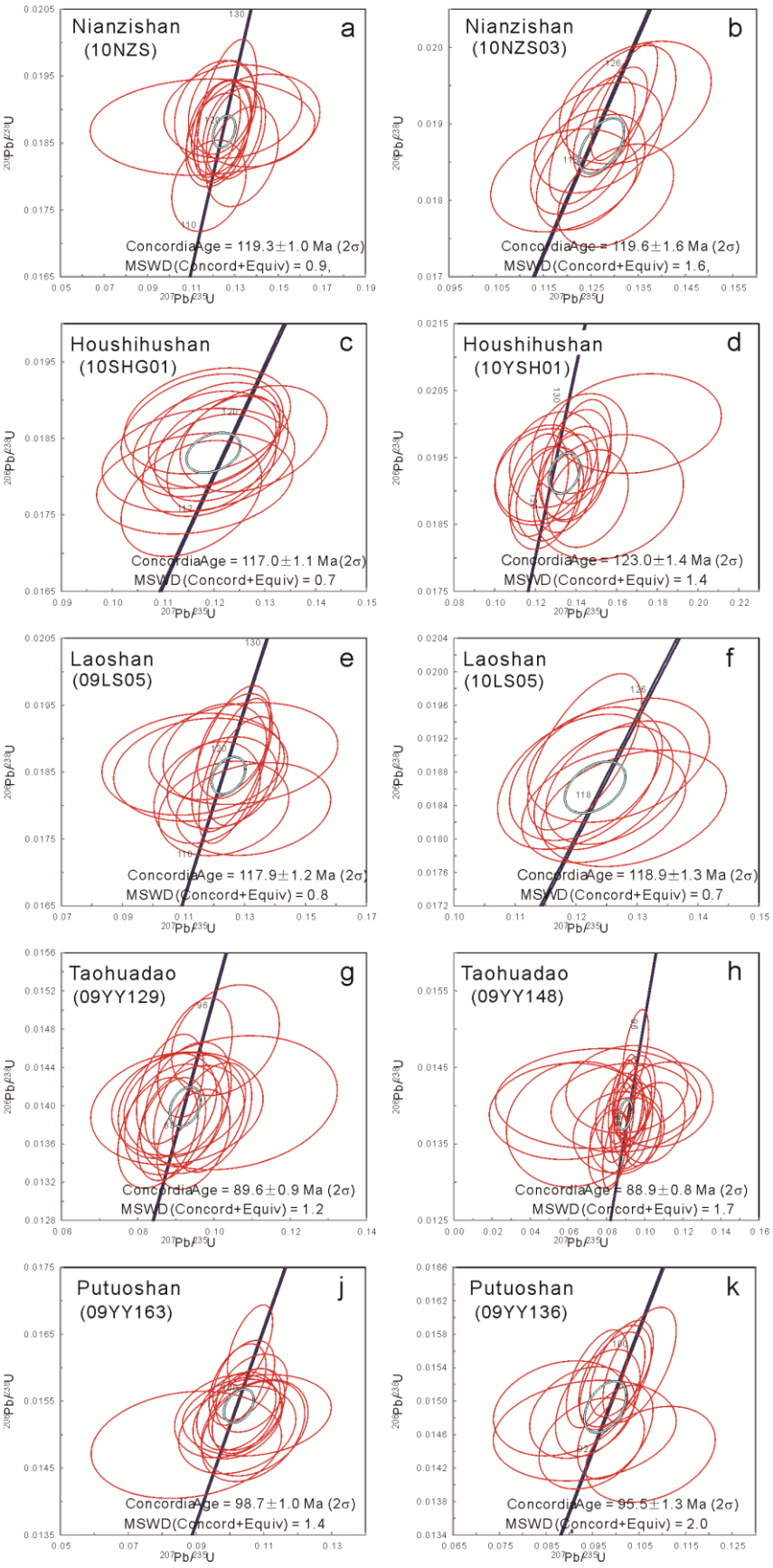


Figure 7.11 U-Pb concordia diagram for zircons from the six A-type granites.

Houshihushan

Zircons from the Houshihushan alkaline A-type granite (10SHG01) range from 50 to 200 μm in length, and have length to width ratios mostly between 1:1 and 1:2. Most crystals show concentric zoning under CL (Figure 7.10). A portion of the zircons are small and irregular, with complex patterns in CL image. Sixteen analyses of 16 zircons were obtained. Four grains have relatively high U contents and high common Pb and were excluded from the age calculation. The remaining zircons have normal contents of U (190 – 386 ppm) and Th (102 – 432 ppm), with relatively constant Th/U ratios (0.5 – 1.1). All the measured Pb-U isotopic ratios are concordant within analytical errors. The weighted mean of $^{206}Pb/^{238}U$ is 0.01835 ± 0.00030 (1σ), corresponding to an age of 117 ± 1.1 (2σ, MSWD = 0.7, Figure 7.11c), which is taken as the best estimate of the crystallization age for the Houshihushan A-type granites. This age is consistent with the LA-ICP U-Pb zircon age of 117 ± 1 Ma from Yang, 2008.

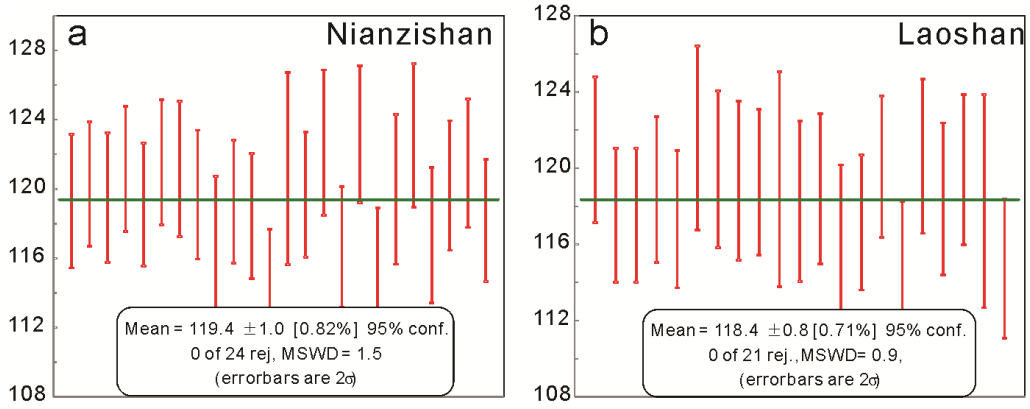


Figure 7.12 Weighted average of the a) Nianzishan and b) Laoshan plutons

Zircons from the Houshihu rhyolite (10YSH01) are smaller than those from the alkaline granite, ranging from 50 to 150 μm in length. Most crystals show concentric zoning under CL (Figure 7.10). Fourteen analyses were obtained on 14 zircons. All the zircons have relatively low contents of U (45 – 111 ppm) and Th (30 – 96 ppm), with Th/U ratios (0.5 – 1.0). All the analysed spots have very low common Pb with f_{206} <

1.1%. The weighted mean of $^{206}Pb/^{238}U$ is 0.01928 ± 0.00034 (1σ), corresponding to an age of 123.0 ± 1.4 (2σ, MSWD = 1.4, Figure 7.11d). The volcanic rocks of the Houshihushan ring complex thus have similar ages to those of the intrusive rocks, confirming it as a volcanic-intrusive complex.

Laoshan

Zircons from the Laoshan alkaline A-type granite (09LS05) and I-type quartz syenite (10LS05) are mostly euhedral, range from 50 to 150 μm in length, and have length to width ratios mostly between 1:1 and 1:2. Most zircons show a clear euhedral concentric zoning under CL (Figure 7.10). Twelve analyses were obtained of 12 zircons from 09LS10. These zircons have moderate contents of U (57 – 387 ppm) and Th (89 – 601 ppm), with Th/U ratios 1.3 – 2.4. The proportion of common ^{206}Pb in total measured ^{206}Pb is quite low with values of 0 – 1.2%. The measured Pb/U isotopic ratios are concordant within analytical errors (Figure 7.11). The weighted mean of $^{206}Pb/^{238}U$ is 0.01846 ± 0.00031 (1σ), corresponding to a Concordia age of 117.9 ± 1.2 (2σ, MSWD = 0.8).

Nine analyses were obtained from 9 zircons from the I-type granite (10LS05). These zircons have higher contents of U (167 – 606 ppm) and Th (135 – 992 ppm) than zircons from the alkaline granites. All the analytical spots have low common Pb, with f_{206} values 0.0–0.4%. The weighted mean of $^{206}Pb/^{238}U$ is 0.01863 ± 0.00024 (1SD), corresponding to a concordia age of 118.9 ± 1.3 (2σ, MSWD = 0.7). The ages of the two phases of the Laoshan pluton are identical within analytical errors (Figure 7.12b). Therefore, the crystallization age for the Laoshan granite is taken as 118.4 ± 0.8 Ma.

Taohuadao

Zircons from the Taohuadao alkaline A-type granite sample (09YY129) are relatively small, range from 50 to 300 μm in length, and have length to width ratios

mostly between 1:1 and 1:2. They are are characterized by irregular crystal forms indicative of corrosion. Sixteen zircons were selected for U-Pb dating and 16 analyses were obtained. These zircons have normal contents of U (157 – 380 ppm) and Th (140 – 708 ppm) with Th/U ratios 0.9 – 3.2. Three spots with high proportions of common ^{206}Pb were eliminated from the age calculation. The measured Pb/U ratios are concordant within analytical errors (Figure 7.11g). The concordia age is 89.6 ± 0.9 Ma (2σ, MSWD = 1.2).

Zircons from Sample 09YY148 are large (200-500 μm in length) and show complex patterns in CL images. Zircons from this sample are. These zircons have highly variable contents of U (238 – 1299 ppm) and Th (182 – 2140 ppm), with Th/U ratios between 0.2 and 1.7. Twenty-three analyses were obtained from 16 zircons with relatively simple and bright CL images. Ten analytical spots have high common Pb with f_{206} > 1%; two of them with extremely large errors were eliminated from the age calculation. The concordia age is 88.9 ± 0.8 (2σ, MSWD = 1.7, 95% confidence interval), overlapping within analytical errors with 09YY129. Therefore, the crystallization age for the Taohuadao granite is accepted as 88.9 ± 0.5 Ma (Figure 7.13a).

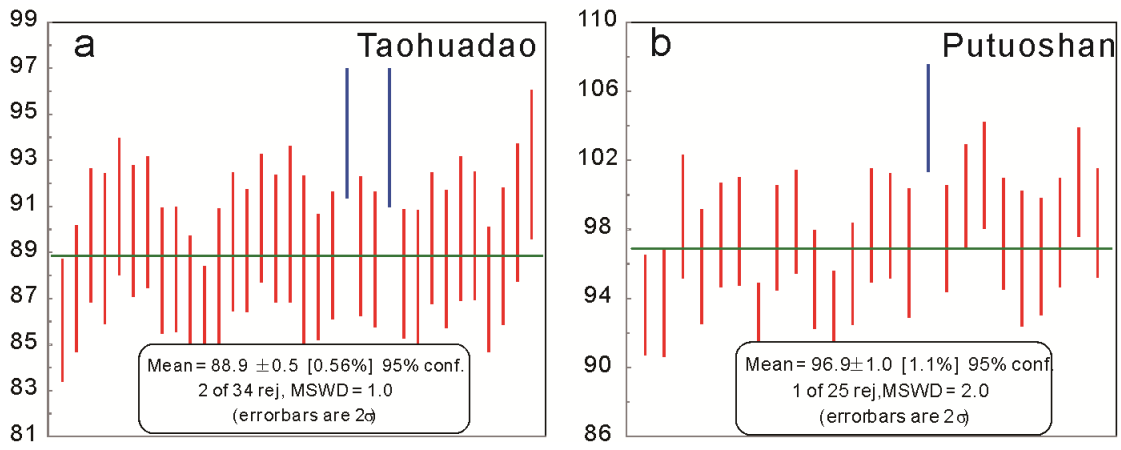


Figure 7.13 Weighted average of the a) Taohuadao and b) Putuoshan plutons

Putuoshan

Zircons from the Putuoshan I-type biotite granite phase (09YY163) are relatively small and rectangular, 100 – 200 μm in length, and have length to width ratios of 1:1 to 1:3. Most of the crystals have euhedral oscillatory zoning. Among them, some show dark CL images, indicative of very high U and Th contents. Sixteen analyses were obtained on 16 zircons. The Putuoshan zircons have highly variable concentrations of U, from 43 – 1373 ppm, and Th from 73 – 1331 ppm, with Th/U ratios (0.2 – 2.4). Apart from three spots, all analyses have very low common Pb with f_{206} = 0.0% – 0.9%. The weighted mean $^{206}Pb/^{238}U$ age is 98.7 ± 1.0 Ma (2σ, MSWD = 1.4) (Figure 7.11)

Zircons from the alkaline A-type granite (09YY136) are mostly prismatic and 50~150μm in length, with length to width ratios of 1:2 to 1:4. Most of the crystals have euhedral oscillatory zoning. All of the zircons except two have normal concentrations of U (83 – 854 ppm) and Th (156 – 463 ppm). Most zircons have very low common Pb with f_{206} < 0.04 ~ 0.82%. Excluding the one high-U zircon, the weighted mean of $^{206}Pb/^{238}U$ age is 95.5 ± 1.3 Ma (2σ, MSWD = 2.0), overlapping with the alkaline granite phases within analytical errors (Figure 7.13b).

.

Table 7-1 Summaries of Hf-O-Li isotopes of six studied plutons

	Zircon *in situ* Hf	**$\delta^{18}O$ ‰**		**$\delta^{7}Li$ ‰**			**Quartz *in situ* $\delta^{18}O$ ‰**		**Whole-rock**	
	$\varepsilon Hf_{(t)}$	**Range**	**Average**	**Li ppm**	**max**	**min**	**Range**	**Average**	**Li**	**$\delta^{7}Li$ ‰**
10NZS	8.0 ±1.5	3.8 – 5.2	4.5 ±0.4	0.2 ±0.5	11.8	-2.1	6.5 – 7.6	7.0 ±0.3	46.3	3.1 ±0.3
10NZS03	9.0 ±0.9	3.8 – 5.3	4.4 ±0.4	0.3 ±0.1	6.8	-10.5	6.9 – 7.6	7.1 ±0.2	36.7	2.6 ±0.6
10NZS01	-	4.1 – 5.0	4.6 ±0.2	0.2 ±0.3	9.3	-10.7	6.4 – 7.9	7.3 ±0.3	50.6	2.5 ±0.4
10NZS04	-	4.0 – 5.4	4.7 ±0.4	-	-	-	6.6 – 7.7	7.1 ±0.2	42.7	1.6 ±0.4
10NZS05	-	4.2 – 5.1	4.5 ±0.2	-	-	-	6.6 – 7.5	7.0 ±0.2	38.7	2.3 ±0.5
Summary	8.5 ±1.4	3.8 – 5.4	4.6 ±0.3	-	0.7 ±1.7	-5.2 ±1.0	6.4 – 7.9	7.2 ±0.3	-	-
HSH01	-10.1 ±1.3	5.2 – 5.7	5.4 ±0.2	0.2 ±0.2	2.3	-15.4	7.4 – 8.8	7.8 ±0.3	25.0	1.2 ±0.6
HSH02	-13.7 ±1.0	5.5 – 5.8	5.7 ±0.1	-	-	-	-	-	31.0	2.3 ±0.5
HSH03	-12.8 ±1.2	5.0 – 5.6	5.3 ±0.2	-	-	-	-	-	9.9	3.9 ±0.3
Summary	-13.3 ±1.2	5.0 – 5.8	5.5 ±0.2	-	-5.3 ±2.0	-13.1 ±1.4	7.4 – 8.8	7.8 ±0.3	-	-
LS-A	-20.2 ±1.4	5.1 – 6.0	5.6 ±0.3	0.7 ±0.7	9.1	-5.4	7.1 – 8.7	8.1 ±0.3	13.1	3.2 ±0.4
LS-I	-19.0 ±1.2	4.8 – 6.0	5.3 ±0.3	-			7.5 – 8.4	8.0 ±0.2	57.9	3.3 ±0.3
Summary	-	-	-	-	5.9 ±2.3	-1.1 ±2.1	-	8.1 ±0.3	-	-

THD-01	-3.4 ±1.0	4.6 – 5.1	4.8 ±0.1	0.1 ±0.2	-0.3	-14.8	7.0 – 7.8	7.4 ±0.2	18.6	1.4 ±0.3
THD-02	-	3.4 – 4.8	4.2 ±0.4	1.4 ±2.0	-10.9	-10.9	6.3 – 7.5	7.2 ±0.4	483.9	6.1 ±0.2
	-	-	-	0.1 ±0.2	-4.7	-11.4	7.0 – 7.7	7.3 ±0.2	-	-
	-	-	-	1.5 ±2.2	16.7	-10.7	6.9 – 7.4	7.2 ±0.2	-	-
	-	-	-		5.9	-5.8	6.7 – 8.7	7.7 ±0.6	-	-
Summary	-	-	-	-	6.1 ±2.0	-8.6 ±1.6	-	7.3 ±0.2	-	-
PTS-A	1.2 ±1.5	5.2 – 5.9	5.6 ±0.2	0.8 ±1.2	11.4	-13.3	2.1 – 7.9	4.1 ±1.5	10.7	3.3 ±0.3
PTS-I	-3.5 ±1.2	4.9 – 5.9	5.2 ±0.2	0.2 ±0.1	13.0	-3.1	7.8 – 8.6	8.0 ±0.2	11.5	1.8 ±0.2
	-	-	-	-	-	-	7.7 – 8.6	8.1 ±0.2	-	-
	-	-	-	-	-	-	7.8 – 8.5	8.1 ±0.2	-	-
Summary	-	4.9 – 5.9	5.4 ±0.3	-	5.5 ±3.3	-7.7 ±3.7	-	8.1 ±0.1	-	-
SZ-01	-5.3 ±1.8	4.6 – 5.7	5.4 ±0.3	0.4 ±0.8	6.9	-6.3	7.5 – 8.3	7.8 ±0.2	21.4	2.7 ±0.2
SZ-02	-5.7 ±1.9	4.4 – 6.0	5.4 ±0.3	0.5 ±0.4	10.7	-3.2	7.1 – 8.2	7.5 ±0.3	13.5	10.7 ±1.2
SZ-03	-5.9 ±1.0	3.7 – 5.6	5.3 ±0.4	0.9 ±1.5	3.7	-13.6	7.2 – 8.0	7.7 ±0.2	69.2	1.4 ±0.1
SZ-04	-5.3 ±1.2	4.0 – 5.6	5.3 ±0.3	0.3 ±0.2	4.6	-7.5	7.3 – 8.8	7.8 ±0.4	83.3	3.2 ±0.4
Summary	-5.5 ±1.5	3.7 – 6.0	5.3 ±0.5	-	3.2 ±0.8	-3.1 ±0.9	-	7.7 ±0.3	-	-

7.1.3 *In situ* Hf-O-Li isotopes

Zircons dated for U–Pb ages were also analysed for Lu-Hf, O and Li isotopes; Quartz grains from corresponding samples also were analysed for O isotopes. The data are presented in Appendix table iv - viii and results are summarised in Table 7-1. Initial $^{176}Hf/^{177}Hf$ ratios, denoted as $\varepsilon Hf_{(t)}$ values, and Hf model ages were calculated based on crystallization ages from the U-Pb dating

Nianzishan

Fifty-one *in situ* Hf, thirty-six *in situ* Li, and one hundred and eighty-seven O isotopic analyses were conducted on the Nianzishan zircons (including zircons that were measured for U-Pb). One hundred and seven O isotopic analyses were conducted on the Nianzishan quartz grains. The measured zircons have homogeneous Hf compositions: $^{176}Hf/^{177}Hf$ = 0.283015 – 0.282851, corresponding to $\varepsilon Hf_{(t)}$ = 5.2 – 10.9. The measured Hf isotopes define a normal Gaussian distribution (Figure 7.14a), with an average of $^{176}Hf/^{177}Hf$ = 0.282940 ± 0.000040. Five zircons and corresponding quartz samples of the Nianzishan A-type granites have been analysed. The results of the five samples are identical within error and a summary of each sample is listed in Table 7-1. As in the Suzhou granites, the zircons of Nianzishan can be divided into two groups based on reflected-light photos, CL imagery and U content. The group with high U and Th has a D_{dpa} higher than 0.08 and shows the "high-U matrix effect". These results have been screened and eliminated from data plot. The screened $\delta^{18}O$ values range from 3.8‰ – 5.4‰, and define a normal Gaussian distribution (Figure 7.14c), with an average of $\delta^{18}O$ = 4.6‰ ± 0.6‰ (2σ). The $\delta^{18}O$ of quartz grains range from 6.5 to 7.6 and form a normal Gaussian distribution (Fig 7.14d) with an average of 7.2 ± 1.0 ‰.

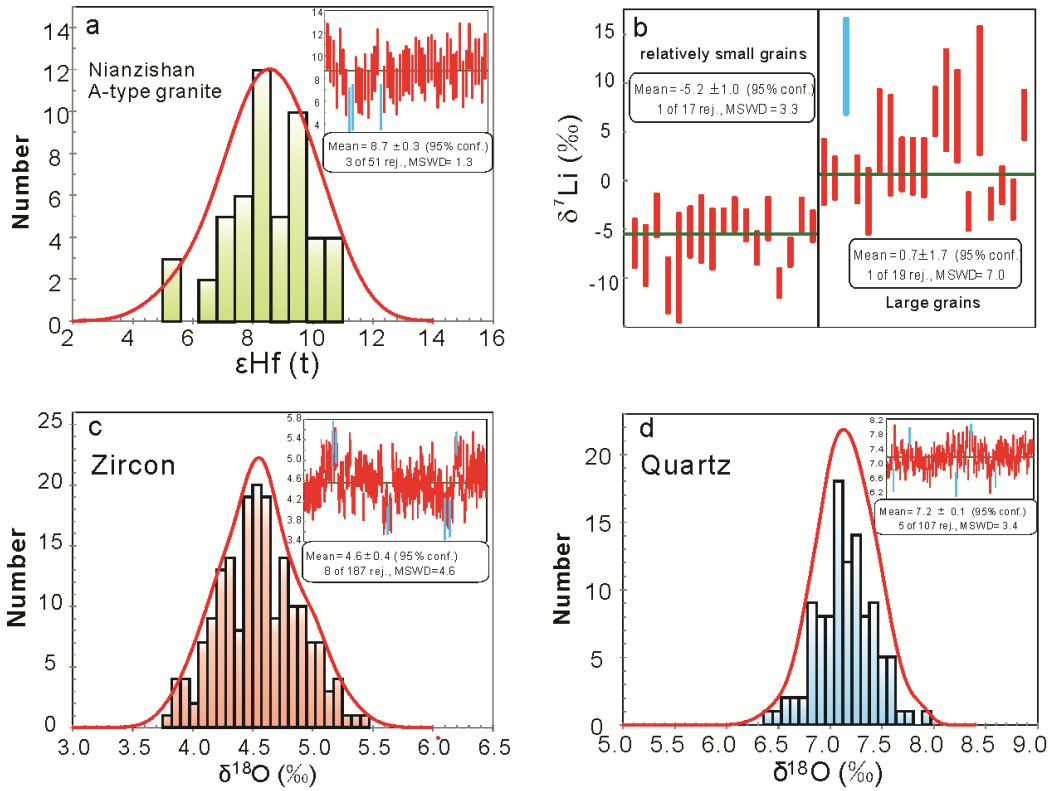


Figure 7.14 a) Histogram and weighted average of $\varepsilon Hf_{(t)}$ values for the Nianzishan zircons; b) Weighted average of δ^7Li values for Nianzishan zircons; Histogram and weighted average of $\delta^{18}O$ values for the Nianzishan: c) zircon and d) quartz.

Zircon *in situ* Li isotope data are collected from the center of the select grains (see chapter 5 and 6). The results can be divided into two groups (Figure 7.14b) based on the grain size and zircon crystal shape. Large and euhedral zircons have a weighted average $\delta^7Li = 0.7 \pm 1.7$ ‰ while the smaller and broken grains have a weighted average $\delta^7Li = -5.2 \pm 1.0$ ‰.

Houshihushan

Sixty-two *in situ* Hf, fifteen *in situ* Li, and thirty-eighty O isotopic analyses were conducted on the Houshihushan zircons (including zircons that were measured for U-Pb). Twenty-five O-isotope analyses were conducted on quartz grains from Houshihushan.

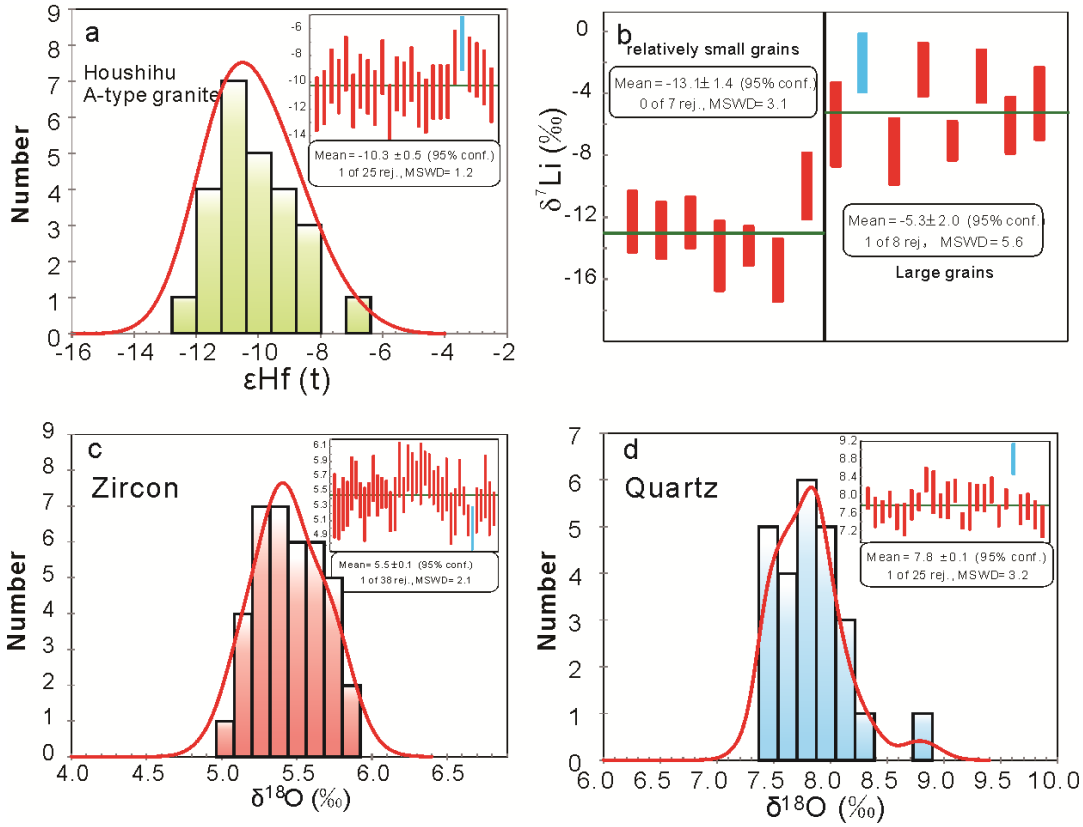


Figure 7.15 a) Histogram and weighted average of $\varepsilon Hf_{(t)}$ values for the Houshihushan zircons; b) Weighted average of δ^7Li values for Houshihushan zircons; Histogram and weighted average of $\delta^{18}O$ values for the Houshihushan: c) zircon and d) quartz.

The two measured zircon samples from alkaline A-type granites have homogeneous Hf compositions ranging from 0.282284 – 0.282505, corresponding to $\varepsilon Hf_{(t)}$ = –14.7 to –7.1. The zircons from the rhyolite have similar $\varepsilon Hf_{(t)}$ from –14.9 to –11.6. Moreover, in terms of O isotopes, zircons from alkaline A-type granites and rhyolite are identical within error. Three zircons and one corresponding quartz sample of the Houshihushan complex have been analysed. As in the Suzhou granites, the zircons of the Houshihushan also have high U contents and the show "high-U matrix effect". These results have been screened and eliminated from the data plots. The screened O isotopic data range from 5.0‰ – 5.8‰, and form a normal Gaussian distribution (Figure 7.15c), with an average of $\delta^{18}O$ = 5.5‰ ± 0.4‰ (2σ). The $\delta^{18}O$ of quartz ranges from 7.4 to 7.8, with an average of 7.8 ± 0.6 ‰.

Zircon *in situ* Li isotopes have been divided into two groups as the Nianzishan zircons (Figure 7.15b). Zircons with large grains have a weighted mean of δ^7Li = -5.3 ± 2.0 ‰ while the smaller grains have a weighted mean of δ^7Li = -13.1 ± 1.4 ‰.

Laoshan

Forty-six *in situ* Hf, fifteen *in situ* Li, and sixty-one O isotopic analyses were carried out on zircons from the Laoshan alkaline granite and the related quartz syenite. Forty-eight O-isotope analyses were conducted on the corresponding quartz samples. The zircons from the Laoshan alkaline granites and quartz syenite have similar Hf-O isotopes. The results are listed in Table 7-1 and presented in Figure 7.16 a-d.

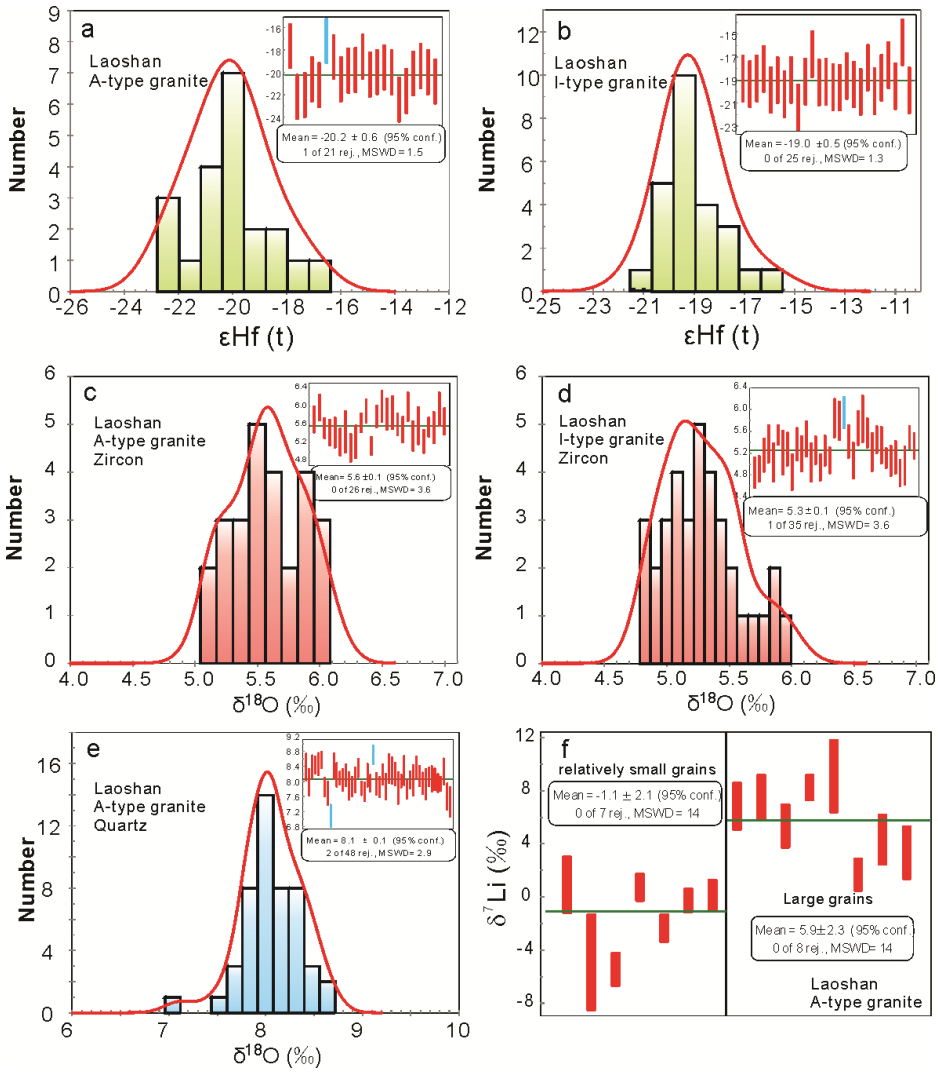


Figure 7.16 Histogram and weighted average of $\varepsilon Hf_{(t)}$ valuse of zircon from the Laoshan

a) A-type granite; b) Histogram and weighted average of $\delta^{18}O$ values for Laoshan c) zircon from A-type granite; d) zircon from I-type granite; e) quartz from A-type granite; f) Weighted average of $\delta^{7}Li$ values of zircons from Laoshan A-type granite.

The $^{176}Hf/^{177}Hf$ ranges from 0.282071 to 0.282266, corresponding to $\varepsilon Hf_{(t)}$ from -22.4 to -15.7. The oxygen isotopes give typical mantle values with an average of $\delta^{18}O$ = 5.4‰ ± 0.6‰ (2σ). The $\delta^{18}O$ values of quartz range from 6.5 to 7.6 and define a Gaussian distribution (Figure 7.16e) with an average of 8.1 ± 0.6 ‰ (2σ).

Zircon *in situ* Li isotopes have also been divided into two groups (Figure 7.16f). Zircons with large grains have a weighted average of $\delta^{7}Li$ = 5.9 ± 2.3 ‰ while the smaller grains have a weighted average of $\delta^{7}Li$ = -1.1 ± 2.1 ‰.

Suzhou

Seventy-four Hf-isotope analyses were taken in the same zones of the zircons used for U-Pb analyses (Figure 7.17).

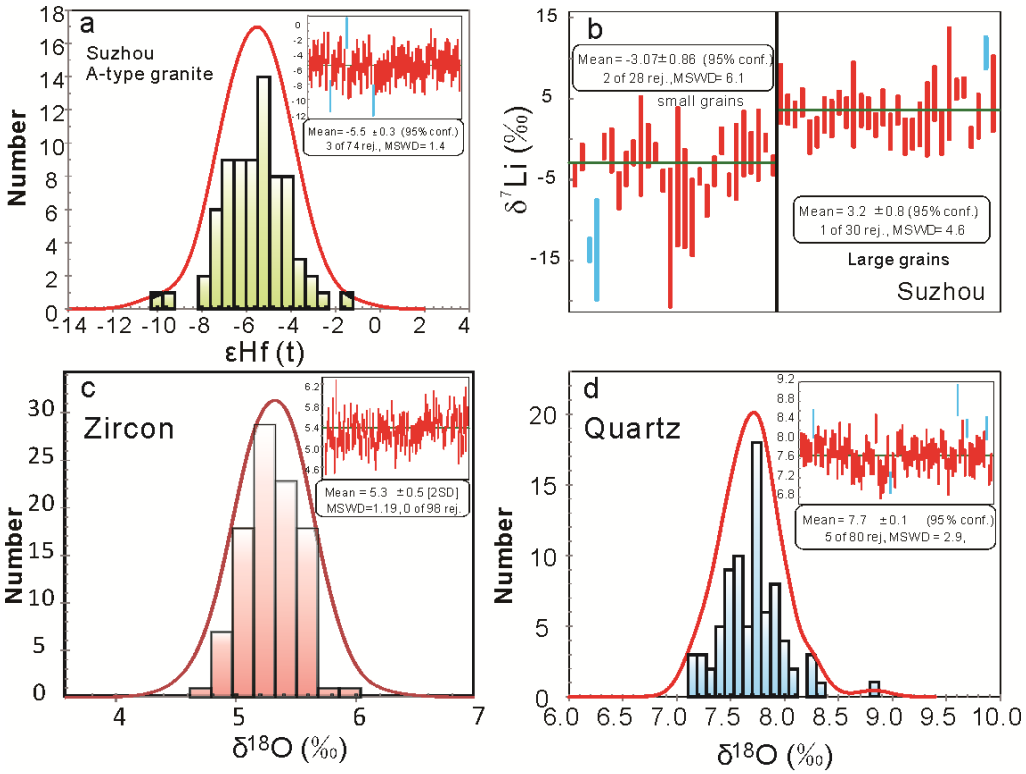


Figure 7.17 a) Histogram and weighted average of $\varepsilon Hf_{(t)}$ values for the Suzhou zircons; b) Weighted average of $\delta^{7}Li$ values for Suzhou zircon; Histogram and weighted average

$\delta^{18}O$ values for the Suzhou c) zircon and d) quartz.

They fall in a tight range of $^{176}Hf/^{177}Hf$ ratios, from 0.282435 to 0.282667, with $\varepsilon Hf_{(t)}$ values ranging from -10.1 to -1.3. The highest and lowest values are both found in the albitized K-feldspar granite, in which zircon has higher U concentrations than other zircon grains. The results display a gaussian distribution with weighted average $\varepsilon Hf_{(t)}$ of -5.6. The oxygen isotopes of the Suzhou granites are in the mantle range and have been discussed in detail in Chapter 4.

Zircon *in situ* Li isotopes has been divided into two groups (Figure 7.17b). Zircons with large grains have a weighted average $\delta^7Li = 3.2 \pm 0.8$ ‰ while the smaller grains have a weighted average $\delta^7Li = -3.1 \pm 0.9$ ‰.

Taohuadao

Twenty-five *in situ* Hf-isotope, thirty-five *in situ* Li-isotope, and fifty-two O-isotope analyses were conducted on the Taohuadao zircons (including 20 zircons that were analysed for U-Pb). Eighty-five O-isotope analyses were conducted on the corresponding quartz grains. The measured zircons have very homogeneous Hf compositions: $^{176}Hf/^{177}Hf = 0.282574 – 0.282695$, corresponding to $\varepsilon Hf_{(t)} = -5.2 – -1.0$. The measured Hf isotopes form a Gaussian distribution (Figure 7.18a), with an average value of $^{176}Hf/^{177}Hf = 0.282620 \pm 0.000030$. Zircons from two samples and five corresponding quartz samples of the Taohuadao A-type granites have been analysed. Zircons from 09YY148 have unique CL images which indicates that they might be hydrothermal. The screened O isotopes of the Taohuadao zircons range from 4.6‰ – 5.1‰. The $\delta^{18}O$ values of the five quartz samples are identical within error. The measured O isotopes form a Gaussian distribution (Figure 7.18d), with an average $\delta^{18}O = 7.3‰ \pm 0.4‰$ (2σ).

Zircon *in situ* Li isotopes have been divided into two groups (Figure 7.18b).

Zircons with large grains have a weighted average δ^7Li = 6.1 ± 2.0 ‰ while the smaller grains have a weighted average δ^7Li = -8.6 ± 1.6 ‰.

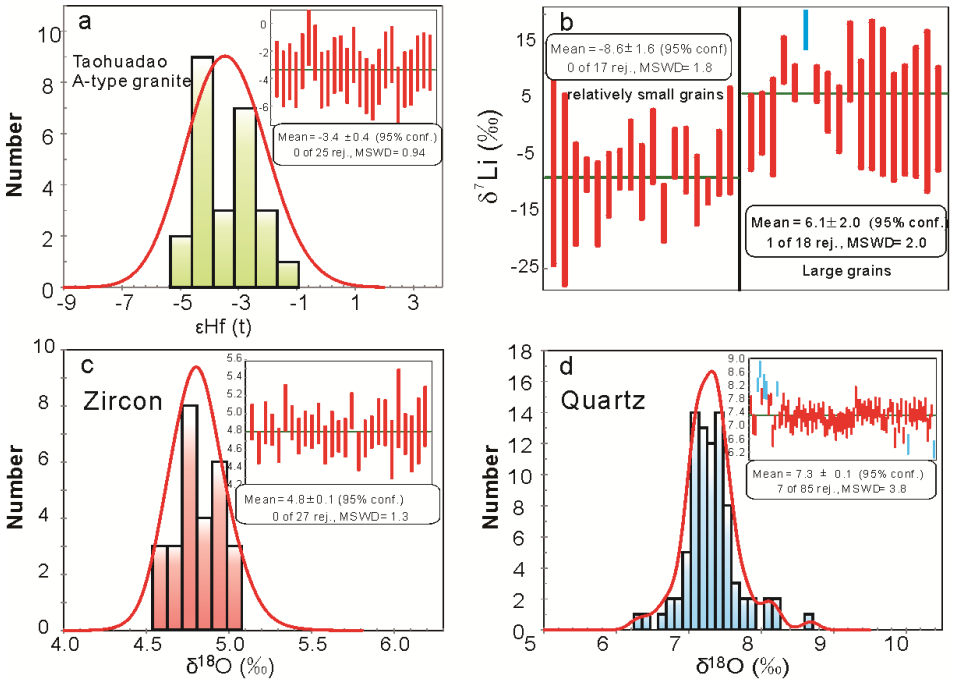


Figure 7.18 a) Histogram and weighted average of $\varepsilon Hf_{(t)}$ values for the Taohuadao zircons; b) Weighted average of δ^7Li values for Taohuadao zircons; Histogram and weighted average $\delta^{18}O$ for the Taohuadao: c) zircon and d) quartz.

Putuoshan

Sixteen *in situ* Hf-isotope analyses and eighteen O-isotope analyses were conducted on zircons from the Putuoshan alkaline granites. $^{176}Hf/^{177}Hf$ ranges from 0.282681 to 0.282862, corresponding to $\varepsilon Hf_{(t)}$ from -1.4 to 5.1. The oxygen isotopes of zircons give mantle values with an average of $\delta^{18}O$ = 5.6‰ ± 0.4‰ (2σ). Twenty *in situ* Hf- and O-isotope analyses were conducted on zircons from the Putuoshan biotite granites. $^{176}Hf/^{177}Hf$ ranges from 0.282551 to 0.282670, corresponding to $\varepsilon Hf_{(t)}$ from -5.7 to -1.6, a little lower than the $\varepsilon Hf_{(t)}$ of the alkaline granites. The zircons from biotite granites have $\delta^{18}O$ = 5.2 ± 0.4 ‰ (2σ). The alkaline and biotite granites have identical zircon and quartz oxygen isotopes. The $\delta^{18}O$ values of quartz range from 7.7 to 8.7 and

define a normal distribution (Figure 7.19e) with an average $\delta^{18}O$ of 8.1 ± 2.0 ‰ (2σ).

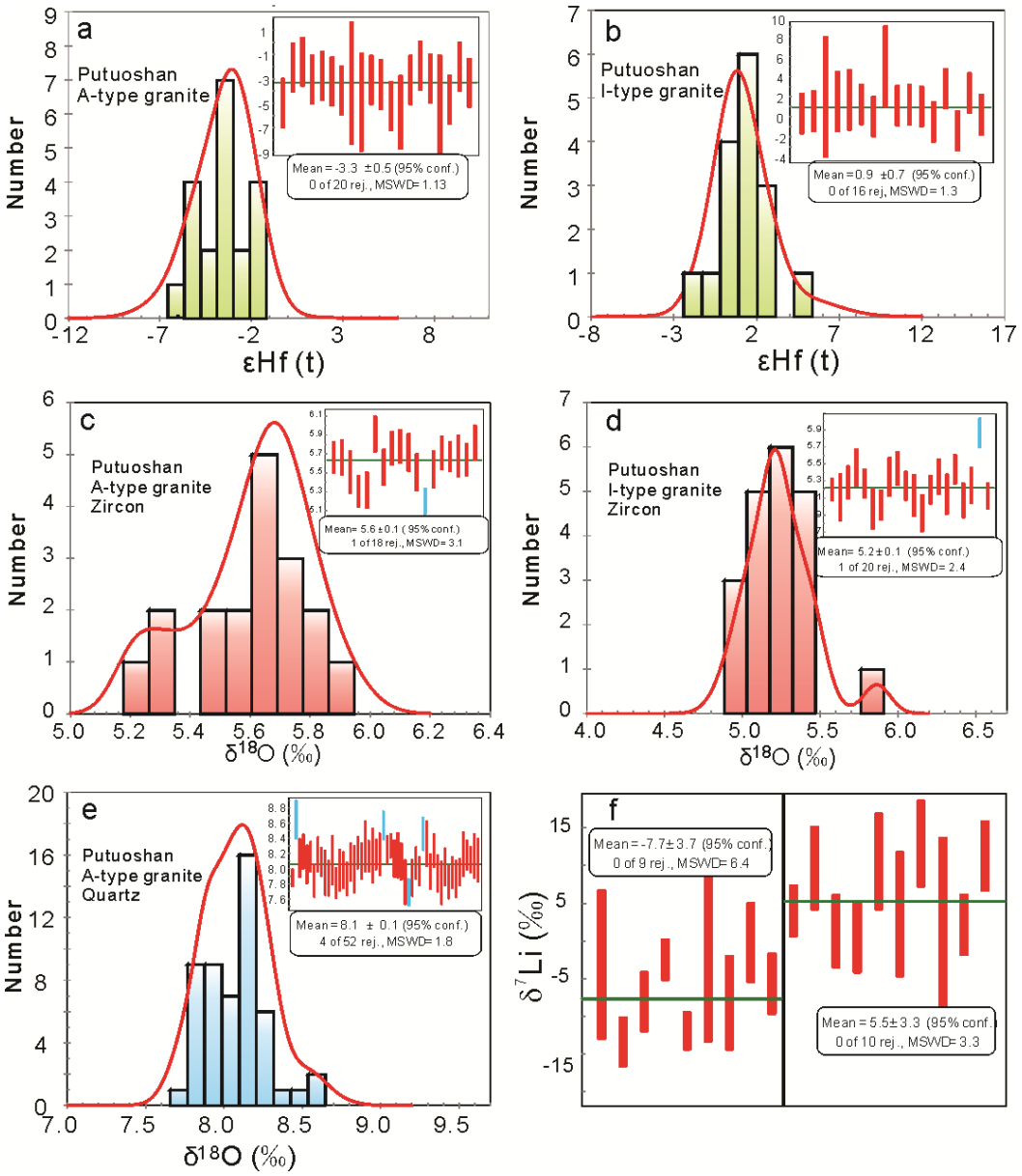


Figure 7.19 Histogram and weighted average of $\varepsilon Hf_{(t)}$ value of zircon from the Putuoshan a) A-type granite; b) I-type granite; Histogram and weighted average of $\delta^{18}O$ values for the Putuoshan c) zircon from A-type granite; d) zircon from I-type granite; e) quartz from A-type granite; f) Weighted average of $\delta^{7}Li$ value of zircons from Putuoshan A-type granite.

Zircon *in situ* Li isotopes have been divided into two groups (Figure 7.19f). Zircons with large grains have a weighted average $\delta^{7}Li$ = 5.5 ± 3.3 ‰ while the smaller grains have a weighted average $\delta^{7}Li$ = -7.7 ± 3.7 ‰.

7.1.4 Whole-rock Lithium isotopes

The samples used *in situ* Hf-O-Li isotope analysis of zircons and quartz were used for analysis of whole-rock Li isotopes; results are summarised in Table 7-1.

The Nianzishan pluton (5 samples) shows a limited range of Li abundances (37–51 ppm) and δ^7Li (1.6 to +3.1‰). The Suzhou granite (4 samples) has variable Li concentrations (13 – 83 ppm) and δ^7Li (1.4 to +10.7‰). The Taohuadao granite (2 samples) shows a uniform [Li] = 15 to 19 ppm, but variable δ^7Li (1.4 to 6.1‰). Except for one sample from the Taohuadao pluton and one sample from the Suzhou pluton, which have relatively high δ^7Li (6.1‰ and 10.7‰, respectively), the δ^7Li of the six plutons are very similar. The mean δ^7Li value of 1.4 ± 0.80‰ (2SD) for the Taohuadao pluton is the lowest, whereas the highest average δ^7Li of 3.2 ± 0.2‰ (n = 3) is found in the Laoshan pluton. The average δ^7Li values for the Nianzishan (2.5 ± 1.2‰ (n = 4)), Houshihushan (2.7 ± 2.4‰ (n = 2)), Suzhou (2.4 ± 1.8‰ (n = 3) and Putuoshan (2.5 ± 2.2‰ (n = 2)) plutons are identical within error. The two samples with higher δ^7Li are considered to be caused by later weathering, which is confirmed by their slightly higher LOI.

7.2 DISCUSSION

7.2.1 The A-type granite magmatic episode

Although several studies have previously reported aspects of the geochronology of six studied A-type granites, there is still inconsistency among references concerning their age (Yang et al., 2008). For example, the Suzhou A-type granites have long been regarded as consisting of multiple intrusions that can be divided into 3 stages (Ouyang, 1985, Wang et al., 1993, Chen et al., 1993, Charoy and Raimbault 1994). However, it is now proved to be formed of a single magmatic period (Gao et al., 2014)(see chapter 4).

The SIMS U-Pb dating in this study provides high precision, high quality geochronology data for the six studied granites. Table 7-2 summarises the present dating results for these A-type granites. The previous Rb-Sr isochron and K-Ar ages usually have large differences because of the relatively low closure temperature of the Rb-Sr and K-Ar systems. Most of the previous U-Pb dating results are from LA-ICP-MS and are consistent with our SIMS results. The high-precision SIMS results show that the Nianzishan, Houshihushan and Laoshan plutons are coeval and are consistent with the age peak (110 – 130 Ma) of the Mesozoic magmatism in the eastern North China Craton (Sun and Yang, 2009). These granites are therefore coeval with the mineralization age of large-scale gold deposits and the formation of the metamorphic core complexes in the eastern North China Craton. This is consistent with the geological evidence for an extensional setting in the Northeast China during the Early Cretaceous. It is suggested that the A-type granites and related alkaline rocks were formed in such an extensional setting and were the shallow responses to the lithospheric thinning and decratonization; the granites thus mark the peak of lithospheric thinning and craton-root destruction in the North China Craton.

The Suzhou, Putuoshan and Taohuadao plutons are important components of the Late Yanshanian magmatic belt. A compilation of present and previous geochronological data for all the intrusive rocks along the southeastern coast of China indicates that the large-scale Late Yanshanian magmatism occurred mainly from around 126 to 89 Ma ago. The Suzhou A-type granites and other coeval A-type granites mark the beginning of the extension during the Early Cretaceous. The subsequent development of bimodal magmatism at 115 to 89 Ma suggests that this major igneous event was the product of extension of the overlying continental lithosphere driven by the break-off and rollback of the flat-subducting Palaeo-Pacific Plate during the

Cretaceous (Li et al., 2007; Li and Li, 2007; Li et al., 2012; Zhu et al., 2013). The Taohudao granites mark the end of the Late Yanshanian regional tectono-magmatic evolution in the area.

Table 7-2 present dating results of studied A-type granites.

Pluton	**Petrology**	**Dating method**	**Age (Ma)**	**Reference**
Nianzishan	Alkaline granite	K-A r	123 ±2	Li, 1993
		Rb-Sr isochron	123 ±8. 6	Li, 1993
		SIMS U-Pb	119 ±1	this study
		SIMS U-Pb	119.6 ±1.6	this study
Houshihushan	Alkaline granite	Rb-Sr isochron	113 ±12	Xu, 1998
	Trachydacite	K-Ar	125	Xu, 1999
	Volcanic tuff	K-Ar	117	Xu, 1999
	Alkaline granite	LA-ICP-MS	118 ±1	Yang, 2008
	Syenite	LA-ICP-MS	120 ±1	Yang, 2008
	Rhyolite	LA-ICP-MS	120 ±1	Yang, 2008
	Trachydacite	LA-ICP-MS	119 ±1	Yang, 2008
	Quartz Syenite	LA-ICP-MS	119 ±3	Wen, 2013
	Granite porphyry	LA-ICP-MS	121 ±2	Wen, 2013
	Alkaline granite	SIMS U-Pb	117.1 ±1.1	this study
	Trachydacite	SIMS U-Pb	123.0 ±1.4	this study
Laoshan	Alkaline granite	K-Ar	104. 5 ±1. 2	Zhao, 1998
	K-feldspar	K-Ar	101. 3 ±1. 3	Zhao, 1998
	Alkaline granite	Rb-Sr isochron	134 ±2. 2	Zhao, 1998
	Alkaline granite	Rb-Sr isochron	110. 7 ±3. 9	Gui, 1989
	Biotite granite	Rb-Sr isochron	～146	Gui, 1989
	Alkaline granite	TIMS U-Pb	110. 8 ±0. 8	Zhao, 1997
	Alkaline granite	TIMS U-Pb	113 ±1	Zhao, 1997
	Alkaline granite	SHRIMP	115	Goss, 2010
	Alkaline granite	SIMS U-Pb	117.9 ±1.2	this study

	Syenogranite	SIMS U-Pb	118.9 ±1.3	this study
Suzhou	Alkaline granite	Bi Ar–Ar	123	Chen, 1993
	Alkaline granite	Rb-Sr isochron	108 ±10	Wei, 2001
	Alkaline granite	TIMS U-Pb	110 ±1	Zhao,1997
Putuoshan	Alkaline granite	TIMS U-Pb	93.6 ±0.4	Xie, 2000
	Biotite granite	SIMS U-Pb	95.53 ±1.3	this study
	Alkaline granite	SIMS U-Pb	98.88 ±1.0	this study
Taohuadao	Alkaline granite	TIMS U-Pb	92.9 ±0.6	Qiu, 1999
	Alkaline granite	SIMS U-Pb	89.6 ±0.8	this study
	Alkaline granite	SIMS U-Pb	89.2 ±1.2	this study

7.2.1 Oxygen isotopes of A-type granites

The Nianzishan, Houshihushan (also known as Shanhaiguan in some of the literature), Laoshan and Suzhou granites have been defined as low-$\delta^{18}O$ A-type granites by bulk analysis of zircon separates (Wei et al., 2008). Table 7-3 summarises the oxygen isotope data of whole-rock samples, bulk zircon and quartz from the previous studies. The average bulk-zircon $\delta^{18}O$ values for the Nianzishan, Houshihushan, Suzhou and Laoshan are 3.79 ± 0.80‰ (2SD, n = 17), 4.86 ± 0.84‰ (n = 12), 4.92 ± 0.26‰ (n = 43) and 5.05 ± 0 .28‰ (n = 17), respectively (Wei et al., 2008).

Table 7-3 Summaries the oxygen isotope of whole-rock, bulk zircon and quartz in the previous studies

Pluton	Mineral	$\delta^{18}O_{min}$(‰)	$\delta^{18}O_{max}$(‰)	$\delta^{18}O_{mean}$(‰)	Reference
Nianzishan	Whole-rock	2.4	2		(Zhao et al., 2001)
	Whole-rock	-1	4.7		(Yu et al.,1990)
	Whole-rock	-1.6	2		(Wei et al., 2001)
	Whole-rock			2.1 ±2.4	(Wei et al., 2001)
	Whole-rock	-1.1	5		(Li et al., 1990)
	Quartz	0	5.8		(Zhao et al. 2001)
	Quartz	0.9	5.8		(Wei et al., 2001a)
	Zircon	3.12	4.17		(Zhao et al. 2001)

	Zircon	3.1	4.27	3.79 ±0.8	(Wei et al., 2008)
Houshihushan	Whole-rock	1.6	6.7		(Li and Yu, 1989)
	Whole-rock			4.9 ±1.2	(Wei et al., 2001)
	Zircon	4.07	5.39	4.86 ±0.84	(Wei et al., 2008)
Laoshan	Whole-rock	5.4	8.8		(Li and Wan, 1994)
	Whole-rock			7.1 ±1.6	(Wei et al., 2001b)
	Whole-rock	4.0	11.2		(Zhao and Wang, 1997)
	Whole-rock	5.7	8.2		(Yu et al., 1990)
	Zircon	4.83	5.46	5.05 ±0.28	(Wei et al.,2008)
Suzhou	Whole-rock	5.9	7.7		(Yu et al.,1990)
	Whole-rock	3.5	9.2		(Wei et al., 1999)
	Whole-rock			7.6 ±1.0	(Wei et al., 2001)
	Zircon	4.79	5.06	4.92 ±0 .26	(Wei et al., 2008)

In this study, low-$\delta^{18}O$ zircons (< 4.7‰) have been found in the Nianzishan, Suzhou, Taohuadao and Houshihushan plutons while the SIMS *in situ* oxygen-isotope analyses of zircons from the Laoshan and Putuoshan granites are within the mantle range (5.3 ± 0.6‰, 2SD, Valley et al., 1998; Cavosie et al. 2009).

In the Suzhou granites, there is a strong linear correlation of $\delta^{18}O$ with [U], which is caused by metamictization (see chapter 4). The Nianzishan and Houshihushan granites are similar to the Suzhou granites, which have many high-U zircons. The high-U zircons of the Nianzishan granites have quite low $\delta^{18}O$ (~3.8 ‰). The screened oxygen isotopes of the Nianzishan granites are the lowest of the six granites ($\delta^{18}O$ = 4.56‰). The screened data of the Houshihushan granites give $\delta^{18}O$ 5.45‰ and shows that these are not really low-$\delta^{18}O$ granites. The Taohuadao pluton is a little lower ($\delta^{18}O$ = 4.80‰), but still overlaps with normal mantle $\delta^{18}O$ values.

The oxygen isotope compositions of quartz are an internal check for whether the zircons formed in equilibrium with their host magmas. Figure 7.20 shows the O-isotope fractionation between zircon and quartz in the analysed samples. With the exception of the two hydrothermally-altered samples, $\delta^{18}O$ values of quartz are close to the equilibrium fractionation with zircon at high temperature.

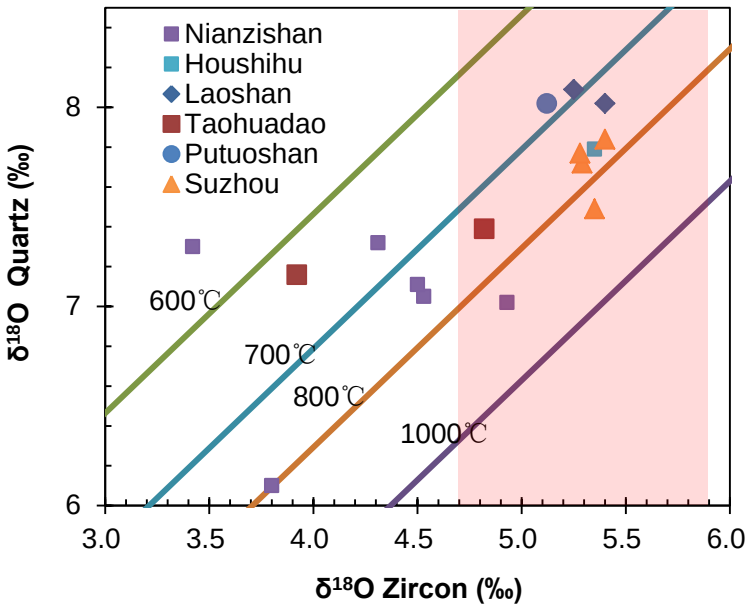


Figure 7.20 Oxygen isotope fractionation between quartz and zircon from the six studied plutons. Thin solid bar of data points represents the 2SD. Solid isotherms are from Valley et al. (2003). The mantle range is shown by the pink box.

The $\delta^{18}O$ values of equilibrium quartz-zircon pairs are interpreted to reflect the primary magmatic oxygen isotopic compositions. Based on the correlation of $\delta^{18}O$ values between zircon and whole rock: $\delta^{18}O_{(Zrc\text{-}WR)} = \delta^{18}O_{(Zrc)} - \delta^{18}O_{(WR)} \approx -0.0612$ (wt% SiO_2) + 2.5 (Valley et al., 2005), the calculated whole-rock $\delta^{18}O$ values of the Nianzishan, Houshihushan, Laoshan, Putuoshan and Taohuadao pluton range from 6.5 – 6.8‰, 7.4 – 7.8‰, 7.4 – 7.7‰, 7.4 – 7.8‰ and 7.1 – 7.5‰, respectively. Therefore, except for the Nianzishan pluton which has slightly lower $\delta^{18}O$, none of the plutons can be considered as 'low-$\delta^{18}O$' A-type granites.

Previous oxygen-isotope studies by the conventional BrF5 method have shown that the Nianzishan A-type granites underwent strong hydrothermal alteration during magmatic emplacement. However, it has been controversial whether the low-$\delta^{18}O$ values are due to post-magmatic alteration or the partial melting of a ^{18}O-depleted protolith. Combined with previous studies, the oxygen isotopes of the Nianzishan

pluton has the following features: 1). the whole-rock and rock-forming minerals (feldspar, magnetite) have widely variable $\delta^{18}O$ values, and show significant isotopic disequilibrium between common rock-forming minerals; 2). the observed zircon $\delta^{18}O$ values of the Nianzishan A-type granite are slightly low and relatively uniform; 3). most of the zircon - quartz pairs exhibit equilibrium oxygen isotope fractionation at magma temperatures. Several models have been proposed to explain the formation of the Nianzishan low-$\delta^{18}O$ A-type granites: 1). The relatively low oxygen isotopes and disequilibrium $\delta^{18}O$ between rock-forming minerals has been reasonably ascribed to meteoric-hydrothermal alteration during subsolidus conditions (Li et al., 1990); 2). water-rock interactions at high temperatures (> 400 ^{o}C) over long periods (> 1 Ma) (Yu et al., 1990; Zhao et al., 2001); 3). partial melting of subducted lower oceanic crust which was isotopically equilibrated with seawater at high temperatures (Wei et al., 2001b; Wei et al., 2008). However, none of above possibilities can be totally ruled out.

7.2.3 Fingerprinting the sources of low-$\delta^{18}O$ A-type granites with Li isotopes

Elliott et al. (2004) have shown potential utility of Li isotopes to track the evolution of the Earth's crust-mantle system. Magna (2010) showed that Li is quite useful in constraining the petrogenesis of A-type granites. Li is quite mobile and Li isotopes are sensitive to fluid/melt-mineral interaction and can be used to provide new constraints on the 'low-$\delta^{18}O$' A-type granites studied here. The fractionation of Li isotopes is dominated by partitioning of Li between solid phases and fluids. There are two main processes that may potentially change $\delta^{7}Li$: 1). Rayleigh-type fractionation (e.g. metamorphic devolatilisation, fractional crystallisation, dehydration, and fluid exsolution); 2). kinetic diffusion driven by mineral-scale concentration gradients.

The upper mantle is inferred to have a $\delta^{7}Li$ equal to that of average MORB, ~ +4 ± 2‰ (Chan et al., 1992, 2002; Tomascak and Langmuir, 1999). Compared to the mantle,

the upper continental crust has an even lighter δ^7Li of 0 ± 2‰ (Teng et al., 2004). Seawater appears to have uniformly high δ^7Li values of ~32‰. The enrichment of isotopically light Li in the continental crust has been explained by magmatic reworking (recycling) of weathered terranes (Teng et al., 2004; Bryant et al., 2004) that had lost their originally heavy Li component during extensive continental weathering (Kısakűrek et al., 2005; Pistiner and Henderson, 2003; Rudnick et al., 2004). Loss of heavy Li also happens during dehydration as ^{7}Li partitions into fluids or melts relative to solid phases. Higher δ^7Li values recorded in the sea water also are attributed to weathering and substantial low-temperature alteration of the oceanic crust to hydrous minerals (such as smectite and phillipsite). Altered oceanfloor basalts have notably heavier δ^7Li values than the mantle (3 – 13‰) and potentially can be used as a tracer to identify ocean-crust recycling (Elliott et al., 2006).

Constraints on the formation of low δ^{18}O magma from Li isotopes

Bindeman and Valley (2001) summarised mechanisms for the generation of low-δ^{18}O magmas: 1). direct, sometimes 'catastrophic' addition of surface fluids into magma (Friedman et al., 1974; Hildreth et al., 1984); 2). more gradual, multistage assimilation of hydrothermally altered rocks (Taylor and Sheppard, 1986; Hildreth et al., 1991); 3). partial melting of the ^{18}O-depleted walls of a magma chamber (Bacon et al., 1989); and 4) wholesale melting and caldera collapse. All of these models require interaction either direct or indirectly with hydrothermal fluids. Thus, Bindeman concludes that the low-δ^{18}O signature ultimately is derived from surface waters. Therefore, it can be anticipated that the low-δ^{18}O rocks will have heavier Li isotope compositions as surface water are characteristically enriched in ^{7}Li (~23‰) relative to most of reservoirs.

In the Nianzishan case, the three models proposed to lower the δ^{18}O also require

the participation of hydrothermal fluids. However, neither whole-rock (δ^7Li = 1.6 to +3.1‰) nor *in situ* (δ^7Li = 0.7 ± 1.7 ‰) Li–isotope analyses of the Nianzishan pluton show isotopically heavy Li. Open-system magma degassing during ascent and emplacement follows the principles of Rayleigh distillation. The process can occur in both deeper and shallow crust (Gerlach, 1986; Dixonetal et. al, 1991; Kyser, 1990; Zheng, 1992). Figure 7.21 shows the variation in δ^{18}O during magma degassing under different temperatures. For a pluton with a primary mantle δ^{18}O value (5.3‰), 20% degassing will account for a 0.7‰ decrease at 300°C and lower the δ^{18}O value to 4.6‰. Moreover, during the degassing of H_2O and CO_2, Li isotopes are most likely remaining the same. Therefore, the possible process that slightly lowers the δ^{18}O of the Nianzishan Pluton is magma degassing from the ascending magma.

Previous δD studies (Li et al., 1992; Chen, 1995; Li, 1995) suggest that the Nianzishan pluton has experienced extreme magma degassing. Integrating the new zircon δ^7Li data, we can suggest that the slightly depleted δ^{18}O of the Nianzishan A-type granites mostly likely was generated during magma degassing.

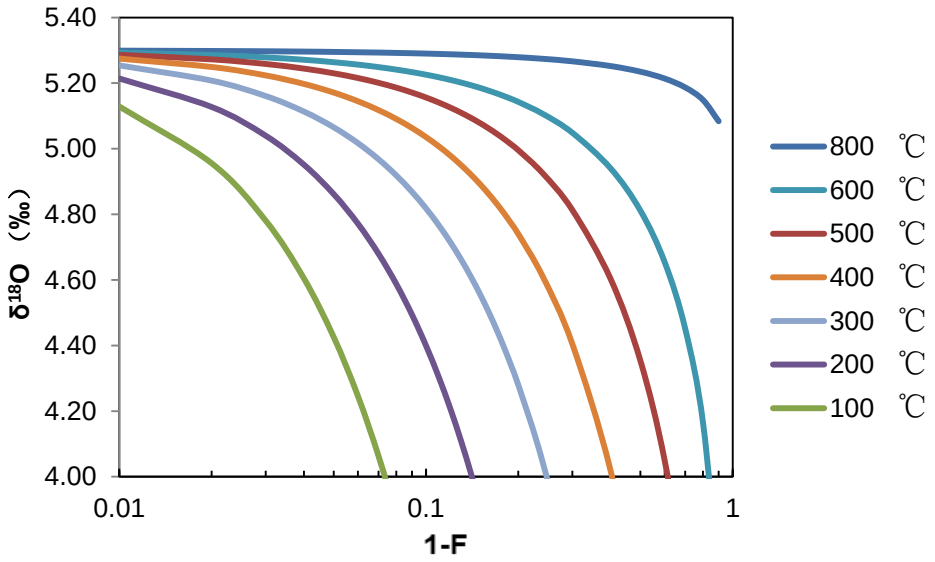


Figure 7.21 δ^{18}O variation during magma degassing under different temperatures

Application of Li isotopes to A-type granites

The origin and genesis of A-type granites has been hotly debated for a long time (seven petrogenetic models were summarised in chapter 1). Primitive-mantle, depleted-mantle, enriched-mantle, mixed crust-mantle and crust-dominant sources have all been proposed in earlier studies. The proposed petrogenetic processes include extraction of melts, magma mixing, extreme fractionation and partial melting. As large δ^7Li variation is observed in fluid-mediated processes, dehydration processes and near-surface processes (Magna et al., 2006a; Tomascak et al., 1999; Wunder et al., 2006), it is anticipated to be quite useful in constraining the origin and petrogenesis of A-type granites.

For example, the partial melting of a F- and/or Cl-enriched, dry, lower crustal granulitic residue left after an earlier extraction of I-type granitic melts (Collins et al., 1982; Clemens et al., 1986) will produce lighter δ^7Li as ^{7}Li and the LILE inventory has been lost by partitioning into the earlier melt. Anatexis of relatively refractory intermediate calc-alkaline meta-igneous crust (Creaser et al., 1991; Skjerlie and Johnston, 1993; Patiño Douce, 1997) produces even lower δ^7Li due to ^{7}Li loss during dehydration process. Derivation from mixed OIB-crustal sources (Eby, 1990; Eby, 1992) and extreme fractionation of mantle-derived magmas emplaced to shallower crustal levels (Turner et al., 1992; Barbarin, 1999) will have produce low [Li] with homogeneous mantle δ^7Li values because Li is only moderately incompatible during mantle melting (Bonin et al., 1998) and fractional crystallization of δ^7Li under high-T conditions is rather limited (Tomascak et al., 1999). The Li signature of magmas derived from mixed crust-mantle sources (Yang et al., 2006) of course depends on the proportion of the end members.

Generally, highly evolved A-type granites are characterized by high abundance of

fluorine (and maybe boron)，as indicated by the presence of fluorite. High F contents in magma system would significantly lower the solidus temperature and viscosity of magmas, which would prolong magma evolution and facilitate extreme fractionation. These highly evolved granites normally were emplaced into high crustal levels, and thus would be in contact with circulating waters. Interaction between granitic melt and UCC country rocks (and circulating fluids therein) should be much more intense than in normal granites.

7.2.4 Origin and Petrogenesis of A-type granites in Eastern China

Zircon is a robust mineral that is highly retentive during most geologic processes. A combined use of *in situ* zircon Hf-O-Li isotopes can place strong constraints on the origin of granites, particularly on deciphering the roles of near-surface weathering, crust/mantle recycling and mantle-derived magmas in granite genesis. $\delta^{18}O$ can restrict the origin of a magma to mantle or crust, while radiogenic $\varepsilon Hf_{(t)}$ traces the time of melting and the evolution of magmas; Li isotopes provides effective constraints on fluid/melt-mineral interaction.

For the analysed samples, aside from two slightly altered ones, the whole-rock Li isotopes are homogeneous and fall into the granite range given by Teng (2004). The *in situ* zircon Li isotopes can be divided into two groups, based on the discussion in Chapter 5 and 6, the negative $\delta^{7}Li$ is caused by diffusion and the higher $\delta^{7}Li$ most likely represents the primitive magma value.

The Nianzishan A-type granites

The Cretaceous Nianzishan A-type granites have an (A_1) anorogenic affinity. Studies suggest that their formation was associated with rifting in eastern China, related to the onset of paleo-Pacific subduction (Wu et al., 2002). Previous Nd-isotope studies of these A-type granites indicate their derivation from a dominantly juvenile crustal

sources which is consistent with the new zircon Hf-isotope data ($\varepsilon Hf_{(t)}$ = +8.7). Previous H-isotope studies suggest the Nianzishan granites experienced magma degassing (Yu et al., 1990; Li et al., 1992; Li, 1995) which can also explain the slightly depleted $\delta^{18}O$ values (~4.6‰) as discussed above. The $\delta^{7}Li$ of the Nianzishan granites is 0.7 ± 1.7 ‰, within the range of upper continental crust ($\delta^{7}Li$ of 0 ± 2‰, Teng et al., 2004).

During the late Mesozoic, the tectonics of NE China were controlled by subduction of the Pacific Plate in the east, which also resulted in lithospheric delamination and was followed by emplacement of the Early Cretaceous anorogenic A-type granites. Therefore, the Nianzishan A-type granites probably are derived from partial melting of a juvenile upper crustal source in response to rise of hot asthenospheric mantle.

The Houshihushan ring complex

The Houshihushan complex is an alkaline ring complex associated with a collapsed caldera. Geochemically, the Houshihushan pluton is very similar to the late Mesozoic Baicha and Kulongshan A-type granites in the Yanshan belt (Wang, 2009). Alkali-feldspar granites are characterized by high $Na_2O + K_2O$, FeO_t/MgO, Ga/Al, Zr, Nb and REE, and low abundances of Al_2O_3, CaO, MgO, Ba, Sr and Eu. They show high zircon saturation temperatures (780 – 801^{o}C).

Based on the previous radiogenic Sr-Nd-Hf isotopic data the Houshihushan granites plot near the field of lower crustal granulites and gneisses and are proposed to be derived from mixing of alkali basaltic magma with crustal-derived melts (Yang et al., 2008).

The Houshihushan alkaline granites and rhyolite have $\varepsilon Hf_{(t)}$ = -13, Hf model ages of T_{DM} = 1.77 - 1.96 Ga and crustal model ages of T_{DM}^{C} = 1.9 - 2.4 Ga, indicating that

an ancient lower crustal component was involved in their genesis. The $\delta^{18}O$ of the Houshihushan pluton is homogeneous and within the mantle range, which indicates that the Houshihushan A-type granite originated either from a dominantly mantle source, or by re-melting of mafic to intermediate igneous rocks, with little involvement of supracrustal materials. The $\delta^{7}Li$ (-5.3‰) of the Houshihushan is the lowest of the six studied granites. High fluorine contents in A-types would significantly increase the solubility of hydrous fluids in granite melt, but they would be released mostly through the fluid exclusion process in a late-stage of the magma evolution which might to some extent lower $\delta^{7}Li$. A meta-sedimentary source is also good to explain for low Li isotopes, however, $\delta^{18}O$ of meta-sedimentary rocks usually quite high (Huang, 2011) and inconsistent with the Houshihushan mantle like $\delta^{18}O$. The unusually low $\delta^{7}Li$ value of the Houshihushan pluton is consistent with the depleted Li-isotope signature of the subcontinental lithospheric mantle under NCC (Tang et al., 2014). The subduction of the Pacific plate during Mesozoic could have generated a large mantle wedge above the subducted oceanic slab and significantly affected the lithospheric mantle beneath eastern China (Zhao et al., 2007). Previous studies have proposed that low $\delta^{7}Li$ in the lithospheric mantle could be generated by reaction between peridotites and low-$\delta^{7}Li$ melt derived from recycled dehydrated Pacific plate since the Late Mesozoic (Tang et al., 2014).

Therefore, the Hf-O-Li isotopic data suggest that the Houshihushan A-type granites were mainly generated by partial melting of a dehydrated mantle source, mixed with some component of lower crustal-derived magmas. The Houshihushan complex formed over a short period in an extensional setting related to destruction of the eastern North China Craton during Early Cretaceous, possibly associated with subduction of paleo-Pacific plate.

The Laoshan granites

The Laoshan A-type granites are closely associated with I-type granites. Based on major and trace elements and Sr, Nd, Pb isotopes, Yan and Shi (2014) suggested that the magma sources of the Laoshan granitic complex were a mixture of EMI-like eclogitic rocks (previously enriched by fluids released from the Mesozoic Pacific subducted slab) and the LCC consisting of granulites or metamorphic residues of prior I-type granites. This conclusion is quite consistent with the new zircon δ^7Li data (5.9 ± 2.3‰). This is isotopically heavier than mantle Li and is extremely rare in granites (Teng, 2004; Magna, 2010); it requires fluid metasomatism. Magna (2010) proposed that the remelting of a modified mantle wedge/lower-crust may account for a significant δ^7Li increase in the magmas produced. In the Laoshan case, a mantle previously enriched by fluids released from the Mesozoic Pacific subducted slab can account for the high δ^7Li. Combined with Hf-O isotopes, we suggest that the ancient lower crust is the other major source, accounting for the highly negative $\varepsilon Hf_{(t)}$ values and mantle-like δ^{18}O.

The petrogenesis of the Laoshan A-type granites is closely related to the overall tectonic evolution of the Jiaodong Peninsula. It is suggested that the Laoshan A-type granites were formed in an extensional setting and were the shallow responses to the lithospheric thinning and decratonization of the North China craton.

The Suzhou A-type granite

Charoy (1994) postulated that a mantle source is indispensable in the generation of the Suzhou granite, even there is no evidence of a "mantle signature" in its geochemistry. Previous studies show the confusion about the origins of the Suzhou A-type granite. The suggested sources include: (a) sedimentary rocks rich in biotite, or feldspar-quartz sandstone (Wang et al., 1998); (b) fractionation of partial melts of residual lower-crustal granulites (Zhou et al., 1997); (c) recycled oceanic crust affected

by high-temperature alteration (Wei et al., 2002; Wei et al., 2008); (d) dominantly crustal materials reworked along rifted continental margins (Fu et al., 1996; Wei et al., 2008); (e) a low degree of partial melting under anhydrous conditions deep in a lower crust metasomatically enriched in F-, LILE-, and HFSE, triggered by an influx of basic magma or by mantle uplift (heat supply) (Charoy and Raimbault, 1994).

Previous data on the radiogenic Sr-Nd isotopes suggest the Suzhou granite was derived from Palaeozoic crust. However, it is possible that metasomatic processes have a greater effect on changing initial $^{87}Sr/^{86}Sr$ ratios in A-type granites, relative to other granites; the $^{87}Sr/^{86}Sr$ ratio is variable because Suzhou A-type granite has low Sr concentrations, making the isotopes sensitive to small additions or removals.

As discussed in chapter 4, the whole-rock $\delta^{18}O$ of the Suzhou pluton is homogeneous and ranges from 6.5 - 7.6‰. The Hf-O isotopes data ($\varepsilon Hf_{(t)}$ = -5.5 and T_{DM}^{C} = 1521~1562 Ma) for the Suzhou A-type granite indicate that ancient igneous rocks are more likely to be the major source of the magmas. The Li isotopes of the Suzhou granite are also in the mantle range. Applying the Hf-O-Li isotopic data for the Suzhou A-type granites, we suggest that mantle-derived magmas played a very important role in the formation of A-type granite. It is generally accepted that mantle material is involved in the A-type granite formation directly or indirectly in three ways: 1). High degree of crystallization and differentiation of basaltic magma intruded in an extension environment may form A-type granites directly (Loiselle and Wones, 1979; Turner et al., 1992); 2). crust-mantle interaction during emplacement of mantle magmas (for example, felsic igneous rock contamination) resulting in SiO_2 saturated A-type granites (Foland and Allen, 1991; Harris, 1995); 3). high-temperature mafic magma underplating the overlying crust to generate A-type granite through anatexis (Gliko et al., 1985; Furlong and Fountain, 1986; Huppert and Sparks, 1988). Integration of the

petrography, major- and trace-element geochemistry suggests the genesis of Suzhou A-type granite was more likely by the 3rd model, except that the mantle both provides heat indirectly, and contributes material directly.

The Taohuadao granites

The Taohuadao granites are located at the eastern coastal area of China. Trace-element features such as high Ga/Al and high contents of HFSE (Zr, Y, and Nb) plot within the field of A-type granites, suggesting post-orogenic extensional settings.

Previous Sr-Nd isotopic data suggested that the Taohuadao A-type granites were dominantly formed from lower crust material, mixing with small volumes of mantle-derived magma. This is consist with the new Hf-isotope data ($\varepsilon Hf_{(t)}$ = -3.3) which also point to a hybrid mantle-crust source. The screened zircon O isotopes of the Taohuadao granite are in the lower end of the mantle value range. The whole-rock $\delta^{18}O$ of the Taohuadao pluton is 6.5 - 7.6‰. Like the Laoshan granites,the Taohuadao granites show higher $\delta^{7}Li$ (6.1 ± 1.6‰) than normal A-type granites, which indicates the involvement of metasomatized lower crust.

The Putuoshan granites

Besides the temporal and spatial coexistence of the Putuoshan I-type and A-type granites, the two intrusive rocks have similar geochemical patterns and isotopic compositions. Published Sr-Nd isotopic data indicate that the Putuoshan granites were derived from partial melting of mixed mantle-crust. The debates focused on whether I-type and A-type granites were derived from the same source. Some suggested that I-type and A-type granites are derived from the same source and A-type granites are the product of long-term magma fractional crystallization (Hong, 1987; Zhou et.al., 1994). Others believe A-type granites formed from deeper source (Huang, 1986; Peng, 1991; Martin et a1., 1994).

The Putuoshan A-type granites were emplaced later than the I-type granites. Compared to the I-type granites, they have higher silica and more alkalis, which suggests higher degrees of fractionation. Moreover, I-type granites have higher LREE/HREE than A-type granites while A-type granites have higher Eu anomalies. The zircon Hf isotopes of the A-type granites are heavier than those of the I-type granites, which indicates more involvement of mantle material. Zircon δ^7Li values for the I-type granites from the Putuoshan composite are not statistically different from those of the coexisting A-type granites, although some of zircon δ^7Li values marginally overlap the high end of the range of normal mantle (MORB：$+4 \pm 2$‰).

Integration of geochemical data and zircon Hf-O-Li isotopic correlations suggests that the two intrusive rocks were derived from the same sources with different degrees of fractionation and involvement of mantle material. The Putuoshan A-type granites were generated by re-melting of ancient mafic-intermediate igneous rocks, triggered by underplating or intrusion of depleted mantle-derived magmas that provided not only the heat source but also part of the mass for the formation of the Putuoshan A-type granites.

7.3 CONCLUSIONS

The following conclusions are drawn on the basis of the present study:

1. Except for the Nianzishan A-type granites, the screened zircon δ^{18}O of the other five plutons are all in the mantle range and in equilibrium with quartz at magma temperatures.
2. The Nianzishan granites have zircon δ^{18}O of 4.6 ‰ after screening. Since the Li isotopes (0.7 ± 1.7‰) indicate little involvement of fluids, the slightly low δ^{18}O values of the Nianzishan granites most probably reflect degassing of H_2O and CO_2 during magma emplacement.
3. Geochemical evidence from Hf-O-Li isotopes indicates that the source region

of Cretaceous A-type granites in eastern China has a more complex history than previously thought. Their genesis could involve partial melting of a juvenile upper crustal source (Nianzishan), re-melting of ancient igneous protoliths, triggered by input of depleted mantle-derived magmas (Suzhou, Putuoshan), a hybrid origin from metasomatized mantle and lower crust (Laoshan, Taohuadao), or a dehydrated mantle source mixed with some component of lower crustal-derived magmas (Houshihushan). Their melting was most likely triggered by the upwelling of the asthenosphere related to the delamination of a flat-subducting oceanic slab and the thinning of the subcontinental lithosphere.

CHAPTER 8. CONCLUSIONS

In this study, six Cretaceous A-type granites (Nianzishan, Houshihushan, Laoshan, Suzhou, Taohuadao, and Putuoshan) along eastern China were examined systematically for their geochronology, petrography, whole-rock geochemistry, whole-rock Li isotope compositions, and *in situ* zircon Hf-O-Li isotopes.

The study emphasizes that the degree of radiation damage accumulated by a zircon crystal through geological time is rarely negligible. SIMS analyses of zircons with extreme radiation damage can show an apparent increase in U-Pb age and a real decrease in $\delta^{18}O$ that are correlated with the D_{dpa}. The higher apparent U-Pb ages and lower $\delta^{18}O$ values typical of high-U zircon are both related to radiation damage, but are caused by different mechanisms. The "high D_{dpa} effect" on SIMS U-Pb age determinations is a matrix effect specific to SIMS analysis, while the low-$\delta^{18}O$ zircons reflect compositional (oxygen-isotope) exchange due to oxygen diffusion in hydrous (metamict) zircons. The U-Pb isotope system in zircon is more stable than the oxygen-isotope system, and zircons with concordant U-Pb ages may thus have disturbed $\delta^{18}O$ values.

In order to obtain more reliable U-Pb and O isotope data from these highly evolved granites, a screening criterion (D_{dpa}) has been developed to quantify the degree of radiation damage by taking both time and [U], [Th] into consideration. The threshold of

[U] that causes the "high-U matrix effect" decreases with increasing age while the D_{dpa} remains the same. Raman spectroscopy can be used to measure the crystallinity of zircons and should be used together with D_{dpa} to select grains for isotopic studies. This provides a new procedure for screening the zircon $\delta^{18}O$ values and SIMS U-Pb ages in order to improve the data quality. The primary conclusion is that at $D_{dpa} > 0.03$, a hydrous phase can infiltrate the zircon structure, accelerating the diffusion of oxygen and leading to low $\delta^{18}O$ values, while $D_{dpa} > 0.08$ will trigger the "high U matrix effect" which causes high U-Pb ages in SIMS dating. Moreover, contrary to general understanding, quartz appears to better preserve its primary $\delta^{18}O$ than zircons, since quartz does not undergo radiation damage. Except for the Nianzishan A-type granites ($\delta^{18}O$ = 4.6‰), the screened zircon $\delta^{18}O$ values of the other five plutons are all in mantle range (4.8 – 5.5‰) and in equilibrium with the corresponding quartz (6.8 – 8.0‰) under magmatic conditions. Therefore, most of the Cretaceous A-type plutons in eastern China are not really "low-$\delta^{18}O$" granites as previous assumed.

In addition to conventional geochemical data, a non-traditional geochemical tracer, the isotopic composition of lithium in zircon, has been used to constrain the source regions of six Cretaceous A-type granites and provides a parallel explanation for the low-$\delta^{18}O$ Nianzishan A-type granites.

Methods for *in situ* lithium-isotope analysis have been improved in the process. Accuracy and precision can be improved by carefully balancing the beam size and analysis time. For the 10 μm beam size, the $^{7}Li/^{6}Li$ ratio of the M257 zircon standard

can be analysed with an internal precision of 2.0‰ (2SE),and an external precision around 2.5‰ (2SD). Special attention is required when dealing with the data from the rim in a profile analysis. The count rate and error of the rim data should be compared with those from the scattered spots, in order to avoid those affected by the rim and charge effects.

With the new *in situ* lithium-isotope analytical methods, the hypothesis of diffusion-driven fractionation of Li in zircon is firstly corroborated by ion imaging on three zircon standards (Plešovice, Qinghu and Temora). All the zircon grains have a rim 5-10 μm wide with Li concentrations 10 to 50 times higher than the core. Extreme isotopic fractionation (up to ~20‰) is observed at zircon rims on a small scale (~50 μm) due to the different diffusivities of ^{6}Li and ^{7}Li. The measured δ^{7}Li values range from -14.3 to +3.7‰ for Plešovice, from -22.8 to +1.4‰ for Qinghu and from -4.1 to 16.1‰ for Temora zircon. There is a linear relationship between [Li] and δ^{7}Li at the rims, but both [Li] and δ^{7}Li are homogeneous within error in the cores of the grains, which suggests that large isotopic variations of Li in zircons can be caused by diffusion. Interpreting the significance of δ^{7}Li values in zircons requires much more effort in understanding of the possible effects of the late diffusion fractionation on [Li] and δ^{7}Li distribution. This requires analysis of profiles to identify whether the δ^{7}Li signature has been affected by diffusion. Homogeneous heavy δ^{7}Li in the cores of large zircon grains most likely carries reliable information about the isotopic signatures of their source magmas.

The Nianzishan granites have zircon $\delta^{18}O$ of 4.6 ‰ after screening. This slightly depleted $\delta^{18}O$ value most probably was caused by degassing of H_2O and CO_2 during magma emplacement. Geochemical evidence from robust zircon Hf-O-Li isotopes indicates that the source region of Cretaceous A-type granites in eastern China has a more complex history than previously thought. This source region could be generated from partial melting of a juvenile upper crustal source (Nianzishan), re-melting of ancient igneous protoliths, triggered by input of depleted mantle-derived magmas (Suzhou, Putuoshan), a hybrid origin from metasomatized mantle and lower crust (Laoshan, Taohuadao), or a dehydrated mantle source mixed with some component of lower crustal-derived magmas (Houshihushan). Their melting was most likely triggered by the upwelling of the asthenosphere related to the delamination of a flat-subducting oceanic slab and the thinning of the subcontinental lithosphere.

Li-isotope geochemistry is still a novel research area. There is an accumulating dataset of Li isotope analyses on major natural reservoirs. Several reservoirs show a significant range in Li isotopes, and substantial overlap is observed among different reservoirs. Systematic study of the Li isotope ratios of igneous rocks is far from mature. Interpreting the significance of $\delta^{7}Li$ values in zircons requires much more effort on understanding the possible effects of late diffusion fractionation on the distribution [Li] and $\delta^{7}Li$ in zircons. Thus the interpretations of the Hf-O-Li isotopic systems to constrain the source regions of A-type granites are still at the frontier stage. This study has laid the groundwork for understanding Li-isotope behavior in granites and in

zircons, and developed Hf-O-Li isotope fingerprints as a useful geochemical tracer for future studies of granites.

REFERENCES

Aines, R. D. and Rossman, G. R. 1986. Relationships between radiation damage and trace water in zircon, quartz, and topaz. American Mineralogist 71(9-10): 1186-1193.

Anderson, J. L. and Bender, E. E. 1989. Nature and origin of Proterozoic A-type granitic magmatism in the southwestern United States of America. Lithos 23: 19–52.

Aulbach, S. and Rudnick, R. L. 2009. Origins of non-equilibrium lithium isotopic fractionation in xenolithic peridotite minerals: Examples from Tanzania. Chemical Geology 258(1-2): 17-27.

Bacon, C. R., Adami, L. H. and Lanphere, M. A. 1989. Direct evidence for the origin of low-o-18 silicic magmas - quenched samples of a magma chambers partially-fused granitoid walls, crater lake, oregon. Earth And Planetary Science Letters 96(1-2): 199-208.

Balan, E., Neuville, D. R., Trocellier, P., Fritsch, E., Muller, J. P. and Calas, G. 2001. Metamictization and chemical durability of detrital zircon. American Mineralogist 86(9): 1025-1033.

Balsley, S. D. and Gregory, R. T. 1998. Low-$\delta^{18}O$ silicic magmas: why are they so rare? Earth And Planetary Science Letters 162(1-4): 123-136.

Barbarin, B. 1999. A review of the relationships between granitoid types, their origins and their geodynamic environments. Lithos 46(3): 605-626.

Be'eri-Shlevin, Y., Katzir, Y., Blichert-Toft, J., Kleinhanns, I. C. and Whitehouse, M. J. 2010. Nd-Sr-Hf-O isotope provinciality in the northernmost Arabian-Nubian Shield: implications for crustal evolution. Contributions To Mineralogy And Petrology 160(2): 181-201.

Beck, P., Chaussidon, M., Barrat, J., Gillet, P. and Bohn, M. 2006. Diffusion induced Li isotopic fractionation during the cooling of magmatic rocks: the case of pyroxene phenocrysts from nakhlite meteorites. Geochimica Et Cosmochimica Acta 70(18): 4813-4825.

Bell, D., Hervig, R., Buseck, P. and Aulbach, S. 2009. Lithium isotope analysis of olivine by SIMS: Calibration of a matrix effect and application to magmatic phenocrysts. Chemical Geology 258(1-2): 5-16.

Bibikova, Y. V., Ustinov, V. I., Gracheva, T. V., Kiselevskiy, M. A. and Shukolyukov, Y. A. 1982. Variations of isotopic composition of oxygen in accessory zircons. Doklady Akademii Nauk SSSR 264: 698-700.

Bindeman, I. N., Brooks, C. K., McBirney, A. R. and Taylor, H. P. 2008. The Low-$\delta^{18}O$ Late-Stage Ferrodiorite Magmas in the Skaergaard Intrusion: Result of Liquid Immiscibility, Thermal Metamorphism, or Meteoric Water Incorporation into Magma? Journal Of Geology 116(6): 571-586.

Bindeman, I. N. and Valley, J. W. 2000. Formation of low-$\delta^{18}O$ rhyolites after caldera collapse at Yellowstone, Wyoming, USA. Geology 28(8): 719-722.

Bindeman, I. N. and Valley, J. W. 2001. Low-$\delta^{18}O$ rhyolites from Yellowstone: Magmatic evolution based on analyses of zircons and individual phenocrysts. Journal Of Petrology 42(8): 1491-1517.

Bindeman, I. N. and Valley, J. W. 2003. Rapid generation of both high- and low-delta O-18, large-volume silicic magmas at the Timber Mountain/Oasis Valley caldera complex, Nevada. Geological Society Of America Bulletin 115(5): 581-595.

Bindeman, I. N., Watts, K. E., Schmitt, A. K., Morgan, L. A. and Shanks, P. W. C. 2007. Voluminous low δ18O magmas in the late Miocene Heise volcanic field, Idaho: Implications for the fate of Yellowstone hotspot calderas. Geology 35(11): 1019.

Black, L. P. and Gulson, B. L. 1978. The age of the Mud Tank carbonatite, Strangways Range, Northern Territory. BMR Journal of Australian Geology and Geophysics 3: 227-232.

Black, L. P., Kamo, S. L., Allen, C. M., Aleinikoff, J. N., Davis, D. W., Korsch, R. J. and Foudoulis, C. 2003. TEMORA 1: a new zircon standard for Phanerozoic U–Pb geochronology. Chemical Geology 200(1-2): 155-170.

Black, L. P., Kamo, S. L., Allen, C. M., Davis, D. W., Aleinikoff, J. N., Valley, J. W., et. al. 2004. Improved 206Pb/238U microprobe geochronology by the monitoring of a trace-element-related matrix effect; SHRIMP, ID–TIMS, ELA–ICP–MS and oxygen isotope documentation for a series of zircon standards. Chemical Geology 205(1–2): 115-140.

Blevin, P. L. and Chappell, B. W. 1995. Chemistry, origin, and evolution of mineralized granites in the Lachlan fold belt, Australia; the metallogeny of I- and S-type granites. Economic Geology 90(6): 1604-1619.

Blichert-Toft, J. and Albarede, F. 1997. The Lu-Hf isotope geochemistry of chondrites and the evolution of the mantle-crust system. Earth And Planetary Science Letters

148(1-2): 243-258.

Bonin, B. 2007. A-type granites and related rocks: Evolution of a concept, problems and prospects. Lithos 97(1-2): 1-29.

Bonin, B., Azzouni-Sekkal, A., Bussy, F. and Ferrag, S. 1998. Alkali-calcic and alkaline post-orogenic (PO) granite magmatism: petrologic constraints and geodynamic settings. Lithos 45(1-4): 45-70.

Booth, A., Kolodny, Y., Chamberlain, C., McWilliams, M., Schmitt, A. and Wooden, J. 2005. Oxygen isotopic composition and U-Pb discordance in zircon. Geochimica Et Cosmochimica Acta 69(20): 4895-4905.

Bouman, C., Vroon, P. Z., Elliott, T. R., Schwieters, J. B. and Hamester, M. 2002. Determination of lithium isotope compositions by MC-ICPMS (Thermo Finnigan MAT Neptune). Geochimica Et Cosmochimica Acta 66(15A): A97-A97.

Bouvier, A.-S., Ushikubo, T., Kita, N. T., Cavosie, A. J., Kozdon, R. and Valley, J. W. 2011. Li isotopes and trace elements as a petrogenetic tracer in zircon: insights from Archean TTGs and sanukitoids. Contributions To Mineralogy And Petrology 163(5): 745-768.

Butera, K. M., Williams, I. S., Blevin, P. L. and Simpson, C. J. 2001. Zircon U–Pb dating of Early Palaeozoic monzonitic intrusives from the Goonumbla area, New South Wales. Australian Journal Of Earth Sciences 48(3): 457-464.

Carmichael, I. S. E. 1991. The redox states of basic and silicic magmas: a reflection of their source regions? Contributions To Mineralogy And Petrology 106(2): 129-141.

Carter, B. T., Hibbard, J. P., Tubrett, M. and Sylvester, P. 2006. Detrital zircon geochronology of the Smith River Allochthon and Lynchburg Group, southern Appalachians: Implications for Neoproterozoic-Early Cambrian paleogeography. Precambrian Research 147(3–4): 279-304.

Cavosie, A. J., Wilde, S. A., Liu, D., Weiblen, P. W. and Valley, J. W. 2004. Internal zoning and U–Th–Pb chemistry of Jack Hills detrital zircons: a mineral record of early Archean to Mesoproterozoic (4348–1576Ma) magmatism. Precambrian Research 135(4): 251-279.

Chan, L. H., Edmond, J. M., Thompson, G. and Gillis, K. 1992. Lithium Isotopic Composition of Submarine Basalts - Implications for the Lithium Cycle in the Oceans. Earth And Planetary Science Letters 108(1-3): 151-160.

Chan, L. H., Gieskes, J. M., You, C. F. and Edmond, J. M. 1994. Lithium Isotope

Geochemistry of Sediments and Hydrothermal Fluids of the Guaymas Basin, Gulf of California. Geochimica Et Cosmochimica Acta 58(20): 4443-4454.

Chan, L. H., Alt, J. C. and Teagle, D. A. H. 2002. Lithium and lithium isotope profiles through the upper oceanic crust: a study of seawater-basalt exchange at ODP Sites 504B and 896A. Earth And Planetary Science Letters 201(1): 187-201.

Chan, L. H. and Frey, F. A. 2003. Lithium isotope geochemistry of the Hawaiian plume: Results from the Hawaii Scientific Drilling Project and Koolau volcano. Geochemistry Geophysics Geosystems 4: -.

Chappell, B. W. and White, A. J. R. 1974. Two contrasting granite types. Pacific Geology 8(173-174).

Charoy, B. and Raimbault, L. 1994. Zr-rich, Th-rich, and REE-rich biotite differentiates in the A-type granite pluton of Suzhou (Eastern China)-The key role of fluorine. Journal Of Petrology 35(4): 919-962.

Chen, H. 1995. A comment on hydrogen isotopic composition and related problems of alkaline granites. Geochimica 24(2): 193-195, (in Chinese with English Abstract).

Chen, J. Y. 2015. Petrogenesis of the Cretaceous diorite-granite-syenite in northeastern Fujian: Implications for reworking of continental crust. Institute of Geology and Geophysics, Chinese Acadamy of Sciences. Ph.D Thesis (in Chinese with English Abstract).

Chen, J. F., Foland, K. A. and Liu, Y. M. 1993. Precise 40Ar-39Ar dating of the Suzhou composite granite. Acta Petrologica Sinica 9(01): 77-85 (in Chinese with English Abstract).

Chen, J. Y., Yang, J. H., Zhang, J. H., Sun, J. F. and Wilde, S. A. 2013. Petrogenesis of the Cretaceous Zhangzhou batholith in southeastern China: Zircon U-Pb age and Sr-Nd-Hf-O isotopic evidence. Lithos 162: 140-156.

Cherniak, D. J. and Watson, E. B. 2003. Diffusion in zircon. Reviews in Mineralogy and Geochemistry. 53: 113.

Cherniak, D. J. and Watson, E. B. 2010. Li diffusion in zircon. Contributions To Mineralogy And Petrology. 160: 383-390.

Cherniak, D. J. 2010. Diffusion in accessory minerals: zircon, titanite, apatite, monazite and xenotime. Reviews in Mineralogy and Geochemistry 72(1): 827-869.

Chu, N. C., Taylor, R. N., Chavagnac, V., Nesbitt, R. W., Boella, R. M., Milton, J. A., Burton, K. 2002. Hf isotope ratio analysis using multi-collector inductively coupled plasma mass spectrometry: an evaluation of isobaric interference

corrections. Journal Of Analytical Atomic Spectrometry 17(12): 1567-1574.

Clarke, D. B., Ed. 1992. Granitoid Rocks. Topics in the Earth Sciences. London, Chapman and Hall.

Clarke, D. B. 1996. Two centuries after Hutton's 'Theory of the Earth': the status of granite science. Geological Society of America Special Papers 315: 353-359.

Clemens, J. D., Holloway, J. R. and White, A. J. R. 1986. Oringin of an A-type granite - Experimental constraints. American Mineralogist 71(3-4): 317-324.

Collins, W. J., Beams, S. D., White, A. J. R. and Chappell, B. W. 1982. Nature and origin of A-type granites with particular reference to southeastern Australia. Contributions To Mineralogy And Petrology 80: 189-200.

Creaser, R. A., Price, R. C. and Wormald, R. J. 1991. A-type granites revisited: Assessment of a residual-source model. Geology 19(2): 163-166.

Creaser, R. A. and White, A. J. R. 1991. Yardea Dacite — Large-volume, high-temperature felsic volcanism from the Middle Proterozoic of South Australia. Geology 19(1): 48-51.

Dall'Agnol, R. and de Oliveira, D. C. 2007. Oxidized, magnetite-series, rapakivi-type granites of Carajás, Brazil: Implications for classification and petrogenesis of A-type granites. Lithos 93(3–4): 215-233.

Dall'Agnol, R. and Ramo, O. T. 2009. The petrogenesis of A-type granites and related rocks preface. Canadian Mineralogist 47(6): 1297-1300.

Dall'Agnol, R., Scaillet, B. and Pichavant, M. 1999. An Experimental Study of a Lower Proterozoic A-type Granite from theEastern Amazonian Craton, Brazil. Journal Of Petrology 40(11): 1673-1698.

Dan, W., Li, X.-H., Guo, J., Liu, Y. and Wang, X.-C. 2012. Paleoproterozoic evolution of the eastern Alxa Block, westernmost North China: Evidence from in situ zircon U-Pb dating and Hf-O isotopes. Gondwana Research 21(4): 838-864.

Deng, F. L. and Macdougall, J. D. 1992. Proterozoic depletion of the lithosphere recorded in mantle xenoliths from Inner Mongolia. Nature 360(6402): 333-336.

Dohmen, R., Kasemann, S. A., Coogan, L. and Chakraborty, S. 2010. Diffusion of Li in olivine. Part I: Experimental observations and a multi species diffusion model. Geochimica Et Cosmochimica Acta 74(1): 274-292.

Eby, G. N. 1990. The A-type granitoids - A review of their occurrence and chemical characteristics and speculations on their petrogenesis. Lithos 26(1-2): 115-134.

Eby, G. N. 1992. Chemical subdivision of the A-type granitoids - Petrogenetic and

tectonic implications. Geology 20(7): 641-644.

Elliott, T., Jeffcoate, A. and Bouman, C. 2004. The terrestrial Li isotope cycle: light-weight constraints on mantle convection. Earth And Planetary Science Letters 220(3-4): 231-245.

Elliott, T., Thomas, A., Jeffcoate, A. and Niu, Y. L. 2006. Lithium isotope evidence for subduction-enriched mantle in the source of mid-ocean-ridge basalts. Nature 443(7111): 565-568.

Ewart, A. 1982. The mineralogy and petrology of Tertiary-Recent orogenic volcanic rocks: with special reference to the andesitic-basaltic compositional range. Andesites: Orogenic Andesites and Related Rocks, John Wiley and Sons. R. S. Thorp. New York: 25-95.

Ewing, R. C., Meldrum, A., Wang, L. M., Weber, W. J. and Corrales, L. R. 2003. Radiation effects in zircon. Zircon. J. M. Hanchar and P. W. O. Hoskin. Washington, Mineralogical Soc America. 53: 387-425.

Foland, K. and Allen, J. 1991. Magma sources for Mesozoic anorogenic granites of the White Mountain magma series, New England, USA. Contributions to Mineralogy and Petrology 109(2): 195-211.

Friedman, I., Lipman, P. W., Obradovi, J. D., Gleason, J. D. and Christia, R. l. 1974. Meteoric water in magmas. Science 184(4141): 1069-1072.

Frost, C. D. and Frost, B. R. 1997. Reduced rapakivi-type granites: The tholeiite connection. Geology 25(7): 647-650.

Frost, C. D., Frost, B. R., Chamberlain, K. R. and Edwards, B. R. 1999. Petrogenesis of the 1 center dot 43 Ga Sherman batholith, SE Wyoming, USA: A reduced, rapakivi-type anorogenic granite. Journal Of Petrology 40(12): 1771-1802.

Frost, B. R., Barnes, C. G., Collins, W. J., Arculus, R. J., Ellis, D. J. and Frost, C. D. 2001. A Geochemical classification for granitic rocks Journal Of Petrology 42: 2033-2048.

Frost, C. D., Frost, B. R., Bell, J. M. and Chamberlain, K. R. 2002. The relationship between A-type granites and residual magmas from anorthosite:evidence from the northern Sherman batholith,Laramie Mountains,Wyoming,USA.

Frost, C. D. and Frost, B. R. 2010. On Ferroan (A-type) Granitoids: their Compositional Variability and Modes of Origin. Journal Of Petrology 52(1): 39-53.

Fu, B., Wei, C. S. and Zheng, Y. F. 1996. The Suzhou A-type granite of low δ18O

magmatic origin. Bulletin of Mineralogy, Petrology and Geochemistry 15(4): 211-215, (in Chinese with English Abstract).

Furlong, K. and Fountain, D. 1986. Continental crustal underplating: Thermal considerations and seismic-petrologic consequences. Journal of Geophysical Research 91(B8): 8285-8294.

Gao, S., Rudnick, R. L., Yuan, H. L., Liu, X. M., Liu, Y. S. and Xu, W. L. 2004. Recycling lower continental crust in the North China craton. Nature 432: 892–897.

Gao, Y.-Y., Li, X.-H., Griffin, W. L., O'Reilly, S. Y. and Wang, Y.-F. 2014. Screening criteria for reliable U–Pb geochronology and oxygen isotope analysis in uranium-rich zircons: A case study from the Suzhou A-type granites, SE China. Lithos 192-195: 180-191.

Geisler, T., Pidgeon, R. T., van Bronswijk, W. and Kurtz, R. 2002. Transport of uranium, thorium, and lead in metamict zircon under low-temperature hydrothermal conditions. Chemical Geology 191(1-3): 141-154.

Gliko, A., Grachev, A. and Magnitsky, V. 1985. Thermal model for lithospheric thinning and associated uplift in the neotectonic phase of intraplate orogenic activity and continental rifts. Journal of Geodynamics 3(1-2): 137-153.

Goss, S. C., Wilde, S. A., Wu, F. and Yang, J. 2010. The age, isotopic signature and significance of the youngest Mesozoic granitoids in the Jiaodong Terrane, Shandong Province, North China Craton. Lithos 120(3-4): 309-326.

Griffin, W. L., Andi, Z., O'Reilly, S. Y. and Ryan, C. G. 1998. Phanerozoic evolution of the lithosphere beneath the Sino-Korean Craton. Mantle Dynamics and Plate Interactions in East Asia 27: 107-126.

Griffin, W. L., Pearson, N. J., Belousova, E., Jackson, S. E., Achterbergh, E. v., O'Reilly, S. Y. and Shee, S. R. 2000. The Hf isotope composition of cratonic mantle: LAM-MC-ICPMS analysis of zircon megacrysts in kimberlites. Geochimica Et Cosmochimica Acta 64(1): 133–147.

Halama, R., Savov, I., Rudnick, R. and McDonough, W. 2009. Insights into Li and Li isotope cycling and sub-arc metasomatism from veined mantle xenoliths, Kamchatka. Contributions To Mineralogy And Petrology 158(2): 197-222.

Harris, C. 1995. Oxygen isotope geochemistry of the Mesozoic anorogenic complexes of Damaraland, northwest Namibia: evidence for crustal contamination and its effect on silica saturation. Contributions to Mineralogy and Petrology 122(3):

308-321.

Hawkesworth, C. J. and Kemp, A. I. S. 2006. Evolution of the continental crust. Nature 443: 811-817.

Hildreth, W., Christiansen, R. L. and Oneil, J. R. 1984. Catastrophic isotopic modification of rhyolitic magma at times of caldera subsidence, Yellowstone plateau volcanic field. Journal Of Geophysical Research 89(B10): 8339-8369.

Hildreth, W., Halliday, A. N. and Christiansen, R. L. 1991. Isotopic and chemical evidence concerning the genesis and contamination of basaltic and rhyolitic magma beneath the Yellowstone Plateau volcanic field. Journal Of Petrology 32(1): 63-138.

Holland, H. D. and Gottfried, D. 1955. The effect of nuclear radiation on the structure of zircon. Acta Crystallographica 8(6): 291-300.

Hong, D. W., G., W. S., Han, B. F. and Qi, M. Y. 1995. The tectonic environment of the alkali granite Science in China: B 25(4): 418-426-in Chinese with English Abstract, (in Chinese with English Abstract).

Hu, J., Qiu, J. S., Wang, D. Z., Wang, R. C. and Zhang, X. L. 2005. Comparative investigations of A-type granites in the coastal and the Nanling inland areas of SE China, and their tectonic significance

Geological Journal of China Universities 11(3): 404-414, (in Chinese with English Abstract).

Huang, H. Q., Li, X. H., Li, W. X. and Li, Z. X. 2011. Formation of high δ18O fayalite-bearing A-type granite by high-temperature melting of granulitic metasedimentary rocks, southern China. Geology 39(10): 903-906.

Huang, K. F., You, C. F., Liu, Y. H., Wang, R. M., Lin, P. Y. and Chung, C. H. 2010. Low-memory, small sample size, accurate and high-precision determinations of lithium isotopic ratios in natural materials by MC-ICP-MS. Journal of Analytical Atomic Spectrometry 25(7): 1019-1024.

Huh, Y., Chan, L. H. and Edmond, J. M. 2001. Lithium isotopes as a probe of weathering processes: Orinoco River. Earth And Planetary Science Letters 194(1-2): 189-199.

Huppert, H. and Sparks, R. 1988. The generation of granitic magmas by intrusion of basalt into continental crust. Journal of Petrology 29(3): 599.

Jackson, S. E., Pearson, N. J., Griffin, W. L. and Belousova, E. A. 2004. The application of laser ablation-inductively coupled plasma-mass spectrometry to in

situ U–Pb zircon geochronology. Chemical Geology 211: 47-69.

James, R. H. and Palmer, M. R. 2000. The lithium isotope composition of international rock standards. Chemical Geology 166(3-4): 319-326.

Jeffcoate, A. B., Elliott, T., Kasemann, S. A., Ionov, D., Cooper, K. and Brooker, R. 2007. Li isotope fractionation in peridotites and mafic melts. Geochimica Et Cosmochimica Acta 71(1): 202-218.

Jeffcoate, A. B., Kasemann, S. A. and Elliott, T. 2004. High-spatial resolution lithium isotope variation in mantle minerals. Geochimica Et Cosmochimica Acta 68(11): A52-A52.

Jiang, X. Y. and Li, X. H. 2014. In situ zircon U-Pb and Hf-O isotopic results for ca. 73 Ma granite in Hainan Island: Implications for the termination of an Andean-type active continental margin in southeast China. Journal Of Asian Earth Sciences 82: 32-46.

Jiang, Y. H., Zhao, P., Zhou, Q., Liao, S. Y. and Jin, G. D. 2011. Petrogenesis and tectonic implications of Early Cretaceous S- and A-type granites in the northwest of the Gan-Hang rift, SE China. Lithos 121(1-4): 55-73.

Jochum, K. P., Stoll, B., Herwig, K., Willbold, M., Hofmann, A. W., Amini, M., et. al. 2006. MPI-DING reference glasses for in situ microanalysis: New reference values for element concentrations and isotope ratios. Geochemistry Geophysics Geosystems 7(2): Q02008.

Kasemann, S. A., Jeffcoate, A. B. and Elliott, T. 2005. Lithium isotope composition of basalt glass reference material. Analytical Chemistry 77(16): 5251-5257.

Kemp, A. I. S., Hawkesworth, C. J., Foster, G. L., Paterson, B. A., Woodhead, J. D., Hergt, J. M., et. al. 2007. Magmatic and crustal differentiation history of granitic rocks from Hf-O isotopes in zircon. Science 315(5814): 980-983.

Kemp, A. I. S., Wormald, R. J., Whitehouse, M. J. and Price, R. C. 2005. Hf isotopes in zircon reveal contrasting sources and crystallization histories for alkaline to peralkaline granites of Temora, southeastern Australia. Geology 33(10): 797-800.

King, E. M., Barrie, C. T. and Valley, J. W. 1997a. Hydrothermal alteration of oxygen isotope ratios in quartz phenocrysts, Kidd Creek mine, Ontario: Magmatic values are preserved in zircon. Geology 25(12): 1079–1082.

King, P. L., Chappell, B. W., Allen, C. M. and White, A. J. R. 2001. Are A-type granites the high-temperature felsic granites? Evidence from fractionated granites of the Wangrah Suite. Australian Journal Of Earth Sciences 48(4): 501-514.

King, P. L., White, A. J. R., Chappell, B. W. and Allen, C. M. 1997b. Characterization and origin of aluminous A-type granites from the Lachlan Fold Belt, Southeastern Australia. Journal Of Petrology 38(3): 371-391.

Kita, N. T., Ushikubo, T., Fu, B. and Valley, J. W. 2009. High precision SIMS oxygen isotope analysis and the effect of sample topography. Chemical Geology 264(1-4): 43-57.

Klimm, K., Holtz, F., Johannes, W. and King, P. L. 2003. Fractionation of metaluminous A-type granites: an experimental study of the Wangrah Suite, Lachlan Fold Belt, Australia. Precambrian Research 124(2-4): 327-341.

Kobayashi, K., Tanaka, R., Moriguti, T., Shimizu, K. and Nakamura, E. 2003. Lithium, boron and lead isotope systematics on glass inclusions in olivine phenocrysts from Hawaiian lavas. Geochimica et Cosmochimica Acta 67(18): A223-A223.

Kobayashi, K., Tanaka, R., Moriguti, T., Shimizu, K. and Nakamura, E. 2004. Lithium, boron, and lead isotope systematics of glass inclusions in olivines from Hawaiian lavas: evidence for recycled components in the Hawaiian plume. Chemical Geology 212(1-2): 143-161.

Krogh, T. E. 1982. Improved accuracy of U-Pb zircon ages by the creation of more concordant systems using an air abrasion technique. Geochimica Et Cosmochimica Acta 46(4): 637-649.

Layne, G. D. 2009. Li, B and Cl isotope determination by SIMS. Secondary Ion Mass Spectrometry in the Earth Sciences: Gleaning the big picture from a small spot. M. Fayek. Toronto, Mineralogical Association of Canada. 41: 89-108.

le Roux, P. J. 2009. In situ lithium isotope analysis by LA-MC-ICP-MS. Geochimica Et Cosmochimica Acta 73(13): A744-A744.

le Roux, P. J. 2010. Lithium isotope analysis of natural and synthetic glass by laser ablation MC-ICP-MS. Journal Of Analytical Atomic Spectrometry 25(7): 1033-1038.

Lee, J. K. W., Williams, I. S. and Ellis, D. J. 1997. Pb, U and Th diffusion in natural zircon. Nature 390(6656): 159-162.

Leech, M. 2008. Does the Karakoram fault interrupt mid-crustal channel flow in the western Himalaya? Earth And Planetary Science Letters 276(3-4): 314-322.

Li, H., Zhang, H., Ling, M. X., Wang, F. Y., Ding, X., Zhou, J. B., . . . Sun, W. D. 2011a. Geochemical and zircon U-Pb study of the Huangmeijian A-type granite: implications for geological evolution of the Lower Yangtze River belt.

International Geology Review 53(5-6): 499-525.

Li, J. Z. and Wan, Z. J. 1994. Lithodemic division and generation of composite batholith of the Laoshan granites. Geology of Shandong Province, (02): 1-12, (in Chinese with English Abstract).

Li, P. Z. 1995. Reply to the "A comment on hydrogen isotopic composition and related problems of alkaline granites"by Chen Hui. Geochimica 24(2): 196-197, (in Chinese with English Abstract).

Li, P. Z., Shen, Y. L., Li, C. L. and Yu, J. S. 1990. Research on the δ18O and fossil hydrothermal system of the Nianzishan alkaline granites, Heilongjiang. Science in China: B, (08): 862-869, (in Chinese).

Li, P. Z., Yu, F. J., Liu, D. P. and Yu, J. S. 1992. The Relationship Between deltaD and Magma Degassing of the Nianzishan Miarolitic alkaline Granite, Heilongjiang. Geochimica, (01): 70-76, (in Chinese with English Abstract).

Li, P. Z. and Yu, J. S. 1989. δD and δ18O composition of the Shanhaiguan alkaline granites. Science Letters, (1): 51-52, (in Chinese).

Li, P. Z. and Yu, J. S. 1993. Nianzishan Miarolitic Alkaline Granite Stock, Heilongjiang--Its ages and Geological Implications. Geochimica, (4): 389-398, (in Chinese with English Abstract).

Li, Q.-L., Li, X.-H., Liu, Y., Tang, G.-Q., Yang, J.-H. and Zhu, W.-G. 2010a. Precise U-Pb and Pb-Pb dating of Phanerozoic baddeleyite by SIMS with oxygen flooding technique. Journal Of Analytical Atomic Spectrometry 25(7): 1107-1113.

Li, X. H. 2000. Cretaceous magmatism and lithospheric extension in Southeast China. Journal Of Asian Earth Sciences 18(3): 293-305.

Li, X. H., Sun, M., Wei, G. J., Liu, Y., Lee, C. Y. and Malpas, J. 2000. Geochemical and Sm-Nd isotopic study of amphibolites in the Cathaysia Block, southeastern China: evidence for an extremely depleted mantle in the Paleoproterozoic. Precambrian Research 102(3-4): 251-262.

Li, X. H., Qi, C. S., Liu, Y., Liang, X. R., Tu, X. L., Xie, L. W. and Yang, Y. H. 2005. Petrogenesis of the Neoproterozoic bimodal volcanic rocks along the western margin of the Yangtze Block: New constraints from Hf isotopes and Fe/Mn ratios. Chinese Science Bulletin 50(21): 2481-2486.

Li, X. H., Li, Z. X., Li, W. X., Liu, Y., Yuan, C., Wei, G. J. and Qi, C. S. 2007. U-Pb zircon, geochemical and Sr-Nd-Hf isotopic constraints on age and origin of Jurassic I- and A-type granites from central Guangdong, SE China: A major

igneous event in response to foundering of a subducted flat-slab? Lithos 96(1-2): 186-204.

Li, X. H., Li, W. X., Wang, X. C., Li, Q. L., Liu, Y. and Tang, G. Q. 2009a. Role of mantle-derived magma in genesis of early Yanshanian granites in the Nanling Range, South China: in situ zircon Hf-O isotopic constraints. Science In China Series D-earth Sciences 52(9): 1262-1278.

Li, X. H., Liu, Y., Li, Q. L., Guo, C. H. and Chamberlain, K. R. 2009b. Precise determination of Phanerozoic zircon Pb/Pb age by multicollector SIMS without external standardization. Geochemistry Geophysics Geosystems 10.

Li, X. H., Li, W.-X., Li, Q.-L., Wang, X.-C., Liu, Y. and Yang, Y.-H. 2010b. Petrogenesis and tectonic significance of the ~850Ma Gangbian alkaline complex in South China: Evidence from in situ zircon U-Pb dating, Hf-O isotopes and whole-rock geochemistry. Lithos 114(1-2): 1-15.

Li, X. H., Long, W. G., Li, Q. L., Liu, Y., Zheng, Y. F., Yang, Y. H., et. al. 2010c. Penglai Zircon Megacrysts: A Potential New Working Reference Material for Microbeam Determination of Hf-O Isotopes and U-Pb Age. Geostandards and Geoanalytical Research 34(2): 117-134.

Li, X. H., Li, Q. L., Liu, Y. and Tang, G. Q. 2011b. Further characterization of M257 zircon standard: A working reference for SIMS analysis of Li isotopes. Journal Of Analytical Atomic Spectrometry 26(2): 352.

Li, X. H., Tang, G. Q., Gong, B., Yang, Y. H., Hou, K. J., Hu, Z. C., et. al. 2013. Qinghu zircon: A working reference for microbeam analysis of U-Pb age and Hf and O isotopes Chinese Science Bulletin 58(36): 4647-4654

Li, Z.-X. and Li, X.-H. 2007. Formation of the 1300-km-wide intracontinental orogen and postorogenic magmatic province in Mesozoic South China: A flat-slab subduction model. Geology 35(2): 179-182.

Li, Z.-X., Li, X.-H., Chung, S.-L., Lo, C.-H., Xu, X. and Li, W.-X. 2012. Magmatic switch-on and switch-off along the South China continental margin since the Permian: Transition from an Andean-type to a Western Pacific-type plate boundary. Tectonophysics 532-535: 271-290.

Liu, Y., Li, X. H., Li, Q. L., Tang, G. Q. and Yin, Q. Z. 2011. Precise U-Pb zircon dating at <5 micron scale by Cameca 1280 SIMS using Gaussian illumination probe. Journal Of Analytical Atomic Spectrometry, (26): 845-851.

Loiselle, M. C. and Wones, D. R. 1979. Characteristics and origin of anorogenic

granites. Geological Society of America Abstracts with Programs 11, (no. 7): 468.

Ludwig, K. R. 2001. Users Manual for Isoplot/Ex rev.2.49: A geological toolkit for. Microsoft Excel. Berkeley Geochronology Centre, Special publication 1a: 56.

Lumpkin, G. R. and Ewing, R. C. 1988. Alpha-decay damage in minerals of the pyrochlore group. Physics And Chemistry Of Minerals 16(1): 2-20.

Lundstrom, C. C., Chaussidon, M., Hsui, A. T., Kelemen, P. and Zimmerman, M. 2005. Observations of Li isotopic variations in the Trinity Ophiolite: evidence for isotopic fractionation by diffusion during mantle melting. Geochimica Et Cosmochimica Acta 69(3): 735-751.

Magna, T., Janousek, V., Kohut, M., Oberli, F. and Wiechert, U. 2010a. Fingerprinting sources of orogenic plutonic rocks from Variscan belt with lithium isotopes and possible link to subduction-related origin of some A-type granites. Chemical Geology 274(1-2): 94-107.

Magna, T., Mezger, K. and Fehr, M. A. 2010b. Lithium isotope composition of Mars - Corollary of radial heterogeneity in the early Solar System? Geochimica Et Cosmochimica Acta 74(12): A656-A656.

Magna, T., Wiechert, U., Grove, T. L. and Halliday, A. N. 2006a. Lithium isotope fractionation in the southern Cascadia subduction zone. Earth And Planetary Science Letters 250(3-4): 428-443.

Magna, T., Wiechert, U. and Halliday, A. N. 2006b. Lithium isotope composition of the inner solar system materials. Meteoritics & Planetary Science 41(8): A110-A110.

Magna, T., Wiechert, U. and Halliday, A. N. 2006c. New constraints on the lithium isotope compositions of the Moon and terrestrial planets. Earth And Planetary Science Letters 243(3-4): 336-353.

Magna, T., Wiechert, U. H. and Halliday, A. N. 2004. Low-blank isotope ratio measurement of small samples of lithium using multiple-collector ICPMS. International Journal of Mass Spectrometry 239(1): 67-76.

Maniar, P. D. and Piccoli, P. M. 1989. Tectonic discrimination of granitoids. Geological Society Of America Bulletin 101(5): 635-643.

Mao, J. W. and Wang, Z. L. 2000. Discussion of the timing and geodynamics of massive metallogenic in eastern China. Bulletin of Mineralogy ,Petrology and Geochemisty, (04): 403-405, (in Chinese).

Marks, M. A. W., Rudnick, R. L., Ludwig, T., Marschall, H., Zack, T., Halama, R., et. al. 2008. Sodic pyroxene and sodic amphibole as potential reference materials for

in situ lithium isotope determinations by SIMS. Geostandards and Geoanalytical Research 32(3): 295-310.

Marschall, H. R., Elliott, T. and Abell, R. 2006. The metamorphic record of lithium and boron isotope fractionation in subduction zonesdoi. Geochimica Et Cosmochimica Acta 70(18): A394-A394.

Martin, R. F. 2006. A-type granites of crustal origin ultimately result from open-system fenitization-type reactions in an extensional environment. Lithos 91(1-4): 125-136.

Matsuhisa, Y. 1974. 18O/16O ratios of NBS-28 and some silicate reference samples. Geochemical Journal 8: 103-107.

McLaren, A. C., Gerald, J. D. F. and Williams, I. S. 1994. The microstructure of zircon and its influence on the age determination from Pb/U isotopic ratios measured by ion microprobe. Geochimica Et Cosmochimica Acta 58(2): 993-1005.

McMillan, P. 1984. Structural studies of silicate glasses and melts—applications and limitations of Raman spectroscopy. American Mineralogist 69(7-8): 622-644.

Meldrum, A., Boatner, L. A., Weber, W. J. and Ewing, R. C. 1998. Radiation damage in zircon and monazite. Geochimica Et Cosmochimica Acta 62(14): 2509-2520.

Miller, C. F., McDowell, S. M. and Mapes, R. W. 2003. Hot and cold granites? Implications of zircon saturation temperatures and preservation of inheritance. Geology 31(6): 529-532.

Monani, S. and Valley, J. W. 2001. Oxygen isotope ratios of zircon: magma genesis of low delta O-18 granites from the British Tertiary Igneous Province, western Scotland. Earth And Planetary Science Letters 184(2): 377-392.

Moriguti, T. and Nakamura, E. 1998. Across-arc variation of Li isotopes in lavas and implications for crust/mantle recycling at subduction zones. Earth And Planetary Science Letters 163(1-4): 167-174.

Murakami, T., Chakoumakos, B. C., Ewing, R. C., Lumpkin, G. R. and Weber, W. J. 1991. Alpha-decay event damage in zircon. American Mineralogist 76: 5l0-1532,.

Nakamura, E., Moriguti, T. and Kobayashi, K. 2008. Lithium isotopic systematics of peridotite xenoliths from Hannuoba,North China Craton:Implications for melt-rock interaction in the considerably thinned lithospheric mantle. Conference, China Beijing.

Nasdala, L., Irmer, G. and Jonckheere, R. 2002a. Radiation damage ages: Practical concept or impracticalvision? - Reply to two comments on "Metamictisation of

natural zircon: Accumulation versus thermal annealing of radioactivity-induced damage", and further discussion. Contributions To Mineralogy And Petrology 143(6): 758-765.

Nasdala, L., Lengauer, C. L., Hanchar, J. M., Kronz, A., Wirth, R., Blanc, P., Seydoux-Guillaume, A. M. 2002b. Annealing radiation damage and the recovery of cathodoluminescence. Chemical Geology 191(1-3): 121-140.

Nasdala, L., Wenzel, M., Vavra, G., Irmer, G., Wenzel, T. and Kober, B. 2001. Metamictisation of natural zircon: accumulation versus thermal annealing of radioactivity-induced damage. Contributions To Mineralogy And Petrology 141(2): 125-144.

Oi, T., Kawada, K., Hosoe, M. and Kakihana, H. 1991. Fractionation of Lithium Isotopes in Cation-Exchange Chromatography. Separation Science And Technology 26(10-11): 1353-1375.

Oi, T., Odagiri, T. and Nomura, M. 1997. Extraction of lithium from GSJ rock reference samples and determination of their lithium isotopic compositions. Analytica Chimica Acta 340(1-3): 221-225.

Ooi, K., Miyai, Y., Makita, Y. and Kanoh, H. 1999. Fractionation of lithium isotopes in ion exchange chromatography with titanium phosphate exchanger. Separation Science And Technology 34(6-7): 1133-1144.

Ouyang, X. W. 1985. The geochemical characteristics and petrogenesis of Suzhou and Geyuan granites. Institute of Geochemistry, Chinese Academy of Sciences, Guiyang (in Chinese). MSc.

Paces, J. B. and Miller, J. D. 1993. Precise U-Pb ages of Duluth Complex and related mafic intrusions, northeastern Minnesota: Geochronological insights to physical, petrogenetic, paleomagnetic, and tectonomagmatic processes associated with the 1.1 Ga Midcontinent Rift System. Journal of Geophysical Research: Solid Earth 98(B8): 13997-14013.

Palenik, C. S., Nasdala, L. and Ewing, R. C. 2003. Radiation damage in zircon. American Mineralogist 88(5-6): 770-781.

Parkinson, I. J., Hammond, S. J., James, R. H. and Rogers, N. W. 2006. Lithium isotope fractionation at magmatic temperatures: Evidence for diffusional fractionation in phenocrysts. Geochimica et Cosmochimica Acta 70(18): A472-A472.

Parkinson, I. J., Hammond, S. J., James, R. H. and Rogers, N. W. 2007.

High-temperature lithium isotope fractionation: Insights from lithium isotope diffusion in magmatic systems. Earth And Planetary Science Letters 257(3-4): 609-621.

Patiño Douce, A. E. 1997. Generation of metaluminous A-type granites by low-pressure melting of calc-alkaline granitoids. Geology 25(8): 743-746.

Peck, W. H., Valley, J. W., Wilde, S. A. and Graham, C. M. 2001. Oxygen isotope ratios and rare earth elements in 3.3 to 4.4 Ga zircons, Ion microprobe evidence for high 18O continental crust and oceans in the Early Archean. Geochimica Et Cosmochimica Acta 65(22): 4215–4229.

Pistiner, J. S. and Henderson, G. M. 2003. Lithium-isotope fractionation during continental weathering processes. Earth And Planetary Science Letters 214(1-2): 327-339.

Qiu, J. S., Wang, D. Z. and McInnes, B. 1999. Geochemistry and petrogenesis of the I- and A-type composite granite masses in the coastal area of Zhejiang and Fujian province. Acta Petrologica Sinica 15(02): 237-246, (in Chinese with English Abstract).

Qiu, J. S., Wang, D. Z., McInnes, B. I. A., Jiang, S. Y., Wang, R. C. and Kanisawa, S. 2004. Two subgroups of A-type granites in the coastal area of Zhejiang and Fujian Provinces, SE China: age and geochemical constraints on their petrogenesis. Transactions of the Royal Society of Edinburgh: Earth Sciences 95(1-2): 227-236.

Qiu, J. S., Wang, D. Z., Peng, Y. M. and Zhou, J. C. 1996. Petrology, geochemistry and genesis of Taohuadao alkali granite in Zhoushan, Zhejiang province. Journal of nanjing university (natural sciences) 32(1): 79–89, (in Chinese with English Abstract).

Ríos, S., Salje, E. K. H., Zhang, M. and Ewing, R. C. 2000. Amorphization in zircon: evidence for direct impact damage. Journal Of Physics: condensed Matter 12(11): 2401-2412.

Rajesh, H. M. 2000. Characterization and origin of a compositionally zoned aluminous A-type granite from South India. Geological Magazine 137(3): 291-318.

Ratcliffe, N. M. and Aleinikoff, J. N. 2000. Silurian age of the Braintree Complex, VT: bearing on the age of the Cram Hill and Shaw Mountain formations. Abstract Programs- Geological Society of America 32: A-68.

Richter, F., Dauphas, N. and Teng, F. 2009. Non-traditional fractionation of non-traditional isotopes: Evaporation, chemical diffusion and Soret diffusion.

Chemical Geology 258(1-2): 92-103.

Richter, F. M., Davis, A. M., DePaolo, D. J. and Watson, E. B. 2003. Isotope fractionation by chemical diffusion between molten basalt and rhyolite. Geochimica Et Cosmochimica Acta 67(20): 3905-3923.

Rudnick, R. L. and Nakamura, E. 2004. Preface to "Lithium isotope geochemistry". Chemical Geology 212(1-2): 1-4.

Rudnick, R. L., Tomascak, P. B., Njo, H. B. and Gardner, L. R. 2004. Extreme lithium isotopic fractionation during continental weathering revealed in saprolites from South Carolina. Chemical Geology 212(1-2): 45-57.

Schuessler, J. A., Schoenberg, R. and Sigmarsson, O. 2009. Iron and lithium isotope systematics of the Hekla volcano, Iceland - Evidence for Fe isotope fractionation during magma differentiation. Chemical Geology 258(1-2): 78-91.

Seitz, H. M., Brey, G. P., Lahaye, Y., Durali, S. and Weyer, S. 2004. Lithium isotopic signatures of peridotite xenoliths and isotopic fractionation at high temperature between olivine and pyroxenes. Chemical Geology 212(1-2): 163-177.

Seitz, H. M., Brey, G. P., Zipfel, J., Ott, U., Weyer, S., Durali, S. and Weinbruch, S. 2007. Lithium isotope composition of ordinary and carbonaceous chondrites, and differentiated planetary bodies: Bulk solar system and solar reservoirs. Earth And Planetary Science Letters 260(3-4): 582-596.

Silver, L. 1963. The relation between radioactivity and discordance in zircons. Nuclear Physics 1075: 34-39.

Silver, L. T. and Sarah, D. 1963. Uranium-lead isotopic variations in zircons: A case study. The Journal of Geology 71(6): 721-758.

Skjerlie, K. P. and Johnston, A. D. 1993. Fluid-absent melting behavior of an F-rich tonalitic gneiss at mid-crustal pressures: Implications for the generation of anorogenic granites. Journal Of Petrology 34(4): 785-815.

Sláma, J., Košler, J., Condon, D. J., Crowley, J. L., Gerdes, A., Hanchar, J. M., et. al. 2008. Plešovice zircon — A new natural reference material for U–Pb and Hf isotopic microanalysis. Chemical Geology 249(1-2): 1-35.

Soderlund, U., Patchett, P. J., Vervoort, J. D. and Isachsen, C. E. 2004. The 176Lu decay constant determined by Lu-Hf and U-Pb isotope systematics of Precambrian mafic intrusions. Earth And Planetary Science Letters 219(3-4): 311-324.

Solá, A. R., Williams, I. S., Neiva, A. M. R. and Ribeiro, M. L. 2009. U-Th-Pb

SHRIMP ages and oxygen isotope composition of zircon from two contrasting late Variscan granitoids, Nisa-Albuquerque batholith, SW Iberian Massif: Petrologic and regional implications. Lithos 111(3-4): 156-167.

Sonntag, I., Ludwig, T. and Altherr, R. 2007. Diffusion profiles of Li in plagioclase/clinopyroxene and plagioclase/olivine intergrowths. Geochimica Et Cosmochimica Acta 71(15): A957-A957.

Stacey, J. S. and Kramers, J. D. 1975. Approximation of terrestrial lead isotope evolution by a two-stage model. Earth And Planetary Science Letters 26(2): 207-221.

Su, B. X., Zhang, H. F., Deloule, E., Sakyi, P. A., Xiao, Y., Tang, Y. J., . . . Liu, P. P. 2012. Extremely high Li and low δ7Li signatures in the lithospheric mantle. Chemical Geology 292-293: 149-157.

Sun, J.-F. 2010. Petrogenesis of the Early Cretaceous A-type granites in the northern Liaodong Peninsula: implications for decratonization of the North China Craton. Institute of Geology and Geophysics, Chinese Acadamy of Sciences. Ph.D Thesis (in Chinese with English Abstract).

Sun, J. F. and Yang, J. H. 2009. Early cretaceous A-type granites in the eastern north china block with relation to destruction of the craton. Earth Science-Journal of China University of Geosciences 34(1): 137-147, (in Chinese with English Abstract).

Sun, N. 1958. Suzhou two stages granites and their metamorphism. Acta Geologica Sinica 38(3): 279-291 (in Chinese with English Abstract).

Sun, S.-s. and McDonough, W. F. 1989. Chemical and isotopic systematics of oceanic basalts: implications for mantle composition and processes. Magmatism in the ocean basins. A. D. Saunders and M. J. Norry, Geological Society Special Publication. 42: 313-345.

Sun, W. D., Ding, X., Hu, Y. H. and Li, X. H. 2007. The golden transformation of the Cretaceous plate subduction in the west Pacific. Earth And Planetary Science Letters 262(3-4): 533-542.

Sylvester, P. J. 1989. Post-collisional alkaline granites. Journal Of Geology 97(3).

Tang, Y. J., Zhang, H. F., Deloule, E., Su, B. X., Ying, J. F., Santosh, M. and Xiao, Y. 2014. Abnormal lithium isotope composition from the ancient lithospheric mantle beneath the North China Craton. Scientific Reports 4.

Tang, Y. J., Zhang, H. F. and Ying, J. F. 2007. Review of the lithium isotope system as a

geochemical tracer. International Geology Review 49(4): 374-388.

Tang, Y. J., Zhang, H. F. and Ying, J. F. 2010. A brief review of isotopically light Li — a feature of the enriched mantle? International Geology Review 52: 964-976.

Taylor, H. P. and Sheppard, S. M. F. 1986. Igneous rocks .1. Processes of isotopic fractionation and isotope systematics. Reviews In Mineralogy 16: 227-271.

Teng, F.-Z. 2005. Lithium isotopic systematics of the continental crust. Geology, University of Maryland (College Park, Md.). Ph.D.

Teng, F. Z., Li, W. Y., Rudnick, R. L. and Gardner, L. R. 2010. Contrasting lithium and magnesium isotope fractionation during continental weathering. Earth And Planetary Science Letters 300(1-2): 63-71.

Teng, F. Z., Mcdonough, W. F. and Rudnick, R. L. 2006a. Diffusion-driven lithium isotope fractionation: Models and implications. Geochimica Et Cosmochimica Acta 70(18): A643-A643.

Teng, F. Z., McDonough, W. F., Rudnick, R. L., Dalpe, C., Tomascak, P. B., Chappell, B. W. and Gao, S. 2004. Lithium isotopic composition and concentration of the upper continental crust. Geochimica Et Cosmochimica Acta 68(20): 4167-4178.

Teng, F. Z., McDonough, W. F., Rudnick, R. L., Walker, R. J. and Sirbescu, M. L. C. 2006b. Lithium isotopic systematics of granites and pegmatites from the Black Hills, South Dakota. American Mineralogist 91(10): 1488-1498.

Teng, F. Z., Rudnick, R. L., McDonough, W. F., Gao, S., Tomascak, P. B. and Liu, Y. 2008. Lithium isotopic composition and concentration of the deep continental crust. Chemical Geology 255(1-2): 47-59.

Teng, F. Z., Rudnick, R. L., McDonough, W. F. and Wu, F. Y. 2009. Lithium isotopic systematics of A-type granites and their mafic enclaves: Further constraints on the Li isotopic composition of the continental crust. Chemical Geology 262(3-4): 370-379.

Tomascak, P. B., Ed. 2004. Developments in the understanding and application of lithium isotopes in the earth and planetary sciences. Reviews in Mineralogy and Geochemistry: Geochemistry of Non-Traditional Stable Isotopes. WASHINGTON, Mineralogical society of America geochemical society.

Tomascak, P. B., Carlson, R. W. and Shirey, S. B. 1999. Accurate and precise determination of Li isotopic compositions by multi-collector sector ICP-MS. Chemical Geology 158(1-2): 145-154.

Tomascak, P. B., Langmuir, C. H., le Roux, P. J. and Shirey, S. B. 2008. Lithium

isotopes in global mid-ocean ridge basalts. Geochimica Et Cosmochimica Acta 72(6): 1626-1637.

Tomascak, P. B., Ryan, J. G. and Defant, M. J. 2000. Lithium isotope evidence for light element decoupling in the Panama subarc mantle. Geology 28(6): 507-510.

Turner, S. P., Foden, J. D. and Morrison, R. S. 1992. Derivation of some A-type magmas by fractionation of basaltic magma - An example from the padthaway ridge, south Australia Lithos 28(2): 151-179.

Ushikubo, T., Kita, N. T., Cavosie, A. J., Wilde, S. A., Rudnick, R. L. and Valley, J. W. 2008. Lithium in Jack Hills zircons: Evidence for extensive weathering of Earth's earliest crust. Earth and Planetary Science Letters 272(3-4): 666-676.

Utsunomiya, S., Valley, J. W., Cavosie, A. J., Wilde, S. A. and Ewing, R. C. 2007. Radiation damage and alteration of zircon from a 3.3 Ga porphyritic granite from the Jack Hills, Western Australia. Chemical Geology 236(1–2): 92-111.

Valley, J. W. 2003. Oxygen isotope in zircon. Reviews in Mineralogy and Geochemistry.

Valley, J. W., Chiarenzelli, J. R. and Mclelland, J. M. 1994. Oxygen isotope geochemistry of zircon. Earth And Planetary Science Letters 126(4): 187-206.

Valley, J. W., Lackey, J. S., Cavosie, A. J., Clechenko, C. C., Spicuzza, M. J., Basei, M. A. S., et. al. 2005. 4.4 billion years of crustal maturation: oxygen isotope ratios of magmatic zircon. Contributions To Mineralogy And Petrology 150(6): 561-580.

Vlastelic, I., Koga, K., Chauvel, C., Jacques, G. and Telouk, P. 2009. Survival of lithium isotopic heterogeneities in the mantle supported by HIMU-lavas from Rurutu Island, Austral Chain. Earth And Planetary Science Letters 286(3-4): 456-466.

Wang, D. Z., Zhao, G. T. and Qiu, J. S. 1995. The tectonic constraint on the late Mesozoic A-type granitoids in Easten China. Geological Journal of Universities 1(2): 13-21, (in Chinese with English Abstract).

Wang, J.-m., Yang, N.-q., Li, K.-q. and Ding, G. 1993. The metallogenesis and magmatic differentiation of Suzhou A-type granite. Acta Petrologica Sinica 9(1): 33-43.

Wang, Q., Zhao, Z. H. and Xiong, X. L. 2000. The Ascertainment of Late-Yanshanian A-type Granite in Tongbai-Dabie Orogenic Belt. Acta Petrologica et Mineralogica 19(4): 297-306,315, (in Chinese with English Abstract).

Wang, Q. L. 2006. MC-ICP-MS analysis of Li isotopes of nature samples. Master

thesis of Institute of Geochemistry, Chinese Academy of Sciences., (in Chinese with English Abstract).

Wang, R. C., Fontan, F., Xu, S. J., Chen, X. M. and Monchoux, P. 1997. The association of columbite, tantalite and tapiolite in the Suzhou granite, China. Canadian Mineralogist 35: 699-706.

Wang, R. C., Shen, W. Z., Xu, J. S., Xu, K. Q. and Lai, M. Y. 1998. Oxygen isotope study on the Suzhou granite. Acta Mineralogica Sinica 18(3): 303-308, (in Chinese with English Abstract).

Wang, Y. 2009. Geochemistry of the Baicha A-type granite in Beijing Municipality: Petrogenetic and tectonic implications. Acta Petrologica Sinica, (01): 13-24, (in Chinese with English Abstract).

Watson, E. B. and Cherniak, D. J. 1997. Oxygen diffusion in zircon. Earth And Planetary Science Letters 148(3-4): 527-544.

Wei, C. S., Zheng, Y. F. and Zhao, Z. F. 1999. The hydrogen and oxygen isotope geochemistry of the Suzhou A-type granite. Acta Petrologica Sinica 15(02): 224-236, (in Chinese with English Abstract).

Wei, C. S., Zheng, Y. F. and Zhao, Z. F. 2000. Hydrogen and oxygen isotope geochemistry of A-type granites in the continental margins of eastern China. Tectonophysics 328(1-2): 205-227.

Wei, C. S., Zheng, Y. F., Zhao, S. F. and Valley, J. W. 2001a. Oxygen isotope evidence for two-stage water-rock interactions of the Nianzishan A-type granite in NE China. Chinese Science Bulletin 46(9): 727-731.

Wei, C. S., Zheng, Y. F. and Zhao, Z. F. 2001b. Nd-Sr-O isotopic geochemistry constraints on the age and origin of the A-type granites in eastern China. Acta Petrologica Sinica 17(1): 95-111.

Wei, C. S., Zheng, Y. F., Zhao, Z. F. and Valley, J. W. 2002. Oxygen and neodymium isotope evidence for recycling of juvenile crust in northeast China. Geology 30(4): 375-378.

Wei, C. S., Zheng, Y. F. and Zhao, Z. F. 2006. Pulsed lithospheric extension? A case study of the Suzhou A-type granite in eastern China. Geochimica Et Cosmochimica Acta 70(18): A693-A693.

Wei, C. S., Zhao, Z. F. and Spicuzza, M. J. 2008. Zircon oxygen isotopic constraint on the sources of late Mesozoic A-type granites in eastern China. Chemical Geology 250(1-4): 1-15.

Wen, X., Ma, C. Q., Sang, L. K., Roger, M., She, Z. B. and Xiong, F. H. 2013. The origin and evolution of the Houshihushan alkaline ring complex in the Yanshan orogenic belt. Earth Science-Journal of China University of Geosciences 38(4): 689-714, (in Chinese with English Abstract).

Wetherill, G. W. 1956. Discordant uranium-lead ages. Transactions, American Geophysical Union 37(3): 320–326.

Whalen, J. B., Currie, K. L. and Chappell, B. W. 1987. A-type granites - geochemical characteristics, discrimination and petrogenesis. Contributions To Mineralogy And Petrology 95(4): 407-419.

White, A. J. R. 1979. Sources of Granitic Magma. Annual Meetings of the Geological Society of America and Associated Societies, San Diego, California.

White, L. T. and Ireland, T. R. 2012. High-uranium matrix effect in zircon and its implications for SHRIMP U–Pb age determinations. Chemical Geology 306–307: 78-91.

Wiedenbeck, M., Hanchar, J. M., Peck, W. H., Sylvester, P., Valley, J., Whitehouse, M., . . . Zheng, Y. F. 2004. Further characterisation of the 91500 zircon crystal. Geostandards and Geoanalytical Research 28(1): 9-39.

Williams, I. S. and Hergt, J. M. 2000. U-Pb dating of Tasmanian dolerites: a cautionary tale of SHRIMP analysis of high-U zircon. Beyond 2000:New Frontiers in Isotope Geoscience Abstract Proceedings: 185–188.

Wong, J., Sun, M., Xing, G. F., Li, X. H., Zhao, G. C., Wong, K., . . . Wu, F. Y. 2009. Geochemical and zircon U-Pb and Hf isotopic study of the Baijuhuajian metaluminous A-type granite: Extension at 125-100 Ma and its tectonic significance for South China. Lithos 112(3-4): 289-305.

Woodhead, J. and Hergt, J. 2005. A preliminary appraisal of seven natural zircon reference materials for in situ Hf isotope determination. Geostandards and Geoanalytical Research 29(2): 183-195.

Woodhead, J. A., Rossman, G. R. and Thomas, A. P. 1991. Hydrous species in zircon. American Mineralogist 76(9-10): 1533-1546.

Woodland, A., Seitz, H.-M., Altherr, R., Marschall, H., Olker, B. and Ludwig, T. 2002. Li abundances in eclogite minerals: a clue to a crustal or mantle origin? Contributions To Mineralogy And Petrology 143(5): 587-601.

Wu, F., Yang, Y., Xie, L., Yang, J. and Xu, P. 2006. Hf isotopic compositions of the standard zircons and baddeleyites used in U-Pb geochronology. Chemical

Geology 234(1-2): 105-126.

Wu, F. Y., Ge, W. C., Sun, D. Y. and Guo, C. L. 2003a. Discussions on the lithospheric thinning in eastern China. Earth Science Frontiers 10(3): 51-60, (in Chinese with English Abstract).

Wu, F. Y., Jahn, B. M., Wilde, S. A., Lo, C. H., Yui, T. F., Lin, Q., et. al. 2003b. Highly fractionated I-type granites in NE China (I): geochronology and petrogenesis. Lithos 66(3-4): 241-273.

Wu, F. Y., Lin, J. Q., Wilde, S. A., Zhang, X. O. and Yang, J. H. 2005. Nature and significance of the Early Cretaceous giant igneous event in eastern China. Earth And Planetary Science Letters 233(1-2): 103-119.

Wu, F. Y. and Sun, D. Y. 1999. The Mesozoic magmatism and lithospheric thinning in eastern China. Journal of Changchun University of Science and technology 29(4): 313~ 318, (in Chinese with English Abstract).

Wu, F. Y., Sun, D. Y., Li, H. M., Jahn, B. M. and Wilde, S. 2002. A-type granite in northeastern China-age and geochemical constraints on their petrogenesis. Chemical Geology 187: 143-173.

Xie, L., Wang, R. C., Wang, D. Z. and Qiu, J. S. 2005. Contrasting Accessory Mineral Assemblages in the Taohuadao Peralkaline and Putuoshan Aluminous A-type Granites，Zhejiang Province. Geological Journal of China Universities 11(3): 390-403, (in Chinese with English Abstract).

Xu, P., Wu, F., Xie, L. and Yang, Y. 2004. Hf isotopic compositions of the standard zircons for U-Pb dating. Chinese Science Bulletin 49(15): 1642-1648.

Xu, Y. G. 2001. Thermo-tectonic destruction of the archaean lithospheric keel beneath the Sino-Korean Craton in China: Evidence, timing and mechanism. Physics And Chemistry Of The Earth Part A-solid Earth And Geodesy 26(9-10): 747-757.

Yamada, R., Tagami, T., Nishimura, S. and Ito, H. 1995. Annealing kinetics of fission tracks in zircon- an experimental study. Chemical Geology 122(1-4): 249-258.

Yan, Q. S. and Shi, X. F. 2014. Geochemistry and petrogenesis of the Cretaceous A-type granites in the Laoshan granitic complex, eastern China. Island Arc, 10.1111/iar.12070: n/a-n/a.

Yang, J. H., Wu, F.-Y. and Wilde, S. A. 2003. A review of the geodynamic setting of large-scale Late Mesozoic gold mineralization in the North China Craton: an association with lithospheric thinning. Ore Geology Reviews 23(3–4): 125-152.

Yang, J. H., Wu, F. Y., Chung, S. L., Wilde, S. A. and Chu, M. F. 2006. A hybrid origin for the Qianshan A-type granite, northeast China: Geochemical and Sr-Nd-Hf isotopic evidence. Lithos 89(1-2): 89-106.

Yang, J. H., Wu, F. Y., Wilde, S. A., Chen, F., Liu, X. M. and Xie, L. W. 2008. Petrogenesis of an alkali Syenite-Granite-Rhyolite suite in the Yanshan Fold and Thrust Belt, Eastern North China Craton: Geochronological, geochemical and Nd-Sr-Hf isotopic evidence for lithospheric thinning. Journal Of Petrology 49(2): 315-351.

Yang, S. Y., Jiang, S. Y., Zhao, K. D., Jiang, Y. H., Ling, H. F. and Luo, L. 2012. Geochronology, geochemistry and tectonic significance of two Early Cretaceous A-type granites in the Gan-Hang Belt, Southeast China. Lithos 150: 155-170.

Yu, J. S., Gui, X. T., Huang, L., Li, X. H. and Hu, R. Z. 1990. Sr-O isotopic system of granites in China. Science in China: B, (7): 738-748, (in Chinese).

Yuan, Z. X. 2001. A Discussion on the naming of A-type granites. Acta Petrologica et Mineralogica 20(3): 293-304, (in Chinese with English Abstract).

Yuan, Z. X., Zhang, M. and Wan, D. F. 2003. A discussion on the petrogenesis of δ18O-low alkali granite—A case study of Baerzhe alkali granite in Inner Mongolia. Acta Petrologica Et Mineralogica, (02): 119-124, (in Chinese with English Abstract).

Zack, T., Tomascak, P. B., Rudnick, R. L., Dalpe, C. and McDonough, W. F. 2003. Extremely light Li in orogenic eclogites: The role of isotope fractionation during dehydration in subducted oceanic crust. Earth And Planetary Science Letters 208(3-4): 279-290.

Zhang, H. F., Deloule, E., Tang, Y.-J. and Ying, J.-F. 2009. Melt/rock interaction in remains of refertilized Archean lithospheric mantle in Jiaodong Peninsula, North China Craton: Li isotopic evidence. Contributions To Mineralogy And Petrology 160(2): 261-277.

Zhang, H. F., Tang, Y. J., Zhao, X. M. and Yang, Y. H. 2007. Significance and propective of non-traditional isotopic systems in mantle geochemistry. Earth Science Frountier 14(2): 37-57, (in Chinese).

Zhang, M., Salje, E. K. H., Farnan, I., Graeme-Barber, A., Daniel, P., Ewing, R. C., et. al. 2000. Metamictization of zircon: Raman spectroscopic study. Journal Of Physics-condensed Matter 12(8): 1915-1925.

Zhang, S. B. and Zheng, Y. F. 2011. On the origin of low δ18O magmatic rocks. Acta

Petrologica Sinica 27(2): 520-530, (in Chinese with English Abstract).

Zhang, X. L., Wang, J. B. and Shen, B. C. 1988. A study on A-type granites in Suzhou, China. Geochemistry 7(1): 29-45.

Zhang, Y. X., Ed. 2010. Diffusion in minerals and melts: Theoretical background. Diffusion in Minerals and Melts, Reviews in Mineralogy and Geochemistry.

Zhao, G. T. and Wang, D. Z. 1997. The geochemistry and genesis of the Laoshan granitoids, Shandong province. Geological Journal of China Universities 3(1): 1-15, (in Chinese with English Abstract).

Zhao, G. T., Wang, D. Z., Cao, Q. C. and Yu, L. S. 1998. Thermal evolution and its significance of I-A type granitoid complex - The Laoshan Granitoid as an example. Science In China Series D-earth Sciences 41(5): 529-536.

Zhao, Z. F., Zheng, Y. F. and Wei, C. S. 2001. Kinetics of oxygen isotope exchange between water and minerals of miarolitic alkaline granite from Nianzishan. Geochimica 30(02): 177-185, (in Chinese with English Abstract).

Zhou, X. H. 2006. Major transformation of subcontinental lithosphere beneath eastern China in the Cenozoic-Mesozoic: review and prospect. Earth Science Frontiers 13(2): 50-64, (in Chinese with English Abstract).

Zhou, X. M. and Li, W. X. 2000. Petrogenesis of Late Mesozoic igneous rock in southeast China. Nature Science letters 10(03): 50-57, (in Chinese).

Zhou, X. M., Sun, T., Shen, W. Z., Shu, L. S. and Niu, Y. L. 2006. Petrogenesis of Mesozoic granitoids and volcanic rocks in South China: A response to tectonic evolution. Episodes 29(1): 26-33.

Zhou, X. R., Yang, J. and Ren, J. 1997. Comparative study of the characteristics and genesis between I and A-type granite of Suzhou area. Earth Science--Journal of China University of Geosciences 15(4): 240-246, (in Chinese with English Abstract).

Zhu, J., Hu, R.-Z., Bi, X.-W., Zhong, H. and Chen, H. 2011. Zircon U-Pb ages, Hf-O isotopes and whole-rock Sr-Nd-Pb isotopic geochemistry of granitoids in the Jinshajiang suture zone, SW China: Constraints on petrogenesis and tectonic evolution of the Paleo-Tethys Ocean. Lithos 126(3-4): 248-264.

Zhu, K.-Y., Li, Z.-X., Xu, X.-S. and Wilde, S. A. 2013. Late Triassic melting of a thickened crust in southeastern China: Evidence for flat-slab subduction of the Paleo-Pacific plate. Journal Of Asian Earth Sciences 74: 265-279.

APPENDIX TABLE i. List of samples studied

No.	Sample name	Lithology	Thin section	Whole-rock	Mount
Nianzishan (47°31'52"N, 122°50'31"E)					
1	10NZS	alkaline granite	yes	yes	A1193
2	GW04190	alkaline granite	yes	-	A1193
3	11-NZS-01	alkaline granite	yes	yes	A1777
4	11-NZS-02	alkaline granite	yes	yes	A1777
5	11-NZS-03	alkaline granite	yes	yes	A1777
6	11-NZS-04	alkaline granite	yes	yes	A1777
7	11-NZS-05	alkaline granite	yes	yes	A1777
Houshihushan (40°02'17"N, 119°41'54"E)					
1	10SHG-01	miarolitic K-feldspar granite	yes	yes	A1193
2	10YSH-03	MME	yes	-	
3	10YSH-04	miarolitic K-feldspar granite	yes	yes	A1195
4	10YSH-05	miarolitic K-feldspar granite	yes	-	
5	HSH01	miarolitic K-feldspar granite	-	yes	
6	HSH02	miarolitic K-feldspar granite	-	yes	
7	HSH03	miarolitic K-feldspar granite	-	yes	
8	HSH04	miarolitic K-feldspar granite	-	yes	
9	HSH05	miarolitic K-feldspar granite	-	yes	
10	HSH06	miarolitic K-feldspar granite	-	yes	
11	HSH07	miarolitic K-feldspar granite	-	yes	
12	10YSH-01	rhyolite	yes	yes	A1195
13	10YSH-02	rhyolite	yes	yes	
14	HSH08	rhyolite	-	yes	
15	HSH09	rhyolite	-	yes	
16	HSH10	rhyolite	-	yes	
Laoshan (36°14'12"N, 120°39'42"E)					
1	09LS02	quartz syenite	yes	yes	
2	09LS03	Bi granite	yes	yes	
3	09LS04	Bi granite	yes	yes	
4	09LS06	Bi granite	yes	yes	
5	09LS07	quartz syenite	yes	yes	
6	10LS01	quartz syenite	yes	yes	
7	10LS05	quartz syenite	yes	yes	A1193
8	09LS01	middle to fine grain granite	yes	-	
9	09LS08	Bi granite	yes	yes	
10	09LS09	granite-porphyry	yes	-	
11	09LS10	K-feldspar granite	yes	yes	
12	09LS11	K-feldspar granite	yes	yes	
13	09LS12	K-feldspar granite	-	yes	
14	09LS14	K-feldspar granite	-	yes	
15	09LS05	K-feldspar granite	-	yes	A1193
16	10LS02	K-feldspar granite	-	yes	
17	10LS03	K-feldspar granite	-	yes	
18	10LS04	K-feldspar granite	-	yes	
19	10LS06	K-feldspar granite	-	yes	

20	10LS07	K-feldspar granite	-	yes	
Suzhou pluton (31°18'48" N， 120°29'55" E)					
1	09YY085	Bi-K-feldspar granite	yes	yes	A806, A1538
2	09YY086	MME	yes	-	
3	09YY087	Bi-K-feldspar granite	yes	yes	
4	09YY088	MME	yes	-	
5	09YY089	Bi-K-feldspar granite	yes	yes	
6	09YY090	Bi-K-feldspar granite	yes	yes	
7	09YY091	Bi-K-feldspar granite	yes	yes	
8	09YY092	Bi-K-feldspar granite	yes	yes	
9	09YY093	Bi-K-feldspar granite	yes	yes	
10	09YY094	K-feldspar granite	yes	-	A1198
11	09YY095	albitized K-feldspar granite	yes	yes	
12	09YY096	albitized K-feldspar granite	yes	yes	A1198
13	09YY097	albitized K-feldspar granite	yes	yes	A806, A1538
14	09YY098	Bi-K-feldspar granite	yes	yes	A1198
15	09YY099	Bi-K-feldspar granite	yes	yes	A1198
16	09YY100	albitized K-feldspar granite	yes	yes	
17	09YY101	Am porphyritic K-feldspar granite	yes	yes	
18	09YY102	Am porphyritic K-feldspar granite	yes	yes	
19	09YY103	Am porphyritic K-feldspar granite	yes	yes	A806, A1538
20	09YY104	MME	-	-	
21	09YY105	Am porphyritic K-feldspar granite	-	yes	A806, A1538
22	09YY106	Half granite half MME	-	-	
23	09YY107	Am porphyritic K-feldspar granite	-	yes	
24	09YY108	Am porphyritic K-feldspar granite	-	yes	
25	09YY109	Am porphyritic K-feldspar granite	-	yes	
26	09YY110	Am porphyritic K-feldspar granite	-	yes	
27	09YY111	Am porphyritic K-feldspar granite	-	yes	
28	09YY112	albitized K-feldspar granite	-	yes	
29	09YY113	albitized K-feldspar granite	-	yes	
30	09YY114	Bi-K-feldspar granite	-	-	A1198
31	09YY115	Bi-K-feldspar granite	yes	-	
Taohuadao (29°48'44" N,122°17'27" E)					
1	09YY118	fine grain granite	yes	yes	
2	09YY119	middle grain miarolitic granite	yes	yes	
3	09YY120	fine grain granite	yes	yes	
4	09YY121	middle grain granite	yes	yes	
5	09YY122	middle grain miarolitic granite	yes	yes	
6	09YY123	J3 dacite	yes	-	
7	09YY124	J3 dacite	yes	-	
8	09YY125	middle grain miarolitic alkaline granite	yes	yes	
9	09YY126	middle to fine grain miarolitic alkaline granite	-	yes	A1199, A1539
10	09YY127	fine grain alkaline granite	yes	yes	
11	09YY128	fine grain alkaline granite	yes	yes	
12	09YY129	fine grain alkaline granite	yes	yes	A806, A1538
13	09YY130	middle to fine grain miarolitic alkaline granite	yes	yes	A1199, A1539
14	09YY131	fine grain K-feldspar granite	yes	yes	
15	09YY132	fine grain K-feldspar granite	-	yes	
16	09YY133	J3 dacite	-	-	

17	09YY145	J3 dacite	-	-	
18	09YY146	middle grain miarolitic granite	-	yes	
19	09YY147	fine grain K-feldspar granite	-	yes	
20	09YY148	fine grain miarolitic K-feldspar granite	-	yes	A806, A1538
21	09YY149	fine grain K-feldspar granite	-	yes	
22	09YY150	fine grain K-feldspar granite	-	yes	
23	09YY151	fine grain K-feldspar granite	yes	yes	
24	09YY152	middle tofine grain K-feldspar granite	yes	yes	
25	09YY153	middle grain miarolitic granite	yes	yes	
26	09YY154	middle grain	yes	yes	
27	09YY155	middle grain	yes	-	A1199, A1539
28	09YY156	Am cumulates	-	-	
Putuoshan (29°58'51"N，122°23'9"E)					
1	09YY134	K-feldspar granite	yes	yes	
2	09YY135	alkaline granites	yes	yes	
3	09YY136	Bi granites	yes	yes	A807, A1539
4	09YY137	K-feldspar granite	-	yes	
5	09YY138	K-feldspar granite	yes	yes	
6	09YY139	alkaline granites	yes	yes	
7	09YY140	dyke	yes	-	
8	09YY141	MME	yes	-	
9	09YY142	alkaline granites	yes	yes	A1199, A1539
10	09YY143	alkaline granites	yes	yes	
11	09YY144	MME	-	-	
12	09YY157	Bi granites	yes	yes	
13	09YY158	dyke	yes	-	
14	09YY159	K-feldspar granite	yes	yes	
15	09YY160	Bi granites	yes	yes	
16	09YY161	Bi granites	yes	yes	
17	09YY162	K-feldspar granite	-	yes	
18	09YY163	K-feldspar granite	yes	yes	A807, A1539
19	09YY164	MME	-	yes	
20	09YY165	K-feldspar granite	-	yes	
21	09YY166	alkaline granites	-	yes	
22	09YY167	MME	-	yes	
23	09YY168	MME	yes	yes	
24	09YY169	MME	-	yes	
25	09YY170	alkaline granites	yes	yes	A1199, A1539

Appendix Table ii. Major(%) and trace element(ppm) analyses for the studied granites

	Nianzishan alkaline granite									Houshihu
Sample#	10NZS	10NZS01	10NZS02	10NZS03	10NZS04	10NZS05	10SHG01	10YSH04	HSH01	HSH02
Oxide(wt%)										
SiO2	74.57	74.40	73.80	74.50	74.40	72.20	76.31	74.71	75.47	76.03
TiO2	0.22	0.22	0.18	0.22	0.22	0.28	0.15	0.14	0.18	0.12
Al2O3	11.96	12.20	13.00	12.30	12.50	13.80	11.64	13.05	12.21	11.64
FeOt	3.38	1.23	1.49	1.48	1.53	1.23	2.55	2.09	2.40	1.16
MnO	0.11	0.14	0.09	0.15	0.13	0.14	0.09	0.05	1.44	0.40
MgO	0.06	0.05	0.05	0.04	0.05	0.11	0.04	0.09	0.03	0.10
CaO	0.26	0.17	0.23	0.26	0.31	0.49	0.18	0.28	0.16	0.21
Na2O	4.13	4.63	4.88	4.82	4.77	5.22	3.99	3.77	3.76	3.89
K2O	4.60	4.50	4.64	4.50	4.49	5.07	4.56	5.33	4.69	4.65
P2O5	0.02	0.03	0.01	0.01	0.02	0.02	0.01	0.01	0.02	0.01
LOI	0.50	0.26	0.17	0.13	0.22	0.17	0.29	0.29	0.02	0.01
Total	99.81	97.82	98.53	98.41	98.64	98.73	99.81	99.81	100.38	98.23
A/CNK	0.98	0.95	0.97	0.93	0.94	0.92	0.98	1.05	1.06	0.99
Traceelement(ppm)										
Zn	24.8	18.7	20.1	24.5	23.5	22.3	23.9	27.9	25.0	25.2
Ga	25.8	23.0	27.2	21.6	25.7	25.5	27.0	25.8	27.4	26.2
Rb	194	199	186	186	193	198	243	180	212	212
Sr	7.45	6.71	6.79	6.32	6.99	7.63	3.20	24.30	5.49	7.02
Y	66.6	71.0	73.9	68.7	83.9	65.5	60.4	59.8	60.2	59.6
Zr	1336	1334	1429	1392	1088	1180	976	527	752	752
Nb	106.0	111.3	88.5	105.3	84.4	87.3	97.8	55.6	76.4	76.2
Cs	1.70	1.81	1.95	1.93	1.73	1.46	2.68	3.47	3.24	2.93
Ba	86.3	93.2	80.6	73.7	77.0	86.8	8.5	73.9	40.1	41.2
La	95	96	85	109	117	117	99	97	99	98
Ce	212	174	211	231	241	248	219	188	204	205
Pr	24.2	21.0	22.9	22.9	24.2	24.2	24.3	20.6	24.5	22.4
Nd	81.5	76.6	84.6	83.9	86.7	90.7	79.1	72.7	77.4	76.9
Sm	15.1	13.9	17.0	16.7	15.0	17.4	14.6	13.0	14.7	13.9
Eu	0.484	0.384	0.417	0.459	0.520	0.497	0.050	0.060	0.080	0.030
Gd	14.2	12.9	14.7	16.3	14.5	14.3	13.8	9.9	11.7	12.3
Tb	2.12	2.16	1.98	2.18	1.61	1.98	2.05	1.61	1.52	1.88
Dy	12.8	10.7	12.0	11.4	13.3	14.1	12.4	9.4	10.7	10.9
Ho	2.53	2.60	2.56	2.50	2.37	3.00	2.44	1.65	2.18	2.01
Er	7.36	6.58	7.24	7.41	7.12	7.07	7.04	4.78	5.84	5.91
Tm	1.06	0.99	1.09	1.04	1.13	1.06	1.05	0.72	0.83	1.04
Yb	6.99	7.40	8.04	6.97	5.97	8.35	7.11	5.42	6.46	6.28
Lu	1.03	1.00	0.98	0.99	1.02	0.98	1.06	0.87	0.96	1.09
Hf	33.2	27.0	30.5	35.1	28.9	26.2	27.9	15.2	21.4	21.3
Ta	5.69	5.99	4.72	6.37	6.65	4.91	5.59	3.51	6.49	4.18
Pb	36.2	29.9	43.3	32.4	34.7	33.9	34.0	28.6	31.3	31.3
Th	21.5	20.1	24.1	24.2	18.9	20.1	25.6	16.8	19.4	21.1
U	3.99	3.30	4.28	4.44	4.29	4.63	5.20	5.24	5.34	5.52
Zr+Nb+Ce+Y	1721	1690	1803	1796	1497	1581	1354	830	1092	1093
Tzr	1004	1001	1008	1000	972	972	970	904	948	940
Eu*	0.10	0.09	0.08	0.08	0.11	0.10	0.01	0.02	0.02	0.01
10^4Ga/Al	4.1	3.6	4.0	3.3	3.9	3.5	4.4	3.7	4.2	4.2

Analytical precision is 2% 5% for major elements, and better than 3% for trace elements.

Note: LOI stands for loss on ignition; A/CNK = mole $Al_2O_3/(CaO+K_2O+Na_2O)$;

$T_{Zr} = 12900/[2.95 + 0.85M + \ln(496000/Zr_{melt})]$, M = (Na + K + 2*Ca)/(Al*Si)

ıshan alkaline granite					**Houshihushan rhyolite**					**Laoshan**
HSH03	HSH04	HSH05	HSH06	HSH07	10YSH01	10YSH02	HSH08	HSH09	HSH10	09LS08
75.23	75.44	75.18	75.36	74.22	72.47	73.98	69.04	68.73	68.53	72.47
0.17	0.19	0.19	0.18	0.23	0.26	0.12	0.29	0.45	0.53	0.32
12.38	12.47	12.90	11.76	12.43	14.66	14.00	14.86	14.66	14.66	14.48
3.17	2.19	2.40	2.58	2.28	3.38	1.14	3.48	3.43	3.48	1.64
0.20	0.75	0.01	0.49	0.98	0.02	0.01	0.14	0.15	0.14	0.05
0.05	0.14	0.05	0.11	0.04	0.07	0.05	0.17	0.40	0.28	0.41
0.15	0.23	0.17	0.20	0.42	0.14	0.31	0.66	0.71	0.68	1.08
3.41	3.31	4.01	3.50	3.89	6.85	2.80	5.21	5.46	5.11	4.09
5.38	5.11	6.03	6.12	5.25	1.37	5.86	1.37	1.18	1.21	4.81
0.03	0.02	0.01	0.01	0.02	0.03	0.04	0.22	0.05	0.17	0.08
0.03	0.02	0.01	0.01	0.02	0.53	0.77	0.22	0.05	0.17	0.35
100.20	99.87	100.96	100.32	99.78	99.78	99.08	95.66	95.27	94.96	99.78
1.06	1.09	0.96	0.92	0.97	1.13	1.22	1.32	1.27	1.34	1.04
25.8	25.9	25.7	26.0	25.6	26.2	73.2	73.4	73.2	73.1	38.6
25.6	26.5	26.8	26.3	25.5	27.7	27.2	27.0	26.6	27.2	18.3
212	212	212	212	212	38	94	94	94	94	144
6.18	6.70	6.76	5.99	7.85	30.69	52.18	52.24	52.26	52.39	159.51
60.2	61.1	58.0	59.7	59.9	23.3	32.3	32.0	32.0	32.8	25.8
752	751	752	753	752	516	463	463	463	463	231
77.3	76.1	77.7	76.8	77.4	39.7	39.8	39.6	39.8	39.4	26.7
3.10	2.95	3.42	4.27	3.18	0.39	1.04	1.19	0.89	1.20	1.03
41.2	40.6	41.4	39.9	41.8	38.6	91.5	91.4	91.7	91.6	713.5
98	98	98	99	98	24	24	24	24	24	70
204	204	203	204	204	83	119	119	119	120	115
22.5	22.2	22.5	22.4	22.5	5.1	11.4	11.4	11.5	11.3	10.7
75.9	75.6	76.0	76.2	75.6	17.8	42.7	42.9	42.8	42.8	35.1
13.9	14.0	14.6	13.9	13.8	3.3	7.5	7.6	7.4	7.3	5.5
0.080	0.110	0.050	0.060	0.090	0.180	0.540	0.440	0.470	0.290	0.840
12.3	12.6	13.7	11.5	11.9	3.7	6.3	6.1	6.1	6.1	4.2
1.78	1.96	1.97	2.06	1.97	0.67	1.13	0.81	0.94	1.15	0.62
10.8	11.3	10.4	10.9	11.0	4.6	5.5	5.6	6.0	5.9	3.6
1.94	1.78	2.02	2.25	2.21	0.96	1.19	1.24	1.21	1.11	0.64
5.87	6.29	7.62	5.70	5.96	2.67	3.47	3.60	3.58	3.45	1.96
0.87	0.92	0.96	0.85	1.01	0.38	0.45	0.49	0.42	0.45	0.31
6.84	6.24	6.67	6.19	7.23	2.55	3.09	3.47	3.28	3.36	2.41
1.04	0.93	0.99	0.94	1.03	0.39	0.40	0.39	0.38	0.47	0.39
22.4	21.3	21.5	22.0	22.3	12.1	10.1	9.9	10.3	10.4	6.6
4.69	4.95	3.83	4.54	4.73	2.32	1.88	1.92	2.01	2.04	1.67
31.4	31.4	31.2	30.4	31.0	7.9	11.8	11.6	11.2	11.5	24.1
21.4	21.1	20.3	22.2	21.3	8.1	8.2	8.1	8.1	8.1	14.0
5.31	5.00	6.82	4.55	4.65	0.90	0.53	0.93	0.79	0.52	2.07
1093	1092	1090	1093	1093	662	654	654	654	655	398
946	952	931	928	933	906	908	912	907	914	817
0.02	0.03	0.01	0.01	0.02	0.15	0.24	0.20	0.21	0.13	0.54
3.9	4.0	3.9	4.2	3.9	3.6	3.7	3.4	3.4	3.5	2.4

quartz syenite							La			
09LS07	09LS04	10LS05	09LS06	09LS02	10LS01	09LS03	09LS10	10LS04	09LS05	10LS06
72.64	74.00	74.63	75.88	75.83	76.33	76.61	76.54	76.65	76.70	76.87
0.39	0.20	0.32	0.12	0.16	0.14	0.14	0.17	0.14	0.18	0.10
14.13	14.14	13.13	13.31	13.06	12.92	12.83	13.14	12.61	12.90	12.58
1.75	1.20	1.64	0.85	0.95	1.13	0.93	0.78	1.24	0.84	0.99
0.06	0.02	0.10	0.05	0.04	0.09	0.05	0.02	0.09	0.01	0.03
0.47	0.07	0.19	0.08	0.16	0.05	0.13	0.05	0.08	0.12	0.08
1.18	0.21	0.42	0.50	0.49	0.05	0.41	0.10	0.06	0.34	0.25
3.93	4.53	4.11	4.06	3.84	4.12	3.69	3.73	4.11	3.58	4.12
4.80	5.06	4.93	4.56	4.81	4.66	4.59	4.77	4.60	4.75	4.44
0.09	0.01	0.03	0.01	0.03	0.01	0.03	0.01	0.02	0.03	0.01
0.35	0.36	0.30	0.39	0.44	0.31	0.40	0.51	0.22	0.36	0.35
99.79	99.80	99.80	99.81	99.81	99.81	99.81	99.82	99.82	99.81	99.82
1.02	1.06	1.02	1.06	1.05	1.08	1.09	1.14	1.06	1.11	1.05
43.5	23.9	21.0	17.4	27.9	24.5	23.3	18.2	24.4	25.0	25.6
18.3	17.5	20.6	18.2	16.7	20.8	18.9	17.5	22.0	17.6	23.7
137	224	136	179	199	184	232	211	204	206	257
179.78	46.09	16.30	14.87	87.87	20.39	57.70	13.28	4.68	54.81	6.08
32.5	10.4	53.3	15.1	10.8	28.5	9.6	14.9	22.6	8.5	27.4
276	127	446	153	136	232	157	192	261	149	253
29.4	29.5	40.8	28.3	28.1	40.5	30.1	54.5	48.6	28.7	53.9
0.93	1.70	0.92	0.86	1.03	0.55	1.10	0.54	0.69	1.23	2.43
784.8	197.3	96.6	38.8	383.6	115.2	216.6	17.2	37.6	235.9	34.8
78	48	61	47	49	30	46	52	29	22	47
135	59	135	75	68	61	66	87	41	19	59
13.0	4.6	15.3	6.3	5.3	4.5	5.1	5.7	4.9	3.0	5.1
44.3	12.9	52.8	16.6	15.4	14.4	14.0	15.1	15.4	9.8	14.1
7.2	1.7	10.2	2.3	2.1	2.7	1.8	2.0	2.9	1.5	2.1
1.020	0.260	0.630	0.180	0.350	0.230	0.310	0.090	0.190	0.230	0.150
5.4	1.4	10.0	2.4	1.7	2.5	1.9	1.8	2.4	1.1	1.9
0.81	0.20	1.53	0.33	0.23	0.48	0.23	0.27	0.44	0.17	0.32
4.6	1.2	9.4	2.1	1.3	3.2	1.4	1.7	2.9	1.1	2.2
0.83	0.23	1.92	0.47	0.25	0.65	0.30	0.35	0.56	0.20	0.51
2.47	0.77	5.55	1.60	0.83	2.12	1.02	1.19	1.84	0.71	1.90
0.37	0.14	0.79	0.27	0.15	0.36	0.18	0.21	0.33	0.13	0.37
2.92	1.34	5.00	2.03	1.35	2.92	1.48	1.81	2.80	1.29	3.48
0.46	0.26	0.70	0.32	0.26	0.49	0.27	0.30	0.47	0.25	0.63
7.7	5.1	11.8	5.8	5.1	8.0	5.8	7.5	9.9	5.6	10.3
1.87	1.79	2.13	1.59	1.79	2.16	1.78	3.02	2.54	1.92	2.88
25.1	29.0	16.3	25.6	25.5	30.2	22.3	23.2	12.8	23.8	13.1
14.4	25.6	10.5	21.1	20.8	24.9	25.3	23.6	20.7	30.5	32.2
2.42	2.73	1.28	3.59	2.88	2.71	2.98	4.29	4.08	2.49	5.75
474	227	676	272	243	361	263	349	373	206	393
833	769	883	788	777	828	794	817	838	791	833
0.50	0.51	0.19	0.23	0.56	0.27	0.50	0.14	0.22	0.54	0.23
2.4	2.3	3.0	2.6	2.4	3.0	2.8	2.5	3.3	2.6	3.6

ıoshan alkaline granite						**Suzhou Amphibole-bearing porph**				
10LS02	10LS03	10LS07	09LS11	09LS12	09LS14	09YY101	09YY102	09YY103	09YY105	09YY107
77.11	77.07	77.85	78.15	77.58	77.32	71.76	72.39	70.20	78.19	73.35
0.08	0.12	0.10	0.08	0.11	0.11	0.38	0.33	0.46	0.09	0.23
13.05	12.62	12.53	11.91	12.03	12.27	13.65	13.67	14.12	11.86	13.55
0.51	1.04	0.63	0.93	1.10	1.04	2.33	2.37	3.19	1.09	1.89
0.03	0.08	0.00	0.01	0.09	0.08	0.07	0.05	0.07	0.02	0.08
0.11	0.07	0.06	0.04	0.05	0.05	0.82	0.60	0.87	0.06	0.37
0.08	0.05	0.05	0.21	0.21	0.19	1.64	1.27	1.60	0.46	0.94
3.50	3.99	3.83	3.99	4.00	4.12	3.63	3.65	3.70	3.39	3.62
4.89	4.47	4.38	4.16	4.31	4.38	5.03	5.00	4.87	4.55	5.47
0.01	0.01	0.01	0.01	0.01	0.01	0.07	0.07	0.10	0.00	0.04
0.46	0.31	0.35	0.33	0.31	0.26	0.71	0.69	0.89	0.41	0.60
99.83	99.83	99.79	99.82	99.80	99.83	100.09	100.09	100.07	100.12	100.14
1.17	1.10	1.13	1.04	1.03	1.03	0.95	1.00	0.99	1.05	1.00
22.8	20.4	24.5	24.8	21.8	21.6	79.67	88.24	53.64	52.95	90.23
18.3	22.1	23.0	23.4	21.1	20.9	19.27	21.00	21.90	19.80	19.96
263	200	300	242	216	198	278	314	293	375	294
29.67	2.60	5.31	5.59	2.41	1.51	124.11	105.49	71.92	20.17	72.64
19.1	8.6	7.1	16.8	29.9	24.9	65.26	76.71	66.48	61.33	63.17
90	162	208	174	230	153	219	255	223	157	215
48.2	34.0	56.8	54.6	40.1	32.9	29.3	46.8	53.4	56.1	36.6
1.20	0.64	1.34	0.67	1.51	1.41	8.76	8.67	6.39	5.40	9.27
120.9	15.9	29.8	33.4	11.3	6.5	547.50	513.24	416.06	100.11	492.16
20	19	40	45	31	31	71	53	64	43	62
36	29	48	59	53	50	131	99	123	93	115
2.7	3.4	2.9	4.0	4.5	4.3	13.25	10.71	12.53	8.70	11.87
7.3	9.4	6.6	10.1	13.6	12.6	46.21	38.23	43.87	29.66	41.98
1.3	1.7	0.7	1.5	2.6	2.3	8.93	8.25	8.85	6.44	8.42
0.070	0.140	0.070	0.110	0.120	0.100	0.760	0.680	0.550	0.180	0.640
1.3	1.6	0.7	1.4	2.3	2.1	9.34	7.81	9.41	6.41	8.64
0.25	0.25	0.10	0.23	0.45	0.39	1.57	1.50	1.59	1.19	1.48
1.8	1.6	0.7	1.5	3.0	2.6	8.46	8.59	8.65	6.96	8.08
0.39	0.34	0.17	0.34	0.64	0.53	1.89	2.11	1.96	1.79	1.82
1.40	1.17	0.75	1.27	2.16	1.75	4.97	5.45	5.13	4.38	4.77
0.26	0.21	0.18	0.25	0.38	0.29	0.93	1.12	1.03	0.90	0.92
2.25	1.73	1.92	2.47	3.21	2.39	5.13	6.15	6.02	5.04	5.08
0.38	0.29	0.39	0.46	0.54	0.38	0.87	1.04	1.03	0.83	0.88
5.0	5.5	9.8	7.8	8.4	5.7	6.88	8.48	8.16	6.68	7.09
3.29	1.67	2.65	2.99	2.16	1.75	2.58	3.06	3.15	3.95	4.16
17.9	16.5	18.6	14.0	22.3	19.2	42.01	44.26	30.94	72.58	52.66
29.9	12.9	34.6	36.7	17.5	15.1	27.73	36.46	37.66	34.95	26.98
3.17	2.36	7.02	8.55	6.56	3.54	7.37	10.88	10.29	9.18	7.86
194	234	320	304	353	261	445	478	466	367	429
753	798	824	800	825	787	801	822	806	792	808
0.17	0.26	0.31	0.23	0.15	0.14	0.25	0.26	0.18	0.08	0.23
2.7	3.3	3.5	3.7	3.3	3.2	2.67	2.90	2.93	3.15	2.78

yritic K-feldspar granite				Biotite-K-feldspar granite						
09YY108	09YY109	09YY110	09YY111	09YY85	09YY87	09YY89	09YY90	09YY91	09YY92	09YY93
73.58	73.10	73.60	75.92	74.45	73.85	74.77	74.61	76.29	73.62	76.43
0.22	0.25	0.22	0.17	0.21	0.23	0.24	0.16	0.06	0.22	0.04
13.54	13.56	13.30	13.12	12.97	13.27	12.86	13.39	12.93	13.55	13.20
1.78	2.07	1.57	0.91	1.92	2.16	2.08	1.46	1.25	1.72	0.76
0.09	0.07	0.05	0.07	0.05	0.05	0.05	0.03	0.04	0.04	0.04
0.37	0.47	0.39	0.29	0.20	0.19	0.25	0.18	0.11	0.34	0.19
0.92	1.06	1.22	0.74	0.70	0.69	0.95	0.64	0.34	0.85	0.18
3.50	3.58	3.56	3.80	3.87	3.89	3.95	4.01	4.28	3.26	3.82
5.33	5.15	5.10	4.70	5.04	5.02	4.80	5.12	4.28	5.20	4.70
0.04	0.04	0.03	0.02	0.03	0.03	0.04	0.02	0.00	0.03	0.00
0.77	0.53	1.07	0.46	0.71	0.69	0.15	0.58	0.64	1.28	0.84
100.14	99.88	100.11	100.20	100.15	100.07	100.14	100.20	100.22	100.11	100.20
1.03	1.01	0.98	1.03	0.99	1.01	0.96	1.01	1.05	1.08	1.13
97.11	108.41	52.86	47.02	75.52	87.09	76.47	54.70	34.46	49.80	32.55
20.22	19.86	19.52	18.98	23.37	24.94	23.56	23.08	21.63	19.76	29.06
307	316	286	256	309	308	328	326	636	282	727
75.41	79.45	91.05	62.51	34.45	37.59	37.07	36.50	4.39	57.19	5.20
62.67	69.30	65.67	57.27	97.24	104.50	98.84	78.96	65.74	68.94	49.86
217	183	204	190	303	316	257	227	127	236	127
32.6	41.3	36.4	46.1	63.5	67.2	65.2	47.7	94.4	45.8	71.2
9.68	11.26	7.65	5.58	3.52	3.53	4.97	4.95	12.12	5.28	12.90
503.12	447.80	470.84	353.04	204.65	222.50	193.10	216.46	16.28	317.19	12.90
63	60	53	52	70	93	76	58	49	57	59
115	109	100	103	142	178	143	117	121	110	137
11.88	11.34	10.89	10.73	14.67	17.77	15.62	12.75	11.98	11.39	12.21
42.71	39.71	39.60	39.45	52.06	62.63	54.76	44.02	37.76	40.00	38.23
8.52	8.05	7.86	7.63	11.47	13.53	11.98	9.74	8.11	8.19	7.68
0.670	0.590	0.610	0.460	0.400	0.440	0.360	0.390	0.050	0.440	0.120
8.90	8.69	8.17	8.09	10.99	13.35	11.55	9.28	8.74	8.48	8.77
1.52	1.49	1.44	1.36	2.08	2.38	2.15	1.74	1.48	1.47	1.31
8.21	8.31	7.95	7.28	11.89	13.26	12.15	9.84	8.39	8.18	6.95
1.87	2.00	1.87	1.62	2.92	3.17	2.93	2.36	1.97	1.92	1.50
4.84	5.14	4.88	4.40	7.21	7.92	7.20	5.71	5.11	4.94	4.36
0.92	1.06	0.96	0.89	1.43	1.52	1.38	1.08	1.03	0.96	0.90
5.16	5.88	5.39	5.10	7.70	8.16	7.60	5.89	5.94	5.47	5.23
0.88	0.99	0.92	0.84	1.30	1.38	1.27	1.00	1.03	0.94	0.91
7.06	6.84	6.59	6.80	10.58	10.85	9.43	8.50	8.18	8.24	9.26
2.68	4.59	4.03	3.67	4.26	3.11	3.38	3.35	7.12	2.54	10.04
49.87	47.45	56.02	33.01	36.37	36.40	34.05	32.77	33.39	23.35	29.30
28.18	33.81	33.88	30.99	31.22	32.10	25.95	24.36	41.14	33.02	50.34
8.37	10.78	9.16	8.50	6.38	7.82	12.96	11.57	3.87	5.40	1.99
427	403	406	397	606	665	564	470	408	461	385
812	795	802	804	841	847	821	815	771	827	778
0.23	0.21	0.23	0.18	0.11	0.10	0.09	0.12	0.02	0.16	0.04
2.82	2.77	2.77	2.73	3.40	3.55	3.46	3.26	3.16	2.76	4.16

		Albitized K-feldspar granite						Taohuadao alkaline granite		
09YY98	09YY99	09YY95	09YY96	09YY97	09YY100	09YY112	09YY113	09YY118	09YY119	09YY120
77.15	74.76	74.79	73.80	77.39	76.95	74.72	75.10	78.05	77.77	77.76
0.05	0.18	0.20	0.19	0.09	0.09	0.22	0.18	0.16	0.17	0.14
12.94	13.20	13.05	13.59	12.08	12.69	12.98	12.85	12.08	11.95	11.93
0.37	1.43	1.48	1.76	0.99	0.81	1.99	1.56	0.86	1.28	1.11
0.01	0.03	0.04	0.04	0.02	0.02	0.05	0.04	0.02	0.04	0.07
0.08	0.22	0.25	0.18	0.11	0.12	0.24	0.21	0.07	0.10	0.07
0.32	0.85	0.82	0.69	0.53	0.59	0.68	0.70	0.08	0.09	0.15
3.94	3.90	3.64	4.08	3.60	3.82	3.81	3.78	4.13	4.31	4.24
5.03	5.02	5.10	5.29	4.75	4.54	4.83	5.07	4.52	4.16	4.44
0.00	0.02	0.03	0.02	0.00	0.00	0.03	0.02	0.00	0.00	0.00
0.69	0.15	0.74	0.52	0.61	0.58	0.59	0.65	0.28	0.36	0.31
100.58	99.76	100.14	100.16	100.17	100.21	100.14	100.16	100.24	100.22	100.23
1.03	0.99	1.00	0.99	1.00	1.03	1.02	0.99	1.02	1.02	0.99
10.38	44.42	53.46	69.75	36.06	24.30	64.49	47.85	98.09	806.76	194.24
21.84	22.22	21.81	23.30	22.18	23.72	21.72	20.60	22.04	38.95	22.79
346	359	324	320	422	473	275	275	223	391	207
17.60	48.41	63.24	39.47	8.80	12.72	51.05	51.92	3.53	10.25	1.93
107.46	88.90	74.30	80.69	76.09	111.19	77.96	66.77	6.93	38.91	20.55
132	221	262	273	222	149	294	246	258	600	230
90.5	52.6	50.1	53.7	73.6	80.1	47.3	40.0	31.1	77.0	28.1
2.66	6.43	6.35	7.13	7.05	5.96	3.41	3.32	0.55	1.16	0.77
66.10	273.18	328.25	261.83	42.93	51.48	296.60	283.21	14.57	22.85	4.07
26	64	66	57	49	30	79	66	27	54	31
80	120	127	108	84	68	150	124	52	77	74
9.07	12.47	13.16	11.66	8.88	8.09	15.55	13.23	4.93	9.65	4.97
35.12	43.71	46.86	43.40	29.20	29.82	54.47	46.75	13.28	28.88	13.75
9.38	9.62	9.26	9.87	6.59	7.90	11.37	9.44	1.73	4.71	2.30
0.130	0.430	0.470	0.470	0.090	0.120	0.510	0.480	0.071	0.212	0.107
7.20	9.44	9.33	9.53	6.68	6.50	11.53	10.19	1.41	4.03	2.43
1.63	1.77	1.63	1.82	1.25	1.52	1.99	1.72	0.18	0.72	0.41
9.91	10.18	8.99	10.29	7.56	9.85	10.73	9.25	1.17	4.51	2.88
2.66	2.57	2.14	2.40	2.04	2.84	2.39	2.02	0.27	1.18	0.70
6.69	6.40	5.46	6.10	5.24	7.17	6.15	5.35	1.00	3.80	2.44
1.57	1.29	1.07	1.17	1.17	1.66	1.14	0.99	0.19	0.69	0.45
9.26	7.07	6.20	6.47	6.59	9.31	6.48	5.60	1.58	4.99	3.35
1.62	1.20	1.08	1.09	1.13	1.61	1.09	0.95	0.29	0.92	0.57
13.14	8.04	9.74	9.31	10.87	8.13	9.65	8.02	8.87	20.81	8.73
23.21	2.91	3.09	3.20	7.18	6.69	2.47	2.75	1.76	3.93	1.53
33.72	23.14	27.43	36.12	38.21	32.45	36.03	33.60	12.60	25.03	88.41
46.99	34.41	44.36	25.93	33.70	53.11	30.35	29.15	24.76	77.58	17.59
9.38	8.73	8.10	5.76	9.55	16.14	6.03	4.27	2.03	4.68	2.50
411	483	514	516	456	409	570	478	348	793	353
774	811	829	830	818	785	842	822	834	919	819
0.05	0.14	0.15	0.15	0.04	0.05	0.13	0.15	0.14	0.15	0.14
3.19	3.18	3.16	3.24	3.47	3.53	3.16	3.03	3.45	6.16	3.61

09YY121	09YY122	09YY125	09YY126	09YY127	09YY128	09YY129	09YY130	09YY131	09YY132	09YY146
77.50	77.46	77.56	76.99	76.76	77.40	77.36	78.03	77.97	75.21	76.47
0.15	0.14	0.16	0.16	0.17	0.15	0.19	0.12	0.13	0.13	0.13
11.81	12.15	11.80	12.12	12.01	12.15	12.22	11.88	11.92	13.76	12.40
1.16	0.94	1.14	1.08	1.18	1.05	1.10	1.18	1.18	1.00	1.17
0.20	0.05	0.03	0.08	0.08	0.09	0.05	0.02	0.01	0.07	0.16
0.07	0.08	0.28	0.14	0.27	0.09	0.09	0.12	0.13	0.32	0.10
0.28	0.24	0.23	0.23	0.24	0.08	0.12	0.16	0.16	0.26	0.25
4.22	4.37	4.27	4.48	4.52	4.40	4.36	3.82	3.83	3.16	4.68
4.39	4.42	4.20	4.54	4.54	4.52	4.49	4.35	4.34	5.47	4.51
0.00	0.00	0.00	0.00	0.00	0.00	0.00	0.00	0.00	0.01	0.00
0.44	0.39	0.54	0.42	0.46	0.31	0.26	0.52	0.52	0.79	0.37
100.22	100.25	100.21	100.25	100.23	100.25	100.24	100.20	100.20	100.17	100.25
0.97	0.98	0.99	0.95	0.94	0.99	1.00	1.05	1.06	1.19	0.95
255.97	262.01	611.43	246.96	301.11	110.05	231.95	191.41	279.12	144.99	201.0
23.55	40.56	39.57	39.63	38.21	23.33	40.42	25.37	25.15	39.15	23.4
217	384	369	380	363	206	374	278	273	391	213
10.80	12.34	21.14	23.62	11.78	2.82	7.92	5.54	5.75	145.77	4.47
44.21	85.17	84.27	71.12	73.91	30.39	80.12	20.87	25.20	66.10	37.1
390	622	711	553	636	297	775	430	427	359	227
45.0	69.2	83.0	65.8	76.3	34.7	73.1	66.4	50.9	45.6	27.6
0.82	3.08	1.35	2.87	2.25	0.85	1.44	1.30	1.12	5.31	0.68
7.75	22.60	30.60	10.34	4.41	2.67	7.61	11.23	10.08	285.37	16.9
35	55	88	64	60	48	70	40	39	93	22
74	100	101	120	116	57	123	51	65	183	43
6.06	9.71	16.19	11.53	11.37	9.37	13.23	5.27	5.24	19.64	4.4
17.75	31.72	52.29	37.96	37.71	29.22	44.09	13.72	13.86	73.91	14.6
3.72	7.01	10.92	7.87	8.18	5.61	9.07	2.07	2.21	15.19	3.2
0.197	0.323	0.462	0.361	0.369	0.238	0.425	0.109	0.122	0.873	0.194
4.32	7.09	8.68	7.13	7.65	5.23	8.08	2.06	2.35	12.43	3.6
0.86	1.46	1.65	1.38	1.48	0.83	1.55	0.36	0.42	1.97	0.67
6.17	9.63	9.90	8.63	9.06	5.16	9.64	2.69	3.11	10.65	4.7
1.45	2.55	2.53	2.19	2.30	1.12	2.56	0.71	0.81	2.40	1.09
4.94	8.07	8.08	6.93	7.18	3.52	8.09	2.85	3.12	6.68	3.66
0.86	1.40	1.42	1.21	1.26	0.59	1.42	0.58	0.62	1.06	0.60
6.21	9.65	10.18	8.43	8.95	4.29	9.93	4.86	4.99	6.95	4.14
1.01	1.63	1.70	1.41	1.53	0.70	1.71	0.87	0.90	1.10	0.67
15.74	21.91	24.24	18.89	22.01	11.13	25.16	18.17	18.37	12.64	8.4
2.39	3.91	4.86	4.00	4.43	2.06	4.41	4.08	2.91	3.03	1.46
69.68	58.03	196.01	121.29	53.72	15.26	35.08	32.93	425.86	73.31	35.7
30.21	48.35	45.90	40.10	37.68	18.94	44.05	34.18	32.14	40.87	10.9
3.92	10.11	9.25	7.91	10.39	4.48	11.55	6.65	8.15	7.94	2.10
554	877	979	810	903	418	1051	569	568	654	335
868	918	934	901	913	843	945	889	888	879	811
0.15	0.14	0.15	0.15	0.14	0.13	0.15	0.16	0.16	0.19	0.17
3.77	6.31	6.33	6.18	6.01	3.63	6.25	4.03	3.99	5.38	3.6

								Putuoshan alkaline granites		
09YY147	09YY148	09YY149	09YY150	09YY151	09YY152	09YY153	09YY154	09YY134	09YY135	09YY137
78.11	78.03	78.15	78.01	77.70	77.76	74.89	77.68	77.33	77.43	75.41
0.14	0.12	0.12	0.12	0.11	0.14	0.21	0.12	0.10	0.11	0.17
11.95	12.00	11.88	11.92	11.92	11.72	13.14	11.97	12.82	12.81	13.66
1.01	1.03	0.94	1.04	1.24	1.48	1.01	0.86	0.00	0.00	0.94
0.01	0.02	0.01	0.02	0.02	0.01	0.01	0.34	0.05	0.06	0.05
0.10	0.10	0.08	0.09	0.08	0.05	0.10	0.08	0.11	0.12	0.23
0.09	0.21	0.25	0.21	0.23	0.37	0.36	0.14	0.35	0.34	0.47
3.22	3.94	3.95	4.01	4.25	4.15	3.62	4.29	4.04	3.76	3.81
4.72	4.31	4.29	4.40	4.24	4.17	6.43	4.33	4.65	4.72	4.72
0.00	0.00	0.00	0.00	0.00	0.00	0.01	0.00	0.00	0.00	0.02
0.81	0.47	0.54	0.40	0.44	0.33	0.43	0.44	0.38	0.37	0.61
100.16	100.22	100.22	100.22	100.22	100.20	100.21	100.24	99.81	99.72	100.10
1.13	1.04	1.03	1.02	0.99	0.97	0.97	1.00	1.04	1.08	1.12
94.6	31.1	196.6	103.9	161.5	35.3	150.7	127.2	29.53	26.52	30.06
38.2	18.2	24.3	23.4	24.2	24.1	38.2	24.9	29.90	29.83	30.40
322	285	243	248	245	226	550	245	467	499	511
21.27	18.89	7.53	6.85	6.29	6.30	84.38	11.72	46.90	29.48	35.06
28.5	23.5	36.7	30.3	24.6	33.0	110.1	26.3	41.28	33.77	46.50
489	104	358	349	77	412	642	428	178	109	141
57.7	30.9	40.1	36.9	21.5	47.4	60.9	56.3	44.6	42.3	43.8
0.97	3.53	0.64	0.57	0.61	0.77	2.81	0.93	5.29	5.58	4.90
114.2	43.0	11.1	10.0	9.1	23.2	66.8	19.5	127.67	63.71	81.99
43	28	39	40	39	40	86	39	57	45	54
83	51	60	60	57	64	150	79	105	84	99
7.8	5.2	5.4	4.8	4.5	5.7	21.5	5.8	9.51	7.62	9.07
24.5	15.3	14.5	12.4	11.7	15.6	83.4	15.8	29.61	23.50	28.26
3.9	2.6	2.4	2.1	1.9	2.7	20.3	2.8	5.21	4.14	4.91
0.273	0.168	0.138	0.121	0.110	0.141	1.585	0.164	0.432	0.305	0.345
3.2	2.5	2.7	2.4	2.2	2.9	17.4	3.1	4.39	3.50	4.12
0.52	0.43	0.53	0.44	0.39	0.54	3.06	0.56	0.77	0.62	0.73
3.2	3.0	3.9	3.2	2.7	4.1	16.8	4.0	4.67	3.71	4.54
0.85	0.70	1.04	0.86	0.66	1.08	3.76	1.00	1.17	0.95	1.17
2.98	2.44	3.93	3.30	2.33	4.03	10.06	3.76	3.70	3.01	3.80
0.58	0.43	0.74	0.63	0.40	0.78	1.52	0.73	0.66	0.53	0.67
4.45	3.23	5.92	5.17	2.83	6.20	9.34	5.78	4.72	3.75	4.83
0.85	0.53	1.02	0.91	0.47	1.08	1.48	1.01	0.80	0.65	0.84
16.4	5.4	13.6	14.7	3.2	16.2	18.5	17.6	8.04	5.61	6.60
3.50	2.44	2.43	2.51	0.83	2.75	3.89	3.10	3.32	3.07	3.03
21.1	28.5	21.9	21.4	10.5	11.8	26.7	25.3	52.05	54.63	54.24
34.3	38.2	25.4	30.5	10.9	38.5	36.1	38.4	60.60	52.79	63.72
4.56	6.23	6.16	5.94	2.08	7.59	8.83	7.70	13.55	7.87	26.02
658	210	496	477	180	556	962	590	369	269	330
911	756	867	863	727	874	915	881	801	762	785
0.24	0.20	0.16	0.16	0.16	0.15	0.26	0.17	0.28	0.24	0.23
6.0	2.9	3.9	3.7	3.8	3.9	5.5	3.9	4.41	4.40	4.20

								Putuoshan biotite granites		
09YY138	09YY142	09YY143	09YY159	09YY162	09YY165	09YY166	09YY163	09YY136	09YY157	09YY160
78.09	75.59	76.68	77.38	77.60	77.10	77.39	77.35	76.85	75.46	75.74
0.08	0.19	0.12	0.10	0.11	0.06	0.12	0.10	0.10	0.17	0.17
12.41	13.21	12.92	12.94	12.68	12.25	12.64	12.87	13.10	13.63	13.09
0.64	0.80	0.51	0.38	0.00	1.16	0.80	0.44	0.49	1.01	0.88
0.03	0.04	0.06	0.03	0.07	0.10	0.08	0.03	0.02	0.06	0.05
0.07	0.25	0.16	0.10	0.11	0.08	0.08	0.10	0.14	0.25	0.27
0.28	0.49	0.54	0.35	0.49	0.54	0.32	0.35	0.50	0.59	0.68
3.85	3.69	4.03	3.88	3.99	3.84	3.84	3.90	3.90	3.79	3.71
4.61	5.33	4.63	4.63	4.50	4.76	4.62	4.63	4.74	4.66	4.83
0.02	0.02	0.01	0.00	0.00	0.01	0.01	0.00	0.00	0.03	0.03
0.00	0.50	0.53	0.39	0.24	0.00	0.00	0.45	0.38	0.56	0.74
100.08	100.11	100.17	100.19	99.79	99.90	99.90	100.23	100.23	100.20	100.18
1.05	1.04	1.03	1.08	1.03	0.98	1.06	1.07	1.05	1.10	1.04
13.80	34.79	35.44	47.34	56.85	39.16	248.68	21.66	15.58	10.50	22.96
17.42	29.73	29.18	30.20	26.14	28.73	29.89	32.60	17.20	9.07	16.57
279	466	467	453	399	377	307	569	263	114	245
14.10	75.90	86.19	224.79	387.55	97.05	552.22	45.80	24.95	61.78	137.71
15.29	35.44	33.21	36.15	34.11	45.45	32.06	47.49	15.98	7.66	15.57
87	163	169	196	243	211	376	178	86	64	119
24.9	45.0	37.8	33.0	31.1	47.5	25.6	74.7	21.7	11.7	21.3
2.78	4.59	5.33	3.72	2.27	2.64	2.11	3.87	3.42	0.89	1.78
37.58	123.95	148.16	534.68	1179.65	462.85	1982.32	49.07	81.58	169.23	324.36
28	51	65	78	77	62	88	58	31	15	35
54	71	78	125	136	113	152	96	58	24	61
5.03	8.51	9.88	12.25	12.92	10.79	14.57	10.81	5.38	2.54	6.21
14.62	26.69	30.15	39.05	44.25	35.66	50.32	34.54	15.64	7.76	18.84
2.33	4.67	4.74	6.37	7.40	6.55	7.77	6.77	2.42	1.27	2.96
0.175	0.429	0.451	0.768	1.120	0.669	1.691	0.344	0.231	0.190	0.404
2.13	3.83	3.81	5.23	5.64	5.48	5.79	5.61	2.20	1.19	2.61
0.33	0.68	0.63	0.83	0.86	0.96	0.84	1.01	0.35	0.18	0.39
2.14	4.17	3.77	4.67	4.66	5.71	4.54	6.10	2.25	1.18	2.41
0.48	1.06	0.94	1.11	1.07	1.40	1.02	1.51	0.50	0.26	0.53
1.60	3.34	2.97	3.29	3.06	4.16	2.91	4.78	1.72	0.87	1.72
0.29	0.59	0.51	0.56	0.49	0.70	0.47	0.89	0.29	0.15	0.29
2.22	4.32	3.56	3.90	3.34	4.82	3.24	6.37	2.24	1.11	2.13
0.38	0.73	0.60	0.67	0.55	0.79	0.53	1.06	0.37	0.18	0.35
4.35	7.74	7.03	7.22	7.85	8.77	9.74	9.81	4.01	2.65	4.67
2.00	3.47	2.99	2.98	3.22	4.37	2.03	5.42	1.61	0.94	1.76
26.44	48.52	48.09	36.60	54.55	49.95	93.45	56.73	26.86	8.72	20.39
38.11	60.55	59.64	54.14	61.55	51.26	28.65	72.56	35.03	16.64	31.47
7.02	7.87	6.91	7.38	9.68	9.70	5.66	12.90	6.63	3.13	5.83
181	314	317	390	445	417	586	396	181	107	217
742	790	794	813	829	810	869	803	740	719	765
0.24	0.31	0.32	0.41	0.53	0.34	0.77	0.17	0.31	0.47	0.44
2.65	4.25	4.27	4.41	3.90	4.43	3.83	4.78	2.48	1.26	2.39

		Putuoshan MME				
09YY161	170.00	09YY139	09YY164	09YY167	09YY168	09YY169
75.88	72.98	51.17	54.19	53.55	64.95	68.34
0.17	0.26	1.08	1.00	0.93	0.68	0.53
13.14	14.73	18.56	17.33	15.15	16.01	15.36
0.91	1.18	7.82	8.35	8.32	4.41	2.99
0.07	0.29	0.11	0.14	0.21	0.09	0.05
0.29	0.39	4.38	4.64	7.87	1.95	1.03
0.74	1.12	5.51	7.35	7.56	4.39	2.36
3.83	4.18	4.04	3.18	3.33	3.80	4.10
4.75	4.44	2.55	1.81	1.18	2.65	4.03
0.03	0.04	0.30	0.28	0.26	0.16	0.14
0.40	0.59	4.22	1.33	1.24	0.83	1.13
100.20	100.19	99.75	99.61	99.60	99.92	100.06
1.03	1.07	0.96	0.84	0.74	0.94	1.00
13.73	43.29	102.44	173.45	147.90	111.66	69.01
16.93	18.13	21.18	35.10	17.87	37.10	20.63
247	222	80	126	51	238	155
111.81	109.75	768.36	1404.57	599.79	1036.95	629.38
18.13	16.39	18.38	41.59	18.25	33.35	7.83
114	131	221	314	134	294	178
23.4	24.9	6.7	15.6	7.7	21.7	21.8
1.57	1.19	1.80	10.29	2.34	6.06	3.43
333.83	374.81	640.27	1208.80	323.88	1167.48	1962.18
36	30	37	54	28	53	48
66	55	73	107	55	102	80
6.33	5.83	8.53	11.93	6.36	11.08	8.05
19.31	18.63	33.26	49.45	24.99	44.15	26.73
3.09	3.32	5.75	9.88	4.70	8.92	3.79
0.406	0.348	1.742	2.756	1.411	2.165	1.043
2.86	2.84	5.06	8.22	4.48	7.19	2.91
0.44	0.44	0.68	1.24	0.63	1.08	0.33
2.80	2.74	3.81	6.51	3.63	5.43	1.74
0.61	0.59	0.73	1.47	0.73	1.12	0.32
1.96	1.85	2.06	3.84	2.04	2.87	0.89
0.32	0.32	0.28	0.56	0.29	0.41	0.13
2.38	2.29	1.84	3.49	1.87	2.55	0.86
0.39	0.38	0.29	0.56	0.29	0.40	0.14
4.73	5.54	5.31	7.55	3.59	8.32	4.66
1.80	2.27	0.40	1.59	0.56	2.74	1.34
17.90	31.06	10.92	19.01	18.55	38.16	14.30
34.57	31.51	2.63	8.69	5.78	36.96	14.47
4.58	5.31	6.63	1.64	1.42	9.21	3.00
221	227	320	478	215	451	288
759	771	761	777	685	814	783
0.42	0.35	0.98	0.93	0.93	0.83	0.96
2.43	2.33	2.16	3.83	2.23	4.38	2.54

APPENDIX TABLE iii. *In situ* zircon U-Th-Pb isotope compositions

Sample/ spot	U (ppm)	Th (ppm)	Th/U	f_{206}* (%)	$^{207}Pb/^{206}Pb$	±1σ (%)	$^{207}Pb/^{235}U$	±1σ (%)	$^{206}Pb/^{238}U$	±1σ (%)	$T_{207/235}$ (Ma)	±1σ	$T_{206/238}$ (Ma)	±1σ	note
Nianzishan															
10NZS-01	330	200	0.61	0.27	0.04763	4.62	0.12268	4.90	0.0187	1.63	117.5	5.4	119.3	1.9	
10NZS-02	207	116	0.56	0.42	0.04630	6.11	0.12112	6.32	0.0190	1.63	116.1	7.0	121.2	2.0	
10NZS-03	348	217	0.62	7.14	0.04460	18.21	0.11523	18.28	0.0187	1.57	110.7	19.4	119.7	1.9	
10NZS-04	194	103	0.53	0.00	0.05288	4.81	0.13341	5.09	0.0183	1.67	127.2	6.1	116.9	1.9	
10NZS-05	230	129	0.56	0.00	0.05004	4.01	0.12883	4.28	0.0187	1.50	123.0	5.0	119.3	1.8	
10NZS-06	179	91	0.51	0.57	0.04771	4.57	0.12198	4.82	0.0185	1.54	116.9	5.3	118.4	1.8	
10NZS-07	127	55	0.43	0.00	0.04797	5.68	0.11814	5.89	0.0179	1.56	113.4	6.3	114.1	1.8	
10NZS-08	274	167	0.61	0.00	0.04832	3.76	0.12641	4.42	0.0190	2.31	120.9	5.0	121.2	2.8	
10NZS-09	272	160	0.59	0.13	0.04801	4.32	0.12401	4.58	0.0187	1.52	118.7	5.1	119.7	1.8	
10NZS-10	166	83	0.50	1.09	0.05421	8.07	0.14079	8.21	0.0188	1.51	133.7	10.3	120.3	1.8	
10NZS-11	352	219	0.62	0.26	0.04729	3.21	0.12201	3.58	0.0187	1.58	116.9	4.0	119.5	1.9	
10NZS-12	147	74	0.50	1.19	0.04938	9.90	0.12916	10.01	0.0190	1.51	123.3	11.7	121.1	1.8	
10NZS-13	223	124	0.56	0.00	0.05079	3.95	0.13060	4.23	0.0186	1.51	124.6	5.0	119.1	1.8	
10NZS-14	160	74	0.46	0.52	0.04725	4.80	0.12401	5.03	0.0190	1.50	118.7	5.7	121.5	1.8	
Weighted Average (2σ) = 119.3 ±1.0 Ma, N=14															
10NZS03-1	52	29	0.55	13.92	0.03601	52.84	0.09141	52.89		2.22	88.8	46.0			high Pb
10NZS03-2	64	21	0.32	1.57	0.05488	10.65	0.14085	10.77		1.56	133.8	13.6			high Pb
10NZS03-3	92	39	0.42	5.23	0.03495	41.90	0.07953	41.93		1.53	77.7	31.9			high Pb
10NZS03-4	178	131	0.73	0.00	0.04962	3.14	0.13144	3.59	0.0192	1.73	125.4	4.2	122.7	2.1	
10NZS03-5	138	52	0.38	0.32	0.04740	5.09	0.11934	5.30	0.0183	1.50	114.5	5.8	116.7	1.7	
10NZS03-6	818	657	0.80	0.03	0.04967	1.45	0.13209	2.18	0.0193	1.62	126.0	2.6	123.1	2.0	
10NZS03-7	139	117	0.84	0.10	0.05231	3.52	0.13027	3.84	0.0181	1.53	124.3	4.5	115.4	1.7	
10NZS03-8	323	179	0.55	0.18	0.04837	2.33	0.12530	2.96	0.0188	1.82	119.9	3.4	120.0	2.2	
10NZS03-9	90	35	0.39	0.61	0.05056	4.57	0.13439	4.88	0.0193	1.70	128.0	5.9	123.1	2.1	
10NZS03-10	296	128	0.43	0.00	0.04935	3.35	0.12498	3.75	0.0184	1.68	119.6	4.2	117.3	2.0	
10NZS03-11	252	136	0.54	0.57	0.04878	4.06	0.12658	4.35	0.0188	1.57	121.0	5.0	120.2	1.9	
10NZS03-12	1010	473	0.47	0.08	0.04924	1.93	0.12916	2.47	0.0190	1.54	123.3	2.9	121.5	1.9	
10NZS03-13	185	104	0.56	0.00	0.04809	3.11	0.12267	3.46	0.0185	1.51	117.5	3.8	118.2	1.8	
Weighted Average (2σ) = 119.6 ±1.6 Ma, N=13															
Houshihushan															
10SHG01-01	201	125	0.62	0.46	0.04656	6.44	0.11695	6.62	0.0182	1.52	112.3	7.1	116.4	1.8	
10SHG01-02	202	128	0.63	0.46	0.04759	4.25	0.11909	4.51	0.0181	1.50	114.3	4.9	115.9	1.7	
10SHG01-03	207	115	0.56	0.00	0.04796	4.14	0.12146	4.42	0.0184	1.53	116.4	4.9	117.3	1.8	

10SHG01-04	339	178	0.52	0.35	0.04731	4.57	0.11557	4.89	0.0177	1.75	111.0	5.2	113.2	2.0	
10SHG01-05	386	432	1.12	0.44	0.05012	4.36	0.12781	4.62	0.0185	1.54	122.1	5.3	118.1	1.8	
10SHG01-06	190	102	0.54	5.69	0.05593	20.91	0.14345	20.96	0.0186	1.52	136.1	27.1	118.8	1.8	high Pb
10SHG01-07	258	148	0.58	0.31	0.04597	5.41	0.11872	5.62	0.0187	1.51	113.9	6.1	119.6	1.8	
10SHG01-08	207	122	0.59	0.00	0.04706	6.61	0.11622	6.78	0.0179	1.51	111.6	7.2	114.4	1.7	
10SHG01-09	281	168	0.60	0.31	0.04591	5.28	0.11769	5.54	0.0186	1.65	113.0	5.9	118.8	1.9	
10SHG01-10	314	217	0.69	0.00	0.04830	3.33	0.12193	3.73	0.0183	1.69	116.8	4.1	117.0	2.0	
10SHG01-11	282	169	0.60	0.00	0.04650	4.62	0.11816	4.87	0.0184	1.53	113.4	5.2	117.7	1.8	
10SHG01-12	202	122	0.60	0.00	0.04696	4.14	0.12008	4.41	0.0185	1.51	115.1	4.8	118.4	1.8	
10SHG01-19	822	1027	1.25	8.46	0.04609	26.50	0.11502	26.54	0.0181	1.52	110.5	28.2	115.6	1.7	
10SHG01-20	1895	10595	5.59	46.28	0.10598	110.47	0.23524	111.05	0.0161	11.28	214.5	194.8	103.0	11.5	high U
10SHG01-21	800	1720	2.15	73.13	0.45771	76.93	1.17601	87.73	0.0186	42.18	789.5	652.6	119.0	49.9	high U
10SHG01-22	655	1036	1.58	55.75	0.45098	7.14	2.10305	8.56	0.0338	4.72	1149.8	60.7	214.4	10.0	high U
Weighted Average (2σ) = 117.0 ±1.1 Ma, N=16															
10YSH01-01	89	66	0.74	0.14	0.05984	9.43	0.15601	9.64	0.0189	2.02	147.2	13.3	120.7	2.4	
10YSH01-02	48	41	0.86	0.00	0.05215	6.59	0.14170	6.77	0.0197	1.54	134.6	8.6	125.8	1.9	
10YSH01-03	45	30	0.66	0.00	0.04672	7.69	0.12376	7.84	0.0192	1.53	118.5	8.8	122.7	1.9	
10YSH01-04	111	96	0.86	0.00	0.04865	5.09	0.12715	5.31	0.0190	1.51	121.5	6.1	121.0	1.8	
10YSH01-05	49	44	0.88	1.14	0.04629	7.39	0.12298	7.55	0.0193	1.53	117.8	8.4	123.0	1.9	
10YSH01-06	67	56	0.83	0.37	0.05215	4.88	0.13945	5.18	0.0194	1.73	132.6	6.5	123.8	2.1	
10YSH01-07	60	52	0.86	0.38	0.04774	5.34	0.12439	5.59	0.0189	1.66	119.0	6.3	120.7	2.0	
10YSH01-08	59	51	0.87	0.00	0.06165	9.83	0.17009	9.94	0.0200	1.52	159.5	14.8	127.7	1.9	
10YSH01-09	79	38	0.47	0.64	0.04620	4.64	0.12158	4.93	0.0191	1.64	116.5	5.4	121.9	2.0	
10YSH01-10	72	45	0.62	0.00	0.05257	4.62	0.13955	4.86	0.0193	1.51	132.6	6.1	122.9	1.8	
10YSH01-11	98	62	0.63	0.25	0.05278	3.92	0.14256	4.24	0.0196	1.62	135.3	5.4	125.0	2.0	
10YSH01-12	50	45	0.90	0.00	0.05595	5.38	0.14571	5.61	0.0189	1.58	138.1	7.3	120.6	1.9	
10YSH01-13	69	38	0.55	0.52	0.04801	6.67	0.12887	6.84	0.0195	1.50	123.1	8.0	124.3	1.8	
10YSH01-14	84	81	0.97	0.00	0.05144	4.34	0.13557	4.61	0.0191	1.57	129.1	5.6	122.1	1.9	
Weighted Average (2σ) = 123.0 ±1.4 Ma, N=14															
Laoshan															
09LS05-01	299	543	1.82	0.00	0.04876	3.47	0.12572	4.21	0.0187	2.38	120.2	4.8	119.4	2.8	
09LS05-02	113	153	1.35	0.00	0.04855	5.81	0.12278	6.00	0.0183	1.53	117.6	6.7	117.2	1.8	
09LS05-03	119	191	1.61	0.47	0.04641	5.54	0.12032	5.75	0.0188	1.56	115.4	6.3	120.1	1.9	
09LS05-04	57	89	1.58	0.00	0.05374	7.61	0.13299	7.77	0.0179	1.58	126.8	9.3	114.7	1.8	
09LS05-05	274	525	1.91	0.00	0.04873	3.57	0.12690	3.95	0.0189	1.69	121.3	4.5	120.6	2.0	
09LS05-06	105	253	2.40	0.54	0.04526	9.94	0.11567	10.08	0.0185	1.70	111.1	10.7	118.4	2.0	
09LS05-07	111	218	1.97	0.00	0.05008	9.62	0.12966	9.76	0.0188	1.65	123.8	11.4	119.9	2.0	
09LS05-08	387	601	1.55	0.00	0.04962	2.89	0.12668	3.75	0.0185	2.39	121.1	4.3	118.3	2.8	
09LS05-09	74	95	1.29	1.17	0.04977	6.88	0.12323	7.07	0.0180	1.61	118.0	7.9	114.7	1.8	
09LS05-10	310	498	1.60	0.00	0.05081	3.30	0.12972	3.75	0.0185	1.80	123.8	4.4	118.3	2.1	

09LS05-11	130	309	2.37	0.90	0.04410	10.67	0.11320	10.80	0.0186	1.67	108.9	11.2	118.9	2.0	
09LS05-12	196	287	1.46	0.31	0.04693	5.80	0.11775	6.05	0.0182	1.71	113.0	6.5	116.2	2.0	
Weighted Average (2σ) = 117.9 ±1.2 Ma, N=12															
10LS05-01	221	350	1.58	0.16	0.04861	4.53	0.12696	4.81	0.0189	1.60	121.4	5.5	121.0	1.9	
10LS05-02	300	474	1.58	0.19	0.04909	4.15	0.12454	4.41	0.0184	1.51	119.2	5.0	117.5	1.8	
10LS05-03	300	474	1.58	0.19	0.04909	4.15	0.12454	4.41	0.0184	1.51	119.2	5.0	117.5	1.8	
10LS05-04	303	529	1.75	0.00	0.04852	3.37	0.12452	3.74	0.0186	1.62	119.2	4.2	118.9	1.9	
10LS05-05	167	135	0.81	0.00	0.05112	4.53	0.12945	4.79	0.0184	1.55	123.6	5.6	117.3	1.8	
10LS05-06	606	992	1.64	0.14	0.04625	2.42	0.12144	3.14	0.0190	2.00	116.4	3.5	121.6	2.4	
10LS05-07	332	563	1.70	0.42	0.04697	3.84	0.12163	4.21	0.0188	1.73	116.5	4.6	119.9	2.1	
10LS05-08	294	400	1.36	0.18	0.04669	4.10	0.12028	4.46	0.0187	1.77	115.3	4.9	119.3	2.1	
10LS05-09	382	578	1.51	0.14	0.04928	3.44	0.12687	3.80	0.0187	1.61	121.3	4.4	119.3	1.9	
Weighted Average (2σ) = 118.9 ±1.3 Ma, N=9															
Taohuadao															
09YY129-02	217	296	1.36	0.00	0.04678	5.61	0.08937	5.86	0.0139	1.70	86.9	4.9	88.7	1.5	
09YY129-03	239	424	1.77	1.26	0.04697	7.75	0.09076	7.91	0.0140	1.56	88.2	6.7	89.7	1.4	
09YY129-05	380	658	1.73	0.38	0.05028	3.83	0.09463	4.13	0.0136	1.57	91.8	3.6	87.4	1.4	
09YY129-06	191	327	1.71	0.00	0.05201	3.93	0.09951	4.28	0.0139	1.68	96.3	3.9	88.8	1.5	
09YY129-07	176	568	3.24	1.20	0.04686	10.07	0.09029	10.22	0.0140	1.72	87.8	8.6	89.5	1.5	high Pb
09YY129-08	231	408	1.77	0.00	0.04529	3.71	0.08851	4.06	0.0142	1.65	86.1	3.4	90.7	1.5	
09YY129-09	218	467	2.14	0.38	0.04753	3.81	0.09503	4.20	0.0145	1.75	92.2	3.7	92.8	1.6	
09YY129-11	195	336	1.73	0.44	0.04891	3.94	0.09404	4.30	0.0139	1.71	91.3	3.8	89.3	1.5	
09YY129-12	220	374	1.70	0.63	0.04936	5.68	0.09430	5.92	0.0139	1.67	91.5	5.2	88.7	1.5	
09YY129-13	356	708	1.99	0.00	0.05396	10.76	0.10439	10.96	0.0140	2.04	100.8	10.6	89.8	1.8	
09YY129-14	295	516	1.75	2.22	0.06831	14.63	0.12807	14.75	0.0136	1.92	122.4	17.2	87.1	1.7	high Pb
09YY129-15	193	325	1.68	0.46	0.05087	5.38	0.10302	5.61	0.0147	1.61	99.6	5.3	94.0	1.5	
09YY129-16	225	395	1.75	0.38	0.04688	3.79	0.08890	4.12	0.0138	1.60	86.5	3.4	88.1	1.4	
09YY129-17	157	140	0.89	0.00	0.04511	4.73	0.08531	5.03	0.0137	1.72	83.1	4.0	87.8	1.5	
09YY129-18	214	375	1.76	0.59	0.04548	5.78	0.08779	6.00	0.0140	1.60	85.4	4.9	89.6	1.4	
09YY129-20	165	269	1.63	1.13	0.04809	4.65	0.09324	4.97	0.0141	1.75	90.5	4.3	90.0	1.6	
Weighted Average (2σ) = 89.6 ±0.9 Ma, N=16															
09YY148-01	534	655	1.23	0.82	0.04401	5.30	0.08154	5.52	0.0134	1.56	79.6	4.2	86.0	1.3	
09YY148-02	1299	2140	1.65	0.91	0.04556	2.95	0.08826	3.35	0.0140	1.59	85.9	2.8	89.9	1.4	
09YY148-03	558	556	1.00	3.85	0.04799	8.31	0.09003	8.45	0.0136	1.51	87.5	7.1	87.1	1.3	
09YY148-04	915	218	0.24	0.35	0.04566	2.67	0.08437	3.07	0.0134	1.51	82.2	2.4	85.8	1.3	
09YY148-05	797	241	0.30	0.33	0.04918	4.51	0.09318	4.81	0.0137	1.67	90.5	4.2	88.0	1.5	
09YY148-06	577	268	0.46	13.60	0.04630	17.43	0.08920	17.51	0.0140	1.70	86.8	14.7	89.5	1.5	high Pb
09YY148-09	710	547	0.77	1.67	0.04539	5.76	0.08708	5.96	0.0139	1.50	84.8	4.9	89.1	1.3	
09YY148-10	535	496	0.93	3.81	0.04588	11.17	0.08639	11.28	0.0137	1.58	84.1	9.2	87.4	1.4	

09YY148-11	740	182	0.25	4.58	0.05674	9.62	0.10966	9.76	0.0140	1.62	105.7	9.8	89.7	1.4	
09YY148-12	866	818	0.94	5.82	0.03131	28.21	0.06012	28.27	0.0139	1.85	59.3	16.4	89.2	1.6	
09YY148-13	1051	688	0.65	3.63	0.04625	14.31	0.09064	14.40	0.0142	1.64	88.1	12.2	91.0	1.5	
08YY148-14	745	244	0.33	4.79	0.03891	29.02	0.07562	29.08	0.0141	1.89	74.0	21.0	90.2	1.7	
08YY148-15	483	534	1.10	3.85	0.03379	23.24	0.06410	23.36	0.0138	2.43	63.1	14.4	88.1	2.1	
09YY148-20	515	521	1.01	1.00	0.04848	4.58	0.09429	4.85	0.0141	1.59	91.5	4.3	90.3	1.4	
09YY148-21	767	563	0.73	0.84	0.04880	4.91	0.08427	5.30	0.0125	1.98	82.2	4.2	80.2	1.6	
08YY148-22	368	485	1.32	0.19	0.05242	3.66	0.09926	3.98	0.0137	1.56	96.1	3.7	87.9	1.4	
08YY148-23	357	377	1.06	0.00	0.04775	3.02	0.09139	3.40	0.0139	1.57	88.8	2.9	88.9	1.4	
08YY148-25	304	500	1.64	4.16	0.04480	35.48	0.08010	35.55	0.0130	2.20	78.2	27.1	83.1	1.8	high Pb
09YY148-26	958	837	0.87	4.59	0.05484	6.47	0.10415	6.66	0.0138	1.56	100.6	6.4	88.2	1.4	
09YY148-27	641	692	1.08	0.54	0.04521	3.71	0.08593	4.02	0.0138	1.55	83.7	3.2	88.3	1.4	
08YY148-2-3	998	714	0.72	0.40	0.04696	2.49	0.09530	2.91	0.0147	1.50	92.4	2.6	94.2	1.4	
09YY148-2-13	1262	1438	1.14	0.17	0.04613	2.14	0.08991	2.64	0.0141	1.54	87.4	2.2	90.5	1.4	
09YY148-2-25	238	304	1.28	0.36	0.04897	3.61	0.09451	3.92	0.0140	1.55	91.7	3.4	89.6	1.4	
Weighted Average (2σ) = 88.9 ±0.8 Ma, N=23															
Putuoshan															
09YY163-01	211	417	1.98	0.19	0.04952	3.54	0.10482	3.92	0.0154	1.69	101.2	3.8	98.2	1.6	
09YY163-02	101	82	0.81	0.39	0.04815	4.42	0.10190	4.69	0.0153	1.55	98.5	4.4	98.2	1.5	
09YY163-03	80	159	1.99	0.00	0.05153	5.68	0.10730	6.01	0.0151	1.95	103.5	5.9	96.6	1.9	
09YY163-04	729	156	0.21	0.16	0.04704	2.09	0.10595	2.57	0.0163	1.50	102.3	2.5	104.5	1.6	
09YY163-05	143	262	1.83	0.86	0.04871	5.02	0.10231	5.27	0.0152	1.59	98.9	5.0	97.5	1.5	
09YY163-06	1373	1331	0.97	2.24	0.04940	3.75	0.10640	4.05	0.0156	1.52	102.7	4.0	99.9	1.5	
09YY163-07	192	239	1.25	0.21	0.04777	3.22	0.10413	3.57	0.0158	1.54	100.6	3.4	101.1	1.5	
09YY163-08	74	119	1.62	0.30	0.04723	6.27	0.09947	6.49	0.0153	1.66	96.3	6.0	97.7	1.6	
09YY163-09	62	121	1.94	0.37	0.05149	5.46	0.10686	5.83	0.0151	2.05	103.1	5.7	96.3	2.0	
09YY163-10	43	73	1.69	0.00	0.04918	6.69	0.10218	6.92	0.0151	1.77	98.8	6.5	96.4	1.7	
09YY163-14	77	89	1.16	0.51	0.05123	8.14	0.10799	8.30	0.0153	1.62	104.1	8.2	97.8	1.6	
09YY163-15	311	468	1.50	0.00	0.04709	2.97	0.10226	3.36	0.0157	1.58	98.9	3.2	100.7	1.6	
09YY163-16	356	703	1.97	0.21	0.04951	4.08	0.10496	4.39	0.0154	1.62	101.3	4.2	98.4	1.6	
09YY163-11	55	88	1.62	1.29	0.04258	12.98	0.08717	13.17	0.0148	2.20	84.9	10.8	95.0	2.1	high Pb
09YY163-12	139	283	2.04	24.61	0.05563	35.91	0.12240	35.98	0.0160	2.24	117.2	40.6	102.0	2.3	high Pb
09YY163-13	514	773	1.50	19.57	0.05044	29.93	0.10147	30.01	0.0146	2.12	98.1	28.5	93.4	2.0	high Pb
Weighted Average (2σ) = 98.7 ±1.0 Ma, N=16															
09YY136-01	246	226	0.92	0.48	0.04951	2.93	0.09986	3.32	0.0146	1.56	96.7	3.1	93.6	1.5	
09YY136-02	93	156	1.67	0.82	0.04620	8.45	0.09332	8.62	0.0146	1.68	90.6	7.5	93.7	1.6	
09YY136-03	854	302	0.35	0.04	0.04939	2.46	0.10511	3.06	0.0154	1.82	101.5	3.0	98.7	1.8	
09YY136-05	4133	2887	0.70	0.08	0.04766	0.77	0.10542	1.71	0.0160	1.52	101.8	1.7	102.6	1.6	high U
09YY136-06	313	409	1.31	0.07	0.04655	3.45	0.09614	3.86	0.0150	1.74	93.2	3.4	95.8	1.7	
09YY136-07	379	327	0.86	0.15	0.04557	2.33	0.09594	2.81	0.0153	1.56	93.0	2.5	97.7	1.5	

09YY136-11	268	304	1.14	0.09	0.04732	2.75	0.09983	3.19	0.0153	1.62	96.6	2.9	97.9	1.6	
09YY136-12	83	177	2.15	0.25	0.05425	5.04	0.10744	5.30	0.0144	1.63	103.6	5.2	91.9	1.5	
09YY136-14	342	423	1.24	0.14	0.04723	2.43	0.09925	2.89	0.0152	1.57	96.1	2.7	97.5	1.5	
09YY136-15	4149	3124	0.75	0.31	0.04662	4.14	0.11561	4.41	0.0180	1.52	111.1	4.7	114.9	1.7	high U
09YY136-16	492	410	0.83	0.14	0.04772	2.28	0.10125	2.75	0.0154	1.53	97.9	2.6	98.4	1.5	
09YY136-18	233	257	1.10	0.47	0.04526	4.73	0.09276	4.97	0.0149	1.50	90.1	4.3	95.1	1.4	
09YY136-19	292	270	0.93	1.42	0.04839	7.51	0.08039	7.69	0.0120	1.64	78.5	5.8	77.2	1.3	high Pb
09YY136-20	272	463	1.70	2.57	0.04744	4.63	0.09481	4.88	0.0145	1.54	92.0	4.3	92.8	1.4	
09YY136-21	129	243	1.88	0.57	0.04285	6.50	0.08810	6.69	0.0149	1.56	85.7	5.5	95.4	1.5	
Weighted Average (2σ) = 95.5 ± 1.3 Ma, N=15															

* f_{206} is the proportion of common ^{206}Pb in total measured ^{206}Pb

APPENDIX TABLE iv. *In situ* zircon Hf isotope compositions

Sample	$^{176}Lu/^{177}Hf_{corr}$	2σ	$^{176}Hf/^{177}Hf_{corr}$	2σ	$^{176}Hf/^{177}Hf_i$	$\varepsilon Hf_{(0)}$	$\varepsilon Hf_{(t)}$	T_{DM}	T_{DM}^C	T_{DM2}	2σ	$f_{Lu/Hf}$
Nianzishan												
10NZS-01	0.004579	0.000018	0.283015	0.000024	0.283005	8.2	10.8	372	485	636	13	-0.86
10NZS-02	0.004590	0.000067	0.282983	0.000027	0.282972	7.1	9.7	422	558	739	15	-0.86
10NZS-03	0.005435	0.000046	0.282975	0.000031	0.282963	6.7	9.3	446	580	771	15	-0.84
10NZS-04	0.003060	0.000025	0.282914	0.000025	0.282907	4.8	7.4	507	706	948	19	-0.91
10NZS-05	0.005164	0.000031	0.283004	0.000028	0.282993	7.8	10.4	395	512	674	13	-0.84
10NZS-06	0.002018	0.000027	0.282946	0.000023	0.282941	6.0	8.6	447	629	839	17	-0.94
10NZS-07	0.003116	0.000014	0.282897	0.000025	0.282890	4.2	6.8	534	744	1003	20	-0.91
10NZS-08	0.002239	0.000042	0.282851	0.000021	0.282846	2.6	5.2	589	845	1146	23	-0.93
10NZS-09	0.003409	0.000024	0.282861	0.000027	0.282853	2.9	5.5	593	828	1122	22	-0.90
10NZS-10	0.003145	0.000050	0.282929	0.000027	0.282922	5.3	7.9	486	672	901	18	-0.91
10NZS-11	0.002270	0.000038	0.282900	0.000023	0.282895	4.4	7.0	517	733	987	20	-0.93
10NZS-12	0.003436	0.000014	0.282900	0.000025	0.282892	4.3	6.9	534	740	996	20	-0.90
10NZS-13	0.003848	0.000030	0.282938	0.000025	0.282929	5.6	8.2	483	656	878	18	-0.88
10NZS-14	0.001351	0.000012	0.282886	0.000023	0.282883	3.9	6.5	524	760	1025	20	-0.96
10NZS-15	0.002101	0.000012	0.282933	0.000021	0.282928	5.5	8.1	466	658	881	18	-0.94
10NZS-16	0.004111	0.000050	0.282958	0.000027	0.282949	6.2	8.9	455	612	815	16	-0.88
10NZS-17	0.004230	0.000058	0.283001	0.000022	0.282991	7.8	10.4	390	515	678	14	-0.87
10NZS-18	0.003765	0.000028	0.282862	0.000023	0.282854	2.9	5.5	597	827	1120	22	-0.89
10NZS-19	0.001684	0.000028	0.282901	0.000024	0.282898	4.4	7.1	507	728	979	20	-0.95
10NZS-20	0.003298	0.000112	0.282967	0.000025	0.282960	6.6	9.2	431	587	780	16	-0.90
10NZS-21	0.004652	0.000053	0.282943	0.000024	0.282933	5.7	8.3	486	648	867	17	-0.86
10NZS-22	0.002602	0.000084	0.282925	0.000026	0.282919	5.2	7.8	485	679	910	18	-0.92
10NZS-23	0.003937	0.000037	0.282900	0.000025	0.282891	4.2	6.8	541	741	999	20	-0.88
10NZS-24	0.002922	0.000024	0.282933	0.000025	0.282927	5.5	8.1	477	662	886	18	-0.91
10NZS-25	0.004111	0.000048	0.282947	0.000024	0.282938	5.9	8.5	471	635	848	17	-0.88
10NZS03-01.	0.001356	0.000003	0.282941	0.000023	0.282938	5.9	8.9	445	625	826	17	-0.96
10NZS03-01-	0.001952	0.000015	0.282936	0.000021	0.282931	5.6	8.6	460	640	847	17	-0.94
10NZS03-02	0.002861	0.000037	0.282922	0.000025	0.282915	5.1	8.1	492	677	900	18	-0.91
10NZS03-03	0.002793	0.000035	0.282967	0.000021	0.282960	6.6	9.6	425	576	756	15	-0.92
10NZS03-04	0.001970	0.000043	0.282956	0.000021	0.282951	6.3	9.4	430	594	782	16	-0.94
10NZS03-05	0.002389	0.000031	0.282939	0.000019	0.282933	5.7	8.7	461	636	841	17	-0.93
10NZS03-06	0.001952	0.000008	0.282920	0.000020	0.282915	5.1	8.1	483	676	899	18	-0.94
10NZS03-07	0.002054	0.000035	0.282965	0.000019	0.282960	6.6	9.7	419	575	756	15	-0.94
10NZS03-08	0.002242	0.000029	0.282972	0.000019	0.282966	6.9	9.9	411	561	736	15	-0.93
10NZS03-09	0.001953	0.000044	0.282956	0.000020	0.282951	6.3	9.3	431	595	783	16	-0.94
10NZS03-10	0.002082	0.000017	0.282902	0.000019	0.282897	4.4	7.4	511	718	958	19	-0.94
10NZS03-11	0.002209	0.000011	0.282937	0.000015	0.282932	5.6	8.7	461	639	846	17	-0.93
10NZS03-12	0.002214	0.000008	0.282918	0.000014	0.282913	5.0	8.0	489	682	907	18	-0.93
10NZS03-13	0.002593	0.000084	0.282977	0.000018	0.282970	7.0	10.0	408	551	722	14	-0.92
10NZS03-14	0.001731	0.000014	0.282960	0.000014	0.282955	6.5	9.5	423	585	769	15	-0.95
10NZS03-15	0.001468	0.000067	0.282921	0.000015	0.282917	5.1	8.1	476	672	893	18	-0.96
10NZS03-16	0.001469	0.000030	0.282927	0.000023	0.282923	5.4	8.4	467	657	872	17	-0.96
10NZS03-17	0.001908	0.000067	0.282998	0.000021	0.282994	7.8	10.9	368	498	647	13	-0.94
10NZS03-18	0.001926	0.000006	0.282904	0.000024	0.282899	4.5	7.5	507	714	952	19	-0.94
10NZS03-19	0.001285	0.000014	0.282929	0.000023	0.282926	5.4	8.4	462	652	865	17	-0.96
10NZS03-20	0.003752	0.000065	0.283003	0.000025	0.282994	7.8	10.9	380	498	646	13	-0.89
10NZS03-21	0.002502	0.000006	0.282927	0.000018	0.282920	5.2	8.3	480	664	882	18	-0.92
10NZS03-22	0.002236	0.000028	0.282961	0.000020	0.282955	6.5	9.5	427	585	770	15	-0.93
10NZS03-23	0.002475	0.000010	0.282962	0.000018	0.282956	6.5	9.5	428	584	768	15	-0.93
10NZS03-24	0.001876	0.000024	0.282915	0.000018	0.282910	4.9	7.9	490	688	916	18	-0.94
10NZS03-25	0.002827	0.000053	0.282976	0.000025	0.282969	7.0	10.0	411	555	727	15	-0.91
Houshihushan												
10SHG01-01	0.001588	0.000022	0.282375	0.000022	0.282371	-14.2	-11.6	1260	1908	2660	53	-0.95
10SHG01-02	0.003030	0.000043	0.282391	0.000022	0.282385	-13.7	-11.1	1286	1878	2615	52	-0.91
10SHG01-03	0.001570	0.000033	0.282433	0.000020	0.282430	-12.1	-9.5	1176	1778	2474	49	-0.95
10SHG01-04	0.001797	0.000035	0.282412	0.000020	0.282408	-12.9	-10.3	1214	1827	2543	51	-0.95
10SHG01-05	0.002755	0.000074	0.282462	0.000025	0.282456	-11.2	-8.6	1172	1720	2390	48	-0.92
10SHG01-06	0.001400	0.000017	0.282381	0.000021	0.282378	-13.9	-11.4	1245	1894	2639	53	-0.96
10SHG01-07	0.001898	0.000021	0.282423	0.000024	0.282419	-12.5	-9.9	1201	1802	2508	50	-0.94
10SHG01-08	0.001476	0.000025	0.282411	0.000019	0.282407	-12.9	-10.3	1205	1828	2545	51	-0.96
10SHG01-09	0.001542	0.000053	0.282387	0.000020	0.282384	-13.7	-11.2	1240	1880	2619	52	-0.95
10SHG01-10	0.002394	0.000073	0.282454	0.000023	0.282449	-11.4	-8.9	1172	1735	2413	48	-0.93

10SHG01-11	0.001582	0.000019	0.282358	0.000020	0.282355	-14.8	-12.2	1284	1945	2712	54	-0.95
10SHG01-12	0.001680	0.000020	0.282417	0.000021	0.282414	-12.7	-10.1	1202	1814	2525	50	-0.95
10SHG01-13	0.004324	0.000098	0.282412	0.000025	0.282403	-13.1	-10.5	1302	1838	2558	51	-0.87
10SHG01-14	0.001486	0.000012	0.282437	0.000021	0.282434	-11.9	-9.4	1167	1768	2460	49	-0.96
10SHG01-15	0.001560	0.000008	0.282383	0.000023	0.282380	-13.9	-11.3	1247	1888	2631	53	-0.95
10SHG01-16	0.002479	0.000080	0.282372	0.000024	0.282367	-14.3	-11.8	1295	1918	2673	53	-0.93
10SHG01-17	0.001749	0.000008	0.282400	0.000021	0.282396	-13.3	-10.7	1229	1853	2580	52	-0.95
10SHG01-18	0.001549	0.000023	0.282400	0.000019	0.282397	-13.3	-10.7	1222	1851	2578	52	-0.95
10SHG01-19	0.001386	0.000044	0.282400	0.000014	0.282397	-13.2	-10.7	1217	1850	2576	52	-0.96
10SHG01-20	0.002554	0.000007	0.282475	0.000019	0.282470	-10.7	-8.1	1146	1689	2347	47	-0.92
10SHG01-21	0.002928	0.000061	0.282505	0.000026	0.282499	-9.7	-7.1	1114	1624	2254	45	-0.91
10SHG01-22	0.002514	0.000028	0.282460	0.000023	0.282455	-11.2	-8.7	1167	1723	2394	48	-0.92
10SHG01-23	0.001829	0.000020	0.282447	0.000022	0.282443	-11.6	-9.1	1164	1748	2431	49	-0.94
10SHG01-24	0.001415	0.000003	0.282431	0.000020	0.282428	-12.2	-9.6	1175	1783	2481	50	-0.96
10SHG01-25	0.001747	0.000008	0.282393	0.000020	0.282390	-13.5	-11.0	1239	1867	2601	52	-0.95
10SHG01-26	0.003181	0.000047	0.282444	0.000020	0.282437	-11.9	-9.2	1213	1759	2443	49	-0.90
10SHG01-27	0.003204	0.000013	0.282437	0.000023	0.282430	-12.1	-9.4	1224	1775	2466	49	-0.90
10SHG01-28	0.002087	0.000039	0.282444	0.000022	0.282439	-11.8	-9.1	1178	1754	2437	49	-0.94
10SHG01-29	0.003952	0.000019	0.282446	0.000019	0.282437	-11.9	-9.2	1238	1760	2444	49	-0.88
10YSH04-01	0.001029	0.000006	0.282306	0.000018	0.282304	-16.6	-13.9	1337	2054	2865	57	-0.97
10YSH04-02	0.002592	0.000046	0.282317	0.000020	0.282311	-16.3	-13.6	1379	2037	2840	57	-0.92
10YSH04-03	0.002870	0.000040	0.282342	0.000019	0.282336	-15.4	-12.7	1353	1984	2763	55	-0.91
10YSH04-05	0.003136	0.000011	0.282330	0.000020	0.282323	-15.9	-13.2	1381	2011	2803	56	-0.91
10YSH04-06	0.002804	0.000021	0.282328	0.000017	0.282321	-15.9	-13.2	1371	2015	2809	56	-0.92
10YSH04-07	0.002012	0.000016	0.282307	0.000023	0.282302	-16.6	-13.9	1372	2058	2870	57	-0.94
10YSH04-08	0.003256	0.000071	0.282345	0.000023	0.282338	-15.4	-12.7	1363	1979	2757	55	-0.90
10YSH04-09	0.002419	0.000050	0.282352	0.000022	0.282346	-15.1	-12.4	1322	1960	2731	55	-0.93
10YSH04-10	0.002239	0.000010	0.282343	0.000020	0.282338	-15.4	-12.7	1328	1979	2757	55	-0.93
10YSH04-11	0.002485	0.000055	0.282387	0.000022	0.282382	-13.8	-11.1	1273	1882	2618	52	-0.93
10YSH04-12	0.002685	0.000024	0.282290	0.000021	0.282284	-17.3	-14.6	1423	2099	2928	59	-0.92
10YSH04-13	0.002667	0.000053	0.282329	0.000022	0.282323	-15.9	-13.2	1364	2011	2803	56	-0.92
10YSH04-14	0.002406	0.000068	0.282346	0.000018	0.282341	-15.3	-12.6	1330	1973	2748	55	-0.93
10YSH04-16	0.002169	0.000078	0.282411	0.000021	0.282406	-13.0	-10.3	1228	1828	2542	51	-0.93
10YSH04-17	0.003778	0.000016	0.282305	0.000021	0.282297	-16.8	-14.1	1443	2069	2885	58	-0.89
10YSH04-18	0.003122	0.000083	0.282356	0.000025	0.282349	-14.9	-12.3	1341	1953	2720	54	-0.91
10YSH04-20	0.001602	0.000024	0.282284	0.000025	0.282280	-17.4	-14.7	1390	2106	2939	59	-0.95
10YSH04-21	0.003762	0.000059	0.282394	0.000019	0.282386	-13.7	-11.0	1308	1873	2605	52	-0.89
10YSH04-22	0.003498	0.000037	0.282389	0.000023	0.282381	-13.8	-11.1	1307	1883	2620	52	-0.89
10YSH01-01	0.001174	0.000005	0.282295	0.000024	0.282292	-17.0	-14.3	1359	2080	2903	58	-0.96
10YSH01-02	0.001365	0.000011	0.282338	0.000023	0.282335	-15.4	-12.8	1304	1984	2765	55	-0.96
10YSH01-03	0.001032	0.000007	0.282313	0.000022	0.282310	-16.3	-13.6	1328	2039	2844	57	-0.97
10YSH01-05	0.001072	0.000002	0.282277	0.000021	0.282275	-17.6	-14.9	1380	2118	2957	59	-0.97
10YSH01-06	0.001751	0.000038	0.282294	0.000023	0.282290	-17.0	-14.4	1381	2084	2908	58	-0.95
10YSH01-07	0.001572	0.000014	0.282292	0.000022	0.282289	-17.1	-14.4	1376	2087	2912	58	-0.95
10YSH01-08	0.001888	0.000034	0.282295	0.000024	0.282290	-17.0	-14.3	1385	2084	2907	58	-0.94
10YSH01-09	0.001807	0.000019	0.282347	0.000025	0.282343	-15.2	-12.5	1306	1966	2740	55	-0.95
10YSH01-10	0.001745	0.000002	0.282290	0.000025	0.282286	-17.2	-14.5	1387	2094	2922	58	-0.95
10YSH01-11	0.001745	0.000010	0.282372	0.000024	0.282368	-14.3	-11.6	1269	1912	2662	53	-0.95
10YSH01-12	0.001154	0.000003	0.282279	0.000019	0.282276	-17.5	-14.8	1380	2114	2951	59	-0.97
10YSH01-13	0.001273	0.000009	0.282320	0.000020	0.282317	-16.1	-13.4	1326	2024	2822	56	-0.96
10YSH01-14	0.001195	0.000001	0.282311	0.000020	0.282308	-16.4	-13.7	1336	2044	2851	57	-0.96
10YSH01-15	0.001455	0.000004	0.282313	0.000019	0.282310	-16.4	-13.7	1343	2041	2847	57	-0.96
10YSH01-16	0.001604	0.000007	0.282280	0.000023	0.282276	-17.5	-14.8	1395	2115	2952	59	-0.95
10YSH01-17	0.001208	0.000004	0.282301	0.000022	0.282298	-16.8	-14.1	1351	2067	2883	58	-0.96
10YSH01-19	0.001425	0.000004	0.282354	0.000022	0.282350	-14.9	-12.2	1284	1951	2717	54	-0.96
10YSH01-20	0.001505	0.000008	0.282319	0.000023	0.282316	-16.1	-13.4	1336	2027	2827	57	-0.95
Laoshan												
09LS05-01	0.002172	0.000041	0.282205	0.000018	0.282201	-20.2	-17.6	1524	2284	3196	64	-0.93
09LS05-02	0.001192	0.000022	0.282074	0.000018	0.282072	-24.8	-22.2	1668	2567	3603	72	-0.96
09LS05-03	0.001963	0.000048	0.282080	0.000018	0.282076	-24.6	-22.0	1694	2558	3588	72	-0.94
09LS05-04	0.002254	0.000024	0.282122	0.000020	0.282117	-23.2	-20.6	1648	2469	3461	69	-0.93
09LS05-05	0.001979	0.000022	0.282106	0.000017	0.282102	-23.7	-21.1	1658	2502	3508	70	-0.94
09LS05-06	0.001325	0.000025	0.282216	0.000018	0.282213	-19.8	-17.2	1475	2257	3158	63	-0.96
09LS05-07	0.002153	0.000044	0.282177	0.000017	0.282173	-21.2	-18.6	1564	2346	3285	66	-0.94
09LS05-08	0.001856	0.000009	0.282121	0.000020	0.282117	-23.2	-20.6	1632	2469	3461	69	-0.94
09LS05-09	0.001958	0.000025	0.282143	0.000018	0.282138	-22.4	-19.8	1605	2421	3392	68	-0.94

09LS05-10	0.002974	0.000184	0.282147	0.000019	0.282140	-22.3	-19.8	1644	2417	3385	68	-0.91
09LS05-11	0.001828	0.000042	0.282178	0.000020	0.282174	-21.2	-18.6	1549	2343	3281	66	-0.94
09LS05-12	0.001749	0.000035	0.282132	0.000022	0.282128	-22.8	-20.2	1611	2443	3424	68	-0.95
09LS05-13	0.001775	0.000028	0.282138	0.000020	0.282135	-22.5	-20.0	1603	2430	3405	68	-0.95
09LS05-14	0.002752	0.000022	0.282153	0.000018	0.282147	-22.1	-19.5	1625	2402	3365	67	-0.92
09LS05-15	0.003472	0.000017	0.282143	0.000017	0.282135	-22.5	-19.9	1674	2429	3402	68	-0.90
09LS05-16	0.002439	0.000017	0.282071	0.000020	0.282065	-25.0	-22.4	1730	2582	3622	72	-0.93
09LS05-17	0.001005	0.000037	0.282089	0.000017	0.282087	-24.2	-21.7	1639	2534	3555	71	-0.97
09LS05-18	0.002625	0.000069	0.282137	0.000017	0.282131	-22.7	-20.1	1643	2437	3414	68	-0.92
09LS05-19	0.000933	0.000007	0.282153	0.000017	0.282151	-22.0	-19.4	1548	2394	3355	67	-0.97
09LS05-20	0.001804	0.000021	0.282138	0.000019	0.282134	-22.5	-20.0	1605	2430	3405	68	-0.95
09LS05-21	0.002131	0.000051	0.282116	0.000018	0.282111	-23.4	-20.8	1651	2481	3478	70	-0.94
10LS05-01	0.002406	0.000011	0.282171	0.000015	0.282166	-21.4	-18.8	1584	2361	3305	66	-0.93
10LS05-02	0.002065	0.000015	0.282156	0.000016	0.282152	-21.9	-19.3	1590	2391	3349	67	-0.94
10LS05-03	0.002471	0.000024	0.282171	0.000017	0.282165	-21.5	-18.9	1587	2362	3306	66	-0.93
10LS05-04	0.002581	0.000093	0.282195	0.000016	0.282189	-20.6	-18.0	1557	2310	3232	65	-0.92
10LS05-05	0.002583	0.000046	0.282143	0.000016	0.282137	-22.4	-19.8	1632	2423	3394	68	-0.92
10LS05-06	0.001725	0.000017	0.282166	0.000014	0.282162	-21.6	-19.0	1562	2369	3317	66	-0.95
10LS05-07	0.002225	0.000010	0.282132	0.000017	0.282127	-22.8	-20.2	1633	2446	3428	69	-0.93
10LS05-08	0.002494	0.000065	0.282168	0.000016	0.282162	-21.6	-19.0	1593	2369	3316	66	-0.92
10LS05-09	0.002678	0.000053	0.282100	0.000016	0.282094	-24.0	-21.4	1699	2518	3529	71	-0.92
10LS05-10	0.002256	0.000021	0.282163	0.000018	0.282158	-21.7	-19.1	1589	2379	3331	67	-0.93
10LS05-11	0.002363	0.000020	0.282230	0.000019	0.282225	-19.3	-16.7	1496	2230	3118	62	-0.93
10LS05-12	0.002578	0.000038	0.282161	0.000018	0.282155	-21.8	-19.2	1606	2384	3338	67	-0.92
10LS05-13	0.002541	0.000017	0.282163	0.000016	0.282157	-21.8	-19.1	1602	2380	3332	67	-0.92
10LS05-14	0.001614	0.000024	0.282148	0.000015	0.282144	-22.2	-19.6	1583	2408	3373	67	-0.95
10LS05-15	0.001854	0.000010	0.282147	0.000015	0.282143	-22.2	-19.6	1594	2410	3376	68	-0.94
10LS05-16	0.002418	0.000050	0.282177	0.000016	0.282172	-21.2	-18.6	1576	2348	3286	66	-0.93
10LS05-17	0.001639	0.000002	0.282154	0.000018	0.282151	-22.0	-19.4	1575	2393	3353	67	-0.95
10LS05-18	0.002760	0.000012	0.282138	0.000017	0.282132	-22.6	-20.0	1647	2434	3410	68	-0.92
10LS05-19	0.000859	0.000002	0.282193	0.000019	0.282191	-20.5	-17.9	1488	2304	3225	65	-0.97
10LS05-20	0.002104	0.000014	0.282139	0.000016	0.282134	-22.5	-19.9	1617	2429	3404	68	-0.94
10LS05-21	0.002341	0.000012	0.282172	0.000018	0.282167	-21.4	-18.8	1579	2358	3301	66	-0.93
10LS05-22	0.001932	0.000020	0.282203	0.000022	0.282198	-20.3	-17.7	1518	2289	3203	64	-0.94
10LS05-23	0.001680	0.000014	0.282150	0.000018	0.282147	-22.1	-19.5	1582	2403	3366	67	-0.95
10LS05-24	0.004983	0.000020	0.282266	0.000021	0.282254	-18.3	-15.7	1557	2165	3023	60	-0.85
10LS05-25	0.000886	0.000013	0.282138	0.000015	0.282136	-22.5	-19.9	1566	2426	3400	68	-0.97
Suzhou												
09YY85-01	0.001663	0.000011	0.282521	0.000017	0.282517	-9.0	-6.2	1053	1578	2184	44	-0.95
09YY85-02	0.001222	0.000018	0.282543	0.000015	0.282540	-8.2	-5.4	1010	1527	2112	42	-0.96
09YY85-03	0.002724	0.000141	0.282518	0.000015	0.282512	-9.2	-6.4	1089	1590	2200	44	-0.92
09YY85-08	0.001134	0.000003	0.282564	0.000019	0.282561	-7.5	-4.7	978	1480	2044	41	-0.97
09YY85-15	0.001874	0.000011	0.282579	0.000020	0.282574	-7.0	-4.2	976	1450	2002	40	-0.94
09YY85-16	0.003401	0.000022	0.282610	0.000021	0.282601	-6.0	-3.3	972	1390	1916	38	-0.90
09YY85-17	0.004116	0.000058	0.282512	0.000015	0.282503	-9.5	-6.8	1141	1611	2230	45	-0.88
09YY85-18	0.005485	0.000034	0.282616	0.000025	0.282603	-6.0	-3.2	1023	1386	1910	38	-0.83
09YY85-28	0.015545	0.000263	0.282461	0.000022	0.282424	-12.3	-9.5	1819	1784	2469	49	-0.53
09YY85-29	0.000866	0.000004	0.282557	0.000024	0.282555	-7.7	-4.9	981	1494	2064	41	-0.97
09YY85-30	0.002633	0.000019	0.282581	0.000018	0.282575	-7.0	-4.2	993	1449	2000	40	-0.92
09YY97-01	0.001626	0.000017	0.282524	0.000014	0.282521	-8.9	-6.1	1048	1570	2173	43	-0.95
09YY97-02	0.001093	0.000001	0.282539	0.000015	0.282536	-8.3	-5.6	1012	1535	2123	42	-0.97
09YY97-03	0.003804	0.000069	0.282516	0.000014	0.282507	-9.4	-6.6	1126	1601	2216	44	-0.89
09YY97-04	0.001157	0.000025	0.282571	0.000016	0.282568	-7.2	-4.4	969	1465	2023	40	-0.97
09YY97-05	0.001870	0.000066	0.282593	0.000017	0.282589	-6.5	-3.7	956	1419	1957	39	-0.94
09YY97-06	0.007499	0.000059	0.282505	0.000017	0.282487	-10.1	-7.3	1277	1644	2276	46	-0.77
09YY97-07	0.002523	0.000060	0.282545	0.000015	0.282539	-8.2	-5.5	1043	1529	2114	42	-0.92
09YY97-08	0.004041	0.000278	0.282667	0.000024	0.282658	-4.0	-1.3	902	1263	1736	35	-0.88
09YY97-09	0.005167	0.000035	0.282484	0.000013	0.282472	-10.6	-7.8	1222	1679	2327	47	-0.84
09YY97-10	0.001272	0.000011	0.282480	0.000017	0.282477	-10.4	-7.7	1101	1668	2312	46	-0.96
09YY97-11	0.001390	0.000068	0.282538	0.000017	0.282535	-8.4	-5.6	1022	1539	2129	43	-0.96
09YY97-12	0.001113	0.000011	0.282527	0.000017	0.282524	-8.8	-6.0	1030	1562	2162	43	-0.97
09YY97-13	0.011312	0.000131	0.282435	0.000019	0.282408	-12.9	-10.1	1590	1821	2524	50	-0.66
09YY97-14	0.003177	0.000170	0.282584	0.000026	0.282577	-6.9	-4.1	1004	1444	1993	40	-0.90
09YY97-15	0.005491	0.000017	0.282555	0.000018	0.282542	-8.1	-5.3	1120	1522	2103	42	-0.83
09YY97-16	0.000897	0.000012	0.282491	0.000017	0.282489	-10.0	-7.2	1074	1641	2274	45	-0.97
09YY97-17	0.005508	0.000053	0.282584	0.000022	0.282571	-7.1	-4.3	1075	1458	2013	40	-0.83

09YY97-18	0.001680	0.000012	0.282562	0.000024	0.282558	-7.6	-4.8	995	1486	2053	41	-0.95
09YY97-19	0.008379	0.000104	0.282530	0.000020	0.282511	-9.2	-6.5	1270	1593	2202	44	-0.75
09YY97-20	0.003471	0.000180	0.282602	0.000023	0.282594	-6.3	-3.5	985	1406	1939	39	-0.90
09YY97-21	0.001013	0.000003	0.282530	0.000018	0.282528	-8.6	-5.9	1022	1554	2150	43	-0.97
09YY103-01	0.005785	0.000024	0.282499	0.000013	0.282485	-10.1	-7.4	1221	1649	2284	46	-0.83
09YY103-02	0.003095	0.000022	0.282505	0.000012	0.282498	-9.7	-6.9	1120	1622	2246	45	-0.91
09YY103-03	0.002346	0.000089	0.282512	0.000016	0.282506	-9.4	-6.6	1087	1603	2219	44	-0.93
09YY103-04	0.002164	0.000037	0.282502	0.000016	0.282497	-9.7	-7.0	1096	1624	2249	45	-0.93
09YY103-06	0.001875	0.000025	0.282528	0.000016	0.282523	-8.8	-6.0	1050	1564	2164	43	-0.94
09YY103-07	0.001987	0.000042	0.282505	0.000017	0.282500	-9.6	-6.9	1087	1617	2239	45	-0.94
09YY103-08	0.001036	0.000016	0.282538	0.000017	0.282535	-8.4	-5.6	1013	1538	2127	43	-0.97
09YY103-09	0.005197	0.000031	0.282503	0.000015	0.282491	-9.9	-7.2	1193	1637	2266	45	-0.84
09YY103-10	0.001008	0.000006	0.282556	0.000019	0.282553	-7.7	-5.0	986	1497	2069	41	-0.97
09YY103-11	0.002691	0.000055	0.282592	0.000022	0.282586	-6.6	-3.8	979	1425	1965	39	-0.92
09YY103-12	0.001464	0.000056	0.282517	0.000017	0.282513	-9.1	-6.4	1054	1586	2196	44	-0.96
09YY103-13	0.002476	0.000013	0.282551	0.000018	0.282545	-8.0	-5.2	1033	1516	2095	42	-0.93
09YY103-14	0.005908	0.000063	0.282562	0.000014	0.282548	-7.9	-5.1	1123	1508	2084	42	-0.82
09YY103-15	0.001258	0.000086	0.282560	0.000019	0.282557	-7.6	-4.8	986	1488	2056	41	-0.96
09YY103-16	0.006007	0.000085	0.282560	0.000017	0.282546	-8.0	-5.2	1130	1513	2090	42	-0.82
09YY103-17	0.003213	0.000077	0.282527	0.000019	0.282520	-8.9	-6.1	1090	1572	2176	44	-0.90
09YY103-18	0.002092	0.000099	0.282557	0.000020	0.282552	-7.8	-5.0	1014	1501	2074	41	-0.94
09YY103-19	0.001728	0.000083	0.282573	0.000019	0.282569	-7.2	-4.4	980	1461	2018	40	-0.95
09YY103-20	0.001657	0.000021	0.282515	0.000016	0.282511	-9.2	-6.5	1062	1592	2204	44	-0.95
09YY103-21	0.000915	0.000011	0.282533	0.000018	0.282531	-8.5	-5.7	1015	1546	2139	43	-0.97
09YY103-22	0.004637	0.000046	0.282552	0.000016	0.282542	-8.2	-5.4	1096	1524	2106	42	-0.86
09YY103-24	0.001514	0.000005	0.282496	0.000017	0.282492	-9.9	-7.1	1085	1634	2264	45	-0.95
09YY103-25	0.004608	0.000009	0.282556	0.000016	0.282545	-8.0	-5.3	1091	1517	2096	42	-0.86
09YY105-01	0.001241	0.000013	0.282499	0.000015	0.282496	-9.8	-7.0	1073	1626	2252	45	-0.96
09YY105-02	0.001712	0.000030	0.282490	0.000018	0.282486	-10.1	-7.3	1100	1648	2284	46	-0.95
09YY105-03	0.001058	0.000004	0.282553	0.000018	0.282550	-7.8	-5.1	992	1504	2079	42	-0.97
09YY105-04	0.001560	0.000010	0.282564	0.000020	0.282561	-7.5	-4.7	989	1481	2045	41	-0.95
09YY105-05	0.002484	0.000102	0.282622	0.000018	0.282616	-5.5	-2.7	929	1356	1868	37	-0.93
09YY105-06	0.000652	0.000034	0.282547	0.000017	0.282546	-8.0	-5.2	989	1514	2093	42	-0.98
09YY105-07	0.002020	0.000039	0.282586	0.000016	0.282581	-6.8	-4.0	970	1436	1981	40	-0.94
09YY105-08	0.001146	0.000005	0.282507	0.000014	0.282505	-9.5	-6.7	1058	1606	2224	44	-0.97
09YY105-09	0.003252	0.000077	0.282546	0.000028	0.282538	-8.3	-5.5	1064	1532	2117	42	-0.90
09YY105-10	0.002112	0.000021	0.282540	0.000018	0.282535	-8.4	-5.6	1039	1538	2127	43	-0.94
09YY105-11	0.001450	0.000019	0.282538	0.000016	0.282534	-8.4	-5.6	1024	1540	2129	43	-0.96
09YY105-12	0.002674	0.000055	0.282574	0.000019	0.282568	-7.2	-4.5	1005	1465	2023	40	-0.92
09YY105-14	0.001525	0.000010	0.282584	0.000020	0.282581	-6.8	-4.0	959	1436	1982	40	-0.95
09YY105-15	0.000746	0.000008	0.282567	0.000024	0.282565	-7.3	-4.5	964	1471	2032	41	-0.98
09YY105-16	0.001646	0.000007	0.282521	0.000016	0.282517	-9.0	-6.2	1053	1578	2184	44	-0.95
09YY105-17	0.001553	0.000016	0.282544	0.000024	0.282540	-8.2	-5.4	1018	1526	2111	42	-0.95
09YY105-18	0.005174	0.000051	0.282566	0.000017	0.282554	-7.7	-4.9	1093	1497	2067	41	-0.84
09YY105-19	0.004422	0.000058	0.282512	0.000017	0.282501	-9.6	-6.8	1153	1613	2234	45	-0.87
09YY105-20	0.005400	0.000097	0.282589	0.000015	0.282576	-6.9	-4.2	1064	1446	1996	40	-0.84
Taohuadao												
09YY129-01	0.002541	0.000015	0.282627	0.000017	0.282623	-5.3	-3.3	923	1364	1896	38	-0.92
09YY129-02	0.001820	0.000015	0.282612	0.000018	0.282609	-5.8	-3.8	927	1395	1941	39	-0.95
09YY129-03	0.001859	0.000046	0.282656	0.000015	0.282653	-4.2	-2.3	864	1297	1801	36	-0.94
09YY129-04	0.002144	0.000015	0.282574	0.000018	0.282570	-7.1	-5.2	990	1482	2064	41	-0.94
09YY129-05	0.001405	0.000015	0.282604	0.000015	0.282602	-6.0	-4.1	928	1411	1964	39	-0.96
09YY129-06	0.002325	0.000016	0.282609	0.000012	0.282606	-5.9	-3.9	944	1403	1952	39	-0.93
09YY129-07	0.001650	0.000009	0.282637	0.000014	0.282635	-4.9	-2.9	886	1338	1859	37	-0.95
09YY129-08	0.001703	0.000008	0.282644	0.000014	0.282641	-4.6	-2.7	879	1324	1840	37	-0.95
09YY129-09	0.001983	0.000024	0.282640	0.000012	0.282636	-4.8	-2.8	891	1334	1854	37	-0.94
09YY129-10	0.001645	0.000006	0.282606	0.000012	0.282603	-6.0	-4.0	932	1409	1960	39	-0.95
09YY129-11	0.003108	0.000057	0.282623	0.000011	0.282618	-5.5	-3.5	944	1376	1913	38	-0.91
09YY129-12	0.001630	0.000012	0.282604	0.000012	0.282601	-6.0	-4.1	934	1412	1965	39	-0.95
09YY129-13	0.002582	0.000016	0.282643	0.000013	0.282639	-4.7	-2.7	900	1328	1845	37	-0.92
09YY129-14	0.004337	0.000039	0.282695	0.000018	0.282687	-3.0	-1.0	867	1220	1691	34	-0.87
09YY129-15	0.002733	0.000048	0.282662	0.000014	0.282657	-4.1	-2.1	877	1288	1788	36	-0.92
09YY129-16	0.001816	0.000051	0.282603	0.000012	0.282600	-6.1	-4.1	939	1415	1969	39	-0.95
09YY129-17	0.001495	0.000011	0.282607	0.000013	0.282604	-5.9	-4.0	926	1406	1956	39	-0.95
09YY129-18	0.003850	0.000045	0.282637	0.000016	0.282631	-5.0	-3.0	943	1347	1871	37	-0.88
09YY129-19	0.003264	0.000030	0.282640	0.000015	0.282635	-4.9	-2.9	923	1338	1859	37	-0.90

09YY129-20	0.001751	0.000005	0.282656	0.000011	0.282653	-4.2	-2.3	863	1298	1802	36	-0.95
09YY129-21	0.002382	0.000054	0.282606	0.000013	0.282602	-6.0	-4.0	950	1410	1962	39	-0.93
09YY129-22	0.002782	0.000009	0.282593	0.000013	0.282589	-6.5	-4.5	980	1441	2006	40	-0.92
09YY129-23	0.001816	0.000024	0.282579	0.000014	0.282576	-6.9	-5.0	975	1470	2048	41	-0.95
09YY129-24	0.001341	0.000017	0.282609	0.000014	0.282607	-5.8	-3.9	919	1400	1947	39	-0.96
09YY129-25	0.002041	0.000012	0.282645	0.000014	0.282642	-4.6	-2.6	884	1322	1836	37	-0.94
Putuoshan												
09YY163-01	0.001920	0.000010	0.282630	0.000026	0.282626	-5.2	-3.1	904	1353	1878	38	-0.94
09YY163-02	0.001120	0.000035	0.282551	0.000021	0.282549	-7.9	-5.7	996	1523	2119	42	-0.97
09YY163-03	0.002027	0.000027	0.282623	0.000015	0.282619	-5.4	-3.3	916	1369	1900	38	-0.94
09YY163-04	0.001497	0.000018	0.282567	0.000022	0.282564	-7.4	-5.2	984	1490	2072	41	-0.95
09YY163-05	0.002873	0.000028	0.282575	0.000020	0.282570	-7.1	-5.0	1009	1479	2056	41	-0.91
09YY163-06	0.003262	0.000022	0.282619	0.000020	0.282613	-5.6	-3.4	954	1380	1914	38	-0.90
09YY163-07	0.002803	0.000026	0.282662	0.000017	0.282657	-4.1	-2.0	878	1283	1778	36	-0.92
09YY163-08	0.001550	0.000028	0.282627	0.000027	0.282624	-5.2	-3.1	899	1355	1880	38	-0.95
09YY163-09	0.002834	0.000072	0.282634	0.000020	0.282629	-5.0	-3.0	920	1346	1868	37	-0.91
09YY163-10	0.000816	0.000008	0.282574	0.000020	0.282573	-7.1	-4.9	956	1471	2045	41	-0.98
09YY163-11	0.001849	0.000024	0.282620	0.000023	0.282616	-5.5	-3.3	917	1374	1906	38	-0.94
09YY163-12	0.002669	0.000026	0.282664	0.000026	0.282659	-4.0	-1.9	872	1279	1773	35	-0.92
09YY163-13	0.001998	0.000034	0.282603	0.000023	0.282600	-6.1	-3.9	944	1411	1958	39	-0.94
09YY163-14	0.002169	0.000043	0.282624	0.000023	0.282620	-5.4	-3.2	918	1364	1893	38	-0.93
09YY163-15	0.002386	0.000036	0.282638	0.000025	0.282633	-4.9	-2.7					
09YY163-16	0.002231	0.000026	0.282629	0.000023	0.282625	-5.2	-3.0	913	1354	1877	38	-0.93
09YY163-17	0.002408	0.000026	0.282670	0.000025	0.282666	-3.8	-1.6	857	1262	1747	35	-0.93
09YY163-18	0.002807	0.000018	0.282658	0.000030	0.282653	-4.2	-2.0	884	1291	1788	36	-0.92
09YY163-19	0.002401	0.000019	0.282584	0.000019	0.282580	-6.8	-4.7	982	1456	2025	40	-0.93
09YY163-20	0.002748	0.000078	0.282576	0.000024	0.282571	-7.1	-5.0	1004	1475	2050	41	-0.92
09YY136-01	0.003018	0.000033	0.282726	0.000026	0.282720	-1.8	0.3	789	1141	1574	31	-0.91
09YY136-02	0.002464	0.000009	0.282716	0.000027	0.282711	-2.1	0.0	791	1160	1602	32	-0.93
09YY136-03	0.003012	0.000031	0.282724	0.000024	0.282719	-1.9	0.2	790	1145	1582	32	-0.91
09YY136-04	0.003048	0.000039	0.282786	0.000019	0.282780	0.3	2.4	700	1007	1386	28	-0.91
09YY136-05	0.002629	0.000093	0.282751	0.000031	0.282746	-0.9	1.2	743	1083	1492	30	-0.92
09YY136-06	0.004471	0.000159	0.282681	0.000018	0.282673	-3.5	-1.4	891	1247	1727	35	-0.87
09YY136-07	0.003506	0.000029	0.282765	0.000029	0.282759	-0.5	1.7	740	1054	1451	29	-0.89
09YY136-08	0.004125	0.000022	0.282800	0.000017	0.282792	0.7	2.8	700	980	1348	27	-0.88
09YY136-09	0.002936	0.000098	0.282759	0.000029	0.282754	-0.6	1.5	737	1065	1466	29	-0.91
09YY136-10	0.003075	0.000034	0.282774	0.000026	0.282768	-0.1	2.0	718	1033	1421	28	-0.91
09YY136-11	0.002034	0.000132	0.282702	0.000030	0.282699	-2.6	-0.5	801	1190	1647	33	-0.94
09YY136-12	0.002493	0.000096	0.282747	0.000031	0.282743	-1.0	1.1	746	1092	1507	30	-0.92
09YY136-13	0.003215	0.000010	0.282733	0.000027	0.282727	-1.6	0.6	782	1124	1551	31	-0.90
09YY136-14	0.002885	0.000087	0.282752	0.000025	0.282747	-0.9	1.2	747	1083	1493	30	-0.91
09YY136-15	0.002331	0.000052	0.282749	0.000023	0.282745	-0.9	1.1	739	1086	1498	30	-0.93
09YY136-16	0.003279	0.000152	0.282862	0.000036	0.282856	3.0	5.1	590	837	1145	23	-0.90

APPENDIX TABLE v. *In situ* zircon O isotope compositions

Sample	IP(nA)	Intensity ^{16}O	$^{16}O/^{18}O_{mean}$	$\delta^{18}O$	2SE	note
Nianzishan						
10NZS-01	1.30	1.313E+9	2.008E-3	4.33	0.24	
10NZS-02	1.29	1.326E+9	2.009E-3	4.78	0.29	
10NZS-03	1.27	1.300E+9	2.009E-3	4.79	0.30	
10NZS-04	1.26	1.313E+9	2.010E-3	5.03	0.27	
10NZS-05	1.25	1.312E+9	2.008E-3	4.41	0.22	
10NZS-06	1.24	1.301E+9	2.009E-3	4.60	0.21	
10NZS-07	1.20	1.291E+9	2.009E-3	4.93	0.45	
10NZS-08	1.20	1.302E+9	2.009E-3	4.88	0.23	
10NZS-09	1.18	1.163E+9	2.009E-3	4.91	0.28	
10NZS-10	1.17	1.281E+9	2.009E-3	4.98	0.38	
10NZS-11	1.15	1.282E+9	2.010E-3	5.08	0.21	
10NZS-12	1.14	1.272E+9	2.009E-3	4.81	0.40	
10NZS-13	1.09	1.237E+9	2.010E-3	5.24	0.34	
10NZS-14	1.08	1.238E+9	2.010E-3	5.44	0.32	
10NZS-15	1.08	1.229E+9	2.009E-3	5.05	0.48	
10NZS-16	1.07	1.227E+9	2.010E-3	5.22	0.41	
10NZS-17	1.05	1.222E+9	2.010E-3	5.25	0.30	
10NZS-18	1.05	1.212E+9	2.010E-3	5.10	0.22	
10NZS-20	1.26	1.293E+9	2.013E-3	4.28	0.27	
10NZS-21	1.26	1.295E+9	2.013E-3	4.26	0.24	
10NZS-22	1.26	1.290E+9	2.014E-3	4.49	0.24	
10NZS-23	1.26	1.290E+9	2.013E-3	4.26	0.28	
10NZS-24	1.26	1.289E+9	2.013E-3	4.24	0.26	
10NZS-25	1.26	1.295E+9	2.013E-3	4.32	0.28	
10NZS-27	1.26	1.296E+9	2.014E-3	4.55	0.29	
10NZS-28	1.26	1.296E+9	2.013E-3	4.41	0.27	
10NZS-29	1.26	1.288E+9	2.013E-3	4.03	0.20	
10NZS-30	1.26	1.293E+9	2.013E-3	4.34	0.34	
10NZS-31	1.26	1.304E+9	2.013E-3	4.24	0.18	
10NZS-32	1.26	1.276E+9	2.013E-3	4.32	0.30	
10NZS-33	1.26	1.294E+9	2.014E-3	4.43	0.35	
10NZS-34	1.26	1.298E+9	2.014E-3	4.45	0.31	
10NZS-35	1.26	1.296E+9	2.013E-3	4.33	0.26	
10NZS-36	1.26	1.289E+9	2.014E-3	4.64	0.23	
11NZS01-01	0.39	1.251E+9	2.033E-3	4.49	0.26	
11NZS01-02	0.38	1.237E+9	2.034E-3	4.80	0.31	
11NZS01-03	0.38	1.240E+9	2.034E-3	5.20	0.33	
11NZS01-04	0.38	1.232E+9	2.034E-3	5.15	0.24	
11NZS01-05	0.37	1.242E+9	2.033E-3	4.50	0.20	
11NZS01-06	0.36	1.215E+9	2.034E-3	4.29	0.33	
11NZS01-07	0.35	1.216E+9	2.035E-3	4.38	0.30	

11NZS01-09	0.33	1.215E+9	2.034E-3	4.26	0.32
11NZS01-10	0.32	1.206E+9	2.034E-3	4.33	0.36
11NZS01-11	0.32	1.195E+9	2.034E-3	4.34	0.35
11NZS01-12	0.32	1.197E+9	2.035E-3	4.66	0.32
11NZS01-13	0.31	1.193E+9	2.035E-3	4.45	0.20
11NZS01-14	0.32	1.187E+9	2.035E-3	4.58	0.39
11NZS01-15	0.32	1.183E+9	2.034E-3	4.13	0.22
11NZS01-16	0.31	1.173E+9	2.034E-3	4.14	0.28
11NZS01-17	0.30	1.175E+9	2.036E-3	4.89	0.19
11NZS01-18	0.30	1.170E+9	2.035E-3	4.71	0.28
11NZS01-19	0.29	1.162E+9	2.036E-3	5.01	0.14
11NZS02-01	1.31	1.349E+9	2.013E-3	4.81	0.24
11NZS02-02	1.31	1.363E+9	2.013E-3	4.82	0.28
11NZS02-03	1.31	1.354E+9	2.012E-3	4.44	0.28
11NZS02-04	1.30	1.366E+9	2.013E-3	4.93	0.26
11NZS02-05	1.30	1.362E+9	2.013E-3	4.77	0.25
11NZS02-06	1.30	1.355E+9	2.013E-3	4.84	0.32
11NZS02-07	1.30	1.366E+9	2.013E-3	5.01	0.30
11NZS02-08	1.30	1.371E+9	2.012E-3	4.62	0.25
11NZS02-10	1.30	1.362E+9	2.013E-3	4.75	0.26
11NZS02-11	1.29	1.359E+9	2.013E-3	4.77	0.25
11NZS02-12	1.30	1.357E+9	2.013E-3	4.73	0.24
11NZS02-13	1.30	1.366E+9	2.013E-3	4.84	0.34
11NZS02-14	1.29	1.363E+9	2.013E-3	4.68	0.25
11NZS02-15	1.29	1.358E+9	2.014E-3	4.92	0.26
11NZS02-16	1.29	1.340E+9	2.013E-3	4.63	0.22
11NZS02-17	1.28	1.344E+9	2.012E-3	4.09	0.27
11NZS02-18	1.28	1.326E+9	2.014E-3	4.84	0.27
11NZS02-19	1.28	1.342E+9	2.013E-3	4.69	0.30
11NZS02-20	1.28	1.333E+9	2.013E-3	4.68	0.28
11NZS02-21	1.28	1.335E+9	2.013E-3	4.56	0.28
11NZS02-22	1.28	1.342E+9	2.013E-3	4.71	0.20
11NZS02-24	1.28	1.339E+9	2.013E-3	4.63	0.31
11NZS02-25	1.28	1.339E+9	2.013E-3	4.53	0.27
11NZS02-26	1.28	1.339E+9	2.013E-3	4.64	0.37
11NZS02-27	1.28	1.343E+9	2.013E-3	4.50	0.30
11NZS02-28	1.29	1.341E+9	2.013E-3	4.33	0.28
11NZS02-29	1.28	1.337E+9	2.013E-3	4.52	0.29
11NZS02-30	1.28	1.336E+9	2.013E-3	4.53	0.22
11NZS03-01	1.26	1.287E+9	2.013E-3	4.04	0.26
11NZS03-02	1.26	1.287E+9	2.013E-3	3.97	0.33
11NZS03-03	1.26	1.287E+9	2.013E-3	4.07	0.28
11NZS03-04	1.26	1.282E+9	2.012E-3	3.92	0.34
11NZS03-05	1.26	1.279E+9	2.012E-3	3.90	0.35

11NZS03-06	1.26	1.282E+9	2.013E-3	3.97	0.31
11NZS03-07	1.26	1.296E+9	2.013E-3	4.21	0.21
11NZS03-08	1.25	1.262E+9	2.013E-3	4.19	0.39
11NZS03-09	1.25	1.277E+9	2.012E-3	3.81	0.26
11NZS03-10	1.25	1.260E+9	2.012E-3	3.89	0.24
11NZS03-11	1.06	1.160E+9	2.014E-3	5.08	0.48
11NZS03-12	1.07	1.168E+9	2.013E-3	4.61	0.33
11NZS03-17	1.06	1.173E+9	2.013E-3	4.74	0.26
11NZS03-18	1.07	1.169E+9	2.013E-3	4.76	0.33
11NZS03-19	1.07	1.173E+9	2.013E-3	4.56	0.27
11NZS03-20	1.07	1.178E+9	2.013E-3	4.86	0.29
11NZS03-21	1.07	1.173E+9	2.013E-3	4.63	0.25
11NZS03-22	1.07	1.172E+9	2.013E-3	4.70	0.32
11NZS03-23	1.07	1.173E+9	2.012E-3	4.41	0.34
11NZS03-24	1.07	1.165E+9	2.013E-3	4.89	0.34
11NZS03-25	1.07	1.167E+9	2.014E-3	5.02	0.29
11NZS03-26	1.07	1.166E+9	2.013E-3	4.58	0.31
11NZS03-27	1.07	1.166E+9	2.014E-3	4.93	0.23
11NZS03-28	1.07	1.164E+9	2.013E-3	4.49	0.21
11NZS03-29	1.07	1.174E+9	2.014E-3	4.91	0.38
11NZS03-30	1.07	1.173E+9	2.013E-3	4.82	0.41
11NZS03-31	1.07	1.174E+9	2.013E-3	4.64	0.20
11NZS04-01	0.54	1.334E+9	2.034E-3	5.08	0.25
11NZS04-02	0.52	1.379E+9	2.033E-3	4.46	0.28
11NZS04-04	0.54	1.377E+9	2.033E-3	4.44	0.20
11NZS04-05	0.54	1.383E+9	2.032E-3	4.22	0.38
11NZS04-06	0.54	1.377E+9	2.033E-3	4.51	0.23
11NZS04-07	0.55	1.374E+9	2.033E-3	4.54	0.30
11NZS04-08	0.55	1.372E+9	2.033E-3	4.52	0.23
11NZS04-09	0.54	1.393E+9	2.033E-3	4.74	0.25
11NZS04-10	1.27	1.312E+9	2.014E-3	4.75	0.26
11NZS04-11	1.27	1.310E+9	2.014E-3	4.58	0.18
11NZS04-12	1.27	1.303E+9	2.013E-3	4.44	0.26
11NZS04-13	1.27	1.306E+9	2.014E-3	4.75	0.40
11NZS04-14	1.26	1.306E+9	2.013E-3	4.37	0.41
11NZS04-15	1.26	1.307E+9	2.014E-3	4.65	0.20
11NZS04-16	1.26	1.305E+9	2.013E-3	4.28	0.32
11NZS04-17	1.26	1.303E+9	2.014E-3	4.76	0.24
11NZS04-18	1.26	1.306E+9	2.014E-3	4.59	0.21
11NZS04-19	1.26	1.305E+9	2.014E-3	4.54	0.28
11NZS04-20	1.26	1.294E+9	2.013E-3	4.26	0.28
11NZS04-21	1.25	1.298E+9	2.013E-3	4.26	0.39
11NZS04-22	1.25	1.300E+9	2.014E-3	4.50	0.19
11NZS04-23	1.25	1.302E+9	2.014E-3	4.50	0.39
11NZS04-24	1.25	1.296E+9	2.014E-3	4.54	0.26

11NZS04-25	1.25	1.298E+9	2.014E-3	4.46	0.16
11NZS04-26	1.25	1.304E+9	2.014E-3	4.60	0.46
11NZS04-27	1.26	1.299E+9	2.014E-3	4.50	0.25
11NZS05-01	1.28	1.323E+9	2.013E-3	4.20	0.32
11NZS05-02	1.28	1.323E+9	2.013E-3	4.46	0.27
11NZS05-03	1.28	1.326E+9	2.013E-3	4.57	0.36
11NZS05-04	1.28	1.332E+9	2.013E-3	4.26	0.20
11NZS05-05	1.28	1.327E+9	2.014E-3	4.98	0.39
11NZS05-06	1.28	1.330E+9	2.013E-3	4.19	0.26
11NZS05-08	1.28	1.328E+9	2.014E-3	4.60	0.17
11NZS05-09	1.28	1.326E+9	2.014E-3	4.67	0.34
11NZS05-10	1.28	1.328E+9	2.014E-3	4.58	0.22
11NZS05-11	1.28	1.325E+9	2.013E-3	4.37	0.22
11NZS05-12	1.28	1.323E+9	2.014E-3	5.00	0.27
11NZS05-13	1.28	1.329E+9	2.014E-3	4.79	0.35
11NZS05-14	1.28	1.322E+9	2.014E-3	4.74	0.33
11NZS05-15	1.28	1.320E+9	2.013E-3	4.32	0.29
11NZS05-16	1.27	1.318E+9	2.014E-3	4.62	0.27
11NZS05-17	1.27	1.320E+9	2.013E-3	4.27	0.31
11NZS05-19	1.27	1.315E+9	2.013E-3	4.39	0.31
11NZS05-20	1.27	1.314E+9	2.014E-3	4.54	0.35
11NZS05-21	1.27	1.281E+9	2.014E-3	4.83	0.28
GW04190-01	1.16	1.219E+9	2.007E-3	4.64	0.14
GW04190-03	1.15	1.229E+9	2.009E-3	5.14	0.31
GW04190-04	1.15	1.232E+9	2.009E-3	5.33	0.22
GW04190-05	1.16	1.233E+9	2.009E-3	5.03	0.33
GW04190-06	1.15	1.221E+9	2.009E-3	5.05	0.23
GW04190-08	1.12	1.217E+9	2.008E-3	4.54	0.23
GW04190-09	1.12	1.187E+9	2.009E-3	5.18	0.30
GW04190-10	1.11	1.196E+9	2.008E-3	4.57	0.14
GW04190-11	1.11	1.206E+9	2.008E-3	4.43	0.22
GW04190-12	1.10	1.204E+9	2.009E-3	4.98	0.41
GW04190-13	1.08	1.251E+9	2.008E-3	4.06	0.27
GW04190-14	1.17	1.257E+9	2.008E-3	4.12	0.32
GW04190-15	1.07	1.167E+9	2.012E-3	4.20	0.30
GW04190-15	1.19	1.275E+9	2.008E-3	4.32	0.30
GW04190-16	1.20	1.298E+9	2.009E-3	4.92	0.39
GW04190-17	1.27	1.299E+9	2.009E-3	4.66	0.21
GW04190-18	1.07	1.176E+9	2.012E-3	4.21	0.36
GW04190-18	1.30	1.347E+9	2.009E-3	4.50	0.23
GW04190-19	1.08	1.183E+9	2.012E-3	4.34	0.35
GW04190-20	1.08	1.176E+9	2.012E-3	4.48	0.36
GW04190-21	1.07	1.174E+9	2.011E-3	4.17	0.29
GW04190-22	1.07	1.176E+9	2.012E-3	4.43	0.37

GW04190-23	1.07	1.167E+9	2.012E-3	4.36	0.20
GW04190-25	1.07	1.170E+9	2.011E-3	4.20	0.37
GW04190-26	1.07	1.164E+9	2.011E-3	4.09	0.27
GW04190-27	1.08	1.176E+9	2.011E-3	3.85	0.40
GW04190-28	1.07	1.175E+9	2.011E-3	4.06	0.33
GW04190-30	1.07	1.177E+9	2.012E-3	4.52	0.36
GW04190-32	1.07	1.179E+9	2.011E-3	3.96	0.28
GW04190-34	1.07	1.182E+9	2.011E-3	4.07	0.40
GW04190-35	1.07	1.184E+9	2.011E-3	3.86	0.36
GW04190-37	1.08	1.179E+9	2.012E-3	4.49	0.19
GW04190-38	1.08	1.185E+9	2.012E-3	4.19	0.31
GW04190-39	1.08	1.182E+9	2.012E-3	4.15	0.37
GW04190-40	1.07	1.182E+9	2.013E-3	4.57	0.32
Houshihushan					
10SHG01-01	1.05	1.145E+9	2.015E-3	5.31	0.43
10SHG01-03	0.95	1.159E+9	2.010E-3	5.19	0.34
10SHG01-04	0.94	1.166E+9	2.011E-3	5.33	0.36
10SHG01-05	0.94	1.169E+9	2.011E-3	5.33	0.30
10SHG01-06	0.91	1.168E+9	2.011E-3	5.61	0.36
10SHG01-07	1.02	1.202E+9	2.011E-3	5.65	0.25
10SHG01-08	1.01	1.210E+9	2.011E-3	5.38	0.23
10SHG01-10	0.99	1.180E+9	2.010E-3	5.19	0.36
10SHG01-12	0.97	1.161E+9	2.011E-3	5.39	0.23
10SHG01-13	1.00	1.191E+9	2.011E-3	5.67	0.31
10SHG01-14	1.03	1.205E+9	2.011E-3	5.44	0.28
10SHG01-15	1.04	1.207E+9	2.011E-3	5.48	0.21
10SHG01-16	1.04	1.190E+9	2.011E-3	5.46	0.18
10SHG01-17	1.03	1.194E+9	2.010E-3	5.23	0.27
10SHG01-18	1.03	1.190E+9	2.011E-3	5.33	0.35
10YSH01-07	0.45	1.127E+9	2.008E-3	5.79	0.36
10YSH01-08	0.43	1.114E+9	2.007E-3	5.45	0.23
10YSH01-11	0.55	1.163E+9	2.008E-3	5.82	0.31
10YSH01-13	0.56	1.162E+9	2.007E-3	5.70	0.32
10YSH01-15	0.57	1.160E+9	2.007E-3	5.69	0.21
10YSH01-16	0.57	1.154E+9	2.008E-3	5.74	0.41
10YSH01-17	0.58	1.144E+9	2.008E-3	5.81	0.22
10YSH01-18	0.59	1.161E+9	2.008E-3	5.71	0.29
10YSH04-01	0.54	1.233E+9	2.007E-3	5.55	0.22
10YSH04-02	0.54	1.228E+9	2.007E-3	5.53	0.30
10YSH04-03	0.56	1.227E+9	2.007E-3	5.40	0.28
10YSH04-04	0.54	1.223E+9	2.007E-3	5.59	0.35
10YSH04-06	0.55	1.212E+9	2.006E-3	5.13	0.34

10YSH04-07	0.54	1.201E+9	2.007E-3	5.22	0.31
10YSH04-08	0.54	1.203E+9	2.007E-3	5.62	0.31
10YSH04-09	0.52	1.191E+9	2.007E-3	5.37	0.18
10YSH04-10	0.52	1.185E+9	2.006E-3	5.11	0.20
10YSH04-11	0.51	1.176E+9	2.006E-3	5.00	0.29
10YSH04-12	0.52	1.176E+9	2.007E-3	5.25	0.30
10YSH04-13	0.50	1.167E+9	2.007E-3	5.31	0.21
10YSH04-16	0.49	1.153E+9	2.007E-3	5.57	0.42
10YSH04-17	0.49	1.149E+9	2.007E-3	5.27	0.36
10YSH04-18	0.51	1.151E+9	2.007E-3	5.26	0.22
Laoshan					
09LS05-01	0.99	1.200E+9	2.011E-3	5.78	0.24
09LS05-03	0.97	1.177E+9	2.012E-3	6.00	0.35
09LS05-05	0.96	1.169E+9	2.011E-3	5.83	0.34
09LS05-06	0.95	1.156E+9	2.011E-3	5.86	0.36
09LS05-07	0.91	1.134E+9	2.011E-3	5.61	0.25
09LS05-08	0.89	1.136E+9	2.010E-3	5.49	0.29
09LS05-09	0.87	1.106E+9	2.011E-3	5.99	0.32
09LS05-10	0.87	1.103E+9	2.010E-3	5.35	0.33
09LS05-12	0.84	1.077E+9	2.011E-3	5.58	0.42
09LS05-14	0.80	1.049E+9	2.010E-3	5.23	0.26
09LS05-16	0.78	1.047E+9	2.011E-3	5.55	0.21
09LS05-17	0.78	1.032E+9	2.011E-3	5.54	0.34
09LS05-18	0.76	1.010E+9	2.011E-3	5.93	0.37
09LS05-19	0.89	1.077E+9	2.011E-3	5.67	0.29
09LS05-21	1.06	1.155E+9	2.015E-3	5.71	0.29
09LS05-22	1.06	1.158E+9	2.016E-3	5.98	0.29
09LS05-23	1.06	1.143E+9	2.015E-3	5.52	0.23
09LS05-25	1.06	1.160E+9	2.015E-3	5.42	0.29
09LS05-26	1.06	1.161E+9	2.015E-3	5.42	0.33
09LS05-27	1.06	1.161E+9	2.014E-3	5.22	0.30
09LS05-30	1.06	1.152E+9	2.015E-3	5.44	0.46
09LS05-31	1.06	1.161E+9	2.014E-3	5.09	0.31
09LS05-32	1.06	1.149E+9	2.015E-3	5.22	0.36
09LS05-33	1.06	1.153E+9	2.015E-3	5.65	0.21
09LS05-34	1.06	1.159E+9	2.016E-3	5.89	0.26
09LS05-35	1.06	1.153E+9	2.014E-3	5.13	0.20
10LS05-01	0.77	1.161E+9	2.011E-3	5.85	0.35
10LS05-02	0.94	1.203E+9	2.011E-3	5.80	0.36
10LS05-03	0.97	1.202E+9	2.012E-3	5.95	0.29
10LS05-04	1.00	1.198E+9	2.011E-3	5.42	0.30
10LS05-05	1.00	1.204E+9	2.010E-3	5.07	0.33
10LS05-06	1.00	1.198E+9	2.011E-3	5.67	0.32
10LS05-07	0.99	1.191E+9	2.012E-3	5.83	0.43

10LS05-08	0.99	1.183E+9	2.011E-3	5.57	0.27
10LS05-09	0.97	1.168E+9	2.010E-3	5.23	0.35
10LS05-10	0.97	1.177E+9	2.011E-3	5.45	0.25
10LS05-11	0.96	1.157E+9	2.011E-3	5.35	0.34
10LS05-12	0.95	1.150E+9	2.010E-3	5.11	0.18
10LS05-13	1.05	1.213E+9	2.010E-3	5.07	0.28
10LS05-14	1.06	1.216E+9	2.010E-3	5.13	0.30
10LS05-15	1.06	1.209E+9	2.010E-3	4.84	0.24
10LS05-16	1.05	1.200E+9	2.010E-3	4.98	0.36
10LS05-17	1.04	1.204E+9	2.011E-3	5.50	0.20
10LS05-18	1.06	1.153E+9	2.014E-3	4.85	0.28
10LS05-18	1.02	1.160E+9	2.010E-3	5.34	0.24
10LS05-19	1.06	1.159E+9	2.014E-3	4.92	0.24
10LS05-20	1.06	1.166E+9	2.015E-3	5.17	0.30
10LS05-21	1.05	1.147E+9	2.015E-3	5.38	0.34
10LS05-22	1.05	1.148E+9	2.014E-3	5.04	0.35
10LS05-23	1.06	1.153E+9	2.015E-3	5.54	0.18
10LS05-25	1.06	1.155E+9	2.015E-3	5.21	0.40
10LS05-26	1.05	1.157E+9	2.015E-3	5.28	0.30
10LS05-27	1.05	1.154E+9	2.014E-3	4.86	0.33
10LS05-28	1.06	1.153E+9	2.015E-3	5.37	0.30
10LS05-29	1.06	1.147E+9	2.015E-3	5.20	0.33
10LS05-30	1.06	1.160E+9	2.015E-3	5.47	0.33
10LS05-31	1.06	1.153E+9	2.014E-3	5.03	0.35
10LS05-32	1.06	1.151E+9	2.015E-3	5.26	0.26
10LS05-33	1.06	1.151E+9	2.014E-3	4.95	0.24
10LS05-34	1.06	1.140E+9	2.015E-3	5.25	0.28
10LS05-35	1.06	1.159E+9	2.015E-3	5.08	0.24
Putuoshan					
09YY163-01	1.91	1.781E+9	2.011E-3	5.67	0.17
09YY163-04	1.96	1.789E+9	2.011E-3	5.67	0.19
09YY163-05	1.96	1.788E+9	2.011E-3	5.51	0.22
09YY163-06	1.95	1.793E+9	2.011E-3	5.31	0.17
09YY163-07	1.96	1.767E+9	2.011E-3	5.32	0.19
09YY163-08	1.96	1.767E+9	2.012E-3	5.91	0.19
09YY163-09	1.95	1.780E+9	2.011E-3	5.56	0.19
09YY163-10	1.96	1.780E+9	2.012E-3	5.76	0.18
09YY163-11	1.97	1.772E+9	2.012E-3	5.78	0.18
09YY163-12	1.99	1.806E+9	2.011E-3	5.72	0.20
09YY163-13	1.98	1.764E+9	2.011E-3	5.51	0.19
09YY163-15	1.96	1.795E+9	2.010E-3	5.20	0.13
09YY163-16	1.98	1.782E+9	2.011E-3	5.54	0.19
09YY163-17	1.96	1.766E+9	2.011E-3	5.71	0.18
09YY163-18	1.97	1.767E+9	2.011E-3	5.68	0.16
09YY163-19	1.97	1.758E+9	2.011E-3	5.68	0.22

09YY163-20	1.96	1.783E+9	2.011E-3	5.64	0.17
09YY163-22	1.97	1.770E+9	2.012E-3	5.82	0.19
09YY136-01	1.94	1.780E+9	2.010E-3	5.20	0.13
09YY136-02	1.95	1.759E+9	2.010E-3	5.11	0.27
09YY136-03	1.94	1.793E+9	2.010E-3	5.28	0.19
09YY136-05	1.97	1.772E+9	2.011E-3	5.46	0.22
09YY136-06	1.97	1.782E+9	2.010E-3	5.27	0.17
09YY136-09	1.96	1.763E+9	2.010E-3	4.98	0.24
09YY136-11	1.96	1.782E+9	2.010E-3	5.02	0.18
09YY136-12	1.96	1.778E+9	2.010E-3	5.35	0.23
09YY136-13	1.96	1.783E+9	2.011E-3	5.45	0.20
09YY136-14	1.97	1.775E+9	2.010E-3	5.25	0.17
09YY136-16	1.97	1.779E+9	2.010E-3	5.13	0.24
09YY136-17	1.96	1.777E+9	2.009E-3	4.92	0.21
09YY136-18	1.97	1.773E+9	2.010E-3	5.20	0.17
09YY136-19	1.95	1.753E+9	2.010E-3	5.35	0.21
09YY136-20	1.96	1.774E+9	2.010E-3	5.15	0.23
09YY136-21	1.96	1.765E+9	2.010E-3	5.44	0.17
09YY136-22	1.96	1.764E+9	2.010E-3	5.08	0.20
09YY136-23	1.95	1.731E+9	2.010E-3	5.25	0.21
09YY136-24	1.95	1.733E+9	2.011E-3	5.86	0.17
09YY136-25	1.93	1.739E+9	2.010E-3	5.13	0.15
Taohuadao					
09YY129-01	1.90	1.671E+9	2.010E-3	4.91	0.20
09YY129-02	1.92	1.685E+9	2.009E-3	4.56	0.17
09YY129-03	1.91	1.666E+9	2.009E-3	4.63	0.17
09YY129-04	1.92	1.695E+9	2.010E-3	4.90	0.23
09YY129-05	1.91	1.679E+9	2.010E-3	4.83	0.17
09YY129-06	1.90	1.686E+9	2.009E-3	4.65	0.18
09YY129-07	1.90	1.691E+9	2.010E-3	5.07	0.25
09YY129-08	1.90	1.688E+9	2.010E-3	4.90	0.18
09YY129-09	1.91	1.681E+9	2.009E-3	4.76	0.19
09YY129-10	1.92	1.684E+9	2.010E-3	4.84	0.19
09YY129-11	1.91	1.669E+9	2.009E-3	4.80	0.18
09YY129-12	1.91	1.677E+9	2.010E-3	4.90	0.22
09YY129-13	1.91	1.659E+9	2.011E-3	5.78	0.22
09YY129-14	1.90	1.673E+9	2.009E-3	4.66	0.21
09YY129-15	1.89	1.676E+9	2.009E-3	4.78	0.25
09YY129-16	1.90	1.679E+9	2.009E-3	4.75	0.17
09YY129-17	1.88	1.682E+9	2.009E-3	4.74	0.21
09YY129-18	1.90	1.684E+9	2.010E-3	5.04	0.19
09YY129-19	1.90	1.657E+9	2.009E-3	4.59	0.21
09YY129-20	1.91	1.689E+9	2.009E-3	4.73	0.20
09YY129-21	1.91	1.690E+9	2.009E-3	4.80	0.17

09YY129-22	1.91	1.647E+9	2.008E-3	4.36	0.24	
09YY129-23	1.90	1.680E+9	2.009E-3	4.92	0.25	
09YY129-24	1.91	1.689E+9	2.009E-3	4.90	0.25	
09YY129-25	1.91	1.660E+9	2.008E-3	4.41	0.16	
09YY129-26	1.91	1.689E+9	2.011E-3	5.51	0.19	
09YY129-2-01	1.20	1.127E+9	2.008E-3	4.35	0.31	
09YY129-2-02	1.20	1.133E+9	2.008E-3	4.61	0.32	
09YY129-2-03	1.20	1.135E+9	2.008E-3	4.58	0.42	
09YY129-2-04	1.19	1.127E+9	2.009E-3	5.06	0.43	
09YY129-2-05	1.20	1.127E+9	2.008E-3	4.78	0.22	
09YY129-2-06	1.19	1.119E+9	2.008E-3	4.48	0.19	
09YY129-2-07	1.20	1.127E+9	2.008E-3	4.67	0.31	
09YY129-2-08	1.20	1.114E+9	2.008E-3	4.50	0.37	
09YY129-2-09	1.20	1.134E+9	2.008E-3	4.43	0.35	
09YY129-2-10	1.20	1.139E+9	2.008E-3	4.42	0.25	
09YY129-2-11	1.20	1.124E+9	2.008E-3	4.81	0.36	
09YY129-2-12	1.20	1.118E+9	2.009E-3	4.98	0.33	
09YY129-2-13	1.19	1.122E+9	2.007E-3	4.27	0.32	
09YY129-2-14	1.20	1.124E+9	2.008E-3	4.45	0.28	
09YY129-2-15	1.19	1.117E+9	2.008E-3	4.55	0.22	
09YY148-2-01	1.22	1.170E+9	2.008E-3	3.96	0.18	high-U
09YY148-2-02	1.21	1.186E+9	2.008E-3	3.90	0.33	
09YY148-2-03	1.22	1.167E+9	2.007E-3	3.85	0.28	
09YY148-2-04	1.22	1.161E+9	2.008E-3	4.03	0.23	
09YY148-2-05	1.21	1.170E+9	2.008E-3	3.98	0.34	
09YY148-2-06	1.21	1.157E+9	2.007E-3	3.86	0.20	
09YY148-2-07	1.20	1.159E+9	2.008E-3	4.24	0.41	
09YY148-2-08	1.21	1.120E+9	2.008E-3	4.02	0.37	
09YY148-2-09	1.20	1.161E+9	2.007E-3	3.49	0.37	
09YY148-2-10	1.21	1.161E+9	2.009E-3	4.43	0.31	
09YY148-2-11	1.20	1.166E+9	2.008E-3	4.18	0.41	
09YY148-2-12	1.21	1.160E+9	2.007E-3	3.74	0.33	
09YY148-2-13	1.21	1.168E+9	2.007E-3	3.63	0.23	
09YY148-2-14	1.20	1.170E+9	2.007E-3	3.77	0.26	
09YY148-2-15	1.18	1.155E+9	2.008E-3	4.04	0.44	
09YY148-2-16	1.19	1.154E+9	2.008E-3	3.93	0.37	
09YY148-2-17	1.19	1.159E+9	2.008E-3	4.03	0.21	
09YY148-2-18	1.20	1.168E+9	2.006E-3	3.02	0.27	
09YY148-2-19	1.20	1.160E+9	2.008E-3	4.34	0.25	
09YY148-2-20	1.24	1.179E+9	2.007E-3	3.82	0.28	
09YY148-01	1.88	1.772E+9	2.010E-3	4.78	0.14	
09YY148-02	1.86	1.783E+9	2.009E-3	4.44	0.20	
09YY148-03	1.91	1.808E+9	2.009E-3	4.48	0.15	

09YY148-04	1.89	1.764E+9	2.009E-3	4.60	0.22
09YY148-05	1.83	1.750E+9	2.009E-3	4.40	0.23
09YY148-06	1.85	1.751E+9	2.008E-3	4.06	0.11
09YY148-07	1.83	1.762E+9	2.008E-3	4.21	0.17
09YY148-08	1.85	1.757E+9	2.009E-3	4.70	0.18
09YY148-09	1.87	1.768E+9	2.009E-3	4.57	0.20
09YY148-10	1.84	1.754E+9	2.009E-3	4.35	0.19
09YY148-11	1.86	1.763E+9	2.007E-3	3.35	0.19
09YY148-12	1.84	1.745E+9	2.009E-3	4.42	0.21
09YY148-13	1.86	1.739E+9	2.008E-3	3.86	0.15
09YY148-14	1.87	1.738E+9	2.008E-3	4.18	0.22
09YY148-15	1.85	1.749E+9	2.008E-3	4.10	0.19
09YY148-16	1.84	1.764E+9	2.009E-3	4.54	0.17
09YY148-17	1.85	1.723E+9	2.008E-3	4.11	0.26
09YY148-18	1.84	1.727E+9	2.009E-3	4.42	0.15
09YY148-19	1.86	1.752E+9	2.008E-3	4.16	0.20
09YY148-20	1.85	1.726E+9	2.008E-3	3.78	0.17
09YY148-21	1.86	1.776E+9	2.007E-3	3.52	0.14
09YY148-22	1.86	1.734E+9	2.009E-3	4.26	0.15
09YY148-23	1.85	1.741E+9	2.008E-3	3.83	0.22
09YY148-24	1.83	1.744E+9	2.009E-3	4.36	0.20
09YY148-25	1.88	1.728E+9	2.008E-3	3.86	0.17

APPENDIX TABLE vi. *In situ* quartz O isotope compositions

Sample	IP(nA)	Intensity O^{16}	O^{16}/O^{18} mean	$\delta^{18}O$ (‰)	2SE
Nianzishan					
10NZSQ1	1.10	1.258E+9	2.012E-3	6.80	0.22
10NZSQ2	1.10	1.262E+9	2.012E-3	6.77	0.17
10NZSQ3	1.09	1.261E+9	2.013E-3	6.97	0.15
10NZSQ4	1.10	1.261E+9	2.013E-3	7.16	0.34
10NZSQ5	1.10	1.257E+9	2.012E-3	6.52	0.30
10NZSQ6	1.10	1.249E+9	2.014E-3	7.56	0.48
10NZSQ7	1.10	1.260E+9	2.013E-3	7.10	0.30
10NZSQ8	1.10	1.260E+9	2.013E-3	7.13	0.31
10NZSQ9	1.10	1.260E+9	2.013E-3	7.10	0.22
10NZSQ10	1.11	1.258E+9	2.012E-3	6.78	0.24
10NZSQ11	1.10	1.255E+9	2.014E-3	7.44	0.18
10NZSQ12	1.11	1.260E+9	2.013E-3	7.30	0.35
10NZSQ13	1.10	1.255E+9	2.013E-3	7.06	0.31
10NZSQ14	1.10	1.258E+9	2.013E-3	6.87	0.35
10NZSQ15	1.09	1.249E+9	2.013E-3	7.06	0.29
10NZSQ16	1.09	1.258E+9	2.013E-3	7.18	0.34
11NZS01Q1	1.18	1.335E+9	2.014E-3	7.73	0.24
11NZS01Q2	1.18	1.332E+9	2.014E-3	7.28	0.21
11NZS01Q3	1.18	1.339E+9	2.013E-3	7.10	0.30
11NZS01Q4	1.18	1.340E+9	2.013E-3	6.85	0.19
11NZS01Q5	1.18	1.337E+9	2.013E-3	6.92	0.25
11NZS01Q6	1.18	1.336E+9	2.014E-3	7.26	0.33
11NZS01Q7	1.17	1.337E+9	2.013E-3	7.14	0.27
11NZS01Q8	1.18	1.333E+9	2.013E-3	7.04	0.28
11NZS01Q9	1.18	1.329E+9	2.013E-3	7.15	0.29
11NZS01Q10	1.18	1.334E+9	2.013E-3	7.08	0.24
11NZS01Q11	1.17	1.328E+9	2.013E-3	6.83	0.34
11NZS01Q12	1.17	1.331E+9	2.013E-3	6.84	0.30
11NZS01Q13	1.17	1.326E+9	2.013E-3	7.03	0.21
11NZS01Q14	1.17	1.328E+9	2.012E-3	6.66	0.19
11NZS01Q16	1.16	1.329E+9	2.013E-3	7.02	0.21
11NZS01Q17	1.16	1.324E+9	2.012E-3	6.65	0.31
11NZS01Q18	1.17	1.326E+9	2.013E-3	7.12	0.29
11NZS01Q19	1.16	1.332E+9	2.013E-3	6.92	0.29
11NZS01Q20	1.17	1.326E+9	2.014E-3	7.30	0.27
11NZS01Q21	1.17	1.333E+9	2.013E-3	6.94	0.32
11NZS01Q22	1.17	1.329E+9	2.013E-3	7.04	0.38
11NZS01Q23	1.17	1.334E+9	2.013E-3	7.17	0.29

11NZS01Q24	1.17	1.325E+9	2.013E-3	7.23	0.26
11NZS01Q25	1.17	1.330E+9	2.013E-3	7.06	0.22
11NZS02Q1	1.20	1.341E+9	2.013E-3	7.25	0.24
11NZS02Q2	1.21	1.346E+9	2.012E-3	7.09	0.29
11NZS02Q3	1.20	1.339E+9	2.012E-3	7.03	0.22
11NZS02Q4	1.20	1.341E+9	2.013E-3	7.30	0.30
11NZS02Q5	1.19	1.340E+9	2.013E-3	7.54	0.29
11NZS02Q6	1.20	1.336E+9	2.012E-3	7.18	0.26
11NZS02Q8	1.18	1.337E+9	2.012E-3	6.93	0.35
11NZS02Q9	1.18	1.335E+9	2.013E-3	7.23	0.27
11NZS02Q11	1.19	1.338E+9	2.013E-3	7.60	0.28
11NZS02Q12	1.19	1.334E+9	2.013E-3	7.46	0.29
11NZS02Q13	1.18	1.341E+9	2.011E-3	6.41	0.33
11NZS02Q14	1.18	1.345E+9	2.012E-3	6.97	0.38
11NZS02Q15	1.17	1.324E+9	2.013E-3	7.42	0.40
11NZS02Q16	1.18	1.340E+9	2.012E-3	7.18	0.32
11NZS02Q17	1.19	1.345E+9	2.012E-3	7.20	0.28
11NZS02Q18	1.19	1.315E+9	2.013E-3	7.56	0.28
11NZS02Q19	1.19	1.344E+9	2.012E-3	7.03	0.27
11NZS02Q20	1.19	1.343E+9	2.013E-3	7.28	0.32
11NZS02Q21	1.19	1.338E+9	2.014E-3	7.70	0.29
11NZS02Q22	1.19	1.333E+9	2.012E-3	6.83	0.28
11NZS02Q23	1.19	1.322E+9	2.013E-3	7.53	0.33
11NZS02Q24	1.18	1.331E+9	2.014E-3	7.89	0.17
11NZS02Q25	1.19	1.341E+9	2.013E-3	7.57	0.26
11NZS04Q1	1.18	1.329E+9	2.013E-3	7.07	0.35
11NZS04Q2	1.17	1.328E+9	2.014E-3	7.35	0.39
11NZS04Q3	1.15	1.315E+9	2.013E-3	6.82	0.21
11NZS04Q4	1.15	1.316E+9	2.014E-3	7.25	0.28
11NZS04Q5	1.15	1.303E+9	2.013E-3	7.07	0.28
11NZS04Q6	1.14	1.309E+9	2.014E-3	7.35	0.28
11NZS04Q7	1.14	1.302E+9	2.014E-3	7.27	0.26
11NZS04Q8	1.13	1.303E+9	2.013E-3	7.11	0.27
11NZS04Q9	1.14	1.305E+9	2.014E-3	7.50	0.20
11NZS04Q10	1.13	1.307E+9	2.014E-3	7.25	0.26
11NZS04Q11	1.13	1.301E+9	2.013E-3	6.86	0.30
11NZS04Q12	1.13	1.300E+9	2.013E-3	6.95	0.33
11NZS04Q13	1.13	1.304E+9	2.012E-3	6.56	0.40
11NZS04Q14	1.13	1.307E+9	2.013E-3	6.85	0.22
11NZS04Q15	1.13	1.304E+9	2.013E-3	7.11	0.27
11NZS04Q16	1.13	1.295E+9	2.013E-3	7.06	0.28
11NZS04Q17	1.14	1.297E+9	2.012E-3	6.60	0.26

11NZS04Q18	1.14	1.301E+9	2.014E-3	7.29	0.22
11NZS04Q19	1.13	1.303E+9	2.014E-3	7.28	0.35
11NZS04Q20	1.13	1.298E+9	2.013E-3	6.98	0.29
11NZS04Q21	1.14	1.300E+9	2.014E-3	7.39	0.36
11NZS04Q22	1.13	1.302E+9	2.014E-3	7.26	0.30
11NZS04Q23	1.13	1.300E+9	2.013E-3	7.17	0.26
11NZS05Q1	1.16	1.313E+9	2.014E-3	7.39	0.25
11NZS05Q2	1.16	1.312E+9	2.014E-3	7.28	0.32
11NZS05Q3	1.16	1.315E+9	2.013E-3	7.21	0.31
11NZS05Q4	1.15	1.318E+9	2.013E-3	6.95	0.28
11NZS05Q6	1.15	1.312E+9	2.013E-3	7.15	0.29
11NZS05Q7	1.15	1.322E+9	2.013E-3	7.08	0.29
11NZS05Q8	1.15	1.325E+9	2.014E-3	7.42	0.35
11NZS05Q9	1.15	1.313E+9	2.013E-3	6.86	0.29
11NZS05Q10	1.15	1.317E+9	2.013E-3	6.93	0.27
11NZS05Q11	1.14	1.315E+9	2.014E-3	7.31	0.33
11NZS05Q12	1.14	1.314E+9	2.013E-3	7.09	0.34
11NZS05Q13	1.14	1.315E+9	2.014E-3	7.37	0.32
11NZS05Q15	1.15	1.312E+9	2.014E-3	7.47	0.23
11NZS05Q16	1.15	1.311E+9	2.014E-3	7.59	0.18
11NZS05Q17	1.15	1.318E+9	2.014E-3	7.31	0.21
11NZS05Q18	1.15	1.315E+9	2.014E-3	7.53	0.34
11NZS05Q19	1.15	1.309E+9	2.013E-3	6.99	0.29
11NZS05Q20	1.15	1.317E+9	2.013E-3	7.21	0.31
11NZS05Q21	1.15	1.413E+9	2.014E-3	7.44	0.19
11NZS05Q22	1.24	1.372E+9	2.014E-3	7.39	0.24
11NZS05Q23	1.18	1.338E+9	2.014E-3	7.45	0.19
Houshihushan					
10SHG01Q01	1.15	1.266E+9	2.013E-3	7.41	0.35
10SHG01Q02	1.15	1.264E+9	2.013E-3	7.42	0.18
10SHG01Q03	1.14	1.268E+9	2.013E-3	7.78	0.33
10SHG01Q04	1.15	1.280E+9	2.013E-3	7.45	0.36
10SHG01Q05	1.15	1.276E+9	2.013E-3	7.51	0.28
10SHG01Q06	1.15	1.266E+9	2.014E-3	7.79	0.28
10SHG01Q07	1.15	1.273E+9	2.013E-3	7.63	0.24
10SHG01Q08	1.15	1.269E+9	2.013E-3	7.61	0.33
10SHG01Q09	1.15	1.273E+9	2.014E-3	7.93	0.23
10SHG01Q10	1.15	1.278E+9	2.013E-3	7.56	0.31
10SHG01Q11	1.15	1.270E+9	2.013E-3	7.74	0.28
10SHG01Q12	1.14	1.281E+9	2.013E-3	7.67	0.32
10SHG01Q13	1.13	1.264E+9	2.016E-3	8.79	0.34
10SHG01Q14	1.13	1.271E+9	2.014E-3	7.90	0.22

10SHG01Q15	1.14	1.271E+9	2.013E-3	7.53	0.23
10SHG01Q16	1.14	1.254E+9	2.014E-3	8.11	0.28
10SHG01Q17	1.14	1.275E+9	2.014E-3	7.92	0.30
10SHG01Q18	1.15	1.275E+9	2.014E-3	7.93	0.29
10SHG01Q19	1.14	1.271E+9	2.014E-3	7.74	0.52
10SHG01Q20	1.14	1.273E+9	2.014E-3	8.10	0.25
10SHG01Q21	1.14	1.266E+9	2.014E-3	7.88	0.40
10SHG01Q22	1.13	1.273E+9	2.014E-3	7.76	0.26
10SHG01Q23	1.14	1.271E+9	2.014E-3	8.06	0.47
10SHG01Q24	1.13	1.267E+9	2.015E-3	8.33	0.27
10SHG01Q25	1.13	1.270E+9	2.014E-3	7.84	0.19
Laoshan					
10LS01Q1	1.11	1.258E+9	2.015E-3	8.38	0.36
10LS01Q2	1.12	1.266E+9	2.014E-3	7.98	0.36
10LS01Q3	1.12	1.262E+9	2.015E-3	8.39	0.31
10LS01Q4	1.12	1.265E+9	2.015E-3	8.44	0.23
10LS01Q5	1.12	1.261E+9	2.015E-3	8.46	0.30
10LS01Q6	1.12	1.261E+9	2.016E-3	8.58	0.22
10LS01Q7	1.11	1.259E+9	2.014E-3	7.86	0.25
10LS01Q8	1.12	1.268E+9	2.014E-3	7.69	0.32
10LS01Q9	1.11	1.266E+9	2.013E-3	7.09	0.30
10LS01Q10	1.12	1.270E+9	2.015E-3	8.41	0.35
10LS01Q12	1.12	1.263E+9	2.015E-3	8.17	0.32
10LS01Q13	1.11	1.257E+9	2.015E-3	8.09	0.18
10LS01Q14	1.10	1.253E+9	2.015E-3	8.04	0.29
10LS01Q15	1.11	1.253E+9	2.015E-3	8.17	0.30
10LS01Q16	1.10	1.260E+9	2.014E-3	7.88	0.37
10LS01Q17	1.10	1.250E+9	2.014E-3	7.86	0.27
10LS01Q18	1.10	1.254E+9	2.015E-3	8.05	0.34
10LS01Q19	1.09	1.258E+9	2.015E-3	8.36	0.25
10LS01Q20	1.09	1.259E+9	2.014E-3	7.82	0.19
10LS01Q21	1.09	1.260E+9	2.014E-3	7.73	0.25
10LS01Q22	1.10	1.269E+9	2.015E-3	8.16	0.31
10LS01Q23	1.10	1.263E+9	2.014E-3	7.95	0.23
10LS01Q24	1.11	1.265E+9	2.016E-3	8.70	0.26
10LS01Q25	1.11	1.261E+9	2.014E-3	7.94	0.29
10LS01Q26	1.10	1.258E+9	2.014E-3	7.86	0.28
10LS01Q27	1.11	1.251E+9	2.015E-3	8.19	0.28
10LS05Q1	1.10	1.254E+9	2.014E-3	7.86	0.34
10LS05Q2	1.11	1.252E+9	2.015E-3	8.34	0.39
10LS05Q3	1.12	1.259E+9	2.015E-3	8.28	0.36
10LS05Q4	1.11	1.267E+9	2.015E-3	8.20	0.31

10LS05Q5	1.11	1.268E+9	2.014E-3	7.83	0.43
10LS05Q6	1.11	1.261E+9	2.015E-3	8.01	0.18
10LS05Q7	1.11	1.264E+9	2.015E-3	8.29	0.39
10LS05Q8	1.11	1.252E+9	2.014E-3	7.78	0.24
10LS05Q9	1.11	1.262E+9	2.015E-3	8.04	0.24
10LS05Q10	1.10	1.257E+9	2.015E-3	8.03	0.41
10LS05Q11	1.10	1.254E+9	2.015E-3	8.37	0.29
10LS05Q12	1.10	1.252E+9	2.015E-3	8.15	0.27
10LS05Q13	1.10	1.254E+9	2.015E-3	7.95	0.29
10LS05Q14	1.09	1.249E+9	2.015E-3	7.93	0.41
10LS05Q15	1.08	1.252E+9	2.015E-3	8.12	0.26
10LS05Q16	1.09	1.248E+9	2.015E-3	8.07	0.34
10LS05Q17	1.09	1.249E+9	2.015E-3	8.05	0.29
10LS05Q18	1.09	1.257E+9	2.015E-3	7.96	0.25
10LS05Q19	1.10	1.257E+9	2.015E-3	7.94	0.19
10LS05Q20	1.10	1.250E+9	2.015E-3	8.27	0.35
10LS05Q21	1.09	1.255E+9	2.014E-3	7.60	0.35
10LS05Q22	1.10	1.267E+9	2.014E-3	7.46	0.40
Putuoshan				**7.04**	**1.91**
09YY136Q1	1.54	1.539E+9	2.008E-3	7.88	0.11
09YY136Q2	1.51	1.519E+9	2.010E-3	8.65	0.26
09YY136Q3	1.54	1.524E+9	2.009E-3	8.14	0.25
09YY136Q4	1.52	1.525E+9	2.009E-3	8.23	0.23
09YY136Q5	1.54	1.522E+9	2.009E-3	8.06	0.25
09YY136Q6	1.50	1.516E+9	2.009E-3	8.16	0.20
09YY136Q7	1.51	1.518E+9	2.008E-3	7.85	0.22
09YY136Q8	1.52	1.512E+9	2.009E-3	8.19	0.23
09YY136Q9	1.51	1.506E+9	2.009E-3	8.09	0.19
09YY136Q10	1.52	1.513E+9	2.009E-3	7.95	0.29
09YY136Q11	1.49	1.511E+9	2.008E-3	7.88	0.23
09YY136Q12	1.49	1.510E+9	2.009E-3	8.12	0.32
09YY136Q13	1.51	1.516E+9	2.008E-3	7.81	0.20
09YY136Q14	1.48	1.514E+9	2.009E-3	7.98	0.28
09YY136Q15	1.53	1.517E+9	2.009E-3	7.98	0.24
09YY136Q16	1.53	1.519E+9	2.008E-3	7.87	0.22
09YY136Q17	1.50	1.517E+9	2.009E-3	8.09	0.25
09YY136Q18	1.51	1.513E+9	2.009E-3	8.00	0.31
09YY142Q1	1.48	1.488E+9	2.009E-3	8.22	0.21
09YY142Q2	1.47	1.488E+9	2.009E-3	8.10	0.24
09YY142Q3	1.48	1.487E+9	2.009E-3	8.29	0.33
09YY142Q4	1.49	1.487E+9	2.009E-3	8.16	0.21
09YY142Q5	1.49	1.484E+9	2.009E-3	8.17	0.36

09YY142Q6	1.47	1.485E+9	2.009E-3	8.19	0.20
09YY142Q7	1.48	1.477E+9	2.009E-3	8.19	0.28
09YY142Q8	1.47	1.490E+9	2.010E-3	8.57	0.19
09YY142Q9	1.48	1.475E+9	2.009E-3	8.26	0.18
09YY142Q10	1.47	1.487E+9	2.009E-3	8.31	0.16
09YY142Q11	1.45	1.477E+9	2.009E-3	8.14	0.24
09YY142Q12	1.46	1.473E+9	2.009E-3	8.18	0.30
09YY142Q13	1.47	1.491E+9	2.009E-3	8.10	0.24
09YY142Q14	1.46	1.469E+9	2.008E-3	7.83	0.30
09YY142Q15	1.47	1.474E+9	2.008E-3	7.69	0.18
09YY142Q16	1.47	1.476E+9	2.008E-3	7.88	0.24
09YY142Q17	1.46	1.468E+9	2.009E-3	8.08	0.21
09YY142Q18	1.49	1.472E+9	2.008E-3	7.97	0.19
09YY170Q1	1.46	1.466E+9	2.009E-3	8.46	0.22
09YY170Q3	1.46	1.474E+9	2.009E-3	8.33	0.30
09YY170Q4	1.47	1.479E+9	2.008E-3	7.97	0.23
09YY170Q6	1.47	1.465E+9	2.009E-3	8.24	0.22
09YY170Q7	1.45	1.458E+9	2.008E-3	7.94	0.24
09YY170Q8	1.46	1.454E+9	2.008E-3	7.81	0.28
09YY170Q9	1.46	1.453E+9	2.008E-3	8.03	0.25
09YY170Q10	1.45	1.439E+9	2.008E-3	7.83	0.22
09YY170Q11	1.44	1.449E+9	2.008E-3	7.95	0.21
09YY170Q12	1.42	1.434E+9	2.008E-3	7.87	0.24
09YY170Q13	1.45	1.450E+9	2.008E-3	7.96	0.18
09YY170Q14	1.42	1.436E+9	2.009E-3	8.20	0.29
09YY170Q15	1.42	1.438E+9	2.009E-3	8.18	0.19
09YY170Q16	1.42	1.438E+9	2.009E-3	8.12	0.17
09YY170Q17	1.42	1.424E+9	2.009E-3	8.17	0.29
09YY170Q18	1.41	1.417E+9	2.009E-3	8.11	0.29
09YY163Q1	1.39	1.370E+9	1.999E-3	3.44	0.36
09YY163Q2	1.41	1.373E+9	2.001E-3	4.23	0.19
09YY163Q3	1.38	1.301E+9	2.008E-3	7.95	0.26
09YY163Q4	1.39	1.370E+9	2.001E-3	4.27	0.27
09YY163Q5	1.41	1.372E+9	1.999E-3	3.26	0.35
09YY163Q6	1.39	1.364E+9	2.002E-3	4.71	0.24
09YY163Q7	1.38	1.374E+9	2.000E-3	3.74	0.32
09YY163Q8	1.40	1.392E+9	1.997E-3	2.15	0.21
09YY163Q9	1.41	1.389E+9	2.000E-3	3.72	0.26
09YY163Q10	1.39	1.367E+9	1.999E-3	3.42	0.26
09YY163Q11	1.39	1.360E+9	1.999E-3	3.39	0.34
09YY163Q12	1.39	1.356E+9	1.999E-3	3.35	0.22
09YY163Q13	1.38	1.372E+9	2.000E-3	3.82	0.33

09YY163Q14	1.40	1.354E+9	2.003E-3	5.42	0.34
09YY163Q15	1.38	1.340E+9	2.006E-3	6.53	0.30
09YY163Q16	1.38	1.353E+9	1.999E-3	3.41	0.31
09YY163Q17	1.40	1.367E+9	1.998E-3	2.79	0.19
09YY163Q18	1.40	1.368E+9	1.998E-3	2.84	0.23
09YY163Q19	1.39	1.349E+9	2.006E-3	6.83	0.22
Taohuadao					
09YY155Q1	1.51	1.514E+9	2.008E-3	7.63	0.26
09YY155Q2	1.51	1.503E+9	2.007E-3	7.04	0.28
09YY155Q3	1.49	1.495E+9	2.007E-3	7.01	0.28
09YY155Q4	1.49	1.511E+9	2.011E-3	-	-
09YY155Q5	1.49	1.504E+9	2.009E-3	8.21	0.19
09YY155Q6	1.49	1.532E+9	2.010E-3	8.68	0.23
09YY155Q7	1.49	1.510E+9	2.008E-3	7.87	0.24
09YY155Q8	1.47	1.504E+9	2.009E-3	8.16	0.35
09YY155Q9	1.50	1.475E+9	2.002E-3	-	-
09YY155Q10	1.48	1.504E+9	2.009E-3	8.05	0.26
09YY155Q11	1.49	1.506E+9	2.008E-3	7.61	0.29
09YY155Q12	1.51	1.503E+9	2.008E-3	7.78	0.17
09YY155Q13	1.50	1.505E+9	2.004E-3	-	-
09YY155Q14	1.50	1.493E+9	2.006E-3	6.69	0.31
09YY155Q15	1.47	1.486E+9	2.004E-3	-	-
09YY155Q16	1.50	1.516E+9	2.002E-3	-	-
09YY155Q17	1.49	1.481E+9	2.007E-3	7.09	0.20
09YY155Q18	1.48	1.487E+9	2.009E-3	8.10	0.20
09YY155Q19	1.50	1.489E+9	2.007E-3	7.16	0.23
09YY155Q20	1.48	1.475E+9	2.011E-3		
09YY126Q1	1.42	1.412E+9	2.007E-3	7.31	0.29
09YY126Q2	1.41	1.423E+9	2.008E-3	7.72	0.25
09YY126Q3	1.42	1.432E+9	2.007E-3	7.27	0.31
09YY126Q4	1.44	1.427E+9	2.007E-3	7.44	0.31
09YY126Q5	1.42	1.431E+9	2.007E-3	7.04	0.25
09YY126Q6	1.42	1.445E+9	2.006E-3	7.00	0.29
09YY126Q7	1.41	1.427E+9	2.007E-3	7.22	0.22
09YY126Q8	1.43	1.435E+9	2.007E-3	7.26	0.31
09YY126Q10	1.43	1.434E+9	2.007E-3	7.52	0.30
09YY126Q11	1.42	1.428E+9	2.007E-3	7.14	0.30
09YY126Q12	1.43	1.428E+9	2.007E-3	7.36	0.25
09YY126Q13	1.42	1.440E+9	2.007E-3	7.23	0.27
09YY126Q14	1.40	1.421E+9	2.007E-3	7.05	0.31
09YY126Q15	1.40	1.438E+9	2.007E-3	7.45	0.28
09YY126Q16	1.41	1.419E+9	2.007E-3	7.15	0.35

09YY126Q17	1.40	1.405E+9	2.007E-3	7.37	0.26
09YY126Q18	1.43	1.404E+9	2.007E-3	7.14	0.23
09YY130Q1	1.39	1.389E+9	2.007E-3	7.44	0.22
09YY130Q2	1.40	1.415E+9	2.007E-3	7.31	0.21
09YY130Q3	1.42	1.398E+9	2.007E-3	7.35	0.34
09YY130Q4	1.40	1.397E+9	2.006E-3	6.95	0.28
09YY130Q5	1.42	1.413E+9	2.006E-3	6.94	0.22
09YY130Q6	1.42	1.396E+9	2.007E-3	7.23	0.33
09YY130Q8	1.41	1.387E+9	2.007E-3	7.24	0.24
09YY130Q9	1.38	1.394E+9	2.007E-3	7.06	0.27
09YY130Q10	1.40	1.386E+9	2.006E-3	6.90	0.33
09YY130Q11	1.42	1.402E+9	2.007E-3	7.09	0.26
09YY130Q12	1.42	1.386E+9	2.007E-3	7.12	0.29
09YY130Q13	1.41	1.376E+9	2.007E-3	7.06	0.30
09YY130Q14	1.41	1.371E+9	2.007E-3	7.11	0.21
09YY130Q16	1.40	1.369E+9	2.007E-3	7.08	0.45
09YY130Q17	1.39	1.359E+9	2.007E-3	7.21	0.26
09YY130Q18	1.38	1.354E+9	2.007E-3	7.07	0.33
09YY130Q19	1.41	1.345E+9	2.007E-3	7.24	0.28
09YY129Q1	1.50	1.404E+9	2.008E-3	7.85	0.32
09YY129Q2	1.50	1.405E+9	2.007E-3	7.45	0.31
09YY129Q3	1.51	1.427E+9	2.007E-3	7.55	0.22
09YY129Q4	1.51	1.406E+9	2.007E-3	7.33	0.31
09YY129Q6	1.50	1.409E+9	2.007E-3	7.47	0.25
09YY129Q7	1.45	1.408E+9	2.007E-3	7.35	0.20
09YY129Q8	1.49	1.414E+9	2.007E-3	7.53	0.25
09YY129Q9	1.50	1.403E+9	2.007E-3	7.40	0.32
09YY129Q10	1.49	1.408E+9	2.007E-3	7.25	0.23
09YY129Q11	1.49	1.407E+9	2.007E-3	7.54	0.31
09YY129Q13	1.50	1.399E+9	2.007E-3	7.34	0.22
09YY129Q14	1.49	1.391E+9	2.007E-3	7.54	0.28
09YY129Q15	1.48	1.405E+9	2.006E-3	7.10	0.22
09YY129Q16	1.48	1.411E+9	2.007E-3	7.16	0.31
09YY129Q17	1.47	1.408E+9	2.006E-3	7.00	0.22
09YY129Q18	1.49	1.405E+9	2.007E-3	7.36	0.15
09YY129Q19	1.49	1.403E+9	2.007E-3	7.60	0.18
09YY129Q20	1.47	1.414E+9	2.007E-3	7.36	0.32
09YY148Q1	1.48	1.355E+9	2.006E-3	6.64	0.28
09YY148Q2	1.49	1.384E+9	2.009E-3	-	-
09YY148Q3	1.49	1.388E+9	2.007E-3	7.38	0.27
09YY148Q4	1.49	1.332E+9	1.998E-3	-	-

09YY148Q5	1.48	1.392E+9	2.007E-3	7.12	0.32
09YY148Q6	1.48	1.393E+9	2.007E-3	7.53	0.26
09YY148Q7	1.48	1.333E+9	2.006E-3	6.70	0.22
09YY148Q8	1.48	1.400E+9	2.007E-3	7.39	0.34
09YY148Q9	1.50	1.363E+9	2.005E-3	6.44	0.29
09YY148Q10	1.48	1.391E+9	2.007E-3	7.39	0.26
09YY148Q11	1.47	1.313E+9	2.001E-3	-	-
09YY148Q12	1.47	1.389E+9	2.007E-3	7.24	0.25
09YY148Q13	1.48	1.386E+9	2.007E-3	7.48	0.35
09YY148Q14	1.47	1.387E+9	2.007E-3	7.18	0.29
09YY148Q15	1.47	1.388E+9	2.007E-3	7.47	0.28
09YY148Q16	1.48	1.350E+9	2.001E-3	-	-
09YY148Q17	1.47	1.399E+9	2.007E-3	7.43	0.27
09YY148Q18	1.46	1.344E+9	1.999E-3	-	-
09YY148Q19	1.48	1.382E+9	2.007E-3	7.34	0.21
09YY148Q20	1.47	1.390E+9	2.007E-3	7.48	0.35
09YY148Q21	1.52	1.292E+9	2.000E-3	-	-
09YY148Q22	1.53	1.393E+9	2.006E-3	6.87	0.34
09YY148Q23	1.53	1.440E+9	2.007E-3	7.11	0.21
09YY148Q24	1.54	1.430E+9	2.008E-3	7.45	0.16
09YY148Q25	1.54	1.379E+9	2.005E-3	6.28	0.25
09YY148Q26	1.54	1.389E+9	2.003E-3	-	-

APPENDIX TABLE vii. In situ zircon Li isotope compositions

Name	Time	IP	$^{7}Li/^{6}Li_{mean}$	1σ	^{7}Li	1σ	$\delta^{7}Li_{corr}$ (‰)	1σ	Li ppm	1σ	note
Nianzishan											
10NZS-01	2013-9-23 10:36	27.6	12.417	0.166	8012.0	1.8	0.9	1.7	0.05	0.001	
10NZS-02	2013-9-23 10:56	27.5	12.321	0.963	14423.0	4.5	-	-	0.09	0.004	high 7Li error
10NZS-03	2013-9-24 1:42	26.5	12.384	0.143	10450.3	1.0	1.5	1.4	0.06	0.001	
10NZS-04	2013-9-24 2:02	26.5	12.382	0.150	10954.5	0.7	1.4	1.5	0.06	0.000	
10NZS-05	2013-9-24 2:21	26.4	12.452	0.024	390477.8	0.6	7.2	0.2	2.08	0.012	
10NZS-06	2013-9-24 2:41	26.4	12.470	0.514	1089.6	1.4	-	-	0.01	0.000	low 7Li
10NZS-08	2013-9-24 3:01	26.4	12.465	0.260	3443.2	1.7	8.3	2.6	0.02	0.000	
10NZS-10	2013-9-24 3:20	26.4	12.433	0.929	24805.4	2.0	-	-	0.13	0.003	high 7Li error
10NZS-11	2013-9-24 3:40	26.4	12.369	0.108	19188.7	1.0	0.3	1.1	0.10	0.001	
10NZS-12	2013-9-24 3:59	26.4	12.335	0.949	30828.0	2.3	-	-	0.16	0.004	high 7Li error
10NZS-13	2013-9-24 4:19	26.4	12.508	0.248	6472.5	1.6	11.8	2.5	0.03	0.001	
10NZS-14	2013-9-24 4:39	26.3	12.367	0.121	16268.0	0.6	0.2	1.2	0.09	0.001	
10NZS-15	2013-9-24 4:58	26.4	12.340	0.168	8826.1	0.7	-2.1	1.7	0.05	0.000	
10NZS-17	2013-9-24 5:38	26.3	12.426	0.216	5232.5	1.6	5.1	2.2	0.03	0.000	
10NZS-19	2013-9-24 5:18	26.3	12.410	0.255	18570.9	0.6	3.7	2.6	0.10	0.001	
10NZS-23	2013-9-24 5:57	26.3	12.386	0.135	13758.7	0.6	1.7	1.4	0.07	0.000	
11NZS02-01	2013-9-22 0:03	24.6	12.524	0.236	103679.1	1.1	6.7	2.4	0.86	0.035	
11NZS02-02	2013-9-22 0:23	24.6	12.336	0.279	12199.7	2.1	-8.9	2.8	0.10	0.002	
11NZS02-03	2013-9-22 0:43	24.6	12.220	0.726	14112.9	2.5	-	-	0.12	0.003	high 7Li error
11NZS02-04	2013-9-22 1:02	24.6	12.208	1.164	27752.8	4.2	-	-	0.23	0.010	high 7Li error
11NZS02-05	2013-9-22 1:41	24.6	12.376	1.218	33282.0	4.9	-	-	0.28	0.014	high 7Li error
11NZS02-06	2013-9-22 2:01	24.5	12.381	0.129	12792.0	1.3	-5.2	1.3	0.11	0.001	
11NZS02-07	2013-9-22 2:20	24.5	12.385	0.171	9691.8	0.1	-4.9	1.7	0.08	0.000	
11NZS02-08	2013-9-22 2:40	24.5	12.372	0.155	12637.6	1.0	-6.0	1.5	0.11	0.001	
11NZS02-09	2013-9-22 3:00	24.5	12.119	0.842	25025.5	3.6	-	-	0.21	0.008	high 7Li error
11NZS02-10	2013-9-22 3:39	24.5	12.366	0.123	12883.0	1.6	-6.4	1.2	0.11	0.002	
11NZS02-11	2013-9-22 3:58	24.5	12.352	0.154	13969.2	1.6	-7.6	1.5	0.12	0.002	
11NZS02-12	2013-9-22 4:18	24.4	12.183	0.778	17824.9	3.4	-	-	0.15	0.005	high 7Li error
11NZS02-13	2013-9-22 4:38	24.4	12.401	0.111	12859.9	1.2	-3.5	1.1	0.11	0.001	
11NZS02-14	2013-9-22 4:57	24.4	12.301	0.946	151689.6	3.4	-	-	1.27	0.043	high 7Li error
11NZS02-15	2013-9-22 5:37	24.3	12.406	0.096	26357.6	1.4	-3.1	1.0	0.22	0.003	
11NZS02-16	2013-9-22 5:56	24.4	12.315	0.143	14671.2	1.0	-10.7	1.4	0.12	0.001	
11NZS02-17	2013-9-22 6:19	24.3	14.221	1.478	2233663.0	12.6	-	-	-	-	[Li] too high
11NZS02-18	2013-9-22 6:39	24.3	12.399	0.978	9353.9	2.8	-	-	0.08	0.002	high 7Li error
11NZS02-19	2013-9-22 6:58	24.4	12.555	0.329	1839.9	0.5	9.3	3.3	0.02	0.000	
Gw04190-1	2013-9-23 9:57	27.6	12.355	0.064	74228.4	1.0	-4.1	0.6	0.45	0.005	
Gw04190-12	2013-9-23 19:21	27.0	12.290	0.770	118989.8	16.4	-	-	0.62	0.101	high 7Li error
Gw04190-13	2013-9-23 20:08	27.0	12.324	0.085	39368.4	0.7	-3.4	0.8	0.21	0.001	
Gw04190-15	2013-9-23 20:28	27.0	12.311	0.080	46076.9	0.7	-4.5	0.8	0.24	0.002	
Gw04190-16	2013-9-23 20:48	27.0	12.337	0.080	39184.6	1.5	-2.3	0.8	0.20	0.003	
Gw04190-18	2013-9-23 21:07	27.0	12.283	0.084	39891.2	0.8	-6.9	0.8	0.21	0.002	
Gw04190-19	2013-9-23 21:27	27.0	12.360	0.095	36287.6	2.0	-0.4	1.0	0.19	0.004	
Gw04190-2	2013-9-23 10:17	27.6	12.359	0.108	19535.5	0.1	-3.9	1.1	0.12	0.000	
Gw04190-3	2013-9-23 17:03	27.1	12.382	0.102	37818.4	1.2	-1.9	1.0	0.23	0.003	
Gw04190-4	2013-9-23 17:23	27.1	12.279	0.073	33126.6	0.1	-10.5	0.7	0.20	0.000	
Gw04190-6	2013-9-23 17:43	27.1	12.318	0.073	48979.0	0.9	-7.3	0.7	0.30	0.003	
Gw04190-7	2013-9-23 18:02	27.1	12.364	0.086	41639.1	0.9	-3.5	0.9	0.25	0.002	
Gw04190-8	2013-9-23 18:42	27.1	12.447	0.126	18050.7	0.8	6.8	1.3	0.09	0.001	
Gw04190-9	2013-9-23 19:01	27.1	12.310	0.079	37832.6	0.3	-4.6	0.8	0.20	0.001	
Houshihu											
10SHG-10-1	2013-9-23 15:06	27.3	12.334	0.134	20922.7	2.6	-6.0	1.3	0.13	0.003	
10SHG-10-10	2013-9-23 23:25	26.8	12.393	0.057	175045.5	2.5	2.3	0.6	0.92	0.023	
10SHG-10-11	2013-9-23 23:44	26.8	12.272	0.107	19648.0	0.4	-7.7	1.1	0.10	0.000	
10SHG-10-12	2013-9-24 0:04	26.8	12.218	0.098	31976.9	0.6	-12.2	1.0	0.17	0.001	
10SHG-10-14	2013-9-24 0:23	26.8	12.290	0.626	18573.7	3.6	-	-	0.10	0.004	high 7Li error
10SHG-10-15	2013-9-24 0:43	26.8	12.336	0.086	49513.3	1.2	-2.4	0.9	0.26	0.003	
10SHG-10-16	2013-9-24 1:03	26.5	12.211	0.091	34858.3	0.3	-12.8	0.9	0.19	0.001	
10SHG-10-17	2013-9-24 1:22	26.5	12.281	0.063	38535.2	0.7	-7.0	0.6	0.20	0.001	
10SHG-10-2	2013-9-23 15:25	27.2	12.257	0.081	40844.4	0.2	-12.3	0.8	0.25	0.000	
10SHG-10-3	2013-9-23 15:45	27.2	12.232	0.112	65558.7	0.3	-14.4	1.1	0.40	0.001	
10SHG-10-4	2013-9-23 16:04	27.2	12.371	0.084	43257.0	0.7	-2.8	0.8	0.26	0.002	
10SHG-10-5	2013-9-23 16:24	27.2	12.239	0.063	55084.6	0.6	-13.8	0.6	0.34	0.002	
10SHG-10-6	2013-9-23 22:06	26.9	12.293	0.090	44714.2	0.1	-6.0	0.9	0.23	0.000	

10SHG-10-7	2013-9-23 22:26	26.8	12.310	0.116	25719.5	1.0	-4.6	1.2	0.13	0.001	
10SHG-10-8	2013-9-23 22:45	26.8	12.180	0.101	24307.5	0.3	-15.4	1.0	0.13	0.000	
10SHG-10-9	2013-9-23 23:05	26.9	12.246	0.107	24588.6	1.2	-9.9	1.1	0.13	0.002	
Laoshan											
09LS05-1	2013-9-23 11:36	27.6	12.314	1.530	526856.5	12.1	-	-	3.16	0.384	high 7Li error
09LS05-13	2013-9-24 9:14	26.0	12.448	0.087	49187.1	0.4	6.9	0.9	0.27	0.001	
09LS05-2	2013-9-23 11:56	27.5	12.496	0.084	72836.7	3.2	7.5	0.8	0.44	0.014	
09LS05-5	2013-9-24 8:15	26.1	12.430	0.080	47886.7	0.7	5.4	0.8	0.26	0.002	
09LS05-6	2013-9-24 8:34	26.0	12.465	0.046	175415.8	1.2	8.3	0.5	0.95	0.011	
09LS05-9	2013-9-24 8:54	26.0	12.475	0.135	15892.4	1.7	9.1	1.4	0.09	0.001	
10LS01-2	2013-9-23 13:14	27.4	12.417	0.105	35998.5	1.1	1.0	1.1	0.22	0.002	
10LS01-7	2013-9-23 13:34	27.4	12.347	0.180	23459.4	0.9	-4.9	1.8	0.14	0.001	
10LS05-1	2013-9-23 12:15	27.5	12.340	0.062	90870.3	1.4	-5.4	0.6	0.55	0.008	
10LS05-11	2013-9-24 6:56	26.2	12.386	0.059	86484.4	1.0	1.7	0.6	0.46	0.005	
10LS05-14	2013-9-24 7:16	26.2	12.375	0.050	143978.6	0.5	0.8	0.5	0.77	0.004	
10LS05-19	2013-9-24 7:55	26.1	12.418	0.092	30095.6	0.8	4.4	0.9	0.16	0.001	
10LS05-2	2013-9-23 12:35	27.4	12.378	0.051	109535.5	0.3	-2.3	0.5	0.66	0.002	
10LS05-21	2013-9-24 7:35	26.1	12.406	0.098	150004.2	1.1	3.4	1.0	0.81	0.009	
10LS05-5	2013-9-24 6:17	26.3	12.363	0.044	195926.1	0.4	-0.2	0.4	1.05	0.004	
10LS05-9	2013-9-24 6:37	26.3	12.368	0.056	87080.1	0.4	0.2	0.6	0.47	0.002	
Taohuadao											
09YY129-01	2010-10-9 23:33	24.9	12.375	0.144	14515.2	2.2	-7.9	1.4	0.09	0.002	
09YY129-02	2010-10-9 23:51	24.9	12.313	0.369	2197.6	0.5	-13.1	3.7	0.01	0.000	
09YY129-04	2010-10-10 0:09	24.9	12.278	0.802	7730.5	5.9	-	-	0.05	0.003	high 7Li error
09YY129-06	2010-10-10 0:38	24.9	12.088	1.056	10435.5	2.7	-	-	0.06	0.002	high 7Li error
09YY129-10	2010-10-10 6:23	25.0	12.353	0.282	3773.8	1.1	-9.7	2.8	0.02	0.000	
09YY129-11	2010-10-10 6:41	25.0	12.293	1.342	74099.7	24.9	-	-	0.45	0.111	high 7Li error
09YY129-13	2010-10-10 6:59	24.9	12.387	0.171	14095.0	0.8	-7.0	1.7	0.09	0.001	
09YY129-14	2010-10-10 7:17	24.9	12.466	0.312	78764.1	4.9	-0.3	3.1	0.48	0.023	
09YY129-16	2010-10-10 7:35	24.9	12.418	0.302	3340.2	1.5	-4.4	3.0	0.02	0.000	
09YY129-17	2010-10-10 7:53	24.9	12.360	0.327	2767.0	2.4	-9.2	3.3	0.02	0.000	high 7Li error
09YY129-19	2010-10-10 8:11	24.8	12.436	0.325	2839.1	0.6	-2.9	3.3	0.02	0.000	
09YY129-21	2010-10-10 8:28	24.8	12.293	0.252	8892.2	0.9	-14.8	2.5	0.05	0.000	
09YY129-22	2010-10-10 8:46	24.8	12.133	0.206	6985.3	0.9	-	-	0.04	0.000	cracks
09YY129-23	2010-10-10 9:04	24.7	12.218	0.344	2496.2	0.9	-	-	0.02	0.000	low 7Li
09YY129-24	2010-10-10 9:22	24.7	12.346	0.441	2019.5	1.4	-	-	0.01	0.000	low 7Li
09YY148-04	2010-10-10 9:40	24.6	12.173	0.718	91102.6	26.6	-	-	0.56	0.148	high 7Li error
09YY148-03	2010-10-10 9:58	24.7	12.122	0.720	52113.3	8.1	-	-	0.32	0.026	high 7Li error
09YY148-14	2010-10-10 10:16	24.6	12.339	0.106	44645.4	0.7	-10.9	1.1	0.27	0.002	
09YY148-01	2010-10-10 10:35	24.6	12.513	2.435	729776.3	42.9	-	-	4.47	1.918	high 7Li error
09YY130-01	2014-12-13 23:23	8.8	12.361	1.006	36677.7	16.2	-	-	0.56	0.091	high 7Li error
09YY130-02	2014-12-13 23:37	8.7	12.470	0.254	7625.0	1.4	1.2	2.5	0.12	0.002	
09YY130-03	2014-12-13 23:51	8.7	12.154	1.099	58371.7	13.0	-	-	0.90	0.117	high 7Li error
09YY130-04	2014-12-14 0:05	8.6	12.104	1.379	227408.0	17.8	-	-	3.52	0.626	high 7Li error
09YY130-05	2014-12-14 0:19	8.4	12.406	0.215	11940.8	1.5	-4.1	2.2	0.19	0.003	
09YY130-06	2014-12-14 0:33	8.2	12.504	1.657	23761.2	7.3	-	-	0.39	0.028	high 7Li error
09YY130-07	2014-12-14 0:47	8.2	12.462	0.399	5973.7	1.7	0.6	4.0	0.10	0.002	
09YY130-08	2014-12-14 1:01	7.8	11.684	3.011	134027.8	20.3	-	-	2.29	0.464	high 7Li error
09YY130-09	2014-12-14 1:14	7.5	12.596	0.189	32492.9	1.9	11.7	1.9	0.58	0.011	
09YY130-10	2014-12-14 1:28	7.4	12.391	0.287	5912.5	1.4	-5.3	2.9	0.11	0.001	
09YY130-11	2014-12-14 1:42	7.5	12.381	0.934	37622.1	7.1	-	-	0.67	0.048	high 7Li error
09YY130-12	2014-12-14 1:56	7.2	12.551	0.146	37122.9	2.0	7.9	1.5	0.69	0.014	
09YY130-13	2014-12-14 2:10	7.6	12.400	0.921	52489.0	6.7	-	-	0.93	0.062	high 7Li error
09YY130-14	2014-12-14 2:24	7.6	12.079	0.599	157024.9	7.7	-	-	2.75	0.213	high 7Li error
09YY130-15	2014-12-14 2:38	7.2	12.327	0.305	70675.4	1.9	-10.7	3.0	1.32	0.025	
09YY130-16	2014-12-14 2:52	7.4	11.881	1.592	33267.1	4.6	-	-	0.60	0.028	high 7Li error
09YY130-17	2014-12-14 3:06	7.2	12.193	1.014	105193.5	4.6	-	-	1.96	0.091	high 7Li error
09YY130-18	2014-12-14 3:20	7.2	12.013	2.247	126770.3	9.7	-	-	2.36	0.229	high 7Li error
09YY130-19	2014-12-14 3:33	7.0	12.656	0.160	30828.2	1.8	16.7	1.6	0.59	0.011	
09YY130-20	2014-12-14 3:47	6.9	11.899	2.945	279421.2	13.2	-	-	5.44	0.718	high 7Li error
09YY130-21	2014-12-14 4:01	6.8	12.387	0.428	8180.3	1.4	-	-	0.16	0.002	cracks
09YY130-22	2014-12-14 4:15	6.7	12.548	0.148	40081.3	1.4	7.7	1.5	0.80	0.011	
09YY130-23	2014-12-14 4:29	6.5	12.512	0.245	8819.3	1.5	4.7	2.4	0.18	0.003	
09YY130-24	2014-12-14 4:43	4.4	12.478	0.273	9351.3	1.6	1.9	2.7	0.28	0.004	
09YY130-25	2014-12-14 4:57	5.0	12.207	1.561	386522.6	12.7	-	-	10.35	1.319	high 7Li error
09YY130-26	2014-12-14 5:11	5.3	12.254	1.176	122571.3	14.3	-	-	3.08	0.442	high 7Li error
09YY130-27	2014-12-14 5:25	5.4	12.593	0.326	8765.6	2.7	11.4	3.3	0.22	0.006	

09YY126-01	2014-12-14 5:39	5.4	11.987	1.414	18575.7	15.0	-	-	0.46	0.069	high 7Li error
09YY126-02	2014-12-14 5:52	5.1	12.398	0.963	1338.9	1.3	-4.7	9.6	0.04	0.000	
09YY126-03	2014-12-14 6:06	5.1	12.327	0.848	697.2	1.3	-10.6	8.5	0.02	0.000	
09YY126-04	2014-12-14 6:20	5.2	12.318	0.450	1548.8	0.8	-11.4	4.5	0.04	0.000	
09YY126-05	2014-12-14 6:34	5.4	12.256	1.451	6273.2	6.5	-	-	0.15	0.010	high 7Li error
09YY126-06	2014-12-14 6:48	5.0	12.794	1.291	384.3	0.8	-	-	0.01	0.000	low 7Li
09YY155-02	2014-12-15 10:03	7.0	12.385	0.283	4310.4	0.9	-5.8	2.8	0.08	0.001	
09YY155-03	2014-12-15 10:16	7.0	12.697	0.570	1114.2	2.5	-	-	0.02	0.001	high 7Li error
09YY155-04	2014-12-15 10:30	7.0	12.488	0.446	2761.5	1.6	2.7	4.5	0.05	0.001	
09YY155-05	2014-12-15 10:44	7.0	12.390	1.199	225.3	1.2	-	-	0.00	0.000	low 7Li
09YY155-06	2014-12-15 10:57	7.1	12.433	0.471	2031.1	2.3	-1.8	4.7	0.04	0.001	
09YY155-07	2014-12-15 11:11	7.0	12.526	0.617	1839.5	2.1	5.9	6.2	0.03	0.001	
09YY155-08	2014-12-15 11:24	7.0	12.243	0.487	2589.2	1.3	-	-	0.05	0.001	?
09YY155-09	2014-12-15 11:38	7.0	12.369	0.663	823.0	1.2	-	-	0.02	0.000	low 7Li
09YY155-10	2014-12-15 11:51	7.0	12.512	0.606	2030.0	1.7	4.7	6.1	0.04	0.001	
09YY155-11	2014-12-15 12:05	7.0	12.462	0.444	2107.5	2.7	0.5	4.4	0.04	0.001	
09YY155-12	2014-12-15 12:18	7.0	12.476	0.454	2312.8	0.6	1.7	4.5	0.04	0.000	
09YY155-13	2014-12-15 12:32	7.0	12.493	0.539	2487.8	2.7	3.1	5.4	0.05	0.001	
09YY155-14	2014-12-15 12:45	7.0	12.494	0.669	1841.8	1.4	3.2	6.7	0.04	0.000	
09YY155-15	2014-12-15 12:59	7.0	12.479	0.429	2216.9	1.5	2.0	4.3	0.04	0.001	
Putuoshan											
09YY142-1	2014-12-15 13:13	7.0	12.505	0.167	19151.8	1.4	4.1	1.7	0.37	0.005	
09YY142-02	2014-12-15 13:26	7.1	12.419	0.493	3649.2	4.6	-3.1	4.9	0.07	0.003	
09YY142-03	2014-12-15 13:40	7.1	12.572	0.272	5786.4	1.4	9.7	2.7	0.11	0.002	
09YY142-04	2014-12-15 13:53	7.0	12.472	0.239	12312.5	0.9	1.4	2.4	0.23	0.002	
09YY142-05	2014-12-15 14:07	7.1	11.907	1.182	10932.9	9.6	-	-	0.21	0.020	high 7Li error
09YY142-06	2014-12-15 14:20	7.1	12.462	0.232	10849.0	2.2	0.6	2.3	0.21	0.004	
09YY142-07	2014-12-15 14:34	7.0	12.003	0.242	8467.8	0.9	-	-	0.16	0.001	near pit
09YY142-08	2014-12-15 14:47	7.0	12.583	0.316	6642.2	1.0	10.6	3.2	0.13	0.001	
09YY142-09	2014-12-15 15:01	7.0	12.499	0.410	4603.1	2.8	3.6	4.1	0.09	0.002	
09YY142-10	2014-12-15 15:15	7.0	12.612	0.283	10874.8	6.0	13.0	2.8	0.21	0.012	
09YY142-11	2014-12-15 15:28	7.1	12.486	0.561	1308.5	1.2	2.5	5.6	0.02	0.000	
09YY170-1	2014-12-15 15:42	7.1	12.295	0.161	28519.4	1.3	-13.3	1.6	0.54	0.007	
09YY170-02	2014-12-15 15:55	6.8	12.482	0.199	13547.0	1.7	2.2	2.0	0.27	0.004	
09YY170-03	2014-12-15 16:09	6.7	12.359	0.195	59633.9	1.4	-8.0	2.0	1.19	0.016	
09YY170-04	2014-12-15 16:22	6.7	12.426	0.132	222045.3	3.0	-2.4	1.3	4.44	0.132	
09YY170-05	2014-12-15 16:36	6.7	12.592	0.229	15307.7	2.5	11.4	2.3	0.31	0.008	
09YY170-06	2014-12-15 16:50	6.7	12.313	0.123	63149.4	1.4	-11.8	1.2	1.26	0.017	
09YY170-07	2014-12-15 17:03	6.7	12.358	1.088	15400.9	6.5	-	-	0.31	0.020	high 7Li error
09YY170-08	2014-12-15 17:17	6.8	12.427	0.546	8539.1	2.8	-2.3	5.5	0.17	0.005	
09YY170-09	2014-12-15 17:30	6.7	12.586	0.565	5085.4	3.1	-	-	0.10	0.003	high 7Li error
09YY170-10	2014-12-15 17:44	6.8	12.357	0.308	5748.7	2.0	-8.2	3.1	0.11	0.002	
09YY170-11	2014-12-15 17:57	6.8	12.454	0.261	17360.2	2.0	-0.1	2.6	0.34	0.007	
09YY170-12	2014-12-15 18:11	6.7	12.388	0.200	14992.7	0.2	-5.6	2.0	0.30	0.001	
Suzhou											
09YY097-1	2010-10-9 21:16	25.2	12.325	0.426	85313.9	3.8	-12.1	4.3	0.51	0.020	high 7Li error
09YY097-4	2010-10-9 21:34	25.2	12.415	0.426	27961.9	2.1	-4.6	4.3	0.17	0.004	
09YY097-5	2010-10-9 21:52	25.2	12.383	0.303	3241.6	0.5	-7.3	3.0	0.02	0.000	
09YY097-6	2010-10-9 22:10	25.1	12.355	0.237	5307.2	0.9	-9.6	2.4	0.03	0.000	
09YY097-2-1	2013-9-26 7:02	26.7	12.337	0.064	89122.7	1.0	-4.4	0.6	0.40	0.004	
09YY097-2-2	2013-9-26 7:21	26.7	12.364	0.081	43247.2	0.6	-2.1	0.8	0.20	0.001	
09YY097-2-3	2013-9-26 8:40	26.8	12.227	0.073	613307.0	2.4	-13.6	0.7	2.77	0.066	
09YY097-2-4	2013-9-26 9:01	26.8	12.227	0.309	1119086.0	1.8	-13.6	3.1	5.06	0.090	
09YY097-2-5	2013-9-26 9:21	26.8	12.380	0.076	65015.1	0.9	-0.8	0.8	0.29	0.003	
09YY097-2-6	2013-9-26 9:40	26.8	12.374	0.133	14893.3	0.2	-1.3	1.3	0.07	0.000	
09YY097-2-7	2013-9-26 7:41	26.7	12.435	0.092	38144.7	3.5	3.7	0.9	0.17	0.006	
09YY097-2-8	2013-9-26 8:20	26.8	12.427	0.077	34212.4	0.5	3.1	0.8	0.15	0.001	
09YY097-2-9	2013-9-26 8:01	26.8	12.317	0.960	324201.5	4.2	-	-	1.47	0.062	high 7Li error
09YY103-03	2010-10-9 22:57	25.0	12.482	0.091	41199.0	2.6	0.9	0.9	0.25	0.007	
09YY103-04	2010-10-10 0:56	24.8	12.507	0.106	26712.0	1.8	3.1	1.1	0.16	0.003	
09YY103-05	2010-10-10 1:14	24.8	12.502	0.113	23582.7	1.2	2.6	1.1	0.14	0.002	
09YY103-06	2010-10-10 1:32	24.8	12.526	0.071	60045.2	2.2	4.6	0.7	0.36	0.008	
09YY103-07	2010-10-10 1:50	24.8	12.511	0.094	34508.7	1.5	3.4	0.9	0.21	0.003	
09YY103-08	2010-10-10 2:08	24.8	12.523	0.261	22445.0	5.5	4.3	2.6	0.14	0.008	
09YY103-09	2010-10-10 2:26	24.8	12.514	0.100	30564.6	3.7	3.6	1.0	0.19	0.007	

09YY103-10	2010-10-10 2:44	24.8	12.510	0.096	33141.4	0.9	3.3	1.0	0.20	0.002	
09YY103-11	2010-10-10 3:02	24.8	12.416	0.047	134244.2	0.9	-4.5	0.5	0.82	0.007	
09YY103-12	2010-10-10 3:19	24.8	12.492	0.071	60538.3	4.9	1.8	0.7	0.37	0.018	
09YY103-13	2010-10-10 3:37	24.8	12.380	0.095	33337.6	1.6	-7.5	0.9	0.20	0.003	
09YY103-14	2010-10-10 3:55	24.8	12.518	0.109	25617.6	2.4	4.0	1.1	0.16	0.004	
09YY103-15	2010-10-10 4:13	24.8	12.482	0.109	24537.8	0.8	1.0	1.1	0.15	0.001	
09YY103-17	2010-10-10 4:31	24.8	12.514	0.088	39265.2	1.8	3.6	0.9	0.24	0.004	
09YY103-18	2010-10-10 4:54	24.8	14.475	0.498	5687038.0	2.9	-	-	-	-	[Li] too high
09YY103-19	2010-10-10 5:12	24.8	12.424	0.089	38177.9	0.5	-3.9	0.9	0.23	0.001	
09YY103-20	2010-10-10 5:30	24.8	12.469	0.082	45433.0	1.6	-0.1	0.8	0.28	0.004	
09YY103-21	2010-10-10 5:48	24.8	12.475	0.110	39258.4	1.1	0.4	1.1	0.24	0.003	
09YY103-23	2010-10-10 6:06	25.0	12.404	0.066	80723.9	1.8	-5.5	0.7	0.49	0.009	
09YY99-1	2013-9-26 4:05	26.5	12.465	0.062	92124.2	0.7	6.2	0.6	0.42	0.003	
09YY99-2	2013-9-26 4:24	26.5	12.386	0.053	269728.3	0.9	-0.4	0.5	1.23	0.011	
09YY99-3	2013-9-26 4:44	26.5	12.333	0.572	200640.8	2.2	-	-	0.91	0.020	near cracks
09YY99-4	2013-9-26 5:04	26.6	12.468	0.060	88045.6	0.6	6.5	0.6	0.40	0.002	
09YY99-5	2013-9-26 5:24	26.6	12.352	0.059	106131.0	0.4	-3.2	0.6	0.48	0.002	
09YY99-6	2013-9-26 5:43	26.7	12.393	0.063	100786.4	0.3	0.3	0.6	0.46	0.001	
09YY99-7	2013-9-26 6:03	26.6	12.425	0.135	19240.5	0.9	2.9	1.3	0.09	0.001	
09YY99-8	2013-9-26 6:23	26.7	12.519	0.098	121037.8	2.0	10.7	1.0	0.55	0.011	
09YY99-9	2013-9-26 6:43	26.7	12.458	0.233	143914.9	4.8	5.7	2.3	0.65	0.031	
09YY99-10	2013-9-26 7:03	25.1	12.437	0.232	5598.4	1.2	-2.8	2.3	0.03	0.000	
09YY085	2010-10-9 23:15	25.0	12.539	0.183	27108.4	1.7	5.7	1.8	0.16	0.003	
09YY085-1	2013-9-25 21:22	25.8	12.315	0.113	38026.3	2.5	-6.3	1.1	0.18	0.005	
09YY085-2	2013-9-25 22:11	25.9	12.446	0.087	52511.7	0.9	4.6	0.9	0.25	0.002	
09YY085-3	2013-9-25 22:31	26.0	12.371	0.074	55561.5	2.2	-1.6	0.7	0.26	0.006	
09YY085-4	2013-9-25 22:51	26.0	12.381	0.304	819037.2	2.2	-0.8	3.0	3.81	0.083	
09YY085-5	2013-9-25 23:11	26.1	12.032	0.694	246376.1	7.7	-	-	1.14	0.088	
09YY085-6	2013-9-25 23:30	26.1	12.381	0.133	19596.5	1.6	-0.7	1.3	0.09	0.001	
09YY085-7	2013-9-25 23:50	26.2	12.371	0.058	75710.2	0.6	-1.6	0.6	0.35	0.002	
09YY085-8	2013-9-26 0:10	26.2	12.330	0.067	63205.1	0.7	-5.0	0.7	0.29	0.002	
09YY085-9	2013-9-26 0:29	26.2	12.394	0.101	35436.0	0.3	0.3	1.0	0.16	0.001	
09YY085-10	2013-9-26 0:49	26.2	12.347	0.104	26662.8	1.0	-3.6	1.0	0.12	0.001	
09YY085-11	2013-9-26 1:08	26.4	12.399	0.094	33220.6	0.3	0.7	0.9	0.15	0.001	
09YY085-12	2013-9-26 1:28	26.3	12.413	0.133	18282.5	0.8	1.9	1.3	0.08	0.001	high 7Li error
09YY085-13	2013-9-26 1:47	26.4	12.420	0.226	5311.1	0.9	2.5	2.3	0.02	0.000	
09YY085-14	2013-9-26 2:07	26.4	12.385	0.200	6900.5	1.0	-0.5	2.0	0.03	0.000	
09YY085-15	2013-9-26 2:27	26.4	12.459	0.168	8100.9	1.5	5.7	1.7	0.04	0.001	
09YY085-16	2013-9-26 2:47	26.5	12.401	0.137	15129.9	1.0	0.9	1.4	0.07	0.001	
09YY085-17	2013-9-26 3:06	26.5	12.371	0.125	19771.1	0.4	-1.6	1.3	0.09	0.000	
09YY085-18	2013-9-26 3:26	26.4	12.474	0.343	2598.8	0.6	6.9	3.4	0.01	0.000	
09YY085-19	2013-9-26 3:46	26.5	12.382	0.216	14387.5	1.5	-0.7	2.2	0.07	0.001	

APPENDIX TABLE viii. Whole-rock Li isotope compositions

	Li (ppm)	δ^7Li (‰)	±σ
Nianzishan			
Li 11NZS01	46.3	3.1	0.3
Li 11NZS02	36.7	2.6	0.6
Li 11NZS03	50.6	2.5	0.4
Li 11NZS04	42.7	1.6	0.4
Li 11NZS05	38.7	2.3	0.5
Houshihushan			
10SHG01	25.0	1.2	0.6
10YSH01	31.0	2.3	0.5
10YSH04	9.9	3.9	0.3
Laoshan			
09LS05	13.1	3.2	0.4
10LS02	25.0	2.2	0.6
10LS01	26.6	3.9	0.2
10LS05	57.9	3.3	0.3
Suzhou			
09YY085	21.4	2.7	0.2
09YY097	69.2	1.4	0.1
09YY103	83.3	3.2	0.4
09YY105-a	17.7	8.2	0.3
09YY105-b	13.5	10.7	1.2
09YY105-c	15.1	10.1	0.3
09YY086	110.8	2.0	0.4
09YY092	17.6	3.2	0.5
09YY100	78.0	2.8	0.5
Taohuadao			
09YY129-a	18.6	1.6	0.5
09YY129-b	32.4	1.4	0.3
09YY148-a	483.9	6.6	1.5
09YY148-b	483.9	6.1	0.2
Putuoshan			
09YY136-a	13.2	1.3	0.2
09YY136-b	11.5	1.8	0.2
09YY163-a	10.7	3.3	0.3
09YY163-b	10.2	3.4	0.5
RGM			
RGM-1-1	60.6	2.3	0.5
RGM-1-2	59.4	1.5	0.8
RGM1-Li-024	58.7	1.7	0.4

RGM1-Li-056	58.7	1.8	0.2
RGM1-Li-060	58.7	2.3	0.3
RGM1-Li-076	58.7	2.3	0.1
RGM1-Li-088	58.7	3.5	0.3
RGM1-Li-108	58.7	2.4	0.3
RGM1-Li-112	58.7	2.8	0.4
RGM1-Li-136	58.7	2.6	0.1
RGM1-Li-140	58.7	2.0	0.2
RGM1-Li-152	58.7	2.7	0.1
RGM1-Li-172	58.7	1.4	0.3
RGM1-Li-184	58.7	2.5	0.1
GPS			
GSP-2-1	32.5	-1.5	0.2
GSP-2-2	30.5	-1.1	0.4
GSP-2-3	33.2	-0.6	0.5
GSP2-Li-016	30.3	0.0	0.1
GSP2-Li-036	30.3	-0.7	0.4
GSP2-Li-052	30.3	0.7	0.1
GSP2-Li-184	30.3	-0.3	0.2

APPENDIX TABLE ix. SIMS zircon U-Pb isotopic data of the Suzhou granites

Sample/ spot	$^{207}Pb/^{206}Pb$	±1σ (%)	$^{207}Pb/^{235}U$	±1σ (%)	$^{206}Pb/^{238}U$	±1σ (%)	$T_{207/235}$ (Ma)	±1σ	$T_{206/238}$ (Ma)	±1σ	U (ppm)	Th (ppm)	Th/U	f_{206}^{*} (%)
Sz1	nphibole-bearing porphyritic alkaline-feldspar granite													
group1 #01	0.0498	3.45	0.134	3.76	0.0195	1.51	127.7	4.5	124.6	1.9	332	174	0.5	0.06
#02	0.0508	6.23	0.139	6.43	0.0199	1.58	132.3	8.0	126.8	2.0	76	62	0.8	0.00
#03	0.0477	2.67	0.132	3.15	0.0201	1.67	126.0	3.7	128.2	2.1	389	171	0.4	0.05
#04	0.0486	2.97	0.137	3.37	0.0204	1.58	130.0	4.1	130.1	2.0	226	200	0.9	0.23
#05	0.0477	3.31	0.127	3.66	0.0193	1.56	121.6	4.2	123.5	1.9	202	85	0.4	0.38
#06	0.0488	1.83	0.136	2.37	0.0202	1.51	129.4	2.9	129.0	1.9	672	470	0.7	0.00
#07	0.0490	1.62	0.134	2.21	0.0198	1.50	127.6	2.7	126.5	1.9	816	337	0.4	0.23
#08	0.0522	5.31	0.137	5.57	0.0190	1.69	130.0	6.8	121.3	2.0	73	55	0.8	0.79
#09	0.0501	5.18	0.134	5.41	0.0194	1.57	127.9	6.5	124.1	1.9	177	154	0.9	0.12
#10	0.0487	4.09	0.131	4.38	0.0195	1.55	125.3	5.2	124.7	1.9	243	74	0.3	0.08
#11	0.0492	2.91	0.133	3.28	0.0195	1.52	126.4	3.9	124.6	1.9	355	147	0.4	0.21
#12	0.0427	9.95	0.115	10.07	0.0195	1.60	110.4	10.6	124.6	2.0	200	160	0.8	1.97
#13	0.0511	4.17	0.143	4.44	0.0202	1.52	135.5	5.6	129.2	1.9	304	168	0.6	0.83
#14	0.0503	4.71	0.136	4.97	0.0196	1.59	129.3	6.1	125.1	2.0	96	82	0.9	0.43
#15	0.0543	14.57	0.148	14.75	0.0198	2.29	140.4	19.5	126.5	2.9	45	36	0.8	1.24
#16	0.0511	4.09	0.133	4.36	0.0189	1.52	127.2	5.2	121.0	1.8	302	155	0.5	1.30
#17	0.0485	7.45	0.128	7.62	0.0191	1.57	121.9	8.8	121.8	1.9	73	34	0.5	0.95
#18	0.0500	2.97	0.138	3.34	0.0200	1.53	131.1	4.1	127.8	1.9	152	103	0.7	0.28
#19	0.0497	2.70	0.135	3.10	0.0197	1.52	128.8	3.8	126.0	1.9	169	55	0.3	0.09
#20	0.0488	3.03	0.135	3.39	0.0200	1.52	128.4	4.1	127.8	1.9	159	126	0.8	0.20
#21	0.0499	2.33	0.134	2.78	0.0195	1.51	127.8	3.3	124.4	1.9	205	174	0.8	0.31
#22	0.0480	2.79	0.129	3.17	0.0195	1.51	123.5	3.7	124.7	1.9	139	159	1.1	0.17
#23	0.0430	20.26	0.110	20.34	0.0185	1.78	106.0	20.7	118.5	2.1	445	180	0.4	27.14
#24	0.0496	2.55	0.143	2.97	0.0209	1.52	135.7	3.8	133.4	2.0	2495	1740	0.5	1.52
#25	0.0506	2.22	0.140	2.72	0.0201	1.58	133.0	3.4	128.0	2.0	270	114	0.4	0.38
#26	0.0483	2.75	0.139	3.14	0.0209	1.51	132.5	3.9	133.5	2.0	2984	2620	0.9	1.61
#27	0.0486	2.29	0.133	2.74	0.0198	1.50	126.5	3.3	126.4	1.9	340	252	0.7	0.12
#28	0.0489	3.84	0.135	4.15	0.0200	1.59	128.6	5.0	127.8	2.0	322	139	0.4	0.03
#29	0.0445	24.31	0.122	24.37	0.0198	1.71	116.6	27.2	126.6	2.1	354	143	0.4	1.53

#30	0.0460	4.40	0.124	4.65	0.0195	1.52	118.4	5.2	124.5	1.9	464	239	0.5	1.62
group2 #01	0.0850	164.33	0.271	165.23	0.0231	17.18	243.2	306.2	147.3	25.1	4511	2141	0.5	30.59
#02	0.0469	11.24	0.143	11.34	0.0222	1.51	136.1	14.5	141.4	2.1	5993	3163	0.5	15.18
#03	0.0466	18.78	0.135	18.86	0.0211	1.79	128.9	23.1	134.5	2.4	4744	1926	0.4	6.01
#04	0.0407	23.48	0.122	23.56	0.0217	1.85	116.8	26.3	138.6	2.5	6633	3293	0.5	34.89
#05	0.0396	17.87	0.110	17.95	0.0201	1.68	105.8	18.2	128.4	2.1	4653	2385	0.5	32.98
#06	0.0487	0.35	0.155	1.54	0.0231	1.50	146.7	2.1	147.4	2.2	8437	3276	0.4	0.03
#07	0.0483	9.70	0.145	9.83	0.0218	1.57	137.4	12.7	138.8	2.2	5942	2562	0.4	1.79
#08	0.0487	0.47	0.150	1.57	0.0224	1.50	142.2	2.1	142.7	2.1	6542	2172	0.3	0.18
#09	0.0482	1.05	0.140	1.84	0.0210	1.51	132.9	2.3	134.2	2.0	3998	1912	0.5	0.65
#10	0.0478	6.68	0.146	6.85	0.0221	1.53	138.2	8.9	141.0	2.1	6693	2757	0.4	14.53
Weighted Average of group 1 $^{206}Pb/^{238}U$ age (2σ) = 126.2 ±0.9 Ma, N=30, 1 of 30 rejected														
Sz2	GPS（120°29'54.9"E, 31°18'47.9"N） Coarse-grained alkaline-feldspar granite													
group1 #01	0.0474	2.42	0.128	2.86	0.0196	1.52	122.2	3.3	124.9	1.9	423	185	0.4	0.22
#02	0.0499	2.79	0.134	3.19	0.0195	1.54	127.6	3.8	124.2	1.9	263	110	0.4	0.00
#03	0.0478	2.47	0.129	2.91	0.0196	1.54	123.5	3.4	125.3	1.9	346	131	0.4	0.00
#04	0.0489	5.61	0.136	5.85	0.0201	1.65	129.1	7.1	128.4	2.1	86	54	0.6	0.23
#05	0.0482	5.96	0.125	6.36	0.0189	2.21	119.9	7.2	120.6	2.6	121	91	0.8	0.48
#06	0.0486	2.71	0.132	3.13	0.0198	1.56	126.2	3.7	126.1	1.9	368	171	0.5	0.30
#07	0.0491	4.28	0.134	4.58	0.0199	1.62	128.1	5.5	126.8	2.0	113	64	0.6	0.18
#08	0.0480	2.63	0.130	3.05	0.0196	1.55	123.9	3.6	125.2	1.9	308	127	0.4	0.06
#09	0.0497	2.52	0.135	2.95	0.0197	1.54	128.7	3.6	126.0	1.9	332	130	0.4	0.00
#10	0.0486	2.45	0.131	2.88	0.0196	1.52	125.1	3.4	124.8	1.9	356	127	0.4	0.06
#11	0.0478	3.89	0.134	4.25	0.0203	1.71	127.4	5.1	129.3	2.2	134	93	0.7	0.79
#12	0.0473	2.62	0.129	3.08	0.0198	1.63	123.2	3.6	126.2	2.0	308	117	0.4	0.00
#13	0.0477	3.37	0.128	3.71	0.0195	1.55	122.6	4.3	124.5	1.9	260	261	1.0	0.08
#14	0.0486	2.78	0.132	3.18	0.0197	1.54	126.1	3.8	125.9	1.9	296	246	0.8	0.07
#15	0.0511	5.92	0.138	6.18	0.0196	1.75	131.1	7.6	124.9	2.2	131	59	0.5	0.68
#16	0.0490	2.25	0.134	2.72	0.0199	1.52	127.8	3.3	126.7	1.9	475	189	0.4	0.14
#17	0.0449	10.59	0.120	10.70	0.0194	1.53	115.2	11.7	123.9	1.9	193	125	0.6	1.94
#18	0.0471	6.06	0.126	6.28	0.0194	1.63	120.5	7.2	123.9	2.0	90	51	0.6	0.48
#19	0.0487	3.08	0.129	3.45	0.0192	1.55	123.2	4.0	122.7	1.9	238	279	1.1	0.05
#20	0.0483	6.57	0.128	6.76	0.0192	1.59	121.9	7.8	122.3	1.9	33	23	0.7	0.00
#21	0.0479	5.15	0.130	5.38	0.0197	1.58	124.2	6.3	125.6	2.0	108	65	0.6	0.33

#22	0.0515	9.34	0.135	9.47	0.0191	1.56	129.0	11.5	121.9	1.9	1691	719	0.4	1.35
#23	0.0479	1.98	0.130	2.48	0.0196	1.51	123.7	2.9	125.1	1.9	597	325	0.5	0.24
#24	0.0492	1.97	0.136	2.48	0.0200	1.51	129.3	3.0	127.8	1.9	742	702	0.9	0.52
#25	0.0480	4.50	0.127	4.75	0.0192	1.52	121.6	5.5	122.8	1.9	1038	530	0.5	1.77
#26	0.0494	4.85	0.139	5.08	0.0205	1.52	132.6	6.3	130.7	2.0	348	118	0.3	1.71
#27	0.0500	4.04	0.126	4.31	0.0182	1.50	120.2	4.9	116.5	1.7	986	542	0.5	2.43
#28	0.0456	7.54	0.118	7.69	0.0188	1.53	113.3	8.3	119.9	1.8	608	663	1.1	4.60
#29	0.0466	3.01	0.136	3.37	0.0212	1.51	129.4	4.1	135.0	2.0	1795	682	0.4	2.73
#30	0.0488	2.21	0.134	2.69	0.0199	1.53	127.3	3.2	126.8	1.9	276	90	0.3	0.20
#31	0.0485	0.78	0.136	1.70	0.0204	1.50	129.9	2.1	130.1	1.9	2605	1154	0.4	0.06
group2 #01	0.0486	1.10	0.157	2.17	0.0235	1.87	148.4	3.0	149.7	2.8	11134	9265	0.8	0.66
#02	0.0470	7.80	0.130	7.97	0.0201	1.61	124.1	9.4	128.0	2.0	6908	6986	1.0	15.94
#03	0.0549	101.50	0.162	101.73	0.0214	6.87	152.4	134.7	136.4	9.3	3027	1457	0.5	46.02
#04	0.0486	2.57	0.146	2.98	0.0219	1.51	138.7	3.9	139.4	2.1	5681	3094	0.5	0.27
#05	0.0510	18.06	0.150	18.14	0.0213	1.67	141.7	24.3	135.9	2.2	5870	1626	0.3	5.41

Weighted Average group 1 $^{206}Pb/^{238}U$ age (2σ) = 125.5 ±0.8 Ma, N=31, 3 0f 31 rejected

Sz3	GPS（120°28'07.3"E, 31°16'46.0"N） fine-grained alkaline-feldspar granite													
group1 #01	0.0479	4.35	0.125	4.67	0.0189	1.68	119.4	5.3	120.6	2.0	214	152	0.7	0.27
#02	0.0481	4.94	0.132	5.18	0.0200	1.56	126.1	6.2	127.4	2.0	80	49	0.6	0.00
#03	0.0486	4.32	0.132	4.60	0.0198	1.56	126.3	5.5	126.1	2.0	108	34	0.3	0.00
#04	0.0480	2.39	0.129	2.84	0.0195	1.53	123.5	3.3	124.7	1.9	373	154	0.4	0.30
#05	0.0495	2.83	0.139	3.21	0.0203	1.51	131.8	4.0	129.6	1.9	562	266	0.5	0.09
#06	0.0511	4.16	0.136	4.46	0.0193	1.61	129.3	5.4	123.1	2.0	171	135	0.8	0.24
#07	0.0482	2.83	0.134	3.21	0.0201	1.53	127.3	3.9	128.3	1.9	339	164	0.5	0.16
#08	0.1705	2.34	0.483	2.88	0.0205	1.68	400.1	9.6	131.0	2.2	251	115	0.5	15.43
#09	0.0483	2.83	0.133	3.21	0.0200	1.53	127.0	3.8	127.7	1.9	319	163	0.5	0.00
#10	0.0499	3.32	0.133	3.69	0.0193	1.61	126.6	4.4	123.2	2.0	191	127	0.7	0.30
#11	0.0484	0.92	0.138	1.76	0.0207	1.50	131.7	2.2	132.4	2.0	2344	3820	0.6	0.29
#12	0.0494	1.66	0.133	2.25	0.0195	1.53	126.4	2.7	124.3	1.9	789	300	0.4	0.01
#13	0.0489	2.35	0.134	2.80	0.0198	1.51	127.5	3.4	126.7	1.9	433	549	1.3	0.09
#14	0.0491	1.50	0.133	2.12	0.0196	1.50	126.8	2.5	125.3	1.9	2723	1045	0.2	1.61
#15	0.0479	2.40	0.130	2.87	0.0196	1.58	123.7	3.4	125.2	2.0	378	633	1.7	0.00
#16	0.0483	3.89	0.121	4.18	0.0182	1.52	116.4	4.6	116.5	1.8	1065	495	0.5	2.27
#17	0.0495	3.21	0.135	3.57	0.0198	1.56	128.6	4.3	126.3	1.9	145	57	0.4	0.00
#18	0.0479	6.46	0.130	6.63	0.0196	1.51	123.8	7.8	125.4	1.9	321	180	0.6	1.08

#19	0.0484	4.19	0.119	4.45	0.0178	1.50	113.9	4.8	113.6	1.7	634	562	0.9	2.57
#20	0.0487	4.36	0.126	4.62	0.0188	1.53	120.4	5.3	119.8	1.8	433	353	0.8	2.11
#21	0.0524	7.98	0.145	8.13	0.0201	1.55	137.7	10.5	128.2	2.0	2923	826	0.3	1.47
#22	0.0474	20.32	0.130	20.41	0.0199	1.92	124.2	24.1	127.2	2.4	1780	604	0.3	1.50
group2 #01	0.0474	6.70	0.146	6.87	0.0223	1.54	138.4	8.9	142.4	2.2	10856	8563	0.8	3.90
#02	0.0487	0.80	0.143	1.70	0.0213	1.50	135.8	2.2	135.9	2.0	6278	3247	0.5	0.07
#03	0.1383	0.60	0.401	1.63	0.0210	1.52	342.1	4.7	134.1	2.0	7427	4006	0.5	11.78
#04	0.0464	41.34	0.146	41.37	0.0228	1.51	138.5	55.0	145.5	2.2	6266	2593	0.4	13.00
#05	0.0488	0.72	0.153	1.66	0.0227	1.50	144.5	2.2	145.0	2.2	5883	2581	0.4	0.48
#06	0.0525	38.76	0.163	38.90	0.0225	3.31	153.3	56.9	143.6	4.7	10415	4754	0.4	25.31
#07	0.0445	11.29	0.132	11.39	0.0214	1.50	125.6	13.5	136.8	2.0	9363	6124	0.6	10.68
#08	0.1674	10.26	0.500	10.43	0.0217	1.87	412.0	35.9	138.3	2.6	10623	17028	1.6	15.06
#09	0.0487	0.81	0.143	1.71	0.0213	1.51	135.9	2.2	136.1	2.0	4892	457	0.2	0.01
#10	0.0486	2.82	0.165	3.22	0.0247	1.55	155.4	4.6	157.2	2.4	12662	9197	0.7	1.29
#11	0.0419	6.40	0.112	6.77	0.0194	2.19	107.7	6.9	123.7	2.7	3857	1191	0.3	21.17
#12	0.1381	0.76	0.367	1.69	0.0193	1.51	317.4	4.6	123.1	1.8	5977	4419	0.7	11.49
Weighted Average group 1 $^{206}Pb/^{238}U$ age (2σ) = 126.2 ±0.5 Ma N=22, 4 of 22 rejected														
Sz4	GPS（120°28'41.9"E, 31°19'36.1"N） altered porphyritic alkaline-feldspar granite													
group1 #01	0.0499	6.84	0.133	7.03	0.0193	1.61	126.6	8.4	123.2	2.0	252	112	0.5	0.93
#02	0.0502	10.63	0.135	10.74	0.0195	1.52	128.8	13.1	124.7	1.9	1849	1188	0.7	1.67
#03	0.0490	2.29	0.132	2.84	0.0196	1.68	125.9	3.4	124.8	2.1	464	255	0.6	0.09
#04	0.0486	3.22	0.134	3.83	0.0200	2.09	127.8	4.6	127.9	2.6	205	97	0.5	0.37
#05	0.0477	3.11	0.131	3.48	0.0199	1.57	124.6	4.1	126.8	2.0	366	197	0.5	0.10
#06	0.0474	1.64	0.135	2.23	0.0206	1.51	128.2	2.7	131.4	2.0	777	455	0.6	0.05
#07	0.0488	2.77	0.130	3.16	0.0194	1.53	124.4	3.7	123.8	1.9	467	186	0.4	0.12
#08	0.0486	2.92	0.130	3.31	0.0194	1.55	124.2	3.9	124.0	1.9	259	96	0.4	0.31
#09	0.0497	18.62	0.139	18.70	0.0203	1.68	132.3	23.5	129.6	2.2	222	188	0.9	1.59
#10	0.0432	8.94	0.115	9.08	0.0194	1.57	110.9	9.6	123.8	1.9	316	119	0.4	1.89
#11	0.0486	3.76	0.134	4.06	0.0199	1.53	127.3	4.9	127.2	1.9	358	319	0.9	0.31
#12	0.0493	2.75	0.139	3.20	0.0205	1.62	132.3	4.0	130.8	2.1	376	239	0.6	0.15
#13	0.0472	4.75	0.131	4.99	0.0202	1.53	125.4	5.9	129.0	2.0	97	73	0.8	0.59
#14	0.0491	8.90	0.125	9.05	0.0184	1.69	119.2	10.2	117.6	2.0	275	288	1.1	2.39
#15	0.0475	2.47	0.130	2.92	0.0198	1.57	123.8	3.4	126.3	2.0	715	294	0.4	0.42
#16	0.0488	1.42	0.139	2.22	0.0206	1.70	132.1	2.8	131.7	2.2	981	517	0.5	0.14
#17	0.0512	9.65	0.138	9.79	0.0196	1.63	131.5	12.1	125.2	2.0	63	33	0.5	0.34

#18	0.0466	13.01	0.124	13.11	0.0193	1.64	118.8	14.8	123.4	2.0	598	309	0.5	1.58
#19	0.0503	9.12	0.140	9.25	0.0202	1.60	133.1	11.6	128.9	2.0	1246	1515	1.2	1.40
#20	0.0475	1.40	0.131	2.05	0.0199	1.50	124.7	2.4	127.3	1.9	614	779	1.2	0.11
#21	0.0480	1.89	0.131	2.42	0.0197	1.51	124.6	2.8	125.8	1.9	339	202	0.6	0.27
#22	0.0487	1.59	0.133	2.22	0.0198	1.54	126.9	2.6	126.4	1.9	482	166	0.3	0.09
#23	0.0484	2.93	0.131	3.30	0.0196	1.51	125.0	3.9	125.2	1.9	255	110	0.4	0.06
#24	0.0462	3.49	0.130	3.82	0.0204	1.55	123.9	4.5	130.0	2.0	415	310	0.7	1.08
#25	0.0478	1.45	0.132	2.09	0.0200	1.50	125.9	2.5	127.8	1.9	2508	2735	1.1	0.54
#26	0.0459	4.03	0.123	4.32	0.0194	1.55	117.6	4.8	123.9	1.9	214	194	0.9	0.72
#27	0.0475	37.82	0.114	37.88	0.0175	2.11	110.0	40.3	111.6	2.3	549	244	0.4	40.61
#28	0.0509	9.02	0.148	9.15	0.0211	1.52	140.0	12.0	134.4	2.0	2652	1393	0.5	16.99
#29	0.0477	1.20	0.130	1.94	0.0198	1.53	124.4	2.3	126.6	1.9	2922	1874	0.6	0.59
#30	0.0430	11.87	0.116	11.97	0.0196	1.55	111.3	12.7	124.8	1.9	615	248	0.4	1.68
#31	0.0289	47.61	0.071	47.66	0.0178	2.09	69.7	32.6	114.0	2.4	513	264	0.5	37.95
#32	0.0442	55.29	0.109	55.37	0.0179	2.90	105.3	56.9	114.6	3.3	507	327	0.6	57.58
group2 #01	0.0494	1.75	0.155	2.31	0.0228	1.50	146.5	3.2	145.3	2.2	6246	2375	0.4	0.16
#02	0.0488	0.93	0.148	1.77	0.0221	1.50	140.4	2.3	140.6	2.1	6136	2854	0.5	0.43
#03	0.0490	0.40	0.148	1.55	0.0219	1.50	140.0	2.0	139.6	2.1	6631	2895	0.4	0.07
#04	0.0490	0.44	0.150	1.56	0.0222	1.50	141.7	2.1	141.4	2.1	6264	2964	0.5	0.03
#05	0.0488	4.20	0.163	4.46	0.0242	1.50	153.1	6.4	154.0	2.3	13433	12553	0.9	1.21
#06	0.0491	0.42	0.156	1.56	0.0231	1.50	147.3	2.1	147.1	2.2	6953	3337	0.5	0.08
#07	0.0485	0.63	0.141	1.63	0.0210	1.50	133.7	2.0	134.1	2.0	3626	1640	0.4	0.10

Weighted Average group 1 $^{206}Pb/^{238}U$ age (2σ) = 126.6 ±0.9 Ma, N=32, 5 of 32 rej

of common ^{206}Pb in total measured ^{206}Pb

xclude from concordia diagram and age calculatio

APPENDIX TABLE x. Zircon Oxygen-isotopic composition and calculated D_{dpa}

Spot	$\delta^{18}O$(‰)	±σ	$T_{206/238}$	U ppm	Th ppm	Dα	D_{dpa}
Sz1							
group1 #01	5.21	0.29	124.6	332	174	1.52E+14	0.01
#02	5.54	0.26	126.8	76	62	3.75E+13	0.00
#03	4.92	0.24	128.2	389	171	1.81E+14	0.01
#04	5.14	0.25	130.1	226	200	1.17E+14	0.01
#05	5.49	0.22	123.5	202	85	9.01E+13	0.00
#06	5.44	0.49	129.0	672	470	3.31E+14	0.02
#07	5.45	0.30	126.5	816	337	3.72E+14	0.02
#08	5.23	0.42	121.3	73	55	3.41E+13	0.00
#09	5.64	0.43	124.1	177	154	8.69E+13	0.00
#10	5.27	0.31	124.7	243	74	1.07E+14	0.01
#11	5.35	0.38	124.6	355	147	1.60E+14	0.01
#12	5.66	0.35	124.6	200	160	9.71E+13	0.00
#13	4.94	0.36	129.2	304	168	1.46E+14	0.01
#14	5.56	0.39	125.1	96	82	4.73E+13	0.00
#15	5.52	0.62	126.5	45	36	2.23E+13	0.00
#16	5.24	0.34	121.0	302	155	1.34E+14	0.01
#17	5.03	0.17	121.8	73	34	3.23E+13	0.00
#18	5.63	0.17	127.8	152	103	7.38E+13	0.00
#19	5.34	0.18	126.0	169	55	7.53E+13	0.00
#20	5.69	0.24	127.8	159	126	7.93E+13	0.00
#21	5.34	0.15	124.4	205	174	1.01E+14	0.00
#22	5.52	0.11	124.7	139	159	7.23E+13	0.00
#23	5.34	0.18	118.5	445	180	1.89E+14	0.01
#24	4.61	0.19	133.4	2495	1740	1.27E+15	0.06
#25	5.02	0.18	128.0	270	114	1.25E+14	0.01
#26	5.35	0.21	133.5	2984	2620	1.58E+15	0.08
#27	4.95	0.21	126.4	340	252	1.66E+14	0.01
#28	5.69	0.19	127.8	322	139	1.49E+14	0.01
#29	5.10	0.17	126.6	354	143	1.61E+14	0.01
#30	5.63	0.17	124.5	464	239	2.12E+14	0.01
group2 #01	4.15	0.18	147.3	4511	2141	2.43E+15	0.12
#02	4.26	0.22	141.4	5993	3163	3.13E+15	0.15
#03	4.63	0.21	134.5	4744	1926	2.30E+15	0.11
#04	4.72	0.16	138.6	6633	3293	3.38E+15	0.16
#05	4.29	0.18	128.4	4653	2385	2.20E+15	0.10
#06	4.26	0.23	147.4	8437	3276	4.46E+15	0.21
#07	4.96	0.19	138.8	5942	2562	2.99E+15	0.14
#08	4.32	0.17	142.7	6542	2172	3.31E+15	0.16
#09	4.69	0.18	134.2	3998	1912	1.96E+15	0.09
#10	4.18	0.17	141.0	6693	2757	3.40E+15	0.16
Sz2							
group1 #01	5.46	0.17	124.92	423	185	1.91E+14	0.01
#02	5.20	0.20	124.19	263	110	1.18E+14	0.01
#03	5.31	0.18	125.28	346	131	1.55E+14	0.01
#04	5.56	0.17	128.42	86	54	4.17E+13	0.00
#05	5.44	0.13	120.56	121	91	5.63E+13	0.00
#06	5.15	0.19	126.08	368	171	1.69E+14	0.01
#07	5.54	0.16	126.76	113	64	5.33E+13	0.00

#08	5.44	0.19	125.22	308	127	1.39E+14	0.01
#09	5.21	0.17	125.95	332	130	1.50E+14	0.01
#10	5.33	0.27	124.83	356	127	1.58E+14	0.01
#11	5.44	0.17	129.34	134	93	6.64E+13	0.00
#12	5.23	0.18	126.20	308	117	1.39E+14	0.01
#13	5.45	0.22	124.47	260	261	1.31E+14	0.01
#14	5.40	0.20	125.87	296	246	1.46E+14	0.01
#15	5.20	0.18	124.87	131	59	5.95E+13	0.00
#16	5.19	0.25	126.71	475	189	2.16E+14	0.01
#17	5.49	0.18	123.95	193	125	9.06E+13	0.00
#18	5.65	0.15	123.89	90	51	4.17E+13	0.00
#19	5.49	0.19	122.67	238	279	1.22E+14	0.01
#20	5.59	0.18	122.29	33	23	1.52E+13	0.00
#21	5.84	0.13	125.63	108	65	5.11E+13	0.00
#22	5.01	0.27	121.86	1691	719	7.44E+14	0.04
#23	5.33	0.33	125.10	597	325	2.76E+14	0.01
#24	5.20	0.29	127.78	742	702	3.81E+14	0.02
#25	5.38	0.14	122.76	1038	530	4.68E+14	0.02
#26	4.81	0.27	130.69	348	118	1.61E+14	0.01
#27	5.17	0.22	116.54	986	542	4.25E+14	0.02
#28	5.95	0.32	119.95	608	663	3.01E+14	0.01
#29	4.36	0.26	134.97	1795	682	8.67E+14	0.04
#30	5.33	0.31	126.75	276	90	1.24E+14	0.01
#31	4.69	0.18	130.11	2605	1154	1.23E+15	0.06
group2 #01	3.96	0.16	149.67	11134	9265	6.55E+15	0.31
#02	4.87	0.17	128.04	6908	6986	3.60E+15	0.17
#03	4.82	0.33	136.43	3027	1457	1.51E+15	0.07
#04	4.72	0.23	139.40	5681	3094	2.94E+15	0.14
#05	4.41	0.27	135.88	5870	1626	2.79E+15	0.13
Sz3							
group1 #01	5.47	0.17	120.61	214	152	9.87E+13	0.00
#02	4.98	0.31	127.37	80	49	3.84E+13	0.00
#03	5.36	0.26	126.08	108	34	4.80E+13	0.00
#04	5.32	0.33	124.71	373	154	1.67E+14	0.01
#05	5.32	0.38	129.57	562	266	2.66E+14	0.01
#06	5.33	0.23	123.08	171	135	8.19E+13	0.00
#07	5.41	0.15	128.27	339	164	1.59E+14	0.01
#08	4.92	0.20	131.05	251	115	1.20E+14	0.01
#09	5.42	0.27	127.74	319	163	1.50E+14	0.01
#10	5.30	0.17	123.20	191	127	8.94E+13	0.00
#11	4.43	0.24	132.36	2344	3820	1.41E+15	0.07
#12	5.12	0.18	124.27	789	300	3.51E+14	0.02
#13	5.64	0.16	126.67	433	549	2.34E+14	0.01
#14	3.73	0.16	125.30	2723	1045	1.22E+15	0.06
#15	5.08	0.15	125.19	378	633	2.16E+14	0.01
#16	4.86	0.17	116.49	1065	495	4.51E+14	0.02
#17	5.34	0.19	126.34	145	57	6.56E+13	0.00
#18	5.34	0.15	125.43	321	180	1.50E+14	0.01
#19	4.97	0.19	113.62	634	562	2.85E+14	0.01
#20	5.37	0.23	119.76	433	353	2.03E+14	0.01
#21	4.92	0.21	128.21	2923	826	1.31E+15	0.06
#22	4.36	0.20	127.19	1780	604	8.03E+14	0.04
group2 #01	4.48	0.27	142.38	10856	8563	6.02E+15	0.29

#02	4.70	0.17	135.91	6278	3247	3.14E+15	0.15
#03	4.50	0.21	134.08	7427	4006	3.69E+15	0.18
#04	4.45	0.22	145.54	6266	2593	3.29E+15	0.16
#05	3.86	0.14	144.99	5883	2581	3.09E+15	0.15
#06	4.39	0.19	143.64	10415	4754	5.45E+15	0.26
#07	4.18	0.12	136.77	9363	6124	4.86E+15	0.23
#08	4.18	0.17	138.27	10623	17028	6.65E+15	0.32
#09	5.17	0.20	136.15	4892	457	2.24E+15	0.11
#10	4.10	0.21	157.23	12662	9197	7.67E+15	0.37
#11	5.27	0.30	123.65	3857	1191	1.68E+15	0.08
#12	5.01	0.28	123.06	5977	4419	2.83E+15	0.14
Sz4							
group1 #01	5.30	0.23	123.21	252	112	1.13E+14	0.01
#02	4.04	0.30	124.66	1849	1188	8.71E+14	0.04
#03	5.34	0.30	124.82	464	255	2.15E+14	0.01
#04	5.52	0.30	127.89	205	97	9.55E+13	0.00
#05	5.46	0.27	126.84	366	197	1.72E+14	0.01
#06	4.76	0.30	131.43	777	455	3.82E+14	0.02
#07	5.14	0.30	123.77	467	186	2.07E+14	0.01
#08	5.15	0.29	123.99	259	96	1.14E+14	0.01
#09	5.19	0.28	129.59	222	188	1.13E+14	0.01
#10	5.08	0.31	123.77	316	119	1.40E+14	0.01
#11	5.47	0.23	127.19	358	319	1.81E+14	0.01
#12	5.06	0.24	130.77	376	239	1.86E+14	0.01
#13	5.31	0.26	129.00	97	73	4.84E+13	0.00
#14	5.33	0.32	117.64	275	288	1.32E+14	0.01
#15	4.83	0.34	126.32	715	294	3.25E+14	0.02
#16	4.77	0.29	131.75	981	517	4.77E+14	0.02
#17	5.60	0.35	125.17	63	33	2.90E+13	0.00
#18	5.11	0.21	123.41	598	309	2.72E+14	0.01
#19	5.04	0.21	128.87	1246	1515	6.78E+14	0.03
#20	5.13	0.17	127.32	614	779	3.33E+14	0.02
#21	5.36	0.27	125.83	339	202	1.60E+14	0.01
#22	5.61	0.22	126.43	482	166	2.16E+14	0.01
#23	5.23	0.17	125.24	255	110	1.15E+14	0.01
#24	5.32	0.16	129.99	415	310	2.08E+14	0.01
#25	5.12	0.21	127.81	2508	2735	1.32E+15	0.06
#26	5.32	0.18	123.94	214	194	1.06E+14	0.01
#27	5.07	0.19	111.56	549	244	2.22E+14	0.01
#28	4.65	0.21	134.41	2652	1393	1.32E+15	0.06
#29	4.79	0.15	126.58	2922	1874	1.40E+15	0.07
#30	5.24	0.23	124.82	615	248	2.76E+14	0.01
#31	5.30	0.31	113.96	513	264	2.15E+14	0.01
#32	5.25	0.29	114.63	507	327	2.19E+14	0.01
group2 #01	4.80	0.24	145.34	6246	2375	3.25E+15	0.16
#02	4.26	0.23	140.62	6136	2854	3.15E+15	0.15
#03	4.52	0.17	139.61	6631	2895	3.36E+15	0.16
#04	4.70	0.18	141.45	6264	2964	3.24E+15	0.15
#05	4.90	0.28	153.97	13433	12553	8.30E+15	0.40
#06	4.89	0.35	147.10	6953	3337	3.74E+15	0.18
#07	4.86	0.21	134.09	3626	1640	1.77E+15	0.08

APPENDIX TABLE xi. SIMS *in situ* Quartz oxygen isotopic results

Sample	$\delta^{18}O$(‰)	±σ	Sample	$\delta^{18}O$(‰)	±σ	Sample	$\delta^{18}O$(‰)	±σ	Sample	$\delta^{18}O$(‰)	±σ
SZ1-Q01	7.44	0.35	**SZ2-Q01**	7.90	0.24	**SZ3-Q01**	7.63	0.24	**SZ4-Q01**	7.62	0.23
SZ1-Q02	7.40	0.31	**SZ2-Q02**	7.79	0.34	**SZ3-Q02**	7.50	0.26	**SZ4-Q02**	7.27	0.21
SZ1-Q03	7.50	0.27	**SZ2-Q03**	7.78	0.31	**SZ3-Q03**	7.62	0.15	**SZ4-Q03**	7.43	0.27
SZ1-Q04	7.38	0.26	**SZ2-Q04**	7.77	0.23	**SZ3-Q04**	7.75	0.29	**SZ4-Q04**	7.76	0.24
SZ1-Q05	7.20	0.24	**SZ2-Q05**	7.74	0.20	**SZ3-Q05**	7.84	0.25	**SZ4-Q05**	7.53	0.28
SZ1-Q06	7.83	0.27	**SZ2-Q06**	7.79	0.31	**SZ3-Q06**	7.72	0.32	**SZ4-Q06**	7.60	0.35
SZ1-Q07	7.73	0.22	**SZ2-Q07**	7.76	0.30	**SZ3-Q07**	7.46	0.23	**SZ4-Q07**	7.57	0.35
SZ1-Q08	7.54	0.26	**SZ2-Q08**	7.73	0.30	**SZ3-Q08**	7.78	0.20	**SZ4-Q08**	7.50	0.32
SZ1-Q09	7.54	0.26	**SZ2-Q09**	8.05	0.15	**SZ3-Q09**	7.61	0.24	**SZ4-Q09**	7.79	0.30
SZ1-Q10	7.35	0.30	**SZ2-Q10**	7.54	0.26	**SZ3-Q10**	7.92	0.29	**SZ4-Q10**	7.77	0.28
SZ1-Q11	7.17	0.40	**SZ2-Q11**	7.78	0.25	**SZ3-Q11**	7.56	0.35	**SZ4-Q11**	7.77	0.22
SZ1-Q12	7.18	0.28	**SZ2-Q12**	7.88	0.25	**SZ3-Q12**	7.71	0.30	**SZ4-DQ01**	8.83	0.31
SZ1-Q13	7.66	0.42	**SZ2-Q13**	7.48	0.28	**SZ3-Q13**	7.76	0.27	**SZ4-DQ02**	9.20	0.33
SZ1-Q14	7.11	0.22	**SZ2-Q14**	7.58	0.29	**SZ3-Q14**	7.73	0.20	**SZ4-DQ03**	8.05	0.35
SZ1-Q15	7.48	0.25	**SZ2-Q15**	7.78	0.27	**SZ3-Q15**	7.45	0.37	**SZ4-DQ04**	10.29	0.28
SZ1-Q16	7.30	0.30	**SZ2-Q16**	7.73	0.31	**SZ3-Q16**	7.98	0.24	**SZ4-DQ05**	8.24	0.19
SZ1-DQ01	7.48	0.24	**SZ2-DQ01**	8.33	0.29	**SZ3-Q17**	7.69	0.29	**SZ4-DQ06**	9.84	0.28
SZ1-DQ02	8.02	0.31	**SZ2-DQ02**	8.01	0.27	**SZ3-Q18**	7.23	0.38	**SZ4-DQ07**	9.20	0.21
SZ1-DQ03	8.23	0.29	**SZ2-DQ03**	7.92	0.28	**SZ3-DQ01**	7.91	0.26	**SZ4-DQ08**	9.55	0.24
SZ1-DQ04	7.38	0.29	**SZ2-DQ04**	7.98	0.38	**SZ3-DQ02**	7.95	0.25	**SZ4-DQ09**	8.25	0.24
						SZ3-DQ03	7.94	0.36	**SZ4-DQ10**	9.36	0.22
						SZ3-DQ04	7.90	0.28	**SZ4-DQ11**	9.17	0.23

"Q" in sample names represents for quartzes which have clear transmitted and reflected light micrographs;
"DQ" in sample names represents quartzes which have a "dirty" appearance under reflected light
and nearly opaque under transmitted light;

APPENDIX TABLE xii. In situ M257 Li isotope compositions

Name	Time	IP	7Li/6Li	%	7Li	%	X Position	Y Position	δ7Lim (‰)	count rate	δ7Licorr (‰)	1se	ppm	1se	note
M257 5μm Scatter points															
M257-5@1	2014-11-6 16:46	1.17	12.48	0.17	12460	0.68	4218	-1253	36.41	10645	-1.20	1.70	1.06	0.01	
M257-5@2	2014-11-6 17:05	1.17	12.51	0.15	10775	1.75	4130	-1130	39.40	9222	1.79	1.52	0.92	0.02	
M257-5@4	2014-11-6 18:21	1.15	12.51	0.14	10191	1.74	3772	-880	39.51	8878	1.90	1.45	0.88	0.02	
M257-5@6	2014-11-6 20:01	1.06	12.47	0.18	9223	1.65	4002	-1024	36.13	8673	-1.48	1.78	0.86	0.01	
M257-5@7	2014-11-6 20:20	1.07	12.55	0.17	8959	1.59	3670	-815	42.64	8402	5.03	1.67	0.84	0.01	
M257-5@08	2014-11-6 20:39	1.05	12.56	0.19	9329	1.66	4281	-1357	43.26	8844	5.65	1.86	0.88	0.01	
M257-5@09	2014-11-6 21:56	1.07	12.50	0.19	8661	1.61	3922	-311	38.00	8131	0.39	1.93	0.81	0.01	
M257-5@10	2014-11-6 22:15	1.07	12.56	0.18	8720	1.62	3804	-311	43.12	8140	5.51	1.80	0.81	0.01	
M257-5@11	2014-11-6 22:34	1.08	12.51	0.16	8939	1.59	3687	-316	39.08	8278	1.48	1.62	0.82	0.01	
M257-5@12	2014-11-6 22:53	1.09	12.52	0.17	9173	1.72	3829	-920	40.33	8426	2.72	1.69	0.84	0.01	
M257-5@17	2014-11-7 3:01	1.08	12.53	0.17	8804	1.51	3915	-565	41.08	8157	3.48	1.68	0.81	0.01	
M257-5@19	2014-11-7 3:40	1.07	12.53	0.14	8684	1.50	3910	-469	40.60	8094	3.00	1.43	0.81	0.01	
M257-5@21	2014-11-7 5:34	1.02	12.50	0.16	8169	1.35	3411	-305	38.23	8007	0.62	1.65	0.80	0.01	
M257-5@23	2014-11-7 6:12	1.02	12.50	0.18	9174	1.14	3386	12	38.13	9037	0.52	1.77	0.90	0.01	
M257 5μm Line test															
M257-5@3	2014-11-6 18:02	1.16	12.53	0.19	10348	1.74	3888	-953	41.06	8913	3.45	1.90	0.89	0.02	
M257-5@12	2014-11-6 22:53	1.09	12.52	0.17	9173	1.72	3829	-920	40.33	8426	2.72	1.69	0.84	0.01	
M257-5@13	2014-11-7 0:29	1.10	12.54	0.18	8601	1.70	3809	-906	41.54	7825	3.93	1.83	0.78	0.01	
M257-5@14	2014-11-7 0:48	1.10	12.48	0.22	7675	1.59	3850	-931	36.75	6978	-0.85	2.18	0.69	0.01	
M257-5@15	2014-11-7 1:07	1.10	12.48	0.18	8081	1.69	3820	-912	36.71	7341	-0.90	1.80	0.73	0.01	
M257-5@16	2014-11-7 1:26	1.10	12.46	0.21	6641	1.66	3802	-896	35.37	6020	-2.23	2.06	0.60	0.01	
M257-5@25	2014-11-7 6:51	0.94	12.55	0.22	6211	1.41	3871	-946	42.21	6608	4.60	2.24	0.66	0.01	
M257 5μm Rim test															
M257-5@18	2014-11-7 3:20	1.07	12.36	0.42	1417	0.70	4018	-310	26.62	1326	-10.99	4.21	0.13	0.00	right
M257-5@20	2014-11-7 3:59	1.05	12.40	0.41	1729	0.91	4017	-447	29.75	1641	-7.86	4.10	0.16	0.00	right
M257-5@22	2014-11-7 5:53	1.02	12.53	0.23	5916	1.23	3388	-500	40.70	5826	3.09	2.31	0.58	0.01	left
M257-5@24	2014-11-7 6:31	0.97	12.45	0.26	3071	0.39	3469	156	34.49	3182	-3.12	2.56	0.32	0.00	up
M257@26	2014-11-7 10:53	0.71	12.35	0.39	1983	0.91	3960	-1164	25.92	2778	-11.69	3.94	0.28	0.00	left
M257@27	2014-11-7 11:28	0.54	12.66	0.49	1263	0.60	4373	-1221	51.56	2332	13.95	4.93	0.23	0.00	right
M257@28	2014-11-7 11:49	0.50	12.52	0.33	2367	0.74	3516	-702	40.23	4699	2.62	3.27	0.47	0.00	left

M257@29	2014-11-7 12:08	0.46	12.52	0.36	2287	0.68	3664	25	39.88	4972	2.27	3.56	0.49	0.00	
Nist-614 5μm Scatter points															
NIST614@1	2014-11-6 17:24	1.17	12.66	0.21	8425	1.00	-1114	778	51.29	7227	13.68	2.12	0.72	0.01	
NIST614@2	2014-11-6 17:43	1.16	12.67	0.22	7729	2.23	-979	783	52.64	6638	15.03	2.23	0.66	0.01	
NIST614@3	2014-11-6 18:40	1.13	12.71	0.23	7227	2.17	-1074	952	55.75	6376	18.14	2.27	0.63	0.01	
NIST614@4	2014-11-6 18:59	1.12	12.66	0.19	7179	2.26	-1277	980	51.40	6414	13.79	1.93	0.64	0.01	
NIST614@5	2014-11-6 19:19	1.12	12.65	0.24	6817	2.11	-1261	1140	50.58	6067	12.97	2.43	0.60	0.01	
NIST614@6	2014-11-6 20:58	1.07	12.72	0.19	6695	2.22	-1177	964	56.66	6280	19.05	1.90	0.63	0.01	
NIST614@7	2014-11-6 21:17	1.08	12.68	0.19	6606	2.07	-1106	1118	53.39	6111	15.78	1.93	0.61	0.01	
NIST614@8	2014-11-6 21:37	1.06	12.71	0.19	6554	2.23	-1076	1278	56.03	6203	18.42	1.93	0.62	0.01	
NIST614@9	2014-11-6 23:12	1.09	12.75	0.18	6773	2.21	-1246	1273	58.91	6208	21.30	1.81	0.62	0.01	
NIST614@10	2014-11-6 23:31	1.09	12.68	0.18	6784	2.24	-865	929	53.18	6216	15.57	1.84	0.62	0.01	
NIST614@11	2014-11-6 23:50	1.10	12.70	0.20	6866	2.27	-719	920	55.30	6270	17.69	1.97	0.62	0.01	
NIST614@12	2014-11-7 0:09	1.10	12.69	0.23	6934	2.26	-738	1094	54.05	6311	16.44	2.34	0.63	0.01	
NIST614@13	2014-11-7 1:45	1.08	12.66	0.21	6639	2.12	-846	1210	51.62	6128	14.01	2.08	0.61	0.01	
NIST614@15	2014-11-7 2:23	1.08	12.68	0.21	6532	2.15	-609	713	53.57	6045	15.96	2.08	0.60	0.01	
Nist-614 5μm Line test															
NIST614@17	2014-11-7 4:18	1.06	12.74	0.20	6289	2.13	-1044	774	57.88	5930	20.27	1.99	0.59	0.01	
NIST614@18	2014-11-7 4:37	1.06	12.68	0.20	6163	2.07	-1065	773	53.46	5818	15.86	2.02	0.58	0.01	
NIST614@19	2014-11-7 4:56	1.04	12.66	0.26	6050	1.97	-1056	775	51.48	5792	13.87	2.60	0.58	0.01	
NIST614@20	2014-11-7 5:15	1.02	12.70	0.23	5873	2.00	-1080	774	54.95	5736	17.34	2.30	0.57	0.01	
NIST614@21	2014-11-7 7:10	0.93	12.65	0.22	5114	2.11	-1131	775	50.39	5494	12.78	2.17	0.55	0.01	
NIST614@25	2014-11-7 10:04	0.66	12.71	0.32	3363	2.11	-1030	771	55.32	5129	17.71	3.24	0.51	0.01	
NIST614@26	2014-11-7 10:24	0.71	12.69	0.30	3519	1.82	-1020	773	54.00	4983	16.39	3.01	0.50	0.01	
Nist-614 5μm Rim test															
NIST614@16	2014-11-7 2:42	1.08	NaN	NaN	4	4.70	-819	570							down
NIST614@14	2014-11-7 2:04	1.08	12.40	0.32	2647	1.35	-587	930	30.27	2446	-7.34	3.20	0.24	0.00	right
NIST614@22	2014-11-7 7:29	0.92	12.76	0.31	4230	1.95	-1380	701	59.58	4575	21.97	3.11	0.46	0.01	left
M257 10μm scatter points															
M257-10um- scat@1	2014-12-11 2:42	8.52	12.48	0.13	68729	1.40	-979	-234	36.64	8068	2.90	1.30	0.87	0.01	
M257-10um- scat@2	2014-12-11 3:37	8.56	12.46	0.14	71266	1.59	-1042	-274	34.83	8328	1.09	1.43	0.89	0.01	
M257-10um- scat@3	2014-12-11 4:31	8.53	12.47	0.12	68464	1.31	-1050	-335	36.09	8026	2.35	1.24	0.86	0.01	
M257-10um- scat@4	2014-12-11 5:26	8.06	12.51	0.11	66228	1.67	-1118	-317	39.45	8221	5.71	1.09	0.88	0.01	
M257-10um- scat@5	2014-12-11 6:21	8.55	12.47	0.12	66891	2.08	-1155	-322	36.13	7826	2.39	1.21	0.84	0.02	

M257-10um- scat@6	2014-12-11 7:16	8.16	12.46	0.13	65689	1.48	-1203	-319	35.13	8046	1.39	1.31	0.86	0.01
M257-10um- scat@7	2014-12-11 8:11	8.07	12.47	0.10	67954	1.27	-1140	-278	35.76	8422	2.02	1.03	0.90	0.01
M257-10um- scat@8	2014-12-11 9:06	8.20	12.45	0.12	67407	1.46	-1183	-281	34.42	8221	0.68	1.18	0.88	0.01
M257-10um- scat@9	2014-12-11 10:00	8.46	12.45	0.11	70196	1.61	-1242	-302	33.72	8294	-0.02	1.06	0.89	0.01
M257-10um- scat@10	2014-12-11 10:55	8.70	12.48	0.11	73510	1.35	-1106	-239	36.41	8452	2.67	1.06	0.91	0.01
M257-10um- scat@11	2014-12-11 11:50	8.01	12.48	0.10	62352	1.14	-1163	-248	36.95	7785	3.21	0.96	0.84	0.01
M257-10um- scat@12	2014-12-11 12:45	8.17	12.46	0.13	64544	1.72	-1212	-261	35.00	7900	1.26	1.34	0.85	0.01
M257-10um- scat@13	2014-12-11 13:53	6.44	12.49	0.12	48922	1.86	-1007	-185	37.06	7600	3.32	1.23	0.82	0.02
M257-10um- scat@14	2014-12-11 14:48	5.94	12.45	0.14	41833	1.68	-846	-99	34.17	7044	0.43	1.43	0.76	0.01
M257 10µm line test														
M257-10um-line@1	2014-12-16 18:33	5.77	12.49	0.12	38851	1.31	-118	-208	37.76	6732	0.40	1.17	0.83	0.01
M257-10um-line@2	2014-12-16 18:47	5.88	12.53	0.12	39478	1.36	-202	-213	40.43	6714	3.07	1.22	0.83	0.01
M257-10um-line@3	2014-12-16 19:41	5.97	12.51	0.10	40603	1.37	45	-149	38.89	6799	1.53	0.99	0.84	0.01
M257-10um-line@4	2014-12-16 20:35	6.11	12.53	0.13	41946	1.49	57	-286	40.40	6863	3.04	1.26	0.85	0.01
M257-10um-line@5	2014-12-16 21:43	6.15	12.53	0.15	42766	1.45	94	-219	41.10	6949	3.74	1.53	0.86	0.01
M257-10um-line@6	2014-12-16 22:38	6.16	12.50	0.12	43007	1.52	-5	-236	38.48	6986	1.12	1.16	0.86	0.01
M257-10um-line@7	2014-12-16 23:46	6.28	12.49	0.14	44405	1.58	-154	-362	37.45	7068	0.09	1.42	0.87	0.01
M257 10µm Rim effect														
M257-1109-10um- test@1	2014-11-9 16:34	13.94	12.46	0.07	74278	1.79	-873	-456	35.33	5330	-4.87	0.72	0.69	0.01
M257-1109-10um- test@2	2014-11-9 16:45	13.91	12.50	0.07	96294	1.35	-866	-457	38.30	6924	-1.90	0.72	0.90	0.01
M257-1109-10um- test@3	2014-11-9 16:56	13.95	12.48	0.07	93199	1.17	-857	-456	36.87	6683	-3.34	0.66	0.86	0.01
M257-1109-10um- test@4	2014-11-9 17:07	13.92	12.50	0.07	87443	1.51	-848	-456	38.43	6283	-1.78	0.69	0.81	0.01
M257-1109-10um- test@5	2014-11-9 17:18	13.89	12.53	0.10	74421	2.02	-837	-456	40.52	5358	0.31	1.02	0.69	0.01
M257-1109-10um- test@6	2014-11-9 17:36	13.93	12.40	0.10	118277	0.20	-842	-456	29.70	8488	-10.51	0.95	1.10	0.00
M257-1109-10um- test@7	2014-11-9 17:47	13.86	12.39	0.07	125068	0.36	-862	-458	29.20	9022	-11.01	0.71	1.17	0.00
M257-1109-10um@8	2014-11-9 16:02	13.94	12.40	0.10	124986	0.33	-457	-362	29.79	8964	-10.42	0.98	1.16	0.00
M257-1109-10um@9	2014-11-9 16:18	13.96	12.40	0.08	115860	0.54	-534	-390	30.23	8301	-9.98	0.83	1.07	0.01
M257 20µm scatter points														
M257_20nA@1-1	2014-11-7 16:11	23.16	12.38	0.05	122496	0.62	3549	-153	28.09	5290	0.84	0.45	2.08	0.01
M257_20nA@2	2014-11-7 16:30	23.82	12.39	0.05	123091	0.50	3297	-124	29.09	5168	1.83	0.48	2.03	0.01
M257_20nA@3	2014-11-7 16:50	23.69	12.44	0.06	124103	0.57	3931	-751	33.23	5239	5.97	0.56	2.06	0.01
M257_20nA@4	2014-11-7 18:06	23.75	12.37	0.05	124805	0.49	3991	-826	27.71	5254	0.45	0.48	2.07	0.01
M257_20nA@5	2014-11-7 18:25	23.61	12.39	0.05	128991	0.53	4072	-904	29.20	5463	1.94	0.46	2.15	0.01
M257_20nA@6	2014-11-7 18:44	23.62	12.37	0.04	130276	0.49	4137	-993	27.18	5515	-0.08	0.45	2.17	0.01
M257_20nA@7	2014-11-7 20:01	23.67	12.41	0.05	128752	0.47	4220	-1078	31.00	5439	3.74	0.54	2.14	0.01

Nist-614 20μm rim points														
NIST614_20nA@1	2014-11-7 17:09	23.76	12.52	0.06	87182	0.93	-836	702	39.92	3670	12.66	0.56	0.59	0.01
NIST614_20nA@2	2014-11-7 17:28	23.76	12.47	0.06	85896	0.92	-957	657	36.06	3615	8.80	0.56	0.58	0.01
NIST614_20nA@3	2014-11-7 17:47	23.81	12.49	0.05	86219	0.90	-1061	635	37.82	3622	10.56	0.54	0.58	0.01
NIST614_20nA@4	2014-11-7 19:03	23.74	12.48	0.06	84873	0.90	-1167	693	36.45	3575	9.20	0.62	0.58	0.01
NIST614_20nA@5	2014-11-7 19:22	23.73	12.52	0.06	85663	0.90	-1220	768	39.73	3610	12.47	0.59	0.58	0.01
NIST614_20nA@6	2014-11-7 19:41	23.72	12.49	0.05	84613	0.85	-1237	851	37.10	3568	9.84	0.49	0.57	0.00

Appendix Table xiii. *In situ* Li analysis of three zircon standards

Name	Time	IP	^{7}Li	$^{7}Li/^{6}Li$	X Position	Y Position	distance to rim	$\delta^{7}Li_{m}$ (‰)	$\delta^{7}Li_{corr}$ (‰)	1se	Li (ppm)	1se
Plesovice zircon 20µm												
PlesoviceR@01	19-Sep-13	26.2	210770	12.249	-742.0	-2913	63	17.5	3.1	1.1	1.29	0.02
PlesoviceR@02	19-Sep-13	26.0	121638	12.225	-952.0	-2961	243	15.5	1.1	1.4	0.75	0.01
PlesoviceR@03	19-Sep-13	25.6	111673	12.253	-1147.0	-3003	401	17.7	3.4	1.2	0.70	0.00
PlesoviceR@04	19-Sep-13	25.4	107004	12.231	-1369.0	-3065	533	16.0	1.6	1.2	0.68	0.00
PlesoviceR@05	19-Sep-13	25.3	102709	12.241	-1570.0	-3139	502	16.8	2.5	1.5	0.65	0.00
PlesoviceR@06	19-Sep-13	25.2	111188	12.236	-1786.0	-3215	451	16.4	2.1	1.2	0.71	0.00
PlesoviceR@07	19-Sep-13	24.8	94878	12.250	-1968.0	-3480	391	17.6	3.2	1.2	0.62	0.00
PlesoviceR@08	19-Sep-13	24.6	99356	12.248	-2134.0	-3592	284	17.3	3.0	1.5	0.65	0.00
PlesoviceR@09	19-Sep-13	24.7	115634	12.235	-2269.0	-3724	213	16.3	1.9	1.3	0.75	0.01
PlesoviceR@10	19-Sep-13	24.4	203814	12.229	-2449.0	-3796	50	15.8	1.5	1.3	1.34	0.01
PlesoviceR@12	19-Sep-13	24.5	138308	12.174	-1521.0	-3884	66	11.3	-3.1	1.3	0.91	0.01
PlesoviceR@13	19-Sep-13	24.2	95685	12.237	-1558.0	-3661	292	16.5	2.1	1.3	0.64	0.00
PlesoviceR@14	19-Sep-13	24.2	95974	12.240	-1586.0	-3507	449	16.7	2.3	1.5	0.64	0.00
PlesoviceR@15	19-Sep-13	24.1	96872	12.228	-1614.0	-3348	610	15.7	1.3	1.4	0.64	0.00
PlesoviceR@16	19-Sep-13	23.8	93667	12.218	-1660.0	-3030	365	14.9	0.6	1.3	0.63	0.00
PlesoviceR@17	19-Sep-13	23.7	94173	12.224	-1721.0	-2902	223	15.4	1.1	1.3	0.64	0.00
PlesoviceR@18	19-Sep-13	23.7	289645	12.139	-1745.0	-2726	54	8.3	-6.0	1.0	1.96	0.02
PlesoviceR@19	20-Sep-13	24.7	112660	12.197	-813.0	-2920	121	13.1	3.6	1.1	0.78	0.00
PlesoviceR@21	20-Sep-13	24.7	124256	12.183	-2332.0	-3751	153	12.0	2.5	1.1	0.86	0.01
PlesoviceR@22	20-Sep-13	24.2	102347	12.177	-2377.0	-3767	115	11.5	2.0	1.3	0.73	0.00

PlesoviceR@23	20-Sep-13	23.8	242085	12.133	-1539.0	-3804	148	7.8	-1.7	1.4	1.75	0.03
PlesoviceR@24	20-Sep-13	23.7	95779	12.198	-1733.0	-2820	144	13.2	3.7	1.2	0.69	0.00
PlesoviceR@25	20-Sep-13	23.9	316495	12.101	-1573.0	-2618	54	5.2	-4.3	1.0	2.28	0.01
plesoviceRr@1	22-Sep-13	28.6	263772	12.418	-969.0	-3445	51	31.5	0.2	0.7	1.21	0.01
plesoviceRr@11	22-Sep-13	28.6	188051	12.424	-1142.0	-2547	123	32.0	0.6	0.8	0.86	0.01
plesoviceRr@12	23-Sep-13	28.6	174390	12.422	-1168.0	-2659	216	31.9	0.5	0.9	0.80	0.01
plesoviceRr@13	23-Sep-13	28.4	169513	12.424	-1239.0	-2738	298	32.0	0.7	0.8	0.78	0.01
plesoviceRr@14	23-Sep-13	28.4	160809	12.430	-1325.0	-2838	380	32.5	1.2	0.8	0.74	0.01
plesoviceRr@15	23-Sep-13	28.4	150674	12.432	-1414.0	-2956	419	32.7	1.3	0.9	0.69	0.01
plesoviceRr@16	23-Sep-13	28.4	147981	12.426	-1839.0	-3591	408	32.2	0.8	0.9	0.68	0.01
plesoviceRr@17	23-Sep-13	28.4	133632	12.443	-1937.0	-3759	238	33.6	2.3	1.0	0.62	0.01
plesoviceRr@18	23-Sep-13	28.3	196947	12.428	-1985.0	-3872	134	32.3	1.0	0.8	0.91	0.01
plesoviceRr@19	23-Sep-13	28.3	160178	12.432	-1862.0	-3020	291	32.7	1.4	0.7	0.74	0.01
plesoviceRr@2	22-Sep-13	28.6	155662	12.444	-1655.0	-3206	527	33.6	2.3	0.9	0.71	0.01
plesoviceRr@20	23-Sep-13	28.3	179207	12.436	-1950.0	-2930	181	33.0	1.6	0.8	0.83	0.01
plesoviceRr@21	23-Sep-13	28.3	314176	12.407	-2074.0	-2872	50	30.6	-0.7	0.6	1.45	0.01
plesoviceRr@22	23-Sep-13	28.3	152880	12.431	-1347.0	-3397	413	32.5	1.2	0.8	0.71	0.01
plesoviceRr@23	23-Sep-13	28.3	162642	12.432	-1256.0	-3545	268	32.6	1.3	1.0	0.75	0.01
plesoviceRr@24	23-Sep-13	28.2	184384	12.428	-1177.0	-3686	136	32.4	1.0	0.8	0.85	0.01
plesoviceRr@3	22-Sep-13	28.7	148962	12.434	-1748.0	-3400	560	32.8	1.5	1.0	0.68	0.01
plesoviceRr@4	22-Sep-13	28.7	159102	12.443	-1763.0	-3081	370	33.6	2.2	0.8	0.73	0.01
plesoviceRr@5	22-Sep-13	28.7	149116	12.433	-1522.0	-3035	428	32.7	1.4	0.7	0.68	0.01
plesoviceRr@6	22-Sep-13	28.7	145512	12.432	-1474.0	-3270	582	32.7	1.3	0.9	0.66	0.00
plesoviceRr@7	22-Sep-13	28.6	404871	12.288	-2021.0	-3961	43	20.7	-10.7	0.7	1.85	0.01
plesoviceRr@8	22-Sep-13	28.7	341950	12.411	-2194.0	-3153	53	30.9	-0.4	0.6	1.56	0.01
plesoviceRr@9	22-Sep-13	28.6	236802	12.432	-1109.0	-2464	44	32.7	1.3	0.6	1.08	0.01
plesoviceRrr@1	23-Sep-13	28.2	155297	12.407	-754.0	-2873	46	30.6	-0.8	0.8	0.72	0.00
plesoviceRrr@14	23-Sep-13	27.8	136848	12.417	-1602.0	-3690	274	31.4	0.0	0.9	0.64	0.01

plesoviceRrr@2	23-Sep-13	28.2	98959	12.412	-954.0	-2926	231	31.0	-0.4	0.9	0.46	0.00
plesoviceRrr@3	23-Sep-13	28.2	108359	12.413	-1149.0	-2966	404	31.1	-0.3	0.9	0.50	0.00
plesoviceRrr@4	23-Sep-13	28.1	114031	12.415	-1374.0	-3029	501	31.3	-0.1	0.9	0.53	0.00
plesoviceRrr@6	23-Sep-13	28.1	116050	12.423	-1983.0	-3442	362	31.9	0.6	1.0	0.54	0.00
plesoviceRrr@7	23-Sep-13	28.0	112981	12.429	-2127.0	-3551	274	32.4	1.0	1.1	0.53	0.00
plesoviceRrr@8	23-Sep-13	27.9	370120	12.396	-1589.0	-3813	152	29.7	-1.7	0.6	1.74	0.04
10µm												
pleoviceR-1@1	9-Nov-14	11.1	478693	12.460	-1617.0	-2052	1	35.1	-4.0	0.5	5.99	0.01
pleoviceR-1@10	9-Nov-14	11.0	282158	12.510	-1565.0	-2132	6	38.7	-0.4	0.6	3.57	0.03
pleoviceR-1@2	9-Nov-14	10.7	179879	12.470	-1633.0	-2078	14	35.7	-3.5	0.7	2.34	0.02
pleoviceR-1@4	9-Nov-14	10.7	91948	12.530	-1667.0	-2134	45	40.7	1.6	0.8	1.19	0.02
pleoviceR-1@5	9-Nov-14	10.8	82369	12.480	-1693.0	-2162	64	36.7	-2.5	0.9	1.06	0.02
pleoviceR-1@6	9-Nov-14	10.8	78470	12.500	-1714.0	-2192	82	38.3	-0.8	0.8	1.02	0.02
pleoviceR-1@7	9-Nov-14	10.8	237264	12.480	-1646.0	-2045	8	36.5	-2.7	0.6	3.06	0.03
pleoviceR-1@8	9-Nov-14	10.8	348590	12.490	-1590.0	-2092	2	37.2	-1.9	0.6	4.48	0.04
pleoviceR-1@9	9-Nov-14	10.8	126592	12.470	-1606.0	-2116	16	35.5	-3.6	0.7	1.63	0.01
plesoviceR-2@1	9-Nov-14	11.0	465114	12.500	-1402.0	-2310	12	37.9	-1.3	0.5	5.86	0.04
plesoviceR-2@10	9-Nov-14	14.5	95911	12.530	-1455.0	-2320	64	41.2	0.6	0.9	0.82	0.02
plesoviceR-2@2	9-Nov-14	11.0	336248	12.460	-1417.0	-2310	26	35.2	-4.0	0.6	4.25	0.04
plesoviceR-2@3	9-Nov-14	11.0	102383	12.450	-1441.0	-2316	50	34.2	-5.0	0.8	1.29	0.01
plesoviceR-2@4	9-Nov-14	10.8	94159	12.520	-1475.0	-2320	84	39.9	0.7	0.8	1.21	0.02
plesoviceR-2@5	9-Nov-14	10.7	84211	12.510	-1501.0	-2325	111	38.7	-0.5	0.8	1.09	0.01
plesoviceR-2@6	9-Nov-14	10.7	75106	12.520	-1530.0	-2330	140	40.3	1.1	1.1	0.98	0.01
plesoviceR-2@7	9-Nov-14	9.2	62293	12.500	-1563.0	-2338	174	38.4	-0.7	1.0	0.94	0.01
plesoviceR-2@8	9-Nov-14	9.3	52786	12.500	-1604.0	-2341	215	38.6	-0.5	2.2	0.79	0.02
plesoviceR-2@9	9-Nov-14	6.1	36268	12.510	-1650.0	-2351	262	39.3	0.1	2.3	0.83	0.01
plesoviceR-3@1	9-Nov-14	14.5	248706	12.470	-1668.0	-2837	14	35.7	-4.7	0.6	2.14	0.03
plesoviceR-3@2	9-Nov-14	14.5	149927	12.550	-1692.0	-2829	27	42.1	1.7	0.5	1.29	0.03

plesoviceR-3@3	9-Nov-14	14.4	125453	12.540	-1715.0	-2823	38	41.7	1.3	0.8	1.09	0.03
plesoviceR-3@4	9-Nov-14	14.3	114292	12.530	-1744.0	-2810	54	40.7	0.3	0.8	0.99	0.02
plesoviceR-3@5	9-Nov-14	14.3	105349	12.510	-1768.0	-2797	68	39.1	-1.3	0.8	0.92	0.02
plesoviceR-3@6	9-Nov-14	14.3	101794	12.510	-1794.0	-2784	83	39.4	-1.0	1.1	0.89	0.02
plesoviceR-4@1	9-Nov-14	14.2	674636	12.470	-1827.0	-1815	3	36.1	-4.4	0.3	6.14	0.03
plesoviceR-4@2	9-Nov-14	14.1	284321	12.500	-1831.0	-1836	21	38.4	-2.2	0.5	2.60	0.04
plesoviceR-4@3	9-Nov-14	14.0	115309	12.520	-1836.0	-1860	46	39.6	-1.0	0.9	1.06	0.02
plesoviceR-4@4	9-Nov-14	14.0	101676	12.550	-1843.0	-1883	70	42.2	1.6	0.6	0.94	0.02
plesoviceR-4@5	9-Nov-14	14.0	129660	12.540	-1850.0	-1908	96	42.0	1.5	0.7	1.20	0.03
plesoviceR-4@6	9-Nov-14	14.0	122134	12.520	-1856.0	-1931	119	39.6	-1.0	0.9	1.13	0.02
plesoviceR-4@7	9-Nov-14	13.9	123904	12.540	-1869.0	-1988	178	41.3	0.7	0.8	1.15	0.03
plesoviceR-4@8	9-Nov-14	13.9	116122	12.540	-1878.0	-2018	209	42.0	1.5	0.8	1.08	0.02
plesoviceR-4@9	9-Nov-14	13.9	110220	12.530	-1886.0	-2053	245	41.1	0.6	0.9	1.03	0.02
plesoviceR-5@01	9-Nov-14	13.6	574841	12.530	-3035.0	-2622	9	40.5	-0.1	0.5	5.48	0.09
plesoviceR-5@02	9-Nov-14	13.6	616352	12.520	-3060.0	-2676	9	40.3	-0.2	0.5	5.83	0.11
plesoviceR-5@03	9-Nov-14	13.7	701826	12.510	-3087.0	-2735	9	38.7	-1.8	0.4	6.61	0.11
plesoviceR-5@04	9-Nov-14	13.7	605562	12.520	-3119.0	-2802	7	39.6	0.5	0.3	6.08	0.12
plesoviceR-5@05	9-Nov-14	13.7	169846	12.520	-3016.0	-2644	23	40.2	1.1	0.6	1.71	0.03
plesoviceR-5@06	10-Nov-14	13.7	105128	12.540	-2988.0	-2658	38	41.8	2.7	0.7	1.06	0.03
plesoviceR-5@07	10-Nov-14	13.7	95170	12.550	-2960.0	-2675	54	42.2	3.1	0.7	0.95	0.02
plesoviceR-5@08	10-Nov-14	13.7	85957	12.540	-2934.0	-2688	69	41.7	2.6	0.7	0.87	0.02
plesoviceR-5@09	10-Nov-14	13.6	87993	12.530	-2902.0	-2704	87	40.7	1.6	1.1	0.89	0.02
plesoviceR-5@11	10-Nov-14	13.6	411067	12.550	-3068.0	-2712	13	42.3	3.3	0.4	4.17	0.09
plesoviceR-5@12	10-Nov-14	13.6	282695	12.510	-3088.0	-2777	17	38.9	-0.2	0.7	2.85	0.05
plesoviceR-5@13	10-Nov-14	13.6	464587	12.530	-3133.0	-2844	10	41.2	2.1	0.6	4.69	0.09
plesoviceR-5@14	10-Nov-14	13.6	122537	12.520	-3039.0	-2715	26	40.2	1.1	0.8	1.24	0.03
plesoviceR-5@15	10-Nov-14	13.6	117132	12.540	-3037.0	-2775	39	41.6	2.6	0.9	1.19	0.03
plesoviceR-5@16	10-Nov-14	13.5	854220	12.400	-3316.0	-3211	0	30.2	-8.9	0.5	8.70	0.02

plesoviceR-5@17	10-Nov-14	13.6	674842	12.430	-2860.0	-2179	0	32.5	-6.6	0.5	6.85	0.02
5µm												
PlesoviceR_5um@1	26-Sep-13	0.8	79930	12.392	-1534.0	-2792	3	29.3	0.9	1.6	10.06	0.04
PlesoviceR_5um@10	26-Sep-13	0.9	13565	12.416	-1561.0	-2828	45	31.3	2.9	2.3	1.62	0.01
PlesoviceR_5um@17	26-Sep-13	0.9	10591	12.413	-1582.0	-2856	80	31.1	2.6	2.9	1.27	0.02
PlesoviceR_5um@2	26-Sep-13	0.8	60544	12.404	-1537.0	-2796	5	30.3	1.9	1.6	7.68	0.03
PlesoviceR_5um@8	26-Sep-13	0.9	22355	12.406	-1555.0	-2820	35	30.5	2.0	1.9	2.71	0.02
PlesoviceR_5um@9	26-Sep-13	0.9	17086	12.402	-1558.0	-2824	40	30.1	1.7	2.8	2.04	0.01
PleR-2-5um@01	17-Nov-14	0.5	15273	12.520	-1329.0	-2448	18	40.3	3.3	1.5	5.14	0.04
PleR-2-5um@02	17-Nov-14	0.5	11543	12.490	-1336.0	-2448	23	37.3	0.3	1.7	3.91	0.03
PleR-2-5um@03	17-Nov-14	0.5	8635	12.520	-1343.0	-2448	28	39.8	2.8	1.7	2.91	0.03
PleR-2-5um@04	17-Nov-14	0.5	8102	12.460	-1350.0	-2448	34	35.0	-2.0	1.5	2.70	0.02
PleR-2-5um@05	17-Nov-14	0.5	2345	12.480	-1384.0	-2458	65	36.4	-0.6	3.3	0.79	0.01
PleR-2-5um@06	17-Nov-14	0.5	2437	12.430	-1391.0	-2458	72	32.1	-4.9	3.1	0.82	0.01
PleR-2-5um@07	17-Nov-14	0.5	3776	12.480	-1398.0	-2458	79	36.8	-0.2	3.1	1.28	0.01
PleR-2-5um@08	17-Nov-14	0.5	3289	12.520	-1405.0	-2458	86	40.3	3.3	3.3	1.10	0.01
PleR-2-5um@12	17-Nov-14	0.5	2704	12.490	-1433.0	-2458	114	37.6	0.6	3.0	0.95	0.01
PleR-2-5um@13	17-Nov-14	0.5	2977	12.450	-1440.0	-2458	121	33.7	-3.3	2.8	1.04	0.01
PleR-2-5um@14	17-Nov-14	0.5	2557	12.480	-1447.0	-2458	128	36.7	-0.4	3.4	0.89	0.01
PleR-2b-5um@01	18-Nov-14	0.8	27373	12.490	-1319.0	-2463	0	37.1	0.1	1.2	5.46	0.03
PleR-2b-5um@02	18-Nov-14	0.8	27701	12.500	-1326.0	-2463	7	38.0	1.0	1.2	5.70	0.04
PleR-2b-5um@03	18-Nov-14	0.8	17305	12.450	-1333.0	-2463	14	33.9	-3.1	1.2	3.61	0.02
PleR-2b-5um@04	18-Nov-14	0.7	12336	12.480	-1340.0	-2463	21	36.8	-0.2	1.5	2.68	0.02
PleR-2b-5um@06	18-Nov-14	0.7	4262	12.390	-1375	-2463	56	29.5	-7.5	2.0	1.00	0.01
PleR-2b-5um@07	18-Nov-14	0.6	2836	12.440	-1382	-2463	63	33.6	-3.4	3.0	0.70	0.01
PleR-2b-5um@10	18-Nov-14	0.6	3458	12.470	-1398	-2468	79	35.8	-1.2	2.8	0.97	0.01
PleR-2b-5um@11	18-Nov-14	0.6	3853	12.440	-1405	-2468	86	32.9	-4.1	2.7	1.10	0.01

PleR-2b-5um@13	18-Nov-14	0.6	3433	12.460	-1419	-2468	100	34.9	-2.1	2.9	0.92	0.01
PleR-2b-5um@14	18-Nov-14	0.6	3695	12.480	-1426	-2468	107	36.9	-0.2	2.8	1.00	0.01
PleR-5-5um@01	17-Nov-14	0.5	20523	12.470	-2976	-2830	3	36.1	-0.9	1.6	7.01	0.04
PleR-5-5um@02	17-Nov-14	0.5	20973	12.480	-2969	-2830	6	36.3	-0.7	1.5	7.23	0.04
PleR-5-5um@03	17-Nov-14	0.5	13504	12.450	-2962	-2830	9	34.5	-2.5	1.7	4.62	0.04
PleR-5-5um@04	17-Nov-14	0.5	13924	12.460	-2955	-2830	13	34.9	-2.1	1.7	4.74	0.03
PleR-5-5um@05	17-Nov-14	0.5	9959	12.480	-2948	-2830	16	36.6	-0.4	2.3	3.37	0.02
PleR-5-5um@06	17-Nov-14	1.0	55960	12.460	-2984	-2869	7	35.3	-1.7	1.2	8.90	0.08
PleR-5-5um@07	17-Nov-14	1.0	38866	12.490	-2977	-2869	10	37.6	0.6	1.4	6.16	0.06
PleR-5-5um@08	17-Nov-14	1.0	22622	12.510	-2970	-2869	14	39.5	2.5	1.7	3.61	0.03
PleR-5-5um@09	17-Nov-14	1.0	20160	12.480	-2963	-2869	17	36.7	-0.3	1.6	3.26	0.03
PleR-5-5um@10	17-Nov-14	1.0	14906	12.490	-2956	-2869	20	37.5	0.5	1.9	2.42	0.02
PleR-5-5um@11	17-Nov-14	1.0	8749	12.500	-2949	-2869	23	38.6	1.6	2.3	1.43	0.01
PleR-5-5um@12	17-Nov-14	1.0	6561	12.400	-2942	-2869	26	29.7	-7.3	2.4	1.08	0.01
PleR-5-5um@13	17-Nov-14	0.9	5754	12.490	-2935	-2869	30	37.6	0.6	1.9	0.97	0.01
PleR-5-5um@14	17-Nov-14	0.9	4668	12.450	-2928	-2869	33	34.3	-2.7	2.7	0.80	0.01
PleR-5-5um@15	17-Nov-14	0.9	4959	12.430	-2921	-2869	36	32.6	-4.4	2.6	0.85	0.01
PleR-5-5um@16	17-Nov-14	0.9	4640	12.480	-2914	-2869	39	36.8	-0.2	2.4	0.83	0.01
PleR-5-5um@17	17-Nov-14	0.9	4040	12.480	-2907	-2869	42	36.4	-0.6	2.5	0.72	0.01
PleR-5-5um@18	18-Nov-14	0.9	4173	12.500	-2900	-2869	46	38.0	1.0	2.6	0.76	0.01
PleR-5-5um@20	18-Nov-14	0.8	3540	12.490	-2886	-2869	52	37.6	0.6	2.8	0.69	0.01
PleR-5-5um@21	18-Nov-14	0.8	4410	12.450	-2890	-2865	49	34.0	-3.0	2.3	0.87	0.01
PleR-5um-1@02	11-Nov-14	1.0	24142	12.440	-1651.0	-2018	1	33.6	-2.3	1.2	4.02	0.01
PleR-5um-1@03	11-Nov-14	0.9	21593	12.370	-1656.0	-2018	3	27.4	-8.5	1.2	3.69	0.01
PleR-5um-1@05	11-Nov-14	0.9	17666	12.420	-1666.0	-2018	7	31.5	-4.4	1.4	3.06	0.02
PleR-5um-1@06	11-Nov-14	0.9	15272	12.310	-1671.0	-2018	9	22.4	-13.5	1.1	2.67	0.02
PleR-5um-1@09	11-Nov-14	0.9	13341	12.380	-1686.0	-2018	14	28.6	-7.3	1.7	2.37	0.02
PleR-5um-1@1	11-Nov-14	1.0	19633	12.450	-1646.0	-2018	1	34.6	-1.4	1.4	3.24	0.01

PleR-5um-1@11	11-Nov-14	0.9	6042	12.300	-1696.0	-2018	18	21.8	-14.1	2.3	1.10	0.00
PleR-5um-1@12	11-Nov-14	0.9	7685	12.420	-1701.0	-2018	20	31.4	-4.5	1.8	1.42	0.01
PleR-5um-1@13	11-Nov-14	0.9	6228	12.470	-1706.0	-2018	22	35.9	0.0	2.0	1.17	0.01
PleR-5um-1@14	11-Nov-14	0.8	4171	12.320	-1711.0	-2018	24	23.4	-12.5	2.4	0.80	0.00
PleR-5um-1@15	11-Nov-14	0.8	2427	12.330	-1716.0	-2018	26	24.2	-11.7	3.5	0.46	0.00
PleR-5um-1@16	11-Nov-14	0.8	5200	12.510	-1721.0	-2018	27	39.3	3.4	2.1	0.99	0.02
PleR-5um-1@17	11-Nov-14	0.8	7788	12.490	-1726.0	-2018	29	37.5	1.6	1.7	1.51	0.02
PleR-5um-1@18	11-Nov-14	0.8	7314	12.420	-1731.0	-2018	31	32.0	-3.9	1.9	1.43	0.01
PleR-5um-3@02	11-Nov-14	1.1	48283	12.430	-1700	-2936	8	32.6	-3.3	0.9	7.32	0.03
PleR-5um-3@03	11-Nov-14	1.0	49765	12.410	-1705	-2936	10	30.8	-5.1	0.9	7.66	0.03
PleR-5um-3@04	11-Nov-14	1.1	44195	12.360	-1710	-2936	12	26.3	-9.6	0.8	6.73	0.02
PleR-5um-3@05	11-Nov-14	1.1	34281	12.360	-1715	-2936	14	27.1	-8.8	1.0	5.23	0.02
PleR-5um-3@06	11-Nov-14	1.0	26863	12.340	-1720	-2936	17	24.6	-11.3	1.1	4.14	0.02
PleR-5um-3@07	11-Nov-14	1.0	17756	12.340	-1725	-2936	19	24.7	-11.2	1.2	2.74	0.02
PleR-5um-3@09	11-Nov-14	1.0	11851	12.330	-1735	-2936	23	23.8	-12.1	1.7	1.84	0.03
PleR-5um-3@1	11-Nov-14	1.1	38746	12.480	-1695	-2936	5	36.8	0.9	1.0	5.85	0.06
PleR-5um-3@10	11-Nov-14	1.0	13518	12.320	-1740	-2936	26	23.1	-12.8	1.5	2.12	0.03
PleR-5um-3@13	11-Nov-14	1.0	13174	12.340	-1755	-2936	33	25.3	-10.6	1.8	2.10	0.03
PleR-5um-3@17	11-Nov-14	1.0	10041	12.340	-1775	-2936	42	24.8	-11.1	1.5	1.65	0.02
PleR-5um-3@18	11-Nov-14	1.0	10123	12.350	-1780	-2936	44	25.6	-10.3	1.9	1.69	0.02
PleR-5um-3@19	11-Nov-14	1.0	12947	12.380	-1785	-2936	46	28.4	-7.5	1.5	2.07	0.02
PleR-5um-5@02	10-Nov-14	1.0	46197	12.480	-3217	-3014	5	36.3	0.4	1.0	7.17	0.06
PleR-5um-5@03	10-Nov-14	1.0	32374	12.500	-3212	-3014	8	38.2	2.3	1.0	4.99	0.03
PleR-5um-5@04	10-Nov-14	1.0	15730	12.510	-3207	-3014	10	38.9	3.0	1.4	2.43	0.02
PleR-5um-5@05	10-Nov-14	1.1	24472	12.490	-3202	-3014	12	37.2	1.4	1.1	3.74	0.03
PleR-5um-5@06	10-Nov-14	1.1	16098	12.440	-3197	-3014	15	33.0	-3.0	1.3	2.46	0.02
PleR-5um-5@07	10-Nov-14	1.0	7739	12.490	-3192	-3014	17	37.1	1.2	2.0	1.19	0.01
PleR-5um-5@08	10-Nov-14	1.1	4872	12.490	-3187	-3014	19	37.8	1.9	2.4	0.74	0.01

PleR-5um-5@09	10-Nov-14	1.0	8768	12.480	-3182	-3014	21	36.8	0.9	1.6	1.35	0.01
PleR-5um-5@1	10-Nov-14	1.0	59950	12.480	-3222	-3014	3	37.0	1.1	0.7	9.49	0.09
PleR-5um-5@10	11-Nov-14	1.0	6748	12.500	-3177	-3014	24	37.9	2.0	2.2	1.04	0.01
PleR-5um-5@11	11-Nov-14	1.1	4625	12.490	-3172	-3014	26	37.7	1.8	2.2	0.70	0.00
PleR-5um-5@12	11-Nov-14	1.1	4104	12.510	-3167	-3014	28	38.7	2.8	2.2	0.62	0.01
PleR-5um-5@13	11-Nov-14	1.1	7267	12.440	-3162	-3014	31	33.3	-2.6	1.9	1.09	0.01
PleR-5um-5@17	11-Nov-14	1.1	6542	12.490	-3142	-3014	40	37.2	1.3	1.9	0.99	0.01
20μm												
PlesoviceL@01	18-Sep-13	24.3	187572	12.254	2572.0	-2792	112	17.9	0.8	0.9	1.11	0.01
PlesoviceL@02	18-Sep-13	24.0	134186	12.263	2308.0	-2851	332	18.6	1.5	1.1	0.80	0.01
PlesoviceL@04	18-Sep-13	23.4	117060	12.263	1751.0	-3017	778	18.6	1.5	1.1	0.72	0.01
PlesoviceL@05	18-Sep-13	22.8	114751	12.255	1427.0	-3150	734	18.0	0.9	1.2	0.72	0.01
PlesoviceL@06	18-Sep-13	22.7	124058	12.248	1150.0	-3273	525	17.4	0.3	1.1	0.79	0.01
PlesoviceL@07	18-Sep-13	22.3	129717	12.263	923.0	-3461	388	18.6	1.5	1.1	0.84	0.01
PlesoviceL@08	18-Sep-13	21.9	176572	12.242	707.0	-3650	262	16.8	-0.3	1.3	1.16	0.01
PlesoviceL@10	18-Sep-13	26.6	219040	12.174	1603.0	-3892	74	11.2	-3.1	1.0	1.32	0.01
PlesoviceL@11	18-Sep-13	26.2	121499	12.247	1575.0	-3676	291	17.3	2.9	1.0	0.74	0.01
PlesoviceL@12	18-Sep-13	25.9	121248	12.235	1549.0	-3446	522	16.3	2.0	1.2	0.75	0.01
PlesoviceL@13	18-Sep-13	25.5	120894	12.237	1499.0	-3234	739	16.4	2.1	1.2	0.76	0.01
PlesoviceL@14	18-Sep-13	24.3	124615	12.248	1432.0	-3020	688	17.4	3.1	1.2	0.82	0.01
PlesoviceL@15	18-Sep-13	24.0	135216	12.230	1380.0	-2836	569	15.8	1.5	1.2	0.90	0.01
PlesoviceL@16	18-Sep-13	23.8	168795	12.217	1322.0	-2626	401	14.8	0.4	1.2	1.14	0.01
PlesoviceL@17	18-Sep-13	23.6	153136	12.225	1271.0	-2436	221	15.4	1.1	1.1	1.04	0.01
PlesoviceL@18	18-Sep-13	23.0	201141	12.197	1221.0	-2264	55	13.1	-1.2	1.0	1.40	0.01
PlesoviceL@22	20-Sep-13	25.5	132937	12.155	1600.0	-3830	135	9.6	-3.6	1.2	0.88	0.01
PlesoviceL@23	20-Sep-13	25.2	196050	12.105	1681.0	-3882	68	5.5	-4.0	1.4	1.34	0.01
PlesoviceL@24	20-Sep-13	25.0	144378	12.183	2485.0	-2803	188	12.0	2.5	1.1	0.99	0.01
PlesoviceL@25	20-Sep-13	24.8	140034	12.139	1339.0	-2676	451	8.3	-1.2	1.2	0.97	0.01

PlesoviceL@26	20-Sep-13	25.0	101691	12.193	1581.0	-3741	226	12.8	3.3	1.4	0.70	0.00
plesoviceLr@1	22-Sep-13	28.7	174600	12.440	1502.0	-3128	794	33.3	2.0	0.9	0.80	0.01
plesoviceLr@3	22-Sep-13	28.7	410604	12.397	2219.0	-2284	100	29.8	-1.6	0.5	1.87	0.01
10µm												
plesoviceL@2	7-Nov-14	13.3	455806	12.470	-159.0	-3371	7	35.5	-3.8	0.4	4.35	0.03
plesoviceL@03	7-Nov-14	13.3	113499	12.540	-126.0	-3341	30	39.0	-0.5	0.9	1.02	0.01
plesoviceL@04	7-Nov-14	13.2	123725	12.520	-81.0	-3310	56	40.3	1.0	0.6	1.19	0.03
plesoviceL@05	7-Nov-14	13.2	129222	12.530	-37.0	-3281	82	40.8	1.5	0.6	1.25	0.03
plesoviceL@06	8-Nov-14	13.1	125910	12.530	-7.0	-3238	108	41.2	1.9	0.6	1.22	0.03
plesoviceL@07	8-Nov-14	13.2	118761	12.520	25.0	-3199	133	40.3	1.0	0.6	1.15	0.02
plesoviceL@08	8-Nov-14	13.1	112714	12.530	57.0	-3157	159	40.6	1.3	0.4	1.10	0.02
plesoviceL@09	8-Nov-14	13.1	107360	12.520	90.0	-3110	187	40.1	0.8	0.6	1.05	0.02
plesoviceL@10	8-Nov-14	12.2	93803	12.540	127.0	-3066	216	41.2	1.9	0.5	0.98	0.02
plesoviceL@11	8-Nov-14	12.1	87156	12.540	166.0	-3023	245	41.8	2.5	0.7	0.92	0.02
plesoviceL@12	8-Nov-14	12.0	83450	12.520	204.0	-2967	278	40.1	0.8	0.6	0.88	0.02
plesoviceL@13	8-Nov-14	11.9	76871	12.530	250.0	-2928	308	40.8	1.5	0.7	0.82	0.02
plesoviceL@14	8-Nov-14	11.1	70381	12.530	303.0	-2882	343	40.6	1.3	0.7	0.81	0.01
plesoviceL@15	8-Nov-14	11.0	69004	12.510	344.0	-2833	375	39.4	0.1	0.7	0.80	0.02
plesoviceL@16	8-Nov-14	11.1	63680	12.530	394.0	-2792	407	41.1	1.8	0.7	0.73	0.01
plesoviceL@17	8-Nov-14	10.4	62557	12.520	441.0	-2745	440	39.6	0.3	0.6	0.77	0.01
plesoviceL@2-1	8-Nov-14	12.4	174812	12.460	-151.0	-3391	3	35.0	-4.5	0.9	1.75	0.01
plesoviceL-2@1	8-Nov-14	12.4	101300	12.510	-122.0	-3358	25	39.0	-0.5	0.9	1.02	0.01
plesoviceL-2@7	8-Nov-14	12.2	136148	12.520	-110.0	-3108	117	40.2	1.1	1.0	1.56	0.03
plesoviceL-3@1	8-Nov-14	12.1	158739	12.410	711.0	-3402	10	31.2	-8.0	0.7	1.82	0.02
plesoviceL-3@2	8-Nov-14	12.1	110898	12.520	706.0	-3364	29	39.8	0.6	0.9	1.27	0.03
plesoviceL-3@3	8-Nov-14	12.1	93767	12.520	700.0	-3320	51	39.9	0.8	0.8	1.07	0.03
plesoviceL-3@4	8-Nov-14	12.1	83510	12.540	691.0	-3279	72	41.4	2.2	0.8	0.96	0.02
plesoviceL-3@5	8-Nov-14	12.1	68191	12.520	683.0	-3226	99	40.0	0.8	1.2	0.78	0.01

plesoviceL-3@6	8-Nov-14	12.1	64456	12.540	673.0	-3182	122	41.5	2.3	1.0	0.74	0.01
plesoviceL-3@7	8-Nov-14	12.1	67773	12.530	665.0	-3131	147	40.5	1.3	0.9	0.78	0.01
plesoviceL-3@8	8-Nov-14	12.1	65556	12.550	662.0	-3079	173	42.8	3.6	1.1	0.76	0.01
plesoviceL-2@9	8-Nov-14	12.4	964952	12.420	-338.0	-3104	6	32.0	-7.2	0.6	10.80	0.06
plesoviceL-2@12	8-Nov-14	12.4	104244	12.530	-67.0	-3108	138	40.5	1.4	1.0	1.17	0.02
plesoviceL-2@13	8-Nov-14	12.4	97082	12.510	-18.0	-3106	161	39.1	-0.1	0.8	1.09	0.02
plesoviceL-2@14	8-Nov-14	12.5	86742	12.540	38.0	-3130	191	41.5	2.3	0.7	0.97	0.02
plesoviceL-2@15	8-Nov-14	12.5	83585	12.540	99.0	-3132	221	42.0	2.8	0.7	0.93	0.02
plesoviceL-3@9	8-Nov-14	12.5	153798	12.430	683.0	-3400	13	32.8	-6.4	0.8	1.71	0.03
plesoviceL-3@10	9-Nov-14	12.5	108942	12.500	656.0	-3388	21	38.7	-0.5	0.8	1.21	0.02
plesoviceL-3@11	9-Nov-14	12.5	103299	12.510	743.0	-3379	19	38.7	-0.4	0.6	1.15	0.02
plesoviceL-3@12	9-Nov-14	12.5	88616	12.500	762.0	-3362	26	38.2	-1.0	0.8	0.99	0.01
plesoviceL-3@13	9-Nov-14	12.6	63266	12.520	660.0	-3032	197	40.4	1.2	0.8	0.70	0.01
plesoviceL-3@14	9-Nov-14	12.5	264590	12.420	376.0	-3463	4	31.3	-7.9	0.5	2.95	0.04
plesoviceL-3@15	9-Nov-14	12.5	212621	12.430	436.0	-3450	6	32.7	-6.5	1.3	2.37	0.04
plesoviceL-3@16	9-Nov-14	12.5	543611	12.460	496.0	-3439	7	34.7	-4.4	0.5	6.05	0.02
plesoviceL-3@17	9-Nov-14	12.5	131460	12.490	551.0	-3428	9	37.6	-1.5	0.6	1.46	0.02
plesoviceL-3@18	9-Nov-14	12.5	162154	12.430	609.0	-3426	6	32.2	-7.0	0.9	1.81	0.01
plesoviceL4-1@1	9-Nov-14	12.5	747840	12.440	1678.0	-1866	5	33.2	-6.0	0.4	8.32	0.01
plesoviceL4-1@02	9-Nov-14	12.5	419075	12.480	1649.0	-1847	9	36.6	-2.6	0.5	4.67	0.04
plesoviceL4-1@04	9-Nov-14	12.3	344955	12.500	1663.0	-1876	13	38.0	-1.1	0.5	3.91	0.04
plesoviceL4-1@05	9-Nov-14	12.3	186208	12.450	1637.0	-1866	19	34.1	-5.0	0.6	2.11	0.02
plesoviceL4-1@06	9-Nov-14	12.2	363833	12.490	1654.0	-1899	25	37.3	-1.9	0.7	4.14	0.05
plesoviceL4-1@07	9-Nov-14	12.2	477763	12.500	1673.0	-1926	27	38.3	-0.9	1.2	5.44	0.18
plesoviceL4-1@08	9-Nov-14	12.2	189827	12.490	1643.0	-1922	37	37.5	-1.7	0.4	2.16	0.04
plesoviceL4-1@09	9-Nov-14	12.2	129972	12.510	1661.0	-1952	40	38.9	-0.3	0.7	1.48	0.02
plesoviceL4-1@10	9-Nov-14	12.2	190272	12.460	1578.0	-1797	17	35.3	-3.9	0.5	2.17	0.02
plesoviceL4-1@11	9-Nov-14	12.2	118216	12.520	1702.0	-1999	42	39.9	0.8	0.9	1.35	0.02

plesoviceL4-1@12	9-Nov-14	12.1	113478	12.520	1596.0	-1954	65	39.9	0.7	0.8	1.31	0.02
plesoviceL4-1@13	9-Nov-14	12.1	99397	12.510	1561.0	-1996	92	39.2	0.0	0.8	1.15	0.02
plesoviceL4-1@14	9-Nov-14	12.0	84936	12.520	1518.0	-2029	119	39.9	0.7	1.0	0.98	0.02
plesoviceL4-1@15	9-Nov-14	12.0	73224	12.540	1483.0	-2075	147	41.4	2.3	1.9	0.85	0.01
plesoviceL4-1@16	9-Nov-14	11.2	69644	12.540	1446.0	-2120	176	41.5	2.4	1.0	0.87	0.01
plesoviceL4-1@17	9-Nov-14	11.2	67333	12.520	1412.0	-2156	201	39.8	0.6	0.9	0.84	0.01
plesoviceL4-1@18	9-Nov-14	11.2	442280	12.470	1769.0	-1972	8	35.7	-3.5	0.5	5.51	0.03
plesoviceL-5@1	9-Nov-14	14.4	783834	12.450	-48.0	-3533	1	33.9	-6.6	0.7	7.00	0.05
plesoviceL-5@2	9-Nov-14	14.5	230975	12.490	-39.0	-3497	38	37.4	-3.1	0.6	2.06	0.03
plesoviceL-5@3	9-Nov-14	14.4	172399	12.530	-27.0	-3453	84	40.5	-0.1	0.8	1.55	0.04
plesoviceL-5@4	9-Nov-14	14.5	127721	12.540	-17.0	-3414	124	41.8	1.3	0.7	1.14	0.03
plesoviceL-5@5	9-Nov-14	14.2	117789	12.550	-5.0	-3342	197	42.2	1.6	0.9	1.07	0.02
plesoviceL-5@6	9-Nov-14	14.1	112782	12.540	3.0	-3296	243	41.7	1.1	0.7	1.03	0.02
plesoviceL-5@7	9-Nov-14	14.2	111259	12.540	2.0	-3262	277	41.7	1.1	0.8	1.01	0.02
plesoviceL-5@8	9-Nov-14	14.1	108327	12.560	17.0	-3220	321	43.7	3.1	0.9	0.99	0.02
Ple_L_a@1	16-Dec-14	5.9	335136	12.412	2328	-1459	3	31.0	-6.4	0.5	6.97	0.05
Ple_L_a@2	16-Dec-14	5.9	139412	12.461	2314	-1473	20	35.1	-2.3	0.6	2.90	0.03
Ple_L_a@3	16-Dec-14	5.9	105056	12.461	2304	-1485	35	35.0	-2.3	0.8	2.18	0.03
Ple_L_a@4	16-Dec-14	6.0	105128	12.448	2298	-1493	45	34.0	-3.4	0.8	2.15	0.02
Ple_L_a@5	16-Dec-14	6.0	124447	12.397	2293	-1500	54	29.7	-7.7	0.7	2.54	0.02
Ple_L_a@6	16-Dec-14	6.1	244184	12.427	580	-3162	3	32.2	-5.1	0.5	4.96	0.05
Ple_L_a@7	16-Dec-14	6.1	99514	12.428	584	-3148	15	32.3	-5.1	1.0	2.00	0.01
Ple_L_a@8	16-Dec-14	6.1	45901	12.495	589	-3135	28	37.8	0.5	1.3	0.92	0.01
Ple_L_a@9	16-Dec-14	6.1	42199	12.506	597	-3123	43	38.8	1.5	1.2	0.85	0.01
Ple_L_b@1	16-Dec-14	6.1	224617	12.451	796	-1649	3	34.2	-3.2	0.6	4.52	0.06
Ple_L_b@2	16-Dec-14	6.1	114279	12.471	807	-1651	11	35.9	-1.5	0.5	2.30	0.03
Ple_L_b@3	16-Dec-14	6.1	73161	12.522	815	-1659	21	40.2	2.8	0.9	1.47	0.02

Ple_L_b@4	16-Dec-14	6.2	64330	12.497	829	-1669	39	38.1	0.7	0.9	1.29	0.02
Ple_L_b@5	16-Dec-14	6.2	302581	12.402	2288	-2909	3	30.1	-7.2	0.6	6.05	0.08
Ple_L_b@6	16-Dec-14	6.2	104815	12.430	2280	-2898	14	32.5	-4.9	0.7	2.09	0.03
Ple_L_b@7	16-Dec-14	6.3	52168	12.470	2271	-2886	29	35.8	-1.6	0.8	1.03	0.01
Ple_L_b@8	16-Dec-14	6.3	64470	12.489	2259	-2872	47	37.4	0.0	0.8	1.27	0.02
Ple_L_c@02	17-Dec-14	6.3	248390	12.425	2562	-1742	9	32.1	-5.3	0.5	4.90	0.07
Ple_L_c@03	17-Dec-14	6.3	186131	12.377	2553	-1742	18	28.1	-9.3	1.0	3.67	0.04
Ple_L_c@04	17-Dec-14	6.3	112260	12.413	2543	-1742	28	31.1	-6.3	0.7	2.21	0.03
Ple_L_c@05	17-Dec-14	6.3	80496	12.479	2534	-1747	38	36.5	-0.9	0.8	1.58	0.02
Ple_L_c@06	17-Dec-14	6.3	728337	12.317	395	-2965	3	23.1	-14.3	0.6	14.37	0.12
Ple_L_c@07	17-Dec-14	6.2	338420	12.377	408	-2961	14	28.0	-9.3	0.4	6.74	0.07
Ple_L_c@08	17-Dec-14	6.3	286999	12.391	423	-2956	29	29.2	-8.1	0.6	5.66	0.05
Ple_L_c@1	17-Dec-14	6.3	430075	12.355	2571	-1740	3	26.2	-11.1	0.6	8.41	0.08
Plesovice_L_A@02	11-Dec-14	8.0	114979	12.453	1904	-3455	32	34.4	0.6	1.3	1.54	0.03
Plesovice_L_A@03	11-Dec-14	8.2	119052	12.431	1883	-3431	64	32.6	-1.2	0.7	1.57	0.03
Plesovice_L_A@04	11-Dec-14	8.2	118063	12.427	1863	-3407	95	32.2	-1.6	1.1	1.55	0.02
Plesovice_L_A@05	11-Dec-14	8.3	79384	12.455	1843	-3383	126	34.5	0.7	1.4	1.04	0.01
Plesovice_L_A@06	11-Dec-14	8.1	75169	12.445	1822	-3358	159	33.8	-0.1	1.0	1.00	0.02
Plesovice_L_A@07	11-Dec-14	8.2	71388	12.442	1802	-3333	191	33.5	-0.3	1.1	0.93	0.01
Plesovice_L_A@08	11-Dec-14	8.2	65097	12.459	1782	-3308	223	34.9	1.1	1.1	0.85	0.01
Plesovice_L_A@09	11-Dec-14	8.8	62138	12.442	1762	-3283	255	33.5	-0.4	1.4	0.76	0.01
Plesovice_L_A@1	11-Dec-14	8.8	157287	12.434	1925	-3479	10	32.8	-1.0	1.3	1.92	0.02
Plesovice_L_A@10	11-Dec-14	8.3	58092	12.429	1742	-3258	287	32.4	-1.4	1.2	0.75	0.01
Plesovice_L_A@11	11-Dec-14	8.6	61928	12.417	1701	-3208	352	31.4	-2.4	1.0	0.78	0.01
Plesovice_L_A@12	11-Dec-14	8.7	62924	12.471	1661	-3158	416	35.9	2.1	1.0	0.78	0.01
Plesovice_L_A@13	11-Dec-14	8.8	61213	12.442	1620	-3108	480	33.5	-0.3	1.4	0.75	0.01
Plesovice_L_A@14	11-Dec-14	8.6	63406	12.437	1580	-3058	544	33.1	-0.7	1.1	0.80	0.01

Plesovice_L_A@15	11-Dec-14	8.9	62081	12.416	1539	-3008	609	31.3	-2.5	1.2	0.75	0.01
Plesovice_L_A@16	11-Dec-14	8.8	57546	12.445	1499	-2958	673	33.7	-0.1	1.5	0.70	0.01
Plesovice_L_A@17	11-Dec-14	7.6	52222	12.464	1458	-2908	738	35.3	1.5	1.4	0.74	0.01
Plesovice_L_A@18	11-Dec-14	7.3	52465	12.490	1418	-2858	802	37.5	3.7	1.3	0.77	0.02
Plesovice_L_A@19	11-Dec-14	7.9	56977	12.454	1377	-2808	866	34.4	0.6	1.4	0.77	0.01
Plesovice_L_A@20	11-Dec-14	8.0	57451	12.467	1337	-2758	930	35.5	1.7	1.2	0.77	0.01
Plesovice_L_A@21	11-Dec-14	7.8	54689	12.453	1296	-2708	995	34.4	0.6	1.1	0.75	0.01
Plesovice_L_A@22	11-Dec-14	7.4	45289	12.454	1256	-2658	738	34.5	0.7	1.5	0.65	0.01
Plesovice_L_A@23	11-Dec-14	5.9	43922	12.489	1215	-2608	673	37.4	3.5	1.7	0.79	0.02
Plesovice_L_A@24	11-Dec-14	6.5	42148	12.483	1175	-2558	609	36.9	3.1	1.5	0.70	0.01
Plesovice_L_A@25	11-Dec-14	5.9	43318	12.458	1134	-2508	544	34.8	1.0	1.2	0.79	0.01
Plesovice_L_A@28	11-Dec-14	6.2	50054	12.477	1013	-2358	480	36.3	2.5	1.7	0.87	0.01
Plesovice_L_A@29	11-Dec-14	7.7	79270	12.404	972	-2308	418	30.3	-3.2	1.2	1.09	0.01
Plesovice_L_A@30	11-Dec-14	7.7	75283	12.456	932	-2258	354	34.6	1.1	1.1	1.03	0.02
Plesovice_L_A@31	11-Dec-14	7.8	78731	12.433	911	-2233	321	32.7	-0.8	1.0	1.07	0.01
Plesovice_L_A@32	11-Dec-14	7.8	85400	12.426	891	-2208	289	32.1	-1.4	1.2	1.16	0.01
Plesovice_L_A@33	11-Dec-14	7.8	90689	12.445	871	-2183	257	33.7	0.2	1.0	1.23	0.02
Plesovice_L_A@34	11-Dec-14	7.9	102744	12.441	851	-2158	225	33.4	-0.2	1.1	1.38	0.02
Plesovice_L_A@36	11-Dec-14	7.9	92361	12.424	810	-2108	161	32.0	-1.6	1.3	1.23	0.02
Plesovice_L_A@37	11-Dec-14	8.0	91289	12.446	790	-2083	129	33.8	0.2	1.1	1.21	0.02
Plesovice_L_A@38	11-Dec-14	8.0	76062	12.446	770	-2058	97	33.8	0.3	1.1	1.01	0.01
Plesovice_L_A@39	11-Dec-14	7.7	79384	12.461	749	-2033	64	35.1	1.5	1.4	1.09	0.01
Plesovice_L_A@40	11-Dec-14	6.9	94451	12.461	730	-2008	33	35.1	1.5	1.0	1.45	0.02
Plesovice_L_A@41	11-Dec-14	6.9	255324	12.442	709	-1983	10	33.5	0.0	0.9	3.94	0.03
Plesovice_L_B@03	11-Dec-14	6.9	106107	12.430	2148	-2138	80	32.5	-1.0	1.0	1.63	0.03
Plesovice_L_B@04	11-Dec-14	6.8	82069	12.452	2115	-2161	121	34.3	0.7	1.2	1.27	0.02
Plesovice_L_B@05	11-Dec-14	6.8	75555	12.452	2083	-2184	160	34.3	0.8	1.2	1.18	0.02

Plesovice_L_B@06	11-Dec-14	6.8	73121	12.448	2050	-2207	200	34.0	0.4	0.9	1.15	0.02
Plesovice_L_B@07	11-Dec-14	6.8	61257	12.432	2018	-2230	240	32.6	-0.9	1.0	0.95	0.01
Plesovice_L_B@08	11-Dec-14	6.7	58477	12.460	1985	-2253	280	35.0	1.4	1.1	0.92	0.01
Plesovice_L_B@09	11-Dec-14	6.7	57977	12.452	1953	-2276	319	34.3	0.7	1.2	0.91	0.01
Plesovice_L_B@1	11-Dec-14	6.9	223378	12.436	2214	-2092	10	33.0	-0.6	0.9	3.43	0.04
Plesovice_L_B@10	12-Dec-14	6.8	57173	12.469	1920	-2299	360	35.7	2.2	0.9	0.90	0.01
Plesovice_L_B@11	12-Dec-14	6.9	56594	12.463	1888	-2322	399	35.2	1.6	1.2	0.87	0.01
Plesovice_L_B@12	12-Dec-14	6.9	51670	12.463	1855	-2345	439	35.2	1.6	1.3	0.79	0.01
Plesovice_L_B@13	12-Dec-14	6.5	52500	12.457	1823	-2368	479	34.7	1.1	1.1	0.85	0.01
Plesovice_L_B@14	12-Dec-14	6.7	51927	12.449	1790	-2391	519	34.1	0.5	1.6	0.82	0.01
Plesovice_L_B@15	12-Dec-14	6.7	51859	12.458	1758	-2414	558	34.8	1.2	1.3	0.82	0.01
Plesovice_L_B@16	12-Dec-14	6.7	51310	12.437	1725	-2437	598	33.1	-0.5	1.0	0.81	0.01
Plesovice_L_B@17	12-Dec-14	6.7	51402	12.446	1693	-2460	638	33.8	0.2	1.1	0.81	0.01
Plesovice_L_B@18	12-Dec-14	6.7	50460	12.458	1660	-2483	678	34.8	1.2	1.1	0.79	0.01
Plesovice_L_B@19	12-Dec-14	6.8	50685	12.449	1628	-2506	717	34.0	0.5	1.3	0.79	0.01
Plesovice_L_B@20	12-Dec-14	6.7	50842	12.437	1595	-2529	758	33.1	-0.5	0.8	0.80	0.01
Plesovice_L_B@21	12-Dec-14	6.8	50093	12.457	1563	-2552	797	34.8	1.2	1.2	0.78	0.01
Plesovice_L_B@22	12-Dec-14	6.7	49863	12.457	1530	-2575	837	34.7	1.2	1.3	0.79	0.01
Plesovice_L_B@23	12-Dec-14	6.8	49224	12.457	1498	-2598	877	34.7	1.2	1.4	0.77	0.01
Plesovice_L_B@24	12-Dec-14	6.7	49368	12.465	1465	-2621	917	35.4	1.9	1.1	0.79	0.01
Plesovice_L_B@25	12-Dec-14	6.7	48283	12.465	1433	-2644	956	35.4	1.8	1.4	0.76	0.01
Plesovice_L_B@26	12-Dec-14	5.8	45847	12.458	1400	-2667	997	34.8	1.2	1.1	0.83	0.02
Plesovice_L_B@28	12-Dec-14	6.8	48847	12.451	1335	-2713	1076	34.2	0.7	1.0	0.76	0.01
Plesovice_L_B@29	12-Dec-14	6.9	50878	12.475	1303	-2736	1116	36.2	2.7	1.2	0.78	0.01
Plesovice_L_B@30	12-Dec-14	6.9	50096	12.446	1270	-2759	1156	33.8	0.3	1.3	0.77	0.01
Plesovice_L_B@31	12-Dec-14	6.9	52365	12.447	1237	-2782	1196	33.9	0.4	1.2	0.81	0.01
Plesovice_L_B@32	12-Dec-14	7.2	53111	12.474	1205	-2805	1235	36.1	2.5	1.5	0.78	0.01
Plesovice_L_B@34	12-Dec-14	7.2	50918	12.454	1140	-2851	1068	34.5	0.9	1.2	0.75	0.01

Plesovice_L_B@35	12-Dec-14	7.1	50648	12.443	1107	-2874	1028	33.5	0.0	1.4	0.75	0.01
Plesovice_L_B@36	12-Dec-14	7.2	50929	12.450	1075	-2897	988	34.1	0.6	1.5	0.75	0.01
Plesovice_L_B@37	12-Dec-14	7.2	51309	12.439	1042	-2920	948	33.2	-0.3	1.4	0.75	0.01
Plesovice_L_B@39	12-Dec-14	6.8	47981	12.469	977	-2966	868	35.8	2.2	1.3	0.74	0.01
Plesovice_L_B@41	12-Dec-14	6.7	46382	12.476	912	-3012	789	36.3	2.7	1.1	0.73	0.01
Plesovice_L_B@42	12-Dec-14	6.6	46307	12.461	880	-3035	749	35.0	1.5	1.5	0.74	0.01
Plesovice_L_B@44	12-Dec-14	6.7	46815	12.462	815	-3081	670	35.1	1.6	1.1	0.74	0.01
Plesovice_L_B@45	12-Dec-14	6.7	53525	12.456	782	-3104	630	34.6	1.1	1.0	0.85	0.02
Plesovice_L_B@46	12-Dec-14	7.7	55779	12.453	750	-3127	590	34.4	0.8	1.2	0.76	0.01
Plesovice_L_B@48	12-Dec-14	7.6	47084	12.473	685	-3173	511	36.0	2.5	1.3	0.66	0.02
Plesovice_L_B@49	12-Dec-14	7.2	56939	12.458	652	-3195	471	34.8	1.3	1.0	0.84	0.02
Plesovice_L_B@50	12-Dec-14	7.4	60301	12.448	620	-3217	432	34.0	0.4	1.3	0.86	0.01
Plesovice_L_B@51	12-Dec-14	7.5	63642	12.452	587	-3239	392	34.3	0.7	1.0	0.90	0.02
Plesovice_L_B@53	12-Dec-14	7.7	68026	12.464	522	-3283	314	35.3	1.8	1.3	0.94	0.02
Plesovice_L_B@54	12-Dec-14	7.7	74238	12.454	490	-3305	275	34.4	0.9	1.1	1.03	0.02
Plesovice_L_B@56	12-Dec-14	7.8	83143	12.473	425	-3349	197	36.1	2.5	1.1	1.13	0.02
Plesovice_L_B@57	12-Dec-14	8.2	91533	12.457	392	-3371	157	34.8	1.2	1.0	1.18	0.02
Plesovice_L_B@58	12-Dec-14	8.5	89987	12.465	359	-3393	117	35.4	1.9	1.0	1.12	0.02
Plesovice_L_B@59	12-Dec-14	8.6	80882	12.468	327	-3415	78	35.6	2.1	0.9	0.99	0.02
Plesovice_L_B@60	12-Dec-14	8.6	84261	12.450	295	-3437	40	34.2	0.6	1.1	1.04	0.01
Plesovice_L_B@61	12-Dec-14	8.6	182889	12.419	262	-3459	10	31.6	-2.0	0.7	2.26	0.01
5µm												
PlesoviceL_5um@1	27-Sep-13	0.9	114548	12.379	-228.0	-3750	3	28.2	-0.2	2.9	13.82	0.56
PlesoviceL_5um@11	27-Sep-13	0.9	8611	12.245	-178.0	-3750	50	17.1	-11.4	3.5	1.04	0.18
PlesoviceL_5um@12	27-Sep-13	0.9	6063	12.294	-173.0	-3750	55	21.1	-7.3	4.4	0.74	0.24
PlesoviceL_5um@2	27-Sep-13	0.9	111195	12.328	-223.0	-3750	5	24.0	-4.5	2.3	13.43	2.11
PlesoviceL_5um@3	27-Sep-13	0.9	86866	12.297	-218.0	-3750	10	21.5	-7.0	1.9	10.49	0.38
PlesoviceL_5um@4	27-Sep-13	0.9	49999	12.305	-213.0	-3750	15	22.1	-6.3	1.9	6.04	0.28

PlesoviceL_5um@5	27-Sep-13	0.9	33726	12.309	-208.0	-3750	20	22.4	-6.1	2.2	4.08	0.45
PlesoviceL_5um@6	27-Sep-13	0.9	23560	12.269	-203.0	-3750	25	19.1	-9.4	2.6	2.84	0.78
PlesoviceL_5um@7	27-Sep-13	0.9	21758	12.276	-198.0	-3750	30	19.7	-8.7	2.6	2.63	0.91
PlesoviceL_5um@8	27-Sep-13	0.9	12623	12.285	-193.0	-3750	35	20.4	-8.1	3.0	1.52	0.60
PlesoviceL_5um@9	27-Sep-13	0.9	9253	12.236	-188.0	-3750	40	16.4	-12.1	3.6	1.12	0.12
pleL-5um-1@01	13-Nov-14	1.3	77618	12.360	-91.0	-3494	2	26.4	-12.1	0.9	8.24	0.01
pleL-5um-1@02	13-Nov-14	1.3	66295	12.450	-91.0	-3489	0	34.4	-4.1	0.9	6.99	0.07
pleL-5um-1@03	13-Nov-14	1.3	64111	12.480	-91.0	-3484	1	36.8	-1.7	1.2	6.71	0.03
pleL-5um-1@04	13-Nov-14	1.3	81382	12.480	-91.0	-3484	1	36.3	-2.3	1.1	8.42	0.02
pleL-5um-1@05	13-Nov-14	1.4	93744	12.450	-91.0	-3479	3	34.4	-4.2	1.0	9.58	0.07
pleL-5um-1@06	13-Nov-14	1.4	58601	12.480	-91.0	-3474	5	36.8	-1.8	0.9	5.94	0.05
pleL-5um-1@07	13-Nov-14	1.4	55876	12.460	-91.0	-3469	6	34.9	-3.6	0.9	5.63	0.02
pleL-5um-1@08	13-Nov-14	1.4	39849	12.490	-91.0	-3464	8	37.5	-1.0	1.0	3.96	0.02
pleL-5um-1@09	13-Nov-14	1.4	24448	12.430	-91.0	-3459	10	32.2	-6.3	1.1	2.42	0.00
pleL-5um-1@10	13-Nov-14	1.4	24791	12.390	-91.0	-3454	12	29.5	-9.1	1.1	2.48	0.01
pleL-5um-1@11	13-Nov-14	1.4	13831	12.420	-91.0	-3449	13	31.9	-6.7	1.5	1.36	0.00
pleL-5um-1@12	13-Nov-14	1.4	9045	12.450	-91.0	-3444	15	34.5	-4.0	1.9	0.88	0.00
pleL-5um-1@13	13-Nov-14	1.4	8892	12.440	-91.0	-3439	17	33.4	-5.1	1.8	0.86	0.00
pleL-5um-1@14	13-Nov-14	1.4	6370	12.480	-91.0	-3434	18	36.8	-1.8	2.2	0.61	0.00
pleL-5um-1@15	13-Nov-14	1.5	5049	12.390	-91.0	-3429	20	29.3	-9.3	2.3	0.48	0.00
pleL-5um-2@01	12-Nov-14	0.9	84108	12.370	-349.0	-3046	6	27.1	-11.4	1.0	12.64	0.10
pleL-5um-2@02	12-Nov-14	1.0	76534	12.380	-344.0	-3046	4	28.7	-9.8	1.0	10.86	0.09
pleL-5um-2@03	12-Nov-14	1.0	82066	12.400	-339.0	-3046	2	30.3	-8.3	1.1	11.14	0.13
pleL-5um-2@04	12-Nov-14	1.1	102975	12.390	-334.0	-3046	1	29.3	-9.2	0.9	13.29	0.17
pleL-5um-2@05	12-Nov-14	1.1	96088	12.370	-329.0	-3046	3	27.9	-10.6	0.9	12.39	0.02
pleL-5um-2@06	12-Nov-14	1.1	69047	12.400	-324.0	-3046	6	29.7	-8.9	0.9	8.90	0.07
pleL-5um-2@07	12-Nov-14	1.1	58710	12.390	-319.0	-3046	8	29.4	-9.1	0.9	7.42	0.05

pleL-5um-2@08	12-Nov-14	1.2	44666	12.450	-314.0	-3046	11	34.3	-4.3	1.0	5.40	0.05
pleL-5um-2@09	12-Nov-14	1.2	52816	12.390	-309.0	-3046	13	29.3	-9.2	0.9	6.25	0.05
pleL-5um-2@10	12-Nov-14	1.2	49394	12.410	-304.0	-3046	15	30.8	-7.7	1.0	5.76	0.05
pleL-5um-2@11	12-Nov-14	1.2	52829	12.390	-299.0	-3046	18	29.4	-9.2	0.9	5.99	0.05
pleL-5um-2@12	12-Nov-14	1.2	85418	12.340	-294.0	-3046	20	24.9	-13.7	1.3	9.64	0.11
pleL-5um-2@13	13-Nov-14	1.2	22454	12.380	-274.0	-3046	30	28.1	-10.5	1.4	2.51	0.03
pleL-5um-2@15	13-Nov-14	1.3	35251	12.390	-264.0	-3046	35	28.9	-9.6	1.3	3.85	0.03
pleL-5um-2@16	13-Nov-14	1.3	31664	12.420	-259.0	-3046	37	31.4	-7.2	1.2	3.45	0.03
pleL-5um-2@17	13-Nov-14	1.3	24691	12.430	-254.0	-3046	40	32.8	-5.7	1.3	2.67	0.02
Qinghu												
20μm												
qinghu01@1	19-Sep-13	23.4	327688	12.129	239.0	643	49	7.4	-6.9	0.9	1.00	0.01
qinghu01@2	19-Sep-13	23.3	302114	12.105	59.0	634	205	5.5	-8.9	1.1	2.08	0.01
qinghu01@3	19-Sep-13	23.1	45163	12.096	-86.0	623	348	4.7	-9.6	2.0	0.31	0.00
qinghu1@4	22-Sep-13	22.3	198977	12.433	155.0	628	110	32.7	1.4	0.8	1.17	0.01
qinghu1@5	22-Sep-13	22.3	80040	12.337	-31.0	624	293	24.8	-6.5	1.1	0.47	0.00
qinghu1r@2	22-Sep-13	28.1	300226	12.368	60.0	658	210	27.3	-4.0	0.7	1.40	0.01
qinghu1r@1	22-Sep-13	28.4	235080	12.354	-92.0	653	357	26.2	-5.1	1.0	1.08	0.01
10μm												
qinghu1@01	10-Nov-14	11.0	945314	12.540	-459.0	1210	0	41.4	-	-	11.78	0.60
qinghu1@02	10-Nov-14	11.6	328780	12.480	-478.0	1210	9	36.9	-2.1	0.9	3.88	0.08
qinghu1@03	10-Nov-14	11.4	192629	12.450	-500.0	1210	31	34.3	-4.8	1.2	2.32	0.05
qinghu1@04	10-Nov-14	11.7	176395	12.460	-524.0	1206	55	34.8	-4.3	0.7	2.08	0.04
qinghu1@05	10-Nov-14	11.6	101879	12.460	-548.0	1208	79	34.7	-4.4	1.0	1.21	0.02
qinghu1@06	10-Nov-14	11.6	91824	12.460	-575.0	1206	106	35.1	-4.0	0.8	1.09	0.02
qinghu1@07	10-Nov-14	11.4	99819	12.470	-601.0	1209	132	35.9	-3.2	0.9	1.21	0.02

qinghu1@08	10-Nov-14	11.6	68022	12.470	-624.0	1209	155	35.9	-3.2	1.0	0.81	0.02
qinghu1@09	10-Nov-14	11.3	91431	12.460	-649.0	1206	190	34.7	-4.4	1.1	1.11	0.02
qinghu1@10	10-Nov-14	11.5	71915	12.400	-677.0	1202	218	30.0	-9.1	1.3	0.86	0.01
qinghu1@11	10-Nov-14	11.6	55979	12.430	-699.0	1198	240	32.5	-6.6	1.2	0.67	0.01
qinghu1@12	10-Nov-14	11.6	90846	12.470	-730.0	1200	271	35.6	-3.5	1.2	1.08	0.02
qinghu1@13	10-Nov-14	11.6	57544	12.500	-759.0	1202	300	38.5	-0.6	1.3	0.68	0.03
qinghu1@13	10-Nov-14	11.6	57544	12.500	-759.0	1202	68	38.5	-0.6	1.3	0.68	0.03
qinghu1@14	10-Nov-14	11.6	180799	12.490	-764.0	1265	5	37.1	-2.0	0.8	2.14	0.04
qinghu1@15	10-Nov-14	11.5	181532	12.510	-760.0	1246	24	39.0	-0.1	1.0	2.18	0.04
qinghu1@16	10-Nov-14	11.5	52537	12.400	-760.0	1226	44	29.9	-9.2	1.4	0.63	0.01
qinghu1@17	10-Nov-14	11.6	60629	12.310	-759.0	1182	88	22.4	-	-	0.72	0.01
qinghu1@18	10-Nov-14	11.6	27621	12.410	-758.0	1162	108	31.1	-8.0	1.5	0.33	0.01
qinghu1@19	10-Nov-14	11.5	82886	12.370	-760.0	1144	126	27.8	-	-	1.00	0.01
qinghu1@20	10-Nov-14	11.3	296608	12.480	-823.0	1265	5	36.2	-2.8	0.7	3.63	0.06
qinghu1@21	10-Nov-14	11.4	262784	12.480	-823.0	1245	25	36.9	-2.2	0.7	3.17	0.05
qinghu1@22	10-Nov-14	11.4	26413	12.440	-821.0	1219	51	33.3	-5.8	2.2	0.32	0.02
qinghu1@23	10-Nov-14	11.4	31137	12.350	-820.0	1197	350	26.1	-	-	0.38	0.01
qinghu1@23	10-Nov-14	11.4	31137	12.350	-820.0	1197	73	26.1	-	-	0.38	0.01
qinghu1@24	10-Nov-14	11.4	30843	12.360	-818.0	1174	96	26.3	-	-	0.37	0.01
qinghu1@25	10-Nov-14	11.6	54100	12.440	-818.0	1150	120	33.6	-5.5	0.9	0.64	0.01
qinghu1@1	10-Dec-14	11.8	959941	12.226	270.0	1172	3	15.6	-18.3	1.3	8.75	0.43
qinghu1@02	10-Dec-14	11.8	455865	12.384	251.0	1164	11	28.6	-5.2	1.0	4.15	0.02
qinghu1@03	10-Dec-14	11.8	119506	12.330	235.0	1161	37	24.2	-9.7	1.0	1.09	0.01
qinghu1@04	10-Dec-14	11.9	1279427	12.704	273.0	1139	3	55.2	-	-	11.58	0.64
qinghu1@05	10-Dec-14	11.9	1227011	12.262	263.0	1143	11	18.5	-15.3	1.0	11.10	0.06
qinghu1@06	10-Dec-14	11.9	101315	12.048	248.0	1142	25	0.7	-	-	0.92	0.01
qinghu1@07	10-Dec-14	11.9	74128	12.044	237.0	1143	36	0.5	-	-	0.67	0.01

qinghu1@08	10-Dec-14	11.8	52180	12.111	217.0	1142	56	6.0	-	-	0.48	0.02
qinghu1@09	10-Dec-14	11.8	107166	12.359	120.0	1149	153	26.6	-7.3	1.1	0.97	0.03
qinghu1@10	10-Dec-14	11.1	99408	12.266	110.0	1148	163	18.9	-	-	0.97	0.01
qinghu1@11	10-Dec-14	11.3	89303	12.317	96.0	1147	177	23.1	-	-	0.85	0.01
qinghu1@12	10-Dec-14	11.1	83479	12.262	87.0	1147	186	18.5	-	-	0.81	0.00
qinghu1@13	10-Dec-14	10.9	110087	12.244	75.0	1146	198	17.0	-	-	1.09	0.01
qinghu1@14	10-Dec-14	11.0	143712	12.353	59.0	1147	214	26.1	-7.8	1.0	1.41	0.03
qinghu1@15	10-Dec-14	11.0	75687	12.404	40.0	1148	233	30.4	-3.5	1.2	0.74	0.01
qinghu1@16	10-Dec-14	8.2	278746	12.395	221.0	1196	3	29.6	-4.2	0.9	3.68	0.05
qinghu1@17	10-Dec-14	10.7	101517	12.405	217.0	1184	13	30.4	-3.5	1.1	1.02	0.01
qinghu1@18	10-Dec-14	10.9	113595	12.380	215.0	1174	23	28.3	-5.5	1.2	1.12	0.01
qinghu1@19	10-Dec-14	11.0	75240	12.107	212.0	1163	34	5.6	-	-	0.74	0.01
qinghu1@20	10-Dec-14	11.1	506457	12.392	210.0	1079	3	29.3	-4.5	0.8	4.91	0.05
qinghu1@21	10-Dec-14	11.2	236493	12.377	205.0	1091	13	28.0	-5.8	0.7	2.27	0.03
qinghu1@22	11-Dec-14	11.2	229435	12.344	198.0	1103	27	25.4	-8.5	0.8	2.20	0.02
qinghu1@23	11-Dec-14	11.2	118623	12.351	187.0	1116	44	25.9	-7.9	1.1	1.14	0.01
qinghu1@24	11-Dec-14	11.1	110334	12.387	179.0	1129	59	28.9	-4.9	1.1	1.07	0.01
5μm												
qinghu1-5um@01	13-Nov-14	1.0	28355	12.470	237.0	1274	1	35.5	-2.9	1.3	3.99	0.04
qinghu1-5um@02	13-Nov-14	0.9	19494	12.450	232.0	1280	5	34.0	-4.5	1.4	2.84	0.03
qinghu1-5um@03	13-Nov-14	0.9	12179	12.480	227.0	1284	10	36.9	-1.5	1.3	1.81	0.01
qinghu1-5um@04	13-Nov-14	0.8	12326	12.430	222.0	1290	15	32.4	-6.1	1.6	2.05	0.03
qinghu1-5um@05	13-Nov-14	0.8	3959	12.390	217.0	1294	20	29.2	-9.3	2.7	0.68	0.01
qinghu1-5um@06	13-Nov-14	0.8	4126	12.470	212.0	1300	25	35.7	-2.7	2.5	0.72	0.00
qinghu1-5um@07	13-Nov-14	0.7	9800	12.440	207.0	1304	30	33.3	-5.1	1.6	1.81	0.01
qinghu1-5um@08	13-Nov-14	0.7	6325	12.490	202.0	1310	35	37.1	-1.4	2.1	1.19	0.01
qinghu1-5um@09	14-Nov-14	1.2	11463	12.450	195.0	1310	40	33.9	-4.5	1.7	1.34	0.02
qinghu1-5um@10	14-Nov-14	1.1	10409	12.450	188.0	1310	45	34.5	-3.9	1.4	1.33	0.02

qinghu1-5um@11	14-Nov-14	1.1	9559	12.440	181.0	1310	50	33.2	-5.3	1.5	1.22	0.02
qinghu1-5um@12	14-Nov-14	1.0	9155	12.450	174.0	1310	55	33.8	-4.6	1.9	1.21	0.01
qinghu1-5um@13	14-Nov-14	1.0	10408	12.450	167.0	1310	60	33.9	-4.5	1.5	1.47	0.02
qinghu1-5um@14	14-Nov-14	0.9	10475	12.490	160.0	1310	65	37.2	-1.3	1.7	1.53	0.02
qinghu1-5um@15	14-Nov-14	0.9	7226	12.430	153.0	1310	70	32.4	-6.0	2.0	1.11	0.01
qinghu1-5um@16	14-Nov-14	0.8	4412	12.480	146.0	1310	75	36.4	-2.0	2.6	0.73	0.01
qinghu1-5um@17	14-Nov-14	0.7	5504	12.520	139.0	1310	80	39.8	1.4	2.2	1.05	0.01
20μm												
qinghu06@1	19-Sep-13	22.4	253033	12.120	-712.0	1718	278	6.7	-6.6	1.3	1.91	0.01
qinghu06@2	19-Sep-13	22.5	230789	12.157	-859.0	1699	130	9.8	-3.5	1.4	1.74	0.01
qinghubudian@01	19-Sep-13	22.3	224603	12.150	-780.0	1720	212	9.2	-4.1	1.1	1.70	0.01
qinghubudian@2	19-Sep-13	22.0	233715	12.154	-918.0	1704	71	9.6	-3.7	1.3	1.80	0.03
10μm												
qinghu6@01	10-Nov-14	13.6	912365	12.410	-1375.0	2307	3	31.0	-8.1	0.5	9.26	0.03
qinghu6@02	10-Nov-14	13.5	481023	12.460	-1390.0	2303	16	35.3	-3.8	0.5	4.92	0.05
qinghu6@03	10-Nov-14	13.6	302836	12.470	-1407.0	2294	35	35.5	-3.6	0.7	3.07	0.07
qinghu6@04	10-Nov-14	13.5	90339	12.470	-1431.0	2288	59	35.8	-3.3	1.0	0.92	0.02
qinghu6@05	10-Nov-14	13.4	62333	12.510	-1453.0	2284	81	39.3	0.2	1.2	0.64	0.01
qinghu6@06	10-Nov-14	12.3	76582	12.430	-1472.0	2280	101	32.6	-6.5	2.7	0.86	0.01
qinghu6@07	10-Nov-14	8.6	62353	12.490	-1497.0	2278	125	37.4	-1.7	1.5	1.00	0.02
qinghu6@08	10-Nov-14	9.0	91477	12.460	-1520.0	2276	148	35.3	-3.8	1.7	1.41	0.02
qinghu6@09	10-Nov-14	9.3	79471	12.480	-1546.0	2273	174	36.7	-2.4	1.4	1.18	0.02
qinghu6@11	10-Nov-14	10.3	113485	12.470	-1606.0	2271	234	36.1	-2.9	1.1	1.52	0.02
qinghu6@12	10-Nov-14	10.5	96251	12.430	-1631.0	2271	259	32.8	-6.3	1.1	1.26	0.01
qinghu6@13	10-Nov-14	11.1	171175	12.430	-1658.0	2269	286	32.6	-6.5	1.4	2.12	0.03
qinghu6@14	10-Nov-14	10.8	194093	12.410	-1694.0	2268	321	31.2	-7.9	1.2	2.47	0.04
qinghu6@1	11-Dec-14	10.6	741115	12.356	-565.0	2291	3	26.3	-7.5	0.8	7.53	0.02

qinghu6@02	11-Dec-14	10.6	468072	12.396	-579.0	2287	15	29.6	-4.2	0.7	4.76	0.09
qinghu6@03	11-Dec-14	10.4	263605	12.378	-598.0	2280	35	28.1	-5.7	0.7	2.72	0.02
qinghu6@04	11-Dec-14	9.3	80002	12.401	-622.0	2277	59	30.1	-3.7	1.2	0.93	0.01
qinghu6@05	11-Dec-14	9.5	61334	12.440	-643.0	2271	81	33.3	-0.5	1.3	0.70	0.01
qinghu6@06	11-Dec-14	9.5	77131	12.366	-665.0	2270	102	27.2	-6.6	1.3	0.87	0.01
qinghu6@07	11-Dec-14	8.1	60641	12.443	-682.0	2271	119	33.6	-0.2	0.7	0.81	0.01
qinghu6@08	11-Dec-14	8.2	113678	12.391	-706.0	2271	142	29.2	-4.6	0.9	1.50	0.01
qinghu6@09	11-Dec-14	8.3	106842	12.374	-729.0	2270	165	27.9	-6.0	0.9	1.38	0.02
qinghu6@10	11-Dec-14	8.7	83793	12.372	-752.0	2272	188	27.6	-6.2	1.3	1.04	0.01
qinghu6@11	11-Dec-14	8.6	128719	12.375	-777.0	2270	213	27.9	-5.9	1.0	1.60	0.01
qinghu6@12	11-Dec-14	8.7	96921	12.372	-794.0	2270	230	27.7	-6.2	1.0	1.20	0.01
qinghu-9@1	11-Dec-14	8.2	1091065	12.263	-1468.0	1097	3	18.6	-15.2	1.2	14.38	0.31
qinghu-9@2	11-Dec-14	8.2	422036	12.327	-1487.0	1093	19	23.9	-9.9	2.9	5.57	0.23
qinghu-9@3	11-Dec-14	8.2	212407	12.372	-1505.0	1087	38	27.7	-6.1	0.8	2.79	0.03
qinghu-9@5	11-Dec-14	8.0	77811	12.430	-1550.0	1080	84	32.5	-1.4	1.2	1.05	0.02
qinghu-9@6	11-Dec-14	8.0	97301	12.400	-1573.0	1075	107	30.0	-3.9	1.4	1.31	0.02
qinghu-9@7	11-Dec-14	8.6	152705	12.372	-1597.0	1070	132	27.7	-6.1	0.8	1.92	0.03
qinghu-9@8	11-Dec-14	8.7	86008	12.430	-1620.0	1063	156	32.4	-1.4	1.2	1.06	0.01
qinghu_a@1	13-Dec-14	3.6	301082	12.190	-4234.0	4084	3	12.8	-21.4	1.2	11.20	0.12
qinghu_a@2	13-Dec-14	3.0	114740	12.400	-4224.0	4094	14	30.3	-3.9	1.1	5.16	0.04
qinghu_a@3	13-Dec-14	3.1	22558	12.430	-4216.0	4107	29	32.7	-1.5	1.8	0.98	0.01
qinghu_a@4	13-Dec-14	3.5	22306	12.430	-4202.0	4122	50	32.4	-1.8	1.4	0.86	0.02
qinghu_a@5	13-Dec-14	3.8	35021	12.450	-4188.0	4136	69	34.5	0.3	1.3	1.24	0.02
qinghu_a@6	13-Dec-14	3.6	33423	12.420	-4176.0	4146	85	31.7	-2.5	1.6	1.22	0.01
qinghu_a@7	13-Dec-14	3.1	39463	12.370	-4162.0	4158	103	27.6	-6.6	1.4	1.70	0.01

qinghu_a@8	13-Dec-14	3.1	16774	12.380	-4150.0	4173	122	28.4	-5.8	3.5	0.73	0.04
qinghu_a@9	13-Dec-14	1.4	13394	12.370	-4136.0	4188	143	27.4	-6.7	2.0	1.28	0.01
qinghu_a@10	13-Dec-14	1.5	7316	12.370	-4121.0	4204	165	27.8	-6.4	3.8	0.64	0.01
qinghu_b@1	13-Dec-14	1.8	139768	12.360	-3829.0	4118	3	26.3	-7.9	1.6	10.27	0.25
qinghu_b@2	13-Dec-14	2.1	49609	12.400	-3822.0	4136	19	29.6	-4.5	1.5	3.19	0.03
qinghu_b@3	13-Dec-14	2.6	39119	12.420	-3813.0	4153	38	31.9	-2.2	1.4	1.98	0.00
qinghu_b@4	13-Dec-14	2.7	31222	12.440	-3803.0	4170	58	33.5	-0.7	1.7	1.53	0.02
qinghu_b@6	13-Dec-14	3.0	18298	12.430	-3783.0	4204	98	32.7	-1.5	1.8	0.81	0.01
qinghu_b@7	13-Dec-14	3.1	16185	12.430	-3774.0	4223	119	32.6	-1.5	1.5	0.70	0.01
qinghu_b@8	13-Dec-14	2.9	15083	12.390	-3766.0	4244	141	29.0	-5.2	1.9	0.69	0.01
qinghu_c@1	13-Dec-14	2.9	205035	12.330	-3595.0	4410	3	24.1	-10.1	1.0	9.52	0.03
qinghu_c@2	13-Dec-14	2.8	113474	12.370	-3586.0	4423	16	27.9	-6.3	1.2	5.35	0.03
qinghu_c@3	13-Dec-14	2.9	67288	12.410	-3574.0	4438	35	30.5	-3.7	1.1	3.07	0.02
qinghu_c@4	13-Dec-14	3.0	44632	12.390	-3559.0	4450	54	28.8	-5.3	1.4	2.00	0.02
qinghu_c@5	13-Dec-14	2.6	24937	12.400	-3546.0	4464	73	30.0	-4.2	1.7	1.28	0.01
qinghu_c@6	13-Dec-14	2.7	27576	12.420	-3535.0	4477	90	31.4	-2.8	1.6	1.36	0.01
qinghu_c@7	13-Dec-14	2.7	21159	12.430	-3515.0	4491	114	32.4	-1.8	2.3	1.04	0.01
qinghu_c@8	13-Dec-14	3.0	43251	12.410	-3498.0	4507	137	30.6	-3.6	0.9	1.95	0.01
qinghu_c@9	13-Dec-14	3.0	19507	12.460	-3484.0	4523	158	34.9	0.7	2.1	0.88	0.01
qinghu_d@1	13-Dec-14	3.0	74507	12.180	-880.0	4455	3	11.3	-22.8	1.7	3.34	0.04
qinghu_d@02	13-Dec-14	3.0	115909	12.390	-867.0	4457	13	29.5	-4.6	1.2	5.13	0.06
qinghu_d@03	13-Dec-14	3.1	69926	12.420	-854.0	4458	26	31.6	-2.6	1.3	2.99	0.02
qinghu_d@04	13-Dec-14	3.1	31259	12.420	-840.0	4458	40	31.6	-2.5	1.6	1.32	0.01
qinghu_d@05	13-Dec-14	3.2	31714	12.450	-829.0	4458	51	34.3	0.1	1.4	1.31	0.01
qinghu_d@06	13-Dec-14	2.9	17086	12.390	-815.0	4454	65	29.1	-5.1	1.9	0.79	0.00

qinghu_d@07	13-Dec-14	3.0	13664	12.440	-795.0	4461	85	33.4	-0.8	1.8	0.60	0.01
qinghu_d@08	13-Dec-14	3.1	22015	12.440	-776.0	4460	104	32.9	-1.2	1.8	0.94	0.01
qinghu_d@09	13-Dec-14	3.1	20826	12.390	-758.0	4464	122	29.3	-4.9	2.1	0.89	0.00
qinghu_d@11	13-Dec-14	2.7	37354	12.410	-705.0	4477	176	31.1	-3.1	2.1	1.87	0.01
qinghu_d@14	13-Dec-14	2.6	22971	12.400	-638.0	4485	244	29.8	-4.4	2.0	1.18	0.01
qinghu_d@15	13-Dec-14	2.5	23242	12.410	-616.0	4488	266	30.5	-3.7	2.4	1.23	0.01
qinghu_d@16	13-Dec-14	1.6	11777	12.400	-599.0	4488	283	30.1	-4.1	5.9	1.01	0.02
qinghu_e@1	13-Dec-14	1.2	50725	12.280	-372.0	4318	3	19.8	-14.4	1.8	5.50	0.05
qinghu_e@02	13-Dec-14	1.4	73049	12.400	-365.0	4321	8	30.4	-3.8	1.6	6.95	0.06
qinghu_e@03	13-Dec-14	1.6	35020	12.420	-347.0	4321	25	31.8	-2.4	1.9	2.97	0.02
qinghu_e@04	13-Dec-14	1.7	17174	12.400	-328.0	4320	44	30.0	-4.1	1.9	1.38	0.01
qinghu_e@05	13-Dec-14	1.7	18302	12.450	-309.0	4319	63	33.8	-0.3	2.3	1.42	0.01
qinghu_e@06	13-Dec-14	2.0	19704	12.390	-290.0	4319	82	29.4	-4.7	1.8	1.31	0.01
qinghu_e@07	13-Dec-14	2.0	19990	12.370	-271.0	4319	101	27.6	-6.6	2.0	1.34	0.01
qinghu_e@08	13-Dec-14	2.0	16120	12.400	-252.0	4318	120	30.0	-4.2	2.1	1.06	0.00
Temora												
Tem2-20um_1	2013-9-21 12:20	24.6	61242.92	12.47	-3069	-283	153	36.0	1.1	0.7	0.29	0.00
Tem2-20um_2	2013-9-21 12:39	24.6	12043.05	12.53	-3134	-268	89	41.1	6.1	1.6	0.06	0.00
Tem2-20um_3	2013-9-21 12:59	24.6	3926.32	12.62	-3222	-280	0	48.0	13.1	2.8	0.02	0.00
Tem2-20um_4	2013-9-21 22:04	24.7	13204.80	12.55	-3312	-306	-94	42.4	7.5	1.5	0.06	0.00
Tem2-20um_5	2013-9-21 13:38	24.6	20849.54	12.52	-3365	-267	-144	40.2	5.3	1.2	0.1	0.00
Temora_10um-01	2014-12-12 18:10	8.3	425465.20	12.39	-3439	6	193	29.5	-4.7	2.0	6.84	0.20
Temora_10um-02	2014-12-12 18:24	8.4	9616.81	12.51	-3418	3	172	38.9	4.8	2.9	0.15	0.00
Temora_10um-03	2014-12-12 18:37	8.4	6160.70	12.46	-3397	0	151	35.2	1.0	2.8	0.1	0.00
Temora_10um-04	2014-12-12 19:05	8.3	5471.37	12.55	-3376	-3	130	42.5	8.3	3.1	0.09	0.00
Temora_10um-05	2014-12-12 19:19	8.2	4519.56	12.51	-3355	-6	109	39.2	5.1	3.5	0.07	0.00

Temora_10um-06	2014-12-12 19:33	7.9	6029.09	12.58	-3334	-9	87	45.0	10.9	2.8	0.1	0.00
Temora_10um-07	2014-12-12 19:47	8.0	5302.67	12.49	-3313	-12	66	37.7	3.6	3.4	0.09	0.00
Temora_10um-08	2014-12-12 20:14	7.5	4240.49	12.58	-3291	-14	44	44.8	10.6	3.1	0.08	0.00
Temora_10um-09	2014-12-12 20:28	7.6	1561.35	12.45	-3269	-16	22	34.2	-	-	0.03	0.00
Temora_10um-10	2014-12-12 20:42	7.2	1448.02	12.52	-3247	-18	0	40.1	5.9	5.7	0.03	0.00
Temora_10um-11	2014-12-12 21:10	7.0	1430.49	12.41	-3225	-20	-22	30.9	-	-	0.03	0.00
Temora_10um-12	2014-12-12 21:24	7.1	2698.20	12.43	-3203	-22	-44	32.3	-	-	0.05	0.00
Temora_10um-13	2014-12-12 21:38	7.1	5482.21	12.64	-3181	-24	-66	50.2	16.1	3.1	0.1	0.00
Temora_10um-14	2014-12-12 22:05	7.0	3220.67	12.53	-3159	-26	-88	40.8	6.6	4.0	0.06	0.00
Temora_10um-15	2014-12-12 22:19	7.1	3507.49	12.49	-3137	-28	-110	37.2	3.1	4.4	0.07	0.00
Temora_10um-16	2014-12-12 22:33	7.0	3413.70	12.53	-3115	-30	-133	40.9	6.7	4.5	0.06	0.00
Temora_10um-17	2014-12-12 22:47	6.6	4901.93	12.59	-3093	-32	-155	45.8	11.7	3.6	0.1	0.00
Temora_10um-18	2014-12-12 23:15	6.1	73417.32	12.45	-3071	-34	-177	33.9	-0.2	1.2	1.6	0.01
Temora_10um-19	2014-12-12 23:28	6.2	234952.80	12.43	-3049	-36	-199	32.4	-1.8	0.6	5.01	0.03

PUBLICATIONS

PUBLISHED PAPERS

1. Li, X. H., Liu, Y., Tang, Y. J., **Gao, Y. Y.**, Li, Q. L. and Tang, G. Q. 2015. In situ Li isotopes analytical techniques and applications. Earth Science Frontiers in publication, (in Chinese with English Abstract).
2. **Gao, Y.-Y.**, et al. 2014. Screening criteria for reliable U–Pb geochronology and oxygen isotope analysis in uranium-rich zircons: A case study from the Suzhou A-type granites, SE China. Lithos 192-195: 180-191.
3. Li, X.-H., Li, Z.-X., Li, W.-X., Wang, X.-C., **Gao, Y.-Y**. 2013. Revisiting the "C-type adakites" of the Lower Yangtze River Belt, central eastern China: *in situ* zircon Hf–O isotope and geochemical constraints. Chemical Geology 345: 1-15.
4. Li, X.-H., Li, Z.-X, He, B., Li, W.-X., Li, Q.-L., **Gao, Y.-Y** Wang, X.-C.. 2012. The Early Permian active continental margin and crustal growth of the Cathaysia Block: *in situ* U-Pb, Lu-Hf and O isotope analyses of detrital zircons. Chemical Geology 328: 195-207.
5. **Gao, Y.-Y**, Li, X. H., Li, Q. L. and Chung, S. L. 2010. Quaternary zircon geochronology by secondary ion mass spectrometry: A case study of the Chinkuashi dacite from northeastern Taiwan. Earth Science Frontiers 17 (2): 146-155, (in Chinese with English Abstract).
6. Li, X. H., Li, W.-X., Wang, X.-C., Li, Q. L., Liu, Y., Tang, G. Q., **Gao, Y.-Y**, Wu, F. Y.. 2010. SIMS U-Pb zircon geochronology of porphyry Cu-Au-(Mo) deposits in the Yangtze River Metallogenic Belt, eastern China: Magmatic response to early Cretaceous lithospheric extension. Lithos 119(3-4): 427-438.

CONFERENCE ABSTRACTS

1. Yu-ya Gao, Xian-hua Li, Suzane Y. O'Reilly. Low-$\delta^{18}O$ Suzhou A-type granite revisited：Uranium influences *in situ* zircon Oxygen-isotope analyses. 2012 34th International Geological Conference
2. Yu-ya Gao, Xian-hua Li, William L. Griffin, Suzanne Y. O'Reilly, Norman J. Pearson. Li isotopes in zircon: effects of Li substitution and kinetic fractionation. Goldschmidt 2013 conference